Sustainable Operational Oceanography

Proceedings of the Sixth International Conference on EuroGOOS
4–6 October 2011, Sopot, Poland

Edited by

H. Dahlin, EuroGOOS Office, Norrköping, Sweden

N.C. Flemming, National Oceanography Centre, UK

S.E. Petersson, EuroGOOS Office, Norrköping, Sweden

Published by

EuroGOOS Office
SMHI
601 76 Norrköping
Sweden

Tel: +46 11 495 8030
Email: eurogoos@smhi.se
Internet: www.eurogoos.org

and

Poland....

:

Acknowledgements:

First published 2013

EuroGOOS Publication no.

ISBN 978-91-974828----

Conference Organisers

Organising Committee

Jan Piechura	IO-PAN, Poland
Hans Dahlin	EuroGOOS Director
Peter Ehlers	EuroGOOS Chair
Marcin Wichorowski	IO-PAN, Poland
Siân Petersson	EuroGOOS Office

Scientific Steering Committee

Hans Dahlin	EuroGOOS Director
Peter Ehlers	EuroGOOS Chair
Enrique Alvarez Fanjul	Puertos del Estados, Spain
Mike Bell	Met Office, UK
Erik Buch	DMI, Denmark
Alessandro Crise	OGS, Italy
Johnny Johannessen	Nansen Center, Norway
Pierre Yves Le Traon	IFREMER, France
Glenn Nolan	Marine Institute, Ireland
Harm Oterdoom	RWS, The Netherlands
Jan Piechura	IO-PAN, Poland
Kostas Nittis	HCMR, Greece
Nadia Pinardi	MOON, INGV, Italy
Sylvie Pouliquen	IBI-ROOS, IFREMER, France
Kees van Ruiten	NOOS, Deltares, The Netherlands
Stein Sandven	Arctic ROOS, Nansen Center, Norway

Table of Contents

Operational coastal services

Oil-drift forecasting services

Monitoring and modelling marine biogeochemical processes

Indexes

Introduction

The Need for Sustained Operational Oceanographic Services

Peter Ehlers, EuroGOOS Chair

Opening Address at the 6th EuroGOOS Conference

Ladies and gentlemen,

It may be that sometime in the future this century will be addressed as the beginning of a maritime age. The seas and oceans are playing an ever increasing role for our life and for our survival.

The oceans are a basic factor for the global climate. They influence climate change and they are affected by the impacts of climate change, not least in coastal regions. The seas are very sensitive ecological systems which need to be protected. This is quite evident here in the Baltic Sea area, which is still suffering from heavy environmental threats.

Marine life contributes to biological diversity which is an indispensable component of the earth system and must be preserved. Just recently the results of the census of marine life have attracted great public interest. At the same time we are intensifying the utilisation of the seas by which the marine environment is further stressed. Maritime transportation is the drive belt for global commerce.

The marine living resources are being increasingly exploited as a food supply. Fishery has been pursued on an industrial scale worldwide for a long time now, strongly suffering from over-fishing. Aquaculture is the fastest growing part of the food industry. Marine biotechnology is becoming an issue of increasing interest.

As concerns the exploitation of non-living resources industry, it is extending its activities to water depths of several thousand metres and into ice-covered regions. That is true in particular with regard to oil and gas which will still cover a big part of our energy demands for the next decades. Maybe someday it will be replaced by gas hydrates. The increasing demand and the increasing costs for mineral resources lead to new incentives for deep sea mining. The awareness for this need is growing in the light of the current discussion about noble earths.

Offshore wind farms are becoming reality in particular off European coasts. Though the production of renewable marine energy – by using tidal, wave, current and thermal power – is still at its infancy due to the still necessary technological developments, in the longer run it will gain in importance.

Ladies and gentlemen,

All this requires a sustainable marine development, based on good ocean management, following the ecosystem approach to reflect a jointly agreed vision of a healthy marine environment with diverse biological components functioning in balance, resulting in a good ecological status and supporting a wide range of sustainable human activities. No wonder that integrated coastal zone management and maritime spatial planning are upcoming issues.

To meet these challenges, sufficient information about the seas and the oceans is a basic and indispensable requirement. We need to know as much as possible about the complex physical, chemical, biological and geological processes taking place in the ocean, in the coastal waters, on the sea floor and in the seabed. Such knowledge is still largely insufficient, fragmented and not easily accessible. Considering the importance which the oceans and the coastal waters have for us and will have even more in the future, there is a most compelling need to improve our understanding by collecting, processing and managing all data needed for describing the processes, to make the data accessible to all who need them for planning and decision making, and to provide forecast services for a broad range of application.

In the light of these requirements, oceanographic data – and that includes physical, chemical, biological and geological parameters – are gaining in importance. A lot of valuable work has been and will be done by marine research. But due to the time restriction of research programmes and projects, research is not sufficient, but has to be based on, and accompanied and supplemented by sustained, permanent oceanographic monitoring and observation systems. Identification of trends in data series, covering long periods of time, will be indispensable as well as regular products and services based on these data, meeting various and widely differing needs for information. These services must be clearly defined, they must meet the real needs of users, and they must have a solid, reliable financial basis with a long term perspective. They cannot be performed and financed on the basis of time-limited research activities, but they require a firm commitment by governments, ascertaining their sustainability. In this respect we still have to face heavy deficits. Governments are reluctant to enter into long-term binding commitments for ocean observation systems and to acknowledge them as a political priority issue. This is a problem at the global level, where all the efforts of more than 20 years to establish a global ocean observing system have not yet led to the results needed. But it is also a problem for us in Europe. Up to now we do not have a firm and well-grounded structure for such a system although EuroGOOS as a network of institutes in Europe dealing with operational oceanography has already existed for 15 years. It is one of the weaknesses of EuroGOOS that we are an unincorporated association of institutes; and that most of our members are not mandated to act on behalf of their governments and to enter into any far-reaching commitments. We are trying to strengthen the role of EuroGOOS. Currently we are planning to transfer EuroGOOS into an entity with its own legal personality. That will be an important step forward. And in the framework of the MyOcean project we are considering the establishment of a European Centre for Ocean Monitoring and Forecasting. We will hear more about this initiative during this conference.

Ladies and gentlemen,

What is needed from operational oceanography, including recent developments and the installation of sustained services, is the topic of this conference on “Sustainable Operational Oceanography”. I welcome you all most cordially to the 6th EuroGOOS conference here in Sopot. The large number of participants including scientists, engineers, technical experts, policy makers and administrators, representatives from the public sector as well as from industry, from all parts of Europe and other parts of the world is quite promising. I apologise for not addressing all of you individually. That

would go beyond the time frame of my welcome address. But as *partes pro toto* I want to address some participants in person.

I bid a cordial welcome to the President of Sopot, Jacek Karnowski. I cordially welcome the Director of the Polish Institute of Oceanology Janusz Pempkowiak. Your well-renowned institute contributes substantially to improving the knowledge of the seas. And we are very glad that you together with the Polish Maritime Institute and the Polish Institute of Meteorology and Water Management and together with the Polish Government invited us to hold this conference here in Sopot which is a very appropriate venue for this conference. I am sure that the *genius loci* will be inspiring for this meeting. Please, convey our great gratitude to the Polish Government for supporting this conference as part of the national activities of Poland within their Presidency in the European Union. Maritime and marine matters and science have long been important issues in this country, as quite recently has been shown by the very impressive European Maritime Day activities in Gdansk.

I cordially welcome Krzysztof Jan Kurdzydlowski, Director of the Polish National Centre for Research and Development. We appreciate very much your dedication to applied science.

I also want to welcome the representative of the Intergovernmental Oceanographic Commission of UNESCO, Albert Fischer, who is the acting director of the GOOS Project Office. EuroGOOS is very closely related to IOC, contributing to the implementation of the Global Ocean Observing System under the auspices of IOC. IOC is co-sponsoring this conference which marks the end of the 50-year jubilee activities of IOC. And I extend this welcome to the colleagues from other regional ocean observing systems.

It is good that you have joined us from so many different parts of the world. Yesterday we had already a very important and fruitful meeting of our GOOS Regional Alliances Forum aiming at further promoting the global system.

We are very happy that Kostas Nittis, Chair of the Marine Board of the European Science Foundation is with us at this conference.

Last but not least I want to welcome our keynote speakers. Colin Grant from BP representing the users side, and Mike Bell from the UK National Centre for Ocean Forecasting. We are looking forward to your speeches.

Ladies and gentlemen,

This is already the 6th EuroGOOS Conference. All the forgoing Conferences have largely contributed to advancing operational oceanography. The proceedings of the conferences reflect the quite impressive development in this field since the mid-1990s. Looking into this year's conference programme you will see that again we are covering a broad range of subjects to be discussed. This morning we will start by hearing about some user perspectives – and I attach great significance to that aspect, as in the end we have to meet the needs of the users. After that we will hear about operational oceanography, coupled predictions and climate change. Then we will get some latest information about what is going on in the IOC with regard to operational oceanography. Our plenary session will raise the most challenging question of how to make operational oceanography sustainable, and numerous parallel sessions will follow dealing with

- Operational Oceanography for climate monitoring and impact
- Real-time observations from ocean and space
- Nowcasting, forecasting and re-analysis
- Operational coastal services
- Monitoring and modelling marine biogeochemical processes
- Oil drift forecasting services.

My expectation is that we will exchange the latest information available, that we will learn from recent projects and benefit from experience gained, that we will develop new ideas on how to make further progress, that we will promote co-operation and find ways to establish those services which are needed. Eventually my hope is that someday we may state that this conference here in Sopot was an important milestone for establishing and ascertaining sustained operational oceanographic services in Europe to facilitate the use and the protection of the seas.

I must not end without expressing my very great gratitude to all those who have brought this conference to reality: in particular to all our Polish colleagues who did all the preparatory work here in Sopot which was necessary, and to the EuroGOOS Office. I want to express my great appreciation to all the speakers at this conference as well as to the session chairs and the rapporteurs. And ultimately I want to thank you all for coming and for participating pro-actively in the conference.

I wish all of us very interesting, exciting sessions, good presentations and discussions which hopefully will lead to new insights and ideas. Besides that the conference may also help us to intensify personal contacts which quite often are decisive for successful co-operation. I am quite sure that this conference will be an enrichment for all of us and that we will enjoy our stay here in Sopot.

Real-time observations from ocean and space

Coastal monitoring: new experiences in central Tyrrhenian Sea

M. Marcelli*[1], G. Zappalà[2], and V. Piermattei[1]

[1]*Laboratory of Experimental Oceanology and Marine Ecology (DECOS), Tuscia University (Italy)*
[2]*CNR-IAMC Messina (Italy)*

Abstract

Complex decision systems have been implemented for prevention and ecological risk analysis, based on economically sustainable activities including forecasting models, satellite images and sustainable observatory networks. Operational oceanography has been engaged in the development of new acquisition, transmission and assimilation systems in order to have the widest possible coverage of real time information, reflecting the guidelines of the World Meteorological Organization (WMO) and of the Intergovernmental Oceanographic Commission (IOC). The high costs of offshore mooring systems and traditional oceanographic cruises have suggested the use of alternative platforms to collect a large number of oceanographic data in a wide space. In particular the Ship-of-Opportunity Programme (SOOP) realised a network to support different operational needs, first of all the provision of upper ocean data for data assimilation in models, in support of climate prediction. Moreover, marine coastal areas can be monitored using small measure platforms integrating "on demand" sensors and systems to measure air and water parameters, streaming collected data using a cellular modem, able to directly connect to internet. This work shows an integrated real time observing system installed in the Latium coastal area (Central Tyrrhenian Sea). It comprises new low cost technological devices and an automatic multi-purpose buoy equipped with a pumping system developed ad hoc for physical-chemical-biological variables measuring. In particular this last device, because of its geographical location, has a strategic relevance for the ocean colour satellite sensors calibration, allowing investigation of marine coastal areas classified as 'case 2' waters and constituting a reference station for water quality assessment.

Keywords: Coastal platform, low cost technologies, multi-purpose observatory network

1. Introduction

A buoy was installed with the main aim of continuously measuring seawater descriptors at a strategic point characterised by different anthropic pressures (e.g. industrial ports, power plants and industries, aquaculture, freshwater incomes), which overlap with high natural value ecosystems. Due to the multiple stressors affecting the coastal area near the Port of Rome, in the north of Latium, the Environmental Ministry decided to monitor the state of ecosystems in a project conducted by the Port Authority.

* Corresponding author, email: marcomarcell@unitus.it

The installation of this platform in the Civitavecchia coastal area therefore has the objective to contribute to the evaluation and control of the environmental changes, which can be due to natural or anthropic causes.

In particular the presence of a fixed station for continuous measurement of meteorological, oceanographic and, mainly, bioptical parameters is a great support to the evaluation of the marine water trophic state.

The platform was an automatic multi-purpose buoy, allowing the integration of various type of instruments. Thus the buoy will be an important point for remote sensing data and mathematical model calibration. In fact operational forecasting of ocean circulation and marine ecosystem fluctuations requires multi-parametric real-time measurements of physical and biochemical properties (Nittis *et al*., 2003).

Moreover the buoy will be an experimental platform for testing of new, low-cost oceanographic technological devices.

This work represents the first step of a multidisciplinary project to integrate a coastal buoy for testing newly developed low cost sensors and systems, for calibration and validation of satellite sensors. Affordable platforms underpin our ability to make sustained in-situ observations of the ocean (Griffiths *et al*., 1999).

Interdisciplinary sensor suites are important for studying problems such as carbon dioxide cycling and variability, the role of biology in upper ocean heating, phytoplankton productivity, upper ocean ecology, population dynamics, and sediment resuspension (Tokar *et al*., 1999).

This paper shows the upgrade of the platform and the integration of new low cost technological devices for coastal environment monitoring.

2. Coastal buoy

2.1 Architecture of the system

The platform was originally moored in Siracusa (Sicily, Italy) coastal waters as a part of a monitoring network funded by the Italian Ministry for University and Research.

Several versions of the systems have been built, with different sensors and hardware components, and installed in Messina (1995) and Venice (1997) as a part, respectively, of the activities of the CNR Strategical Project for Automatic Monitoring of Marine Pollution in Southern Italy Seas and of the PRISMA 2 programme, aimed at the study and safeguard of the Adriatic Sea (Zappalà *et al.*, 1999).

The platform, installed off the coast of Civitavecchia, in a depth approximately 40 m deep, has a size of 4.0 × 2.4 m with a maximum height of about 3 metres above sea level (due to the presence of a frame for the meteorological station) with a mass around 1100 kg, which can vary depending on the payload.

The configuration of the structure, similar to that of a catamaran, was designed to provide maximum stability.

The entire platform loaded with equipment, the mast-head and two people, placed on either side of the structure, has a tipping capacity of about 40 degrees, sufficient to ensure stability.

The platform is made of stainless steel, which supports 10 cylindrical floating buoys, arranged in two rows. In an upper position, still connected to the stainless steel frame, four other floating buoys can be added to increase to rollover stability.

In the central semi-submerged part, a container houses the equipment for measurement and analysis.

In the middle of the structure there is a stainless steel trellis arch supporting the signalling equipment and the meteorological instrumentation. The signalling system is composed of a marine lantern flashing twilight automatic ignition and, as passive radar reflector, one St. Andrew's cross.

Figure 1 The buoy.

2.2 Buoy management, data acquisition and transmission system

The buoy is managed by a new, improved version of the advanced system for data acquisition and transmission, formerly described by Zappalà *et al*. (2002).

The data acquisition and transmission system uses a PC104 standard form factor implementing a PC-like architecture with low power consumption.

The PC104 uses a CPU-1452, which is an embedded RoHS compliant board based on two modules: a mezzanine CPU module combined with a PC/104-Plus form factor carrier. The mezzanine CPU module features the processor and its Intel® 815E chipset with 100MHz bus frequency. The processor is the Intel® Celeron® 400MHz. The system comes with 256 MB SDRAM soldered on board. No active cooling is required to operate within the standard and extended temperature ranges.

Ten RS232 ports are available to connect instruments, and a 1GB compact flash card is used as mass memory unit and a real time clock. Connections for keyboard and monitor complete the computer system.

A cellular radio modem is used for data acquisition and transmission enabling, thanks to an embedded TCP/IP stack, to easily connect to the internet both to transmit data and receive commands using standard FTP and email protocols; it is always possible also to connect to the buoy simply using a traditional modem dialling the buoy cellular phone number.

The management software is a newer improved version of that formerly described by Zappalà *et al*. (2004). Thanks to the embedded macro-commands the software enables easy management of the maintenance of the buoy and the instruments, operation and measurements, automatically starting measurement cycles, every 10 minutes, which can be altered and are remotely programmable without stopping normal activity.

An unmoored buoy test is performed at the beginning of every measurement cycle, comparing the buoy position read by GPS against the pre-set mean/max latitude and longitude values and sending, if necessary, SMS alarm messages are sent to control centre operators.

The power supply system in its full implementation comprises one 200W wind generator, four 80W solar panels and up to eight 12V 80Ah batteries. The full implementation is necessary only when high energy demanding devices (e.g. pumping systems, chemical analysers) are integrated in the buoy system.

3. Instrumental payload

Progress in solving most oceanographic problems is still significantly limited by technological barriers (Dickey and Bidigare, 2005).

At present the buoy hosts and manages an Idronaut OceanSeven 316 multi-parametric probe for temperature, conductivity, dissolved oxygen, pH, chlorophyll-a fluorescence and turbidity measurements. Moreover a differential dangling measure system is integrated to acquire temperature at five fixed depth by means of SBE 38.

Moorings have been used to obtain chemical, optical, biological and acoustical data in addition to the more common physical data and have proven to be excellent platforms for testing and developing new sensors (Griffiths *et al*., 1999).

In fact the innovation in this work is represented by the application of a low cost technology for temperature, conductivity and fluorescence of chlorophyll-a measure to the buoy system.

3.1 Low cost technology

The low cost instrument was developed during the MFS-TEP project, specifically the T-FLAP (european patent n. EP1962089A1). It was developed because of the possibility of using a continuous profiling probe, with an active fluorescence measurement, and is very important in real time phytoplankton studies; it is the best way to follow the variability of sea productivity (Marcelli *et al*., 2007).

The device is developed with low cost components, but allows a high accuracy of measurements. The measurement components are based on: a pressure transducer, a glass bulb temperature resistor; blue LEDs, interferential filters and a photodiode for the fluorescence measure.

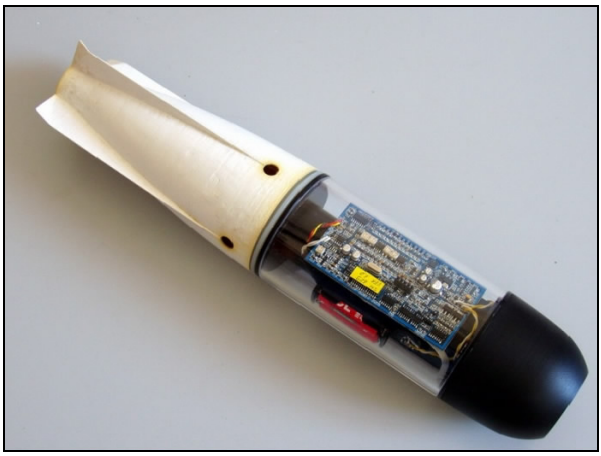

Figure 2 The T-FLAP

To enable continuous measurement, one T-FLAP is plugged in a circuit powered by a surface pumping system and managed by the buoy electronics.

The instrument was calibrated by means of a laboratory calibration system, composed of a closed hydraulic circuit which simulates the buoy pumping system and which includes reference sensors (MicroTSG SBE45, FIAlab Fluorometer).

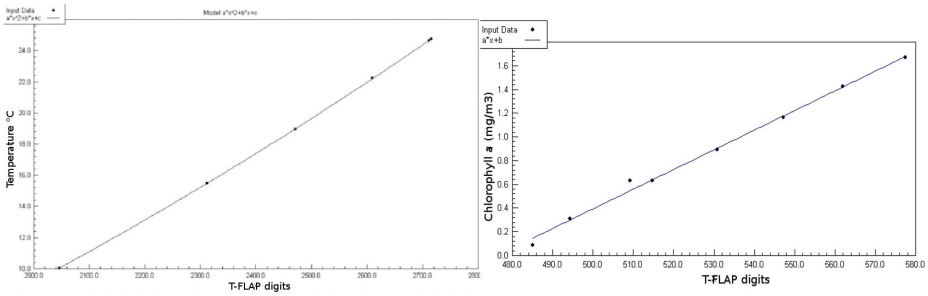

Figure 3 Temperature and Fluorescence calibration of T-FLAP

3.2 Future integrations

In the future also multispectral sensors, water samplers (previously described in their first version by Zappalà *et al*., 2002), pumping systems and a meteorological station will be added in the buoy instrumental payload.

References

Dickey, T.D. and R.R. Bidigare (2005): Interdisciplinary oceanographic observations: the wave of the future, Scientia Marina, 69 (Suppl. 1), 23-42.

Griffiths, G., R. Davis, C. Eriksen, D. Frye, P. Marchand, and T. Dickey (1999): Towards new platform technology for sustained observations. Proc. Of OceanObs 99, www.bom.gov.au/OceanObs99/Papers/Griffiths.pdf

rish, J.D., R.C. Beardsley, W.J. Williams, and K.H. Brink (1999): Long-term moored observations on Georges Bank as part of the U. S. Globec Northwest Atlantic/ Georges Bank program. Proc. of MTS-IEEE OCEANS '99 Conference, I, pp. 273-278.

Marcelli, M., A. Di Maio, D. Donis, U, Mainardi, and G.M.R. Manzella (2007): Development of a new expendable probe for the study of pelagic ecosystems from voluntary observing ships. Ocean,Sci., 3, 1-10.

Nitttis, K., C. Tziavos, I. Thanos, P. Drakopoulos, V. Cardin, M. Gacic, G. Petihakis, and R. Basana (2003):, The Mediterranean Moored Multi-sensor Array (M3A): system development and initial results. Annales Geophysicae, 21, pp. 75-87.

Tokar, J.M., and T.D. Dickey (1999): “Chemical sensor technology - Current and future applications”, chapter in: Chemical Sensors in Oceanography.

Zappalà, G., G. Caruso, and E. Crisafi (2002): Design and use of advanced technology devices for sea water monitoring. Operational Oceanography. Implementation at the european and regional Scales, eds. Flemming N.C., S. Vallerga, N. Pinardi, H.W.A. Behrens, G. Manzella, D. Prandle, and J.H. Stel, Elsevier Oceanography Series, 66.

Zappalà, G. (2004): A software set for environment monitoring networks. Proc. Of the Int. Conf. On Development and Application of Computer Techniques to Environmental Studies X. Envirosoft 2004, eds. G. Latini, G. Passerini, and C.A. Brebbia, WIT Press, Southampton, pp. 3-12.

Zappalà, G., L. Alberotanza, and E. Crisafi (1999): Assessment of environmental conditions using automatic monitoring systems. Proc. of MTS-IEEE OCEANS '99 Conference, II, pp. 796-800.

Activities of the calibration laboratory at HCMR-Crete – progress and challenges

M. Ntoumas*[1], D. Kassis[1], M. Potiris[2], D. Ballas[1], T. Chondronasios[1], P. Pagonis[1], T. Tsagaraki[1], D. Podaras[1], L. Manousakis[1], V. Zervakis[2], P. Drakopoulos[3], G. Petihakis[1], and K. Nittis[1]

[1]*Institute of Oceanography, HCMR*
[2]*Department of Marine Sciences, University of the Aegean*
[3]*Department of Optics, TEI of Athens*

Abstract

The calibration laboratory of HCMR-Crete has been developed to support the POSEIDON weather forecasting and monitoring system. It is set up to work with a range of sensors, which include temperature, conductivity, turbidity, Chl-*a* and oxygen. A large temperature-controlled tank with an approximate volume of 1.5 m^3 is used to achieve salinity and temperature gradients where necessary.

The calibration procedures followed are compliant with manufacturer recommendations; however, our main focus is on data ranges recorded in the eastern Mediterranean area. Processing and evaluation of calibration data focuses on minimising sensor drift by recalculating corrected coefficients at regular intervals. Special effort is made in order to establish a time-dependent filter that would perform dynamic data corrections following the sensor drift.

In the future we aim to utilise pre- and post- deployment calibration procedures to examine biofouling effects and define its contribution to the overall sensor drift. As sensors are expected to contribute to data assimilation as part of an integrated sampling system, we also focus on defining overall errors and their sources in order to improve sensor performance.

Although a large number of sensors are deployed every year in the European seas, calibration procedures vary significantly between laboratories. Thus it would be very constructive to work towards common practices, an approach already in place for observational platforms (buoys, ferryboxes, and gliders) and we believe a similar set-up along with a possible certification method would be very useful.

Keywords: operational oceanography, buoy network, calibration, biofouling

1. Introduction

The POSEIDON monitoring and forecasting system of the Eastern Mediterranean (poseidon.hcmr.gr) uses a variety of platforms ranging from coastal buoys equipped with a few basic met-ocean sensors to open sea stations with an extensive list of sensors targeted to both physical and biochemical process and their coupling at various time scales (Petihakis *et al.*, 2010). Three multi-parametric deep water observatories currently

* Corresponding author, email: mntou@hcmr.gr

operate: the E1-M3A mooring operating in the Cretan Sea since 2000, Athos station in North Aegean and Pylos mooring site that operates in the SE Ionian Sea. These stations host sensors for temperature and salinity at several depths ranging from surface to 1000 m as well as Chl-*a*, dissolved oxygen, PAR and light attenuation at 20, 50, 75 and 100 m (M3A). The surface buoy hosts a complete set of sensors for air-sea interaction studies (wind speed and direction, air pressure, air temperature, wave height and direction, relative humidity, precipitation, radiance, irradiance, radiometer and pyranometer) as well as an ADCP for current speed measurements in the upper 100 m. A total of 20 CTs and CTDs plus the surface sensors are always deployed in the field for a period of 6 up to 8 months before they are replaced. The large number of the deployed sensors and the need for high quality data led to developing of calibration methods and infrastructures to cover the needs of the POSEIDON monitoring and forecasting system.

2. Calibration strategy

In order to minimise the calibration time and expenses, our calibration procedure is designed in such a way as to cover the range of the measured parameters present in Greek seas. For temperature this translates to a range of 11–28 °C. Keeping that in mind and given the regional salinities (31–39.6 psu) as well as the min-max deployment depths we estimate a calibration range for the conductivity sensors between 3.5 and 6.47 $\mathrm{S\,m^{-1}}$. For turbidity and Chl-*a* sensors the calibration procedure is carried out with reference solutions with low concentrations, which correspond to the actual values measured in the oligotrophic open seas around Greece. Dissolved oxygen sensors are calibrated over the range of 0–100% saturated solutions resulting in different concentrations depending on salinity and temperature. Furthermore in the future we are aiming to adjust even further the calibration range of each sensor to the specific local conditions at each deployment site.

3. Equipment

3.1 Infrastructures

The calibration facilities at the HCMR Thalassocosmos complex in Crete include a fully equipped laboratory with a custom-made large calibration tank, two smaller plexiglass tanks and a number of reference sensors and all the necessary apparatus for temperature, salinity, Chl-*a*, turbidity and dissolved oxygen sensor calibration. The support team consists of the HCMR technicians and scientists, who prepare the instrumentation, perform field experiments, service and maintain the instruments and assist users during experiments in the calibration facility.

The T/C calibration tank has an inner diameter of about 122 cm and an inner height of 120 cm, allowing an adequate number of sensors to be immersed in it. The tank walls are PVC with a polyurethane filling and are 9 cm thick, providing the necessary heat insulation. It is equipped with a 2000 W heating element and an electric motor with a propeller for the efficient homogenisation of the tank water (Zervakis, 2008).

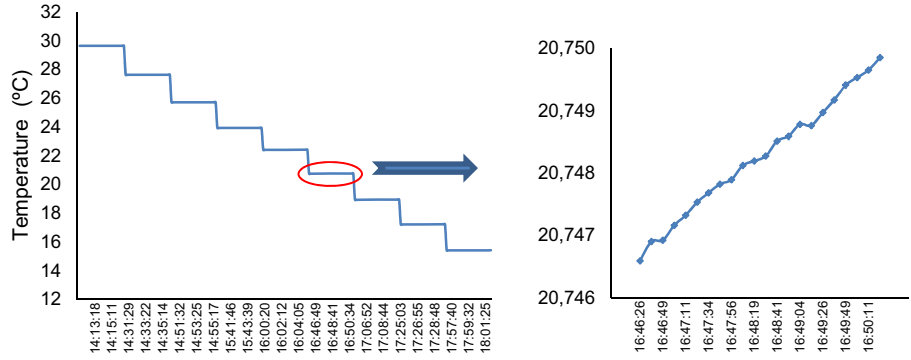

Figure 1 Temperature calibration experiment a) full-range time steps; b) single time step temperature evolution.

The large volume of the T/C tank allows the simultaneous immersion of 4 CTD units (SBE 16 plus) inside the filtered seawater. The continuous stirring and the use of the CTD pumps effectively eliminate salinity spikes without causing any thermal errors, allowing discrete calibration steps (Figure 1a). The water sampling for the salinity analysis is performed from the same water level that the immersed instruments log data.

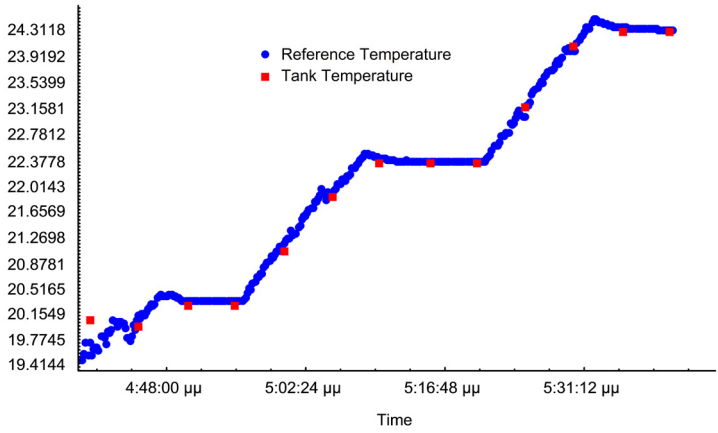

Figure 2 The Haage bath performance in comparison with the SBE-35 Deep Ocean Standards Thermometer.

The two smaller 100 l plexiglass baths are equipped with a laboratory Haage temperature control circuit that permits fast temperature gradients and temperature stabilisation. The baths are used for smaller T/C sensors as well as DO sensors calibration and their stability is validated, during the experiments, by the SBE 35 Standards Thermometer (Figure 2).

3.2 Standards and references

The temperature reference sensor used in the HCMR calibration lab is the SBE 35 Deep Ocean Standards Thermometer manufactured by Seabird Electronics with an accuracy of 0.001°C and stability of 0.001°C per year (www.seabird.com/products/spec_sheets/35data.htm). For salinity measurements we use an Autosal 8400A laboratory salinometer standardised with IAPSO Standard Seawater and an accuracy of 0.003 ppt (www.guildline.com/oceanography.php).

An estimation of the calibration precision for temperature is 0.0054°C as a result of the square root of the sum of squares of the SBE 35 accuracy, the non-uniformity of the temperature distribution in the T/C tank and the tank stability during a calibration step. The non-uniformity of the temperature is considered to be the maximum difference between the reference sensor and a second temperature sensor calibrated by the manufacturer and its valued 0.005°C. This difference in temperature is recorded to the centre of the T/C tank where the sensors under calibration are placed. The stability of the tank is 0.002°C as the maximum difference in temperature recorded by the reference thermometer during a 2 minute calibration step (Figure 1b) (Inoue *et al.*, 2001).

Using the same approach the salinity uncertainly becomes 0.0062 psu as a product of the temperature error and the Autosal accuracy and without the contribution of sampling errors in this result.

For the calibration of the dissolved oxygen sensors the uncertainly lies on the accuracy of the Winkler titration and for the optical sensors measuring turbidity and Chl-*a* the uncertainly is a factor of the error in the production of the reference solutions in the lab.

4. Methodology

4.1 Procedures

The aim is to produce predefined calibration steps at regular intervals with an achieved homogeneity of the seawater mass inside the tank. During this multistep procedure the physical properties of the seawater are monitored and high frequency data and duplicate water samples are collected for later analysis with the high precision salinometer. The calibration of conductivity sensors is performed simultaneously with the temperature calibration and discrete gradients are created for each parameter. Seawater is collected one day prior to the calibration and the procedure begins with the highest temperature of the range selected using the tank-heating element. Using crushed (freshwater) ice, both parameters are gradually decreased to the lower point of the selected range. The procedure is fully controlled as shown in Figure 1a.

Dissolved oxygen sensors are calibrated in the Haage bath where through temperature changes we alter the oxygen concentration of the water covering the whole range of concentrations measured in the station. The turbidity and Chl-*a* sensors are calibrated against different reference solutions.

4.2 Data analysis

Generally the calibration data analysis involves defining the drift and trying to minimise it. In order to achieve that there are two approaches:

Approach A: Linear fit between reference values and sensor measurements (in most cases applied to the data). $T_{ref} = aT_{sens} + b$

An example of temperature calibration results for 4 Seabird 16 plus CTD:

CTD s.n	*a*	*b*
5039	0.99975	+0.0015
5040	0.99977	- 0.0008
5052	0.99999	- 0.0029
5055	0.99961	+ 0.0025

Approach B: Recalculating the calibration coefficients of the sensor itself (applied to the sensor e.g. SBE CTs).

The second approach involves raw sensor data that permits the recalculation of the calibration coefficients of the sensor. Usually we can log the raw and the engineering units of the sensor but in some cases we need to convert engineering units to raw with a small price for accuracy because we are processing mean values. For the calculation of the SBE T/C sensor coefficients we have develop codes and routines that resolve the manufacture relations and fit the response of the sensor to the reference values. A linear least squares fit to the calibration constants will remove some of the random uncertainty associated with each calibration point, and the calibration history can show how a sensor is aging and if the latest calibration is consistent with the past calibrations.

An example is the Seabird temperature sensors. A thermistor is not a linear device; that is, the resistance of the thermistor is not linearly related to temperature. Thermistors behave in a logarithmic manner. Sea Bird has determined that the best fit to the calibration data for the their thermistor is of the form:

$$\text{ITS-90} = \frac{1}{a_0 + a_1[\ln(f_0/f)] + a_2[\ln^2(f_0/f)] + a_3[\ln^3(f_0/f)]} - 273.15$$

Where f_0, f are the sensor frequencies
and a_0, a_1, a_2, a_3 are the sensor calibration coefficients.

This equation can be transformed to a linear third-order polynomial and a linear least squares fit allows the determination of the new calibration coefficients (Figure 3).

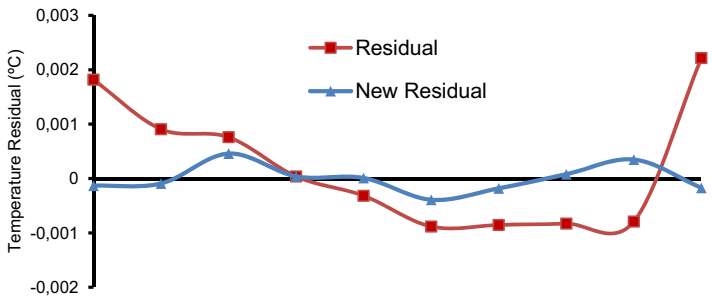

Figure 3 Residuals of a SBE temperature sensor at each calibration point before and after the recalculation of new calibration coefficients.

5. Field validation

5.1 Survey data

Once the calibration procedure is completed a field validation is also performed prior to the deployment on the POSEIDON buoy network. This is a crucial step as errors can occur throughout the calibration procedure, thus avoiding long-term deployment (6–8 month period) errors. The performance of the calibrated instrument is checked against in-situ data and if necessary a correction coefficient is applied to the transmitted data. Especially at the M3A buoy we perform a monthly multi parameter survey that includes CTD casts, equipped with Chl-*a*, turbidity and dissolved oxygen sensors, plus water samples and zooplankton nets from various depths (Figure 4). The data correction for temperature and salinity is performed following the application notes published in the Seabird Electronics webpage (www.seabird.com/application_notes/AN31.htm). This approach computes an offset drift for temperature sensors based on pre- and post-deployment calibration data. Conductivity sensors usually drift by changing span (the slope of the calibration curve) so in this case the data correction involves the calculation of the slope from calibration and survey data.

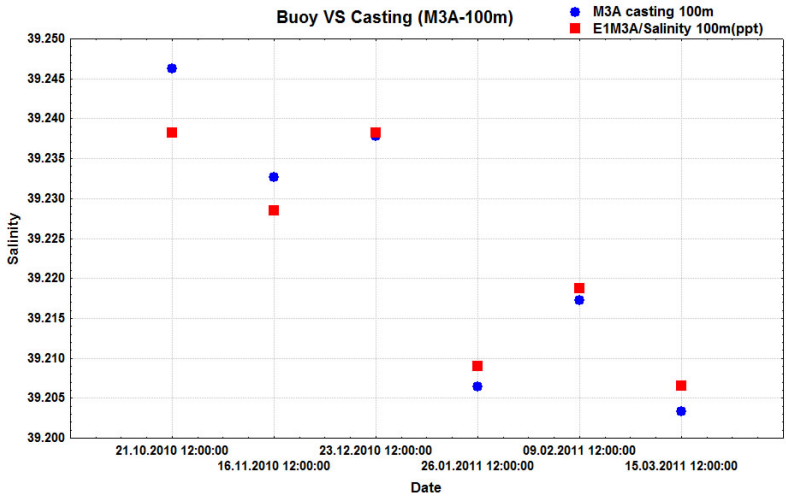

Figure 4 Monthly comparison of the conductivity sensor deployed at the M3A station in depth of 100m against the survey casting.

5.2 Biofouling

The SeaBird conductivity sensor (used on HCMR's moorings and CTDs) uses a Beckman three-electrode conductivity cell as the variable resistance element in an AC Wien Bridge Oscillator. The measurement is contained entirely within the cell so the dimension of the cell is a critical factor. The drift of a conductivity sensor is generally due to electronic component aging, fouling that leads to dimensional changes in the cell geometry, and non-conducting material in the cell. Generally the electronic drift is smooth and smaller compared to the other factors (Saunders *et al.*, 2010). Biofouling is the major limiting factor in conductivity measurements (especially moored observations) in the ocean environment. In an attempt to "quantify" the biofouling contribution to the

sensor overall drift, experiments have been performed using the same CTD unit before and after the cleaning procedures recommended by the manufacturer (Medeot *et al.*, 2010). The results, in this case, indicate that drift due to biofouling is significantly higher than the electronic drift especially after long deployment periods (Figure 5).

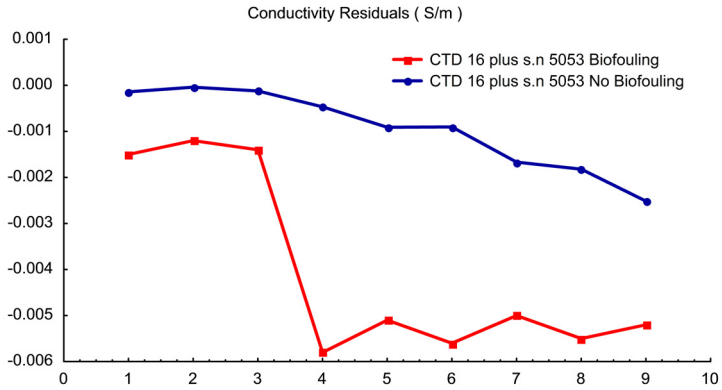

Figure 5 Residuals of a conductivity sensor before and after fouling removal.

6. Future perspectives

A major technical challenge for operational oceanography is to conduct high precision field measurements that produce high quality data available to the scientific community. In the case of extended scientific networks, such as EuroGOOS, the need for harmonisation of procedures and practises is an important issue that affects the overall quality of the produced knowledge. This statement stands out when it comes to calibration. Although several calibration laboratories operate all over Europe there are significant differences in methodologies and procedures as well as on infrastructures. In order to achieve the highest standards of performance for deployed sensors a closer collaboration and sharing of knowledge and practises will lead eventually to common adopted operation methods and significant cost reduction.

Future steps in our calibration activities involve both upgrade of equipment as well as improvement of existing methodologies, especially for optical and dissolved oxygen sensors. Thus by maintaining a detailed track of each sensor history in the field and through pre- and post- deployment calibration experiments and continuous surveys we will examine the contribution of biofouling, in terms of regional and seasonal parameters, to the overall drift. Furthermore due to different sensor technologies and demands we will further develop our analysis and fitting techniques in order to be able to minimise the drift as much as possible. The overall goal is a continuous procedure that will assure the maximum quality and will act as a dynamic filter to previous and future sensors measurements and data assimilations.

References

Inoue, A., M. Miyazaki, K. Izawa, K. Ando, Y. Takatsuki, and K. Mizuno: Stability of water temperature in the conductivity and temperature calibration system and results of calibration experiments, ARGO Technical Report FY2001, JAMSTEC, 9-17.

Medeot, Nevio, Rajesh Nair, Riccardo Gerin (2011). Laboratory Evaluation and Control of Slocum Glider C-T Sensors. J. Atmos. Oceanic Technol., 28, 838-846.

Petihakis, G., K. Nittis, D. Ballas, D. Kassis, P. Pagonis, L. Perivoliotis, and P. Drakopoulos (2009). The POSEIDON reference time-series stations of the Eastern Mediterranean Sea, in Proceedings of the "OceanObs'09: Sustained Ocean Observations and Information for Society" Conference (Annex), Venice, Italy, 21-25 September 2009, Hall, J., Harrison D.E. and Stammer, D., Eds., ESA Publication WPP-306, 2010.

Saunders, P.M., K.-H. Mahrt, and R.T. Williams (1991). Standards and laboratory calibration. WOCE Hydrographic Program Operations and Methods.

Zervakis, V. (2008). Evaluation and protocol of operation of temperature/conductivity calibration tank, HCMR.

CORA3, a comprehensive and qualified ocean in-situ dataset from 1990 to 2010

Cécile Cabanes*[1], Antoine Grouazel[1], Victor Turpin[2], François Paris[2], Christine Coatanoan[2], Karina Von Schuckmann[1], Loic Petit de la Villéon[2], Thierry Carval[2], and Sylvie Pouliquen[1]

[1]*Laboratory of Oceanography from Space (LOS), IFREMER/CNRS, Brest, France*
[2]*Coriolis Data Centre, IFREMER, Brest, France*

Abstract

Coriolis is a French programme basically aimed at contributing to the ocean in-situ measurements as part of the French oceanographic operational system. It has been especially involved in gathering all global ocean in-situ observation data in real time, and developing continuous, automatic, and permanent observation networks.

A new version of the comprehensive and qualified ocean in-situ dataset, the Coriolis dataset for Re-Analysis (CORA), is produced for the period 1990 to 2010. This in-situ dataset of temperature and salinity profiles, from different data types (Argo, GTS data, VOS ships, NODC historical data, and more) on the global scale, is meant to be used for general oceanographic research purposes, for ocean model validation, and also for initialisation or assimilation of ocean models.

To generate this new version, new and updated data have been extracted from the Coriolis database and added to the previous CORA dataset spanning the period 1990–2008. To qualify this dataset, several tests have been developed to improve the quality of the raw database in a homogeneous way, and to fit the level required by the physical ocean re-analysis activities. These tests include some simple systematic tests, a test against climatology and a more elaborate statistical test involving an objective analysis method (for the validation of this dataset). Visual quality control (QC) is performed on all the suspicious temperature (T) and salinity (S) profiles and quality flags are modified in the dataset if necessary.

This Coriolis product is available on request through MyOcean Service Desk (www.myocean.eu).

Keywords: ocean database, in-situ, quality control.

1. Introduction

The Coriolis database is a real time dataset as it is updated every day as new data arrive. In contrast, the CORA database corresponds to an extraction of all in-situ temperature and salinity profiles from the Coriolis database at a given time. All the data are then re-qualified. CORA is meant to fit the needs of both re-analysis and research projects. However, dealing with the quantity of data required by re-analysis projects and the quality of data required by research projects, remains a difficult task.

* Corresponding author, email: Cecile.Cabanes@ifremer.fr

Several important changes have been made since the last release of CORA2, concerning both the production procedure (to be able to release yearly reanalysis) and quality checks applied to the data. Those changes are the following:

- A new procedure is now used to produce the dataset: This procedure was set up to be able to extract only new and updated data from the Coriolis database at each new release of CORA.
- A new set of quality checks is performed on the data.
- A check of duplicates was re-run on the whole dataset
- An XBT bias correction has been applied.
- The CORA3 release has been extended for the period 1990−2010.

2. Description of the dataset

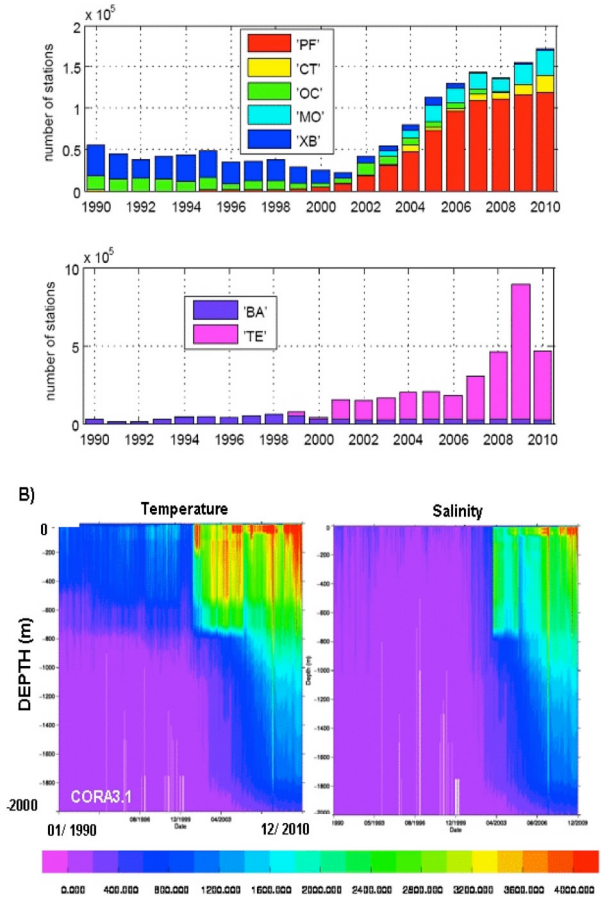

PF Argo Floats
CT CTD data
OC World Ocean Database 2009
MO Mooring data
XB XBT or XCTD
BA GTS (truncated)
TE GTS (truncated)

Figure 1 A) Number of profiles in the Global Ocean in the different file types in CORA3 and B) Number of temperature and salinity data per month over the global Ocean, as a function of depth (from S. Guinehut, CLS, Toulouse).

The Coriolis centre receives data from the Argo programme, French research ships, GTS data, GTSPP, GOSUD, MEDS, voluntary observing and merchants ships, moorings, and the World Ocean Database (the last one not in real time). CORA thus contains data from different types of instruments: mainly Argo floats, XBT, CTD and XCTD, and moorings. The data are stored in 7 file types: PF, XB, CT, OC, MO, BA, and TE. Figure 1 shows the number of temperature and salinity profiles in the CORA3 database for the whole period 1990–2010 and their repartitioning among the different file types. A large amount of data comes from the GTS as a consequence of the real time needs of the Coriolis data centre.

3. Description of data processing

3.1 Data flow

CORA data are retrieved from the Coriolis database which is constantly evolving because new data are submitted, some data are reprocessed, other data are adjusted in delayed mode (Argo data), quality flags are modified in the Coriolis database after quality checks have been performed, etc. Basically, all new and modified data since the previous version of CORA are retrieved from the Coriolis database. This subset of new and updated data are then re-qualified. Other quality checks are performed on the whole dataset to ensure data quality consistency.

3.2 Quality checks

Data received by the Coriolis data centre from different sources are put through a set of quality control procedures (Coatanoan and Petit de la Villéon, 2005) to ensure a consistent dataset.

Besides these tests, several other quality checks have been developed or applied to produce CORA3 in order to reach the quality level required by the physical ocean re-analysis activities. These checks include some simple systematic tests; a test against climatology and a more elaborate statistical test involving an objective analysis method (see Gaillard *et al*., 2009 for further details). Visual quality control (QC) is performed on all suspicious temperature and salinity profiles. After these visual checks a decision is made on whether to change or not change the control quality flag.

- Systematic test on new and updated data

  A profile fails a systematic test when pressure is negative, T and S values are outside an acceptable range depending on depth and region, T or S are equal to zero at bottom or surface, values are constant at depth, values are outside the 10 σ climatological range, if there is large salinity gradient at the surface (more than 5 PSU within 2dB) or a systematic bias. Each time a profile failed a systematic test it was visually checked.

- Tests on the whole database

  A test against climatology that we call Anomaly Method was also applied. In this case, a profile failed the test if at least 50% of its data points lie outside the 5 σ climatological range. This allows detection of smaller deviations compare to the 10 σ check. The statistical test is based on an objective analysis run (Bretherton *et al*., 1976) with a three-week window. Residuals between the raw data and the gridded

field are computed by the analysis. Residuals larger than a defined value produce alerts that are then checked visually. This method combines the advantage of a collocation method since it takes into account all neighbouring sensors, and the comparison with climatology. Finally, Argo floats pointed out by the altimetric test (Guinehut *et al*., 2009; ftp://ftp.ifremer.fr/ifremer/argo/etc/argo-ast9-item13-AltimeterComparison) were systematically verified over all their life period and quality control flags were modified when necessary.

Quality control for the CORA3 database also includes feedback from N. Ferry (Mercator Ocean, Toulouse) who performed the run GLORYS2V1. This feedback provides a list of suspicious profiles detected by a comparison with the model solution. About 50% of the alerts were confirmed after a visual check for the CORA3 database. Figure 2 is an example of a suspicious profile detected. This kind of feedback can help to improve our tests.

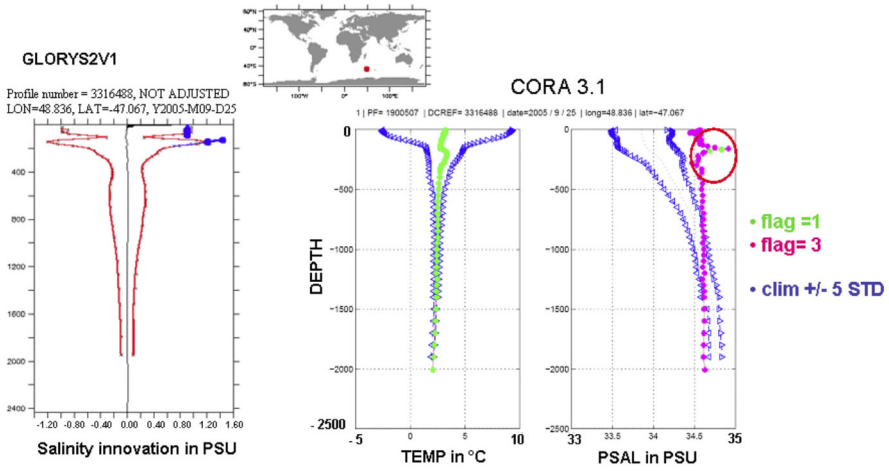

Figure 2 Example of a suspicious profile provided by the feedback of N. Ferry (Mercator Ocean, Toulouse) who performed the GLORY2V1 run. Right: Salinity innovation (PSU) and left: the visual check performed on this alert (temperature in °C and salinity in PSU as a function of depth).

A final test was performed on the whole CORA dataset in order to check for duplicate data.

3.3 XBT bias correction

Different issues with the data of eXpendable BathyThermograph (XBTs) exist and, if not corrected, they are known to contribute to anomalous global heat content variability (e.g Wijffels *et al*. 2008). The XBT system measures the time elapsed since the probe entered the water and thus inaccuracies in the fall rate equation result in depth errors. There are also issues of temperature offset but usually with little dependence on depth.

The correction applied on CORA3 dataset is an application of the method described in Hamon *et al*., 2011. This correction is divided in two parts: first the computation of the thermal offset, then the correction of depth. To evaluate the temperature offset and the error in depth all the co-localised profiles are used for reference (e.g. in a 3 km ray, ±15

days temporal frame, a maximum average temperature difference of 1°C and a bathymetric difference inferior to 1000 m) that are not XBT and with quality flags different from 3 and 4 (suspicious and bad quality). Those references thus gather CTD, Argos profilers and mooring buoys.

Figure 3 shows the impact of the correction on the difference between XBT and reference profiles in the CORA3 database as a function of time and depth. The large positive bias is significantly reduced.

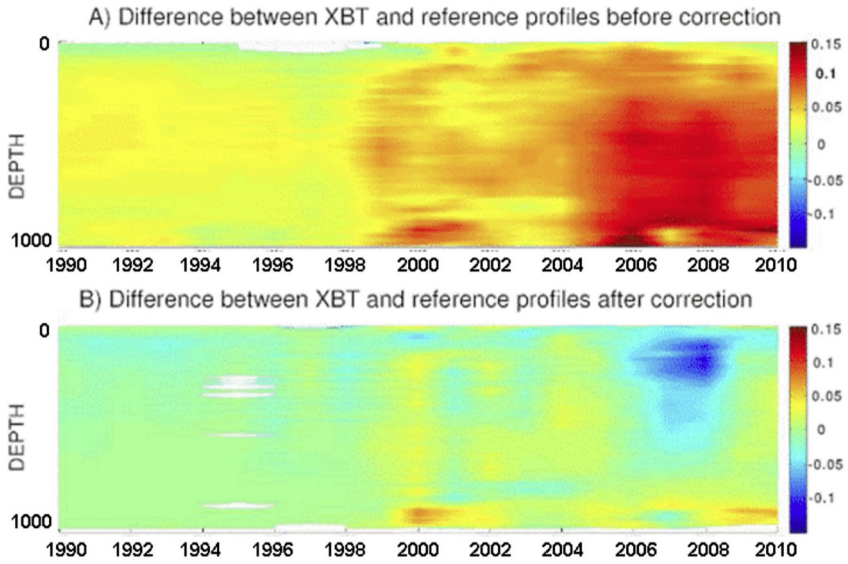

Figure 3 Temperature difference (in °C) between XBT and reference profiles before (top) and after (bottom) correction.

4. Goals and uses of the dataset

4.1 Research

The CORA database is meant to investigate specific scientific questions. Achieving this goal will lead to the improvement of the quality of the dataset, by detecting abnormal data. This will subsequently benefit the Coriolis data centre. Using the CORA database to estimate global ocean temperature, heat and freshwater still need careful comparison and sensitivity studies as these global quantities are very sensitive to any sensor drift or systematic instrumental bias (see Von Schuckmann *et al*, 2011). Although our quality controls are meant to detect such instrument problems, they can still miss unknown drifts or bias.

4.2 Data assimilation in ocean models

An important application of such a database is also its use for ocean reanalyses. Throughout the world, several reanalysis projects are underway which aim to provide a continuous space-time description of the ocean, synthesising the information provided by various observation types (remotely sensed and in-situ) and the constraints provided

by the physics of numerical ocean models. In France, global ocean reanalysis activity is a joint collaboration between Mercator-Océan, the Coriolis data centre and several oceanographic and atmospheric research laboratories in the framework of the GLORYS (GLobal Ocean ReanalYsis and Simulations) project. This project also contributes to the production of coordinated reanalyses at the European level in the context of the EU-funded FP7 project MyOcean, in collaboration with Italian, British, French and Canadian partners. The goal of GLORYS is to produce a series of realistic eddy-resolving global ocean reanalyses. Several reanalyses are planned, with different streams. Each stream can be produced several times with different technical and scientific choices. Stream 2 (GLORYS2) covering the period 1992–2010 has been produced using the CORA3 data set.

Acknowledgements

This work is part of the MyOcean project.

References

Boehme, L., P. Lovell, M. Biuw, F. Roquet, J. Nicholson, S.E. Thorpe, M.P. Meredith, and M. Fedak (2009). Technical Note: Animal-borne CTD-Satellite Relay Data Loggers for real-time oceanographic data collection, Ocean Sci., 5, 685–695.

Boyer, T.P., J.I. Antonov, O.K. Baranova, H.E. Garcia, D.R. Johnson, R.A. Locarnini, A.V. Mishonov, T.D. O'Brien, D. Seidov, I.V. Smolyar, and M.M. Zweng (2009). World Ocean Database 2009. S. Levitus, Ed., NOAA Atlas NESDIS 66, U.S. Gov. Printing Office, Wash., D.C., 216 pp., DVDs.

Bretherton, F., R. Davis, and C. Fandry (1976). A technique for objective analysis and design of oceanic experiments applied to Mode-73. Deep-Sea Res., 23, 559–582.

Coatanoan, C., and L. Petit de la Villéon (2005). Coriolis Data Centre, In-situ data quality control procedures, IFREMER report, 17 pp. www.coriolis.eu.org/cdc/documents/cordo-rap-04-047-quality-control.pdf

Gaillard, F., E. Autret, V. Thierry, P. Galaup, C. Coatanoan, and T. Loubrieu (2009). Quality controls of large Argo datasets, J. Atmos. Ocean. Tech., 26, 337–351.

Guinehut, S., C. Coatanoan, A.-L. Dhomps, P.-Y. Le Traon, and G. Larnicol (2009). On the Use of Satellite Altimeter Data in Argo Quality Control, Journal of Atmospheric and Oceanic Technology, 26, 395–402.

Hamon, M., G. Reverdin, and P.-Y. Le Traon (2012). Empirical correction of XBT data, Journal of Atmospheric and Oceanic Technology.

Von Schuckmann, K., and P.-Y. Le Traon (2011). How well can we derive Global Ocean Indicators from Argo data?, Ocean Sci. Discuss., 8, 999–1024.

Wijffels, S.E., J. Willis, C.M. Domingues, P. Barker, N.J. White, A. Gronell, K. Ridgway, and J.A. Church (2008). Changing Expendable Bathythermograph Fall Rates and Their Impact on Estimates of Thermosteric Sea Level Rise. J. Climate, 21, 5657–5672. doi: 10.1175/2008JCLI2290.1.

Operational Oceanography for climate monitoring and impact

The Polish-Russian-Norwegian co-operation for operational coastal services

Magdalena Kamińska*, Włodzimierz Krzymiński, Marzenna Sztobryn, and Natalia Drgas

Institute of Meteorology and Water Management - National research Institute, Maritime Branch in Gdynia, Poland

Abstract

The Vistula Lagoon is a trans-border lagoon of two countries: Poland and Russian Federation (Kaliningrad Oblast). Because of the economic importance of the Lagoon, e.g. regarding fishery and marine transport, as well as its touristic value, the improvement and preservation of good ecological status in this basin is equally important to both countries.

Investigations of the state of the lagoon – hydrologic, geological, physical, chemical and biological – were performed in cooperation and there was also cooperation on work on the results of historical investigations, when Poland and Russia belonged to one political system. One example is "Hydrometeorological regime of the Vistula Lagoon" issued in 1975, edited by Lazarenko and Majewski. Cooperation diminished after Poland accessed the European Union, but Polish-Russian projects started again around ten years ago. Stronger collaboration is necessary due to the requirements of the EU Water Framework Directive (60/UE/2000) of developing cooperation with non-EU countries in trans-border areas. Russia (Kaliningrad Oblast) is open to cooperation with Poland to keep and, if possible, improve the ecological status of the reservoirs.

Keywords: coastal services, Baltic Sea, Vistula Lagoon, Polish coastal zone, information and data distribution.

1. Introduction

During 2007–2011, the Maritime Branch of the Institute of Meteorology and Water Management, National Research Institute (IMWM NRI), was a beneficiary of two international projects co-financed by the Norwegian Financial Mechanism (NFM) – "Strengthening the administrative capacity in order to improve the management of the Polish coastal zone environment" and "System for the exchange of information on ecosystem state of the Vistula Lagoon within the frame of the Polish-Russian transboundary co-operation". The first project, with the acronym SeA-Man (PL0103) addressed the Polish coastal administration. The second project – SerVis Force (PL0223) – ran between 2008 and 2011 and addressed the Polish and Russian management authorities of the Vistula Lagoon, a cross-border water body belonging to both countries. The budget of each project consisted of 85% from NFM funds and 15% from internal resources of the IMWM NRI. IMWM NRI was the sole contractor for the project PL0103 and was the main executor of project PL0223, with Norwegian and Russian

* Corresponding author, email: Magdalena.Kaminska@imgw.pl

partners: Norwegian Institute for Water Research (Oslo), Federal State Institution "Kaliningrad Provincial Center for Hydrometeorology and Environmental Monitoring" (FSI Kaliningrad PCHEM), Atlantic Branch of the Institute of Oceanology Russian Academy of Sciences P.P. Schirshov (AB IO RAS) and Federal State Institution "Atlantic Research Institute of Fishery and Oceanology" (FSI ARIFO).

2. Results obtained within the projects

2.1 Concurrent monitoring cruises

An analysis of historical and contemporary monitoring programmes carried out by Russian and Polish institutions in the Vistula Lagoon was conducted within the project PL0223 with reference to the requirements of HELCOM and EU Water Framework Directive (WFD). This resulted in the development of a concerted list of parameters and methods compliant with the WFD requirements to be monitored by both Polish and Russian partners in the relevant parts of the Vistula Lagoon (Table 1).

Table 1 List of concerted parameters and methods for monitoring the environmental status of the Vistula Lagoon

Parameter	Method		Compliance
	RUS	PL	
water temperature & salinity	CTD probe	CTD probe	+
oxygen	classic Winkler	classic Winkler	+
pH	potentiometric	potentiometric	+
water transparency	Secchi disc	Secchi disc	+
nutrients: orthophosphate, total phosphorus, nitrate, nitrite, ammonia, total nitrogen	colorimetric	colorimetric	+
chlorophyll-a	spectrophotometric	spectrophotometric	+
phytoplankton: species composition, abundance & biomass	microscopic taxonomic determination	microscopic taxonomic determination	+
macrozoobenthos	microscopic taxonomic determination; gravimetric biomass determination	microscopic taxonomic determination, gravimetric biomass determination	+

Meso-zooplankton, the planktonic size group monitored within the HELCOM COMBINE programme was not included because it is not required by the WFD. The programme of measurements comprised also the setting of a network of measurement stations in both parts of the Vistula Lagoon.

2.2 Results of concurrent monitoring cruises

In-situ measurements and laboratory analyses concerning the Polish part of the Vistula Lagoon in the project PL0223 were conducted by the Maritime Branch of the IMWM NRI in Gdynia while the corresponding activities in the Russian part of the Lagoon were done by three partners: water temperature and salinity were determined by ABIO RAS,

nutrients were analysed by FSI Kaliningrad PCHEM and biological variables were analysed by FSI ARIFO.

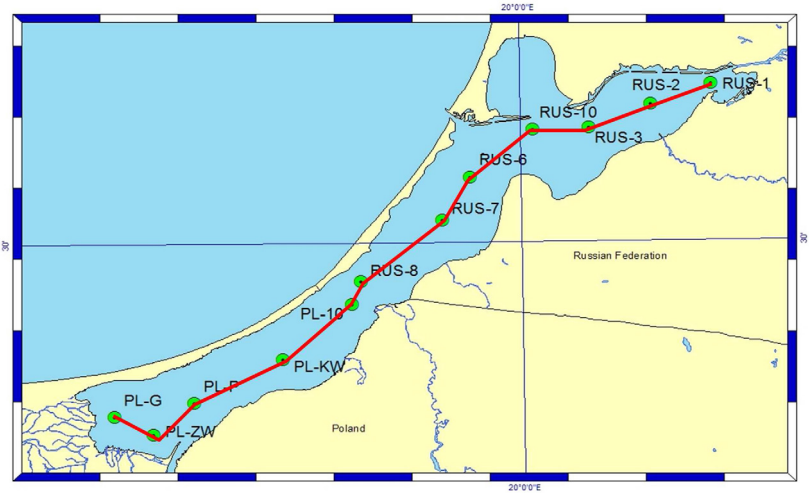

Figure 1 Location of measurements stations in the Polish (PL) and Russian (RUS) parts of the Vistula Lagoon. The Lagoon has a total length of 91 km, and the average width is 9 km.

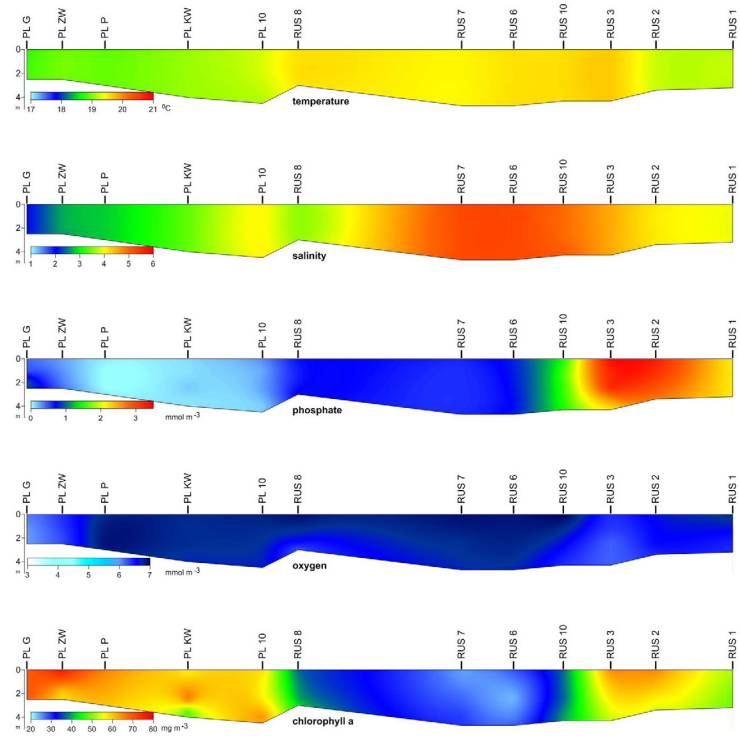

Figure 2 Vertical distribution of selected environmental parameters along the Vistula Lagoon RUS-PL transect in 2009.

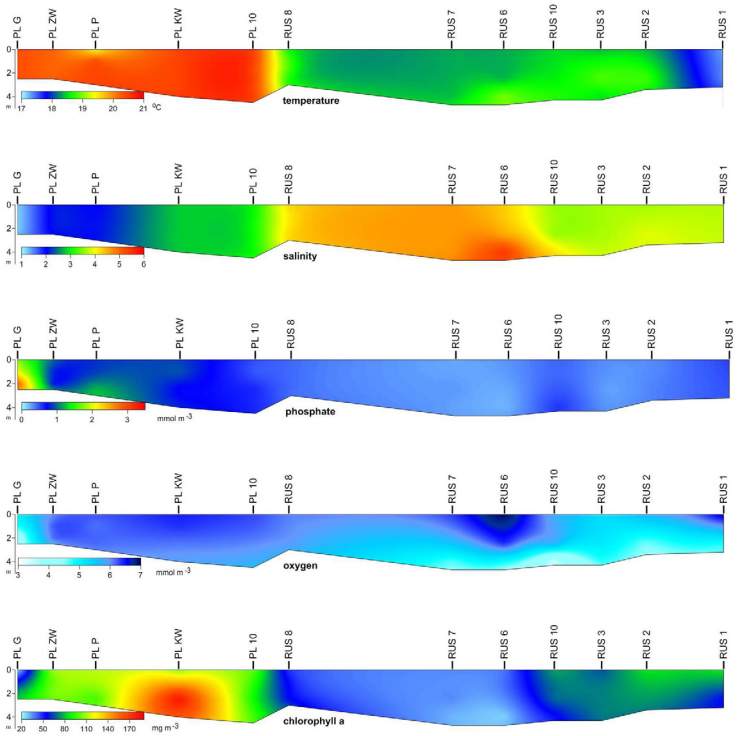

Figure 3 Vertical distribution of selected environmental parameters along the Vistula Lagoon RUS-PL transect in 2010.

In 2009, the measurements were conducted in parallel on one day and at border stations PL-10 and RUS-8 with 30 minute intervals (Figure 2). In 2010, because of the strong SW winds which prevented Russian partners from seagoing, the measurements were done with a 2 days lapse (Figure 3).

2.3 Contribution of the Norwegian partner

The Norwegian partner NILU developed an Environmental Surveillance and Information System (ENSIS), a data base application for riverine monitoring data storage and environmental assessment purposes. Within the project PL0223, ENSIS was adapted to the morphological conditions of the Vistula Lagoon, e.g. to enhanced number of measurement levels (a single measurement level occurs in rivers), enumerated parameters and new measurement units. The adjustment comprised also the environmental status classification system in a five-grade classification system according to the Ministerial Decree[i] (2008). To provide the classification of the ecological status of the Vistula Lagoon, the results of measurements from the project as well as monitoring data supplied by the regional Warmińsko-Mazurski Inspectorate for Environmental Protection

i Decree of the Minister of Environment from 20 August 2008 concerning status classification in unit surface water bodies Journal of bill No. 162, pos. 1008

obtained within the WFD monitoring activities between 2007 and 2009. The classification resulted in poor or bad status (Figure 4).

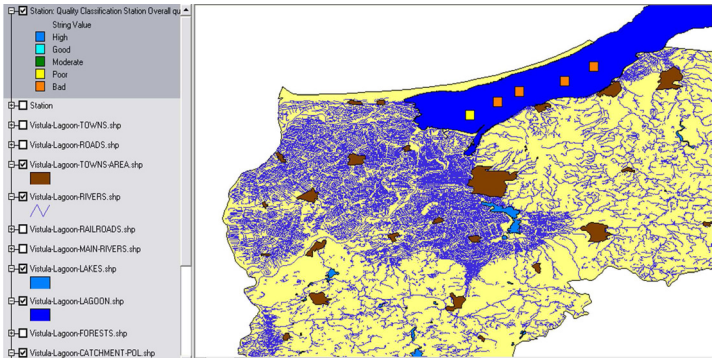

Figure 4 Ecological status classification in the Polish part of the Vistula Lagoon based on project and monitoring data using ENSIS.

2.4 Adaptation of MIKE hydrodynamic model to forecasting of hydrodynamic conditions in the Polish coastal zone and in the Vistula Lagoon

Both projects, PL0103 and PL0223, had a clear prognostic aim in common. It was the forecasting of hydrodynamic conditions and ecological status in the Polish coastal zone and in the Vistula Lagoon for environmental management purposes and open public information.

MIKE 21 ELP III level model was adapted for the forecasting of sea level in the Polish coastal zone, including the Szczeciński Lagoon, and MIKE 3D FM model with ecological module was used in the case of the Vistula Lagoon.

The bathymetry and morphology data on the Polish coastal zone and the Szczecin Lagoon were implemented into the model. MIKE 21 ELP III level model was calibrated with data on 26 storm surges and 8 low water cases during the years 1997–2001. Next, the forcing data – measured meteorological data – were substituted in the model by predicted data and the modelled sea level values were compared with the real data. The model validation in the Szczecin Lagoon was done with water level data from the period 18–22 January 2007 (sea level records every 3 hours). The model MIKE 21 ELP III level was also tested for compatibility with the operational systems of the hydrological service of the IMWM – the Hydrological System (HS) and the Marine Operational Hydrology System (MOHS).

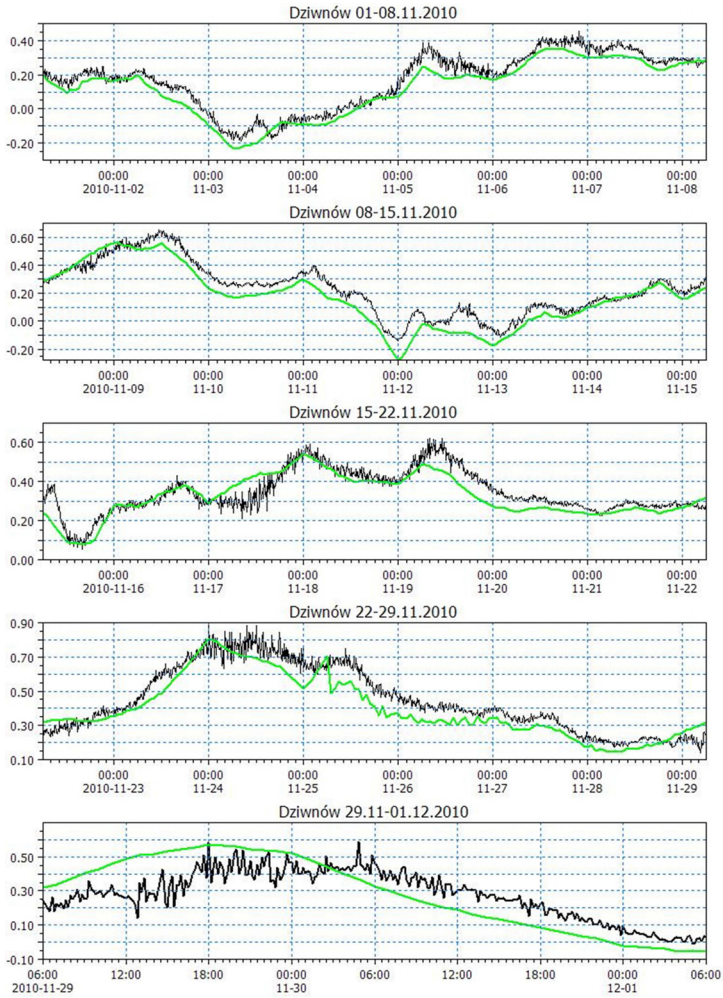

Figure 5 Results of daily sea level model simulations (in metres) at Dziwnów station in November 2010 (black line: real data, green line: modelled data).

In the case of Vistula Lagoon and the MIKE 3D FM model with ecological module Ekolab, the calibration was conducted by a team of Polish and Russian experts. The pre-calibration of the model was done with sea level data from the period 14–30 August 2009 with a time step of 30 s. The open border of the model was set at Pilawska Strait, having a section of ca. 4000 m^2. The calibration of the model took into account the sources of fresh water discharge comprising 5 rivers in the Polish part of the Lagoon and 7 rivers in the Russian part. The set of forcing agents included wind friction, sea level changes at the open border of the model and riverine discharges. An irregular model grid of 200 up to 1300 m was used (Figure 6). Higher horizontal resolution was applied in the vicinity of the Pilawska Strait. The vertical resolution comprised 10 layers of differing thickness (σ). The surface layer was assigned the least thickness, contributing only 2%

of the basin depth. The wind friction coefficient was assumed constant in the entire study area and equal to 0.001255. The specific parameters applied in the model calibration are listed in Table 2.

Table 2 Parameters applied in the calibration of MIKE 3D FM model of the Vistula Lagoon

plane	grid size [m]	bottom friction coefficient (constant) [m]	viscosity coefficient (constant) [m2 s-1]	dispersion coefficient [m2 s-1]	time step [s]
horizontal	200–1300	0.5	0.28	0.02	30
vertical	10 variable layers		logarithmic formula	0.01	30

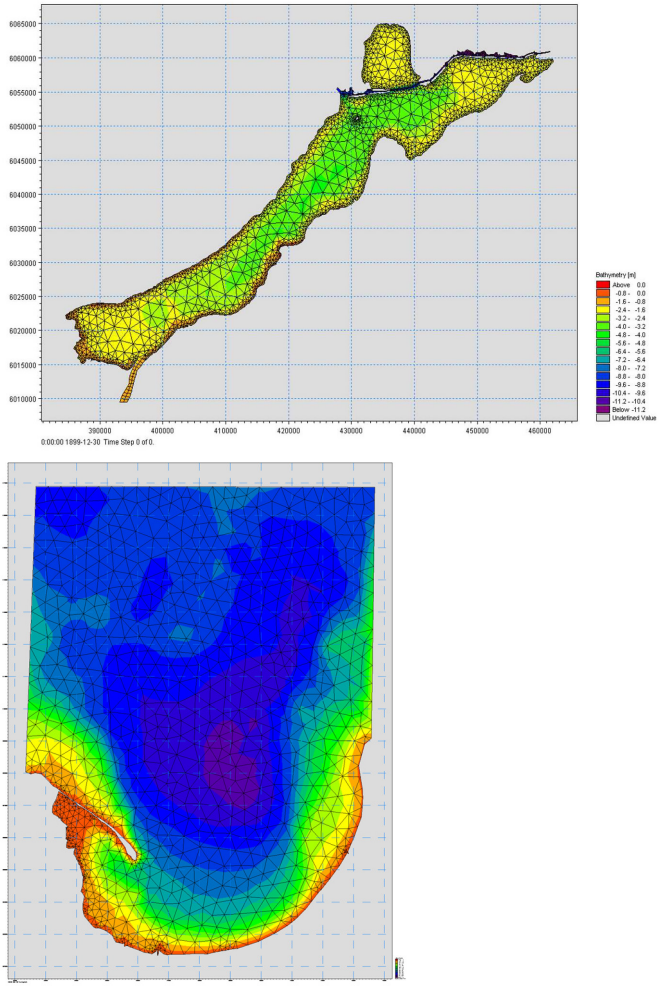

Figure 6 Flexible mesh created with a resolution of 30–150 m.
Top: Vistula Lagoon, Bottom: Gulf of Gdańsk.

The model was validated for surface temperature and salinity simulations using data from the concurrent monitoring cruise in the Vistula Lagoon on 30 August 2009 (Figure 7). The validation of water level (Figure 8) and salinity (Figure 9) was carried out with measurement data from the Tolkmicko station in the Vistula Lagoon obtained by the State Hydrological and Meteorological Service of IMWM.

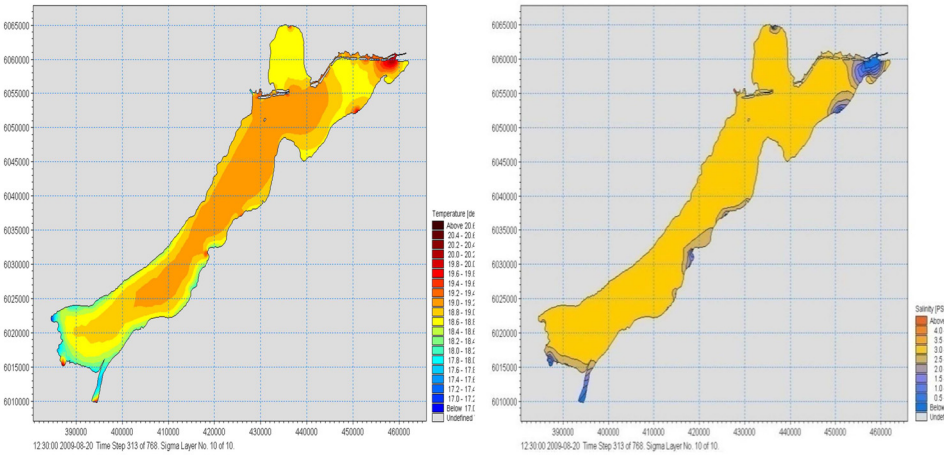

Figure 7 Physical parameter distribution in the Vistula Lagoon obtained in MIKE 3D FM model calibration, Left: temperature, Right: salinity.

Figure 8 Comparison of water level simulated by the MIKE 3D FM model with measurement data from Tolkmicko station in the Vistula Lagoon (modelled data: green line, measurements: orange line).

The comparison in both cases – water level and salinity – between the modelled data and measurements was assumed positive taking into account the short period of the test and little measurement frequency (1 per day).

Since April 2011, the model is predicting daily forecasts of water temperature and salinity, sea currents and oxygen concentration for the Gulf of Gdańsk, Puck Bay (inner part of the Gulf of Gdańsk) and Vistula Lagoon. The model predicts water quality for

selected regions, i.e. chlorophyll-*a* concentration for the Gulf of Gdańsk and Vistula Lagoon, and orthophosphates (PO4) and nitrates (NO3) for the Gulf of Gdańsk.

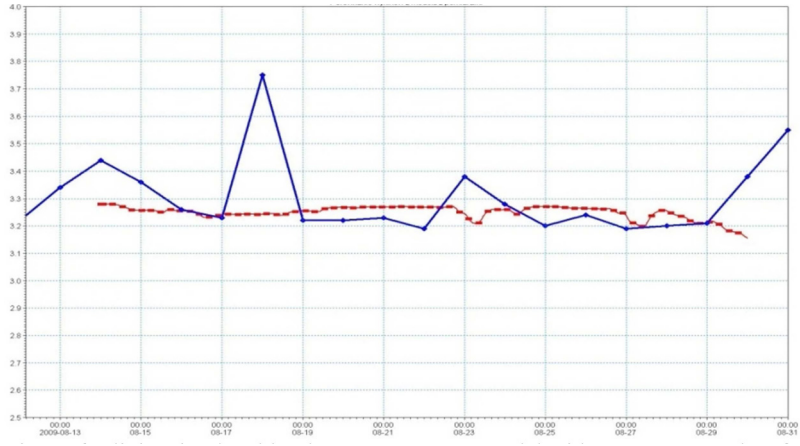

Figure 9 Comparison of salinity simulated by the MIKE 3D FM model with measurement data from Tolkmicko station (salinity between 3.2 and 3.8) in the Vistula Lagoon (modelled data: red line, measurements: blue line).

3. Distribution of information and data

The 24 h forecasts of selected hydrodynamic parameters and water quality indicators in the Gulf of Gdańsk, Puck Bay, Vistula Lagoon and Szczecin Lagoon stand for the operational deliverables of both projects. Direct access to these products is available via a dedicated web site www.baltyk.pogodynka.pl in the folder "Specialized forecasts" which was constructed within the projects and incorporated into the general IT system of the IMWM.

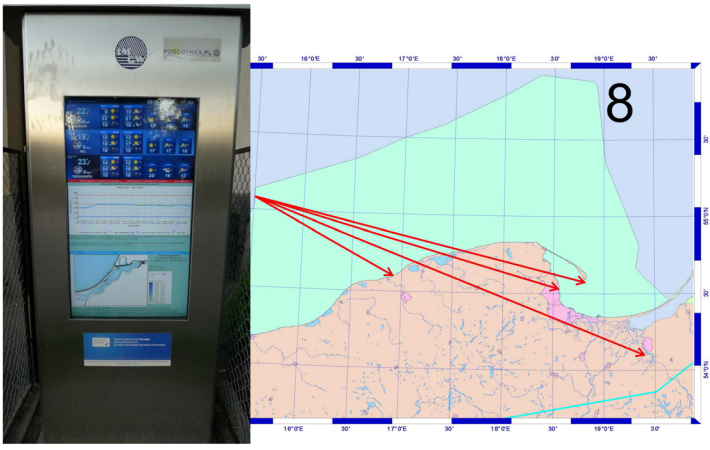

Figure 10 A multimedia kiosk and presentation of hydrodynamic and ecological parameters – here: forecast for the Vistula Lagoon (lower panel).

The operational deliverables can also be accessed via multimedia kiosks. The kiosks with digital displays were situated in 4 locations along the Polish coast: in Ustka, Gdynia, Hel and Elbląg. The display of a kiosk is divided 3 parts with forecasts displayed in the lower panel. Besides the results of numerical models, the kiosks present current weather data (upper panel) and sea level in chart form (middle panel).

4. Summary

The establishment of a formal framework for the exchange of data and information between the neighbouring countries has to be considered a very important result of the project PL0223.

Similarly, the agreements on continued co-operation signed by the partners: IMWM-NRI with FSI "Kaliningrad PCHEM" and IMWM-NRI with AB IO RAS. The platform for the exchange of real time meteorological and hydrological data between the Polish and Russian (Kaliningrad Oblast) respective services has been developed. The hydrodynamic models implemented for the Gulf of Gdańsk and Vistula Lagoon have been put into operation. Operational oceanographic service was implemented along the entire Polish coastal zone.

Acknowledgment

The authors acknowledge the efforts of personnel conducting measurements and sampling during the concurrent monitoring cruises. Mr Sérgio das Neves is acknowledged for completing data series for calibration and technical work on setting in operational mode the model of the Vistula Lagoon.

References

Aleksandrov, S. (2009). Project report "Chlorophyll concentration as indicator of ecological state of the Vistula Lagoon of the Baltic Sea" (in Russian).

Aleksandrov, S. (2010). Project report "Chlorophyll concentration as indicator of ecological state of the Vistula Lagoon of the Baltic Sea in 2010" (in Russian).

Alexeevskaya, L.N. (2009). Project report "Otchet o rezul'tatah raboty po opredelenyu azota ammoniynogo i kisloroda rastvorennogo v Vislinskom zalive v ramkah proyekta PL0223" – Development of the system for the exchange of information on ecosystem state of Vistula Lagoon in frame the Polish-Russian cooperation-SerVis-FORCE" ("Отчет о результатах работы по определению азота аммонийного и кислорода растворенного в Вислинском заливе в рамках проекта PL0223").

Bielecka, M. (2011). Project report "Prace w zakresie modelowania hydrodynamiki Zalewu Wiślanego dla potrzeb wdrożenia modelu ekologicznego Zalewu w ramach realizacji projektu PL0223. Etap III: Analiza i ocena wyników symulacji hydrodynamiki Zalewu Wiślanego, wykonanych z wykorzystaniem modelu MIKE 3D" (in Polish) .

Chubarenko, B.V., and D.A. Domnin. Project report "Tehnicheskiy otchet o nauchno-isledovatel'skoy rabote po teme: 'Analiz funkcyonal'nosti bazy dannyh ENSIS' v ramkah vypolnenya proyekta PL0223 'Sistema obmena informaciyey ob ekologicheskom sostayanii Vislinskogo zaliva v ramkah polsko-rossiyskoy kooperacii'"

(“Технический отчет о научно-исследовательской работе по теме: «Анализ функциональности базы данных ENSIS» в рамках выполнения проекта PL0223 ‘Система обмена информацией об экологическом состоянии Вислинского залива в рамках польско-российской кооперации’”).

Chubarenko, B.V., and A. Kuleshov (2009). Project report “Hydrological automatic probe measurements (30.08.2009) within the mutual monitoring activities in the framework of the Project PL-0223 ‘System for the exchange of information on ecosystem state of the Vistula Lagoon in frame of the Polish-Russian Transboundary Cooperation’” (in Russian).

Chubarenko, B.yV., A. Sokolov, N. Demchenko, and O. Kozlova. Project report “Numerical modeling of the Vistula lagoon (17–23.10.2010) within the mutual activities in the framework of the Project PL-0223 ‘System for the exchange of information on ecosystem state of the Vistula Lagoon in frame of the Polish-Russian Transboundary Cooperation’” (in Russian).

Kirina, E.E. (2009). Project report “Otchet o rezul’tatah raboty po opredelenyu azota nitratnogo i azota nitritnogo v Vislinskom zalive v ramkah proyekta PL0223 – Development of the system for the exchange of information on ecosystem state of Vistula Lagoon in frame the Polish-Russian cooperation-SerVis-FORCE” (“Отчет о результатах работы по определению азота нитратного и азота нитритного в Вислинском заливе в рамках проекта”).

Kirina, E.E. (2010). Project report “Otchet o rezul’tatah raboty po opredelenyu azota nitritnogo, rastvorennogo kisloroda i azota obshchego v Vislinskom zalive v ramkah proyekta PL0223 – Development of the system for the exchange of information on ecosystem state of Vistula Lagoon in frame the Polish-Russian cooperation-SerVis-FORCE” (“Отчет о результатах работы по определению азота нитритного, растворённого кислорода и азота общего в Вислинском заливе в рамках проекта PL0223”).

Lewandowski, A., and T. Olszewski, (2008). Project report „Raport syntetyczny dotyczący współpracy polsko-rosyjskiej w zakresie problematyki środowiska Zalewu Wiślanego, wynikającej z dotychczas realizowanych projektów krajowych i międzynarodowych” (in Polish).

Mas’ko, O.P. (2009). Project report “Otchet o rezul’tatah raboty po opredelenyu fosfatov i fosfora obshchego v Vislinskom zalive v ramkah proyekta PL0223 – Development of the system for the exchange of information on ecosystem state of Vistula Lagoon in frame the Polish-Russian cooperation-SerVis-FORCE” (“Отчет о результатах работы по определению фосфатов и фосфора общего в Вислинском заливе в рамках проекта PL0223”)

Mas’ko, O.P. (2010). Project report “Otchet o rezul’tatah raboty po opredelenyu fosfatov i fosfora obshchego v Vislinskom zalive v ramkah proyekta PL0223 – Development of the system for the exchange of information on ecosystem state of Vistula Lagoon in frame the Polish-Russian cooperation-SerVis-FORCE” (“Отчет о результатах работы по определению фосфатов и фосфора общего в Вислинском заливе в рамках проекта PL0223”) .

Potseluyeva, D.V. (2009). Project report “Otchet o rezul’tatah raboty po opredelenyu azota obshchego i procenta nasyshcheniya vody kislorodom v Vislinskom zalive v ramkah proyekta PL0223 – Development of the system for the exchange of infor-

mation on ecosystem state of Vistula Lagoon in frame the Polish-Russian cooperation-SerVis-FORCE" ("Отчет о результатах работы по определению азота общего и процента насыщения воды кислородом в Вислинском заливе в рамках проекта PL0223") .

Potseluyeva, D.V. (2010). Project report "Otchet o rezul'tatah raboty po opredelenyu azota nitratnogo, azota ammoniynogo I procenta nasyshcheniya vody kislorodom v Vislinskom zalive v ramkah proyekta PL0223 – Development of the system for the exchange of information on ecosystem state of Vistula Lagoon in frame the Polish-Russian cooperation-SerVis-FORCE" ("Отчет о результатах работы по определению азота нитратного, азота аммонийного и процента насыщения воды кислородом в Вислинском заливе в рамках проекта PL0223") .

Rudinskaya, L.V. (2009). Project report "Macrozoobenthos in the Vistula Lagoon of the Baltic Sea in August 2009" (in Russian)

Rudinskaya, L.V. (2010). Project report "Macrozoobenthos of the Vistula Lagoon (Baltic Sea)" (in Russian).

Shchagina, N.V. (2009). Project report "Organizaciya ohrany okruyhazushchei sredy i sistemz nacyonal'nogo ekologicheskogo monitoring na territorii Rossiiskoy Federacii" (in Russian: "Организация охраны окружающей среды и системы национального экологического мониторинга на территории Российской Федерации").

Assessment and comparison of different Mediterranean Sea reanalysis dataset: 1985–2007

M. Adani*[1], G. Coppini[1], S. Dobricic[2], M. Drudi[1], C. Fratianni[1], A. Grandi[1], V. Lyubartsev[2], P. Oddo[1], S. Simoncelli[1], N. Pinardi[3], and M. Tonani[1]

[1]*Gruppo Nazionale di Oceanografia Operativa, INGV, Sezione di Bologna, Bologna, Italy*
[2]*Centro EuroMediterraneo per i Cambiamenti Climatici, Bologna, Italy*
[3]*Department of Environmental Sciences, University of Bologna, Ravenna, Italy*

Abstract

One simulation and two re-analyses have been produced in order to study the Mediterranean Sea circulation for the period 1985 to 2005. The two re-analyses differ only for the assimilation scheme used: in the first a Reduced Order Optimal Interpolation (ROOI) has been applied; the second makes use of a new three-dimensional variational scheme (3dvar). The ocean general circulation model, common to all the numerical experiments, is based on OPA 8.1 code. The observational data sets assimilated consist of vertical temperature and salinity in-situ profiles from thermometers, CTD, XBT, MBT, BOTTLE, ARGO floats; along track satellite sea level anomalies (SLA), daily mean fields of satellite-derived Sea Surface Temperature are used for correcting the fluxes. The results of both re-analyses are comparable and are qualitatively consistent with the known circulation structures in the period of interest. The largest errors are at the thermocline level and in regions with strong eddy activity. However, OceanVar (3dvar assimilation scheme) produces 20% better results for the sea-level anomaly root mean square error.

Keywords: Mediterranean Sea, re-analysis, assimilation

1. Introduction

Historically, climatological studies have been carried out either by analysing past observations dealing with the sampling problem, or by modelling studies which use the known physical laws of the geophysical fluid dynamic to simulate the behaviour of the system with the problem that often the accumulation of uncertainties causes a model drift. In the analyses, assimilations techniques are used to combine model and observation estimates in an optimal way, in order to avoid the problems connected with the previously mentioned methods. In this case the "optimal way" should be designed and applied in such a way that the assimilation minimises the variance of the errors. Unfortunately, analyses are usually inconsistent in time since assumptions are made during the analysed period change (i.e. changes in the assimilation scheme or circulation model) and this may lead to misinterpretation of the results. The solution to this problem is the re-analysis which is like the analysis but done with a consistent model and data assimilation

* Corresponding author, email: mario.adani@bo.ingv.it

scheme for the investigated period, yielding to a temporally homogeneous gridded dataset (Glickman, 2000; see amsglossary.allenpress.com/glossary).

The Mediterranean Sea is a mid-latitude semi-enclosed basin. It communicates with the Atlantic Ocean through the Strait of Gibraltar and with the Marmara Sea through the Dardanelles. Wind stress is mainly responsible for the presence of permanent gyres (Pinardi and Masetti, 2000). The heat and water surface and lateral fluxes drive the thermohaline circulation. The net income of heat and water from the Strait of Gibraltar balances the losses at the air-sea interface over a long-term period. This paper compares two re-analyses, made by changing only the assimilation scheme, and a model simulation. Moreover we assess the capability of the re-analyses in reproducing the long-term variability of the Mediterranean Sea.

2. Experimental setup

The OGCM used in this work is based on OPA 8.1 code (Madec *et al*., 1998), implemented in the Mediterranean Sea. It has 1/16° horizontal resolution and 71 unevenly spaced vertical levels (for a complete description refer to Tonani *et al*., 2008). The only difference with respect to Tonani's implementation is the surface water flux parameterisation. In the present study a realistic surface water flux has been implemented: the evaporation is computed by the model using bulk formulae, the precipitation is a climatological monthly mean from NCEP re-analysis and the river input is a climatological monthly mean from the Global Runoff Data Centre. More information concerning the river implementation can be found in Adani *et al*. (2011). Three numerical experiments have been carried out and compared: a simulation (hereafter SIM) and two re-analyses using the same OGCM but different assimilation schemes: the OceanVar developed by Dobricic and Pinardi (2008) based on the 3dvar scheme and the SOFA (De Mey and Benkiran, 2002) based on Reduced Order Optimal Interpolation. The numerical experiments associated are hereafter called OV-RE and SO-RE respectively. A complete mathematical description of the assimilation schemes can be found in Adani *et al*. (2011); note that the observational error matrix is identical for the two schemes and the multivariate part of the model background error covariance matrix, consisting in vertical Empirical Orthogonal Functions, is common to both schemes.

For the re-analysis a correction to the surface heat flux is applied. The correction is proportional to the difference between model and satellite-derived SST with a relaxation time corresponding to 2.5 days. The model is forced with ERA-15 and ECMWF operational analysis, when available.

The numerical experiments cover the entire period 1985–2007 except for SO-RE, which has only been run for some years in order to save computational time and restarted from the OV-RE solution.

The observational dataset includes:

- Satellite SST objective interpolated map (OISST; Marullo *et al*., 2007)
- In-situ temperature and salinity profiles from MedAtlas (Maillard *et al*., 2005), the Ship-of-Opportunity Programme (Manzella *et al*., 2007) and the MedArgo programme (Poulain *et al*., 2007).

- Altimetry observations from all the available satellites: data and relative corrections are described by Pujol and Larnicol (2005).

3. Quality of the re-analyses

The quality of the re-analysis is evaluated based on observation–background misfits. Except for the SST, observations are independent from model estimates. The upper panels of Figure 1 show the Root Mean Square Error of temperature as a function of time and depth for the three experiments, and the mean of the whole period of reanalysis is shown in the right panel; the lower panels show the same for salinity. The temperature error shows a seasonal behaviour: the highest error is located at the basis of the summer thermocline probably due to not enough vertical resolution of the model for reproducing the very shallow thermocline which characterises the Mediterranean Sea in summer. The two re-analyses have a significantly lower error than the simulation (about 0.45°C). Salinity shows the maximum error at the surface reaching a value of 0.6 psu for SIM and 0.4 psu for OV-RE and SO-RE. It is interesting to note the decrease of the error in the 21st century: this model behaviour is mainly due to a different sampling strategy of the in-situ observations during the Ship-of-Opportunity/MedArgo Programme and the MedAtlas dataset.

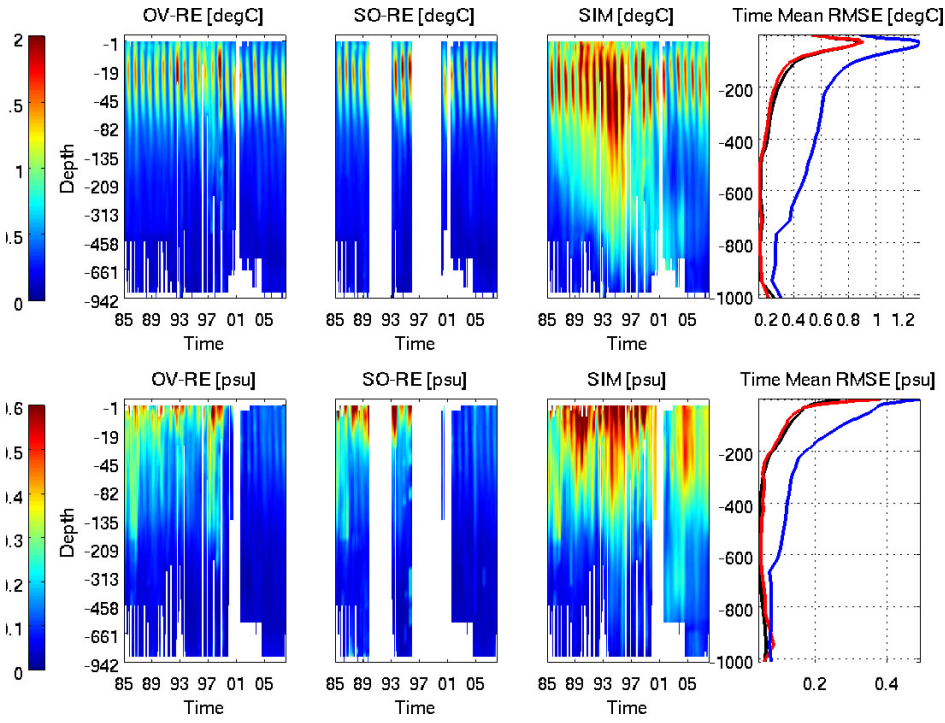

Figure 1 RMSE for temperature (upper panels expressed in ºC) and salinity (lower panels expressed in psu) for the three numerical experiments as function of time and depth. The right panel is the mean of the whole period: OV-RE is the red curve, SO-RE is black and SIM is blue.

The upper panel of Figure 2 shows the Sea Level Anomaly (SLA) RME. The OV-RE solution is the best one giving an average error of about 4 cm, about 20% better than SO-RE. SIM, as expected, has the highest error between 6 and 7 cm. In the lower panel the SST RMSE is presented. OV-RE and SO-RE have the same skill in reproducing the SST, due to the flux correction applied, about 0.5 °C of RMSE (same value associated to the SST observation, Marullo *et al*., 2007) and they are better then the SIM. The error has seasonality with highest error during summer.

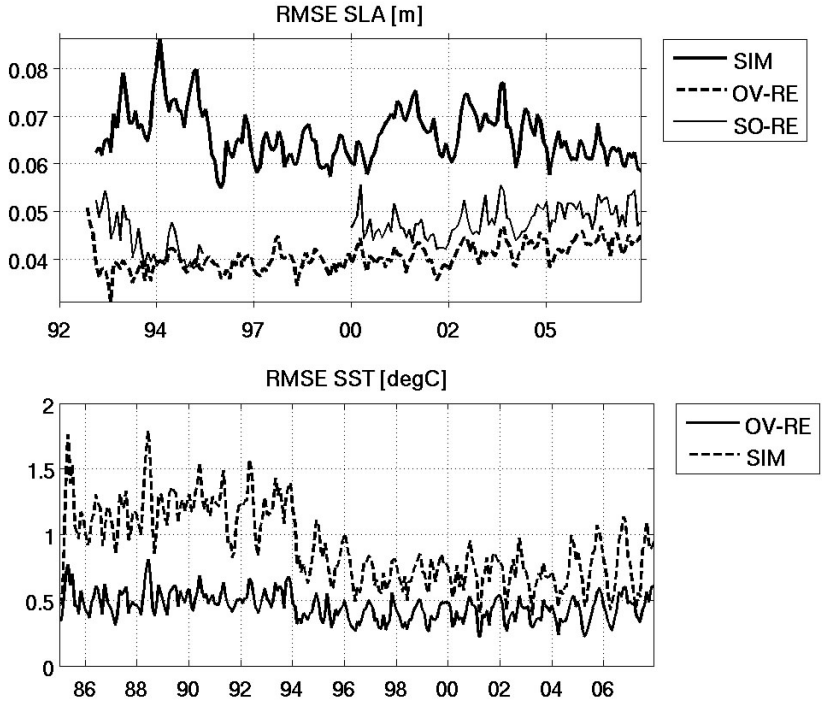

Figure 2 Upper panel RMSE of SLA (m). Lower panel RMSE of SST (°C).

It is important to mention that the surface heat flux correction tends constantly to increase the heat content of the model, reaching 0.4 °C in 2000, and then stabilising. The assimilation tends to decrease the heat content until 2005 and then stabilises reaching 0.8 °C. The two corrections act together to redistribute the heat content along the water column.

4. Decadal variability

The decadal variability from OV-RE has been described in Pinardi *et al*. (2011). Here we will show only a few pictures of the mean circulation of the basin (Figure 3). Many of the structures already described in literature can be found in the re-analysis estimate. Starting from Gibraltar the two anti-cyclone structures (A) are found and the Algerian current (B) is visible. A large cyclonic structure characterises the Gulf of Lion (C) and

three cyclonic gyres are visible in the Tyrrhenian Sea (D). In the Sicily Strait the current splits into three parts (E), one circulating cyclonically in the Tyrrhenian Sea, one passing near the Sicily coast creating the Atlantic-Ionian Stream and one circulating along the African coast creating the African Modified Atlantic Water current (Robinson *et al*., 1999). In the Adriatic Sea the Western Adriatic Costal current and the South Adriatic Cyclonic Gyre (F) are well visible. In the Gulf of Sirte the anti-cyclonic gyre (G) is visible. H is the Pelops Gyre and I is the bifurcation of the current into the Mid-Mediterranean Jet and Southern Levantine current. In the Levantine basin the Mersa-Matruth (L) and the Shikmona (M) Gyre systems are found.

Along the Turkish coast there is the Asian Minor current and the Rhodes Gyre (N). O and P are the Ierapetra Gyre and Western Cretan Gyre respectively.

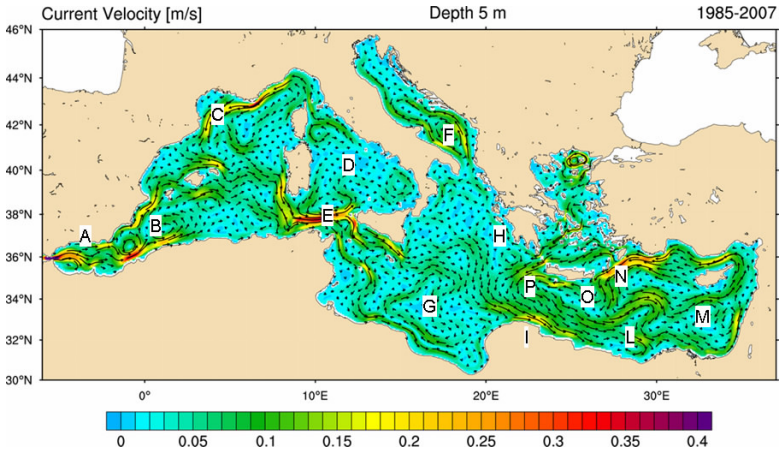

Figure 3 Mean Surface Circulation. Colours indicate the intensity of the current in ms^{-1}

5. Conclusion

Two re-analyses and a simulation have been carried out for the Mediterranean Sea from 1985 to 2007. In the re-analysis experiments all the available in-situ and satellite observations for the past 23 years have been used with two assimilation schemes, a Reduced Order Optimal Interpolation scheme, so-called SOFA, and a three-dimensional variational scheme, so-called OceanVar. OV-RE gives better results for abundant data such as SLA, improving by about 20% the RMSE with respect to SO-RE, but giving the same RMSE of SO-RE for sparse data sets, such as temperature and salinity profiles. Reanalysis estimates are consistent with the observations and the past knowledge of the Mediterranean Sea circulation.

Acknowledgements

This work was supported by the European Commission MyOcean Project (SPA.2007.1.1.01— development of upgrade capabilities for existing GMES fast-track services and related operational services; Grant Agreement 218812-1-FP7-SPACE 2007-1) and by the CIRCE project, founded by the European Commission's 6th

Framework Programme through Contract 036961. We would also like to thank the Istituto Nazionale di Geofisica e Vulcanologia (INGV) and the Centro Euro-Mediterraneo per i Cambiamenti Climatici (CMCC) for facilities support. We are thankful to Dr. M. Vichi for the interesting discussions and personally grateful to Dr. I. Fukumori for his moral, scientific, and financial support.

References

De Mey, P. and M. Benkiran (2002). A multivariate reduced-order optimal interpolation method and its application to the Mediterranean Basin–scale circulation. Ocean Forecasting: Conceptual Basis and Applications, N. Pinardi and J. Woods, Eds., Springer, 281–306.

Dobricic, S. and N. Pinardi (2008). An oceanographic three-dimensional assimilation scheme. Ocean Modell., 22, 89–105.

Glickman, T. (eds.) (2000). Glossary of Meteorology. 2nd ed. Amer. Meteor. Soc., 855 pp.

Leaman, K.D. and F.A. Schott (1991). Hydrographic structure of the convection regime in the Gulf of Lions: Winter 1987, J. Phys.Oceanogra., 21(4), 575-598

Madec, G., P. Delecluse, M. Imbard, and C. Levy (1998). OPA 8.1 ocean general circulation model reference manual. Institut Pierre-Simon Laplace, Note du Pole de Modelisatzion, No. 11, 91 pp. [Available online at http://www.nemo-ocean.eu/content/download/259/1665/version/1/file/Doc_OPA8.1.pdf.]

Maillard, C., M. Fichaut, G. Maudire, C. Coatanoan, E. Balopoulos, A. Iona, A. Lykiardopoulos, P. Karagevrekis, J.-M. Beckers, M. Rixen, M.-J. Garcia, B. Manca, A. Giorgetti, A. Mosetti, N. Mikhailov, E. Vyazilov, A. Kuznetsov, N. Puzova, R. Boukortt, B. Boudjellal, N. Eddalia, H. Dooley, A. Drago, S. El-Agami, G. Kortchev, I. Gertman, Y. Tsehtik, S. Lakkis, G. Manzella, I. Oliounine, A. Orbi, J. Largissi, S. Zizah, M. Ozyal, F. Berkay, N. Pinardi, M. Zavatarelli, A. Suvorov, A. Khaliulin, G. Zodiatis, K. Bilashvili, Z. Savaneli, V. Dadic, V. Diaconu, R. Gelfeld, and C. Sammari (2005). MEDAR/MEDATLAS 1998-2001: A Mediterranean and Black Sea oceanographic data base and network. Boll. Geofis. Teor. Appl., 46, 329–344.

Manca, B.B., V. Kovaevic, M. Gacic, and D. Viezzoli (2002). Dense water formation in the Southern Adriatic Sea and spreading into the Ionian Sea in the period 19971999. J. Marine Systems, 33-34, Pages 133-154.

Marullo, S., B. Buongiorno Nardelli, M. Guarracino, and R. Santoleri (2007). Observing the Mediterranean Sea from space: 21 years of Pathfinder-AVHRR sea surface temperatures (1985 to 2005): Re-analysis and validation. Ocean Sci., 3, 299–310.

Pinardi, N., and E. Masetti (2000). Variability of the large-scale general circulation of the Mediterranean Sea from observations and modelling: A review. Palaeogeogr. Palaeoclimatol. Palaeoecol., 158, 153–173

Pinardi N., M. Adani, G. Coppini, C. Frattianni, P. Oddo, M. Tonani, V. Lyubartsev, S. Dobricic, and M. Zavatarelli. The Mediterranean Sea large scale low frequency ocean variability from 1987 to 2007: a retrospective analysis. To be submitted.

Poulain, P.M., R. Barbanti, J. Font, A. Cruzado, C. Millot, I. Gertman, A. Griffa, A. Molcard, V. Rupolo, S. Le Bras, and L. Petit de la Villeon (2007). MedArgo: A drifting profiler program in the Mediterranean Sea. Ocean Sci., 3, 379–395.

Pujol, M.-I., and G. Larnicol (2005). Mediterranean Sea eddy kinetic energy variability from 11 years of altimetric data. J. Mar.Syst., 58, 121–141.

Robinson A.R., J. Sellschopp, A. Warn-Varnas, W.G. Leslie, C.J. Lozano, P.J.Haley Jr., L.A. Anderson, and P.F.J. Lermusiaux (1999). The Atlantic Ionian Stream. Journal of Marine Systems, 20, 129-156.

Roether W., B.B. Manca, B. Klein, D. Bregant, D. Georgopulos, V. Beitzel, V. Kovacevic, and A. Lucchetta (1995). Recent changes in the eastern Mediterranean deep waters. Science, 271, 333–335.

Smith, R.O., H.L. Bryden, and K. Stanseld (2008). Observations of new western Mediterranean deep water formation using Argo floats 2004-2006, Ocean Sci., 4, 133-149.

Tonani, M., N. Pinardi, S. Dobricic, M.I. Pujol, and C. Fratianni (2008). A high-resolution free-surface model of the Mediterranean Sea. Ocean Sci., 4, 1–14.

The Fram Strait integrated ocean observing and modelling system

Stein Sandven*[1], Hanne Sagen[1], Laurent Bertino[1], Agnieszka Beszczynska-Möller[2], Eberhard Fahrbach[2], Peter F. Worcester[3], Matthew A. Dzieciuch[3], Waldemar Walczowski[4], Piotr Wieczorek[4], Emmanuel Skarsoulis[5], Andrey Morozov[6], Dany Dumont[7], Craig Lee[8], Brian D. Dushaw[1,8], Edmond Hansen[9], and Harald Rohr[10]

[1]*Nansen Environmental and Remote Sensing Center, Bergen, Norway*
[2]*Alfred-Wegener-Institut for Polar and Marine Research, Bremerhaven, Germany*
[3]*Scripps Institution of Oceanography, University of California at San Diego, La Jolla, California, USA*
[4]*Institute of Oceanology, Polish Academy of Sciences, Sopot, Poland*
[5]*Foundation for Research and Technology Hellas, Heraklion, Greece*
[6]*Woods Hole Oceanographic Institution, Woods Hole, Massachusetts, USA*
[7]*Institut des sciences de la mer, Université du Québec à Rimouski, Canada*
[8]*Applied Physics Laboratory, University of Washington, Seattle, Washington, USA*
[9]*Norwegian Polar Institute, Tromsø, Norway*
[10]*OPTIMARE Sensorsysteme GmbH & Co. KG, Bremerhaven, Germany*

Abstract

An innovative integrated observing and model system is under development to contribute to sustainable environmental monitoring in the Arctic, and in particular to improve the estimates of heat, mass and freshwater transfer through the Fram Strait. The ice-ocean model, multipurpose acoustic system, and the oceanographic components are described, including examples of data and comparison of data and model.

Keywords: Fram Strait, ice-ocean models, acoustic measurements, oceanographic moorings, gliders

1. Introduction

The deep and wide Fram Strait, between Greenland and Spitsbergen, is the main passage through which the mass and heat exchanges between the Nordic Seas and the Arctic Ocean take place. On the eastern side of the Strait, the northward West Spitsbergen Current (WSC) brings Atlantic water to the Arctic Ocean, whereas on the western side the southward East Greenland Current (EGC) carries cold and fresh water from the Arctic back to the North Atlantic. To understand the climate changes in the Arctic Ocean, it is important to quantify the heat, freshwater, and mass transports through the Strait. Therefore, the Fram Strait is one of the key sites identified by the Arctic Regional Ocean Observing System (Arctic ROOS; Sandven, 2005) and the integrated Arctic Ocean Observing System, iAOOS (Dickson *et al*., 2008).

* Corresponding author, email: stein.sandven@nersc.no

An oceanographic moored array has been operating since 1997 to monitor the ocean water column properties and oceanic advective fluxes through Fram Strait. An extremely complex circulation pattern has been observed, with pronounced recirculation and mesoscale activity. The spatial resolution of the mooring array varies from 10 to 30 km. It is not sufficient for resolving the mesoscale variability and recirculation, resulting in large errors in estimates of the oceanic fluxes. An improved observing system is required, with high temporal and spatial resolutions capable of quantifying the impact of mesoscale currents and determining the influence of the recirculation on net oceanic transports through the Strait.

Our goal is to develop an innovative integrated observing and model system for long-term environmental monitoring in Fram Strait, combining data from satellites, acoustic systems, moorings, and gliders with high-resolution ice-ocean circulation models through data assimilation (Sagen *et al*., 2010, 2011). In this paper the major components of this system will be presented.

2. Ice-Ocean modelling and data assimilation system

The TOPAZ model and data assimilation system developed at NERSC is the engine of the Arctic reanalysis and daily forecasting services within the MyOcean project (Hackett *et al*., 2012). The TOPAZ system provides lateral boundary conditions to regional high-resolution models covering regions of climatic and economic interest, such as the Fram Strait and the Barents Sea. (See http://topaz.nersc.no for results).

The nested Fram Strait Nansen-HYCOM ice-ocean model has 28 hybrid vertical layers and a horizontal resolution of 3.5 km. It simulates an intense mesoscale eddy activity (Figure 1, left), still without being fully eddy-resolving. The ice model includes a collisional rheology in the Marginal Ice Zone (MIZ). The ECMWF fields are used at 6-hour frequency. Figure 1 shows that the model respects well the overall heat fluxes across Fram Strait but underestimates the transport of a few temperature classes, in particular the coldest waters. The splitting of northward and southward flows at 2º C is also sharper in the observations than in the model.

3. The Fram Strait acoustic network

Ocean acoustic thermometry/tomography uses measurements of acoustic travel times between sources and receivers with an accuracy of a few milliseconds to provide range-averaged temperature and current information along the acoustic tracks at arbitrarily high temporal resolution. To illustrate the efficiency and coverage, the current Fram Strait acoustic system samples six sections (corresponding to a total length of 1215 km) covering an area of 25921 km^2 with water depths ranging from 1450 m down to 4000 m in 15 minutes eight times per day. In comparison, a glider needs approximately 14 days to cover a 300 km section, at a horizontal resolution of 7–9 km and a maximum dive depth of 1000 m.

3.1 DAMOCLES: Single-track acoustic experiment 2008-2009

A pilot acoustic thermometry experiment was carried out in the WSC during 2008–2009 (e.g. Sagen *et al*., 2011) as part of the EU DAMOCLES integrated project (2005–2010). The experiment used state-of-the-art sweeper source and receiver technology. The

acoustic source swept from 190 Hz to 290 Hz in 60 s every 3 hours for a year. The signals were recorded 130 km away on a 700-m vertical array with eight hydrophones spaced 96 m apart. Acoustic travel times, corrected for mooring motion and clock drift, have been inverted to obtain range and depth-averaged temperature estimates (Skarsoulis *et al*., 2010).

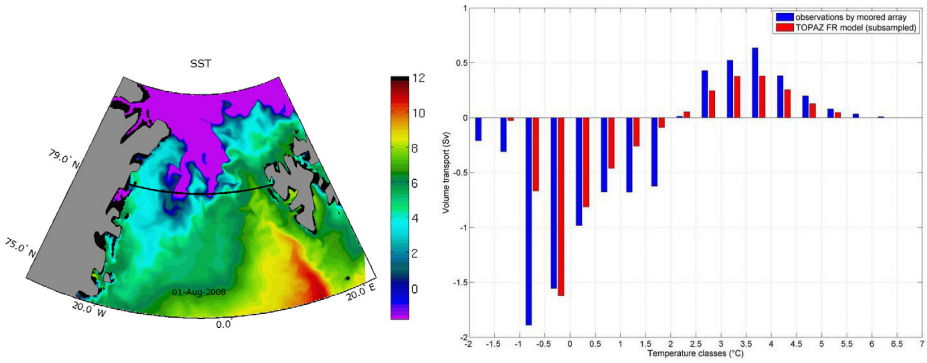

Figure 1 Left: Model sea surface temperature in the Fram Strait on 1 August 2008. The black line is at 79°N, which is close to the oceanographic mooring array. Right: Net volume transport through the Fram Strait section, split into temperature classes, as obtained from the moored observations (blue) (mean Jan 2007 – June 2008) and from the Fram Strait model sub-sampled to the grid points of the moored instruments (red) (mean Jan 2007 – Dec 2009).

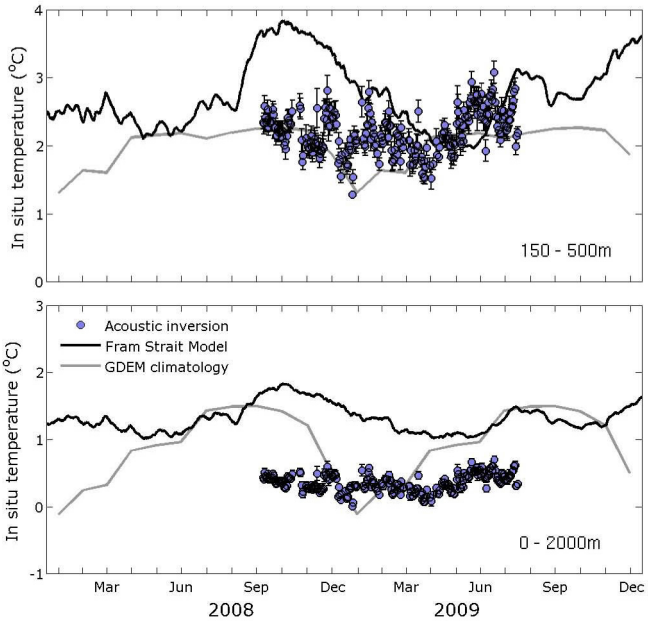

Figure 2 Modelled and acoustically-derived temperatures at 150–500 m depth in the core of the North Atlantic Water (top) and in the upper 2000 m (bottom) along the 130 km acoustic track, compared to GDEM climatology.

In Figure 2, temperatures derived from travel times are compared to the model and climatology, the latter being inaccurate in this area of high inter-annual variability. The model temperatures are warmer than those from the acoustic inversion and climatology. The acoustic inversions show that the temperature minimum did not take place in February 2009, as in the climatology, but rather in late April. The Fram Strait model predicts a minimum at the beginning of June. Furthermore, the subsequent warming of the intermediate waters occurs faster in the acoustic observations than in the model.

Acoustically-derived temperatures for the intermediate layers show stronger variability than the model. Whether the variations are controlled locally or remotely by the advection of North Atlantic Water can be further examined with the analysis of surface and boundary conditions.

A free-running model is used here for evaluation, and the 3-D temperatures should be better constrained in data assimilative mode. The continuous flow of acoustic data should be assimilated to correct the local solution and possibly also remote water properties. The Ensemble Kalman Filter makes it possible to assimilate non-linear observations such as travel times. The question remains how beneficial the acoustic measurements will be in assimilation mode.

3.2 ACOBAR: Triangle acoustic experiment 2010-2012

The first multipurpose acoustic network in the Fram Strait MIZ for tomography, ambient noise, and glider navigation was deployed in 2010 (Sagen *et al*., 2011). The triangle experiment 2010−2012 is designed to provide two-way travel times along each of the sides of the triangle, and one-way travel times along sections between each of the corners of the triangle and the long vertical receiver array in the middle of the triangle (Figure 3). Each of the three sources produces a 60 s linear frequency-modulated (LFM) signal sweeping from 200 Hz to 300 Hz every 3 hours every other day for two years. Moreover, the three sources produce 80 s RAFOS signals at about 260 Hz every six hours during selected time windows for glider navigation. In 2011, the system was partially recovered and provided one-year long time series of acoustic and engineering data along section AD (Figure 3).

Large oceanographic variability is observed for this 181 km long section crossing the WSC in the NW−SE direction. These data will be used for assimilation/inversion exercises and compared to the data from the 2008−2009 experiment. Acoustic data from six tracks will be available for analysis and inversion following recovery of the acoustic array during September−October 2012. Improved assimilation/model-oriented inversion approaches are under development in the ACOBAR project.

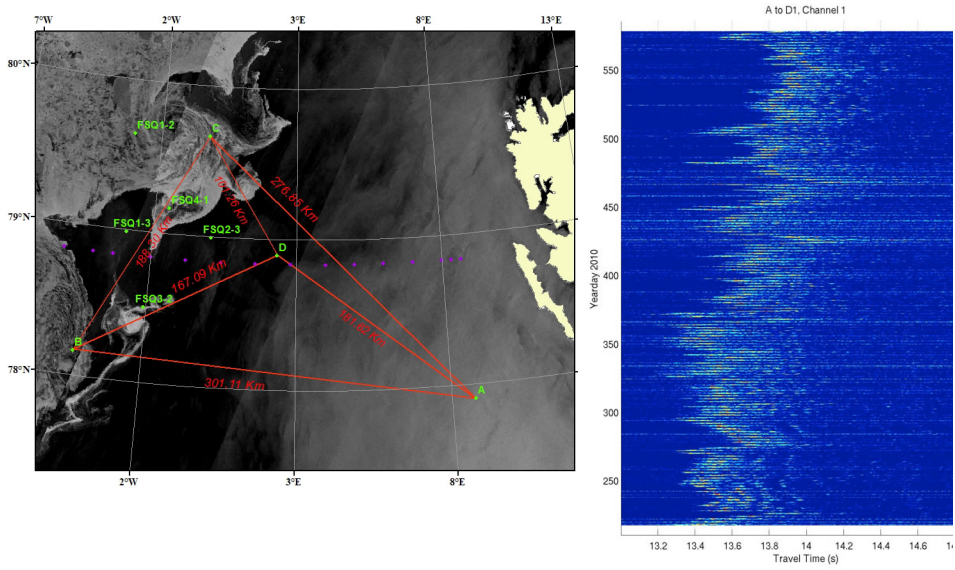

Figure 3 Left: The location of the ACOBAR acoustic network superimposed on two SAR images from ENVISAT (23-24 September 2011), showing the source mooring locations (green) and the oceanographic mooring array (lilac) relative to the ice edge. One transceiver mooring was deployed in each corner of the triangle (A, B, C) and a receiver mooring was deployed in the middle (D). Right: One year of receptions (4 August 2010 – 1 August 2011) at mooring D of the LFM signal transmitted by the source at mooring A. Receptions are not corrected for mooring motion and clock drift.

3.3 Ambient noise observations

The natural part of the ambient noise in the MIZ is generated by processes such as breaking waves; rain/snow/hail falling on the sea surface; ice floe collisions; compression of slush ice between ice floes; cracking and break up of sea ice caused by ocean waves propagating into the ice covered regions; and convergence zones caused by ocean circulation and wind (e.g. Johannessen *et al*., 2003). Human activities such as seismic investigations, oil exploration, fishing activity and shipping contribute significantly from time to time in this region. Figure 4 shows seismic air gun activity in the Fram Strait. The impact of human activities on the noise levels in the Arctic is expected to increase, and it is important to establish benchmark information on the ambient noise in this region. In 2012, ambient noise measurements from five vertical arrays (a total of 20 receivers) over 2 years will be downloaded and analysed at NERSC.

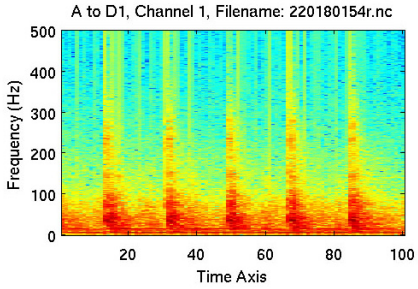

Figure 4 Acoustic data from the deepest receiver at mooring D shown as a spectrogram (left). The strong low frequency signal coming in every 20 s is from a ship borne air gun used for seismic exploration.

4. The oceanographic component of the Fram Strait ocean observing system

4.1 The oceanographic mooring array with operational capability

The array of deep oceanographic moorings (14 moorings before 2002 and 16 afterwards) has been jointly operated by the Alfred Wegener Institute and Norwegian Polar Institute since 1997. It covers the 300 km wide section from the shelf west of Svalbard across the deep part of the Strait to the eastern Greenland shelf. Each mooring carries several instruments from which data are available only after the annual exchange of moorings (Schauer *et al.*, 2004; Beszczynska-Möller *et al.*, 2012). To achieve near-real time (NRT) data transfer from the moored array, the ACOBAR project focused on two objectives: to test long-range acoustic data transfer between the moorings and to develop communication to shore using a moored surface unit capable of satellite data transmission (Figure 5).

To achieve the first goal, in 2009 three low-frequency long-range acoustic modems, interfaced with current meters, were deployed for a one-year long field test in the eastern Fram Strait. Recorded data were transferred in a relay mode (sequential data transfer from the farthest mooring towards the central communication unit). Since acoustic data transmission over the typical range between moorings of O (30 km) proved to be unreliable, the distance between long-range modems was reduced by adding a relay-link mooring with an additional modem between the instrumented moorings. The results of the first field test revealed significant problems related to the high level of ambient noise and low signal-to-noise ratio, resulting in a large number of failed transmissions. Building on this experience, for the next deployment of moorings with acoustic modems in 2011 the output amplitude (and therefore the range of the modems) was increased, and the transmission settings were adjusted to give more frequent transmissions with smaller data packages.

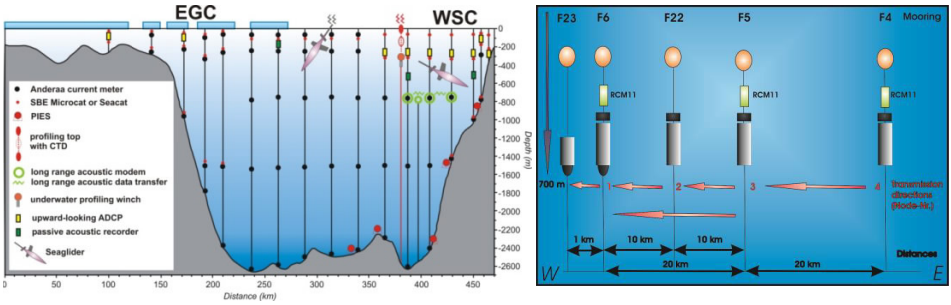

Figure 5 Left: The scheme for the oceanographic observing system in Fram Strait, including deep moorings, the profiling communication mooring for NRT data transfer, and gliders; Right: Acoustic long-range modems for underwater data transmission.

For NRT data transfer to shore, a communication mooring was designed, consisting of an acoustic modem receiving data from other moorings, a central unit, and an underwater winch equipped with a profiling CTD at the top, capable of Iridium data transfer. During summer 2010 and 2011 the underwater winch with a CTD profiler was deployed for the first short-term field tests, without being acoustically linked to the moorings. These field tests of the winch-profiler system revealed that under the strong currents in the eastern Fram Strait, most of the time drag on the profiler body prevented it from surfacing. In addition, drifting sea ice poses a risk for the profiler when at the surface. An improved system is currently under development and will be further tested in 2012.

4.2 Gliders with under ice capability

To complement oceanographic measurements at the moored array with spatially high-resolution CTD sections, autonomous, buoyancy-driven gliders have been deployed since 2008. The Fram Strait integrated observatory employs Seagliders (Eriksen *et al*., 2001) equipped with temperature, conductivity, pressure, fluorescence, optical backscatter and dissolved oxygen sensors. Gliders profile the upper 1000 m with a horizontal resolution of approximately 7–9 km during deep dives. During each surfacing, data are transmitted to shore. Since 2008, six glider missions with a total duration of 416 days have been performed during summer and autumn in the eastern and central Fram Strait, and about 2000 vertical profiles have been measured.

For acoustic positioning and navigation of gliders profiling under the sea ice, an array of three to five RAFOS 260-Hz sound sources have been deployed since 2010 in the northern and western Fram Strait. The tomographic sources also provide RAFOS signals between tomographic transmissions. In collaboration with the Applied Physics Laboratory, University of Washington (APL-UW), Seagliders were equipped with RAFOS receivers and dedicated software for acoustic navigation (Lee *et al*., 2008). This system was developed at APL-UW for under-ice glider missions in the Davis Strait and adopted for glider operations in the Fram Strait.

When RAFOS transmissions were available, the gliders calculated navigational solutions for testing purposes, remaining mostly in open water. The maximum range of RAFOS signals received by the Seagliders in Fram Strait varied between 50 and 300 km, depending on the type of sound source (two RAFOS systems were used, as well as

tomographic sources), sea ice extent between source and glider, and the type of RAFOS receiver carried by the glider. During the glider mission in 2011, 72% of acoustically obtained positions had an error of less than 10 km, while nearly half of the positions were accurate to 5 km. Based on field tests in 2010 and 2011, it can be concluded that for Seagliders equipped with the new RAFOS-2 receivers, sufficient coverage of the western Fram Strait glider section can be achieved with a network of 4-5 RAFOS sources, assuming that transmission ranges comparable to the upper bound of the observed ranges can be achieved.

4.3 Profiling mooring in the West Spitsbergen Current

Since 2008 a profiling mooring has been deployed by the Institute of Oceanology PAS under the DAMOCLES and AWAKE projects to obtain vertical profiles of temperature, salinity, and currents in the core of the West Spitsbergen Current. The mooring, located over the upper shelf slope west of Svalbard, is equipped with a McLane Moored Profiler (MMP). The profiler, carrying a CTD sensor and current meter, travels up and down along a vertical mooring cable twice a day, covering the layer between 130 and 730 m depth. The high resolution, year-round vertical profiles measure seasonal variability of the AW temperature and water column heat content. During the cooling period, the mixing, homogenisation and temperature decrease observed in the upper 500 m implied ocean to atmosphere heat fluxes reaching up to 500 Wm^{-2}. Short-term variability was mostly related to lateral shifts of the WSC core and mesoscale variability. In September 2010 the mooring position was moved closer to the tomographic mooring to provide better comparisons between acoustic and MMP observations, and in September 2011 the mooring was recovered and redeployed at the same position.

5. Conclusions and future perspectives

The first steps have been taken towards implementing components of an integrated data and model system in Fram Strait. A high-resolution ice–ocean model has been established and compared to acoustic and moored array data. An acoustic system was deployed both for ocean acoustic tomography and for positioning and navigation of gliders and floats. Gliders made their first flight under the ice in Fram Strait using acoustic navigation in 2011. Currently, gliders and floats use RAFOS signals provided by the acoustic network to navigate with an accuracy of 5–10 km. To improve navigational accuracy, we recommend using the broadband tomographic signals instead of standard narrowband RAFOS signals for positioning gliders and floats (Sagen *et al*., 2010, 2011). The joint use of tomographic sound sources for ocean measurements and navigation would decrease the overall logistical efforts. This integrated concept can be further developed and used in the Arctic interior, as well as other areas.

A multipurpose acoustic system in the Arctic would be a unique and cost efficient component of an Arctic Ocean Observing System (e.g., Sagen *et al*., 2010, 2011) and a means to validate and constrain climate models. Acoustic sources and receivers can be integrated into cabled networks for long-term operation. To proceed to an operational acoustic network in the Arctic interior, coordinated actions have to be taken across disciplines and countries working with Arctic Ocean research.

Acknowledgments

This work was supported by EU/FP6 in the framework of the DAMOCLES IP project and ESONET NoE and by the EU/FP 7 in the framework of the ACOBAR and Polish-Norwegian Research Fund (AWAKE). Special thanks are to the University of Bergen, the Norwegian Coast Guard, and the crews on board R/V Håkon Mosby and K/V Svalbard. Ocean model ran on the NOTUR2 HPC facilities.

References

Beszczynska-Möller, A., E. Fahrbach, U. Schauer, and E. Hansen (2012). Variability of Atlantic water temperature and transport in the entrance to the Arctic Ocean in 1997-2010. ICES J. Marine Sciences, in press.

Dickson (2008). The integrated Arctic Ocean Observing System (iAOOS) in 2008. A Report of the Arctic Ocean Sciences Board. Written by R.R. Dickson with inputs from iAOOS PIs

Eriksen, C.C., T.J. Osse, R.D. Light, T. Wen, T.W. Lehman, P.L. Sabin, J.W. Ballard, and A.M. Chiodi (2001). Seaglider: A long-range autonomous underwater vehicle for oceanographic research. IEEE J. Oceanic Eng. 26: 424-436.

Hackett, B., L. Bertino, D. Durand, and H. Wehde. Monitoring and forecasting the Arctic Ocean: Norway and MyOcean. This issue.

Johannessen, O. M., H. Sagen, S. Sandven, and K. V. Stark (2003). Hotspots in ambient noise caused by ice edge eddies in the Greenland Sea and the Barents Sea. IEEE J. Oceanic Eng. 28, 2: 212-228.

Lee, C. M., and J. I. Gobat (2008). Acoustic navigation and communications for high latitude ocean research (ANCHOR). J. Acoust. Soc. Am., 123, 2990, doi:10.1121/1.2932529.

Sagen, H., S. Sandven, *et al*. (2010). Acoustic technologies for observing the interior of the Arctic Ocean. in Proc. "Ocean Obs '09: Sustained Ocean Observations and Information for Society" Conference (Annex), Venice, Italy, 21-25 September 2009, Hall, D. E., and Stammer, D., Eds., ESA Publication WPP-306.

Sagen, H., S. Sandven, P. F. Worcester, A. Beszczynska-Möller, E. Fahrbach, and A. K. Morozov (2011). The Fram Strait acoustic system for tomography, navigation and passive listening, in Proc. 4th International Conf. on Underwater Acoustic Measurements: Technologies and Results, 20 24 June, 2001, Greece

Sandven, S., O. M. Johannessen, E. Fahrbach, E. Buch, H. Cattle, L. Toudal Pedersen and T. Vihma (2005). The Arctic Ocean and the Need for an Arctic GOOS. EuroGOOS Publication No. 22, March 2005, 50 pp.

Schauer, U., E. Fahrbach, S. Osterhus, and G. Rohardt (2004). Arctic warming through the Fram Strait: Oceanic heat transport from 3 years of measurements. J. Geophys. Res., 109(C06026), 10.1029/2003JC001823.

Skarsoulis, E., G. Piperakis, M. Kalogerakis, H. Sagen, S. A. Haugen, A. Beszczynska-Möller, and P. F. Worcester (2010). Tomographic inversions from the Fram Strait 2008-9 experiment, in Proc. European Conf. on Underwater Acoustics 2010, pp. 265-271, Istanbul, Turkey.

Hydrodynamic properties of the south Ionian Sea based on the POSEIDON Pylos observatory

D. Kassis*, K. Nittis, L. Perivoliotis, A. Chondronasios, G. Petihakis and P. Pagonis

Institute of Oceanography, Hellenic Centre for Marine Research

Abstract

The multi-platform POSEIDON-Pylos observatory in the south-east Ionian Sea has been in operation since 2007, delivering near real time data for a variety of meteorological, water column and near-seabed oceanographic parameters. It has been designed to contribute to long term monitoring of air-sea interaction and thermohaline processes of this key area of the Eastern Mediterranean where water masses of different origin meet and transform at various temporal and spatial scales. An inductive mooring line, with CTD instruments on in, provides salinity, temperature and pressure real-time data down to a depth of 500−1000 m. An autonomous seabed platform, that delivers data using underwater acoustic technology, was also deployed during 2008 to monitor deep sea (1670 m) temperature, salinity and dissolved oxygen data as well as high frequency pressure measurements for tsunami detection. Analysis of delayed mode data using the combined information of these two datasets as well as CTD profiles obtained during the maintenance visits reveals the dynamic picture of the south Ionian upper thermocline as well as the variation of temperature and salinity in deeper layers. Apart from the synoptic and seasonal scale signals that appear to be dominant in this area, important inter-annual variability can also be observed, such as a strong signal of LIW at intermediate depths during the spring of 2009.

Keywords: Operational oceanography, moored station, water masses, thermohaline properties

1. Introduction

The POSEIDON-II project (2005−2008) implemented major upgrades to the monitoring and forecasting infrastructure of the POSEIDON system that delivers operational services in the Eastern Mediterranean since 2000 (www.poseidon.hcmr.gr). These upgrades included the development of two new multi-parametric observatories in the southern Aegean (E1-M3A) and the south-east Ionian Seas (Pylos). The POSEIDON-Pylos station that started to operate in February 2007 consists of a surface buoy that hosts the meteorological and surface oceanographic sensors, and an inductive mooring line capable of hosting CTD sensors down to 1000 m depth (although a shorter 500 m cable has been used during the past 2 years due to damage to the original mooring line). Furthermore, during 2008 a sea-bed observatory platform was integrated in the system capable of recording sea level, temperature, salinity and dissolved oxygen from the sea bottom (1670 m). With the sea-bed platform, the Pylos station became the first Mediter-

* Corresponding author, email: dkassis@hcmr.gr

ranean open-sea tsunami detection system that can contribute to an integrated warning system for the basin.

Located approximately 15 km from the west coast of southern Peloponnese at the southeast Ionian Sea, the observatory's location is ideal for studies of the Easter Mediterranean Sea thermohaline circulation and its variability attributed to regional or larger scale forcing and climate change. Temperature and salinity time-series from several depths exhibit a complex picture of this transitional area where water masses formed in the Levantine, the Aegean and the Adriatic Seas meet and interact with the water masses of the Western Mediterranean Sea that enter through the Sicily straits (Nittis *et al*., 1993; Malanotte-Rizzoli *et al*., 1997).

2. System description

2.1 Architecture and configuration

The Pylos station is a part of POSEIDON buoy network that consists of 10 oceanographic mooring sites monitoring in the Aegean and Ionian Seas (Figure 1).

Figure 1 The POSEIDON buoy network (yellow dots are Wavescan buoys and green dots are Seawatch buoys). The Pylos station is indicated with a red circle.

It combines a multi-parametric surface buoy with an inductive mooring cable and a deep seabed platform. The buoy used at the Pylos site is a Fugro-Oceanor Wavescan type which is a platform suitable for deployment in deep offshore locations and can host a large number of sensors and different telecommunication systems. The acoustic communication system between the seabed platform and the surface buoy enables real-time data transmission from the sea bottom (Figure 2).

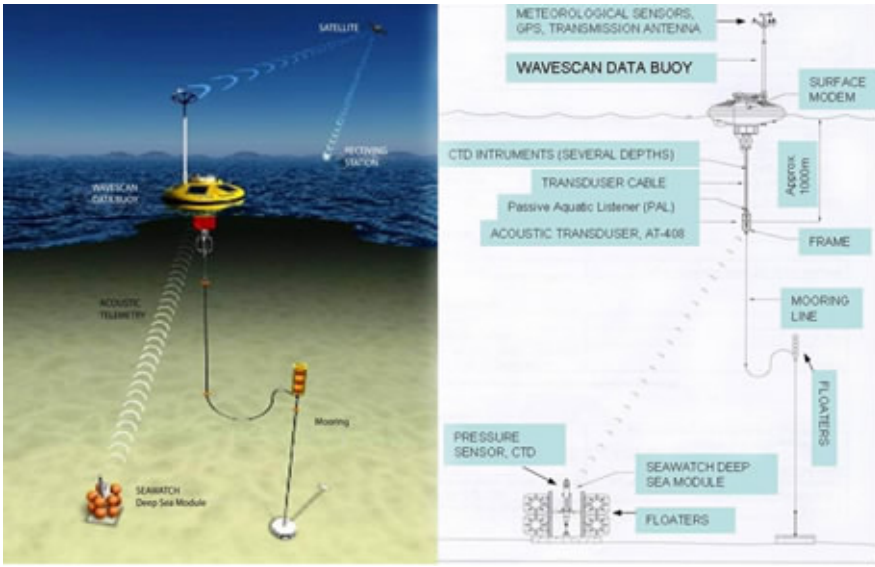

Figure 2 Pylos observatory architecture and components.

Table 1 Configuration of the Pylos observatory during 2010–2011.

Parameter	Depths measured (m)	Sensor(s) used	Accuracy
Air-Sea interface module (surface buoy)			
Wind speed dir	Surface	Young 04106	1 ms^{-1} 10°
Air pressure	Surface	Vaisala PTB 220A	±0.15 hPa
Air temperature	Surface	Omega	±0.1°C
Wave height, direction, period	Surface	Fugro OCEANOR Wavesense	0.1 m, 0.5°, 0.5 s
SST, SSS	Surface (1 m)	Seabird 37 SIP	±0.1°C, 0.05 $mScm^{-1}$
Currents	Surface (1 m)	Nortek, Aquadopp currentmeter	Sp: ±0.5 cms^{-1} Dir: ±2°
Water column module (mooring line)			
Temperature	20, 50, 75, 100, 250, 400, 500 m	Seabird 37-M CT	0.005°C
Salinity	20, 50, 75, 100, 250, 400, 500 m	Seabird 37-M CT	0.0005 Sm^{-1}
Pressure	250 m	Seabird 37-IM CTD	0.1% FS
Bottom module (seabed platform)			
Pressure	Seabed (1680 m)	Paroscientific 43K-101	0.1% FS
Temperature	Seabed (1680 m)	Seabird 16plus CTD	0.005°C
Salinity	Seabed (1680 m)	Seabird 16plus CTD	0.0005 Sm^{-1}
Pressure	Seabed (1680 m)	Seabird 16plus CTD	0.1% FS
Dissolved Oxygen	Seabed (1680 m)	Aanderaa Optode	<5% saturation

The observatory integrates a variety of sensors for monitoring atmospheric and oceanographic parameters as shown in Table 1.

Data are transmitted every 3 hours through a dual GSM/GPRS and INMARSAT-C satellite system. Additionally, most of the sensors used on this site are configured to store the measured data in the internal memory so that if the acquisition system or the cable connecting the sensor to the acquisition system fails, the data can be recovered during the maintenance missions when the sensors are recovered. The transmitted data are collected at the POSEIDON operational centre where automatic near real time quality control processes are applied on a daily basis.

2.2 Seabed component

The SDSM (Seawatch Deep Sea Module) observatory lies in the seabed below the surface buoy at approximately 1700 m depth. It is especially designed for tsunami surveillance and is equipped with a high-resolution pressure sensor that measures the sea level every 15 seconds. Internal processing applies the DART algorithm (Gonzalez *et al*., 1998) to identify a tsunami event based on user defined thresholds. When such a condition is detected the message is immediately communicated to the surface buoy through a hydro acoustic link which in turn is relayed to the operational centre. In normal operation mode the SDSM transmits the measured salinity, temperature, pressure, dissolved oxygen and sea level every 3 hours. These data are also stored on the internal memory of the platform along with the high frequency pressure time series that can be uploaded when the platform is recovered. The SDSM is powered through an on board battery pack and can remain operational for over 2 years. The platform is recovered by activating a releaser.

3. Temperature and Salinity observations

3.1 Data processing

Three years (2008–2010) of temperature and salinity data from 8 SBE-37 CTD instruments are presented. The sensors were mounted on the mooring line at several depths (1, 20, 50, 75, 100, 250, 400 and 500 m). A delayed mode data re-processing was performed including delayed mode data quality control and integration of the time series uploaded from the instruments internal data logger. Thus no-data periods due to transmission or system failures have been filled, although some gaps remained, related to rejected dubious data.

3.2 Upper layer T&S observations

Temperature time series of the first 100 m exhibit an intense variability especially in the surface layers (1–50 m) which is accentuated during the summer period and is propagated to deeper layers (50–100 m) during the late autumn and early winter period when the seasonal thermocline is gradually destroyed (Figure 3). Although this pattern seems to have a seasonal variability, during 2009 a well-mixed subsurface layer can be observed which is destroyed with an abrupt heating of the 20 m layer at the start of August. This is also observed in the salinity time series and becomes more intense during 2010 (Figure 3).

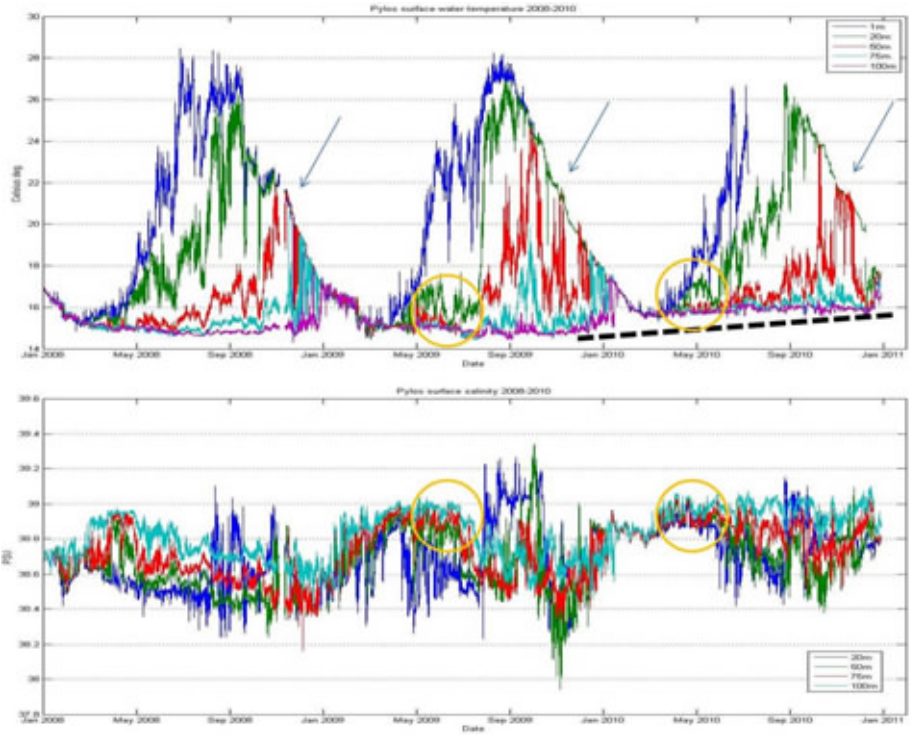

Figure 3 Temperature and salinity time series (2008–2010) for 1–100 m depths

An inter-annual positive trend can also be observed regarding the layers between 50–100 m leading to temperature and salinity differences of almost 1°C and 0.1 PSU respectively between summers of 2008 and 2010 (Figure 3 and Figure 5).

3.3 Intermediate depths T&S observations

The stratification of the intermediate layers during 2008 is destroyed with an intense variability and mixing during spring and summer of 2009. New water masses are introduced with more homogenous characteristics and seem to dominate during 2010 between intermediate depths of 250–500 m. The positive trend of the surface layers is also observed leading to more warm and saline waters during 2010 compared to 2008. Gradually this mass seems to move upwards giving a strong signal at the 250 m layer which presents 1°C and 0.2 PSU higher temperature and salinity values at the end of 2010 and forms a new stratification during the same year as it dissected from the underlying layers (Figure 4 and Figure 5).

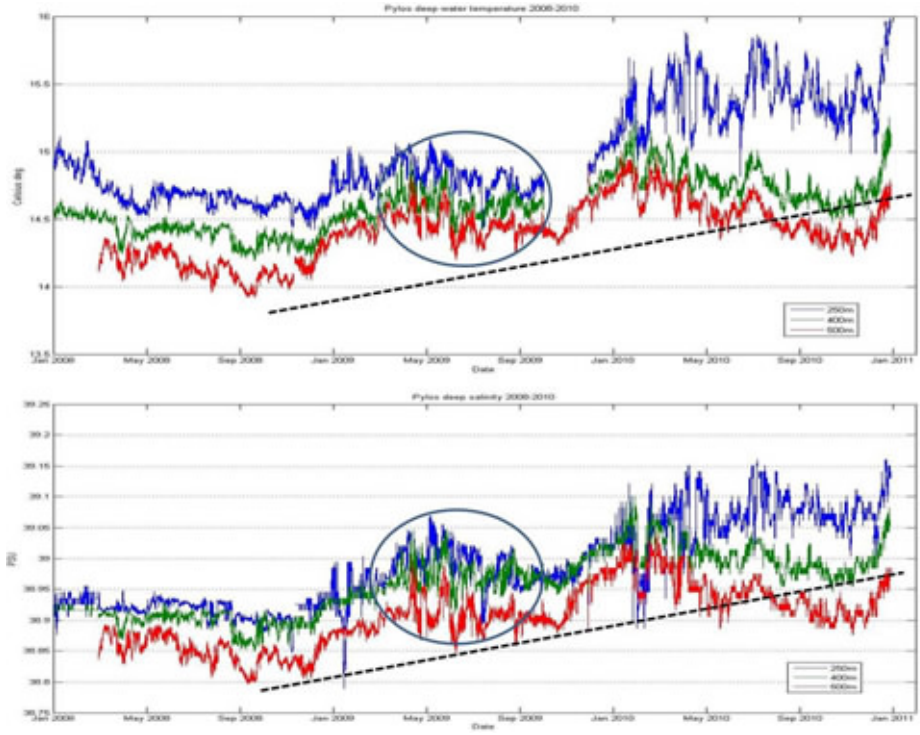

Figure 4 Temperature and salinity time-series (2008–2010) for 250–500 m depths.

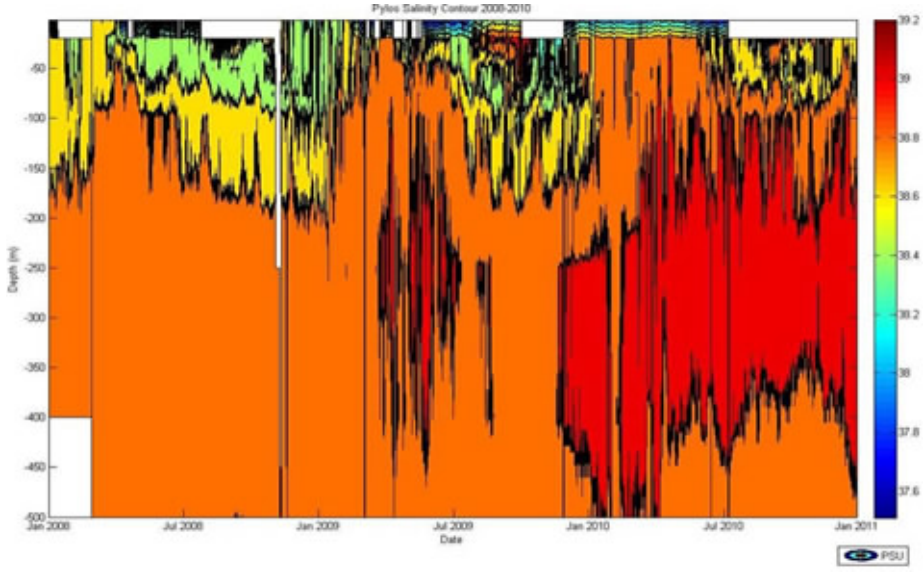

Figure 5 Salinity contour plot of the first 500 m for 3 years (2008–2010) of observations.

Data from CTD casts during the station's maintenance cruises with R/V Aegeo using a Seabird 9 are also analysed. The salinity profiles presented (Figure 6) confirm this increase during 2009 and 2010 covering a wide depth range from the subsurface down to 700 m depth. The low salinity subsurface layer signal, related to Atlantic Water (AW) during the end of 2008 which is replaced with higher salinity values later on, is also observed within the casts of November 2008, November 2009 and July 2010.

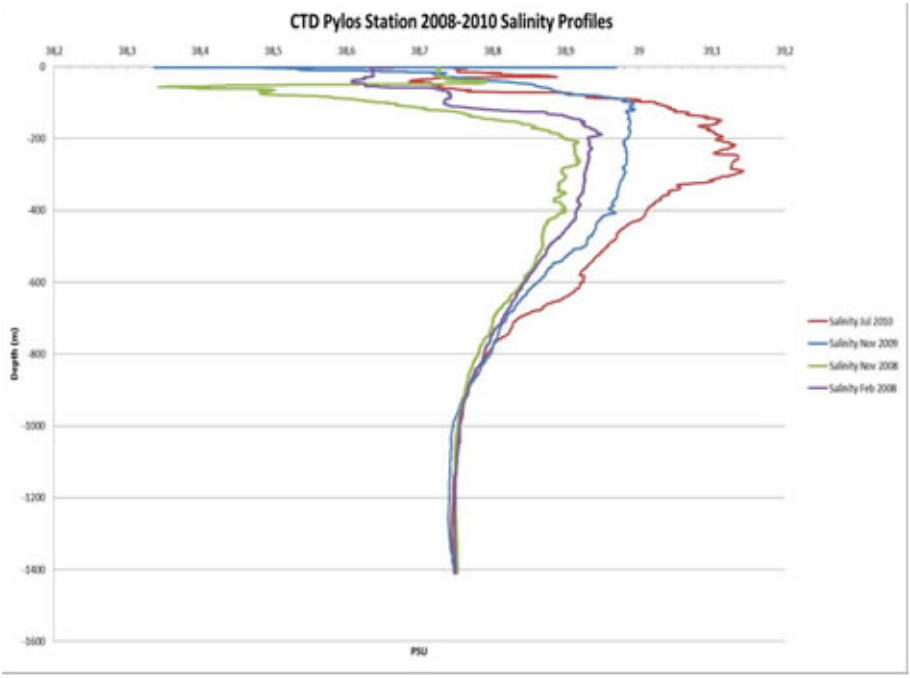

Figure 6 Salinity profiles from 4 different CTD casts during the scheduled maintenance cruises at Pylos station.

4. Conclusions

Operational fixed point observatories deliver valuable data. As well as for operational purposes (assimilation, model validation), these data can also be used for studies of ocean dynamics at different scales, especially when consistent long time series are available. The first 3 years of operation of the POSEIDON-Pylos observatory of the south-east Ionian sea have delivered water column temperature and salinity data that were used for studies of the regional thermohaline circulation. The upper-layers' temperature time-series demonstrate an intense synoptic and seasonal variability, which is the dominant signal in this area. A strong seasonal thermocline has been observed, which is formed at much shallower depths during July and is destroyed between September and October due to diminished insolation, water surface cooling and increased surface turbulence which is propagated to deeper layers. Although the time-series are relatively short, apart from the seasonal, inter-annual variability signals can also be observed, such as a strong signal of LIW at intermediate depths which is introduced during the spring of 2009 and becomes dominant during 2010 covering the subsurface and intermediate

depth area. This temperature and salinity maximum layer has probably been extended into the Ionian Basin by a northward flow through the Antikithira Strait. High salinity intermediate water branches that reach the northern Ionian basin are expected also to affect both the formation processes and the properties of the waters to be produced in the Adriatic (Theocharis *et al*., 2002). The salinity minimum of the subsurface water during the second half of 2008 that is related to presence of AW weakens and disappears during 2009 and is replaced by more saline water as a result of the preceding intense mixing with the underlying layers.

Acknowledgements

The POSEIDON I and II projects were funded by the Financial Mechanism of the European Economic Area and the Hellenic Program of Public Investments.

References

Nittis, K., N. Pinardi and A. Lascaratos (1993). "Characteristics of the summer 1987 flow field in the Ionian Sea", Journal of Geophysical Research, 1993, Vol. 98, pp171−184.

Gonzalez, F.I., H.M. Milburn, E.N. Bernard, and J. Newman (1998). Deep-ocean assessment and reporting of tsunamis (DART): Brief overview and status report. In: THE NTHMP TSUNAMETER NETWORK 37Proceedings of the International Workshop on Tsunami Disaster Mitigation. Tokyo, Japan, pp. 118−129.

Malanotte-Rizzoli, P., B. Manca, M. Ribera D'Alcala, A. Theocharis, A. Bergamasco, D. Bregant, G. Budillon, G. Civitarese, D. Georgopoulos, A. Michelato, E. Sansone, P. Scarazzato, and E. Souvermezoglou (1997). A synthesis of the Ionian Sea hydrography, circulation and water mass pathways during POEM-Phase I., Progress in Oceanography, 39, 153−204.

Theocharis, A., K. Nittis, H. Kontoyannis, E. Papageorgiou, and E. Balopoulos (1999). Climatic changes in the Aegean Sea influence the thermohaline circulation of the Eastern Mediterranean (1986−1997). Geophysical Research Letters 20, 11, 1617−1620.

Theocharis, A., B. Klein, K. Nittis, and W. Roether (2002). Evolution and status of the Eastern Mediterranean Transient (1997−1999) Journal of Marine Systems 33− 34 (2002) 91− 116.

Kassis, D., D. Ballas, K. Nittis, P. Pagonis, and D. Georgopoulos (2009). An integrated ocean observing system in the Ionian Sea. 3rd Conference on Underwater Acoustic Measurements: Technologies and Results, Nafplion, 21−26 June 2009, Book of Abstracts, p.144.

Petihakis, G., K. Nittis, D. Ballas, D. Kassis, P. Pagonis, L. Perivoliotis, and P. Drakopoulos (2009). The POSEIDON reference time-series stations of the Eastern Mediterranean Sea, in Proceedings of the "OceanObs09: Sustained Ocean Observations and Information for Society" Conference (Annex), Venice, Italy, 21−25 September 2009, Hall, J., Harrison D.E. and Stammer, D., Eds., ESA Publication WPP-306, 2010.

Sea surface temperature variations at the automatic MARNET stations in the German Bight and western Baltic Sea

Detlev Machoczek*

Federal Maritime and Hydrographic Agency (BSH), Germany

Abstract

Temperature measurements have been carried out at the Borkumriff/Ems station since 1924, Deutsche Bucht station in the German Bight since 1948, Fehmarn Belt since 1924, and Kiel Lighthouse since 1937. These long-term data series clearly indicate changes in the yearly temperature distribution in the German Bight and in the western Baltic Sea, especially during the past two decades. There is evidence that the change is not attributable mainly to an accumulation of extreme values (hot summers, warm winters), but to a shift in the length of seasons, with summer seasons becoming longer at the expense of spring and autumn, causing an increase in the annual heat balance.

Keywords: German Bight, Western Baltic Sea, temperature variations, time series

1. Introduction

Since September 1872, meteorological and oceanographic measurements have been made on board manned lightships in the German Bight, and since August 1900 also on board manned lightships in the western Baltic Sea. However, there was only sporadic processing of data in the first 50 years, and measurement data were rarely published. Therefore, the first continuous data series begin as late as 1924. The continuation of measurements was threatened when manned lightships were taken out of service. It was decided, therefore, to replace the lightships in the German Bight and western Baltic Sea with automated monitoring stations (Holzkamm, 1988). However, not all of the manned lightships were replaced with automated monitoring stations. Automated monitoring stations replaced only four lightships: two each in the North Sea and in the Baltic Sea (Figure 1). While the Ems and Deutsche Bucht stations are located in the area of the middle-latitude West Wind Drift, where a pronounced maritime climate prevails (BSH, 2009), the maritime nature of climate decreases toward the east. The weather regime in the area of the Kiel and Fehmarn Belt stations has been classified as predominantly maritime because continental weather influences are making themselves felt in this region (Hupfer, 2010).

* Corresponding author, email: detlev.machoczek@bsh.de

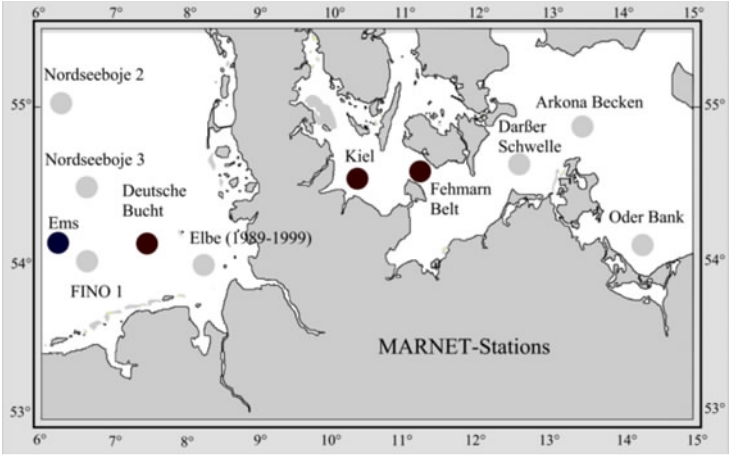

Figure 1 Location of Marnet-Stations in the German Bight and the western Baltic Sea.

2. The data

In 1989, the manned lightship Borkumriff moored in the German Bight was replaced by the unmanned lightship TW Ems which, however, was not located at the same position as the manned lightship but about 22 nm farther to the north. Despite this considerable distance between the stations, combination of the measurement data from both monitoring stations into one series is justified because the horizontal temperature gradient in this part of the German Bight is generally small.

The position in the German Bight where the unmanned lightship Deutsche Bucht has been located since 1989 had been occupied by the manned lightship Deutsche Bucht since 1969. As no lightships were moored at that position prior to that year, measurement data from the two manned lightships P15 and P12, moored at a position more to the southeast for different periods, were included in the data series from the lightship Deutsche Bucht. The two positions are about 17 nm apart.

Compared to the German Bight, the western Baltic Sea is characterised by markedly stronger horizontal temperature gradients. Therefore, a combination of time series data from stations which are too far apart is not an option. As the position of the lighthouse replacing the Kiel lightship is only about 1 nm southwest of the lightship position, the measurement data from the two stations can be combined into a single measurement series.

Also at the Fehmarn Belt station, the two measurement series from the manned Fehmarn Belt lightship and from the automated monitoring station, respectively, can be combined into one data series because measurements at this particular position have been made continuously since 1900, which is an optimum situation.

At the stations located on manned lightships in the German Bight, water temperatures were measured once a day at 8:00 a.m. (UTC). They were additionally measured twice a day, at the time of two consecutive slack tides, during spring, neap, and mean tides. The measurements were made using a surface thermometer with an accuracy of 0.1°K.

Monthly mean values including their standard deviation were computed on the basis of all measurement data available.

At automated monitoring stations, water temperatures are measured hourly using an electrical thermometer with an accuracy of 0.01°K. Both the daily mean value and the monthly mean value including their standard deviations are determined. Mean values are not computed if more than 15% of the hourly or daily values are missing.

On manned lightships in the western Baltic Sea, water temperatures were measured only at 8:00 a.m. (UTC). Otherwise, the methods used both at manned and automated stations are identical to those used at German Bight stations.

While the data series collected on board manned lightships only have minor gaps, mostly during the war and in the after-war years, data gaps have become considerably larger since the introduction of automated measurements. This is due to the fact that manual measurements could be made even during periods of bad weather, and the equipment used was such that malfunctions were nearly impossible, whereas today's sophisticated technology used for automated measurements breaks down easily, and the conditions required to carry out repairs, namely good weather and availability of a ship, are not always readily met (Figure 2).

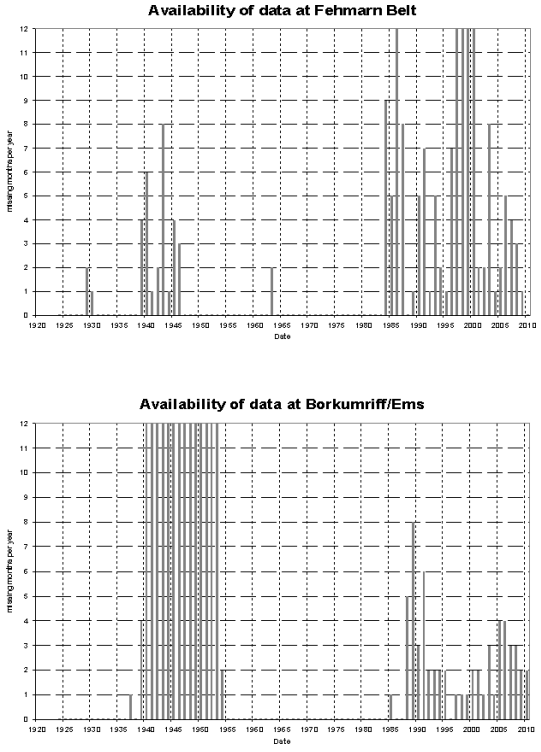

Figure 2 Availability of data, missing months per year, Fehmarn Belt, Ems.

3. Temperature variations at the Ems and German Bight stations

Because of gaps in the data series following the introduction of automated monitoring stations in 1989, the establishment and evaluation of time series of annual mean values is possible only to a limited extent. The Ems station can be given as an example of the trend toward higher annual means over the past 20 years (Figure 3). As the minimum and maximum values of sea surface temperatures are not affected by these limitations, conclusions can be drawn regarding temperature changes over time.

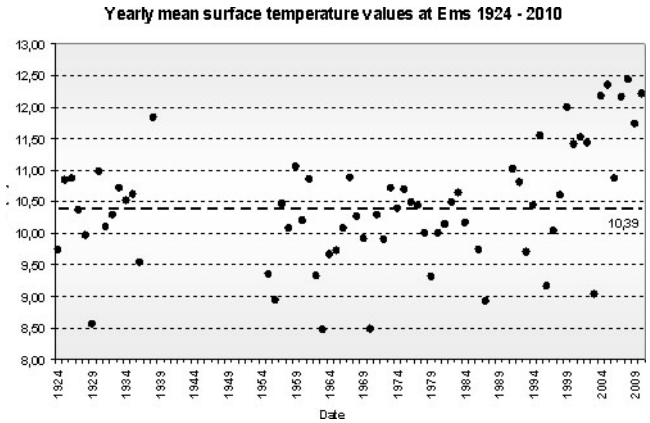

Figure 3 Yearly mean surface temperature values at Ems 1924–2010.

At the German Bight station, a clear trend toward rising temperatures in the period from 1948 to 1981 is not visible in the maximum temperatures, but minimum values rose about 0.5°K during the same period. At the Ems station, neither minimum nor maximum values show a significant trend in the period from 1954 to 1989. Minimum values are nearly constant, and maximum values show a slight downward trend.

However, the picture is quite different looking at the minimum and maximum sea surface temperatures after 1990. At both stations, both the minimum and maximum values have clearly risen. Maxima at the German Bight station increased by 0.56°K in the period from 1992 to 2010, and at the Ems station by 0.62°K in the period from 1991 to 2010. Minimum values at the German Bight and Ems stations are 0.93°K and 0.58°K, respectively (Figure 4). This development has also been described by Loewe *et al*. (2005, 2006) and Loewe, ed. (2009).

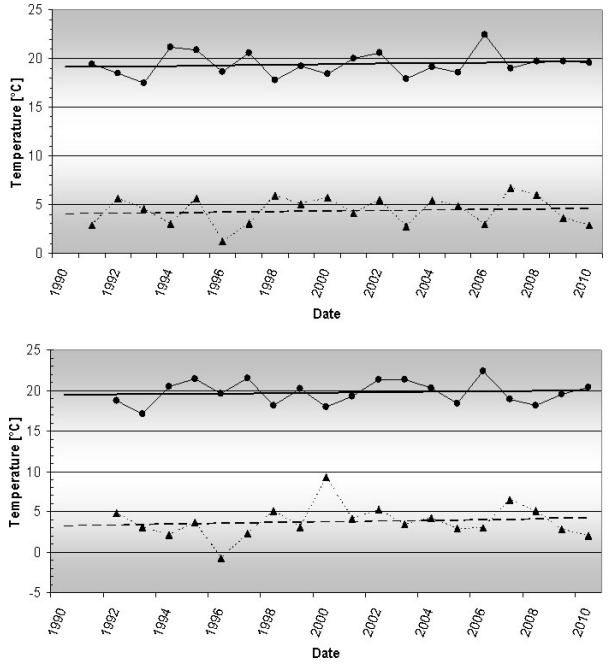

Figure 4 Annual minimum/maximum surface temperatures at Ems (top) and Deutsche Bucht (bottom).

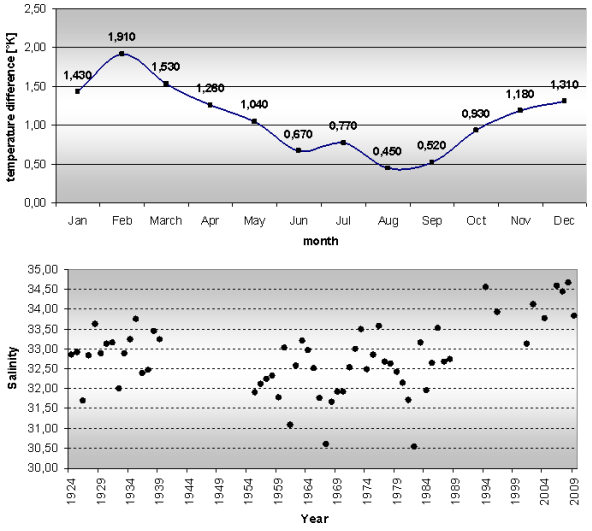

Figure 5 Top: Temperature differences between monthly mean surface temperature values 2000–2009 and 1924–2009 at Ems; Bottom: Yearly mean surface salinity values in February at Ems 1924–2009.

When computing monthly mean values from the data of both time series, those from the Ems station covering the period from 1924 to 2009, and those from the German Bight station covering the period from 1949 to 2009, and subtracting them from the monthly means of the years 2000 to 2009, it is found that all monthly mean values from this period are above the 85-year means at both stations. At the Ems station, the largest positive deviation is found in February, at 1.9°K. The minimum still is 0.45°K in August. The monthly means of surface salinity in February show a marked increase in the years after 2000. This allows the conclusion that there have been increased inflows of warm, high-salinity water of Atlantic origin (CLIVAR, 2007; ICES, 2011), (Figure 5).

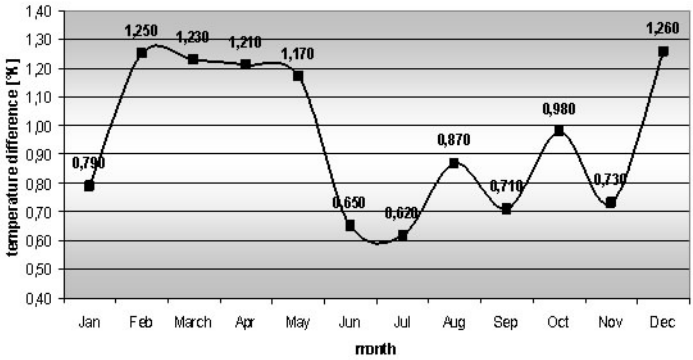

Figure 6 Temperature differences between monthly mean surface temperature values 2000–2009 and 1949–2009 at Deutsche Bucht.

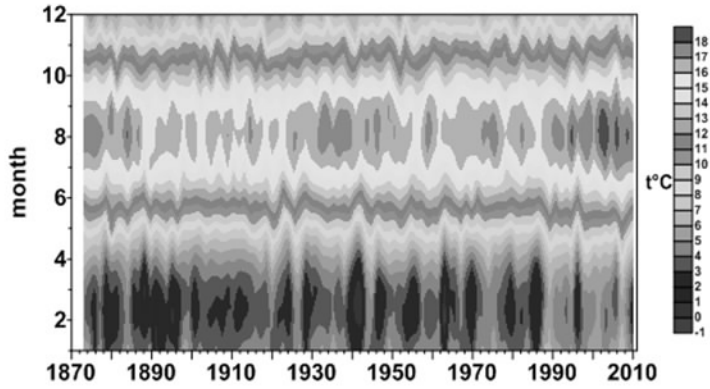

Figure 7 Sea surface temperature at Heligoland Roads.

A comparison of temperatures at the German Bight station shows a similar trend, although the time series at this station covers only 60 years. Here, too, a temperature increase has clearly taken place, but over a wider temporal range than at the Ems station because positive deviations of 1.17°K to 1. 26°K from the 60-year means are found in the months of February, March, April and May, and in December. Here, too, the cause has been increasing in-flows of warm high-salinity water (Wiltshire & Manley, 2004) (Figure 6). The isopleth diagram of sea surface temperatures at the Heligoland Roads station in the period from 1873 to 2010 also shows a trend toward rising summer and

winter temperatures for the period after 1990 (Figure 7).

4. Temperature variations at the Kiel and Fehmarn Belt stations

Time series of the annual means cannot be prepared for these two stations because the data gaps at these automated stations are too large. Besides, the Fehmarn Belt station was out of operation in the time from 1997 to 2000 due to a technical revamp. Unfortunately, the data gap at the Kiel station is considerably larger. After the lightship had been taken out of service in 1967, it proved impossible until 1985 to generate measurement data over a prolonged period of time. Only patchy data which is not suitable for evaluation is available from this period (DHI, 1979). However, the few available annual averages lie in the trend described in the analysis by Lehmann, Getzlaff & Harlaß (2011) of temperature-satellite data from 1990 to 2008.

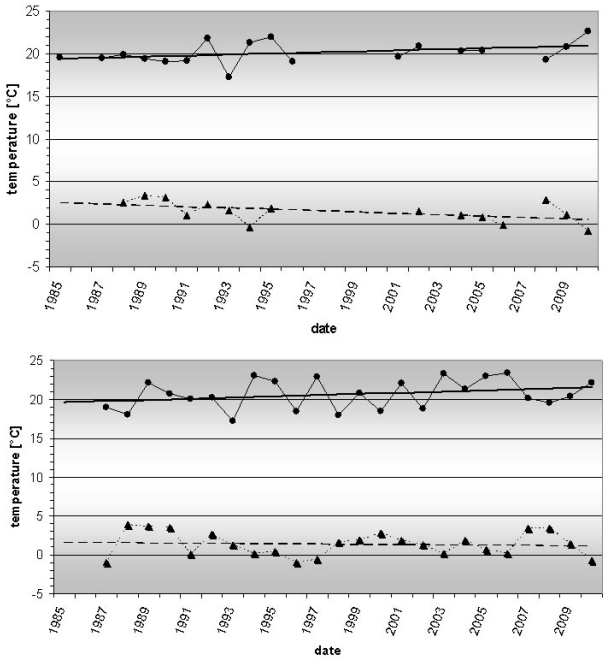

Figure 8 Annual minimum / maximum surface temperatures at Fehmarn Belt and Kiel.

At the Fehmarn Belt station, the measurements made on board the manned lightship cover a period of 61 years without major gaps, whereas the data available from the Kiel lightship only cover the years 1937 to 1967. An evaluation of minimum and maximum temperature data from the manned lightships shows that maximum temperatures had a slightly declining trend in the time from 1924 to 1984. No clear trend has been found in the minimum temperatures because the computed rise of minimum temperatures is within the range of accuracy of the individual values.

The data collected after 1985 show an entirely different temporal behaviour of maximum and minimum temperatures. Over the past 25 years, maximum sea surface temperatures have risen at both stations, Fehmarn Belt by 1.48°K and Kiel by as much as 1.85°K. The

value given for the Fehmarn Belt station is subject to some uncertainty due to three data gaps in the time series covering this period, but the trend of temperature development at this station corresponds to that at the Kiel station.

Minimum temperatures in both time series show a parallel development, but the temperature decrease computed for the Fehmarn Belt station is subject to the reservation referred to above. At the Kiel station, the minimum temperature has decreased by 0.42° K over the past 24 years (Figure 8). When computing monthly means from the Fehmarn Belt data covering the period from 1924 to 2009 and subtracting them from the monthly means of the years 2000 to 2009, it is found that 11 monthly mean values from this period are above the 85-year means.

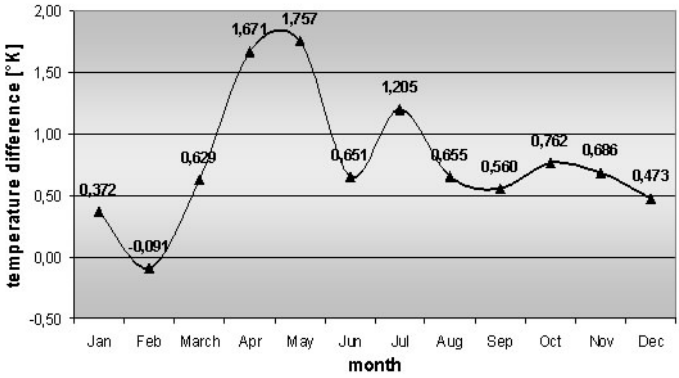

Figure 9 Temperature differences between monthly mean surface temperature values 2001–2009 and 1924–2009 at Fehmarn Belt.

February is the only month in which the mean value from the period 2000–2009 is below the 85-year mean. The strong positive deviation from the 85-year means is particularly obvious in the months of April and May, at 1.67°K and 1.76°K, respectively (Figure 9). The majority of evaluations made by Deutscher Wetterdienst (DWD, Meteorological Service of Germany) have shown positive air temperature anomalies for this region, including some major anomalies, in the period from 2000 to 2009, which probably caused the higher water temperatures. Compared to the 85-year mean values, the transition from low winter temperatures to higher summer temperatures has been taking place within a shorter period of time, extending the warmer period accordingly.

5. Conclusions

The time series of water temperatures at all four automated measuring stations show that annual mean sea surface temperatures in the German Bight and in the Western Baltic Sea have risen over the past two decades. They indicate a rise of maximum temperatures at all stations, whereas minimum temperatures have risen only in the German Bight, not in the western Baltic Sea.

At the Ems and Deutsche Bucht stations, the data indicate an influence of warm, high-salinity water of Atlantic origin in winter, at least until the turn of the century.

At the Kiel and Fehmarn Belt stations, surface water temperatures in spring have changed significantly during the last decade, showing an increase of temperatures in April and May. Winter temperatures apparently do not rise, but the length of the cold season has decreased.

Acknowledgements

The data in Figure 7 was kindly provided by P. Mangelsdorf and K. Wiltshire, Alfred-Wegener-Institut für Polar- und Meeresforschung (AWI), Biologische Anstalt Helgoland. The data processing was done by A. Frohse, BSH.

References

Bundesamt für Seeschifffahrt und Hydrographie (2009). Naturverhältnisse Nordsee und Englischer Kanal. BSH, 20062, 7–40.

CLIVAR (2007). The Oceanography of the North Atlantic and adjacent Seas. Newsletter of the Climate Variability and Predictability Programme, No. 40 (Vol. 12, No. 1), 11–13.

Deutsches Hydrographisches Institut (1979). Technischer Bericht, No. 2, 3, 4, 5 (unpublished manuscript).

Deutscher Wetterdienst (2002, 2004, 2007, 2008, 2009). Die Witterung in Übersee, Global Climate Review. DWD, Vol. 50, No. 4, 5, Vol. 52, No. 4, 5, Vol. 55, No. 4,5, Vol. 56, No. 4, 5, Vol. 57, No. 4, 5.

ICES (2011). ICES Report on Ocean Climate 2010. ICES Cooperative Research Report, No. 309, 50–54.

Holzkamm, F. (1988). Das automatische ozeanographische Messnetz des DHI in Nord- und Ostsee. Wissenschaftlich-Technische Berichte, DHI, No. 1988-3, 15 pp.

Hupfer, P. (2010). Die Ostsee – Kleines Meer mit großen Problemen. Gebrüder Borntraeger, Stuttgart, 65–73.

Lehmann, A., K. Getzlaff, and J. Harlaß (2011). Detailed assessment of climate variability in the Baltic Sea area fort he period 1958 to 2009. Climate Research, Vol. 46, 191–193.

Loewe, P. *et al*. (2005). Nordseezustand 2003. Berichte des BSH, No. 38, 68–92.

Loewe, P. *et al*. (2006). Nordseezustand 2003. Berichte des BSH, No. 40, 92–114.

Loewe, P. ed. (2009). System Nordsee, Zustand 2005 im Konzept langzeitlicher Entwicklungen. Berichte des BSH, No. 44, 111–144.

Wiltshire, K.H., and B.F.J. Manley (2004). The warming trend at Helgoland Roads, North Sea: phytoplankton response. Helgoland Marine Research, No. 58, 269–273.

Sea ice satellite products available at IFREMER/ CERSAT

F. Girard-Ardhuin*[1], D. Croizé-Fillon[2], and S. Pouliquen[1]

[1]*IFREMER/LOS, Plouzané, France*
[2]*IFREMER/CERSAT, Plouzané, France*

Abstract

Polar orbiting satellites enable daily and global coverage of the polar oceans, providing a unique monitoring capability of sea ice dynamics over the Arctic and Antarctic. Operational products available from IFREMER/CERSAT include Arctic and Antarctic ice concentration (and extent), and Arctic sea ice drift. IFREMER/CERSAT hosts a unique database with almost 20 years of winter time series for sea ice data: concentration from SSM/I data, sea ice drift from SSM/I, AMSR-E, QuikSCAT and ASCAT/MetOp data. These time series are ongoing and will continue for long term monitoring using the SSM/Is and MetOps operational sensors. These parameters are used as observations for climate change and also for data assimilation in ocean models.

Keywords: Sea ice, satellite observations, time series, drift.

1. Introduction

This paper presents the sea ice concentration and sea ice drift datasets from satellite, available at IFREMER via the Centre d'Exploitation et de Recherche SATellitaire (CERSAT). IFREMER/CERSAT datasets are unique: the data are systematically produced daily (only during the winter for the drift), at polar scale, since 1992. Sea ice concentration data and sea ice drift data are presented.

2. Arctic and Antarctic sea ice concentrations maps

Since the 1970s, passive microwave radiometers such as the Special Sensor Microwave Imager(s) (SSM/I) have been commonly used to estimate sea ice concentration from the daily brightness temperature data. The final resolution is a 25 × 25 km pixel for the lower frequencies and a 12.5 × 12.5 km resolution for the 85.5 GHz channels. We focus here on the 12.5 km resolution sea ice concentration dataset produced at IFREMER/CERSAT which started in 1992.

Among various algorithms, sea ice concentration is usually estimated either from the NASA team or Bootstrap algorithms. Both algorithms use the low frequency channels of the SSM/I, yielding the 25 × 25 km resolution of the sea ice concentration maps as distributed by the National Snow and Ice Data Center, Boulder, Colorado. The need for higher resolution sea ice concentration data to monitor the marginal ice zones, polynia and lead openings has required the development of new algorithms relying on the 85.5 GHz channel brightness temperature data. Among these algorithms, the Artist Sea Ice

* Corresponding author, email: fanny.ardhuin@ifremer.fr

(ASI) algorithm developed at the University of Bremen (Germany) provides reliable results (Kaleshke *et al*., 2001).

In order to produce the IFREMER/CERSAT sea ice concentration maps and dataset at a resolution of 12.5 × 12.5 km, the ASI algorithm is applied to the whole high frequency brightness temperatures dataset (1992 – present) of the SSM/I. In order to discard artefacts at low latitudes, a monthly climatological sea ice mask is applied. A "neutral area", defined as a three pixel-wide band along the coastline, is flagged because the concentration estimates there are quantitatively not reliable. This is due to the land contamination effect within the footprint of the sensor. Finally, a correction has been applied to dismiss some of the remaining unrealistic concentration values in this area, mainly in the estuaries. Arctic and Antarctic sea ice concentration data and maps at 12.5 km resolution are available daily (see examples in Figure 1). Monthly data and a 15-year long climatology (1992–2006) are also available (Ezraty *et al*., 2007a). These maps are produced systematically because they are used as a background for the sea ice drift estimations presented hereafter. Sea ice concentration data, maps and documentation are available at CERSAT.

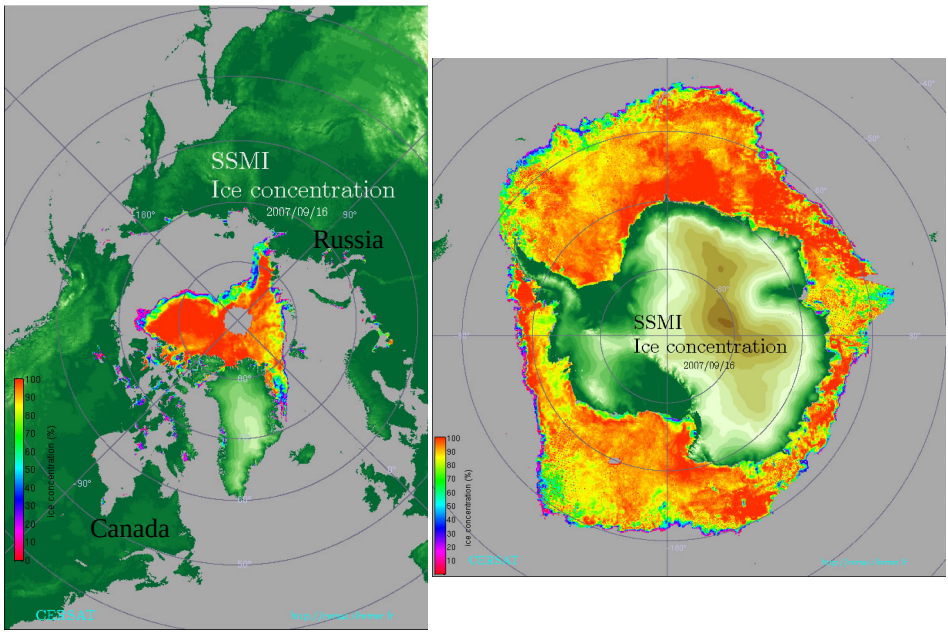

Figure 1 Daily sea ice concentration maps in mid-September 2007. Left: The Arctic at its minimum record area to date; Right: The Antarctic from SSM/I radiometer data. Grid spacing is 12.5 km. Concentration is in percentage.

3. Arctic sea ice drift fields

At IFREMER, sea ice drift are inferred from passive (radiometers) and active microwave sensors (scatterometers) at low resolution, a Merged drift product resulting from the combination of these individual drift maps is presented (Figure 2). A medium resolution

product is also estimated from data of the Advanced Microwave Scanning Radiometer Earth observing system (AMSR-E).

3.1 Low resolution product

Since the 1990s, sea ice drift can be estimated from satellite data, daily and with global coverage of the polar ocean. The ice motion is estimated at the scale of large ice floes, whereas a buoy measures the drift of a single ice floe. Here, we focus on large scale (or polar scale) sea ice drift, inferred from passive (radiometers) and active microwave sensors (scatterometers). High frequency data are very sensitive to atmospheric effects (moisture and liquid water). This implies sea ice drift estimations at periods of low water vapour during winter.

Passive microwave radiometers data like SSM/I brightness temperature data are used to estimate sea ice drift (Emery *et al*., 1997). A scatterometer can also be used for sea ice drift estimation (Ezraty *et al*, 2007b), the benefit of the all-weather, day–night microwave radar measurements has been well established. During the 1999–2009 period, daily averaged backscatter maps at a resolution of 12.5 km have been built from the Ku-band SeaWinds/QuikSCAT scatterometer data. Since 2007, the ASCAT scatterometer onboard MetOp provides C-band backscatter data, processed to give daily averaged backscatter maps (same pixel size resolution). Drift fields are inferred at 3 and 6 day-lags from the SSM/I H & V channels and from QuikSCAT and ASCAT data with the same drift grid resolution (62.5 km). Details about tracking methods to infer sea ice drift fields can be found among others in Ezraty *et al*. (2007a,b), Emery *et al*. (1997), Kwok *et al*. (1998).

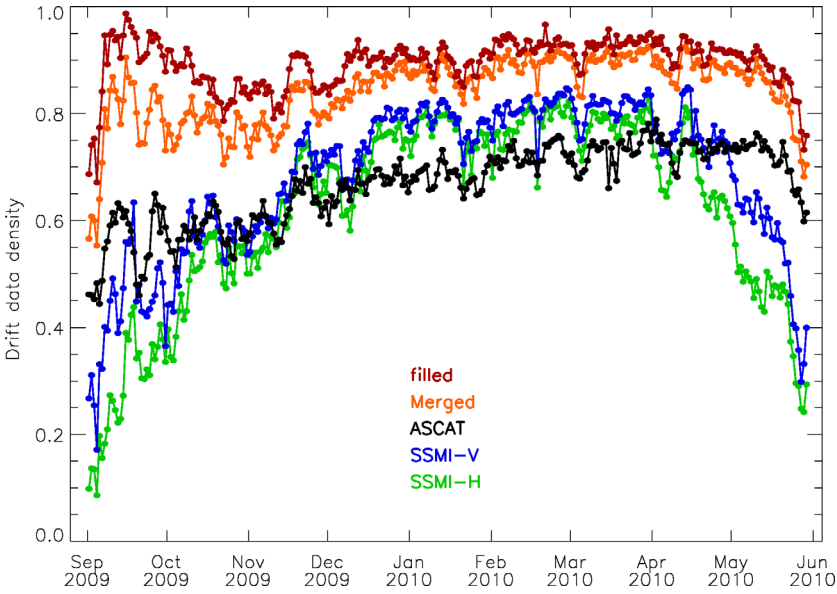

Figure 2 Density of valid data for a winter (2009–2010) for individual products, merged drift product and the filled one.

The combination of these independent drift fields (radiometer and scatterometer fields at the same resolution) provides better confidence in the final resulting field than for the individual ones (Girard-Ardhuin and Ezraty, 2012). First, the data gap at the North Pole is reduced to the smallest one. Second, the sea ice merged drift field enables discrimination of remaining vectors outliers of the individual products. Third, the number of valid drift vectors is higher than the single sensors valid drift vectors: the merging increases the data density up to 90% for December – April and more than 80% in autumn and spring (see Figure 2). We have developed a space and time interpolation to infer drift in some data gaps patches. This is very useful, in particular for autumn estimation. The interpolation enables the time window to be increased in September and May when the drift data density reaches only 20 to 70% for single sensor drift (80 to 90% for the filled product). A monthly drift product is also available. These datasets are produced daily at IFREMER/CERSAT since 1992 each autumn−winter−spring season from September until May.

3.2 Medium resolution product

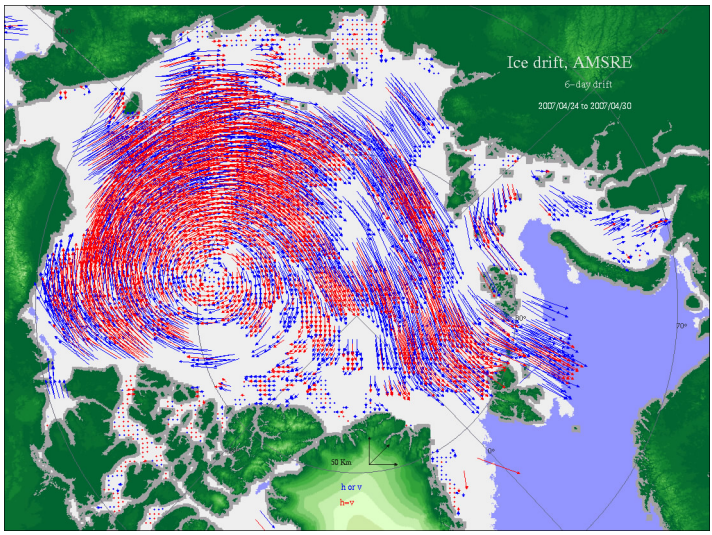

Figure 3 Merged AMSR-E H & V sea ice drift at 6 day-lag (24−30 April, 2007). Drift vectors less than one pixel are marked with a cross. Red: identical drift for H and V polarisations. Blue: selection of one channel.

Since 2002 and until October 4th 2011, the AMSR-E sensor has provided brightness temperature maps at 89 GHz H and V channels. From these maps, a merged drift of the two channels is inferred with a 31.25 km grid spacing which we call “medium resolution” (Ezraty *et al.*, 2007c). The enhanced resolution also translates in greatly reducing the quantification noise, and even enables computation of a 2-day lag dataset. The AMSR-E drift product has a better angular resolution than the low resolution product, but also more patches of data gaps and no data around the North Pole. Figure 3 shows the AMSR-E merged drift field at 6-day lag. The merged medium resolution AMSR-E drifts are in slightly better agreement with buoys than the merged low

resolution scatterometer/radiometer drifts but the AMSR-E product has a lower density drift, in particular at fall and spring. The scatterometer/SSMI merged product has a data density higher than 80% for the period December – mid-April and higher than 60% for early autumn and early spring, whereas AMSR-E provides 50 to 80% data density from December to April, and decreases for early autumn down to 15 to 60%.

4. Conclusion

Passive microwave measurements provide sea ice concentration datasets for both poles. The 12.5 km resolution IFREMER/CERSAT sea ice concentration dataset is available all year round since 1992. Sea ice drifts inferred only from radiometers have a reasonable accuracy but are limited by data gaps and low data density at the beginning and the end of the cold period. The main limitation is the angular resolution for small drifts: for slow motion areas, the ice vectors have a larger uncertainty. Recently, the AMSR-E radiometer has provided a better vector accuracy because of its enhanced ground resolution. Thus the time lag can be reduced to two days. The merging of three independent fields of drift data (two SSM/I and one QuikSCAT or ASCAT) at the same resolution improves the data density and the usable time period over winter. It also enables the discrimination of the vector outliers remaining in the individual products. IFREMER/CERSAT hosts a unique database of almost 20 years of winter time series of sea ice drifts. These datasets are available for oceanic and climate modelling. The time series will continue for Arctic long term monitoring using the new MetOp/ASCAT operational scatterometers, planned to be operated for the next 20 years.

Acknowledgements

The authors thank the CERSAT team for acquisition and archiving of the data and the systematic processing of the sea ice drift maps. The Global Monitoring for Environment and Security European Union projects PolarView and MyOcean support partly the data production and distribution.

References

Emery, W.J., C.W. Fowler, and J. Maslanik (1997). Satellite-derived maps of Arctic and Antarctic sea ice motion: 1988 to 1994. Geophys. Res. Lett. 24 (8): 897−900.

Ezraty, R., F. Girard-Ardhuin, J.F. Piollé, L. Kaleschke, and G. Heygster (2007a). Arctic and Antarctic sea ice concentration and Arctic sea ice drift estimated from Special Sensor Microwave data, User's manual, version 2.1, February 2007. Available at IFREMER/CERSAT.

Ezraty, R., F. Girard-Ardhuin, and J.F. Piollé (2007b). Sea ice drift in the central Arctic combining QuikSCAT and SSM/I sea ice drift data, User's manual, version 2.0, February 2007. Available at IFREMER/CERSAT.

Ezraty, R., F. Girard-Ardhuin, and D. Croizé-Fillon (2007c). Sea-ice drift in the central Arctic using the 89 GHz brightness temperatures of the Advanced Microwave Scanning Radiometer, User's manual, version 2.0, February 2007. Available at IFREMER/CERSAT.

Girard-Ardhuin, F., and R. Ezraty (2012). Enhanced Arctic sea ice drift estimation merging radiometer and scatterometer data. To be printed in IEEE Trans. Geosc. Rem. Sens.

Kaleschke, L., C. Lüpkes, T. Vihma, J. Haarpainter, A. Bochert, J. Hartmann, and G. Heygster (2001). SSM/I sea ice remote sensing for mesoscale ocean-atmosphere interaction analysis. Canadian J. of Remote Sensing, vol. 27 (5), 526−537.

Kwok, R., A. Schweiger, D.A. Rothrock, S. Pang, and C. Kottmeier (1998). Sea ice motion from satellite passive microwave imagery assessed with ERS SAR and buoy motions. J. Geophys. Res. 103 (C4): 8191−8214.

Nowcasting, forecasting and re-analysis

Validation of sea ice results from a real-time forecast system

Arne Melsom* and Bruce Hackett

Norwegian Meteorological Institute

Abstract

Sea ice is a component of the ocean circulation that is unique in the sense that it forms a near-binary field where the fraction of the cover is either 0 or (very close to) 1 nearly everywhere. However, the transition between the open ocean and the (near-)continuous ice cover – the marginal ice zone – is of significant interest, due to, for example, intensive biological activity.

Here, we compare model predictions and observations that are available for the Arctic region from the MyOcean project. For validation we use observations in the forms of sea ice charts of the European sector that are based mainly on expert interpretation of satellite radar data. The observations are thus independent of the radiometer data that are assimilated by the ocean-sea ice model.

We identify and describe validation metrics that are tailored for near-binary fields. Commonly used metrics, such as RMS differences between model results and observations in the full domain, provide the user with information that is difficult to interpret in the present context. Specific validation metrics are proposed here, including displacement of the sea ice edge, and the size and overlap of the each sea ice category, including contingency tables.

Keywords: validation, sea ice, ocean modelling, radar data

1. Introduction

Sea ice is a part of Earth's climate system that develops over time scales which presently range from hours and days due to weather conditions, to several years due to the build-up of a multi-year ice cover. In turn sea ice variability affects the atmosphere by modifying the ocean/atmosphere exchanges of heat, moisture and momentum, and by changing the albedo during summer. Hence, sea ice information is valuable for forecasting conditions in the Arctic region on all of the listed time scales. Further, due to teleconnections in the atmosphere and the ocean, this information is potentially useful for seasonal forecasting (Benestad *et al*., 2010; Melsom, 2009) and studies of Earth's climate (e.g. Deser *et al*., 2000).

Sea ice conditions are of interest to a diverse group of users, including commercial fishing, tourism, off-shore industry and science. The recent decline in sea ice in the Arctic Ocean during summer has also given rise to a renewed interest in using routes in the Arctic Ocean for shipping, particularly between Eastern Asia on one side, and Europe and the east coast of North America on the other. Such a development will intrin-

* Corresponding author, email: arne.melsom@met.no

sically require capabilities related to emergencies, e.g. oil spills in the region of the marginal ice zone (MIZ), and threats from drifting icebergs.

Here, we present the validation system that has been developed for operational use in MyOcean's Arctic Monitoring and Forecasting Centre (ARC-MFC). MyOcean is the Marine Core Service implementation project of the Global Monitoring for Environment and Security in the 7th Framework Programme (FP7) of the European Union.

The present work is an extension and update of the work reported by Melsom (2010). We begin with a presentation of the sources of information that are available. Then we discuss how to best process this information in the context of validation, and define several metrics for sea ice validation. Next, validation results from the ARC-MFC are given, and we conclude with a summary of our results and recommendations.

2. Sea ice–ocean circulation model

TOPAZ is a coupled sea ice–ocean data assimilation model system that has been developed for use in the North Atlantic Ocean, the Nordic Seas, the Arctic Ocean, and adjacent shelf seas. It is the main production system of the ARC-MFC. TOPAZ assimilates observations by means of the ensemble Kalman filter (Evensen, 2003).

TOPAZ' ocean circulation model is the HYbrid Coordinate Ocean Model (HYCOM; Bleck, 2002), which is set up on a horizontal grid of 880×800 nodes, with a non-constant mesh size of 12–16 km. This resolution is eddy-permitting in low latitudes and mid-latitudes, but it does not resolve the mesoscale in the Arctic region. In the vertical direction, the ocean is represented by 28 hybrid layers.

In the TOPAZ system, HYCOM is coupled to a sea ice model which combines elastic-viscous-plastic rheology (Hunke and Dukowicz, 1997) with the thermodynamics from Drange and Simonsen (1996). The model computes advection and local changes in ice concentration, ice thickness and snow depth.

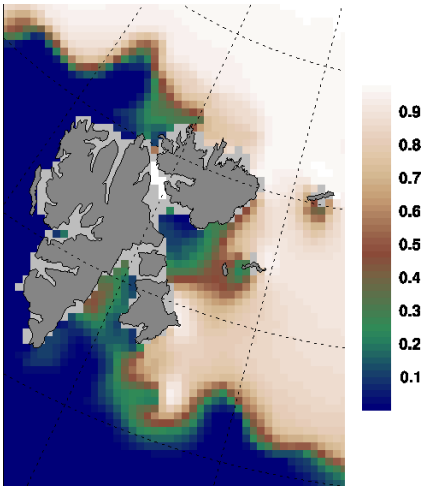

Figure 1 Sample gridded values for sea ice concentration from the sea ice–ocean circulation model. Only results for a limited region near Svalbard are displayed.

TOPAZ is presently run operationally in a weekly cycle in the ARC-MFC. The model is initialised by an assimilation step one week prior to production time. In the assimilation step, data from various observational platforms are used to adjust the initial state of the model, including radiometer data which is affected by sea ice. It is subsequently run for a 17 day period, forced by meteorological analysis fields for the first 7 days, and by forecast fields for the next 10 days. A sample field of sea ice concentration is shown in Figure 1.

3. Validation observations

The observational product for sea ice that is used in this study is available from the MyOcean Sea Ice and Wind Thematic Assembly Centre (Breivik and Dinessen, 2011). The product, which covers the waters from east of Greenland to Novaya Zemlya, and the western Kara Sea, is updated daily on working days. Results for sea ice concentration are provided as gridded fields of sea ice categories, as defined by the World Meteorological Organization. The horizontal resolution of these fields is 1 km × 1 km. Such a high resolution is made possible by extensive use of Synthetic Aperture Radar (SAR) data from Radarsat and Envisat. In order to fill gaps between satellite passes, SAR data are supplemented by visual and infrared data from MODIS and AVHRR.

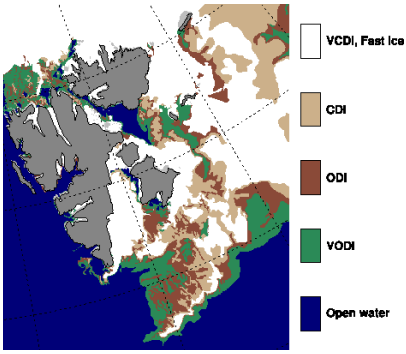

Figure 2 Sample gridded values for sea ice concentration from the observational product (detail). This is approximately the same region as in Figure 1.

In this product sea ice concentration observations are interpreted as multiples of 1/10. These values are subsequently grouped into five sea ice categories, as defined in Table 1.

Table 1 Definition of sea ice categories

Category name	Acronym	Values	Belong to MIZ?
Open water	OW	<0.1	No
Very open drift ice	VODI	0.1, 0.2, 0.3	Yes
Open drift ice	ODI	0.4, 0.5, 0.6	Yes
Close drift ice	CDI	0.7, 0.8	Yes
Very close drift ice	VCDI	0.9, 1	No

4. Processing of observational data and model results

Model results from the ARC-MFC are interpolated onto a regular, polar-stereographic grid, with a resolution of 12.5 km before they are released to users. The present validation is performed in order to shed light upon the quality of the results from a user perspective, so it is the interpolated results that will be considered here.

To make model results and observations comparable, we must choose an algorithm for mapping two sets of 2D data with different resolutions horizontally (1 km×1 km vs. 12.5 km×12.5 km) and different sea ice variables (5 ice categories vs. continuous concentration) onto same-resolution products. In order to illustrate this challenge, a simplified case with a difference in horizontal resolution is displayed in Table 2 and Table 3.

Table 2 Sea ice concentrations with a fine resolution

1.0	1.0	1.0	1.0	0.8	0.2
1.0	1.0	1.0	0.8	0.2	0.0
1.0	1.0	0.8	0.2	0.0	0.0
1.0	0.8	0.2	0.0	0.0	0.0
0.8	0.2	0.0	0.0	0.0	0.0
0.2	0.0	0.0	0.0	0.0	0.0

Table 3 Sea ice concentrations with a coarse resolution

1.00	0.95	0.30
1.00	0.30	0.00
0.30	0.00	0.00

The coarse resolution results in Table 3 are simply averaged values over the corresponding 2×2 cells in Table 2. A well-posed validation algorithm should take this into account, i.e., a “perfect” score should be returned when the one set is validated using the other as “truth”. It is not possible to define a general interpolation function from the coarse to the fine grid which assures such a result. Hence, we will integrate the fine resolution result onto the corresponding representation by the coarser resolution. Note that even this approach does not guarantee a “perfect” score in the general case, since a fine resolution grid cell may bridge two or more coarse resolution grid cells (e.g. when one grid is rotated relative to the other), and the results may be sampled with a time offset or with differences in averaging period.

In the present context, we will therefore integrate the observations onto the 12.5 km×12.5 km resolution of the model product, and we will map the model sea ice concentration values onto the 5 sea ice categories of the observational product. The

observational product is a composite of snap-shots from various satellite-born instruments, while the model results are daily averages.

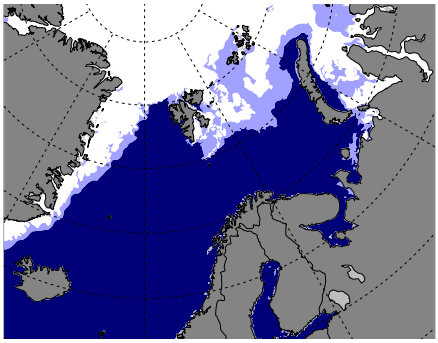

Figure 3 Domain for which the present analysis is performed. Light blue shows MIZ from a sample ice chart.

5. Validation metrics

We wish to validate a two-dimensional field that is characterised by a front whose position has a strong temporal dependence, and can be represented by a sea ice edge according to a standardised definition. Furthermore, at some distance from the front the sea ice concentration is (nearly) uniform, with values of 0 on the open ocean side, and (close to) 1 in the interior of the ice cover. We may thus view sea ice concentration as a near-binary field whose variability is characterised by the motion of the front and variability in the vicinity of the front, a region which is referred to as the marginal ice zone (MIZ). Presently, the MIZ is represented by sea ice classes VODI, ODI and CDI.

5.1 Bias and RMS error of sea ice concentration

The two most commonly used validation metrics are the bias and the root mean square (RMS) error. However, when applied to near-binary field data, these quantities tend to be determined by the two dominant states and do not provide much information about the quality of the model results where they are of most interest to users, i.e., in the MIZ. Since the resolution in sea ice concentration is limited to 5 categories, a better strategy is to investigate the statistics of these categories. A relevant validation metric is defined in subsection 5.3 below.

5.2 RMS error of sea ice edge position

If defined appropriately, the position of the sea ice edge is of interest to many users. Representing the sea ice edge by a sea ice concentration value that corresponds to the limiting conditions for operation of vessels may be appropriate in this context. Here, we set the boundary between VODI and ODI to represent the sea ice edge. Then, assuming that model results and observations have been processed as described in Section 4, we adopt the following algorithm for validation of the model sea ice edge:

1. For both observations and model results, find the set of grid cells that belongs to ice category ODI and that has at least one neighbour cell (up, down, right or left) that

belongs to ice category VODI. The two sets of grid cells that result define the ice edge in their respective products.

2. For each grid cell that belongs to the sea ice edge in the observational product, compute the distance to the nearest sea ice edge grid cell in the model product. The model RMS error is then computed as the root mean square of these distances.

In the case where the domain for validation is dominated by significant coast line undulations, e.g. due to islands and/or fjords, the second item in the algorithm may also limit the computation of distances between cell pairs to pairs that only have ocean cells along the lines where the distances are computed. Although there are archipelagos (Svalbard, Frans Josef Land) in the domain which we consider here, our domain is mostly open ocean, and we have chosen not to implement this extension.

5.3 Errors by sea ice categories

As stated above, the sea ice cover is largely characterised by the position of its edge, and by the variability in the MIZ which spans the region between the open ocean and the near-continuous ice cover. Hence, the validation metric for the position of the sea ice edge described in section 5.2 should be supplemented by a validation metric for the distribution of sea ice in the MIZ. We will adopt two metrics for ice category errors: (1) a contingency table for distribution of observed vs. modelled categories, and (2) time series of the areal extent for each category and each product, plus time series of the total category area where the products overlap.

6. Validation results

For the purpose of demonstration of results from the validation metrics that were defined in section 5, we use observations and model results for day 7+2 in the weekly model production cycle (see section 2); this corresponds to the 2-day forecast relative to the analysis day. This information was available for a period of 20 weeks, from November 2010 to March 2011.

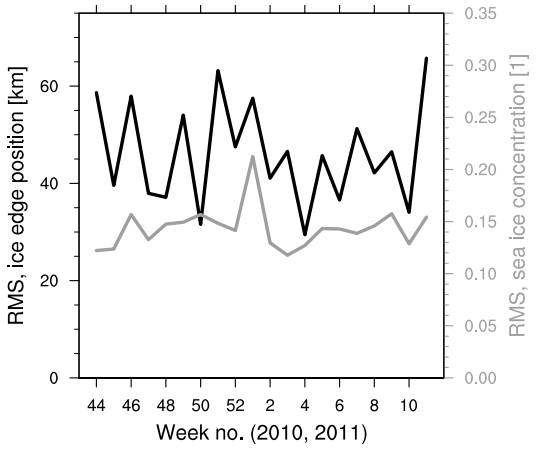

Figure 4 RMS error of model results vs. observations of sea ice concentration (grey, right axis), and position of the ice edge (black, left axis).

First, we examine results for RMS errors of the sea ice concentration and the position of the edge. The time series of these RMS errors are depicted in Figure 1.

The range of values of the RMS error for sea ice concentration is constrained by the large areas away from the MIZ where both model results and observations have values of 0 (ice free) or very close to 1 (ice interior). Hence, the time dependence of this metric is weak, as displayed by the grey curve in Figure 4, and the usefulness is low for both users and developers of the products.

Table 4 Contingency table for the sea ice categories defined in section 3. Regions in which both model and observations indicate either open water or very close drift ice have been excluded. Tabulated values are percentages, computed by aggregating results over a period of 20 weeks. Dark grey shading correspond to matching categories. Light grey shading is used for cells where results from both model and observations are classified as belonging to the MIZ.

		Observations				
		OW	**VODI**	**ODI**	**CDI**	**VCDI**
Model	**OW**		8.3	5.7	5.1	1.9
	VODI	3.1	**2.0**	2.2	2.2	1.2
	ODI	1.8	1.6	**2.2**	2.7	1.8
	CDI	1.3	1.5	2.7	**5.1**	4.5
	VCDI	3.2	3.0	7.4	29.6	

The RMS errors for the position of the ice edge in Figure 4 suggest that the edge can be expected to be found 40−60 km from its position in the model. The variability of these results is dominated by changes from one week to the next.

The results in Table 4 reveal that, after the vast domains away from the MIZ have been excluded, the ice categories from the model results and observations are only matching in less than 10% of the remaining region.

We note from Table 4 that the largest values appear in the top and bottom rows where observations indicate MIZ conditions, while the model results correspond to OW (top row) or VCDI (bottom row).

Table 5 Same as Table 4, but here results have been merged for categories that belong to the MIZ.

		Observations		
		OW	**MIZ**	**VCDI**
Model	**OW**		19	2
	MIZ	6	**22**	7
	VCDI	3	40	

Next, we have condensed the results further in Table 5 by merging the MIZ categories. We still find that the match between model results and observations in the MIZ is fairly low, at 22% of the remaining region.

7. Concluding remarks

Validation may serve several purposes. It may provide users with valuable information about the quality of available products, and it can help developers to become aware of weaknesses in the systems they work with. Thus, future efforts by development teams may be guided in a direction which could lead to significant improvements of the relevant products.

Furthermore, one must be aware that all products, based on observations or based on model results, have sources of errors. Hence, when comparing model results and observations, the term "RMS error", used here in subsections 5.1 and 5.2, may be misleading. A term that perhaps more properly describe these metrics is "RMS differences".

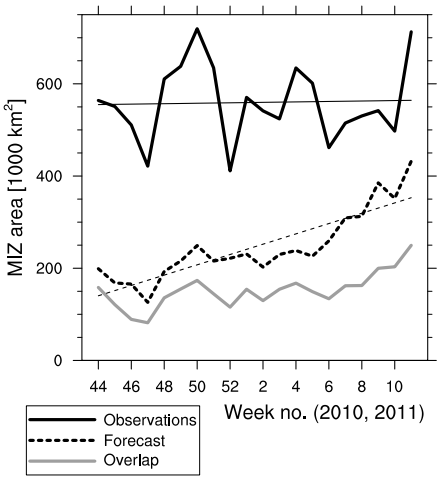

Figure 5 Temporal evolution of the MIZ extent in the observational product (full black line) and model results (dashed black line) during a period of 20 weeks. Thin lines show the least squares linear fit, while the grey line shows the total area where the MIZ overlaps in the two products.

The results in section 6 reveal that the extent of the MIZ is much larger in the observational product when compared to the model results. In fact, almost half of the MIZ region from observations is classified as VCDI in the model results. The magnitude of this discrepancy should be instructive for the modellers and lead to efforts to have a less abrupt transition from open water to the near-continuous ice covered region in the ocean-sea ice model.

In order to gain additional insight into differences between the two products, we examine how the size of the MIZ changes in time, displayed in Figure 5. We find that, while the MIZ area exhibits a strong trend in the model results, nearly doubling in size during the 20 week period, the observations change markedly from week to week, but with almost no trend.

We also note that the MIZ overlap region increases much less than the model MIZ, so much of the growth of the model MIZ takes place in regions outside of the observed MIZ.

We have demonstrated that for the near-binary sea ice concentration field, validation metrics that are tailored for such fields provide much more useful results than the standard metrics. Indeed, the simple RMS error in the ice concentration fields (Figure 4) is shown to be misleadingly low compared to the results from the more MIZ-specific metrics (Table 4, Table 5, and Figure 5). Moreover, we have been able to identify significant discrepancies between model results and observations that could potentially guide model development and/or satellite imagery interpretation to improve one or both of the products that have been examined.

Acknowledgements

This work has been funded by MyOcean/EU Project no. FP7-SPACE-2007-1. The assimilative ocean sea−ice model system TOPAZ has been developed at the Nansen Environmental and Remote Sensing Center, while satellite data were processed by the Sea Ice Service at the Norwegian Meteorological Institute. We are grateful for the efforts by these teams. The analysis was performed using scripts developed for the R programming language (http://www.r-project.org). All figures were made using tools from the NCAR Command Language (NCL; http://ncl.ucar.edu).

References

Benestad, R.E., R. Senan, M. Balmaseda, L. Ferranti, Y. Orsolini, and A. Melsom (2011). Sensitivity of summer 2-m temperature to sea ice conditions. Tellus, 63A, 334-337, doi: 10.1111/j.1600-0870.2010.00488.x

Bleck, R. (2002). An oceanic general circulation model framed in hybrid isopycnic-cartesian coordinates. Ocean Mod., 4, 55-88.

Breivik, L.A., and F. Dinessen (2011). Product user manual: Regional sea ice Svalbard. MyOcean project document 14 pp. Available from http://catalogue.myocean.eu.org/static/resources/user_manual/myocean/USER_MANUAL_SEAICE_ARC_L4_NRT_OBSERVATIONS_011_002-v1.0.pdf

Deser, C., J.E. Walsh, and M.S. Timlin (2000). Arctic sea ice variability in the context of recent atmospheric circulation trends. J. Climate, 13, 617-633.

Drange, H, and K. Simonsen (1996) Formulation of Air-Sea Fluxes in the ESOP2 Version of MICOM. Tech. Rep. No. 125, Nansen Environmental and Remote Sensing Center 23 pp.

Evensen, G. (2003) The ensemble Kalman filter: Theoretical formulation and practical implementation. Ocean Dyn. 53, 343-367.

Hunke, E.C., and J.K. Dukowicz (1997). An elastic-viscous-plastic model for sea ice dynamics. J. Phys. Oceanogr., 27, 1849-1867.

Melsom, A. (2009). Ocean - sea ice - atmosphere heat fluxes over the Arctic Ocean. met.no Note 14/2009, Norwegian Meteorological Institute 7 pp. Available from http://met.no/Forskning/Publikasjoner/Publikasjoner_2009

Melsom, A. (2010). Validation of sea ice concentration in the myOcean Arctic Monitoring and Forecasting Centre. met.no Note 12/2010, Norwegian Met. Inst. 8 pp. Available from http://met.no/Forskning/Publikasjoner/Publikasjoner_2010

Validation of the UK Met Office FOAM ocean forecasting system

John Siddorn*, Alex Arnold, Rosa Barciela, Ed Blockley, Karen Edwards, David Ford, Rachel Furner, Catherine Guiavarc'h, Pat Hyder, Dan Lea, Matt Martin, Enda O'Dea, Andrew Ryan, Alistair Sellar, Dave Storkey, Peter Sykes, Jennie Waters, and James While

Met Office, United Kingdom

Abstract

The UK Met Office produces ocean forecast products on a daily basis with global and regional coverage. The FOAM ocean forecasting system is based on the NEMO ocean model and an analysis correction assimilation scheme. A wide range of data is assimilated including in-situ data from moorings, profiling floats and satellite sea-surface temperature, sea-surface elevation and sea-ice data. Ecosystem models are also run in near-real time to provide information about algal blooms and underwater visibility. This paper describes the systems, briefly details how the system quality is verified, and presents some example evaluation of the system skill for diurnal SST cycles and site-specific current forecasts.

Keywords: FOAM, ocean modelling, operational forecasting, NEMO, SST, currents

1. Introduction

The Forecasting Ocean Assimilation Model (FOAM) system is the operational ocean modelling system, with data assimilation, used for short-range forecasting at the UK Met Office. Recent implementations of FOAM configurations are described in Storkey *et al*. (2010) and O'Dea *et al*. (submitted). The FOAM system is based on the Nucleus for European Modelling of the Ocean (NEMO) framework (Madec, 2008). This is a community model that has a wide user and developer base particularly in Europe. It will also form the ocean model component of the Met Office seasonal forecasting and climate modelling systems in the near future. The FOAM system is made up of a suite of nested configurations, with a global ORCA025 (Drévillon *et al*., 2008) configuration feeding boundary conditions to a North Atlantic rotated grid 1/12° model (the NATL12) and the non-linear free surface tidal model the Atlantic Margin Model at approximately 7 km resolution (the AMM7). Two further 1/12° regional configurations for the Mediterranean Sea and Indian Ocean are nested into the global configuration using one-way lateral boundary conditions,. The sea ice component is currently modelled using the 2nd version of the Louvain-le-Neuve (LIM2) model (Fichefet and Morales Maqueda, 1997). This has viscous-plastic dynamics (Hibler, 1979) and a 3-layer thermodynamic model (Semtner, 1976). The AMM7, is coupled with the ERSEM ecosystem model (Blackford *et al*., 2004).

* Corresponding author, email: john.siddorn@metoffice.gov.uk

Data assimilation is based on a version of the analysis correction scheme. The scheme was originally devised by Lorenc *et al*. (1991) and implemented for FOAM by Bell *et al*. (2000). Analysis steps are performed once per day. Each analysis step consists of a number of iterations. On each iteration the observations are separated into groups which are easily related (thermal profiles, saline profiles, surface temperature, surface height). For the AMM7 at present the only assimilation type is surface temperature. For each group of observations (e.g. the temperature profile data), increments are calculated first for the directly related model variables (e.g. the temperature fields). These increment fields are then used to calculate increments for less directly related model variables (e.g. the velocity fields) using hydrostatic and geostrophic balance relationships, water property conservation or statistical relationships. The univariate components of the model error covariance are specified as the sum of two 3D error covariances, one describing the ocean mesoscale, the other large scales including atmospheric synoptic scales (Martin *et al*., 2007). These and the observation error covariances are estimated from differences between one-day and two-day forecasts verifying at the same time (Parrish and Derber, 1992), combined with statistics of observation minus model values (Hollingsworth and Lönnberg, 1986), obtained from hindcast assimilations. Altimeter data are assimilated by displacement of isopycnal surfaces, an extension of the Cooper and Haines (1996) scheme. A pressure correction technique (Bell *et al*., 2004) is employed to improve the dynamical balance near the equator and analyses performed with large correlation scales are used to attempt to remove large-scale biases in the satellite surface temperature data.

This paper briefly details how the system is routinely validated in operations, and gives some examples of use-specific validation of the real-time products with a view to demonstrating utility of the real-time products from FOAM.

2. Operational Monitoring and Verification

There are two main functions to the real-time validation:

1. Daily monitoring of products to detect major problems, and to identify significant features in the forecast.
2. Monthly examination of accuracy statistics to detect gradual deteriorations in the quality of products, and to confirm that the accuracy level is consistent with the results of the calibration hindcast.

2.1 Daily Monitoring

The purpose of the daily monitoring is to detect major problems with the products, partly through manual checks of the model outputs but also including some automatic checking. All the monitoring information is produced automatically and available for viewing by scientists on a monitoring web page (Figure 1). Interesting or unusual events are recorded in a monitoring log. The plots examined include:

- Maps of all products at various depths.
- Differences between the daily mean surface temperature and the OSTIA analysis for the same day.
- Time-series of the extreme values of the model fields.

- Maps of data assimilation innovations.
- Maps of data assimilation increments.
- Maps of anomalies against climatologies .
- Maps of statistics derived from assimilation innovations.
- Volume transports.

A daily automated assessment of the FOAM is also provided, with the number of available observations for the day, and root mean squared (RMS) and mean errors derived from innovations for each observation type being provided to the monitoring web page.

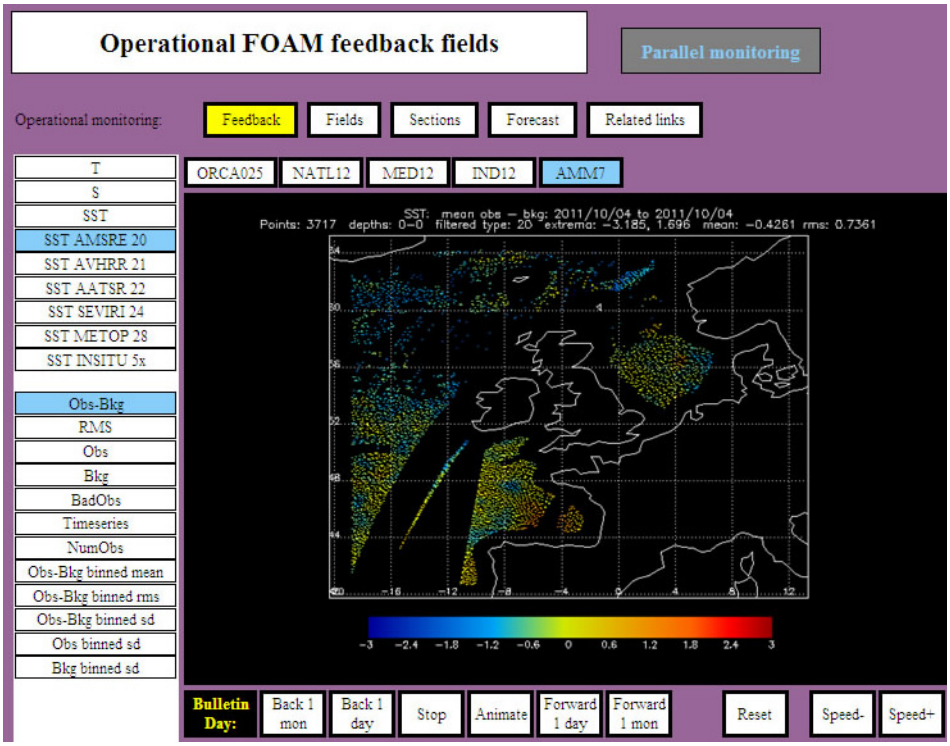

Figure 1 The monitoring page showing SST innovations for observations from the AMSRE satellite.

Automatic email warnings are produced if pre-defined thresholds for each diagnostic variable are exceeded, for example if RMS errors are higher than expected, there are fewer good observations than expected or there are more bad observations than expected. Daily statistics are saved for future reference.

2.2 Accuracy Monitoring

The daily monitoring outlined above will only detect major and immediate problems; it will not detect gradual deteriorations in the accuracy of products. To capture such problems daily accuracy statistics are monitored on a monthly basis. Variations in

accuracy are also compared to the calibration hindcast to detect deviations from the normal seasonal and inter-annual variability of the errors. If potential problems are detected, then the plots from the monitoring section are useful for investigating the cause.

The Global Ocean Data Assimilation Experiment (GODAE; Bell *et al*., 2009) metrics are used as a basis for use in evaluating model-based products. Although these metrics were designed for the GODAE community (and thus assimilating models of the open ocean) the concepts and terminology have been adapted to describe the metrics which are appropriate for the FOAM AMM7 model as well as the FOAM open ocean models. Explanations of the GODAE metric classes can be found in Hernandez and Crosnier (2008). There are two groups of metrics used: analysis statistics and forecast statistics. At present these statistics are all computed in observation space (GODAE class 4), and averaged over pre-defined regions. The analysis statistics are derived from the data assimilation innovations (observation minus model differences). These differences are computed using model background fields before the observations are assimilated, and are therefore indicative of the accuracy of the 1-day forecasts. Because the data assimilation uses an FGAT (First Guess at Appropriate Time) scheme, these differences use the model value at the same time as the observation.

In contrast, the forecast statistics are based on daily-mean fields. These fields are stored until the validity time has passed, and then compared to observations using the methodology defined for the GODAE class 4 inter-comparison (Hernandez *et al*., 2009 and subsequent updates of the methodology). The statistics are derived from the observation minus forecast differences for sea surface temperature for all models and sea surface height, sea ice and profiles of temperature and salinity for models where these are assimilated. For ERSEM, statistics are produced for surface chlorophyll and suspended particulate matter. These errors show the accuracy of the 1-, 3- and 5-day forecasts. The statistics are presented as 30-day running means to smooth out high-frequency variability and enable detection of significant changes in the accuracy (Figure 2).

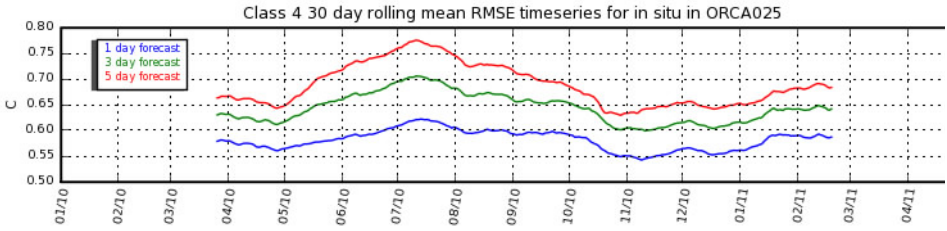

Figure 2 An example of the 30 day rolling mean RMS error in SST of the FOAM ORCA025 model from in-situ observations minus model forecast. Three time-series are presented, in blue the 1 day forecast RMSE, in green the 3 day forecast RMSE and in red the 5 day forecast RMSE.

3. 3. Site-specific Current Validation

An assessment of site-specific current forecast skill of global FOAM (ORCA025) analysis fields has been made using daily-mean output from 2007-08 and hourly instantaneous output from Jan 2007 – Jun 2007. Comparisons were made initially with

PIRATA (Prediction and Research Moored Array in the Atlantic) moored current meters in the eastern tropical Atlantic.

There has been a qualitative analysis involving visual examination of fields and comparing with observations in the vicinity of each buoy. Figure 3 shows an example plot of daily-mean model currents surrounding the PIRATA buoy at 6°S, 8°E with the buoy location superimposed. When the model missed a feature it would quite often be found in the modelled currents either at a nearby location or time. This qualitative analysis of the system shows FOAM appears to be performing sensibly. However, for there to be use made of the FOAM currents for site specific applications, more quantitative assessments need to be done. As many applications of site-specific currents require the prediction of the exceedance of speed thresholds time series of buoy data has been used to determine whether the model can correctly predict when speed thresholds are exceeded. The thresholds 0.25 ms^{-1}, 0.5 ms^{-1}, 0.75 ms^{-1} and 1.0 ms^{-1} were used as these reflect operational user requirements.

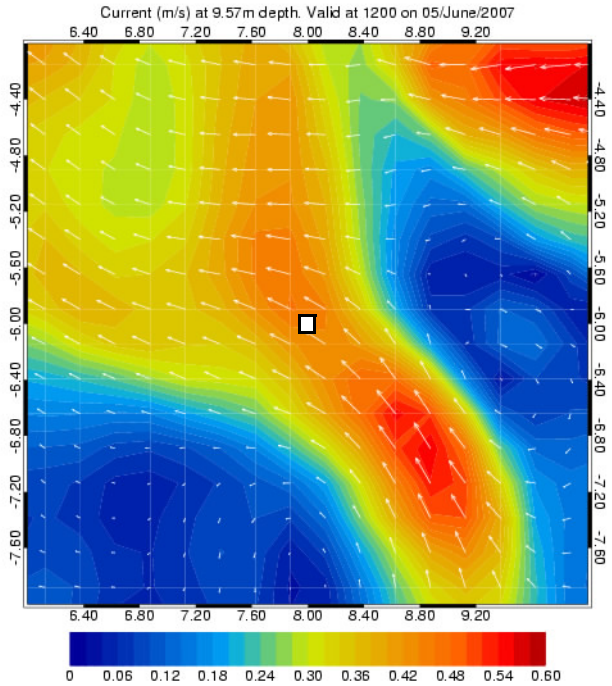

Figure 3 An example plot of current speed (contours) and vectors (arrows) with an analysis site shown (square).

A categorical analysis was performed using these thresholds by producing 2×2 contingency tables and calculating a range of metrics including Receiver Operating Characteristic (ROC) curves, Heidke skill scores and Matthews Correlation Coefficients (phi coefficients). Despite the qualitative analysis that the model currents were capturing the observed features reasonable well there were too many ‘misses’ and ‘false alarms’ for the model to be considered skilful. Therefore we do not have sufficient confidence in the

currents to be deriving daily threshold warnings at this stage. Future assessments will focus on identifying time and space scales over which the modelled currents do have sufficient skill.

Histogram plots of observed and modelled currents (Figure 4) suggest that FOAM-ORCA025 tends to predict too many weak currents and underestimate the largest observed currents. However analysis was performed using 6-hourly wind forcing so time interpolation may perhaps smooth the current fields. Future implementations of ORCA025 will use hourly wind forcing, the impact of which may be seen in this type of analysis.

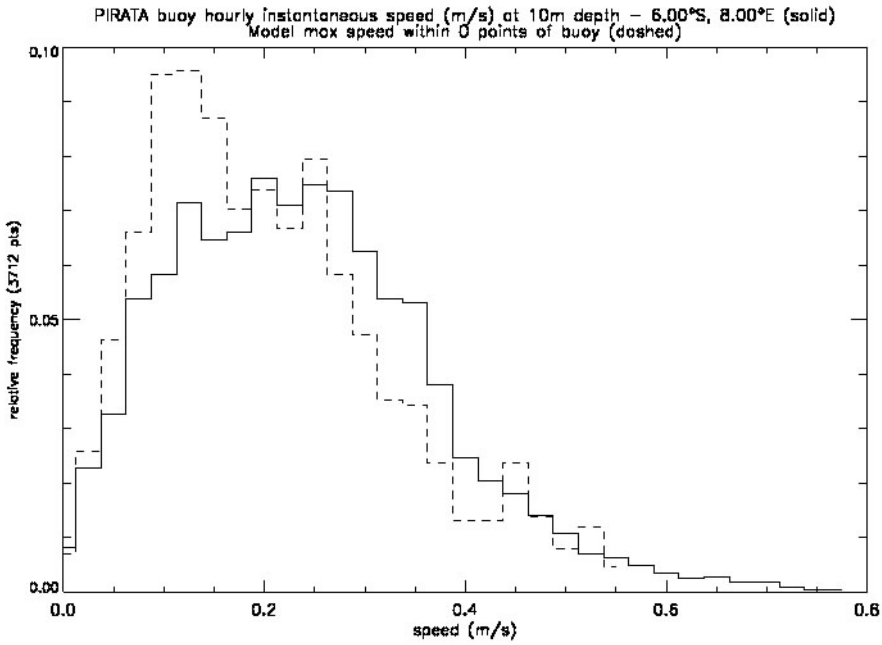

Figure 4 An example plot of relative frequency of current speed from a PIRATA buoy (solid line) and the FOAM ORCA025 model (dashed line).

4. Diurnal SST evaluation

The diurnal cycle of sea surface temperature (SST) is caused by the direct solar heating and night time cooling of the top few metres of the ocean. This cycle can be considered to be on top of long period seasonal changes and variability due to advective and mixing processes. In the absence of wind, cloud, and precipitation, the SST diurnal cycle would follow a predictable oscillatory pattern. However, variations in solar heating due to cloud and the tendency of wind to mix heat to depth, make the diurnal system much more complex.

An assessment of the ability of satellite and buoy observation platforms to observe and resolve this diurnal cycle of SST was performed prior to such data being used to assess diurnal SST in the Met Office's ORCA025 configuration of FOAM (Sykes *et al*., 2011). It was found that for the moored buoys, four evenly spaced observations per day are

required to resolve the SST diurnal cycle in order to satisfy the Nyquist sampling requirements. Satellites are only able to achieve this level of observation frequency if they are geostationary and are sampling areas unaffected by cloud cover. Nevertheless, statistical assessment of the satellite data showed that a diurnal signal is detectable.

FOAM was then assessed for its ability to simulate and predict a diurnal cycle of SST. Hourly SST output covering the Atlantic region from the model was compared to in-situ PIRATA buoys and SEVIRI (Spinning Enhanced Visible and Infrared Imager) geostationary satellite SST measurements. An algorithm was used to identify daily diurnal SST minima, maxima and ranges for the observations and model data over a 1 month period in July 2008. The timings of the diurnal minima and maxima within the buoy and model data were also compared. The assessment showed that FOAM does produce a diurnal cycle with skill across all forecast days. Comparison with all the PIRATA buoys gave anomaly correlations of between 0.6 and 0.75 for prediction of the diurnal SST maxima and minima and between 0.45 and 0.55 for the diurnal SST range. Biases against all the buoys were of the order of 0.05 K for the maxima, minima and ranges; with the model underestimating the diurnal SST range overall.

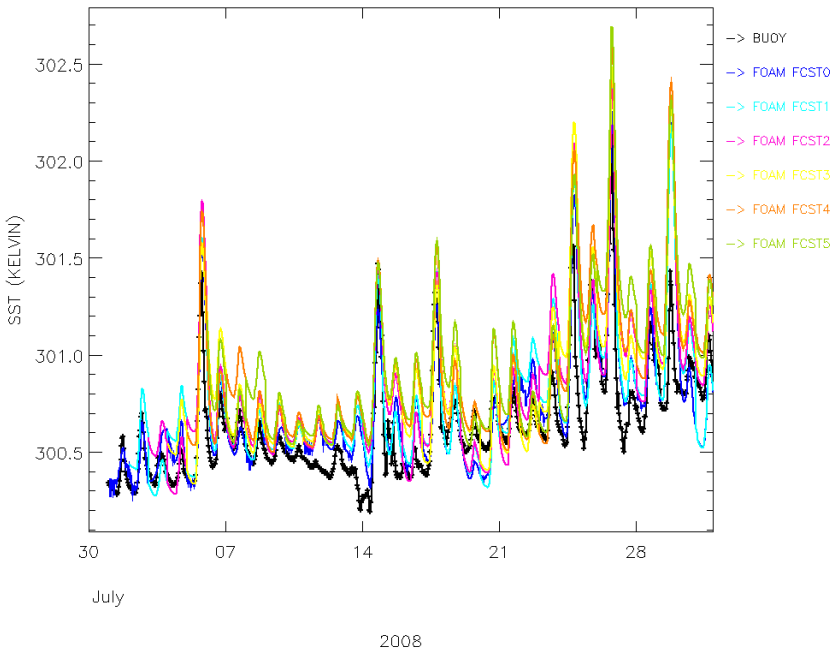

Figure 5 A month of high frequency SST observations from a PIRATA buoy at 11.5°N, 38°W (black line) compared with model outputs at the same point for the analysis (blue), 1 day forecast (cyan), two day forecast (pink), 3 day forecast (yellow), 4 day forecast orange and 5 day forecast (green).

Timings of the diurnal SST maxima and minima were assessed for the model and the PIRATA buoys; the timings for FOAM tended to be of the order of 1 hour early for the minima and 1 hour late for the maxima. Results from the model to satellite assessment showed that FOAM had skill in predicting the diurnal minima and maxima with anomaly

correlations between 0.42 and 0.56 for the minima and 0.54 to 0.62 for the maxima; the correlations showing a decrease with increasing forecast lead time. Biases were of the order of 0.1 K for the minima and -0.1 K for the maxima. Overall the model underestimated the diurnal SST range compared to the satellite by around 0.4 K; however there was skill seen in the model diurnal SST ranges at all forecast lead times with anomaly corrections ranging from 0.47 to 0.68. The underestimate of the model diurnal SST ranges relative to the satellite is thought to be potentially due to an absence of a skin correction in the model (the surface model value being an average for the top 1m compared to the satellite skin measurement) and due to relatively coarse temporal resolution forcing.

5. Conclusions

The FOAM system is well monitored and verified. The utility of FOAM forecasts is something that is highly dependant upon the particular use of the forecast, and detailed assessments are required to quantify the skill of the system. The diurnal cycle in SST is generally well simulated in the system, whereas site specific currents, although qualitatively well predicted, at this stage care should be taken with their use in a quantitative site specific way.

Acknowledgements

Funding for this research is gratefully acknowledged from the UK Ministry of Defence, from the European Community's Seventh Framework Programme FP7/2007−2013 under grant agreement 218812 (MyOcean) and from Ocean2025.

References

Bell, M.J., R.M. Forbes, and A. Hines (2000). Assessment of the FOAM global data assimilation system for real-time operational ocean forecasting. J. Marine Sys., 25, 1-22.

Bell, M.J., M.J. Martin, and N.K. Nichols (2004). Assimilation of data into an ocean model with systematic errors near the equator. Q.J.R. Meteorol. Soc. 130, 873-893.

Bell, M.J., P.-Y. Le Traon, M. Lefebvre, N. Smith, and K. Wilmer-Becker (2009). GODAE: The Global Ocean Data Assimilation Experiment, Oceanography Special Issue, 22 (3).

Blackford, J.C., J.I. Allen, and F.J. Gilbert (2004). Ecosystem dynamics at six contrasting sites: a generic model study. Journal of Marine Systems, 52, 191-215.

Cooper M, and Haines K (1996). Altimetric assimilation with water property conservation. J. Geophys. Res. 101(C1), 1059-1077.

Drévillon, M., R. Bourdallé-Badie, C. Derval, Y. Drillet, J.-M. Lellouche, E. Rémy, B. Tranchant, M. Benkiran, E. Greiner, S. Guinhut, N. Verbrugge, G. Garric, C.-E. Testut, M. Laborie, L. Nouel, P. Bahurel, C. Bricaud, L. Crosnier, E. Dombrowsky, E. Durand, N. Ferry, F. Hernandez, O. Le Galloudec, F. Messal, and L. Parent (2008). The GODAE/Mercator-Océan global ocean forecasting system: results, applications and prospects. J. Operational Ocean. 1: 51-57.

Fichefet, T. and M.A. Morales Maqueda (1997). Sensitivity of a global sea ice model to the treatment of ice thermodynamics and dynamics. J Geophys Res 102:12609-12646.

Hernandez, F. and L. Crosnier (2008). List of internal metrics for the MERSEA-GODAE Global Ocean: Specification for implementation. MERSEA WP5. Project deliverables D5.4.5, MERSEA Project report Rep. MERSEA-WP05-MERCA-STR0015.02A, 75 pp, Mercator Océan, Toulouse.

Hernandez, F., L. Bertino, G. Brassington, E. Chassignet, J. Cummings, F. Davidson, M. Drévillon, G. Garric, M. Kamachi, J.-M. Lellouche, R. Mahdon, M.J. Martin, A. Ratsimandresy, and C. Regnier (2009). Validation and Intercomparison Studies Within GODAE, Oceanography Special Issue, 22 (3), 128-143.

Hibler, W.D. (1979). A dynamic thermodynamic sea ice model. Journal of Physical Oceanography, 9, 815 - 846.

Hollingsworth, A. and P. Lönnberg (1986). The statistical structure of short-range forecast errors as determined from radiosonde data. Part I: The wind field. Tellus, 38A, 111-136.

Lorenc, A.C., R.S. Bell, and B. MacPherson (1991). The Met Office analysis correction data assimilation scheme. Q.J.R. Meteorol. Soc. 117, 59-89.

Madec, G. (2008). “NEMO ocean engine”. Note du Pole de modélisation, Institut Pierre-Simon Laplace (IPSL), France, No 27 ISSN No 1288-1619.

Martin, M.J., A. Hines, and M.J. Bell (2007). Data assimilation in the FOAM operational short-range ocean forecasting system: a description of the scheme and its impact. Q.J.R. Meterol. Soc. 133, 981-995.

O’Dea, E.J., J. While, R. Furner, A. Arnold, P. Hyder, D. Storkey, K.P. Edwards, J.R. Siddorn, M.J. Martin, H. Liu, and J.T. Hol (2011). An operational ocean forecast system incorporating SST data assimilation for the tidally driven European North West European shelf. Submitted to J. Oper. Oceanography.

Parrish, D.F., and J.C. Derber (1992). The National Meteorological Center's spectral statistical-interpolation analysis system. Mon. Weather Rev., 120, 1747-1763.

Semtner, A.J. Jr, (1976). A model for the thermodynamic growth of sea ice in numerical investigations of climate. Journal of Physical Oceanography, 6, 379 - 389.

Storkey, D., E.W. Blockley, R. Furner, C. Guiavarc'h, D. Lea, M.J. Martin, R.M. Barciela, A. Hines, P. Hyder, and J.R. Siddorn (2010). Forecasting the ocean state using NEMO: The new FOAM system. J. Operational Oceanography, 3, 3-15.

Sykes, P, J. While, A. Sellar, and M. Martin (2011). Diurnal Variability in Sea Surface Temperature: Observation and model assessment. Forecasting Research Technical Report, 556, Met Office, Exeter, pp45.

Forecast and hindcast of the Black Sea ecosystem

V. Dorofeyev*[1], T. Oguz[2], G. Korotaev[1] and L. Sukhikh[1]

[1]*Marine Hydrophysical Institute, Sevastopol, Ukraine*
[2]*Institute of Marine Sciences, Middle East Technical University, Turkey*

Abstract

The Black Sea nowcasting and forecasting system, set up and developed at MHI in the framework of FP6 and FP7 projects, has been operating in real-time mode since April 2009. Further improvements of the system includes the development of the Black Sea ecosystem forecast on the basis of the existent 3D biogeochemical model. This model is one way coupled with physical model. It extends from the sea surface to 200 m depth with 26 z-levels. The model includes 15 state variables. Nitrogen is considered as the only limiting nutrients for phytoplankton growth. This model has been used to simulate the Black Sea ecosystem evolution during three decades (1971–2001). The numerical experiments on modelling of the Black Sea ecosystem managed to display the main features of the pelagic ecosystem evolution, which are known from numerous measurements. Further development for the Black Sea ecosystem model is the adaptation to the forecast problems, most importantly the initialisation of the biogeochemical fields. A set of numerical experiments with assimilation of satellite chlorophyll-*a* data was carried out to elaborate the scheme of the Black Sea ecosystem forecast.

Keywords: Black Sea, ecosystem, modelling, biogeochemical model, trophic structure.

1. Introduction

The Black Sea is one of the largest enclosed basins in the world, which receives a high nutrient loading from rivers draining parts of Europe and Asia. The Black Sea marine ecosystem manifested significant changes during the last few decades. The healthy ecosystem which was observed in the 1960s and early 1970s has been altered drastically by the impacts of many factors (eutrophication, over-fishing and a large population growth of gelatinous and opportunistic species in the 1980s). These changes in the Black Sea ecosystem were noted in the biomass of the main components, taxonomic composition and of the phytoplankton community structure, particularly in the northwestern shelf. The natural phytoplankton annual cycle with spring and autumn maxima in biomass has been replaced by a pattern characteristic to eutrophied waters identified by several exceptional maxima – the summer one being the most pronounced. Such evident changes in marine biology were accompanied by a modification of the vertical geochemical structure. The most pronounced signature of the geochemical changes is an increase of nitrate concentration in the oxic/suboxic interface zone from 2 to 3 mmol m^{-3} in the late 1960s to 6–9 mmol m^{-3} during the 1980s and 90s. The goal of this work was

* Corresponding author, email: dorofeyev_viktor@mail.ru

to reconstruct the Black Sea ecosystem evolution during three decades from 1971 until 2001 years on the basis of a three dimensional interdisciplinary model.

2. The Black Sea ecosystem model

The model of the Black Sea ecosystem consists of physical and biogeochemical parts. The physical part is the model of the Black Sea circulation based on POM (Princeton Ocean Model), driven by ERA40 atmosphere forcing. It has 26 sigma levels compressed towards the surface. Boundary conditions on the sea surface are heat and fresh water fluxes and surface temperature, provided by a data set from atmospheric model every 6 hours.

The biogeochemical model is an extension of the set of one-dimensional models given by Oguz *et al*. (1999, 2000 and 2001) with identical parameters describing interactions between its compartments. It has a one-way coupling off-line with the circulation model through current velocity, temperature, salinity and turbulent diffusivity. The biogeochemical model extends from the sea surface to 200 m depth with 26 z-levels, compressed to the sea surface. It includes 15 state variables. Phytoplankton is represented by two groups, typifying diatoms and flagellates. Zooplankton is also separated into two groups: microzooplankton (nominally < 0.2mm) and mesozooplankton (0.2–2 mm). The carnivorous group covers the jellyfish *Aurelia aurita* and the ctenophore *Mnemiopsis leidyi*. The model food web structure identifies the omnivorous dinoflagellate *Noctiluca scintillans* as an additional independent group. It is a consumer feeding on phytoplankton, bacteria, and microzooplankton, as well as particulate organic matter, and is consumed by mesozooplankton. The trophic structure includes also nonphotosynthetic free living bacteriaplankton, detritus and dissolved organic nitrogen. Nitrogen cycling is resolved into three inorganic forms: nitrate, nitrite and ammonium. Nitrogen is considered as the only limiting nutrient for phytoplankton growth. Additional components of the biogeochemical model are dissolved oxygen and hydrogen sulfide.

The spatial resolution for the both parts of the ecosystem model (physical and biogeochemical) is approximately 7 km. As has been mentioned, the biogeochemical model uses hydrophysical fields from the circulation model. For the first 23 years these are the results of reanalysis of the Black Sea dynamics by means of assimilation of archived hydrographic data (Moiseenko *et al*., 2009), and for the last 8 years they are the results of assimilation of the space altimetry (Dorofeyev and Korotaev, 2004).

Fluxes of all biogeochemical variables are set to zero on the sea surface, bottom in shallow part of the basin and on the lateral boundaries, except rivers estuaries, where nitrate fluxes are set up proportional to river discharges and nitrate concentrations. These data are provided by Ludwig (2007) and present a combination of measurements and data derived from the modelling. On the lower liquid boundary in the deep part of the basin, concentrations of all parameters are set to zero except ammonium and hydrogen sulfide (sulfide and ammonium pools).

3. Evolution of the Black Sea ecosystem

On the basis of the biogeochemical model a numerical simulation was carried out of the long-term evolution of the Black Sea ecosystem for the time period 1971 to 2001.

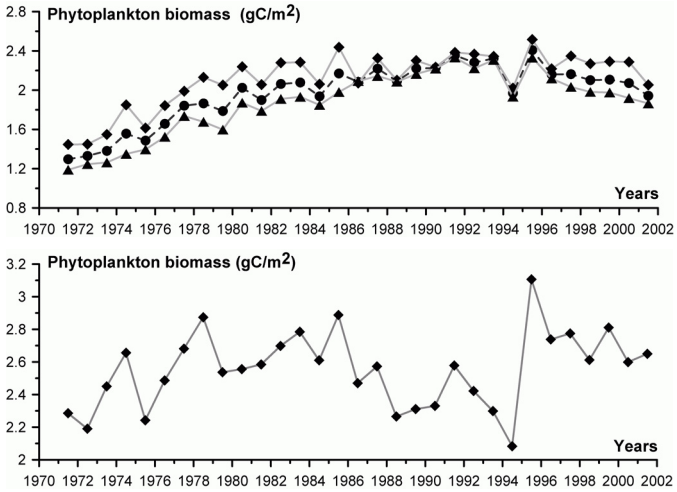

Figure 1 Evolution of the annual-mean phytoplankton biomass in the upper 50 m layer for the deep part of the Black Sea basin (top) and the North Western Shelf (bottom). On the top plot the squares denote values of the phytoplankton biomass for the western part of the interior basin, triangles denote the eastern part, and spots are for the whole deep part of the basin.

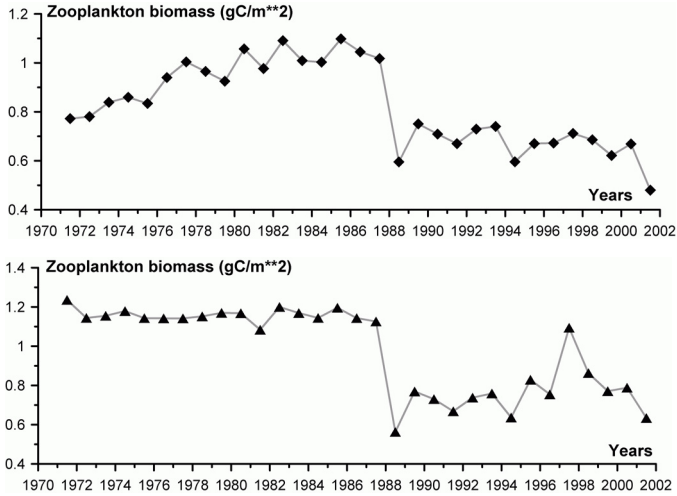

Figure 2 Evolution of the annual-mean zooplankton biomass in the upper 50m layer for the deep part of the Black Sea basin (top) and North Western Shelf (bottom).

Figure 1 demonstrates the evolution of the annual-mean phytoplankton biomass in the upper 50 m layer for the deep part of the Black Sea basin and North Western Shelf. The phytoplankton biomass approximately doubles in value from about 1.2 gCm^{-2} in the early 1970s to 2 gCm^{-2} in the mid-1990s and then decreases. On the northwestern shelf the level of the phytoplankton biomass in general is about 1.5 times as large as in the deep part of the basin. It grows from the early 1970s until the mid-1980s, then decreases

until 1994 and after an abrupt rise continues to decrease. There is a difference in phytoplankton biomass between western and eastern parts of the interior basin due to the exchange between the shallow northwestern part, reach in bio-production, and deep parts of the Black Sea. But after 1985 this difference becomes minor till 1995, when it starts to increase. This can be explained by relatively small amount of phytoplankton on the northwestern shelf during this period of time. As a result influence of the shelf waters on the deep part of the Black Sea was week during this period.

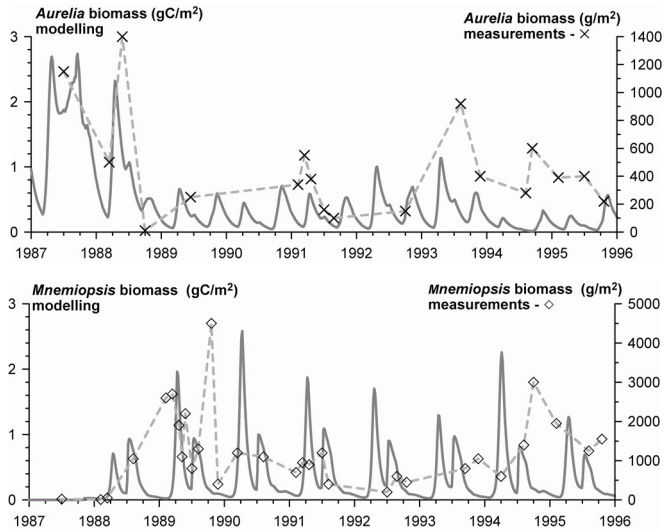

Figure 3 Evolution of the *Aurelia* (top) and *Mnemiopsis* (bottom) biomass in the upper 50 m layer for the deep part of the Black Sea: results of modelling and measurements (Purcell *et al*., 2001).

Figure 2 shows the inter-annual variability of the zooplankton biomass in the upper 50 m layer separately for the deep part of the Black Sea basin and North Western Shelf region. The response on the phytoplankton population growth in the deep part of the basin during the 1970s and 1980s was a zooplankton biomass increase from about 0.8 gCm^{-2} in the early 1970s to about 1 gCm^{-2} in 1987. Then zooplankton biomass reduces rapidly in 1998 and then stabilises at about 0.6 gCm^{-2}. Zooplankton biomass on the northwestern shelf is about 1.2 gCm^{-2} and changes very little during time period until 1987. Then it abruptly reduces as well as in the deep part of the Black Sea. This sudden decrease in zooplankton population in the late 1980s is linked to the *Mnemiopsis leidyi* invasion in the Black Sea. At that time it was observed in different regions of the Black Sea in great quantities. Before the *Mnemiopsis leidyi* invasion *Aurelia aurita* dominated the carnivorous group of the Black Sea ecosystem. The years 1989–1991 constituted the phase of pelagic ecosystem evolution in which *Aurelia* blooms were almost completely replaced by those of *Mnemiopsis* (Figure 3). Following its accidental introduction into the Black Sea in ballast waters of tankers during the early 1980s, the *Mnemiopsis* community quickly dominated the entire ecosystem, because it had no predators in the Black Sea. The sudden increase in the *Mnemiopsis* population caused a reduction in the biomass of the zooplankton community.

The surface layer in the deep part of the Black Sea is supplied with nutrients from deep waters rich in nitrates. During the winter season they are accumulated in the upper layer due to intense winter mixing and then assimilated by phytoplankton. The amount of nitrate near the surface depends directly on the value of nitrate concentration in the layer of maximum, which is situated between upper and lower nitrocline on a depth of approximately 60–70 m. During the considered time period the value of nitrate concentration is characterised by an increase from 2–3 mmolN m^{-3} in the 1960s to 8–9 mmolN m^{-3} in the late 80s and then decrease to the value of about 4 mmolN m^{-3} in the late 1990s – early 2000s (Konovalov and Murray, 2001). Apart from a three-fold increase in the value of the nitrate maximum by over 20 years the nitrate peak shifted about 10 m upward.

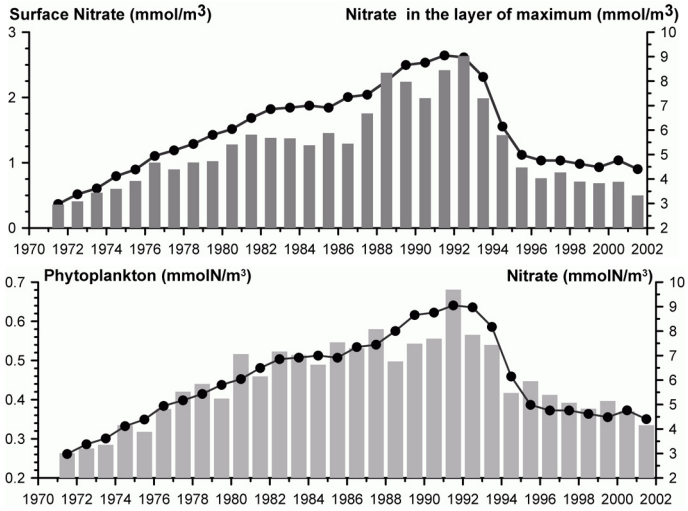

Figure 4 Annual-mean surface nitrate (top) and phytoplankton (bottom) concentrations (bars) in the deep part of the Black Sea and annual-mean nitrate maximum (spots).

Figure 4 shows that the nitrate surface concentration increases about five-fold from 0.4 mmolN m^{-3} in the early 1970s to about 2.5 mmolN m^{-3} in the early 1990s, then it decreases to the level of about 0.5 micromoles. The surface phytoplankton concentration also grows during the time period 1971–1991 from a quarter of micromole in the early 1970s to approximately 0.7 micromoles in 1991. Then it falls to the value of about 0.3 micromoles. Both the values of surface nitrate and phytoplankton closelyfollow the solid line – evolution of the nitrate maximum.

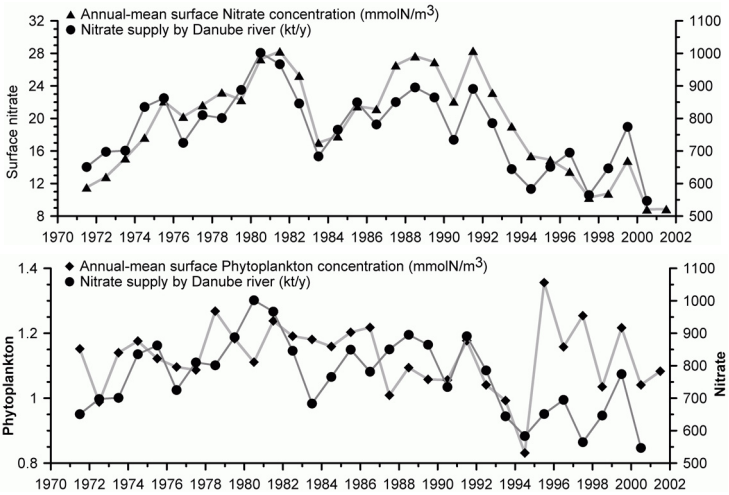

Figure 5 Annual-mean surface nitrate (top) and phytoplankton (bottom) concentrations on the northwestern shelf of the Black Sea and annual-mean nitrate supply by the Danube river (spots).

On the northwestern shelf of the Black Sea the main factor influencing the nutrient amount in the surface layer is supplied by rivers (mainly the Danube which provides about 70 percent of the total nutrient amount incoming in the Black Sea). Figure 5 shows the evolution of the annual-mean surface phytoplankton and nitrate on the northwestern shelf. The annual-mean amounts of nitrate incoming with rivers are represented on the same plots. These data are provided by Ludwig (2007). Surface nitrate concentrations correlate well with annual nitrate fluxes on the shelf supplied by rivers. The surface concentration of the phytoplankton changes slightly around the level of approximately 1.1 mmolN m^{-3} during the first twenty years. Then after an abrupt reduction during 1992–1994 it rises in 1995 and then decreases. But there is no as evident correlation with the nutrient supply as it is in the case of the surface nitrate. It seems to be due to the fact that nitrate concentration on the northwestern shelf is high enough and phytoplankton growth in this case is limited by other factors.

The changes in the Black Sea ecosystem during time period from 1971 until 2001 are visible not only in inter-annual evolution of the main ecosystem components, but also in seasonal variability. The natural phytoplankton annual cycle, which was usual for the pre-eutrophication phase of the Black Sea ecosystem, has been replaced by a more complicated pattern characterised by several maxima. These changes are illustrated in Figure 6, which represents the annual evolution of phytoplankton, zooplankton and medusa *Aurelia aurita* in the upper 100 m layer in the central part of the basin for three years: 1972, 1982 and 1992.

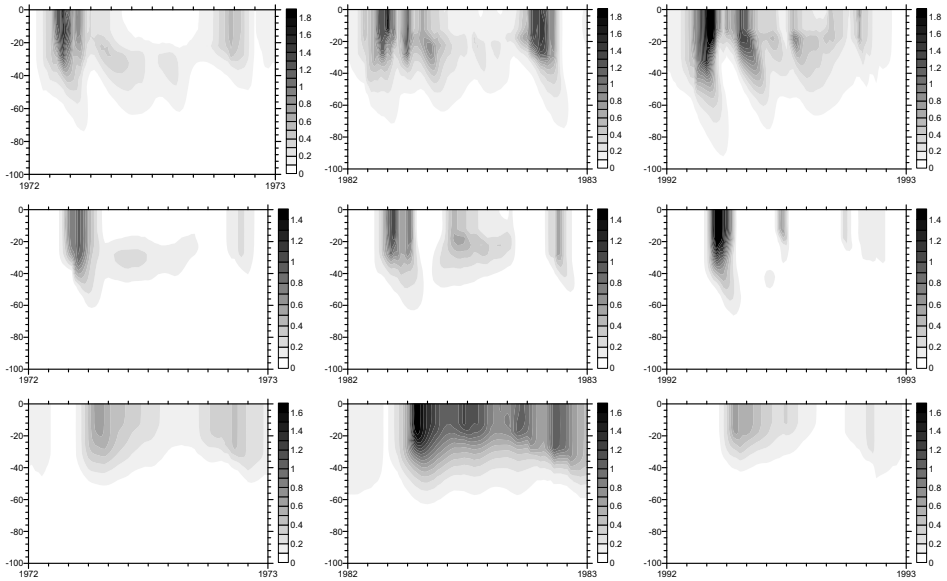

Figure 6 Seasonal evolution of the phytoplankton (top), zooplankton (middle) and *Aurelia aurita* (bottom) in the central part of the Black sea for three years: 1972 (left), 1982 (middle) and 1992 (right).

In 1972 the phytoplankton annual cycle is characterised by spring and autumn maxima in biomass. The phytoplankton community exhibited a major bloom during the late winter–early spring season, following the period of active nutrient accumulation in the surface waters at the end of the winter mixing season and as soon as the water column receives sufficient solar radiation. Distribution of zooplankton closely follows that of phytoplankton with a time lag of about half a month. The jellyfish *Aurelia aurita* has two pronounced maxima in April–May and late autumn. In 1982 (eutrophication phase) the phytoplankton annual cycle includes a few blooms. As in the previous case of 1972 the phytoplankton exhibits a major bloom during the late winter–early spring season. The phytoplankton bloom is first followed by a zooplankton bloom of comparable intensity, which reduces the phytoplankton stock to a relatively low level, and then by an *Aurelia* bloom that similarly reduces the zooplankton biomass. The phytoplankton recovers and produces a weaker late spring bloom. The *Aurelia* population decreases in August after a double maximum in late spring and earlier summer, and then produces blooms in September and November. The September bloom gives rise to phytoplankton and then zooplankton successively blooms during October–November. The years after 1987 (*Mnemiopsis* invasion into the Black Sea) constituted a new phase of the Black Sea ecosystem transformation. The *Mnemiopsis* community dominated the ecosystem. The sudden increase in the *Mnemiopsis* population led to reduction in zooplankton biomass. The *Aurelia* stock decreased abruptly in comparison with 1982. It produces a bloom in late spring and a weak maximum in November. Phytoplankton produces a set of maxima with the summer one being well pronounced. The largest growth of the zooplankton is observed in mid-spring and then it produces only a set of weak maxima.

4. Forecast of the biogeochemical parameters

The described 3D biogeochemical model was used as a basis for part of the new version of the Black Sea forecast system. It provides a five-day model forecast for the phytoplankton and nitrate distribution in the Black Sea. The product covers the whole Black Sea, and is delivered on a horizontal grid with a resolution of 4.8 km, and with 18 vertical depth levels (upper 200 m layer). The model was calibrated in different approaches against climatic data and independent space observations.

One of the key problems for the forecast of the biological fields is initialisation of the ecological model. For these purposes satellite data of chlorophyll-*a* were assimilated into the model. The assimilation procedure is based on the nudging technique. The data used are the standard product MODIS, which is recalculated from surface chlorophyll-*a* concentration to surface phytoplankton. Because of lots of gaps in satellite data they are exposed to additional processing. The MODIS data are optimally interpolated on the regular grid of the biogeochemical model. After this procedure the number of gaps reduces (see for example Figure 7). Then the model runs in spin up mode with assimilation of satellite data and with external parameters corresponding to the initial time.

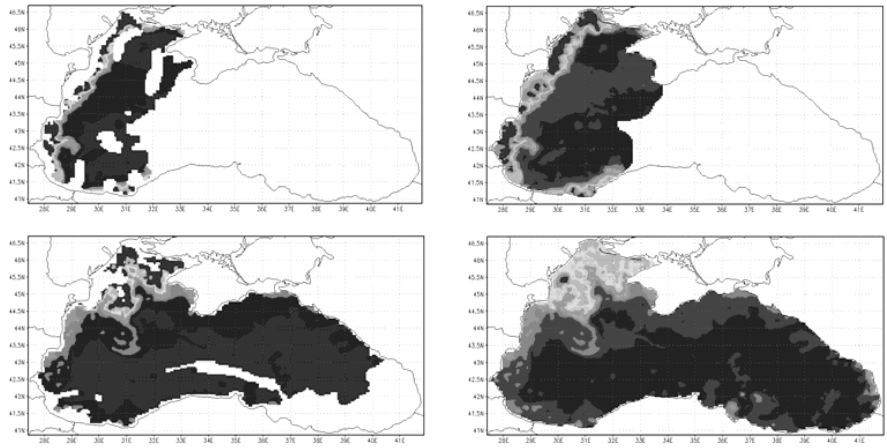

Figure 7 Examples of the satellite data before (left) and after (right) optimal interpolation

5. Summary

The finished numerical experiment on modelling of the Black Sea ecosystem managed to display the main features of the pelagic ecosystem evolution during three decades 1971–2001, which are known from numerous measurements. The phytoplankton biomass grew during the time period from the early 1970s until the early 1990s, characterised by the eutrophication phase of the Black Sea ecosystem. Surface concentration of the phytoplankton increased in the deep part of the basin by about 3 times. As a result zooplankton concentration rose too until after the 1980s, when a *Mnemiopsis* invasion caused a sudden reduction in zooplankton community. This change in biological biomass was accompanied by variations in geochemical vertical structure; the main signature being an increase in nitrate concentration in the layer of maximum at a depth approximately 70 m,

which is a key parameter for the intensity of biological processes in the surface layer of the interior Black Sea. The ecological model was then adapted for the purposes of forecast of the biogeochemical parameters in the Black Sea. In the forecast mode the model uses MODIS satellite chlorophyll-*a* data.

Acknowledgements

The research leading to these results has partially received funding from the European Community's Seventh Framework Programme FP7/2007–2013 under grant agreement no. 218812 (MyOcean) and EU 6th Framework projects SESAME (contract no. 036949-2).

References

Dorofeyev, V.L, and G.K. Korotaev (2004). Satellite altimetry assimilation in eddy-resolved model of the Black sea circulation, Ukrainian Journal of Marine Researches, 1, 52–68.

Konovalov S.K, and J.W. Murray (2001). Variations in the chemistry of the Black Sea on a time scale of decades (1960–1995), J. Mar. Sys., 31, 217–243.

Ludwig, W. (2007). River runoff and nutrient load data synthesis for hindcasting simulations, Deliverable 4.3.2, SESAME project.

Moiseenko, V.A., G.K. Korotaev, V.V. Knysh, A.I. Kubryakov, V.N. Belokopytov, and N.V. Inyushina (2009). Interannual variability of the thermohaline and dynamical characteristics of the Black sea according to results of the reanalysis for time period 1971–1993, Ecological safety of the coastal zone and complex use of the shelf resources. Sebastopol, 19, 216–227.

Oguz, T., H.W. Ducklow, P. Malanotte-Rizzoli, J.W. Murray, E.A. Shushkina, V.I. Vedernikov, and U. Unluata (1999). A physical-biochemical model of plankton productivity and nitrogen cycling in the Black Sea, Deep-Sea Res. 1, 46, 597–636.

Oguz, T., H.W. Ducklow, and P. Malanotte-Rizzoli (2000). Modeling distinct vertical biochemical structure of the Black Sea: Dynamical coupling of the oxic, suboxic, and anoxic layers, Global biochemical cycles, vol.14, 4, 1331–1352.

Oguz, T., H.W. Ducklow, J.E. Purcell, and P. Malanotte-Rizzoli (2001). Modeling the response of top-down control exerted by gelatinous carnivores on the Black Sea pelagic food web, Journal Geophys. Res., vol.106, No C3, 4543–4564.

Purcell, J.E., T.A. Shiganova, M.B. Decker, and E.D. Houde (2001). The ctenophore mnemiopsis in native and exotic habitats: U.S. estuaries versus the Black Sea basin, Hydrobiologia, 451, 145–176.

Monitoring and forecasting the Arctic Ocean: Norway and MyOcean

Bruce Hackett*[1], Laurent Bertino[2], Lars-Anders Breivik[1], Dominique Durand[3] and Henning Wehde[4]

[1]*Norwegian Meteorological Institute, Oslo, Norway*
[2]*Nansen Environmental and Remote Sensing Center, Bergen, Norway*
[3]*Norwegian Institute for Water Research, Bergen, Norway*
[4]*Institute of Marine Research, Bergen, Norway*

Abstract

Four Norwegian institutions – IMR, met.no, NERSC and NIVA – are playing a significant role in the GMES MyOcean project, which is building the European Marine Core Service. The Norwegian contribution is strongly focused on the Arctic region and consists of three main product components: in-situ observations, satellite observations and numerical forecasting and reanalysis. Together these constitute a major part of the MyOcean Arctic node.

In-situ observational products are managed by IMR, as the Arctic node of the MyOcean In-Situ Thematic Assembly Centre (IS-TAC). They include surface and profile data of temperature, salinity, current velocity and direction, water level, chlorophyll and oxygen concentration from research ships, drifting buoys and fixed stations. In addition, NIVA manages Ferrybox data from the entire MyOcean domain, and including the Arctic region. Both near real-time products and multi-year time series are provided.

Satellite observations of sea ice are managed by met.no, who lead the MyOcean Sea Ice and Wind TAC. Arctic data products include sea ice concentration, drift velocity, surface temperature and iceberg concentration, and are provided by met.no, NERSC and partner agencies in Denmark and France. Both near real-time products and multi-year time series sea ice are made available. In addition, met.no provides an Arctic sea surface temperature analysis product via the MyOcean SST-TAC.

Numerical forecasts and reanalyses are produced and managed by met.no and NERSC in the Arctic Monitoring and Forecasting Centre (ARC-MFC), which is led by NERSC. The TOPAZ4 system includes a coupled ocean-ice model and assimilation of in-situ and satellite observations. Forecasts are updated daily, building on a weekly analysis cycle. The reanalysis product, when completed, will cover the period 1991–2010. Products include daily mean 3D fields of temperature, salinity and velocity, in addition to 2D fields of surface height and sea ice parameters.

All Arctic products are freely available to registered MyOcean users. Discovery, viewing and download services are found at www.myocean.eu.

Keywords: Arctic, ocean forecasting, satellite monitoring, real-time observations

* Corresponding author, email: Bruce.Hackett@met.no

1. Introduction

The Arctic Ocean and its adjacent seas are the object of increasing interest for politics, business and science. Not only is the region a bellwether for climate change, it is also a growing arena for transportation and resource exploitation, whose political and commercial ramifications are significant.

Norway has long had vital interests in the Arctic. Historical activities such as fisheries, coastal transportation and scientific exploration have been supplemented in recent years by the offshore petroleum industry and tourism. Insofar as the polar ice cap continues to decline, the northeast passage will become a more heavily used shipping lane, connecting North Atlantic countries with northern Asia. This increased traffic will all pass between Norway and its sovereign territory Spitzbergen. Norway thus has a vested interest in sustainable exploitation of resources, avoiding environmental detriments and ensuring safety at sea. These are all aims that rely directly on the information supplied by operational oceanography and marine meteorology.

A major challenge for the nation is to exercise its vested interests based on a population of only 5 million. The coastline is long and the adjacent sea areas are large. What is more, the sea conditions near Norway are significantly determined by the conditions in the ocean regions further afield: the Nordic Seas, the North Atlantic and the Arctic Ocean. Clearly, Norway relies heavily on scientific knowledge of the ocean environment in order to pursue its interests and has supported marine and weather research for over a century. Over the years this support has resulted in a number of national and independent agencies that address various aspects of marine science. The importance of operational information was understood very early, notably by the establishment of the Norwegian Meteorological Institute (met.no) in 1866, with a specific aim to ensure safety at sea. Support for fisheries management was manifested in the Institute of Marine Research (IMR), which originated in the Norwegian Fisheries Directorate in 1906 and was established as a separate state agency in 1989.

This paper describes the activities of four major Norwegian oceanographic agencies in a specific Arctic research and development endeavour. This endeavour is part of the European Commission R&D project MyOcean (www.myocean.eu), which aims to design and build a marine core service for Europe. The MyOcean model of the core service is based on six regional seas components supplemented by a global component, and provides observations (in-situ and satellite), forecasts and multi-year time series. One regional component of MyOcean is the Arctic, where the four Norwegian agencies play a major role. In addition to met.no and IMR, the Nansen Environmental and Remote Sensing Center (NERSC) and the Norwegian Institute for Water Research (NIVA) participate in MyOcean and its Arctic components.

The next section briefly describes MyOcean, its organisational model and the roles of the Norwegian participants. Thereafter, we will describe more closely the contributions made to the MyOcean service and show some examples.

2. MyOcean and the Arctic

The proposed European marine core service intends to provide value-adding users with ocean data and information products of known quality by efficient and agreed delivery

mechanisms. The MyOcean approach to building the core service is founded on five pillars:

1. integration of models, in-situ observations and satellite data;
2. build on existing capacities;
3. focus on European value;
4. free and open data policy;
5. operationality.

In addition, MyOcean acknowledges that the ocean has strong regional diversity, both in physical and biological characteristics. As a consequence, the existing capacities that MyOcean leverages, some developed over many years, tend also to be regional, and this is reflected in the products and organisation of the production (see Figure 1). The MFCs run assimilating model systems that produce analyses and forecasts, as well as reanalysis time series; they are straightforwardly regional. The TACs produce observational data products, both near-real-time and long time quality-controlled series. They are thematic, essentially by platform; there are four TACs for satellite-based data and one for in-situ observations. Still, each TAC provides regional products analogous to the MFCs.

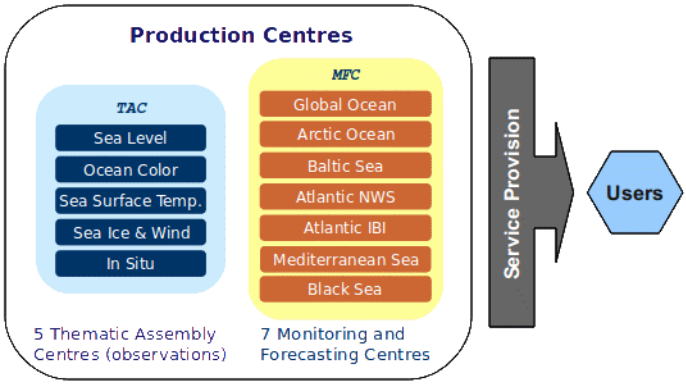

Figure 1 Schematic of the MyOcean production and service to users. Each of the five TACs and seven MFCs are virtual Production Centres that encompass one or more physical Production Units where the data production is performed. Each Production Center also has one or more Dissemination Units for delivery of data products.

The most important MyOcean products for the Arctic are produced in the Sea Ice & Wind TAC (SIW-TAC) and the Arctic MFC (ARC-MFC), along with the Sea Surface Temperature TAC (SST-TAC) and the In-Situ TAC (IS-TAC).

3. Norwegian contributions

The contributions to production are summarised in Table 1. In addition, met.no provides service management components for the SIW-TAC and ARC-MFC.

Table 1 Norwegian participation in MyOcean Arctic production and delivery. "Lead" indicates leadership of the corresponding Work Package in the MyOcean project.

MyOcean Production Centre	Participants	Production Units	Dissemination Units
SIW-TAC	met.no (Lead), NERSC	met.no, NERSC	met.no
SST-TAC	met.no	met.no	
IS-TAC	IMR, NIVA	IMR, NIVA	
ARC-MFC	IMR, met.no, NERSC (Lead)	met.no, NERSC	met.no, NERSC

3.1 In-situ observations

A major challenge for the IS-TAC is to provide ready access to in-situ observations from the wide range of data producers and owners around Europe. In the Arctic, in-situ observing systems are relatively scarce, but the small number of data producers actually makes the organisational problem somewhat easier. In the IS-TAC, both IMR and NIVA provide coordination of data access as well as delivering observational data themselves.

IMR has responsibility for the Arctic regional component of the IS-TAC, coordinating the management of in-situ data from all sources. This is tasked to the Norwegian Marine Data Center, which is a department of IMR. Within the MyOcean system, there is a special emphasis on the provision of near-real-time (NRT) observations to the other production centres, for example for routine validation of model predictions and satellite retrievals. Therefore, much effort has been spent in facilitating access to in-situ observations as soon as possible after measurement. An example of data coverage for one month is shown in Figure 2. The NRT observations include ship measurements (CTD, water samples, Ferrybox) and measurements from autonomous vehicles (ARGO, surface drifters).

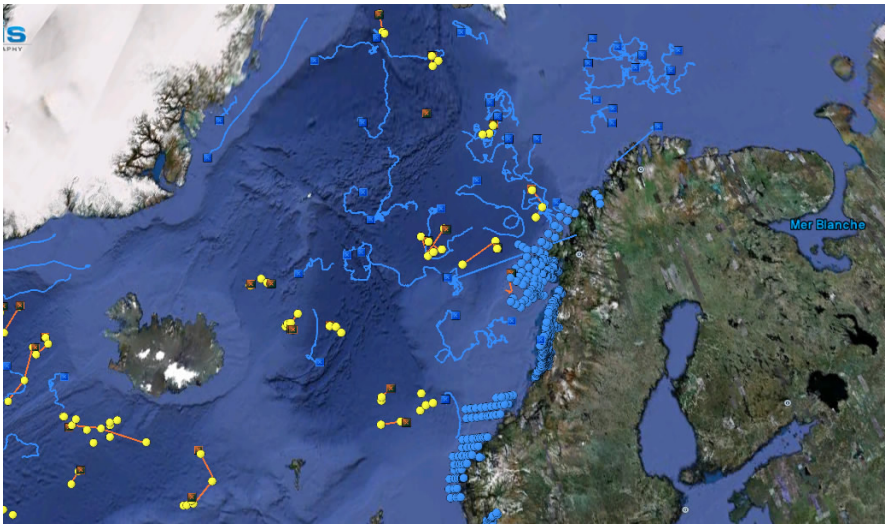

Figure 2 Sample overview of NRT in-situ observations in the European Arctic region available from the In-Situ TAC. Shown are all data collected in April 2011.

NIVA is responsible for coordinating all Ferrybox data available in European waters, which includes some platforms operating in the Arctic and sub-Arctic, and for routines for quality control of biogeochemical data from any types of oceanic observation platforms. Ferrybox lines operating routinely in northern Europe as of September 2011 are shown in Figure 3. As said above, there has been a considerable effort to make these observations available in NRT.

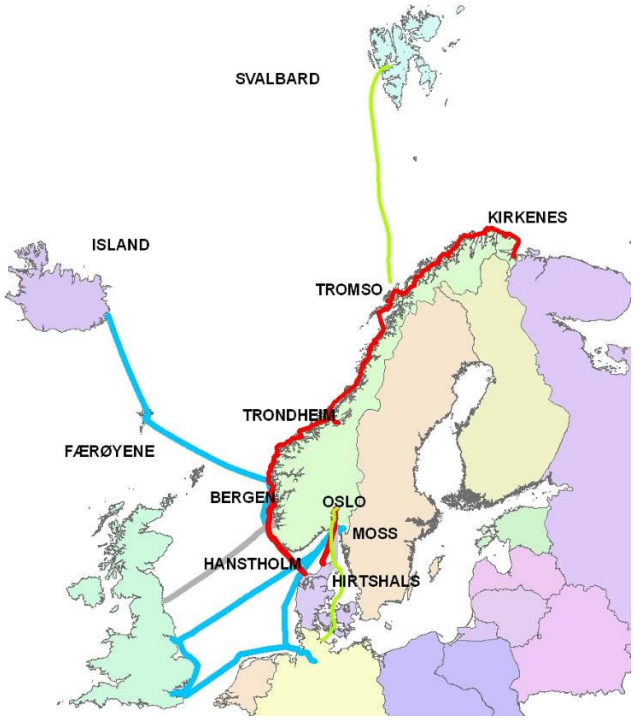

Figure 3 Ferry Box routes accessed in MyOcean, September 2011.

3.2 Satellite observations

The SIW-TAC is managed by met.no, but is organised in two parts: one for sea ice products and one for wind products. Of most interest for the Arctic are the sea ice products; the wind products will not be described further here.

The SIW-TAC provides a collection of existing and new NRT sea ice products from the major European producers. Products include global, i.e., covering both the Arctic and Antarctic, and regional data for the European Arctic, Greenland and the Baltic. The global products derive mainly from the EUMETSAT Ocean and Sea Ice Satellite Application Facility (OSISAF, osisaf.met.no), the high latitude part of which is hosted by met.no. These products include gridded ice concentration (Figure 4), ice type, ice edge and ice drift, and are provided by met.no as a collaboration between EUMETSAT and MyOcean. Among the regional sea ice data products, NERSC produces ice type maps in the European Arctic from Envisat ASAR swath data using an automated neural network technique (Figure 5). The met.no Ice Service provides its daily ice concentration charts for the Svalbard area. These are produced manually using all available satellite infor-

mation and then gridded for digital dissemination. Additional Arctic regional sea ice products are provided to the SIW-TAC by IFREMER, the Danish Meteorological Institute (DMI) and the Danish Technical University (DTU). All SIW-TAC sea ice data products are collated and delivered through the Dissemination Unit at met.no.

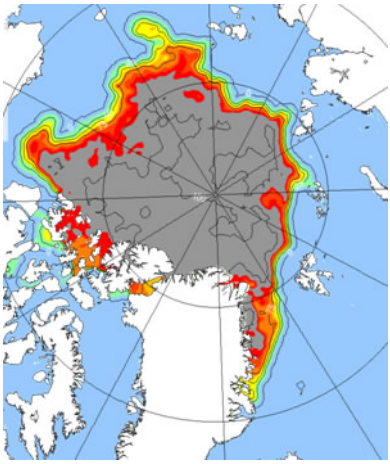

Figure 4 OSISAF northern hemisphere ice concentration, 10 km resolution, daily updated. Ice edge, type and drift also available. Produced by met.no.

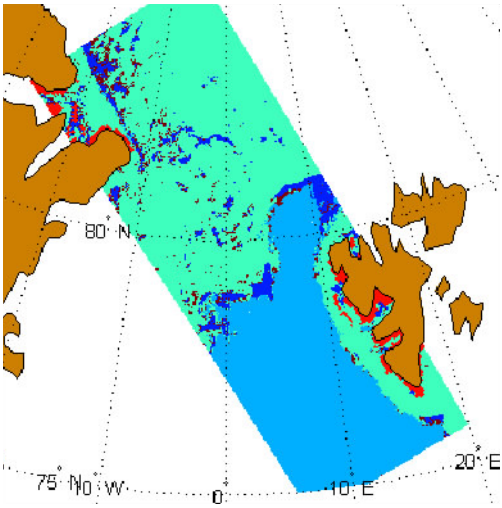

Figure 5 Regional ice type from ASAR swath, 0.5 km resolution, produced by NERSC. Dark blue: “calm open water without sea ice (with wind speed < 3 m/s) or nilas or only some start of freezing stage”; light blue: “open water without sea ice (with wind speed > 3 m/s)”; light green “any type of sea ice”.

In the SST-TAC, met.no provides a daily high-resolution SST analysis for the Arctic. The analysis algorithm is developed in collaboration with DMI and combines data from several satellite sensors, including AATSR, AVHRR SAFNAR, AVHRR NAVO_G,

AMSRE, AVHRR Metop-A, depending on availability. Resolution is 0.05°. An example is shown in Figure 6.

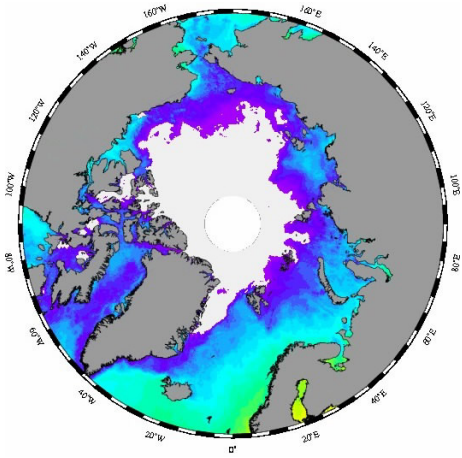

Figure 6 Analysed SST map on 0.05° grid, produced by met.no. Light grey area is ice.

3.3 Analyses and forecasts

The ARC-MFC partnership is dominated by the three Norwegian participants, with NERSC in the management role. For MyOcean, they have agreed on a general division of duties in which NERSC provides the model and assimilation development, met.no carries out the operational implementation and service provision, and IMR is responsible for calibration and validation. This arrangement has proven beneficial since the ocean modelling community in Norway is relatively small, and it is therefore important to exploit the strengths of each partner.

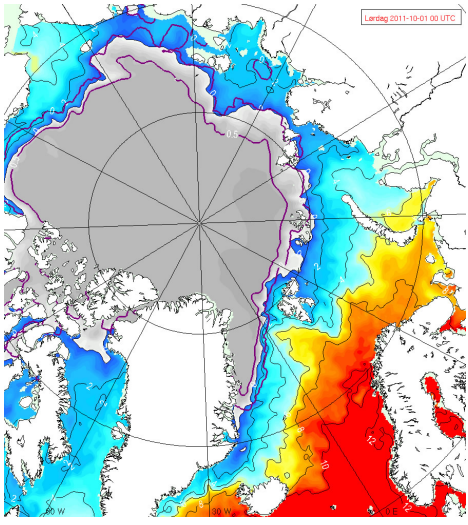

Figure 7 TOPAZ forecast field for sea surface temperature (colours) and ice concentration (heavy purple contour lines).

The model and assimilation system used in the ARC-MFC is the TOPAZ system developed at NERSC (Bertino and Lisæter, 2008, Sakov *et al*., 2011). It is built around the HYCOM hydrodynamic model and includes a two-way coupled sea ice model. Recently, the NORWECOM biological model, developed by IMR, has been coupled to HYCOM in the TOPAZ system (Samuelsen *et al*., 2010). An Ensemble Kalman Filter (EnKF) (Evensen, 2009, Sakov and Oke, 2008) is used to assimilate sea surface height, SST, sea ice concentration and drift, and profiles of temperature and salinity. The model system is run on a stretched grid of 12−16 km resolution covering the Arctic and North Atlantic Oceans. Output is converted to regular grids (12.5 km) and daily mean fields for dissemination to users. An example of the Arctic grid is shown in Figure 7. The output product includes three-dimensional physical and biogeochemical parameters as well as sea surface height and sea ice parameters. At present, the coupled ocean-ice-biology system is run in real-time mode at met.no, using a weekly assimilation cycle and daily forecast updates. It is run in reanalysis mode at NERSC in order to cover the period 1991−2010 with monthly mean user output on a regular 12.5 km grid. Real-time and reanalysis data are delivered from Dissemination Units at met.no and NERSC, respectively.

An important issue for the analysis and forecast system is the accuracy of the predictions. To this end, considerable effort is made to provide the user with information on product quality, quantified as validation metrics calculated against observations. A number of metrics have been defined, and implemented in priority order according to what are considered the most important ones from a user perspective: sea ice concentration first, then ice edge position, ice drift, SST, temperature and salinity profiles, and finally sea surface elevation. Metrics are updated weekly and published at myocean.met.no/ARC-MFC/V1Validation/SeaIceConcentration.

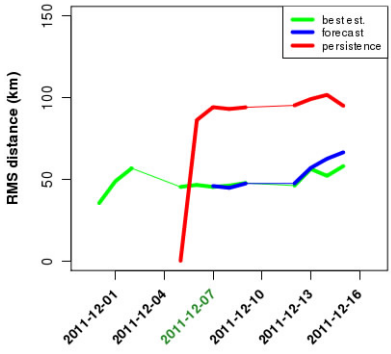

Figure 8 Validation of TOPAZ ice edge location against observation from met.no ice chart in Svalbard region. Metric is rms distance from observed ice edge to nearest ice edge grid point in model.

3.4 Service Provision

Provision of a reliable service to users is a cardinal aim of MyOcean. To that end, the project is implementing a uniform program for service management, in which each Production Center is responsible for practising agreed management processes. For the

SIW-TAC and ARC-MFC, met.no is tasked with managing the service, although all partners must necessarily contribute to its execution.

The primary service to users is dissemination of data products, which is being implemented via three basic functions: discovery, viewing and downloading. Discovery is enabled by the MyOcean Online Catalogue, found at myocean.eu.org/web/24-catalogue.php. Viewing and downloading rely on the THREDDS Data Server technology, which provides MyOcean Dissemination Units with a common platform for viewing by Web Mapping Services (WMS), file-by-file download by http and subset and aggregation download via OpeNDAP. These services, along with standard ftp, are hosted at met.no and IFREMER for the SIW-TAC, and at met.no and NERSC for the ARC-MFC. Products from all MyOcean Production Centres are accessible to registered users through the Catalogue using a uniform user interface.

For the Norwegian participants, MyOcean provides a valuable opportunity to modernise data dissemination methods and to implement needed service management practises.

4. Conclusions

The four major Norwegian marine agencies presented in this paper are making valuable contributions to the MyOcean project and, in return, are improving their ability to provide useful and robust products and services to users. Not least, the collaborative spirit that has been established is a benefit to operational oceanography in Norway. It is not surprising that their most important activities in MyOcean are focused on the Arctic. This is a confirmation of the importance of the Arctic for the nation.

MyOcean is a development project and is a step toward implementing a marine core service for Europe. Norwegian partners have established a very strong presence in the Arctic components of MyOcean and expect to continue as MyOcean transitions to a fully operational marine core service.

Acknowledgements

The MyOcean project is supported in part by he European Community's Seventh Framework Programme FP7/2007−2013 under grant agreement 218812.

References

Bertino, L., and K.A. Lisæter (2008). The TOPAZ monitoring and prediction system for the Atlantic and Arctic Oceans, Journal of Operational Oceanography, Vol. 1, No. 2, 2008

Evensen, G. (2009). Data assimilation, The Ensemble Kalman Filter, 2nd ed., Springer.

Sakov, P., and P.R. Oke (2008). A deterministic formulation of the ensemble Kalman filter: an alternative to ensemble square root filters. Tellus, 60A, 361−371.

Sakov, P., F. Counillon, L. Bertino, K.A. Lisaeter, P.R. Oke, and A. Korablev (2011). TOPAZ4: an ocean-sea ice data assimilation system for the North Atlantic and Arctic, submitted.

Samuelsen A, G. Huse, and C. Hansen (2009). Shelf recruitment of *Calanus finmarchicus* off the west coast of Norway: role of physical processes and timing of diapause termination. Mar. Ecol. Prog. Ser. 386:163−180.

The MyOcean Monitoring and Forecasting Centre for the North West European Continental Shelf

John Siddorn*[1], Alex Arnold[1], Karen Edwards[1], Rachel Furner[1], Bruce Hackett[2], Pat Hyder[1], Enda O'Dea[1], José Ozer[3], Simon Jandt[4], Frank Janssen[4], Stephanie Ponsar[3], Alistair Sellar[1], Morten Skogen[5], Peter Sykes[1], Sarah Wakelin[6], and James While[1]

[1]*Met Office, Exeter, United Kingdom*
[2]*met.no, Oslo, Norway*
[3]*Management Unit of the North Sea Mathematical Models, Belgium*
[4]*Bundesamt für Seeschifffahrt und Hydrographie, 20359 Hamburg, Germany*
[5]*Institute of Marine Research, Bergen, Norway*
[6]*National Oceanography Centre, Liverpool, UK*

Abstract

The North West European Continental Shelf Monitoring and Forecasting Centre (NWS MFC) is one of the operational production centres of the GMES FP7 MyOcean project. It is based around the established operational expertise and infrastructure of the NOOS community, with contributions from operational and research centres around the region. A number of operational services have existed for marine monitoring and forecasting of the region for many years. The NWS MFC builds on these services, and the expertise gained from running them, with the aim of providing a world-leading service delivering the best available ocean hindcast, nowcast and forecast products, free of charge at the point of delivery. The focus of the NWS MFC has been on developing the three strands required to provide a service that users can rely upon: the products, the system (IT infrastructure for robust production and delivery) and the service (documentation, processes and support personnel). Significant advances have been made in all three areas, with a fully supported service now available that provides hindcast, nowcast and forecast physical and biogeochemical ocean data.

Keywords: North West Shelf, NOOS, operational modelling, MyOcean, NEMO, ROMS, ERSEM, NORWECOM

1. Introduction

The North West European Continental Shelf Monitoring and Forecasting Centre (NWS MFC) is one of the operational production centres of the GMES FP7 MyOcean project. At its inception the NWS MFC activities were designed around a community of operational centres that have a history of delivering services to government to industry and to the public. This community had come together under the banner of the North West Shelf Operational Oceanography System (NOOS; www.noos.cc). The MyOcean NWS MFC has built upon that collaboration and cooperation to deliver improved products, systems and services for users of the Marine Core Services in the NOOS region. All partners in

* Corresponding author, email: john.siddorn@metoffice.gov.uk

the NWS MFC are active NOOS contributors, bringing expertise in modelling, observations and product evaluation to the group.

The aim of the MyOcean NWS MFC has been to provide operational, fully validated products free of charge to all marine users. These products include ocean model based information for the past (through hindcasts of the marine environment of the last fifty years), the present and for short-range forecasts. It does not provide observation based products.

The European North West Shelf region is a shallow seas dominated region (Figure 1), with a broad shelf with strong tides. The impact of the North-Atlantic is important in that shelf-slope exchange processes have a significant influence upon the highly utilised coastal areas, and therefore it is important to effectively monitor and predict the behaviour of the North-East Atlantic, although in the context of the NWS MFC the main aim is to provide information on the shelf region.

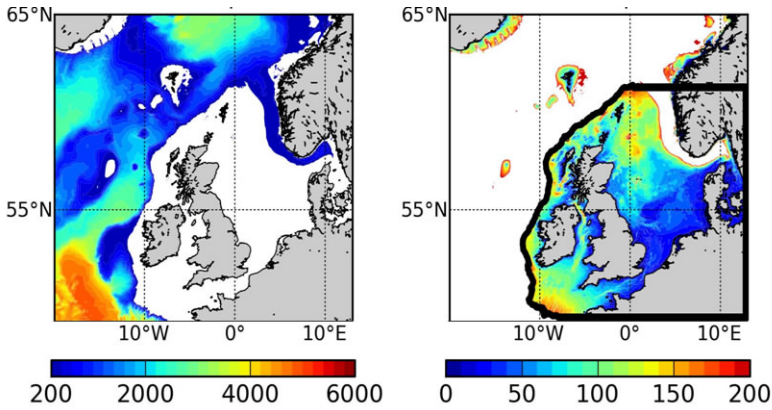

Figure 1 The NWS MFC region, showing the bathymetry of the off-shelf region (left) and the shelf region (right) in metres. The demarcation between the two, with the exception of the Norwegian Trench region, follows the 200 m contour line.

Shipping, oil and gas exploration and fishing industries are significant users of the NWS marine area, whilst the heavily industrialised and densely populated northern European countries that have coastlines around the NWS region mean that human interaction with the marine environment (both as a user and a polluter) is high here. This history of marine activities means that marine services are relatively mature, especially where there is a direct impact upon coastal communities. There are therefore a significant number of advanced operational services, including for example wave and storm surge forecasts, around the region. The use of three-dimensional hydrodynamic ocean models, often coupled to biogeochemistry models, is also relatively mature in the region with many NOOS members operationally supporting services that provide hydrodynamic and ecosystem monitoring and forecasting independently from the Marine Core Service. The challenge for the Marine Core Service NWS MFC is therefore not to build something new, but to develop a service that can add value to the presently available services either

through improving upon them by driving standards of products and service up, or through providing a resource upon which they can gain benefit and therefore improve.

This paper outlines how this added-value has been, or is being, achieved. It will describe the activities of the NWS MFC giving, firstly, a brief description of the products that will be provided then a summary of the progress made or expected in improving the quality of those products. Then the paper will describe how the service to users has been developed to include an in-depth, user-focused, evaluation of the quality of the products.

2. The NWS MFC products

The MyOcean Marine Core Services, and thus the European North West Shelf Monitoring and Forecasting Centre (NWS MFC), categorises its services under four areas of use: maritime safety; marine resources; coastal and marine environment; and weather, seasonal forecasting & climate. Each of these has different requirements both with respect to the service and the products. An important aspect of developing the service is to understand the user requirements for products and to provide a product portfolio that meets these requirements.

The NWS MFC must provide products to support activities that contribute to safety at sea. These include ship routing services, offshore operations and search and rescue operations. The products must also contribute to oil spill response and remediation. Key users expected to take advantage of NWS MFC products are the European Maritime Safety Agency (EMSA), users delivering assessments for the Convention for the Marine Environment of the North East Atlantic (OSPAR) and national maritime safety agencies. The NWS MFC must provide products that contribute to the protection and the sustainable management of living marine resources in particular for aquaculture, fishery research or regional fishery organisations. Any ecosystem-based approach to fish stock management also benefits from this information. Key users in this context are ICES (International Council for the Exploitation of the Sea), the FAO (Food and Agriculture Organization of the United Nations) and national fisheries agencies. The NWS MFC must provide products useful for water quality monitoring and pollution control, in the context of the Marine Strategy Framework Directive in particular. Key users in this context are EEA (The European Environment Agency), OSPAR and national environmental agencies. Finally, the NWS MFC must provide products useful in support of weather, seasonal and climate prediction services. National and European Weather Services and Climate Research centres should benefit from the NWS MFC products, for example as bottom boundary conditions for atmospheric models.

As well as directly supplying these users, the NWS MFC must provide information that allows national bodies the ability to downscale to their coastal regions effectively to provide the above information on a national level. This broad remit introduces often conflicting demands for products, with key users requiring a variety of parameters at a range of resolutions (both temporal and spatial) and over differing timescales (long hindcasts versus short-range forecasts versus long-range predictions). The products that are detailed in Table 1 are a synthesis of these requirements into one product set, although it is anticipated that as resource availability increases and our understanding of user requirements improve, the products may be adapted accordingly. The need for users to have sustainability in the service is, however, well recognised and therefore the

product list will be maintained or expanded, and there is no expectation of products that are used being removed.

The forecast services are provided by the operational meteorological centres of the UK and Norway (the Met Office and met.no), with the nominal service being provided by the Met Office and a backup forecast being available to operational users from met.no. The hindcast products are provided by the Institute of Marine Research, Bergen (IMR) and the National Oceanography Centre, Liverpool (NOC). The dissemination of products is from operationally supported servers maintained at the Met Office and met.no, with full redundancy in the production. Dedicated servers running the MyOcean specific delivery mechanisms are maintained at the Met Office and met.no, providing robust, timely and efficient delivery of the products via mechanisms defined by MyOcean. A subsetting service has been designed by MyOcean that provides a technically advanced, but still evolving, method for delivery of data and the NWS MFC has also retained the more traditional method of data delivery via FTP.

Table 1 The NWS MFC product details

42°N – 60°N, 20°W – 13°E North West European Shelf Monitoring and Forecasting Centre (NWS MFC)					
	Forecast Service (A)	**Forecast Service (B)**		**Hindcast Service**	
Temporal resolution	Hourly instantaneous	25h mean		Monthly mean	
Parameters available	T	T	light atten	T	light atten
	S	S	Chl-*a*	S	Chl-*a*
	SSH		O_2	SSH	O_2
	U	U	DOP	U	DOP
	V	V	DON	V	DON
			plankton biomass		plankton biomass
			1° productivity		1° productivity
Horizontal resolution	~7km	~7km		~12km	
Vertical levels	Top, middle, bottom	0, 3, 10, 15, 20, 30, 50, 75, 100, 125, 150, 200, 250,300, 400, 500, 600, 750, 1000,1500, 2000, 3000, 4000, 5000		0, 3, 10, 15, 20, 30, 50, 75, 100, 125, 150, 200, 250,300, 400, 500, 600, 750, 1000,1500, 2000, 3000, 4000, 5000	
Update frequency	Daily	Daily		~annual – biannual	
Time range	Analysis “best-guess” March 22nd 2011 on 5 day forecast	Analysis “best-guess” March 22nd 2011 on 5 day forecast		January 1960 – December 2004	
Target delivery time	0900 UTC daily	0900 UTC daily		Per version	

Since the beginning of the MyOcean project the NWS MFC team has been developing the products as well as the service. There is a continuous cycle of research and development that leads to incremental improvements in the models that underpin the

production. Some particularly important changes have been made to the modelling systems. The Met Office forecast production has been updated from the Medium-Resolution Continental Shelf (MRCS; Siddorn *et al*., 2006) configuration based upon the POLCOMS ocean model (Holt and James, 2001) coupled with the ERSEM ecosystem model (Blackford *et al*., 2004) system to the Atlantic-Margin Model (AMM; O'Dea *et al*., submitted) configuration based upon the NEMO model (Madec, 2008) coupled to ERSEM. This has meant the ability to use the Optimal Interpolation (OI) data assimilation scheme (Martin *et al.*, 2007) already used at the Met Office for the open ocean Forecasting Ocean Assimilation Model (FOAM; Storkey *et al*., 2010) suite of configurations. For the moment the data assimilation is limited to the use of sea-surface temperature (SST) data, although in future this will be extended to other data types.

The backup forecast is provided from the met.no/IMR ocean-ecosystem model, which covers the NW Shelf and Nordic Seas and includes the MIPOM (Engedahl, 1995) ocean model coupled to the NORWECOM ecosystem model (Søiland and Skogen, 2000) and an ice model. This system is run on native grids of 4 km (MIPOM physics) and 20 km (NORWECOM ecosystem). Output data are interpolated onto the same grid and with the same format as the nominal forecast model, thereby ensuring the user can seamlessly transition from using the nominal forecast to the backup when required. The backup system is also in the process of being overhauled, and a ROMS based configuration (Shchepetkin and McWilliams, 2005, Haidvogel *et al*., 2008) is being trialled in parallel operations. A data assimilation component building on the ROMS 4DVar code (Moore *et al*., 2011a, b, c) is being developed for the system. Transition to delivering the backup products from the ROMS based system is expected shortly for the physics parameters, followed by an offline ecosystem (using NORWECOM) coupling in early 2012.

Two modelling systems are used to produce hindcast products for the NWS MFC, one from the Institute of Marine Research (IMR) and one from the National Oceanography Centre (NOC). These are different systems but they provide products on the same grid and at the same horizontal resolution for ease of interoperability. For the NOC simulations the physical model used is the POLCOMS-ERSEM described above. The IMR simulations use the NORWECOM system (Søiland and Skogen, 2000). NORWECOM, or the NORWegian ECOlogicalModel system, is a coupled 3 dimensional physical, chemical, biological model system for studying of primary production and dispersion of particles (such as fish larvae and pollution). The model was originally developed for simulations in the North Sea and Skagerrak, but has also been used in the Norwegian Sea, the Barents Sea and the Benguela. The set-up for the NORWECOM hindcast is fully described in Hjøllo *et al*., (2009) and Skogen & Mathisen (2009).

The hindcast production systems are also under development and, in the medium-term for example, the NOC production of hindcasts is expected to follow the forecast production at the Met Office and use an assimilative NEMO-ERSEM AMM configuration.

As well as improving the modelling systems underpinning the production, the products are expected to be improved through the improved specification of inputs to the systems. Much of the NWS domain is heavily influenced by river inputs; effort is being made to improve both the quality of the inputs, which are presently climatological, as well as working with the hydrological modelling community to assess the use of real-time

modelled river inputs to the system. Another input that strongly influences the NWS is the exchange of heat and freshwater between the Baltic Sea and the Kattegat through the narrow openings at the Great and Little Belts. Work is being done with colleagues from the Baltic modelling community to better specify the boundary condition in this region, which is expected to lead to improvements in the freshwater distribution through the North Sea.

In the longer term, the community will be looking at more fundamental changes in how we provide marine products, with many of the NWS MFC partners undertaking research in atmosphere-wave-ocean coupling to improve the way air-sea exchange is modelled. Better forecasts are also expected to be possible through the use of ensemble based systems, and in the future there will be effort to develop multi-model ensembles to provide estimates of the uncertainty and/or error in the product, perhaps in the future leading to the ability to provide probabilistic forecasts instead of (or as well as) the presently available deterministic forecasts.

3. Quality Information

As part of the NWS MFC service there are a number of activities that focus on assessing the quality of the products provided. Under the MyOcean nomenclature, which is different from that often used in operational oceanography, there is a “calibration” phase and a “validation” phase. The calibration phase refers to the activity prior to introducing a production change that assesses the suitability of a change to the production system (generally a model or assimilation change) for introduction to operations. It does not directly assess the product or give any information that can be directly associated with the quality as would be seen by users, but does assess whether the change being introduced is likely to lead to improvements. This is normally associated, in the case of forecast models, with running test cases (normally a number of years in the recent past). This generally uses old forcing and different input data (where data assimilation is used) and is confusingly what many of us are used to as referring to as validation. The validation phase refers to the period post implementation where the products are created and assessed (for the forecasts) in close to real-time. For the hindcast production, this is an assessment of the full hindcast and so more closely reflects the normal meaning of validation. MyOcean requires that a scientific calibration and subsequently scientific validation report is produced prior to approval for release of products. This provides assurance that the Marine Core Service products made available for the NWS MFC are of high quality. However, these documents are technical documents designed for internal decision making processes, and do not provide the sort of information that may be of use to users of the NWS MFC products. An additional document has therefore been produced, the Quality Information Document (QuID) that is designed to provide a synthesis of available quality information that allows users to judge when and how to use the products.

These documents are available from the MyOcean web site (www.myocean.eu). A summary of the key quality information as it reflects the quality of NWS MFC products is given in the sections below.

3.1 Synthesis of Forecast Quality

A short synthesis of the quality of the Met Office NWS MFC forecast production, based on extensive evaluation of the system, is given here. More details can be found in O'Dea *et al*. (submitted) or in the NWS MFC QuID.

The propagation of the harmonic tides components shows a RMS error of sea surface elevation of 18 cm for the M2 tide and of 6 cm for the S2 tide. The surge elevations have been compared to a limited number of stations in the North Sea, located in the German Bight, along the Dutch, Belgian and UK coasts. In most cases, the correlation coefficient is high (~0.95). The validation of currents speed against HF radar observations in the Liverpool Bay shows correlations of 0.82 for hourly currents. Because of the lack of observations the transports have been assessed by model inter-comparison to BSH and MUMM models. Results indicate a good agreement between the three models for daily fluxes of volume, heat and salt. The SST is well represented over the whole area. The temperature profiles are well represented by the model and errors in the full domain are dominated by off-shelf observations. For the sea surface salinity, the model underestimates the influence of the freshwater discharge by the rivers Scheldt, Rhine and Meuse in the Belgian waters. This could partly result from the aggregation of the three outflows or from the use of river runoffs from climatology. The chlorophyll-*a* concentration has been analysed at three levels i) the whole domain, ii) regional areas, iii) locally (stations in the Southern North Sea and English Channel). The spatial and temporal variability are significantly underestimated by the model.

3.2 Synthesis of Hindcasts Quality

A short synthesis of the quality of the NWS MFC hindcast production, based on extensive evaluation of the system, is given here. More details can be found in the NWS MFC QuID.

The IMR simulations capture the main features of the hydrography, although the southern North Sea salinity values are too low. For the volume transports, the Skagerrak and English Channel inflows are comparable with observations. In the north, the inflow in the eastern region is close to the estimates based on observations, while the inflow at the Shetland Shelf is weaker than observations suggest. Heat content is well represented by the model compared to observations. For the winter nutrients there is good agreement between the modelled and measured long-term means for three out of four cases. Chlorophyll data show a large discrepancy and less variability in the model compared to measurements. Chlorophyll-*a* is clearly underestimated especially near the coast. This appears to be a problem in many models (OSPAR, 2008), even if most North Sea models give realistic estimates for the primary production (Moll and Radach, 2003). In the Skagerrak the model misses some of the saline and nutrient rich Atlantic water. The water is present at the correct depth further northwest in the Norwegian Trench, but is not found inside the Skagerrak. This is caused by a relatively coarse resolution (see e.g. Albretsen & Røed, 2010). There is also a problem simulating the salinity in the Norwegian Coastal current due to the use of climatological fresh water run off to the Baltic Sea (Røed and Albretsen, 2007).

Comparison of NOC simulated SST with AVHRR satellite data shows broad agreement on seasonal timescales. Mean errors on the continental shelf are generally less than 1°C.

Comparison with World Ocean Database temperature and salinity observations show the model is generally too cold and too fresh. Exceptions to this are a broad region through the central North Sea and isolated regions in the deeper off-shelf water, where the model is too warm and too salty. The dissolved oxygen concentration is mainly underestimated but with skill on the continental shelf, although in the deep water north of 60°N the agreement between model and observations is poor. Nitrate levels are overestimated by the model but with skill in most regions except for the central North Sea. Apart from around the English coasts and the south-eastern North Sea, phosphate is generally overestimated by the model. The modelled chlorophyll tends to be underestimated on the shelf and overestimated compared to the sparse open ocean observations

4. Conclusions

A community of operational and research centres with expertise in numerical ocean prediction, built around the NOOS association, has come together to develop the MyOcean North West Shelf Monitoring and Forecasting Centre. The Centre is a regional component of the emerging European Marine Core Service, whose aim is to deliver a service based on good, and known, quality products freely available to all users. This paper demonstrates the success of the NWS MFC, and the MyOcean project, in taking the steps to providing an operational service that combines products, delivery mechanisms and service infrastructure. An understanding and communication of the quality of the products and service is also being made available.

Acknowledgements

Funding for this research is gratefully acknowledged from the UK Ministry of Defence, from the European Community's Seventh Framework Programme FP7/2007–2013 under grant agreement 218812 (MyOcean) and from Ocean2025: the NERC's core programme in ocean science.

References

Albretsen, J., and L.P. Røed (2010). Decadal long simulations of mesoscale structures in the northern North Sea/Skagerrak using two ocean models. Ocean Dynamics, 60, doi:10.1007/s10236l010-0296-0.

Blackford, J.C., J.I. Allen, and F.J. Gilbert (2004). Ecosystem dynamics at six contrasting sites: a generic model study. Journal of Marine Systems, 52, 191–215.

Engedahl, H., (1995). Implementation of the Princeton Ocean Model (POM/ECOM3D) at the Norwegian Meteorological Institute (DNMI). Res. Rep. No. 5, Norwegian Meteorological Institute, Oslo, Norway.

Haidvogel, D.B., H. Arango, P.W. Budgell, B.D. Cornuelle, E. Curchitser, E. Di Lorenzo, K. Fennel, W.R. Geyer, A.J. Hermann, L. Lanerolle, J. Levin, J.C. McWilliams, A.J. Miller, A.M. Moore, T.M. Powell, A.F. Shchepetkin, C.R. Sherwood, R.P. Signell, J.C. Warner and J. Wilkin (2008). Ocean forecasting in terrain-following coordinates: Formulation and skill assessment of the Regional Ocean Modeling System. J. Comput. Phys., 227(7), 3595–3624.

Hjøllo, S., M. Skogen, and E. Svendsen (2009). Exploring currents and heat within the North Sea using a numerical model. Journal of Marine Systems 78, 180–192. doi:10.1016/j.jmarsys.2009.06.001.

Holt, J.T. and I.D. James (2001). An s coordinate density evolving model of the northwest European continental shelf 1, Model description and density structure, Journal of Geophysical Research, Oceans, 106, C7, 14015–14034.

Madec, G. (2008). NEMO ocean engine. Note du Pole de modélisation, Institut Pierre-Simon Laplace (IPSL), France, No 27 ISSN No 1288–1619.

Martin, M.J., A. Hines and M.J. Bell (2007). Data assimilation in the FOAM operational short-range ocean forecasting system: a description of the scheme and its impact. Q. J. Roy Met Soc, 133, 981–995.

Moll, A., and G. Radach (2003). Review of three-dimensional ecological modelling related to the North Sea shelf system – Part 1: models and their results. Progress in Oceanography, 57:175–217.

Moore, A.M., H.G. Arango, G. Broquet, B.S. Powell, A.T. Weaver and J. Zavala-Garay (2011). The Regional Ocean Modeling System (ROMS) 4-dimensional variational data assimilation systems Part I – System overview and formulation. Progress in Oceanography 91, 34–49.

Moore, A.M., H.G. Arango, G. Broquet, C.A. Edwards, M. Veneziani, B.S. Powell, D. Foley, J.D. Doyle, D. Costa, and P. Robinson (2011). The Regional Ocean Modeling System (ROMS) 4-dimensional variational data assimilation systems: II Performance and application to the California Current system. Progress in Oceanography 91, 50–73.

Moore, A.M., H.G. Arango, G. Broquet, C.A. Edwards, M. Veneziani, B.S. Powell, D. Foley, J.D. Doyle, D. Costa, and P. Robinson (2011). The Regional Ocean Modeling System (ROMS) 4-dimensional variational data assimilation systems: III Observation impact and observation sensitivity in the California Current system. Progress in Oceanography 91, 74–94.

O'Dea, E.J., J. While, R. Furner, A. Arnold, P. Hyder, D. Storkey, K.P. Edwards, J.R. Siddorn, M.J. Martin, H. Liu, and J.T. Holt (2011). An operational ocean forecast system incorporating SST data assimilation for the tidally driven European North West European shelf. Submitted to J. Oper. Oceanography.

OSPAR (2008). Revised draft assessment of the predicted environmental consequences for problem areas following nutrient reductions. Report on the 2nd OSPAR ICG-EMO workshop, OSPAR EUC08/5/2-E(L), 51 pp.

Røed, L.P., and J. Albretsen (2007). The impact of freshwater discharges on the ocean circulation in the Skagerrak/northern North Sea area Part I: model validation. Ocean Dynamics (2007) 57:269–285 DOI 10.1007/s10236-007-0122.

Shchepetkin, A.F., and J.C. McWilliams (2005). The Regional Ocean Modeling System (ROMS): A split-explicit, free-surface, topography-following coordinate ocean model. Ocean Modelling, 9, 347–404.

Siddorn, J.R., J.I. Allen, J.C. Blackford, F.J. Gilbert, J.T. Holt, M.W. Holt, J.P. Osborne, R. Proctor, and D.K. Mills (2006). Modelling the hydrodynamics and ecosystem of the North West European continental shelf for operational oceanography. Journal of Marine Systems, doi:10.1016/j.jmarsys.2006.08.001.

Skogen, M., and L. Mathisen (2009). Long term effects of reduced nutrient inputs to the North Sea. Estuarine Coastal and Shelf Science 82, 433–442.

Storkey, D., E.W. Blockley, R. Furner, C. Guiavarch, D. Lea, M.J. Martin, R.M. Barciela, A. Hines, P. Hyder, and J.R. Siddorn (2010). Forecasting the ocean state using NEMO: The new FOAM System. Journal of Operational Oceanography, 3(1), 3–15.

The Mediterranean Monitoring and Forecasting Centre, a component of the MyOcean system

M. Tonani[1], A. Teruzzi[2], G. Korres[3], N. Pinardi[4], A. Crise[4], M. Adani[1], P. Oddo[1], S. Dobricic[5], C. Fratianni[1], M. Drudi[1], S. Salon[2], A. Grandi[1], G. Girardi[1], V. Lyubartsev[3] and S. Marino[1]

[1]*Istituto Nazionale di Geofisica e Vulcanologia, Gruppo di Oceanografia Operativa, Bologna, Italy*
[2]*Istituto Nazionale di Oceanografia e Geofisica Sperimentale, Trieste, Italy*
[3]*Hellenic Centre for Marine Research, Athens, Greece*
[4]*University of Bologna, Department of Environmental Sciences, Ravenna, Italy*
[5]*Centro EuroMediterraneo per i Cambiamenti Climatici, Bologna, Italy*

Abstract

Within the Global Monitoring for Environment and Security programme (GMES) and its Marine Service Fast Track, MyOcean consolidates the past efforts in pre-operational ocean monitoring and forecasting capacity in Europe. The Mediterranean Monitoring and Forecasting Centre (Med-MFC) is one of the regional production centres of the MyOcean system (www.myocean.eu). The Med-MFC is therefore the operational centre for the provision of basic modelling datasets that are at the basis of the continuous monitoring and forecasting of the marine environment for this region. This system is composed of two key elements coupled off-line: Med-currents for the physical system, and Med-biogeochemistry, for the biogeochemical component. The system produces 10-day forecasts daily for Med-currents and twice weekly for Med-biogeochemistry.

The MyOcean system is operational since December 2009 and is periodically updated.

Keywords: Mediterranean Sea, ocean forecasting, operational oceanography

1. Introduction

The development of the components of the MyOcean Med-MFC started more than ten years ago in the frame of several EU projects and since year 2009 is part of the MyOcean system. This system is composed of two key elements coupled off-line: Med-currents for the physical system, and Med-biogeochemistry, for the biogeochemical component. 10-day forecasts are produced daily by Med-currents and twice weekly by Med-biogeochemistry. Med-currents products also include the daily analyses produced once a week for the past fifteen days. All the Med-MFC products are available via the MyOcean catalogue and MyOcean download facilities.

2. Description of Med-Monitoring and Forecasting System

The Med-MFC system is made up of three different components (Figure 1):

- Med-currents nominal production/dissemination unit

* Corresponding author, email: marina.tonani@bo.ingv.it

- Med-biogeochemistry production/dissemination unit
- Med-current back-up production/dissemination unit.

The three components are developed and maintained respectively by INGV, OGS and HCMR.

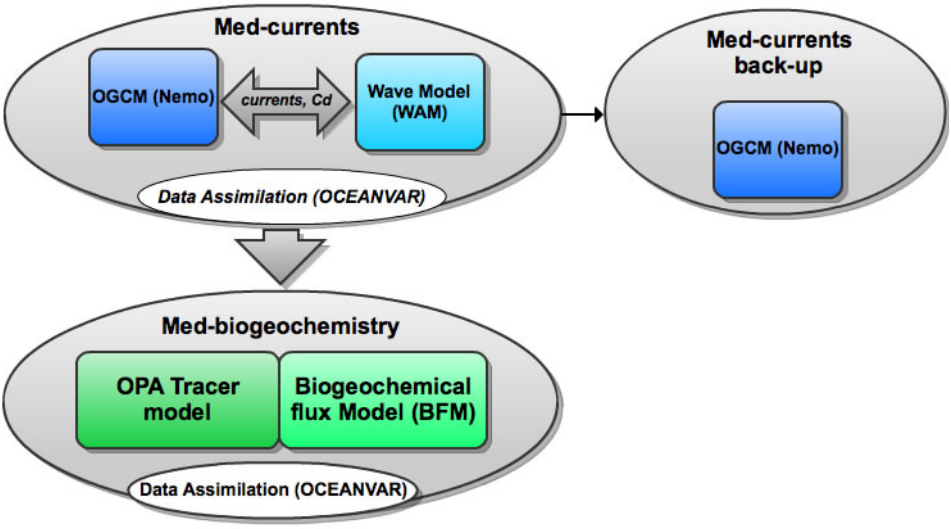

Figure 1 Med-MFC components: Med-currents nominal, Med-biogeochemistry and Med-currents back-up.

The numerical model component of Med-currents is composed of two elements: an Ocean General Circulation Model (OGCM) and a Wave Model. The OGCM code is NEMO-OPA (Nucleus for European Modelling of the Ocean-Ocean PArallelise) version 3.2 (Madec *et al*., 2008). The code is developed and maintained by the NEMO-consortium. The model is a primitive equation in spherical coordinates. The Wave Model is based on the WAM (Wave Analysis Model) code. NEMO-OPA has been implemented in the Mediterranean with a horizontal resolution of 1/16°×1/16° and 72 unevenly spaced vertical levels (Oddo *et al*., 2009). The off-line coupling between NEMO and WAM is done as follows. The NEMO model provides a first guess of SST and surface currents which are used by the WAM model. The neutral drag coefficient computed by WAM is used by the NEMO model and modified in order to take into account the stability conditions at the air-sea interface. The Digital Bathymetric Data Base Variable Resolution (DBDB-V) has been used to make the hydrodynamic and wave model coastline and bathymetry. The bathymetry has been manually interpolated along the Croatian coast by a comparison with detailed nautical chart. The two models cover the entire Mediterranean Sea and also extend into the Atlantic in order to better resolve the exchanges with the Atlantic Ocean at the Strait of Gibraltar.

The wave model takes into consideration the surface currents for wave refraction but assumes no interaction with the ocean bottom. The model uses 24 directional bins (15° directional resolution) and 30 frequency bins (ranging between 0.05 Hz and 0.7931 Hz) to represent the wave spectra distribution.

The hydrodynamic model is nested, in the Atlantic, within the monthly mean climatological fields computed from ten years of daily output of the 1/4°×1/4° global model (Drevillon *et al*., 2008). Details of the nesting technique and major impacts on the model results can be found in Oddo *et al*., 2009. The model uses vertical partial cells to fit the bottom depth shape.

The model is forced by momentum, water and heat fluxes interactively computed by bulk formulae using the 6-h, 0.25° horizontal-resolution operational analyses and forecasts fields from the European Centre for Medium-Range Weather Forecasts (ECMWF) and the model predicted surface temperatures (details of the air-sea physics can be found in Tonani *et al*., 2008). The water balance is computed as Evaporation minus Precipitation and Runoff. The evaporation is derived from the latent heat flux while the precipitation and the runoff are provided by monthly mean datasets: the Climate Prediction Center Merged Analysis of Precipitation (CMAP) Data (Xie and Arkin, 1997); the Global Runoff Data Centre dataset (Fekete *et al*., 1999) for the Ebro, Nile and Rhone and the dataset from Raicich (1996) for the Adriatic rivers (Po, Vjosë, Seman and Bojana). The Dardanelles inflow is parametrised as a river and the climatological net inflow rates are taken from Kourafalou and Barbopoulos (2003).

The horizontal viscosity and diffusion operators are assumed to be bi-laplacian with coefficients of $5\times109\ m s^{-1}$ and $3\times109\ m s^{-1}$ for viscosity and diffusion respectively. The vertical diffusion and viscosity terms are dependent upon the Richardson number. The vertical convective processes are parametrised using the enhanced vertical diffusivity parametrisation. The model time step is of 600 seconds. The advection scheme for active tracers (temperature and salinity) is a mixed up-stream/MUSCL (Monotonic Upwind Scheme for Conservation Laws (Estubier and Lévy, 2000)) scheme. The up-stream scheme is used in proximity of the river mouths, close to the Atlantic lateral boundaries and at the Gibraltar Strait where the large mixing acting in the area of the Strait of Gibraltar, due to the internal wave and tide breaking, is not explicitly resolved by the model and therefore the vertically diffusivity is also artificially increased. The data assimilation system is the OCEANVAR scheme developed by Dobricic and Pinardi (2008). The background error correlation matrix is estimated from the temporal variability of parameters in a historical model simulation. Background error correlation matrices vary seasonally and in 13 regions of the Mediterranean which have different physical characteristics (Dobricic *et al*., 2006). The mean dynamic topography used for the assimilation of SLA has been computed by Dobricic *et al.* (2005). The assimilated data include: sea level anomaly, sea surface temperature, in-situ temperature profiles by VOS XBTs, in-situ temperature and salinity profiles by ARGO floats, and in-situ temperature and salinity profiles from CTD. Satellite OA-SST data are used for the correction of surface heat fluxes with the relaxation constant of 40 $W m^{-2} K^{-1}$.

Med-biogeochemistry is coupled off-line to Med-currents which provides the physical forcing in terms of velocity, temperature, salinity, irradiance, eddy diffusivity and wind speed fields (Lazzari *et al*., 2010). The model of Med-biogeochemistry is based on the OPA Tracer model (v8.1) coupled with the BFM model. The BFM (Biogeochemical Flux Model) is an ERSEM-like (European Regional Seas Ecosystem Model) model based on fluxes of elements (carbon, phosphorous, nitrogen and others) among chemical

functional families and living functional groups. A detailed explanation and description of Med-biogeochemistry can be found in Teruzzi *et al.* (2011).

The Med-currents component has a back-up production and dissemination unit based on a simplified version of the Med-currents system without the wave-currents coupling and data assimilation. The back-up system is initialised every day from the nominal system initial conditions in order to avoid discontinuity between the products of the two production lines. The format of the products is the same in order to reduce as the impact on the users much as possible. The back-up products are released only in case of major failure of the nominal production.

The MyOcean Service Desk provides all the information and support needed to the users to switch to the back-up products in case of unavailability of the nominal products.

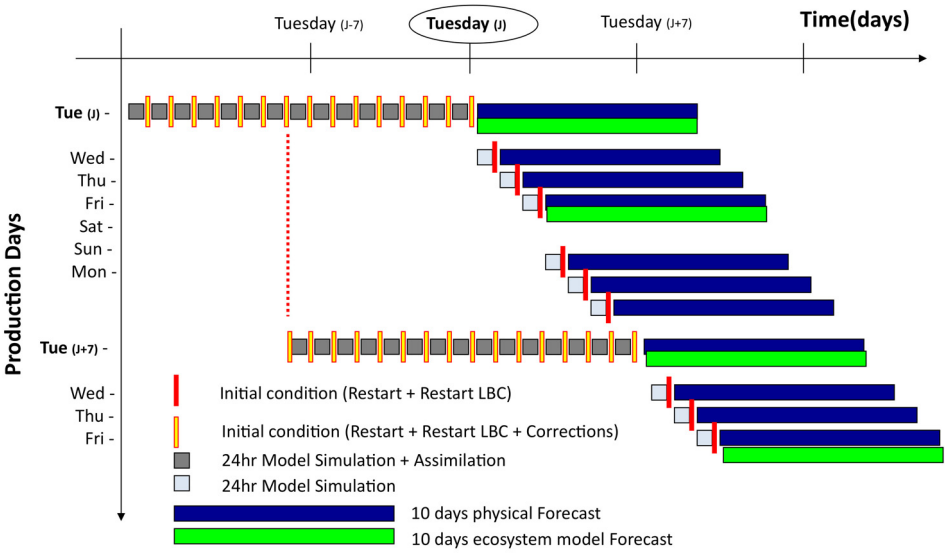

Figure 2 Med-MFC production cycle for the two components Med-currents and Med-biogeochemistry.

3. Med-MFC products

Every day (J) the Med-currents system produces 10 days of forecast from J to J+9, as shown in Figure 2.

On Tuesdays, 15 days of analyses are produced, from J-15 to J-1, with the assimilation of all the available satellite and in-situ data. The Med-biogeochemistry 10-day forecast is produced twice weekly on Tuesdays and Fridays (see Figure 2).

On all days except Tuesdays a 24-hour simulation is computed (from J-1 to J) in order to have the best initial condition for the forecast. The simulation differs from the first day of forecast produced the previous day (J-1) for the atmospheric forcing which is an analysis field instead of a forecast.

Med-currents products are:

- Sea level
- Temperature
- Salinity
- Horizontal currents
- Horizontal currents due to the Stokes drift (from January 2012)
- Wave number (from January 2012).

Med-biogeochemistry products are:

- Chlorophyll
- Nutrients
- Dissolved Oxygen concentration (from January 2012)
- Primary production (from January 2012)
- Phytoplankton biomass (from January 2012)

Some products are already available in the MyOcean catalogue while others will be added in January 2012 when the MyOcean system is going to be upgraded.

The products are available to the users as soon as they are produced and time series of the analysis fields are available for the past years. The users can therefore select the time frame of the datasets and also if needed the geographical sub-domain.

All the production phases are monitored and checked by the MyOcean system in order to manage as soon as possible any possible failures, problems and degradation of the products.

All the products are validated and assessed in near real time via comparison with dependent and semi-independent observations (Tonani *et al*., 2009). A real time network has been developed for this purpose in collaboration with the MOON community (Mediterranean Operational Oceanography Network) in order to collect all the available moored observations for temperature, salinity, currents and sea level. All the information collected via this network are elaborated by *ad hoc*-software in order to evaluate the quality of the Med-MFC products (gnoo.bo.ingv.it/myocean/calval).

The system capabilities to reproduce the Ierapetra gyre (Popov, 2004; Marullo, 2003) has been assessed with work performed in collaboration with the In-situ TAC (Thematic Assembly Centre) of MyOcean. The Iera-Petra gyre is a seasonal structure with inter-annual variability which is located south of Crete in the Levantine basin and has an anticyclonic structure. Figure 3 shows a sequence of Med-currents Sea Surface Height field with the superimposition of the trajectory of an Argo float (dark line) for the period September–December 2010. The model is well able to reproduce the structure and its temporal evolution.

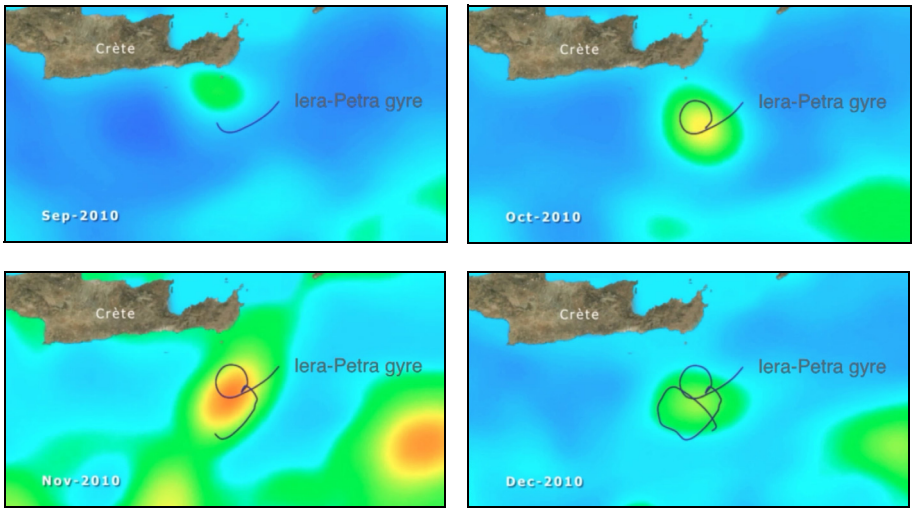

Figure 3 Sea Surface Height maps and Argo float trajectories for September, October, November and December 2010 in the Levantine Basin.

Acknowledgements

This work was supported by the European Commission MyOcean Project (SPA.2007.1.1.01, development of upgrade capabilities for existing GMES fast-track services and related operational services, grant agreement 218812-1-FP7-SPACE 2007-1).

Thanks to all the MyOcean Med-MFC partners involved in products Calibration/ Validation: ISPRA, IFREMER, NKUA, HCMR, IMEDEA, Puertos del Estado, NIB, IORL, CNR, IMS-METU, OC-UCY and UMT-OUI-POU.

References

Dobricic, S., and N. Pinardi (2008). An oceanographic three-dimensional variational data assimilation scheme. Ocean Modelling, 22, 3–4, 89–105.

Dobricic, S. (2005). New mean dynamic topography of the mediterranean calculated front assimilation system diagnostic. GRL, 32.

Dobricic, S., N. Pinardi, M. Adani, M. Tonani, C. Fratianni, A. Bonazzi, and V. Fernandez (2007). Daily oceanographic analyses by Mediterranean Forecasting System at the basin scale. Ocean Sci., 3, 149–157.

Dobricic, S., N. Pinardi, M. Adani, M. Tonani, C. Fratianni, A. Bonazzi, and V. Fernandez (2007). Daily oceanographic analyses by Mediterranean Forecasting System at the basin scale. Ocean Sci., 3, 149–157.

Lazzari, P., A. Teruzzi, S. Salon, S. Campagna, C. Calonaci, S. Colella, M. Tonani, and A. Crise (2010). Pre-operational short-term forecasts for the Mediterranean Sea biogeochemistry. Ocean Science, 6, 25–39.

Marullo, S., E. Napolitano, R. Santoleri, B. Manca and R. Evans (2003). Variability of Rhodes and Ierapetra Gyres during Levantine Intermediate Water Experiment: Observation and model results. JGR, vol. 108, 8119, 18 pp.

Oddo, P., M. Adani, N. Pinardi, C. Fratianni, M. Tonani, and D. Pettenuzzo (2009). A Nested Atlantic-Mediterranean Sea General Circulation Model for Operational Forecasting. Ocean Sci. Discuss., 6, 1093–1127.

Pinardi, N., I. Allen, P. De Mey, G. Korres, A. Lascaratos, P.Y. Le Traon, C. Maillard, G. Manzella, and C. Tziavos (2003). The Mediterranean ocean Forecasting System: first phase of implementation (1998–2001). Ann. Geophys., 21, 1, 3–20.

Popov, Yu.I. (2004). Genesis and structure of the anticyclonic Ierapetra Zone in the Levantine basin. Physical Oc., 14, 4, 234–242.

Roullet, G., and G. Madec (2000): Salt conservation, free surface, and varying levels: a new formulation for ocean general circulation models. J.G.R., 105, C10, 23,927–23,942.

Teruzzi, A., S. Salon, G. Bolzon, P. Lazzari, S. Campagna, F. Ficarelli, C. Solidoro, and A. Crise (2011). Operational forecasts of the biogeochemical state of Mediterranean Sea. Mercator ocean Newsletter, n. 40.

Tonani, M., N. Pinardi, S. Dobricic, I. Pujol, and C. Fratianni (2008). A high-resolution free-surface model of the Mediterranean Sea. Ocean Sci., 4, 1–14.

Tonani, M., N. Pinardi, C. Fratianni, J. Pistoia, S. Dobricic, S. Pensieri, M. de Alfonso and K. Nittis (2009). Mediterranean Forecasting System: forecast and analysis assessment through skill scores, Ocean Sci. 5,649–660.

The MyOcean IBI-MFC: A new operational ocean forecast service for the IBI-ROOS area

M.G. Sotillo*[1], J. Chanut[2], S. Queralt[1], G. Reffray[2], P. Lorente[1], M. Drevillon[2], S. Cailleau[2], B. Levier[2], and E. Álvarez Fanjul[1]

[1]*Puertos de Estado, Madrid, Spain*
[2]*Mercator Océan. Ramonville Saint-Agne, France*

Abstract

The MyOcean project (FP7) is dedicated to implementing the GMES Marine Core Service for ocean monitoring and forecasting, dealing with environment, security and resources. MyOcean aims to deliver regular and systematic reference information on the state of the oceans and European regional seas (www.myocean.eu). Inside the MyOcean sub-system structure, the IBI Monitoring and Forecasting Centre (IBI-MFC) is responsible for operationally generating daily ocean predictions for the IBI-ROOS area.

The IBI-MFC Service provides daily 5-day forecasts of 3D daily mean fields for temperature, salinity, sea surface height, zonal and meridional velocity, as well as hourly mean values of surface fields (sea surface height, surface currents and temperature). This new operational service is available from September 2011.

The IBI-MFC Operational Ocean Forecast system is based on a regional NEMO model application which includes high frequency processes of paramount importance for characterising regional scale marine processes (i.e. tidal forcing, surges and high frequency atmospheric forcing, fresh water river discharge, etc.). This 1/36º eddy resolving application, nested in the MyOcean global system and using ECMWF atmospheric forcing, has been implemented inside new operational suites.

Scientific quality is one of the criteria which will guide continuous improvement of MyOcean products, and therefore product validation arises as a key issue for the IBI-MFC. An exhaustive validation in order to provide an overall assessment is performed by means of a routine check against metrics computed using available observations (both satellite and in-situ sources included). Comparisons with other previous existing ocean forecast systems in the IBI area are also performed.

Keywords: MyOcean, IBI-ROOS, operational forecasting, NEMO, ocean model validation

1. The MyOcean IBI Monitoring and Forecasting Centre

MyOcean is the main European Project (FP7) dedicated to implementing the GMES Marine Core Service for ocean monitoring and forecasting, dealing with environment, security and resources. MyOcean aims to deliver regular and systematic reference information on the state of the oceans and European regional seas (www.myocean.eu). The MyOcean system is composed of 14 subsystems: 5 observation Thematic Assembly

* Corresponding author, email: marcos@puertos.es

Centres (TACs), dealing with observational data organisation and dissemination, 7 Monitoring and Forecasting Centres (MFCs) responsible for operational generation of daily ocean forecasts and analysis and reanalysis products, together with an unified web portal and an Information System.

Inside this MyOcean sub-system structure, the IBI Monitoring and Forecasting Centre (IBI-MFC) is responsible for operationally generating daily ocean prediction for the IBI-ROOS area, covering the whole of the European Atlantic facade and providing services from the Canary Islands to Ireland. Puertos del Estado (PdE) and Mercator Océan (MO) are the two Production Centres in charge of most of the IBI developments, maintenance and production issues. Nevertheless, as can be seen in the full IBI-MFC scheme (Figure 1), some other institutions participate as IBI-MFC partners.

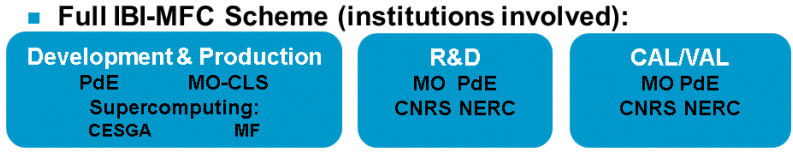

CESGA: Centro de SuperComputación Galicia, Santiago de Compostela, Spain
CLS: Collecte Localisation Satellites, Toulouse, France.
CNRS (POC): *Centre National de la Recherche Scientifique*, Toulouse, France.
MF: Meteo-France, Toulouse, France.
MO: *Mercator Océan*, Toulouse, France.
NERC (POL): *National Environment Research Council*, Liverpool, UK.
PDE: *Puertos del Estado*, Madrid, Spain.

Figure 1 IBI-MFC internal organisation: Partners involved by task.

2. The IBI-MFC Service

The operational IBI Ocean Analysis and Forecasting system provides a daily 5-day hydrodynamic forecast (+ 1 day of hindcast, generated as best estimate) including high frequency processes of paramount importance for characterising regional scale marine processes (i.e. tidal forcing, surges and high frequency atmospheric forcing, fresh water river discharge, etc.). The system is currently based on a (eddy-resolving) NEMO model application run at 1/36º horizontal resolution driven by ocean and meteorological forcing and it provides ocean predictions for the area shown in Figure 2 (left).

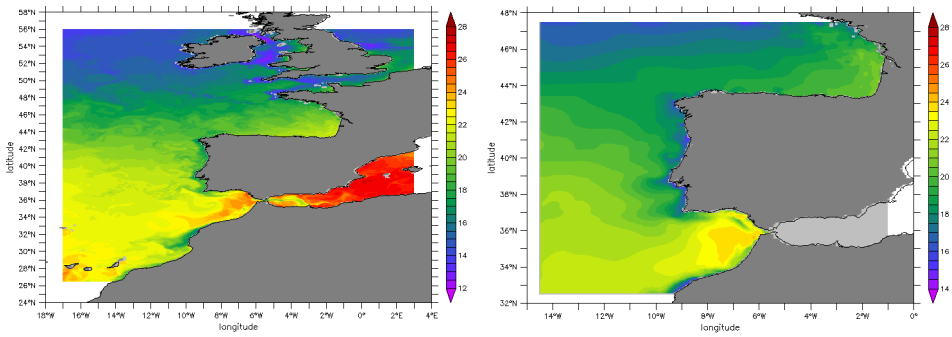

Figure 2 IBI MFC spatial coverage. Left: IBI service domain (available from IBI-V1release; launched on 1st April 2011). Right: coverage of the IBI-V0 (PdE ESEOAT system), starting point of the IBI system at the beginning of MyOcean Project. SST fields depicted.

The operational suite implemented to generate this IBI-MFC service daily consists of complex software that includes procedures that aim to automate and ensure:

1. Availability (and correct use) of input data from different sources (provided by different institutions through different machine servers)
2. Execution of the IBI model application
3. Generation of IBI-MFC products from model outputs
4. Storage and dissemination of IBI-MFC products
5. Validation and quality verification of IBI-MFC products.

The degree of complexity reached by this operational suite in order to ensure the daily IBI-MFC service also means an increase of the associated risk of some component failure, with a potential impact on the service availability. In order to minimise the potential impacts that may lead to a service outage and thus to enhance operational robustness, two mirror systems are being running in parallel – the nominal system at PdE the back-up at MO.

The IBI MFC Forecast System generates a daily Forecast bulletin as the primary user-oriented product, which includes predictions for a 5-day forecast horizon. Daily averages of 3D fields are provided for the following variables: temperature, salinity, zonal and meridional velocity components and sea surface height. Additionally, hourly frequency data is provided for SST, surface currents, sea surface height and barotropic velocities. All the IBI-MFC data products, just like the rest of MyOcean products, are generated in standard NetCDF format (www.unidata.ucar.edu/software/netcdf/).

IBI-MFC products are included in the MyOcean product catalogue, and disseminated through the MyOcean web portal (www.myocean.eu) which works as single point of access to any MyOcean data for advanced download and viewing. Figure 3 illustrates an example of navigation through the MyOcean catalogue for downloading data and an example of on-line viewing of IBI-MFC products. Through these tools, any user can access the IBI-MFC products from a 1-year live rolling archive (starting on 1 April 2011).

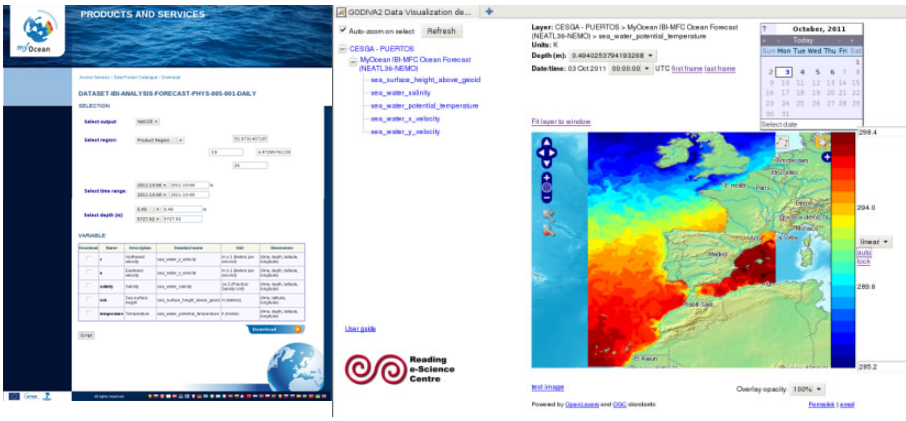

Figure 3 Left: Screenshot of the MyOcean catalogue to download IBI data; Right: Screenshot of the WebMapServer implemented for IBI-MFC products on-line viewing.

Furthermore, and in order to encourage the use of MyOcean products, there is a MyOcean Service Desk which provides end-users with any information needed to start with MyOcean data. This Service Desk also provides answers to any further question that may arise to any user on MyO products.

3. The IBI-MFC Model Application

The NEMO model (Madec, 2008) solves the three-dimensional finite-difference primitive equations in spherical coordinates discretised on an Arakawa-C grid and 50 geopotential vertical levels (z coordinate). It assumes hydrostatic equilibrium and Boussinesq approximation and makes use of a non-linear split explicit free surface to properly simulate fast external gravity waves such as tidal motions. Partial bottom cell representation of the bathymetry allows an accurate representation of the steep slopes characteristic of the area. The model grid is a subset of the global 1/12° ORCA tripolar grid also used by the parent system (that provides initial and lateral boundary conditions) but refined at 1/36° horizontal resolution (~2 km). The delivered products are bilinearly interpolated on a regular longitude/latitude 1/36° grid. Vertical mixing is parametrised according to a k-ε model implemented in the generic form proposed by Umlauf and Burchard (2003) including surface wave breaking induced mixing, while tracers and momentum subgrid lateral mixing is parametrised according to bilaplacian operators.

The IBI run is forced every 3 hours with atmospheric fields (10-m wind, surface pressure, 2-m temperature, relative humidity, precipitations, shortwave and long-wave radiative fluxes) provided by ECMWF. CORE empirical bulk formulae (Large and Yeager, 2004) are used to compute latent sensible heat fluxes, evaporation and surface stress. Solar penetration is parametrised according to a two-band exponential scheme with monthly climatological attenuation coefficients built from Seawif satellite ocean colour imagery. Lateral open boundary data (temperature, salinity, velocities and sea level) are interpolated from the daily outputs from the MyO Global eddy resolving system. These are complemented by 11 tidal harmonics (M2, S2, N2, K1, O1, Q1, M4, K2, P1, Mf, Mm) built from FES2004 and TPXO7.1 tidal models solutions. The atmospheric pressure component, missing in the large scale parent system sea level outputs, is added hypothesing pure isostatic response at open boundaries (inverse barometer approximation). Riverine inputs are implemented as lateral points sources with flowrates based on daily observations (when available) gathered by the PREVIMER project (www.previmer.org). Monthly climatological data from GRDC (www.bafg.de/GRDC) and the French "Banque Hydro" dataset (www.hydro.eaufrance.fr) are used when the previous data source is not available.

The downscaling methodology is inherited from the strategy developed for the ESEOAT (V0) system (Sotillo *et al*., 2007). Every week, on Thursdays (D0), the regional system is initialised 14 days in the past from analysed outputs taken from the MyO Global system and bilinearly interpolated on the refined grid. The model is then integrated until D0 to allow the spin up of small scales and the convergence of physical processes that are not resolved by the parent system. From the analysed output at D0 till D0+7 days, 7 sequences of 5 day forecasts plus a hindcast of the previous day with refreshed atmospheric forcing are performed.

4. IBI-MFC product quality assurance: the scientific Validation

Within the MyOcean project it is explicitly stressed that a useful quality characterisation of MyOcean products disseminated to the user community, using a scientific approach, is required. To generate IBI-MFC products, state-of-the-art ocean sciences tools (i.e. NEMO model) are used to guarantee the best possible description of the marine environment. Furthermore, a scientific assessment of the generated products is done in two phases: firstly, and mainly during the IBI system development phase prior to the IBI-V1 release, a calibration of the IBI-MFC systems under development was performed. Secondly, a routine validation during operations based on scientific best practices is performed daily. It is worth mentioning that the resulting CAL/VAL outputs enhance and orientate the transition to new versions of products, trigger R&D dedicated studies for new advances in the systems, and provide a scientific base for measuring the improvements in the resulting MyOcean system performance.

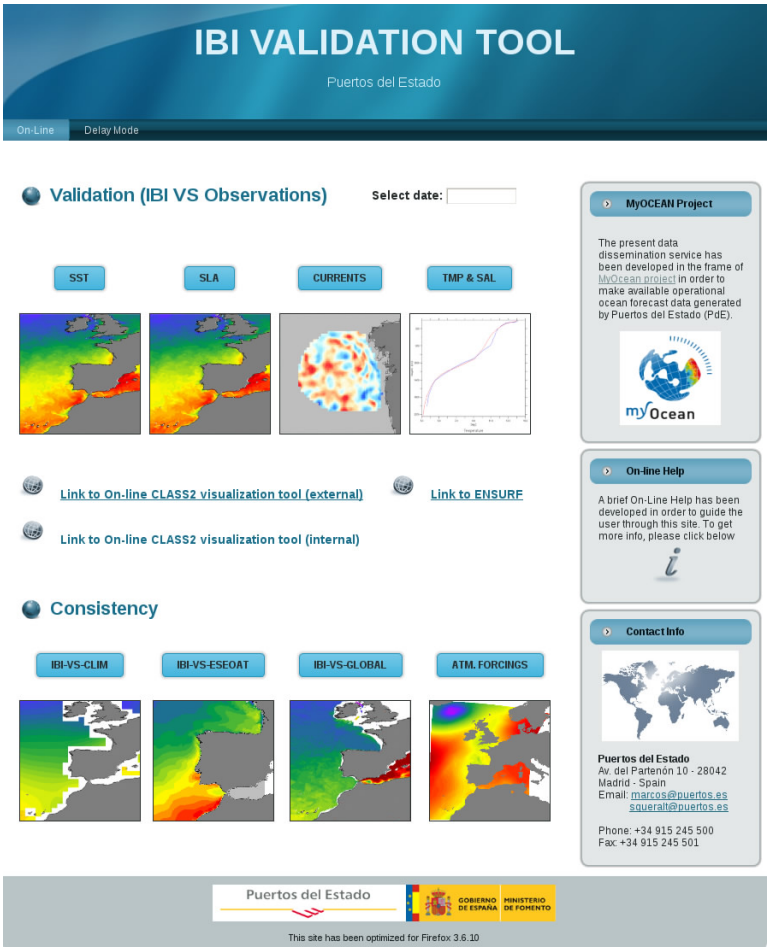

Figure 4 Screenshot of the PdE IBI-MFC dedicated validation web page.

This paper focuses on the automated scientific validation process routinely performed. This on-line IBI validation process has two different modes according to the time frequency performance:

1. “on-line” mode component: Validation procedures launched after the daily IBI forecast cycle.
2. Delayed mode component: Validation procedures launched to compute specific metrics and statistics covering longer periods (different launch time frequencies are considered: p.eg. monthly, seasonal, and annual reviews)

The “on-line” Validation Component is performed daily to check the consistency of IBI forecast products (as soon as they are generated) and to verify the quality of the IBI “best estimates” products from the previous day against available independent observations. On the other hand, the main objectives of the Delayed Mode Validation Component are to provide a global review of the IBI system performance for longer time windows, as well as an automatic generation of information on longer time scales (i.e.: monthly, seasonal, or annual) to routine production of user-oriented long-term IBI bulletins. Furthermore, this delayed mode validation process allows computation of specific metrics focused on physical processes that need observational data available only in delayed mode.

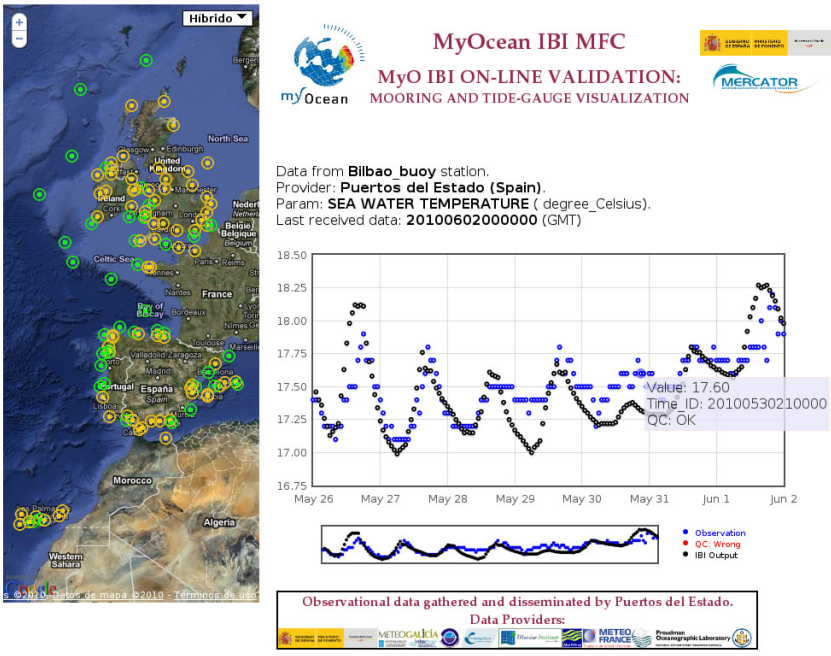

Figure 5 Snapshot of the tool dedicated to daily validation of IBI-MFC products by means of comparing them with available in-situ observations from moorings (measured parameters: surface currents, salinity and temperature) and tide-gauges (sea level and residuals). The map shows geographical locations of moorings (green dots) and tide gauges (orange ones) where comparisons are performed.

Both PdE and MO maintain webpages dedicated to visualisation of the most relevant information provided by their automatic validation process. Both validation webpages are updated daily with all the outputs from the validation processes. The daily update of these web pages (generation of plots, html files, storage, etc.) is fully automated and the web generation procedure is considered to be the last step of the on-line validation process. Figure 4 shows the appearance of the PdE IBI-MFC webpage.

Daily IBI-MFC on-line validation enables an assessment of the precision of IBI products, comparing them with as many available observations as possible for variables such as SST (using satellite L4 & L3 products and measurements from in-situ moorings), sea level (tide gauge observations and satellite sea level anomaly data), surface currents (mooring observations, info from drifters and HF radar data), surface salinity (in-situ observations from moorings) and temperature and salinity profiles (using measurements from ARGO floats). Figure 5, Figure 6 and Figure 7 illustrate some examples of the metrics and comparisons performed between IBI model products and observed data.

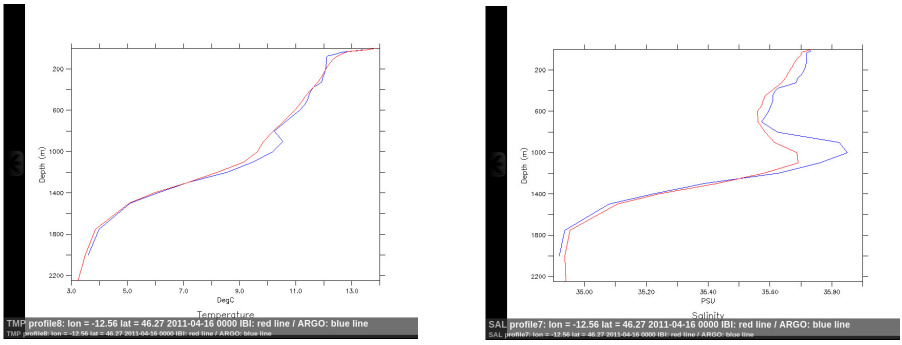

Figure 6 Profiles of temperature (ºC) and salinity (PSU) for the 01/08/2011. The red line is the IBI best estimate, and the blue line corresponds to the ARGO observation.

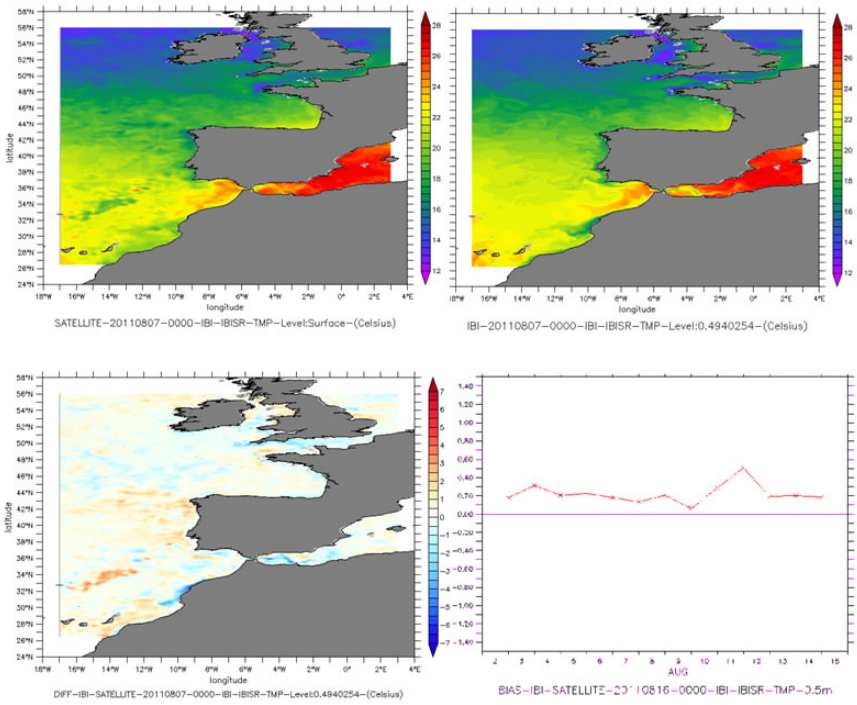

Figure 7 Assessment of SST (ºC) on 07/08/2011. ODYSSEA L4 satellite (upper left panel). IBI-V1 Best estimate (upper right panel). Differences between both fields (lower left panel) and time series of bias (computed the 16/08/2011 for the entire IBI service domain) displaying last 15 days (right lower panel).

References

Large, W.G., and S.G. Yeager, (2004). Diurnal to decadal global forcing for ocean and sea-ice models: the data sets and flux climatologies. NCAR technical notes.

Madec, G. (2008). NEMO Ocean General Circulation Model Reference Manuel. Internal Report. LODYC/IPSL, Paris.

Sotillo, M.G., A. Jordi, M.I. Ferrer, J. Conde, J. Tintoré, and E. Álvarez-Fanjul (2007). The ESEOO Regional Ocean Forecasting System. Proceedings of the seventeenth (2007) International Offshore And Polar Engineering Conference, Vol 1 - 4, 1716 - 1722.

Umlauf, L., and H. Burchard (2003). A generic length-scale equation for geophysical turbulence models, Journal of Marine Research, Volume 61, Number 2, 1 March 2003, pp. 235-265(31)

An analysis of Cantabric coastal trapped disturbances

S. Gaztelumendi*[1,2], J. Egaña*[1,2], M. Ruiz*[1,2], D. Pierna[1,2], K. Otxoa de Alda[1,2], and I.R. Gelpi[1,2]

[1]*Basque Meteorology Agency (EUSKALMET), Álava, Spain*
[2]*TECNALIA, Álava, Spain*

Abstract

One of the most important weather events along the Iberian Peninsula North Coast is the Coastally Trapped Disturbances (CTDs) in which the southerly flow is replaced by northerlies in a narrow zone along the coast. Associated with the arrival of those events, a shift and strengthening of the wind take place, with an increase in pressure and a drop in temperature.

This work presents an analysis of more relevant CTDs produced along the Cantabrian Coast during the 21st century using information available from different sources. We also describe two different representative events.

Keywords: coastally trapped disturbances, wind reversals.

1. Introduction

References

Cantabric Coastally Trapped Disturbances (CTDs) are mesoscale flow phenomena occasionally observed along the Iberian Peninsula North Coast during the late spring and summer months. Their appearance depends on some meteorological aspects ranging in the mesoscale and the presence of elevated terrain along the coast.

In the Basque Country coastal area, this severe weather phenomenon usually manifests itself as an abrupt change in weather. Air cools by as much as 10–15 °C in 20 minutes and the wind shifts suddenly (usually from southerly to northerly) with gusts up to 20–30 $m s^{-1}$. On the other hand humidity and pressure increase and sea conditions get worse. Eastward propagation of CTD along the Basque Country Coastal area is generally energetic but relatively short-lived (hours).

2. Analysis and classification

One of the most important coastal weather events in Basque Country is the so-called “Galerna” phenomena (“Enbata” in Basque language, “Galerne” in French). A “Galerna” episode is a mesoscale phenomenon that can be grouped into two main categories; those that are directly driven by a frontal passage (even a squall line) and those episodes without frontal presence, usually named typical “Galerna”. The latter

* Corresponding authors, email: santiago.gaztelumendi@tecnalia.com, joseba.egana@tecnalia.com, miriam.ruiz@tecnalia.com

ones can be considered as a CTD phenomena where the northerly flow is highly ageostrophic and limited to the coastal zone.

CTDs are mesoscale systems laterally confined against the Cantabrian mountains by Coriolis effects, and vertically by stable stratification. They propagate rapidly with the mountainous barrier on the right. The transition to northerly flow begins in Asturias and propagates eastward along the Cantabrian coast. Abrupt changes in the meteorological variables are intensified as the CTD propagates to the east over the Basque Country coastal area (Figure 1). In addition, there are wind reversals associated with frontal type "Galerna" episodes. In those cases mesoscale effects along the Cantabric coast overintensify the wind reversal (and associated effects) more than expected from synoptic-scale conditions.

This work has focused on the "Galerna" episodes that affect the Basque Country area during the last 10 years (2001–2011 period) and we have summarised most relevant aspects of them in Table 1. The strongest winds reversal events, with gusts above 25 ms^{-1}, are of a frontal type. As can be seen in Figure 2, the most frequent CTDs have a moderate intensity (gusts between 17 ms^{-1} and 25 ms^{-1}). During wind reversal, the directions of the max wind gust registered are from N/NW. A rise in pressure during the phenomena varies from 1–2 mb in one hour in the weak cases, to over 5 mb in the strongest ones. The propagation time of a "Galerna" event along the Basque coast varies from 1 hour for the strongest case, to two hours in the weakest ones.

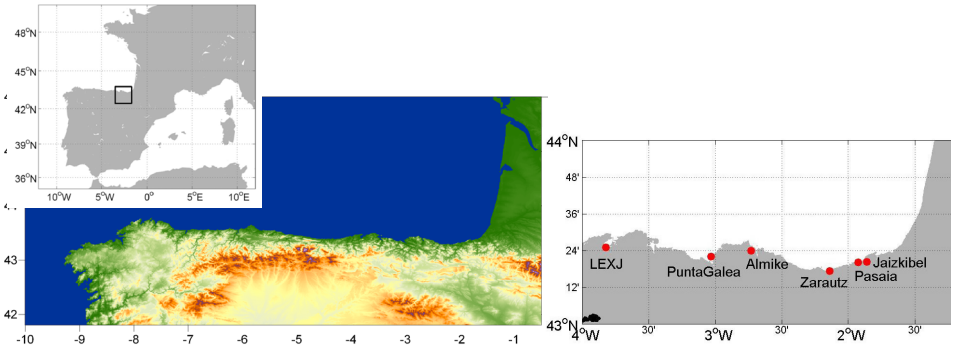

Figure 1 Basque Country location, Cantabric coast topography and locations of coastal stations used in the study.

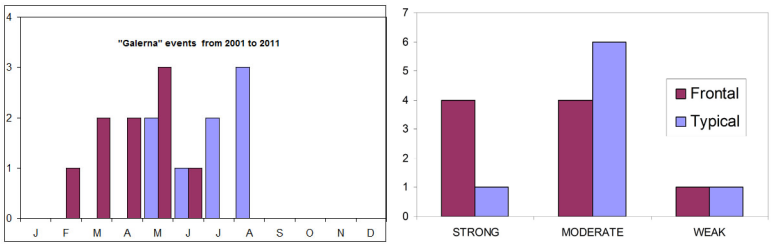

Figure 2 Distribution of "Galerna" events for the period 2001–2011 considering month event occurrence and strength of the wind reversal (strong: vmax > 25 ms^{-1}, moderate: 17 ms^{-1}<vmax <25 ms^{-1} and weak: vmax < 17 ms^{-1}).

3. Example episodes

In this section two cases of both categories of wind reversal are presented as examples.

Table 1 Summary of more relevant "Galerna" events in Basque Country during the 2001−2011.

DATE	Max wind gust (km/h)	Max wind gust (m/s)	Dir	Dir(º)	location	Start time	End time	Duration	p min time	p min	Δp (1h)	ΔT (30 min)	ΔT (1h)	ΔRH(%)	CTD	OTHER
2001 5 12	103,0	28,6	W	291	Pta Galea	20:40	22:20	1:40	19:50	1000,6	2,4	8,2	9	44	X	
2002 5 13	128,0	35,5	W	289	Pta Galea	13:30	14:20	0:50	11:40	1002,4	3,8	13,9	13,6	49		X
2002 5 21	85,0	23,6	W	288	Pta Galea	19:40	21:10	1:30	18:20	990,4	3	10,9	12	66		X
2004 6 22	86	23,8	NW	300	Bermeo	19:10	20:20	1:10	16:40	1000,2	2,6	8,4	9,7	38		X
2005 5 27	89,6	24,8	NW	308	Bilbao harb	18:10	20:10	2:00	17:00	1002,7	2,6	10,7	11,9	18	X	
2005 6 18	59,4	16,5	NW	317	Bilbao harb	14:50	18:00	3:10	13:30	1009,3	0,5	5	6,3	30	X	
2006 5 17	59,4	16,5	W	291	Pta Galea	14:30	17:20	2:50	12:10	1007,3	1	9,4	9,8	24		X
2007 2 14	135,0	37,5	W	282	Almike	8:40	9:50	1:10	7:40	994,1	5,7	7,3	7,6	31		X
2007 3 4	110,9	30,8	NW	324	Pta Galea	16:00	17:30	1:30	14:00	999	3,6	11,3	11,8	49		X
2007 4 24	69,8	19,3	N	339	Pta Galea	15:30	18:40	3:10	15:30	1005,3	1,1	6,1	8,4	29		X
2007 4 30	67,0	18,6	NW	328	Pta Galea	7:50	9:50	2:00	7:20	1001,4	1,4	4,6	5,1	19		X
2007 7 15	82,8	23,0	W	280	Almike	13:50	16:10	2:20	13:50	998,2	1,4	15,3	16,4	58	X	
2009 7 22	79,2	22,0	NW	315	Almike	13:00	15:00	2:00	12:50	996,8	1,4	9,3	11,4	52	X	
2009 8 23	74,7	20,7	NW	319	Pta Galea	16:10	18:30	2:20	16:00	999,8	2,3	5,4	5,7	25	X	
2009 8 31	85,4	23,7	NW	328	Pta Galea	14:50	17:10	2:20	14:30	1000	1,7	10,3	10,4	4	X	
2010 3 29	107,2	29,7	NW	321	Pta Galea	18:50	20:10	1:20	17:40	990,6	2,6	9	9,9	53		X
2011 8 6	70,5	19,5	W	292	Ondarroa	12:10	14:20	2:10	11:40	997,7	1,1	6,5	6,3	31	X	

3.1 Event on 27 May 2005

Synoptic description: At 500 hPa (Figure 3), there is a trough over the eastern Atlantic ocean, southwest the British Isles. The 850 hPa chart indicates offshore flow over the Iberian Peninsula North Coast and an intense temperature gradient (approximately 10ºC) between the east and west parts. Turning to surface charts, there is a low centre to the north-west of the Iberian Peninsula.

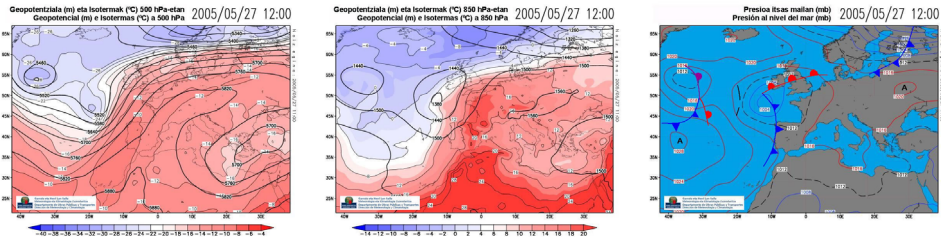

Figure 3 500 and 850hPa geopotential height and isotherm, SLP (2005/05/27-12 UTC)

Mesoscale and local description: NWP mesoscale model mean wind maps (Figure 4) show the wind transition from southerly to northerly along the Basque coast. In Figure 5 we can see temperature and wind data from some representative locations (Figure 1). In Almike (Bermeo) the wind shift takes place at 18:30 UTC, with a northerly flow of over 20 ms^{-1} (22 ms^{-1}). These wind reversals translate eastward along the coast, arriving at Jaizkibel station at 20:00 UTC (22.7 ms^{-1}). In Pasaia the significant wave height rises from 0.5 m to 2 m in a few minutes.

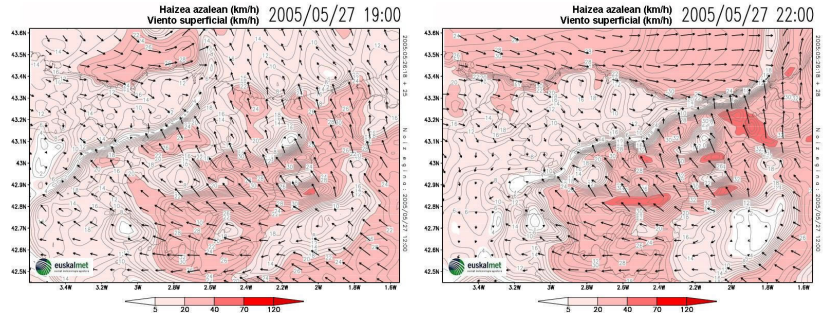

Figure 4 NWP mesoscale model wind data (kmh^{-1}) (2007/05/27 at 19:00 and 22:00 UTC).

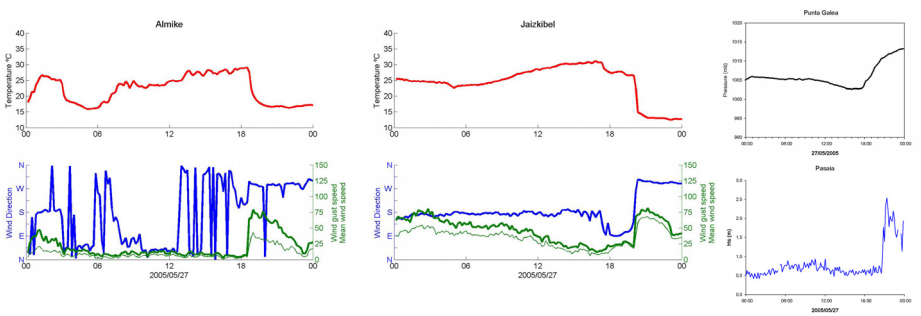

Figure 5 Observed time series evolution of wind and temperature for Almike and Jaizkibel, pressure in Punta Galea and significant wave height in Pasaia.

3.2 Event on 14 February 2007

Synoptic description: The synoptic patterns are characterised by an extensive zone of low pressure over the northern Atlantic. As the front moves eastward, the southerly flow switches to northerly in the Iberian Peninsula (see Figure 6). The temperature distribution shows warm temperature over the Basque Country but over the western part of the Iberian Peninsula there is a cold air mass.

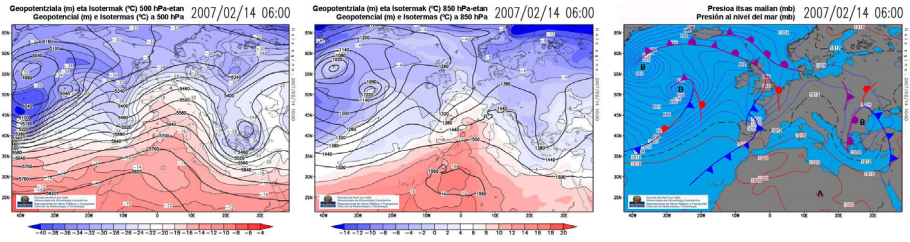

Figure 6 500 and 850hPa geopotential height and isotherms, and SLP (2007/02/14 06 UTC).

Mesoscale and local description: Figure 7 illustrates the evolution of the event as captured by the mesoscale model. At 10:00 UTC the southerly flow has been replaced by a cooler moist maritime flow. Wind data for various stations along the coast is shown in

Figure 8. At 9:00 UTC, the transition from southerly to northerly flow is observed in Almike (Bermeo) and gusts of 37.6 ms^{-1} are measured. In Jaizkibel the wind shift arrives at 9:40 UTC, with wind gusts of 33.4 ms^{-1}. The temperature drops by 6–8–ºC in 30 minutes.

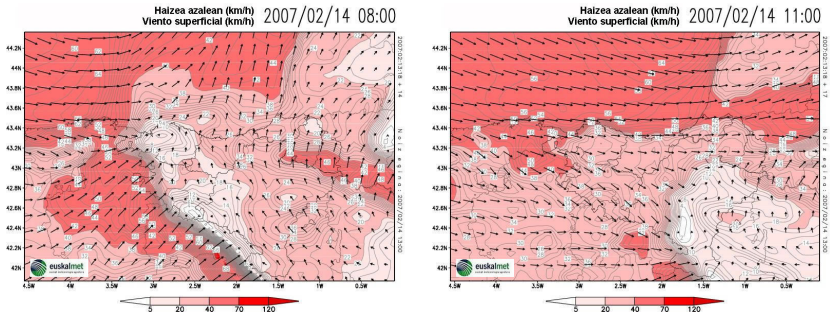

Figure 7 NWP mesoscale model wind data (2007/02/14 at 08:00 UTC and 11:00 UTC)

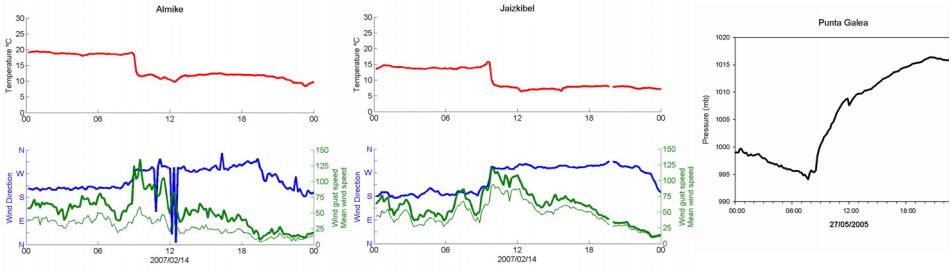

Figure 8 Observed time series evolution of wind and temperature for Almike and Jaizkibel, and pressure evolution for Punta Galea.

4. Conclusions

A preliminary study and classification of “Galerna” events affecting the Basque Country over the last ten years has been made. 2007 was the most active year with five “Galerna” events (just one CTD), while the year 2009 had more CTD events, with three cases. In 2003 and 2008 no “Galerna” events were registered.

CTDs only occur during late spring and summer months. These disturbances usually arrive in the Basque Country coast during the afternoon or early evening. On the other hand, wind reversals associated with fronts decrease in frequency in summer time and can happen at anytime during the day.

The synoptic environment favourable for a CTD event along the Cantabrian Coast is a low centred near the British Isles. This center of low pressure produces a southerly flow in the Bay of Biscay. On the other hand, in 850 hPa and 500 hPa levels, the dominant flow is the offshore flow. While warm continental air sits over the eastern part of the Cantabrian Coast, the western part has cooler air and there is an intense temperature

gradient of around 8–10ºC between both parts, though in the strongest events this difference can be higher.

Comparing both events examined in the previous section, the most intense event with the strongest gusts (37.6 ms^{-1}) is the wind reversal associated with a front. This perturbation also has a faster propagation speed than the CTD that happened on 27 May 2005. If we analyse the temperature changes, the largest fall is associated with the CTD, and the temperature decreases by 10–15ºC within a few minutes.

These disturbances are an important warm-season severe weather coastal problem in Basque Country due to their impact on summer coastal marine activities. Its sudden appearance may surprise fishermen and recreational boaters and also affect beach users.

5. Future work

Further studies need to be done, considering more cases and a deeper analysis of the forcing, propagation, and decay at mesoscale level.

Numerical studies using non-hydrostatic high-resolution mesoscale models are planned in order to improve understanding of the phenomena and to improve operational prediction of coastal meteorological conditions at EUSKALMET.

Acknowledgements

The authors would like to thank the Emergencies and Meteorology Directorate – Interior Department – Basque Government for public provision of data and operational service financial support. We also would like to thank all our colleagues from EUSKALMET for their daily efforts in promoting valuable services for the Basque community.

References

Arasti Barca, E. (2001). Estudio de la galerna típica del Cantábrico. INM. ISBN 84-8320-175-5.

Dorman C.E. (1985). Evidence of Kelvin Waves in California's marine layer and related eddy generation. Mon. Wea. Rev 113, 827–839.

Gaztelumendi, S., R. Hernandez, and K. Otxoa de Alda (2003). Some aspects on the operative use of the automatic stations network of the Basque Country. 3rd ICEAS, Torremolinos, Spain.

Mass, C.F., and M.D. Albright (1987). Coastal southerlies and alongshore surges of the west coast of North America: Evidence of mesoscale topographically trapped response to synoptic forcing. Mon. Wea. Rev, 115, 1707–1738

Nuss, W.A. *et al*. (2000). Coastally trapped wind reversals: Progress toward understanding. Bull. Amer. Meteor. Soc. 81, 719–743.

Reason, C.J.C., K.J. Tory, and P.L. Jackson (2001). A model investigation of the Dynamics of a Coastally Trapped Disturbance. J.Atmos.Sci.

Analysis of an explosive cyclogenesis episode on the Basque Country coastal area

J. Egaña*[1,2], S. Gaztelumendi*[1,2], M. Ruiz*[1,2], D. Pierna[1,2], I.R. Gelpi[1,2], and K. Otxoa de Alda[1,2]

[1]*Basque Meteorology Agency (EUSKALMET) Álava, Spain*
[2]*TECNALIA, Meteo Unit, Álava, Spain*

Abstract

The rapid deepening of a low pressure centre on November 8, 2010 resulted in a deep depression classified as explosive cyclogenesis (known as a "Becky" episode). The cyclone minimum values of pressure, together with its location and movement over the Cantabric Sea, led to serious consequences on the Cantabrian coast. Strong winds and high waves severely affected the coast of the Basque Country. This event is analysed from the perspective of adverse weather situation, considering meteorological and maritime conditions.

Keywords: Becky, deep low, explosive cyclogenesis.

1. Introduction

The pass of the deep low "Becky" over the Cantabric Sea produced an exceptional worsening of maritime conditions on Basque Country area during 8 and November 9, 2010. During this episode, the significant height wave exceeded 8 metres along the coast; causing damage at many places in the Basque coastal area, especially in the San Sebastian area. This paper presents some aspects related to this severe weather episode, including synoptic and meso-meteorological aspects, with special focus on maritime conditions and analysis of wave patterns, including features from wave modelling, oceanometeorological structures and buoy data collected in the area.

2. Meteorological conditions

During November 8, 2010, a deep and extensive low pressure centre was created by explosive cyclogenesis west of the British Isles (a cyclogenesis process can be considered as "explosive" when a cyclone deepens at a rate greater than 1 $hPa\,h^{-1}$ over 24 hours). The cyclone, with a minimum pressure value about 960 mb, caused intense west-northwest fluxes generating high fetch (Figure 1).

The next day, the cyclone approaches coast of France (Brittany), weakening gradually, and on November 10 it moves over to Continental Europe (Figure 1 and Figure 3). Becky generates very intense winds, with gusts surpassing 100 $km\,h^{-1}$ in exposed areas in the western part of the Basque country, especially on November 8.

* Corresponding authors, email: joseba.egana@tecnalia.com, santiago.gaztelumendi@tecnalia.com, miriam.ruiz@tecnalia.com

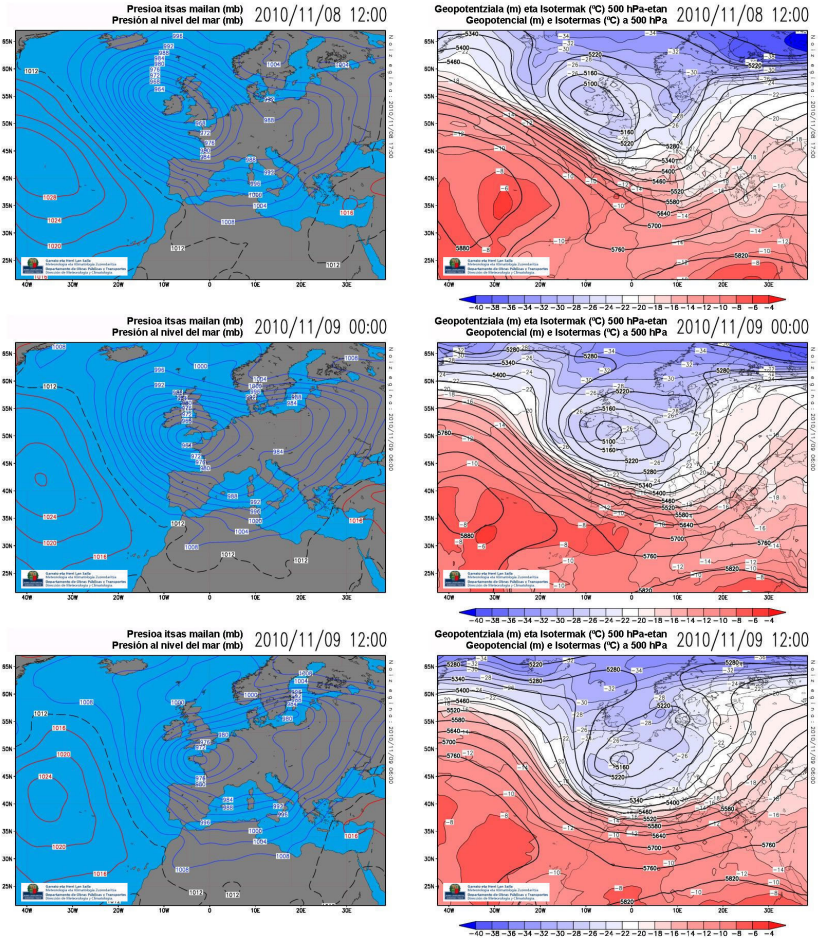

Figure 1 Sea level pressure and 500 hPa geopotential height and isotherm maps every 12 hours from 2010/11/08 12:00 to 2010/11/09 12:00.

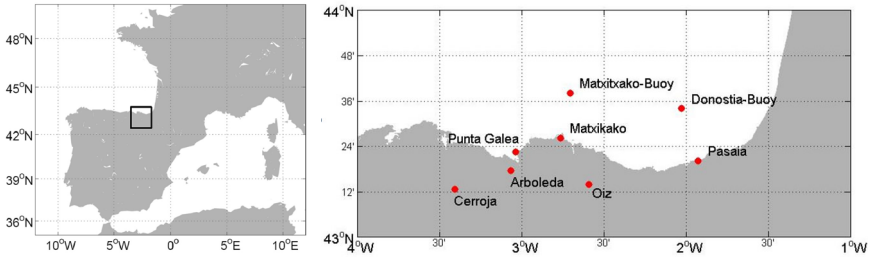

Figure 2 Location of buoys and automatic weather stations.

Wind gusts recorded along the Basque coast reached 130.9 kmh^{-1} in Matxitxako station and 108 kmh^{-1} in Punta Galea. In the mountain areas near the coast the maximum wind gusts reached 132.7 kmh^{-1} (Cerroja), 108.6 kmh^{-1} (Oiz) and 104.4 kmh^{-1} (Arboleda) (Figure 3).

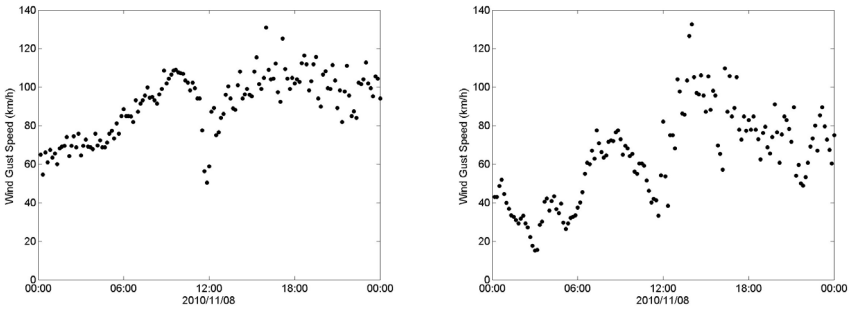

Figure 3 Wind gust speeds (kmh^{-1}) observed in Matxitxako and Cerroja.

3. Maritime conditions

Figure 4 shows how the waves increased over the northeastern Atlantic Ocean. From the Great Sole Bank to Finisterre, due to wind (strength and persistence) and fetch, the significant height wave grew to reach 12 m at 12 UTC November 9, 2010. The waves had a northwest direction with a period of between 10 and 15 seconds. This swell moved along the Cantabrian Coast, from west to east, with significant heights higher than 10 m. Wave maximum values reached the Basque coast around noon on November 9. The feature that produces the worst sea conditions in the Basque Country area is an intense maritime flow that generates high fetch able to produce heavy swells, characteristically observed in this episode.

Analysing the data registered from different Atlantic buoys we can see the time evolution of large waves. The waves generated in the entire western seaboard of Europe are considerable, with significant heights exceeding 10 m in most areas. During the night of November 8, the worst sea conditions first arrived at the buoys situated further north, and later translated southwards (Figure 6). The wave height decreased significantly during November 10.

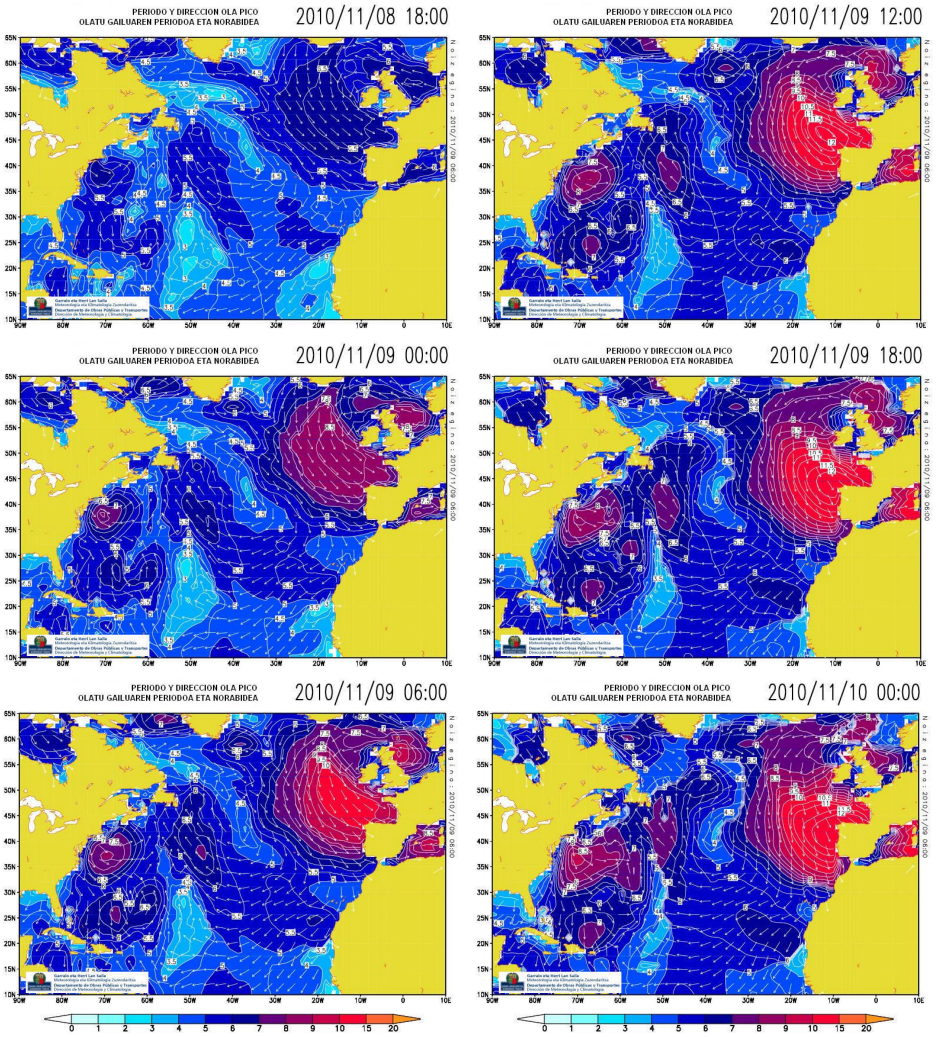

Figure 4 Significant wave height maps every 6 hours from 2010/11/08 18:00 to 2010/11/10 00:00.

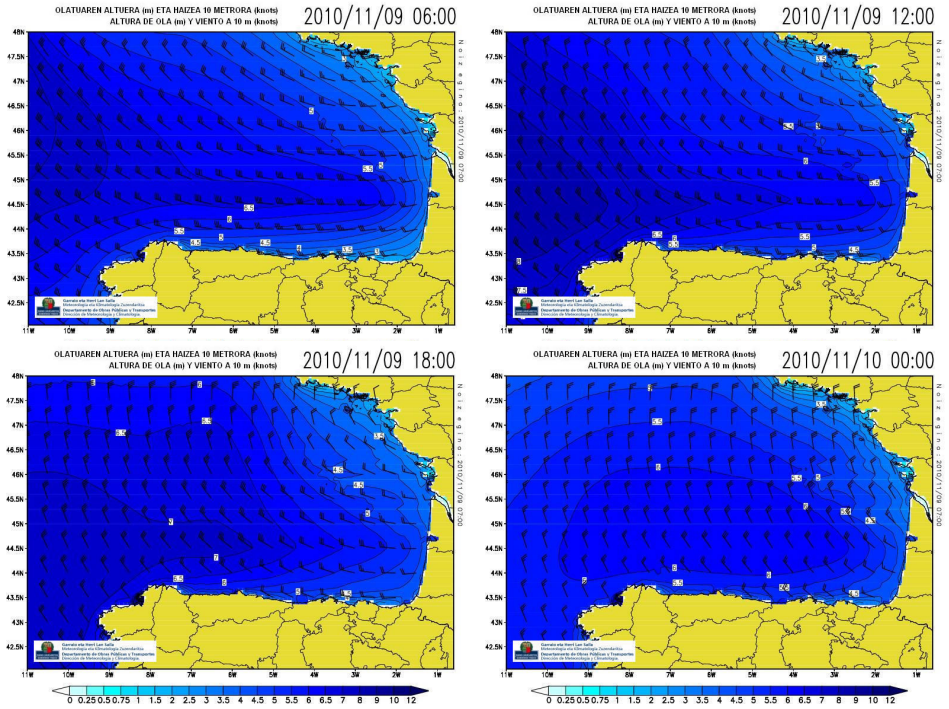

Figure 5 Significant wave height maps for the Bay of Biscay every 6 hours from 2010/11/09 06:00 to 2010/11/10 00:00.

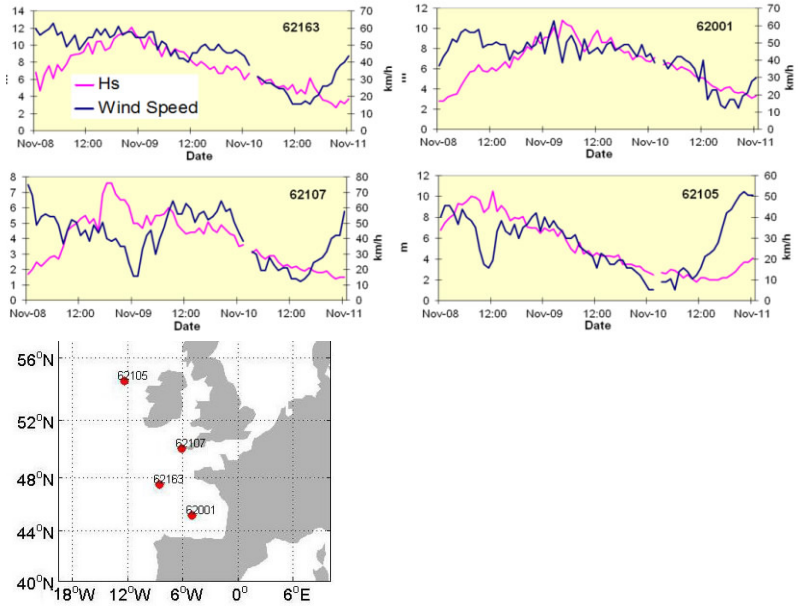

Figure 6 Hs (m) and mean wind speed (kmh^{-1}) at different buoy locations.

Wave height data were recorded by two buoys located about 10 miles offshore and some oceano-meteorological structures in the coastal area, showing that the waves increased during November 8. The largest significant wave height was registered in the morning of November 9 (Matxitxako buoy 10.65 m) and some hours later in Donostia buoy (9.25 m) located in the eastern Bay of Biscay (Figure 7).

The maximum wave heights registered by the Basque buoys reached values of 15 m, recorded during the morning of November 9 by the Matxitxako buoy. In the Pasaia harbour station the maximum significant wave height reached 9 m. During the second half of the day and during November 10, the wave height decreased for all structures and by the end of the day the significant wave heights does not exceed 3.5 m.

The barometric effect during November 9 increased the tide height by 30–35 cm. It should be mentioned that waves hitting the Basque coast had a major swell component of nearly 8 m (Figure 7), due to high fetch.

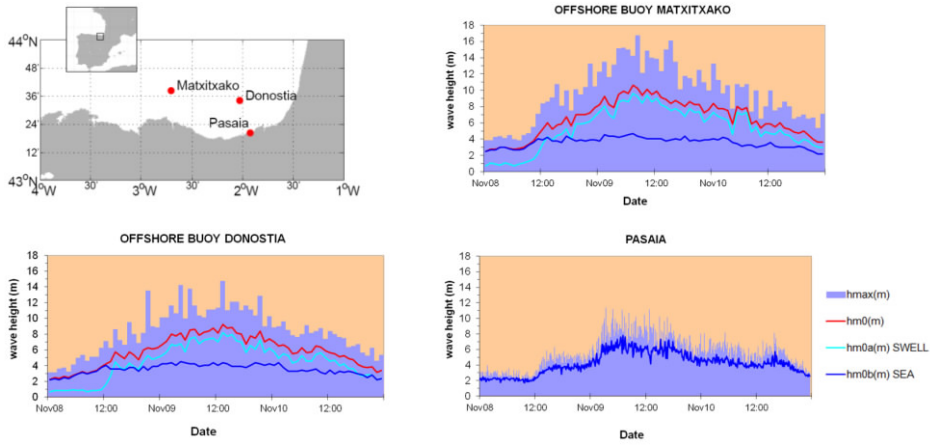

Figure 7 Hs (m) and mean wind speed (kmh^{-1}) for different buoys.

4. Conclusion

The significant wave height reached 8–9 m along the coast and around 10 m at the outer buoys, with maximum values of 15 m. The main component of the surge is the swell.

The coincidence of the spring tides with the barometric tide increased the sea level by 30–35 cm; the heavy swell made a considerable wave effect along the Basque coast.

There was substantial material damage all along the Basque coast. In particular damage was caused in Donostia–San Sebastian, especially in the Paseo Nuevo promenade, where strong waves cause a deep hole (Figure 8).

Based mainly on Euskalmet information, the authorities activated a red level warning for this episode. Considering the information available days in advance, civil protection clamped down in coastal areas, preventing all activities at sea, and on coastal roads and promenades near the sea. These measures reduced damages and avoided personal losses.

Figure 8 Some pictures taken along the Basque Coast during the event.

Acknowledgements

The authors would like to thank the Emergencies and Meteorology Directorate – Interior Department – Basque Government for public provision of data and operational service financial support. We also would like to thank all our colleagues from EUSKALMET for their daily effort in promoting valuable services for the Basque community.

References

Egaña, J., S. Gaztelumendi, I.R. Gelpi, and K. Otxoa de Alda (2010). Analysis of oceano-meteorological conditions during Klaus episode on Basque Country area. 10th EMS, 8th ECAC.

Gaztelumendi, S, J. Egaña, I.R. Gelpi, and K. Otxoa de Alda (2008). The Euskalmet wave forecast system: preliminary results and validation. Proceedings of the Fifth International Conference on EuroGOOS: 168-176.

Gaztelumendi, S., J. Egaña, I.R. Gelpi, and K. Otxoa de Alda (2008). A preliminary implementation of a wind-wave prediction model for the Bay of Biscay. XI International Symposium on Oceanography of the Bay of Biscay.

Gaztelumendi, S., J. Egaña, I.R. Gelpi, N. Alchaarani, K. Otxoa de Alda, L. Ferrer, M. González, M. Grifoll, A. Fontán, J. Mader, and A. Uriarte (2009). Implementación de un sistema operacional océano-meteorológico para el País Vasco. ISMSO9. II International Symposium of Marine Science.

Towards a dynamic coupling between the atmospheric and the ocean wave forecasting models of the POSEIDON system

Anastasios Papadopoulos*[1], Gerasimos Korres[2] and Petros Katsafados[3]

[1]*Institute of Inland Waters, Hellenic Centre for Marine Research, Greece*
[2]*Institute of Oceanography, Hellenic Centre for Marine Research, Greece*
[3]*Department of Geography, Harokopio University of Athens, Greece*

Abstract

The Hellenic Centre for Marine Research (HCMR) developed the POSEIDON system to provide monitoring and forecast services for the marine environmental conditions of the Greek Seas and the Mediterranean region. The POSEIDON weather forecasting system provides high-resolution weather forecasts and also produces the atmospheric forcing for the ocean models. Currently, a one-way coupling approach has been formulated where the atmospheric forcing fields are ingested into the wave and ocean models with a spatial resolution of 5 km and a temporal resolution of 1 h.

This study investigates the possible improvements of wind and ocean wave forecasts, as a result of a two-way interaction between the atmospheric and the wave models of the POSEIDON system. The efficiency of the coupling methodology is assessed on the basis of numerical experiments related to one-way and two-way coupling.

Keywords: air-sea interactions, weather forecast, sea state forecast

1. Introduction

The Hellenic Centre for Marine Research (HCMR) developed the POSEIDON system to provide monitoring and forecast services for the marine environmental conditions of the Greek Seas and the Mediterranean region. The POSEIDON weather forecasting system is the key element that provides timely high-resolution (1/20° × 1/20°) 5-day weather forecasts for the Mediterranean basin and the surrounding countries (Papadopoulos and Katsafados, 2009). It also produces the atmospheric forcing for the ocean numerical prediction models of the POSEIDON system; the ocean wave model, which is based on the WAM Cycle-4, and the ocean general circulation model which is based on POM model code (Blumberg and Mellor, 1987). The weather forecasting system is based on an advanced version of the non-hydrostatic atmospheric Eta/NCEP model. In the operational mode, a 3D data assimilation package, the Local Analysis Prediction System (LAPS) produces high resolution analysis fields for the initial conditions (Albers, 1995) while for the boundary conditions the 0.5° × 0.5° GFS/NCEP global forecasts are used. In the coupled POSEIDON forecasting system a one-way coupling approach has been formulated where the atmospheric forcing fields (surface fluxes of momentum, moisture, heat, radiation and precipitation rates) are ingested into the ocean wave and the ocean circulation models with a spatial resolution of 5 km and a temporal resolution of 1 h.

* Corresponding author, email: tpapa@hcmr

However, wind-generated ocean waves play a key role in the transfer of momentum, heat, and water vapour between air and sea. To this end, this study investigates the possible improvements of wind and ocean wave forecasts, as a result of a two-way interaction between the atmospheric and the wave models of the POSEIDON system. The efficiency of the coupling methodology is assessed on the basis of numerical experiments related to one-way and two-way coupling.

2. Methodology

The relatively high vertical resolution applied in the atmospheric model permits the application of a surface layer model based on the well established Monin–Obukhov similarity theory (Monin and Obukhov, 1954). In order to calculate surface turbulent flux for momentum, the similarity theory requires prescription of boundary conditions at two levels in the air, assuming fluxes between these two levels are constant. The relevant variables at the lowest model level are used as the upper boundary condition. The profiles of the relevant atmospheric variables tend to have the log form as the lower boundary is approached. Since the log function has a singularity at $z=0$, it is usually assumed that the log profile ends at some small but finite height z_0, and that the considered variables take their lower boundary values at this height. This situation is illustrated in Figure 1. The height z_0 is called the roughness height or roughness length.

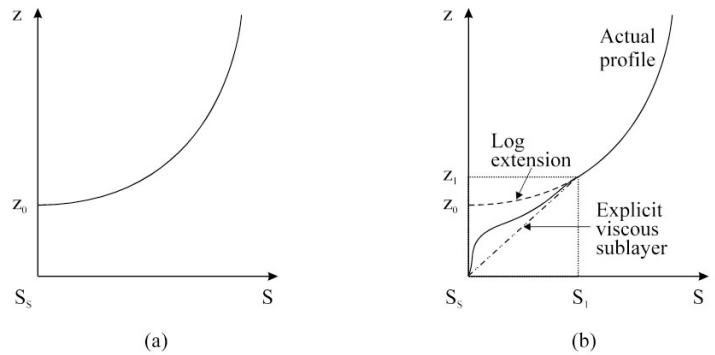

Figure 1 (a) log profile ending, (b) log profile with the viscous sublayer ending.

The situation near the surface is however more complicated than represented in Figure 1(a). More realistic is the profile displayed in Figure 1(b) where a viscous sublayer has been implemented. This thin sublayer reflects the fact that near the surface there is not enough space for turbulent elements to develop. Different viscous sublayer approaches are applied over ground and over water surfaces in the Eta model. The viscous sublayer over water surfaces (Janjic, 1994) is assumed to operate in three different regimes: (i) smooth and transitional, (ii) rough and (iii) rough with spray, depending on the roughness Reynolds number $\mathrm{Re} = (z_0 \cdot u_*)/\nu$. Here, u_* is the friction velocity and ν is the molecular viscosity for momentum, $\nu = 1.5 \cdot 10^{-5}\,\mathrm{m^2 s^{-1}}$. The roughness height z_0 is defined by:

$$z_0 = \frac{(\alpha_{CH} \cdot u_*^2)}{g} \quad (1)$$

where g is the acceleration of gravity and α_{CH} is the Charnock coefficient, which is considered constant.

However, α_{CH} is not constant but depends on the sea state and research to provide the appropriate foundation in terms of data and modelling expertise to support the design and the development of new air-sea exchange techniques is being established. As a starting point for this research, this study investigates the possible improvements of wind and ocean wave forecasts, as a result of a two-way exchange of 10-m wind fields (from atmospheric to wave model) and Charnock coefficient variations (from wave to atmospheric model).

3. Preliminary results

To investigate the sensitivity of simulating the air-sea exchanges, two sets of numerical experiments were performed: one consists of the control runs in which the Charnock coefficient was kept constant (α_{CH} = 0.018 that is typical for rapidly rising seas) and using the simulated wind fields to force the wave model. The second set of simulations, separate fromthe control runs, included the experimental runs in which the Charnock coefficient variations as estimated by the wave model were assimilated back into the atmospheric model which was run again and then the modified wind fields were used to again force the wave model. In both sets of simulations for the initial meteorological conditions the European Centre for Medium range Weather Forecast (ECMWF) operational analysis gridded data on a 0.5-degree horizontal grid increment at 11 standard pressure levels (1000, 925, 850, 700, 500, 400, 300, 250, 200, 150 and 100 hPa) were interpolated on the model grid points using optimal interpolation analysis while the boundary conditions were linearly interpolated at each model time step from the ECMWF data available every 6 hours. To define the initial state of the sea surface temperature field the ECMWF 0.5° × 0.5° gridded data were used. The overall analysis is restricted to the time scale characteristic of the short term weather predictions (from 21 March 2011 at 00 UTC to 28 March 2011 at 00 UTC) but at which sea state and atmospheric circulation present large variations.

The efficiency of the coupling methodology is assessed on the basis of differences in magnitude of the simulated fields (e.g. wind speed, sea wave height, surface latent heat flux, near-surface air temperature at 2 m height). Figure 2 shows the difference in the fields of wind speed and significant wave height at 00 UTC 22 March 2011 (after 24 hours of simulation). On the map, the positive differences indicate that the second simulation experiment (variable α_{CH}) estimated higher values (e.g. wind speed) in relation to the first experiment (constant α_{CH}). In contrast, negative differences indicate that the second set of experiments underestimated the relevant field (i.e. wind speed field). It also appears that the spatial distribution of the wave height is well correlated to the pattern of the wind speed.

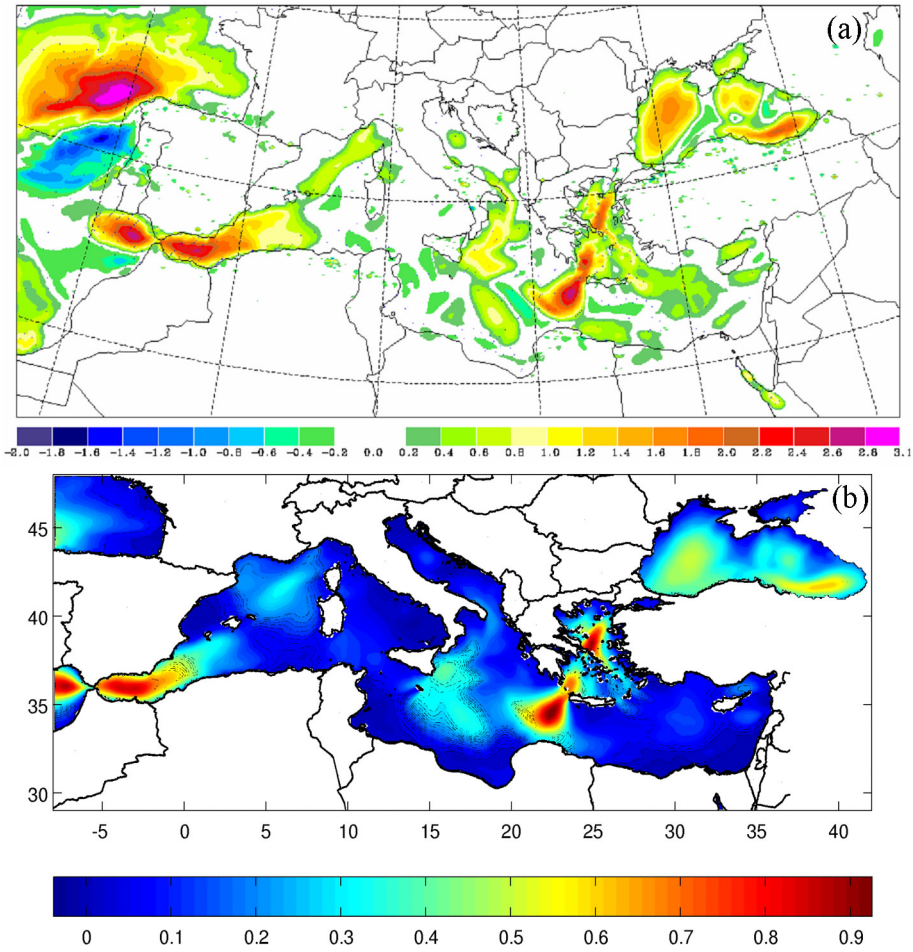

Figure 2 Map of the difference in the fields of (a) wind speed (in $m s^{-1}$) and (b) significant wave height (in m), as derived from the two set of numerical experiments.

Figure 3 also shows the difference in the fields of (a) air temperature at 2 m height and of (b) surface latent heat flux.

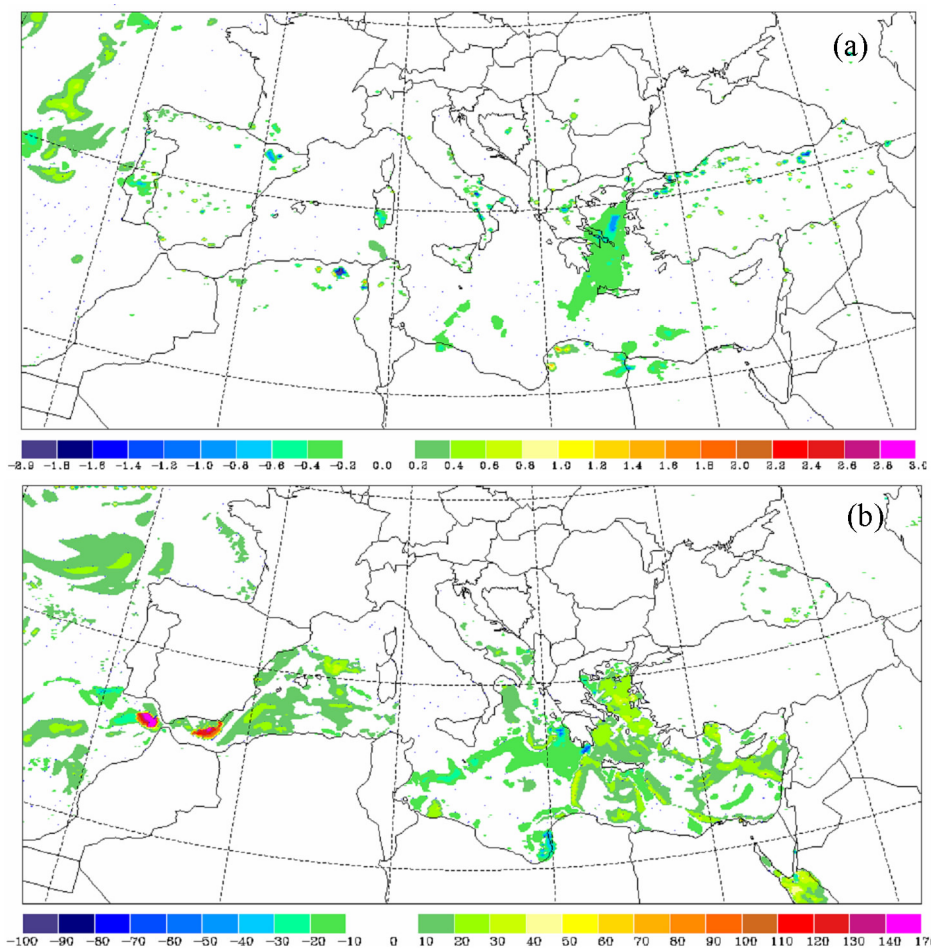

Figure 3 Map of the difference in the fields of (a) air temperature at 2 m height (in °C) and (b) surface latent heat flux (in Wm^{-2}), as derived from the two set of numerical experiments.

The overall effect is also examined with the relative frequency (spaced logarithmically) of the differences between the control and the experimental simulations for the entire simulation and across the model domain. For the specific case study, the mode is shown (Figure 4) to be well above zero and the distribution is skewed to large positive values (higher values when the two-coupling was applied), while we observe fewer cases where values are higher in the control simulation (negative differences). This evidence indicates that the application of the method increases the wind speed, which is quite a significant improvement, taking into account that near the surface the atmospheric models generally underestimate the magnitude of the wind speed.

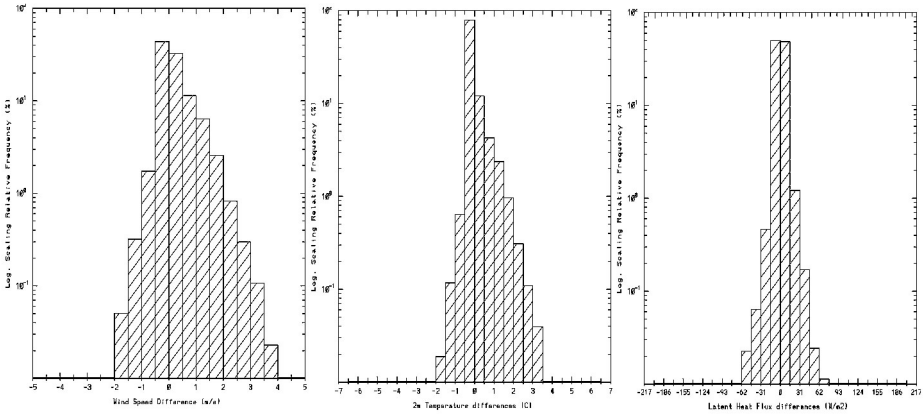

Figure 4 Relative frequency (%) of (a) wind speed (in $m s^{-1}$), (b) air temperature at 2 m height (in °C) and (c) surface latent heat flux (in $W m^{-2}$) differences between the two numerical experiments.

However, the method should be tested in more events and the simulated wind speed and wave height should be compared directly with measurements of the network of the POSEIDON buoys network.

References

Albers, S.C. (1995). The LAPS wind analysis, Weather and Forecasting, 10, 342–352.

Blumberg, A.F., and G.L. Mellor (1987). A description of a three-dimensional coastal ocean model, vol.4, edited by N. Heaps, pp.208, AGU, Washington D.C.

Janjic, Z.I. (1994). The step-mountain Eta coordinate model: Further developments of the convection, viscous sublayer and turbulence closure schemes, Monthly Weather Review, 122, 927–945.

Monin, A.S., and A.M. Obukhov (1954). "Osnovnye zakonomernosti turbulentnogo peremeivani v prizemnem sloie atmosfery". Trudy Geofiz. in-ta AN SSSR, No. 24 (151), 163–187.

Papadopoulos, A. and P. Katsafados (2009). Verification of operational weather forecasts from the POSEIDON system across the Eastern Mediterranean, Natural Hazards and Earth System Sciences, 9, 1299–1306.

Operational coastal services

The SAMPA project: building an operational oceanography system for the Strait of Gibraltar

E. Álvarez Fanjul*[1], F.J. de los Santos Ramos[2], José C. Sánchez-Garrido[3], D. Santos Muñoz[2], M. Gómez Lahoz[1], M.I. Ruiz Gil de la Serna[1], B. Pérez Gómez[1], M.G. Sotillo[1], S. Pérez Rubio[1], P. Lorente[1], J. García Lafuente[3], and J. Conde[4]

[1]*Puertos del Estado, Madrid, Spain*
[2]*Autoridad Portuaria Bahía de Algeciras, Cádiz, Spain*
[3]*Physical Oceanography Group, University of Malaga, Spain*
[4]*Agencia Estatal de Meteorología (AEMET), Madrid, Spain*

Abstract

The Strait of Gibraltar is one of the most important oceanographic regions in the world, both because of the physical processes taking place and its important socio-economic activity, being one of the areas of the world with most intensive maritime traffic. In spite of these facts, there is an important deficit in the marine monitoring and forecasting capacities in the region. To fill this gap, Puertos del Estado and The Algeciras Port Authority launched the 3-year SAMPA project. In the Framework of this initiative, new monitoring instruments (buoys, meteorological stations and tide gauges) were deployed, new state of the art forecast models were developed (waves, wind and 3D circulation) and associated downstream products are being implemented for the operational use of the data produced. In parallel with the SAMPA initiative and closely related, Puertos del Estado is leading the TRADE project, oriented to build an HF radar infrastructure in the area. The combined results of these two projects will open a new panorama both in the scientific knowledge of the straits and in the capability of proper knowledge-based decision-making for daily and extraordinary maritime challenges, such as accidental oil spill and port operations optimisation.

Keywords: Gibraltar straits, ocean modelling, waves, tide gauges, buoy, HF radar, oil spill, forecasting, alert system.

1. The SAMPA concept

The Strait of Gibraltar is one of the key regions in the world maritime traffic. Every year, around 100000 vessels cross the region, of which around 65000, enter or leave the Mediterranean Sea, while the rest cross between Europe and Africa. On top of that, the Algeciras Port Authority is one of the largest European ports, with traffic of 80 million tons and 5 million passengers per year.

Additionally, the Strait of Gibraltar is one of the most important and challenging areas in the world from the point of view of physical oceanography. It is a key point for the water and heat exchange between the Atlantic and the Mediterranean Sea, with all sorts of complex processes occurring in a very limited space. The most characteristic one is the two layer circulation, with cold water entering into the Mediterranean Sea in the form of

* Corresponding author, email: enrique@puertos.es

an intense jet, while saltier water plunges into the Atlantic in the lower layers. At the interface, the intense tidal forcing produces internal waves that propagate eastward.

In spite of the facts, the region has been poorly covered from the point of view of operational oceanography. There has not been enough instrumentation or modelling systems. This deficit could be especially critical in the event of a massive oil spill in the region.

In order to fill this gap, Puertos del Estado and the Algeciras Port Authority have launched the 3-year SAMPA project (Sistema Autónomo de Medición, Predicción y Alerta – Autonomous system for Monitoring, Forecasting and Alert) to build Operational Oceanography at the Strait.

The SAMPA system, as it is common today in operational oceanography, has three components: a monitoring component, consisting of new measuring devices deployed in the region, a forecasting system, based on new numerical models for waves, winds and circulation, and finally a set of user-oriented visualisation and downstream applications. The project links to and is coordinated with TRADE project, led by Puertos del Estado and devoted to building an HF radar capacity in the Strait.

Once developed, the system will be integrated into the Puertos del Estado operational system, ensuring the sustainability of the new developments. Furthermore, there are plans to export the concept to additional regions. Therefore, SAMPA is also an advanced Operational Oceanography laboratory.

SAMPA is now in its final year and most of its components are already in place. This paper gives a general and descriptive overview of the whole system, describing its three components, and detailing the link with TRADE. It is expected that scientific results will come in the following years, when the data being gathered now can be properly analysed.

2. The monitoring component

SAMPA is developing a whole set of new instrumentation in the region (Figure 1). The system is designed to provide a real-time insight of oceanographic conditions in the region, with special focus on the Algeciras Bay, and complements previous Puertos del Estado instrumentation such as the Ceuta harbour buoy on the African coast of the strait. All the instruments are in place, transmitting in real time and fully integrated into the Puertos del Estado system and, additionally, into the GMES-MyOcean in-situ TAC.

New buoys (Tryaxis and Watchkeeper models from AXYS) have been deployed to be permanently operated and maintained, as well as radar-based tide-gauges (Miros) and meteorological stations. It is interesting to note than due to the high traffic in the region, two large protection buoys have been moored close to the buoys. Additionally, the Watchkeeper buoy has been equipped with an AIS system. As a result, the stations have not suffered any collisions, something unfortunately frequent in previous Puertos del Estado attempts in nearby positions.

The data can be accessed in real time both from the Puertos del Estado web page (www.puertos.es) and through the SAMPA specific interface (sampa-apba.puertos.es), to be described later in this paper. The ADCP systems have been deployed temporally, in the framework of model validation campaigns.

The sampling frequency changes depending on the instrument, being as high as 2 Hz in the case of the tide gauges. All the data, before being visualised, pass an automatic quality control.

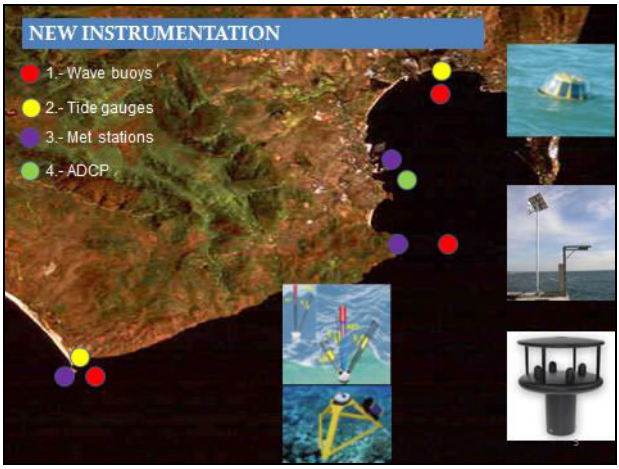

Figure 1 The SAMPA monitoring system.

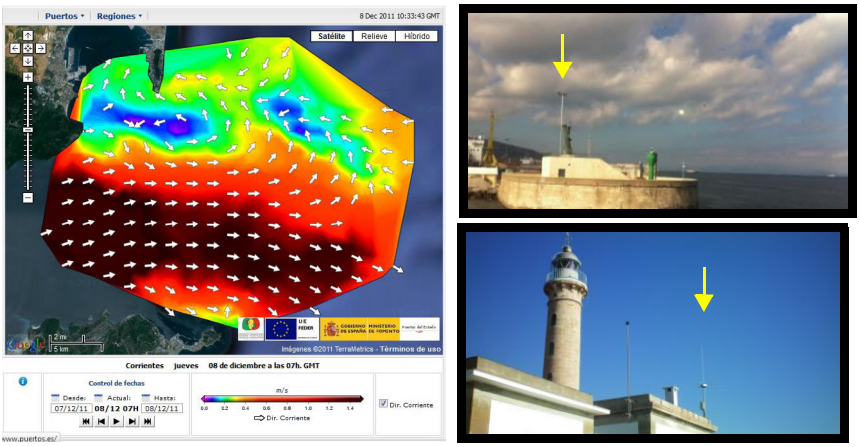

Figure 2 The HF Radar system of the TRADE project. The resulting total vectors are shown in the SAMPA interface and stations at African (upper) and European coast (lower).

This instrumentation is complemented with the installation of Codar's SeaSonde HF radars to monitor the currents. This parallel development is being carried out with FEDER funding in the framework of the TRADE (Trans regional RADars for Environmental applications) project. In an initial stage, two antennas have been deployed, one on each side of the strait (see Figure 2). This system is in place and now is under calibration and validation (drifting buoy experiments led by Cadiz University are being carried out to monitor system performance). It is planned that the fully operational phase will start by mid-2012. By the end of 2012, the whole system will be in place, with an additional

antenna located at Tarifa (southern tip of the Iberian Peninsula), providing better coverage of the western part of the strait.

All systems will be accessible from the Puertos del Estado web page and from the specific SAMPA interface. Figure 2 shows an actual snapshot of the HF radar currents, taken from the SAMPA interface. Data from the most recent days will be accessible, as well as animations of the currents and extraction of time series as selected points.

3. The modelling component

SAMPA takes advantage of the existing forecasting capacities at Puertos del Estado (described in Gómez *et al*., 2005 and Álvarez Fanjul *et al*., 2001) and develops new ones when required to provide a complete forecast of the strait sea state and the general oceanographic and meteorological conditions in the following days. It has three main components: atmosphere, waves and circulation. All systems are based on downscaling and provide a 3-day horizon forecast. This section provides an overview of these components.

3.1 Atmospheric modelling

Atmospheric modelling in SAMPA has been developed in close collaboration with AEMET, the Spanish Meteorological Agency. Its main objective is to improve the wind forecasts, which are very much affected by the orography and local meteorological singularities in the area. The CALMET model (Scire *et al*., 1990) has been implemented. for this purpose. CALMET is a meteorological model that includes diagnostic and prognostic wind fields.

The SAMPA configuration covers a domain of 500×300 grid points with a 1 km horizontal resolution, with 10 vertical levels. It is operationally nested into AEMET's HIRLAM model, providing a 3-day horizon forecast.

In order to prepare CALMET to be operational under Puertos de Estado's Linux- based computer environment, and to make it able to work with such a large domain, important recoding was necessary. Validation results show an improvement of the wind obtained by means of the CALMET downscaling as compared with HIRLAM's original wind fields, with a reduction of bias and RMS in the positions of the meteorological stations used for validations.

Output from this model is operationally employed in the circulation and wave models to be described in next sections.

3.2 Wave modelling

Puertos del Estado had already developed a specific wave forecast for the Strait of Gibraltar region (Gómez *et al*., 2005). It is based on a Wavewatch model (Tolman, 1991) application, nested operationally into two WAM (WAMDI group, 1988) applications, one in the Atlantic and another one in the Mediterranean Sea. This system has a resolution of $1' \times 1'$, which is enough to deal with the Strait of Gibraltar but not with the Algeciras Bay, so the objective of SAMPA in this specific field has been to cover this gap.

This is an especially complex problem due to the orography and strong bathymetric gradients in the region. In addition, due to strong local winds, wave generation inside the Algeciras Bay must be taken into account. To fulfil these modelling requirements, an unstructured grid application of SWAN (Booij *et al*., 1999) has been developed (see Figure 3), nested into the Puertos del Estado system.

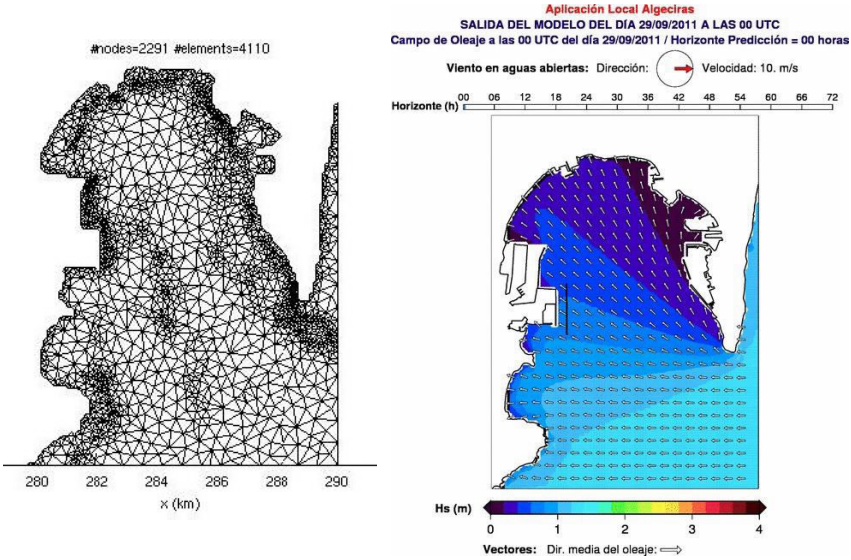

Figure 3 The SAMPA wave forecast. Unstructured grid and snapshot of results.

As in the case of the atmospheric model, the validation with buoys show a good behaviour of the system.

3.3 Circulation modelling

The circulation forecast model has been developed by Malaga University and it is operational in Puertos del Estado, using 4 nodes-32 cores of its supercomputer system.

The MITgcm has been used, with a SAMPA implementation using a non-regular grid, with maximum horizontal resolution of 200 m at the inner part, and 46 z-levels in the vertical. The model is forced by a complex set of input data, including momentum (winds generated by CALMET model), heat and fresh water (from the atmosphere HIRLAM model) and open boundary conditions from the MyOcean model (Mediterranean sea application). Tidal forcing is imposed at the boundaries based on LEGOS-POC/CLS models. Finally, in order to simulate atmospheric pressure forcing, dominant in the subinertial frequency (Garcia Lafuente *et al*., 2002), the system is additionally nested into Puertos del Estado's Nivmar storm surge forecast system based on a barotropic application of the HAMSOM model (Álvarez Fanjul *et al*., 1997) covering the eastern Atlantic and the whole Mediterranean Sea.

Figure 4 shows snapshots of the SAMPA circulation forecast model. Particularly striking is the capability of the system to reproduce the internal waves produced in the strait, as clearly shown by its signature in the free surface, visible in the upper panel.

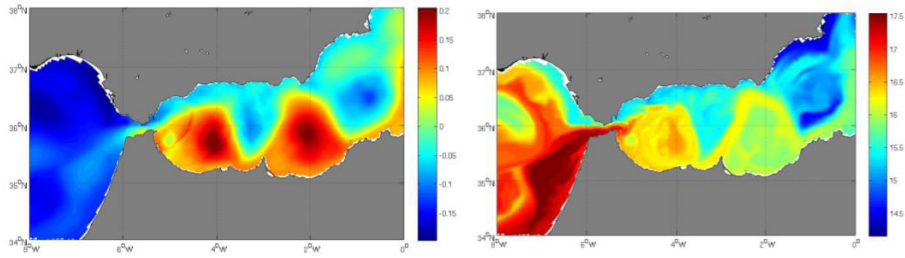

Figure 4 The SAMPA circulation model. Snapshot of sea level (left plot) and SST (right plot).

4. Alert system, visualisation and downstream services

Apart from the modelling and monitoring components previously described, a set of visualisation and downstream applications has been implemented.

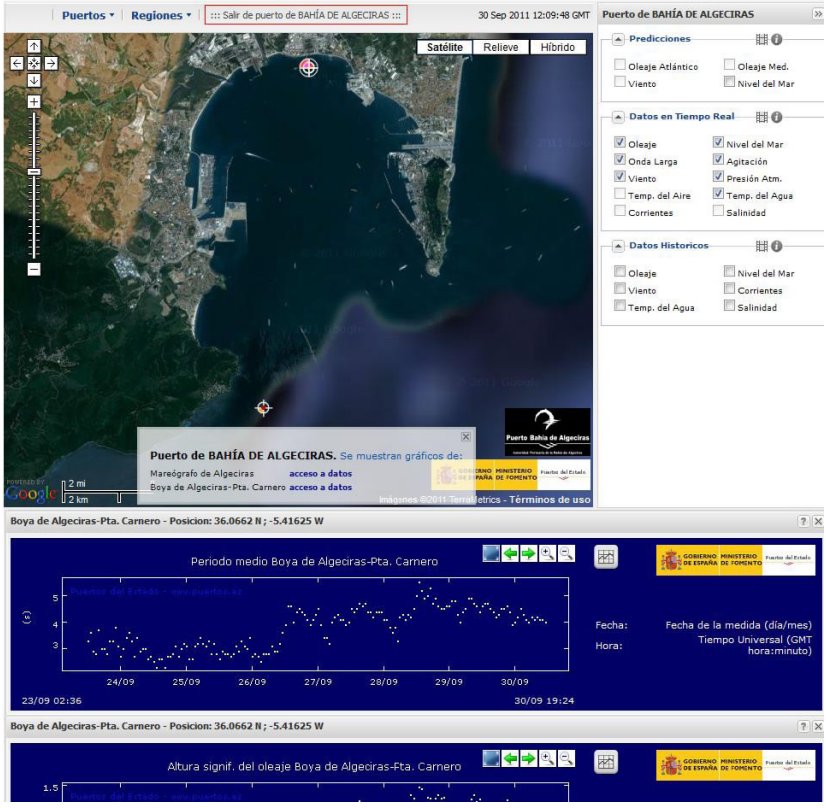

Figure 5 The SAMPA web interface. Time series and location of instruments.

All the model forecasts and in-situ real time data are freely accessible both on the Puertos del Estado website (www.puertos.es) and in the specific SAMPA project web interface (Figure 5). The interface has the capability of showing the data in graphical and

numerical format, and is extremely flexible, allowing the mixing of real time, forecast and historical information on screen at the same time. The time series visualisation software has the capability of zooming or moving to any user-selected time period in the last month. The 2D fields representation (models and HF Radar) can be zoomed to show higher detail in any region, can produce animations or display any selected date in the last 2 weeks (see Figure 2 for an example).

Specific alert indicators have been adapted from developments done previously by Puertos del Estado in the framework of the ECOOP project and are updated in real time on the SAMPA home page. At this moment, the alerts detect risky situations related to waves, sea level and abnormal combinations of these two variables. An alert system capable of detecting rapid sea level oscillations, such as Seiches or Tsunamis, is under development and will be implemented by the end of the project.

The Medslick model (Lardner *et al.*, 2006) has been implemented in the Algeciras Bay (see Figure 6) and is being linked automatically to all forecasting systems for its use by the Port responsible for responding to cases of accidental marine pollution.

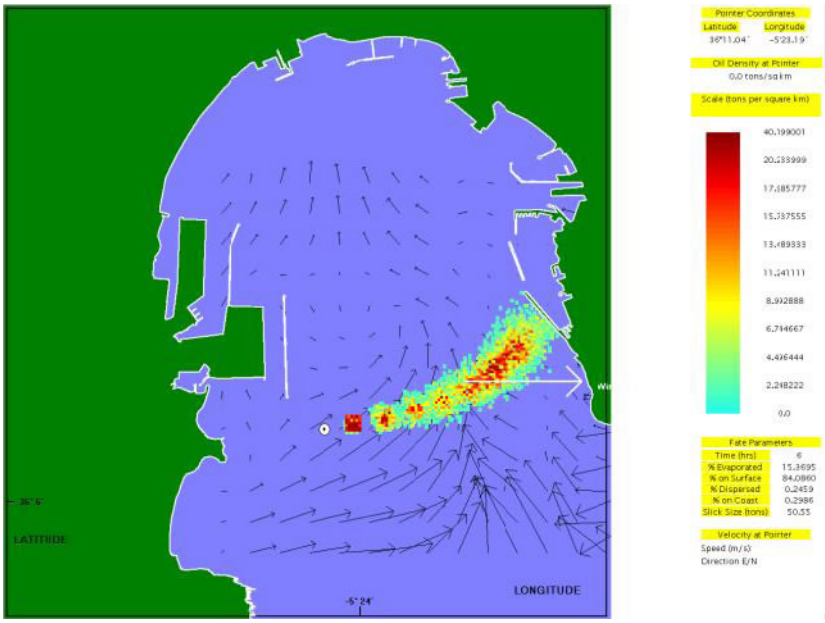

Figure 6 The Medslick model inside SAMPA system.

5. Conclusions and future plans

The SAMPA project, in coordination with TRADE, is creating an operational oceanographic system for the Strait of Gibraltar region that will serve the Algeciras Bay harbour as well as other users. When fully operational by the end of 2012, it is expected to be a key component for better scientific knowledge of the region and for downstream applications

In the final year it is planned to close the contact with final user, specifically with the Algeciras Harbour Authority and with Salvamento Marítimo, the Spanish institution in charge of search and rescue and oil spill combat. The data from SAMPA will be integrated into its Environmental Data Server and serve as input data for its own applications, such as Oilmap, in order to combat marine pollutions and detect the origin of intentional spills by means of backtracking. With the experience gained in this interaction it is planned to launch a SAMPA2 project, more user oriented, to take full advantage of the new tools and present the information in new ways, more tailored to specific user needs.

The idea behind the way SAMPA works is that the architecture and concept can be extended to other regions. This will certainly be the case with other harbours of the Puertos del Estado's system. In this sense SAMPA is working as an operational oceanography laboratory, where advanced ideas are tested and integrated, to be later extended to other harbours in the system.

Acknowledgments

We wish to thank LEGOS/POC and CNES for the provision of tidal constants developed by NOVELTIS/LEGOS in the frame of COMAPI study for its use in the circulation modelling. INGV has kindly provided support to implement the OBC in the model. We are thankful to Dr. Sannino working at the ENEA Italian National Agency for helpful technical support concerning the MITcgm ocean model. We wish to thank SOCIB for providing and implementing the BatTri software at Puertos del Estado. The collaboration of Cadiz University and the Spanish Hydrographic office is critical to the field validation campaigns for model validation and HF Radar calibration. The University of Cyprus has provided Medslick and the necessary support to implement it. We also want to thank the high professionalism and level of compromise of the companies involved in the provision and installation of the instrumentation and in the software development, more specifically Sidmar (buoys, tide gauges and meteorological stations), Qualitas REMOS (HF Radar and Portus) and Nologin (SAMPA web page). IGN has supported us in the levelling of the tide gauges, with ETICA performing the field work. The TRADE project is supported by FEDER funds by means POCTEP, Trans-Regional Cooperation Programme, (Programa Operativo de Cooperación Transfronteriza España-Portugal, in Spanish).

References

Álvarez Fanjul, E., B.P. Gómez, and I.R. Sánchez Arévalo (2001). Nivmar: A storm surge forecasting system for the Spanish waters. Scientia Marina, 65, 145-154.

Álvarez Fanjul, E., B.P. Gómez, and I.R. Sánchez Arévalo (1997). A Description of the Tides in the Eastern North Atlantic. Progress in Oceanography, 40, 217-244.

Booij, N., R.C. Ris, and H.L. Holthuijsen (1999). A third-generation wave model for coastal regions, Part I, Model description and validation. Journal of Geophysical Research, 10, C4, 7649-7666.

García Lafuente, J., E. Álvarez Fanjul, J.M. Vargas, and A.W. Ratsimandresy (2002). Subinertial variability in the flow through the Strait of Gibraltar. Journal of Geophysical Research.

Lardner, R., G. Zodiatis, D. Hayes, and N. Pinardi (2006). "Application of the MEDSLIK Oil Spill Model to the Lebanese Spill of July 2006". European Group of Experts on Satellite Monitoring of Sea Based Oil Pollution. European Communities.

Marshall, J., A. Adcroft, C. Hill, L. Perelman, and C. Heisey (1997). "A finite-volume, incompressible Navier Stokes model for studies of the ocean on parallel computers". J. Geograph. Res. 102 (C3): 5753–5766.

Scire, J.S., E.M. Insley, and R.J. Yamartino, (1990). Model formulation and user's guide for the CALMET meteorological model. Sigma Research Corp., Concord, MA

Tolman, H.L. (1991). A third-generation model for wind waves on slowly varying, unsteady and inhomogeneous depths and currents. Journal of physical Oceanography, 21, 782–797.

WAMDI Group, S. Hasselman, K. Hasselman, P.A.E.M. Janssen, G.J. Komen, L. Bertotti, P. Lionelo, A. Guillaume, V.C. Cardone, J.A. Greenwood, M. Reistad, L. Zambresky, and J.A. Ewing (1988). The WAM model: a third-generation ocean wave prediction model. Journal of Physical Oceanography, 18, 1775–1810.

Estimating real-time river discharge to the sea

Lennart Funkquist

Swedish Meteorological and Hydrological Institute

Abstract

For a long time there has been a pressing need for reasonable estimates of real-time river discharges to seas for driving shelf-sea models including ecological models. This has now been achieved by extending an already running operational river discharge model (HYPE) for the Baltic Sea drainage basin to cover all European rivers. A sustainable operational system has been built up to respond to GMES downstream services such as climate studies, coastal ocean models, regional environmental commissions including HELCOM and OSPAR, regional and national operational institutes, environmental protection agencies, fishery boards, water regulation bodies and SMEs working in coastal areas.

Daily data on river discharge and nutrient supply has been validated against observations at land stations and river outlets. Its impact on regional ocean and ecological models has been assessed by a comparison between model runs using climatology and daily data.

Keywords: River runoff, ocean modelling

1. Introduction

1.1 The HYPE model

The hydrological model HYPE (Lindström *et al*., 2009) is a conceptual, semi-distributed dynamic model. River basins are represented by sub-basins in the form of polygons. Each sub-basin contains different classes according to vegetation, soil type, topography and land-use. Three layers of soil are used to model processes like evapotranspiration, snow-melt, surface runoff, infiltration, percolation and macro-pore flow. Tile drainage and groundwater flow from soil layers to rivers and lakes are modelled for each class. The model simulates the turnover of nitrogen and phosphorus in soil layers and its transformation in rivers and lakes. Transport of water and nutrients between the sub-basins are modelled through a special routing module.

As the HYPE model uses global and regional data bases, there is no limit on its geographical application. The HYPE version for Europe is named E-HYPE and is divided into five main drainage basins, see Figure 1. The resolution ranges from about 10 km^2 for the Swedish drainage basin to approximately 120 km^2 for the whole of Europe, which sums up to about 50000 sub-basins. The operational system consists of the model itself with forcing from ECMWF and is run on daily basis.

* Corresponding author, email: lennart.funkquist@smhi.se

Figure 1 The E-HYPE model for Europe is divided into five subregions according to their geographical outlets, Baltic Sea, NE Atlantic, Mediterranean, Black Sea and Barents Sea. Each subregion is further divided into smaller polygons.

1.2 Users and objectives for ocean applications

The E-HYPE data is used in different areas such as ocean forecasting, research projects, water management, water allocation, eutrophication limitation and climate services

For forecasting, daily updated 10-day prognostic data is accessible by ftp. For reanalysis applications, a 30-year hindcast data set, based on ERAMESAN forcing, has been produced. The data set includes freshwater volume fluxes to the sea for all European rivers and runoff from land areas between river outlets. For some regions, there is the possibility to supply estimates of nutrient concentrations as well.

Questions that could be answered by using E-HYPE data could be divided into three groups: scenarios, forecasting and nowcasting, and water quality questions.

- Typical questions related to scenarios are how changes in landcover and future climate will affect hydrological variables. The model can also give estimates on frequency of extreme flooding or drought.
- For ocean applications, information on nutrient and fresh water supply from rivers is important both for operational ocean forecasts and climate studies and its influence on ecological parameters like phytoplankton growth and the risk of harmful algae bloom. For land use it is of value to know which areas are currently at risk of flooding or for example what is today's value of soil moisture.
- Monitoring of water quality questions has becoming more and more important and in Europe a Water Framework Directive (WFD) and Marine Strategy Framework Directive (MSFD) have been defined to help the answer questions such as how much of the nutrients goes into the sea, where do the nutrients come from and are they above certain risk levels. The biodiversity can be threatened because of low volume flow during breeding periods.

1.3 Input data for model setup and calibration

The setup of the E-HYPE model requires input from a number of global and regional databases. Static information like topography can be found in the global database HydroSHEDS. There are a number of databases for river discharge, nutrient concen-

tration, land use, soil type, major dams, industrial emissions and amount of irrigation. For the daily forcing of the model both operational atmospheric models and re-analysis products are used for precipitation and surface temperature.

2. Validation

Validation of the model results is an important issue and a number of different methods are used for this purpose. Measurements of daily flow rates together with monthly and yearly mean can be compared with model results. Examples of comparisons are shown in Figure 2. Satellite data is helpful for comparison of snow cover with snow water equivalent in the model. Figure 3 shows a comparison of pixel values from MERIS satellite data averaged over the model polygons with model results for a smaller region in Sweden. The plan is to assimilate the satellite snow cover data into the hydrological model.

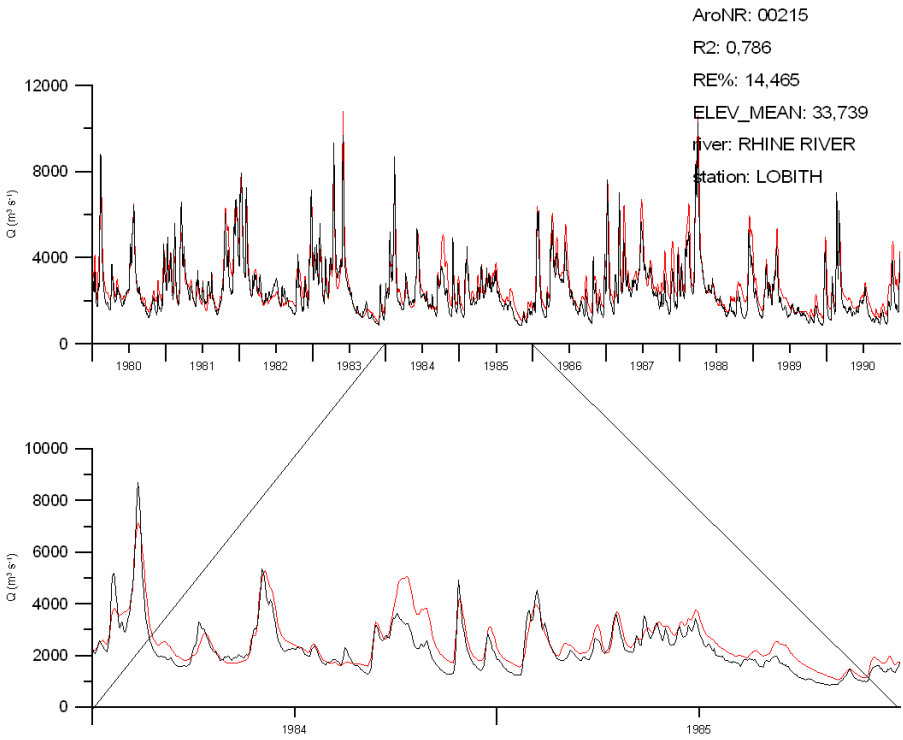

Figure 2 Observed (black) and modelled (red) volume flow for river Rhine at station Lobeth for the period 1980-1990 (upper part). The lower part shows the same for 1984-1985.

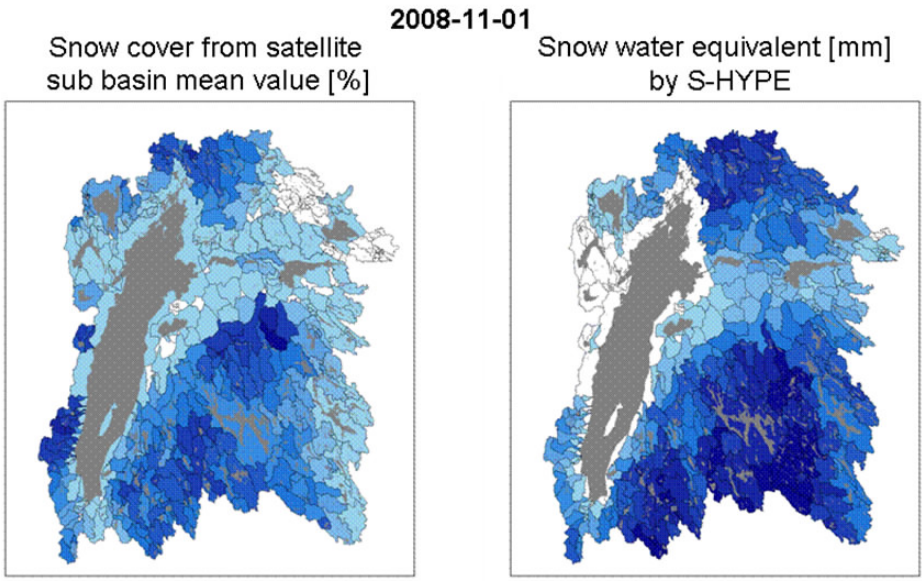

Figure 3 BioPar pixel values averaged over each polygon compared with snow water equivalent from the S-HYPE model for a drainage basin in southern Sweden.

3. Impact on ocean models and access of data

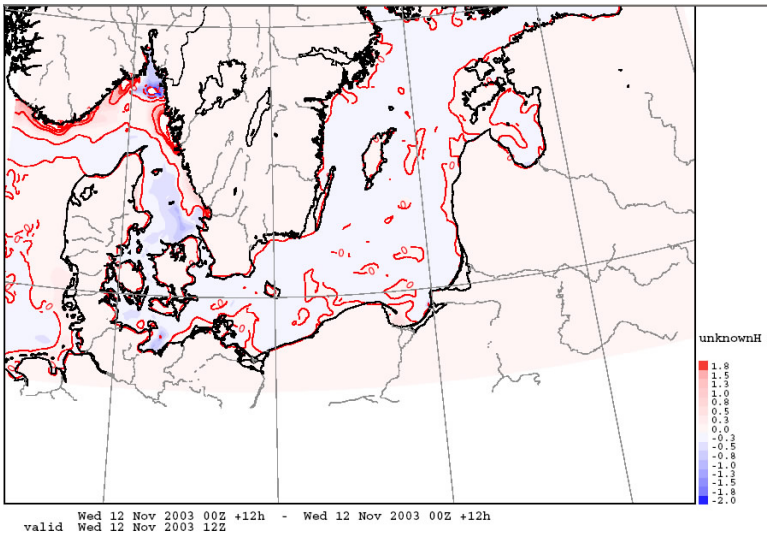

Figure 4 Differences in surface salinity (PSU) in the southern Baltic Sea and Skagerrak/Kattegat after approximately 10 months with daily river runoff compared with monthly means.

Validation studies and assessment of the impact of daily river runoff on operational ocean models are parts of on-going projects. As an example, Figure 4 shows the results for a 12 month simulation with an ocean model for the Baltic Sea/North Sea. Differences

in surface salinity from a run forced with daily river discharge compared with monthly mean values shows up in the whole area, especially close to river outlets.

As can be seen in Figure 5, there are also differences in nutrient supply to the sea. It is noticeable how months with high peaks are underestimated in monthly mean data. As the peaks occur in the most productive period they should have an effect on the start and strength of the blooming.

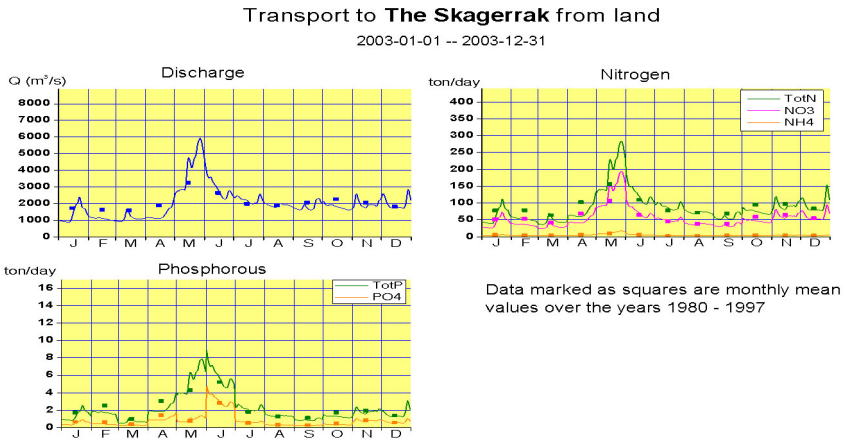

Figure 5 Difference between monthly means and daily data for 2003 on nutrient load to the Skagerrak.

Acknowledgments

The E-HYPE runs were performed by the unit of Hydrological Research at SMHI. Several persons have been involved and I especially acknowledge Henrik Spångmyr, Joel Dahné and Kristina Isberg.

The research leading to these results has received funding from the European Community's Seventh Framework Programme [FP7/2007-2013] under grant agreement n° 263400.

References

Lindström, G., C.P. Pers, R. Rosberg, J. Strömqvist, and B Arheimer (2010). Development and test of the HYPE (Hydrological Predictions for the Environment) model – A water quality model for different spatial scales. Hydrology Research 41.3-4:295-319.

OSERIT: a downstream service dedicated to the Belgian Coastguard Agencies

Sébastien Legrand* and Valérie Dulière

Management Unit of the North Sea Mathematical Models (MUMM), Royal Belgian Institute of Natural Sciences (RBINS), Belgium

Abstract

The research project OSERIT aims to develop an "Oil Spill Evaluation and Response Integrated Tool" for the Belgian Coastguard Agencies. This web-based tool will gather relevant, scientific-based information needed to support the decision-making process in case of oil spilled at sea. OSERIT targets two categories of users. The first category includes operational users who need to access marine and oil spill drift forecasts. The second category of users includes environmental representatives who need to compare several scenarios in order to assess the potential environmental consequences of various combating strategies. To meet this ambitious goal, a new web-based interface and a new 3D oil drift and fate mathematical model are being developed.

This article first explains how OSERIT development is dictated by end-users requirements for its quickness, reliability, user-friendliness, accessibility and inherent quality. The main model features are then presented. Finally, the model performances are illustrated using a real case: the oil leak that happened in the Gannet field in August 2011. OSERIT should be ready for operational use in September 2012.

Keywords: Drift, oil spill, search and rescue, modelling, service, North Sea, Belgium

1. Introduction

Despite its small size, the Belgian part of the North Sea (BPNS) is intensely used (Douvere *et al*., 2007). In addition to areas dedicated to dredging activities, sand and gravel extraction, off-shore wind farms and aquaculture activities, the BPNS is crossed by two of the world's busiest merchant shipping lanes, namely the Westhinder-Noordhinder Traffic Separation Schemes (TSS) and the navigation channel to the Scheldt estuary and the ports of Antwerp, Terneuzen, Vlissigen and Zeebrugge (Figure 1). Altogether, these activities generate more than 100000 AIS recorded ship movements per year (van Iperen *et al*., 2011). In total, approximately 40% of the transport in the BPNS consists of dangerous goods either in package form (2/3) or in bulk (1/3) (Le Roy and Maes, 2006). This high shipping density combined with dangerous currents caused by sand banks makes BPNS a high risk area for ship-ship collisions, ship-offshore structure collisions, ship groundings, loss of cargo, loss of containers, man overboard incidents and – last but not least – oil and HNS pollution of the sea.

* Corresponding author, email: s.legrand@mumm.ac.be

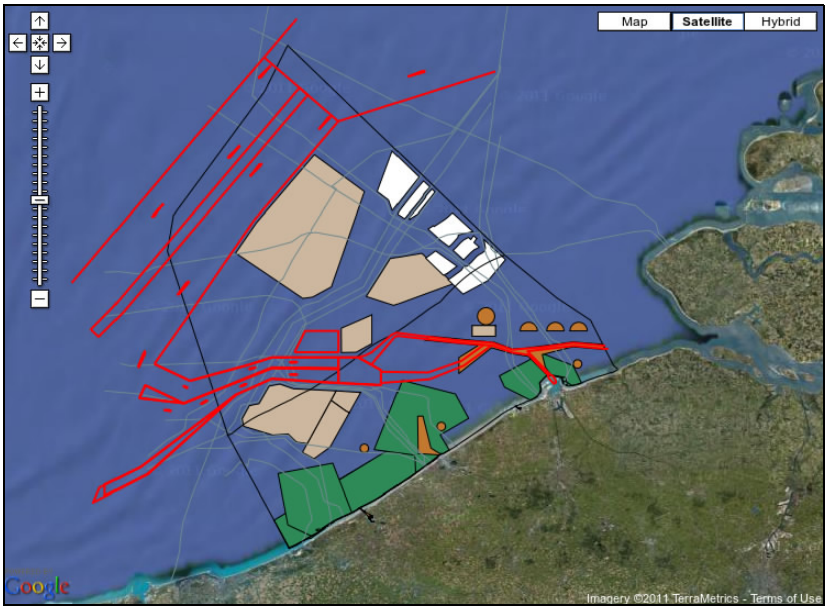

Figure 1 The Belgian part of the North Sea is intensively used: in red the traffic separation scheme, in brown dredging and dumping sites, in bisque sand and gravel extraction sites and in white off-shore wind farms. Marine protected areas are in green.

To efficiently face all these risks and to ensure optimum use of resources, the Belgian Coastguard structure was created in 2003. Its primary mission is to create and coordinate cooperation between the 17 Belgian governmental agencies that have legal responsibilities and competencies at sea or in the ports (www.kwgc.be).

MUMM is a full partner of the Belgian Coastguard, operating the Belgian North Sea Aerial Survey (Lagring *et al*., 2012) and monitoring licensed economic marine activities. In case of marine pollution, MUMM also gives scientific advice for defining the best strategy for fighting pollution and deploys its surveillance aircraft, the *R.V. Belgica* and the surveillance vessel *Tuimelaar*. Finally, the MUMM operational oceanography team provides the Belgian Coastguard Agencies with high resolution marine forecasts and performs on-demand 2D drift simulations of SAR objects and oil spills floating on the sea surface. This latter service also includes automatic drift simulations of satellite-detected pollution reported by EMSA CleanSeaNet.

The MUMM oil drift service is now routinely used by the coastguard's operators. Aiming constantly to improve this service and to answer the operators' needs and suggestions, MUMM is developing a new tool that gathers and provides relevant scientific-based information to perform a 'Net Environmental Benefit Assessment'. This assessment is a legal obligation in Belgium before deciding the best strategy to combat marine oil pollution. This "Oil Spill Evaluation and Response Integrated Tool" (OSERIT) must therefore allow end-users to perform and compare several oil drift and fate simulations in order to estimate the environmental consequences of the pollution on the marine environment. To meet this ambitious goal, a new 3D mathematical model that

directly simulates the time and space evolution of oil concentration in the water column is being developed. This new fate model combines the advantages of the Lagrangian approach for modelling the surface processes and the Eulerian approach to forecast the oil concentration chemically dispersed in the water column.

2. Service definition

The main objective of the research project OSERIT is the development of an integrated tool that gathers relevant, scientific-based information provided by operational oceanography to support the decision-making process of the Belgian Coastguard Agencies in cases of oil pollution.

2.1 End-users requirements

From our end-users feedbacks, we identified three kinds of expectations from two different categories of end-users. The first category includes operational users who need to quickly access high resolution short term marine and drift trajectory forecast. The second category of users includes environmental representatives who need to compare several scenarios in order to assess the environmental consequences of the different possible strategies to combat the oil pollution.

A priori, the first category of end-users needs a very simple and ready-to-go tool while the second category needs a solution that offers more advanced options and scenarios, including the application of chemical dispersant. Both categories agreed with the fact that the success of OSERIT depends on its quickness, reliability, user-friendliness, accessibility and inherent quality (i.e. state-of-the-art system). It should allow visualisation and download of required information.

2.2 A web-based interface

To ensure its accessibility by all the Belgian Coastguard Agencies, the OSERIT service is built around a web-based interface. This interface is voluntary kept as simple and user-friendly as possible. It will offer 3 basic functionalities: a flexible input form, a visualisation tool and an export tool.

The input form will allow users to define the simulation set-up. Basic inputs are the oil type (or the SAR object type), the initial time and place and the simulation type (forward or backward in time). Advanced/optional inputs include the definition of the oil release and spill scenarios. Because oil spill can result from many different situations, OSERIT provides some pre-defined scenarios. The user can chose from a “single point” or “ellipse-shape” oil spill, from an instantaneous or continuous release and finally, from surface, bottom or water column release. Continuous release from a moving source is also implemented.

The visualisation tool will allow users to access marine forecast and various diagnostics derived from the drift simulation such as probability maps for search and rescue operation, oil polluted zones, residence time and exposure times in oil-sensitive areas or oil mass balance. Combining the look and feel of Google Maps with the powerful layers management and rendering of MapServer, the visualisation tool will also allow the model results to be superimposed on relevant environmental and economic GIS layers. Figure 1 and Figure 2 are screenshots from the future visualisation tool.

Finally, the export tool will allow users to download the results of the selected simulation in various file formats and insert them in their own GIS tool.

The web-based interface will interact with MUMM web server and the new 3D oil drift and fate model installed on the MUMM high performance computer. This model is described in the next section.

3. Model description

3.1 A new 3D mathematical model

The OSERIT model is a kinetic model, based on empirical data and parametrisations, that simulates the 3D drift and fate of oil on the sea surface and in the water column. The current version is based on the Lagrangian particle approach that represents a spill of oil by the release of particles. The Lagrangian module computes the displacement of each particle resulting from the combined actions of winds, ocean currents, Stokes drift, buoyancy, turbulent diffusion, gravity, viscosity and surface tension. Beaching is also included. The hydrodynamic model COHERENS (Luyten, 2011) was used as a development platform for OSERIT.

More particularly, the advection at the sea surface is computed as a combined effect of winds, surface water currents and waves. Within the water column, particles move under the action of water currents, waves and buoyancy effects. The turbulent diffusive transport is expressed using the random walk technique following Wang *et al.* (2008). Particles can move from the surface into the water column through the process of vertical natural dispersion mainly due to the action of breaking waves. Surface oil is then split into smaller droplets that are propelled into the water column. The oil natural dispersion follows the kinetic approach of Tkalich and Chan (2002). The oil entrainment rate from a surface slick to the water column is computed along with the intrusion depth of the droplets. Two different parametrisations have been implemented in OSERIT to simulate the horizontal surface spreading of oil over the water surface mainly due to the combined effect of gravity, inertia, interfacial tension and viscosity. The first method is based on Fay (1970) and approaches the spreading due to gravity-viscous forces by computing random velocities in the range of velocities that are assumed proportional to the diffusion coefficients (Garcia *et al.* 1999). The second method, also based on Fay (1970), considers the oil slick as an ellipse which elongates along the wind direction (Lehr *et al.*, 1984). The surface horizontal spreading stops when the terminal thickness is reached based on data from McAuliffe (1987), as done in French (2003).

3.2 Hydro-meteorological forcing

OSERIT offers the availability of various hydro-meteorological forcing. Currently, two forcing data sets have been implemented. The first one comes from MUMM forecasts, and the second one from MyOcean.

3.3 Future model developments

The model is currently undergoing further development, and soon will have new modules to compute oil evaporation and sedimentation be implemented in OSERIT. An Eulerian module is also being developed. Once validated the Eulerian module will be coupled one-way to the Lagrangian one. The Eulerian module will be used to simulate

the evolution of oil dispersed into the water column while the Lagrangian one will be used to simulated the drift of non-dispersed oil at the sea surface and in the water column.

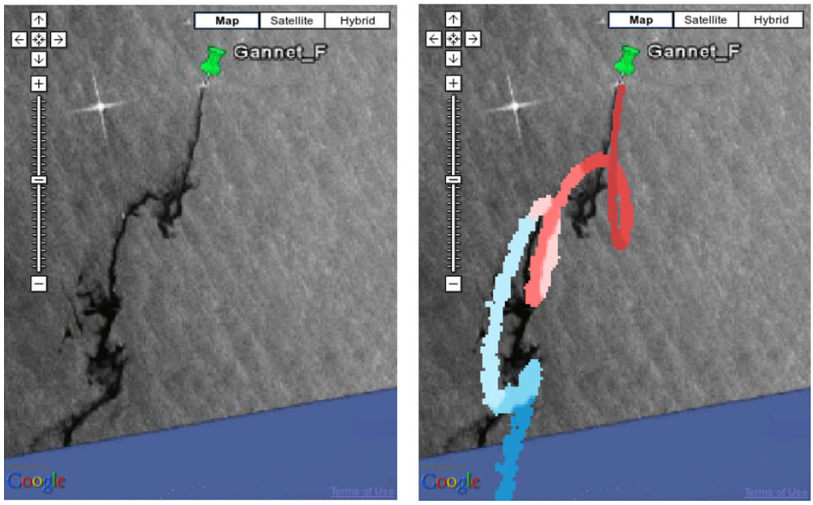

Figure 2 Satellite image taken on 19 August 2011 (5:31 UTC) by the COSMO SkyMed System (left) and the corresponding model estimation of the oil slick position superimposed on the same satellite image (right). The colours on the right panel represent time intervals of 6 hours during which the oil has been released. The dark red part of the slick represents oil that has been released during the 6 hours before the satellite image was taken while the dark blue part of the slick represents oil that has been released between 36 and 48 hours before the satellite image was taken. The Gannet F platform is represented by green drawing pin.

4. Test case

To evaluate the current version of the OSERIT model, the model has been set up to simulate a real test case: the Gannet incident. Model results have been compared to observations.

4.1 The Gannet incident

On 10 August 2011, a subsea structure linking the Gannet F wells to the main platform broke, about 180 km east of Aberdeen (Scotland). Oil leaked until 19 August giving a total oil loss of 218 tons, as estimated by Shell (~1300 barrels). Slicks were observed as far as 30 km from the leak. Most of the oil has been naturally dispersed offshore and did not reach the Scottish coasts. No significant environmental impacts have been reported.

4.2 Observations

After the incident, e-GEOS made some satellite images of the slick available (www.e-geos.it/news/11-08-23-gannet/index.html). These images were taken from radar sensors mounted on satellites of the COSMO-SkyMed system. SITREPs from the UK Maritime and Coastguard Agency were also made available to us through the Bonn Agreement parties.

4.3 Experimental set up

The Gannet incident occurred just out of the domain covered by MUMM's models. Therefore, the model was set up to use the hourly surface ocean current forecast from MyOcean NWS MFC. The 10 m wind forecasts were taken from UK Met-Office forecasts. No wave forecasts was available to us at that time.

The model was set up to simulate the surface drift due to wind and water current, horizontal diffusion and natural vertical dispersion. Due to the lack of information on 3D water currents and sea state, the simulation has been limited to 2D drift (instead of 3D), and the entrainment rate of surface oil into the water column has been taken as constant.

The model release scenario was as follows: the leak was assumed to be continuous and was represented by the surface release of 30 Lagrangian particles every 10 minutes at the Gannet F position.

4.4 Results and discussion

The reports from the UK Maritime and Coastal Agency state that the surveillance flight on 19 August 2011, 7:40 UTC observed a surface oil slick that was 24.5 km long and 0.05 km wide. The satellite image taken earlier the same day (5:31 UTC) by the COSMO SkyMed System shows a continuous slick at least 16 km long, starting at Gannet F and going South (Figure 2, left panel). Note that the satellite image only covers one part of the sea area that is covered by oil.

The first portion of the observed oil slick elongates from the leak location towards SSW over 6.5 km, and then shifts westwards. At the turning point, it presents a ring-shaped oil-covered area. The second portion elongates over ~4 km towards the south and ends in a disk shape. The third portion elongates toward the SSW and includes an oil-covered area of ~2 km radius. Finally, the slick elongates towards the SW until it reaches the limit of the area covered by the satellite.

The OSERIT model simulates the position of the observed oil slick well (Figure 2, right panel). It captures the general shape, orientation and dimensions of the slick and is also able to capture more specific features of the slick such as the ring-shaped oil-covered area at the end of the first portion of the slick. Colours on Figure 2 tell how long the oil has been released before the satellite picture was taken. Each colour corresponds to a 6-hour time frame. So the dark red part of the slick represents oil that has been released 0–6 hours before the satellite image was taken, while the dark blue represents the oil that has been released about 36–42 hours before the satellite picture. These colours clearly show how tides affect the drift and therefore the shape of the slick. It appears that the larger oil-covered areas follow turning points in the tidal regime. Note that the model slightly overestimates the amplitude of the slick movement due to ocean tidal current. This might be due to an overestimation of the amplitude of tidal currents in the ocean forcing. From time to time, a small shift can be noticed in the position of the simulated slick compared to the position of the observed slick. The shift is sometimes to the east, sometimes to the west. It usually remains under 1 km and never exceeds 2 km. This shift in the position can probably be explained by the low resolution of the wind forcing dataset or by the fact that the simulation does not include the Stokes drift (since no wave observations were available at the time the proceeding was written).

5. Conclusion

The research project OSERIT aims at developing an integrated tool that gathers relevant, scientific-based information provided by operational oceanography to support the decision processes of the Belgian coastguards in case of emergencies such as oil pollution of the sea. This tool is designed as a one-stop shop service to access currents, temperature, salinity, wind and waves forecast and allows launching, visualising and downloading both simple and complex 2D and 3D drift simulations. Based on state-of-the-art techniques, special care has been taken to meet the end-users requirement for tool quickness, reliability, user-friendliness, accessibility and inherent quality. The inherent quality of the tool has been illustrated using the Gannet incident. The drift model is able to capture the general features of the slick (shape, orientation and dimensions) as well as more specific features (ring-shaped oil-covered area…).

In September 2012, OSERIT will be at the heart of the next upgrade of the operational service MUMM delivers to the Belgian Coastguard Agencies.

Acknowledgements

OSERIT development is funded by the Belgian Federal Science Policy Office (BELSPO) through the contract SD/NS/10A (programme “Science for a Sustainable Development”). The Gannet study case was performed in the framework of FP7 MyOcean WP18 (Grant FP7-SPACE-2007-1-CT-218812-MYOCEAN). The authors also acknowledge Neil Chapman from the UK Maritime and Coastguard Agency and John Siddorn from the UK Met Office for their grateful help in collecting information on the Gannet incident.

References

Douvere F., F. Maes, A. Vanhulle and J. Schrijvers (2007). The role of marine spatial planning in sea use management: The Belgian case. Marine Policy, 31, 182–191, doi:10.1016/j.marpol.2006.07.003.

Fay (1970). Physical processes in the spread of oil on water surface. Proceedings of Conference on Prevention and Control of Oil Spills, API, Washington D.C., pp. 463–467.

French McCay, D. (2003). Development and application of damage assessment modeling: example assessment for the North Cape oil spill. Marine Pollution Bulletin, 47, 341–359.

Garcia-Martinez, R. and H. Flores-Tovar (1999). Computer modeling of oil spill trajectories with a high accuracy method. Spill Science and Technology Bulletin. Vol. 5 (5/6), 323–330.

Lagring, R., G. de Montpellier, T. Jacques, W. Van Roy and R. Schallier (2012). Twenty years of Belgian North Sea aerial surveillance: a quantitative analysis of results confirms effectiveness of international oil pollution legislation. Marine Pollution Bulletin, in press, doi:10.1016/j.marpolbul.2011.11.029.

Lehr, W.J., R.J. Fraga, M.S. Belen, and H.M. Cekirge (1984). A new technique to estimate initial spill size using a modified Fay-type spreading formula. Marine Pollution Bulletin, 15, 326–329.

Lehr, W.J. (1996). Progress in oil spread modeling. In: Proceedings of the 19th Arctic and Marine Oil Spill Program (AMOP) Technical Seminar. Environment Canada, 889–894.

Le Roy, D. and F. Maes (2006). Risk Analysis of marine activities in the Belgian part of the North Sea: "RAMA", report D/2006/1191/37, Belspo, 203p (Research program SPSD II: "Scientific support plan for a sustainable development policy").

Luyten, P. (2011). COHERENS — A Coupled Hydrodynamical-Ecological Model for Regional and Shelf Seas: User Documentation. Version 2.0. RBINS-MUMM Report, Royal Belgian Institute of Natural Sciences, 1202 pp.

McAuliffe, C.D. (1987). Organism exposure to volatile/soluble hydrocarbons from crude oil spills - a field and laboratory comparison. Proceedings, 1987 Oil Spill Conference, Baltimore, Maryland, USA, 275–288.

Tkalich, P., and E.S. Chan (2002). Vertical mixing of oil droplets by breaking waves. Marine Pollution Bulletin, 44, 1219–1229.

van Iperen, W.H. and C. van der Tak (2011). VEILIGHEIDSSTUDIE OFFSHORE WINDPARK "North Sea Power", MARIN, report 23307.620/B3, 84p.

Wang, S.D., Y.M. Shen, Y.K. Guo, and J. Tang (2008). Three-dimensional numerical simulation for transport of oil spills in seas. Ocean Engineering, 35, 503–510.

Marine Information Services associated with HF radar observing networks

Andrés Alonso-Martirena*[1], Jorge Sánchez[1], Vicente Fernández[1], Chad Whelan[2], Laura Pederson[2], Anton Kjelaas[3], Donald Barrick[2], and Enrique Álvarez Fanjul[4]

[1]*Qualitas Remos S.L.*
[2]*Codar Ocean Sensors Ltd.*
[3]*CodarNor A.S.*
[4]*Puertos del Estado*

Abstract

The expansion of ocean observing networks, both in-situ platforms (buoys, mareographs, etc.) and remote observing technologies, such as coastal HF radars and satellites, together with the increasing ocean modelling capabilities are resulting in a huge growth of data and information on the ocean.

Marine information services associated with HF Radar are experiencing a strong increase in recent years. This paper presents firstly a review of the latest significant advances regarding the technology itself, which have contributed to make its integration into operational ocean observing networks possible; secondly, a snapshot of the recent development that HF Radar observing networks are undergoing in the Iberian Peninsula. We focus then on the information services based on HF Radar data and additional measured and modelled data that are currently being provided.

Keywords: HF radar, oil spill, PORTUS, ocean remote sensing, SeaSonde

1. Key advances around SeaSonde HF Radar technology

1.1 Large antenna arrays evolve into a single antenna solution

One critical issue when planning an HF radar installation is to minimise land occupation in order to keep both ecological and visual impacts to the feasible minimum. This requirement is an absolute must if considering installations on oil platforms, small islands or piers.

The first HF radar to demonstrate and validate current and wave measurement capability was built between 1969–1973 in a program led by DARPA and NOAA, in cooperation with Scripps Institution of Oceanography and Stanford University. Designed by Donald Barrick (nowadays President of CODAR Ocean Sensors, Ltd.) at NOAA Environmental Research Laboratories (ERL), the radar with its original 500-meter long phased-array antenna was bulky and inconvenient for deployment, but proved the point that HF radar is a viable tool for measurement of ocean current and wave parameters.

In 1972, management at NOAA decided to develop an alternative to the large, costly phased-array technology for current and wave mapping. This led to the compact

* Corresponding author, email: andres.alonso-martirena@qualitasremos.com

CODAR approach that replaces large phased arrays with single mast direction-finding (DF) antenna units.

The technology has evolved from the original 1972 CODAR radar and is now the SeaSonde®, for which the latest version has all transmit and receive elements colocated atop a single mast and occupies as little as one square meter for its deployment.

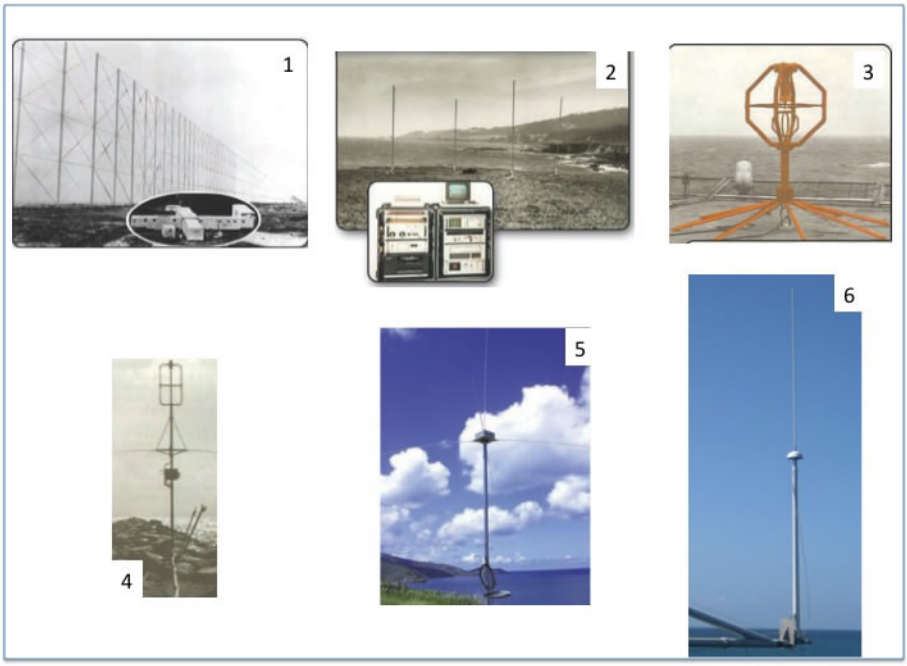

Figure 1 Current mapping HF radar antenna evolution in the last 40 years:
#1: 500-m long phased array radar at San Clemente Island, circa 1972. Smaller inset image shows the trailers used to house the radar electronics and computer system.
#2: the first NOAA-built CODAR antenna system consisting of a square monopole receive array with direction-finding closed-form solutions for bearing. Smaller inset image shows the electronics and DEC PDP-11/23 computer and tape drives used for near-real-time processing and archival.
#3: The first crossed-loop CODAR antenna, built of copper.
#4: a later version of crossed-loop CODAR antenna, built of PVC.
#5: Successor to CODAR, the SeaSonde.
#6: Latest SeaSonde antenna system with all transmit and receive elements colocated atop a single mast.

1.2 Frequency sharing capability by multiple radars

Because the MF/HF/VHF bands have not been used for most radar applications up to now, there have been no frequency bands designated for radar below 430 MHz by the ITU (International Telecommunications Union). Thus, users must apply for “secondary licenses”, meaning they cannot interfere with “primary” users. To avoid interference, each user would like a frequency separate from all other HF radar users (as well as from the conventional radio users of these bands). The problem is exacerbated by the wide signal bandwidths needed for radar operation in contrast with radio communications. To

achieve a 1 km range cell, one needs 150 kHz bandwidth, for example. Typical radio channels occupy 5 kHz bandwidth or less. This means that one radar user monopolises 30 potential radio channels. Finally, a given fixed bandwidth (like 150 kHz) occupies a much larger fractional bandwidth percentage-wise at HF (e.g., 5 MHz) than at microwave (e.g., 5 GHz). All of this makes it clear that each new user will not receive a separate frequency for his own use; multiple users must share the same frequency in a manner that does not cause mutual interference.

CODAR invented and patented a methodology based on GPS timing along with FMCW (frequency-modulated continuous wave) gated signals to control the exact sweep time of multiple transmitters down to nanoseconds so all transmitters can occupy the exact same frequency channel (Barrick, 2008). This enables a single receive antenna to process unambiguously scattered signals from multiple transmitters as described in the next section. The signals from various transmitters are identified and separated in the demodulation phase.

1.3 Multistatic processing for the enhancement of coverage and data quality

The normal mode of radar operation is backscatter (or monostatic). In this mode, transmitter and receiver are collocated, sometimes sharing the same antenna, while in others the transmit and receive antennas may be separated a small distance. Together with the patented frequency sharing method explained in the previous section, CODAR also came up with an inexpensive solution that allowed bistatic operation (Barrick, 2008). This enables a single receive antenna to process unambiguously scattered signals from multiple transmitters. Thus not only mutual interferences are eliminated, but the use of other station's signals is possible. In fact, a single coastal station can simultaneously operate in a backscatter mode (using its own transmitted signal’s sea echoes), but also using the echoes from several adjacent coastal SeaSondes transmissions. This gives rise to the term multistatic instead of bistatic.

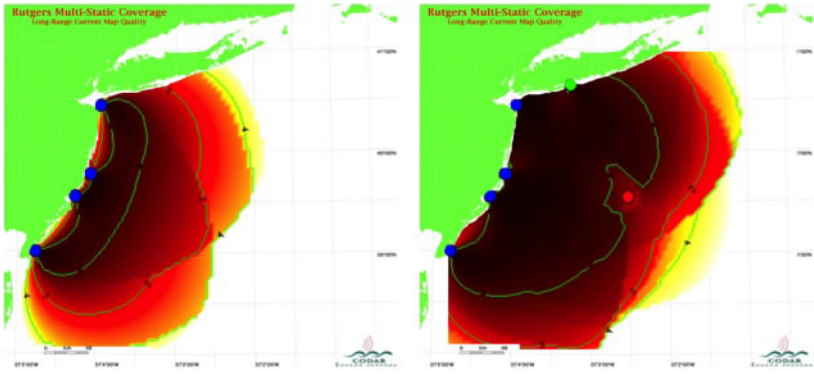

Figure 2 Left: Coverage and quality of four backscatter Long-Range SeaSondes off the coast of New Jersey. Dark red indicates best quality of total vectors; yellow going to white indicates poor or no coverage. Right: Example of 50% coverage extension using an additional multistatic transmitter on a buoy (red point) by adding a transmitter on a buoy 150 km offshore, operating multistatically with the four SeaSondes.

There are two advantages of extending an existing backscatter network to multi-static:

- It extends the area of coverage
- It adds redundancy in the backscatter region, thereby increasing current measurement accuracy and robustness.

2. Iberian Peninsula SeaSonde HF Radar network

In 2002, the Prestige oil spill disaster off the northwestern coast of Spain acted as a wake up call highlighting the importance of preparing for such a crisis. It led to Spanish Institutions prioritising the improvement of maritime protection related activities, operational oceanography and oil spill response preparedness.

Back in 2005 a cooperation agreement aimed to increase marine safety and efficiency in navigation and harbour management was signed between Puertos del Estado, the General Directorate of the Merchant Marine of the Spanish Ministry of Public Works and the Galician Government (Xunta de Galicia). One of the primary focuses of the agreement involved the development of advanced ocean observing infrastructures and, as an essential element, the installation of an HF coastal Radar network.

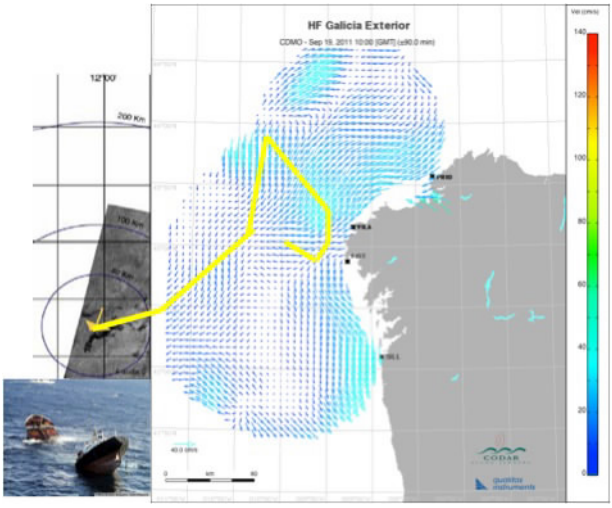

Figure 3 The yellow line represents the trajectory followed by the Prestige ship. The accident occurred inside the radar coverage area but when the ship finally sank 6 days later it was just outside the coverage area.

A successful initial installation led by Puertos del Estado was the beginning of HF radar implementation in the Iberian Peninsula that will result in 20 radars by the end of 2012. We introduce below some of these systems together with their associated operational services and research areas.

2.1 Galicia HF radar network

Today, in 2011, the Galician HF radar network is made up of four SeaSonde long range 5 MHz radars that provide real time surface currents and wave information along the

coast from Silleiro in the south close to the boarder to Portugal to Prior in the North (280 km or 75% of Galicia coast) and with a range of up to 200 km from the coast. The operational-scientific exploitation of data is carried out by to Puertos del Estado and the Galician Regional Government. Puertos del Estado runs an online validation and quality control of the radar observations from the very initial project layout and system start up. In addition to the long range HF Radar network, the Physical Oceanography Group of University of Vigo in Galicia (GOFUVI) has implemented a high-resolution HF radar system in the Ría de Vigo.

The areas of application of Galicia HF radar collected data are very wide. Real-time surface currents information is openly available online with a special focus on its use by Spanish Port Authorities in order to improve safety in navigation. The use of these data has also resulted in a continuous improvement of oil spill trajectory forecast and backtracking models (Abascal *et al*., 2009) and the increase in the quality of both ocean models and observations in the area. As a principal result of all these efforts over the years, Galicia has become one of the most advanced science and knowledge development platforms concerning HF Radar technology in Europe.

2.2 Portugal HF radar network

The first HF radar network in Portugal was deployed in the Sines area by the Hydrographic Institute (IH is the Portuguese Navy's Laboratory for Ocean Sciences), which is a principal operational oceanography institution in Portugal. The system consists of 2 standard-range SeaSonde radars with a spatial resolution of about 1 km. This system is part of the SIMOC (Operational Surface Currents Monitoring System) project. The Sines area, positioned halfway between Lisbon and Algarve, was chosen as the first permanent HF Radar deployment area since it is one of the most sensitive locations of the Portuguese coast, having a major petrochemical harbour, and directly to the south, a natural reserve (Natural Park of the Southwest of Alentejo). Environmental monitoring by means of HF radar in this area is understood as a preventive action to improve safety along one of the heaviest ship traffic corridors in the world. The data series obtained will also contribute to the IH modelling activities in currents and oil spill models.

The Portuguese network will be expanded inside the period 2011 to 2012 by the TRADE initiative (Trans-regional RADars for Environmental applications that is being implemented in partnership by the Spanish Puertos del Estado, the Portuguese Hydrographic Institute and the Cadiz University) along the Iberian Algarve and Andalucía coasts including as part of it also the monitoring of the Gibraltar Strait. Five HF radars will be installed along the coast covering a large part of the area between Cape San Vicente and Gibraltar Strait. This sensitive area, which has several natural parks along the coast and is one important touristic destination in Europe, is the scenario of one of the world's largest vessel concentration and traffic areas in the world. The TRADE project is aimed to contribute significantly to the ocean observing infrastructure required by the region for safe navigation and, at the same time, to help the decision makers in order to improve the coastal management of this area. It is envisioned that additional scientific groups join the original TRADE partners creating a strong permanent environmental applications oriented knowledge base and work team around coastal HF Radar.

2.3 Additional projects and ongoing initiatives

The Basque Government in cooperation with AZTI (a Technological Centre specialised in Marine and Food Research) along the Gulf of Biscay, SOCIB (a Coastal Ocean Observing and Forecasting System located in the Balearic Islands) in the Ibiza Channel and the Spanish Ministry of Environment, Rural and Marine Affairs in the Ebro River Delta have also implemented multipurpose ocean observing networks giving thus life to the largest HF Radar observing infrastructure in Europe.

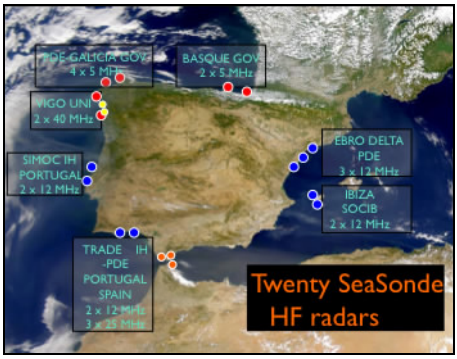

Figure 4 Iberian multipurpose HF Radar network.

3. Marine Information Services and Tools related to HF Radar

3.1 Rapid deployable HF Radar currents information

In January 2009, The Norwegian Clean Seas Association for Operating Companies (NOFO) and the Norwegian Coastal Administration (NCA) announced 18 defined technological challenges concerning oil spill response, seeking new ideas and proposals for solutions. Almost 180 ideas were submitted by private enterprises in Norway and abroad. Following rounds of evaluations, 20 projects were approved with funding from NOFO. “Rapid Deployable HF Radar for Emergency Spill Operations” was one of the most successful projects among these 20. The Norwegian company CODARNOR lead the project in which CODAR Ocean Sensors, the Norwegian Meteorological Institute (met.no) and QUALITAS were partners. The objectives that were reached in this project were:

- To develop a Mobile SeaSonde HF radar unit that can be rapidly deployed to the coast of Norway to aid in effective and efficient oil spill response.
- To develop of a data service that provides high quality SeaSonde-derived 2-D current fields using OMA (Open Mode Analysis) technique (Kaplan and Leiken, 2007) to The Norwegian Meteorological Institute in near real time for spill drift model input and operations planning.
- To demonstrate that SeaSonde-derived 2-D current fields can improve operational oil spill drift model results.

By supplementing models with real time data, calculation of oil drift trajectory and spreading in coastal waters were significantly improved. This is more and more important as oil exploration and production activities move closer to the Norwegian

coast. As a future extension, it is envisioned that forecasters from Norwegian Meteorological Office will be able to use the OMA surface currents to blend with modelled currents to improve their operational 24h emergency oil spill service.

3.2 Tsunami Detection

It was over 32 years ago that Barrick first described how an approaching tsunami could be measured from its HF radar-observed current pattern in a 1979 Remote Sensing of Environment article (Barrick, 1979). With few HF radars operating at that time and sizable tsunamis being a rare or infrequent occurrence, this research went largely unnoticed for many years. Following the 2004 Indian Ocean tsunami, Lipa and Barrick revisited the topic by developing a tsunami pattern recognition algorithm that worked against the ambient background flows. The methods described in their 2006 paper (Lipa *et al*., 2006) formed the basis for the first and only commercial HF radar tsunami detection software package available on the market. The radar measures the velocity of the particle-like Bragg waves arrayed over the surface of the tsunami wave. While the tsunami height increases slowly as depth decreases, the particle/Bragg velocity increases much faster: as the inverse three-quarters power of the depth. Therefore as the water gets shallower, the velocity seen by the radar begins to stand out from the background circulation in that region.

The last Japan catastrophic earthquake and tsunami confirmed the validity of these methods. Two SeaSondes installed in Hokkaido (Japan) observed the Tsunami signature and nine hours later SeaSondes installed in the West Coast of the Continental U.S. could also identify this signature.

3.3 PORTUS Marine Information System

The PORTUS concept was initially developed by Puertos del Estado as the Oceanographic Information System to manage and make observations (more than 200 measurement devices) as well as forecasting information available to its stakeholders and the general public.

PORTUS is a web-based Marine Information System. Its main aim is to make all available marine data & information easily available through a single geographical interface to favour its use and integration.

Some of PORTUS features are:

- Flexible Marine Information System with special focus on SeaSonde HF Radar
- Friendly multisource data visualisation interface
- Secure data storage and management (historic, real-time, forecast)
- Multilayer web based secured access through Internet
- Specialised tools to take the most out of HF Radar (QA/QC, data fusion and forecast products…)
- Powerful export capabilities in a wide range of standard and non-standard formats and data serving to other systems

Today multiple added value advanced applications related to coastal HF Radar operation are nested in this tool providing daily benefits to a large variety of interested users and society in general.

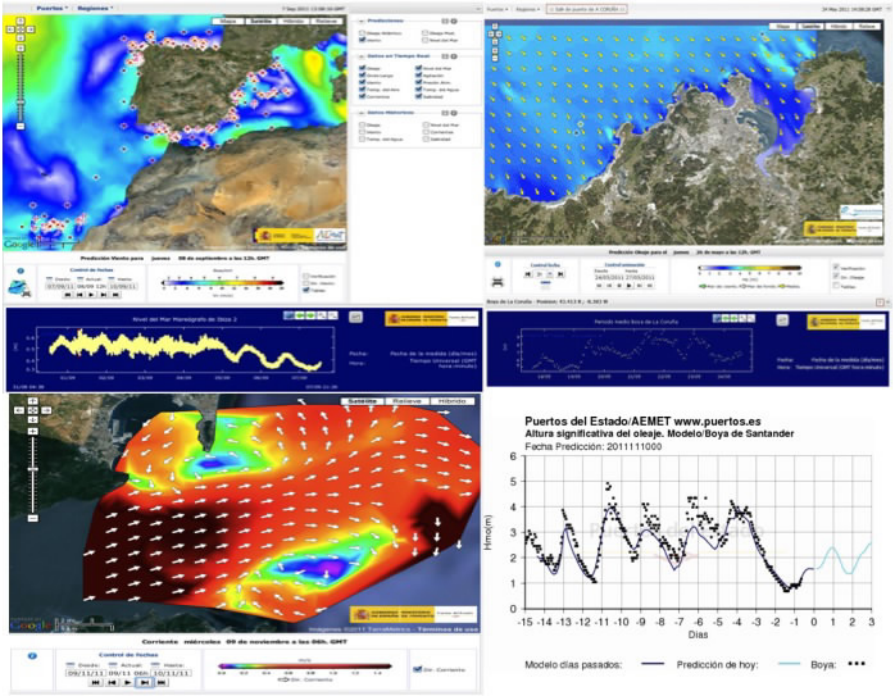

Figure 5 Puertos del Estado general Oceanographic Information System. (www.puertos.es)

References

Barrick, D.E. (2008). 30 years of CMTC and CODAR, Proceedings of IEE/EOES/ CMTC 9th Working Conference on Current Measurement Technology.

Abascal, A.J., S. Castanedo, R. Medina, I.J. Losada, and E. Álvarez Fanjul (2009). Application of HF radar currents to oil spill modelling. Marine Pollution Bulletin, 58, 238–248.

Kaplan D.M., F. Leiken (2007). Spatial interpolation and filtering of surface current data based on open-boundary modal analysis. Journal of Geophysical Research, vol. 112, C12007, 20 pp.

Whelan, C.W., D.E. Barrick, P.M. Lilleboe, Ø. Breivik, A. Kjelaas, V. Fernandez, and A. Alonso-Martirena (2010). Rapid deployable HF RADAR for Norwegian emergency spill operations. Proceedings of Oceans 2010 Sydney IEE Conference.

Barrick, D.E. (1979). A coastal radar system for tsunami warning. Remote Sensing of the Environment, 8, 353–358.

Lipa, B.J. D.E. Barrick, J. Bourg, and B.L. Nyden (2006). HF radar detection of tsunamis. Journal of Oceanography, 2, 705–716.

Real time in-situ data management system for EuroGOOS: A ROOSs–MyOcean joint effort

Sylvie Pouliquen*[1], Thierry Carval[1],Thomas Loubrieu[1], Karina von Schuckmann[2], Henning Wehde[3], Lid Sjur Ringheim[3],Thomas Hammarklint[4], Anders Hartman[4], Kai Soeje[5], Tobias Gies[5], Marta De Alfonso[6], Leonidas Perivoliotis[7], Dimitris Kassis[7],Veselka Marinova[8]

[1]*IFREMER, Brest, France*
[2]*CNRS, Brest, France*
[3]*IMR, Bergen, Norway*
[4]*SHMI, Norrköping, Sweden*
[5]*BSH, Hamburg, Germany*
[6]*Puertos Del Estado, Madrid, Spain*
[7]*HCMR, Athens, Greece*
[8]*IOBAS, Varna, Bulgaria*

Abstract

MyOcean is the implementation project of the GMES Marine Core Service to develop the first concerted and integrated pan-European capacity for Ocean Monitoring and Forecasting. Within this project, the in-situ Thematic Assembly Centre (in-situ TAC, INS-TAC) of MyOcean is a distributed service integrating data from different sources for operational oceanography needs. The MyOcean in-situ TAC collects and carries out quality control in a homogeneous manner on data from outside MyOcean data providers, especially EuroGOOS partners in Europe, to fit the needs of internal and external users. It provides access to integrated datasets of core parameters for initialisation, forcing, assimilation and validation of ocean numerical models. Since the primary objective of MyOcean is to forecast ocean state, the initial focus is on observations from automatic observatories at sea (e.g. floats, buoys, gliders, ferrybox, drifters, SOOP) which transmit to the shore in real-time. The second objective is to set up a system for re-analysis purposes that integrates data over the past 20 years. The global and regional portals set up by the INS-TAC have been extended by the EuroGOOS ROOSs (Arctic ROOS, BOOS, NOOS, IBI-ROOS, MOON together with Black Sea GOOS) to integrate additional parameters important for downstream and national applications.

Keywords: ocean database, in-situ data, operational oceanography, Europe

1. Introduction

In the past decade, the nature of requirements by national and international agencies have changed: they want to know or estimate what the future of the earth will look like and what the impact will be on their territories due to climate change, ocean health monitoring (e.g. Marine Strategy Framework Directive) and fisheries assessment, but they cannot pay the full bill for the data acquisition. Therefore they are pushing, and

* Corresponding author, email: sylvie.pouliquen@ifremer.fr

nowadays more often imposing, a change in data policy and a move towards increased data sharing, in which data acquired with public funds should be freely available to the community.

Moreover, the nature of science itself has changed. Investigators and research funding agencies are looking for context, impacts, and synthesis, rather than just focusing on individual, well-defined processes. Most scientists need the data collected by others as well as their own. They cannot do their work using only the data they have collected by themselves.

The growth of operational oceanographic services, based on downscaling of global model results, is really important. These are in demand by users especially for real/near real-time data such as operational meteorology has been providing for a long time.

The scope of the EuroGOOS ROOSs (Regional Operational Oceanographic Systems) is wide, from observing system operation and maintenance, research activities, ocean modelling and forecasting to the development of downstream services for end users. The needs of the ROOSs in terms of data management are partially addressed by the on-going development carried on within GMES, SeaDataNet and other EU initiatives. It is essential to improve the quantity, quality and accessibility of marine information for decision-making and to open up new economic opportunities in the marine and maritime sectors of Europe, for the benefit of European citizens and the global community.

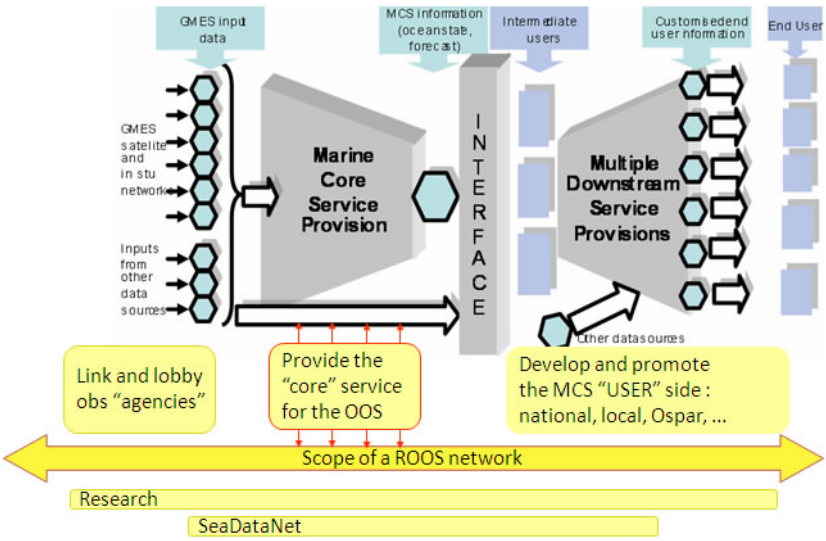

Figure 1 EuroGOOS ROOSs and GMES.

2. Requirements from users

In "The science base of EuroGOOS" (Prandle *et al*., 1998) some limitations related to data exchange were highlighted. The situation has improved but the following statements are still relevant and should be seen as priority actions not only in Europe but around the world.

- *Lack of international infrastructure for operational oceanographic data gathering, transmission, and products, (e.g. as adopted in World Weather Watch), and consequently lack of common standards.* This is still true in general, although the situation has improved a lot in the past 10 years in the physical oceanographic domain. Experience within the GODAE (Global Ocean Data Assimilation Experiment), Argo and GHRSST (Global High Resolution Sea Surface Temperature) programmes have shown that it was possible to reach consensus on common standards (on issues such as data formats, real-time and delayed mode quality control and data distribution). In some domains, such as bio-geochemistry, there is still a long way to go.
- *Lack of clear right or duty to collect and transmit real-time data.* Once again in the past ten years we have seen the concept of "portals" emerging with the duty to serve data to users in real-time: Salto/DUACS for altimetry, Medspiration/GHRSST for SST, Argo and GOSUD (Global Ocean Surface Underway Data) Global Data centres and JCOMMOPS are examples that exist nowadays. It has been shown that sharing data rapidly is not a burden for scientists. On the contrary, it is beneficial as problems are detected more rapidly by comparison with nearby measurements and collaboration to set up appropriate observing system facilitated.
- *Lack of proper design of a services infrastructure, using, for example, multiple data inputs such as wind, waves, and currents, to generate predictions of oil spill movements.* With the GMES (Global Monitoring for Environment and Security) initiative in Europe we have seen a demonstration of the capability to build end-to-end services for users. Some projects like Mersea/MyOcean, Marcoast or PolarView are consolidating the systems that will be needed to be sustained in the future.
- *Imbalance between monitoring (measurement) technology and capacity for post-processing data and subsequent real time use of numerical models.* Money and man power have been allocated to compile homogeneous datasets both at national and international level. This is illustrated by the French Coriolis project, the EU project SeaDataNet and DMAC (Data Management and Communications) in the USA. This effort should be sustained in the future.

In the past decade progress has been driven not only by applications such as Operational Oceanography but also by a fundamental change in cultural behaviour among scientists. This important change started in the satellite community where it was possible to bring together data from missions managed by different countries (altimetry from NASA and ESA, SST from most space agencies) but also in the in-situ world where Argo has been a pilot experience for the other JCOMM (WMO-IOC Joint Technical Commission for Oceanography and Marine Meteorology) networks (Belbeoch *et al*., 2010).

As a summary what a user requires is:

- To know what data is available, to be able to collaborate with other institutes and improve the observation strategy and coordination
- To access the data easily – to be able to use the data without having to consider who processed them as it will be known to have been done in a coherent way and there is access to enough metadata to understand what processing has been carried out.

3. The EuroGOOS strategy

In 2008 the DATAMEQ (DATA Management Exchange and Quality) working group, composed of data managers from the EuroGOOS, ROOSs and EU projects addressing data management issues (Euro-Argo, EuroSites, SeaDataNet, ICES, Ferrybox, INSPIRE, ECOOP, Satellite), issued a set of recommendations (Pouliquen *et al*., 2008) that was endorsed by the EuroGOOS members at the annual EuroGOOS meeting in 2008. It was agreed that the ROOSs should set up regional portals extending what had been benchmarked in ECOOP and consolidated/certified in MyOcean as a basic infrastructure for EuroGOOS Data Exchange. It was also recommended that these portals should use standard vocabularies developed within SeaDataNet and use the OceanSites NetCDF format for data distribution. It was agreed that the ROOSs should maintain regional catalogues of the operational observing systems that should be used to update a European catalogue more easily in a semi-automatic way. Finally it was agreed that a set of quality control procedures applicable in near real time automatically should be assembled by the DATAMEQ working group and used by the EuroGOOS members as a minimum level of quality control processing.

Setting up such a system will reduce the duplication of efforts among the agencies, improve the quality and reduce the cost of the observation distribution, improve access to the observations and therefore increase the benefit of the observation "observed once used multiple". It will necessitate the establishment of key partnerships to increase data availability inside each region making it more sustainable over time and allowing the development of downstream services.

It necessitates agreement on common data policy enabling open and free access to data and agreement on common standards and protocols to share data between institutes.

4. The MyOcean in-situ Thematic Assembly Centre (INS-TAC)

MyOcean aims to provide a sustainable service for Ocean Monitoring and Forecasting validated and commissioned by users. The MyOcean information includes observations, analysis, reanalysis and forecasts describing the physical state of the ocean and its primary biogeochemical parameters. It also contributes to research on climate by providing long time-series of re-analysed parameters. It started in 2009 for 3 years and will continue for an additional 2.5 years through the MyOcean II project that started in April 2012.

Within this project, the in-situ Thematic Assembly Centre of MyOcean is a distributed service integrating data from different sources for operational oceanography needs. The MyOcean in-situ TAC collects and carries out quality control in a homogeneous manner on data from outside MyOcean data providers (national and international networks), to fit the needs of internal and external users. It provides access to integrated datasets of core parameters for initialisation, forcing, assimilation and validation of ocean numerical models which are used for forecasting, analyses (nowcast) and re-analysis (hindcast) of ocean conditions. Since the primary objective of MyOcean is to forecast ocean state, the initial focus is on observations from automatic observatories at sea (e.g. floats, buoys, gliders, ferryboxes, drifters, SOOP) which are transmitted in real-time to the shore at global (V0 2009) and regional (V1 mid-2011) scales both for physical and biogeo-

chemical parameters The second objective is to set up a system for re-analysis purposes that requires products integrated over the past 25 years for temperature and salinity parameters. This will be the main challenge of MyOcean II for the European seas.

Since the elaboration of the proposal, the MyOcean in-situ TAC has been designed to rely on the EuroGOOS ROOSs with regional coordination endorsed by partners from the ROOSs and on a global component based on the Coriolis data centre that acts as a GDAC (Global Data Centre) for some of the JCOMM networks.

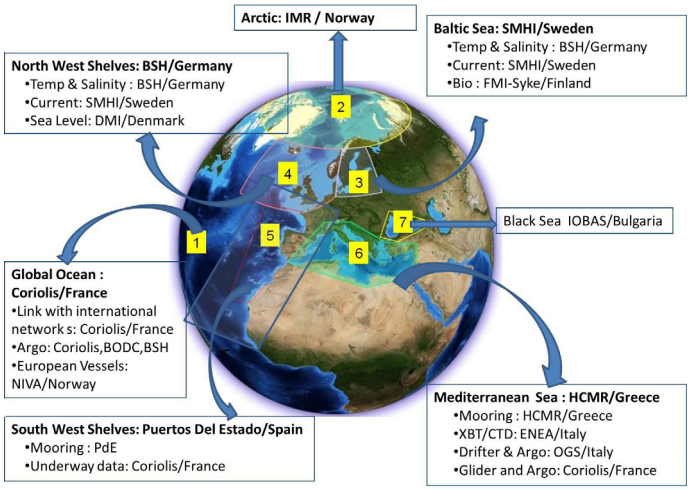

Figure 2 The in-situ TAC global and regional components. Institute responsibilities inside each component.

The MyOcean in-situ TAC is focused on a limited number of parameters:

- *Temperature and salinity*: global and regional, produced in real time (all components) and delayed mode (global, as prototype in other regions)
- *Currents*: global and regional, produced in real time (global, North West Shelves, Mediterranean Sea, Baltic)
- *Sea level*: regional, produced in real time (South West Shelves, North West Shelves, Baltic)
- *Biogeochemical (chlorophyll, oxygen and nutrients)*: global and regional, produced in real time (all components)

The in-situ TAC architecture is decentralised. However, the quality of the products delivered to users must be equivalent wherever the data are processed (Pouliquen *et al*., 2010). The different functions implemented by the global and regional components of the in-situ TAC are summarised in Figure 3.

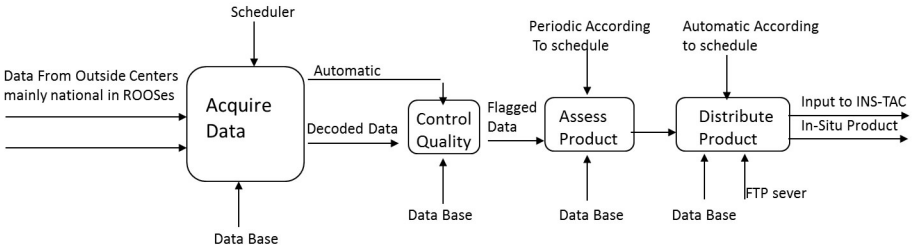

Figure 3 Functions to be implemented by an in-situ TAC component.

Each region has implemented 4 core functions:

- *Acquisition*: Gather data available on international networks or though collaboration with regional partners
- *Quality control*: apply automatic quality controls that have been agreed at the in-situ TAC level. These procedures are defined by parameter, elaborated in coherence with international agreement, in particular SeaDataNet, and documented in MyOcean catalogue
- *Product Assessment*: Assess the consistency of the data over a period of time and an area to detect data not coherent with their neighbours but that could not be detected by automatic quality control (QC). This function has a level of complexity in its implementation which is clearly different from the other three as it is highly reliant on scientific expertise
- *Product distribution*: make the data available within MyOcean and to the external users

Each region has organised the activities according to the expertise and background in data management for operational oceanography.

- The 4 functions are implemented in one institute per region (e.g.: Arctic, Black Sea)
- The 3 functions (Acquisition, QC and Assessment) are implemented by parameter (Baltic and NWS) and only Distribution is centralised
- Acquisition and QC is done by platforms (Mediterranean Sea, SWS and Global), one institute taking care of the assessment and distribution is centralised.

The global component of the in-situ TAC (www.coriolis.eu.org/Data-Services-Products/MyOcean-In-Situ-TAC) collects the data from the regional components and integrates them into the global product acting as a backup of the regional centres. The main distribution channel for the INS-TAC is FTP. The Open Geospatial Consortium (OGC) viewing service (WMS) and OPeNDAP access are under development and is gradually being set up in 2011–2012. (Pouliquen *et al*., 2011).

5. Extension to EuroGOOS needs

As the structure of the FTP portal is based on platforms it was feasible to integrate the measured parameters and also to include platforms that measure parameters not processed by MyOcean in-situ TAC such as wind and waves. This activity has been endorsed by the ROOSs in collaboration with the regional INS-TAC partners and no

additional near real time QC is performed on the new parameters. In collaboration with SeaDataNet, the appropriate vocabularies have been used to integrate the new parameters and SeaDataNet will extend these vocabularies if needed.

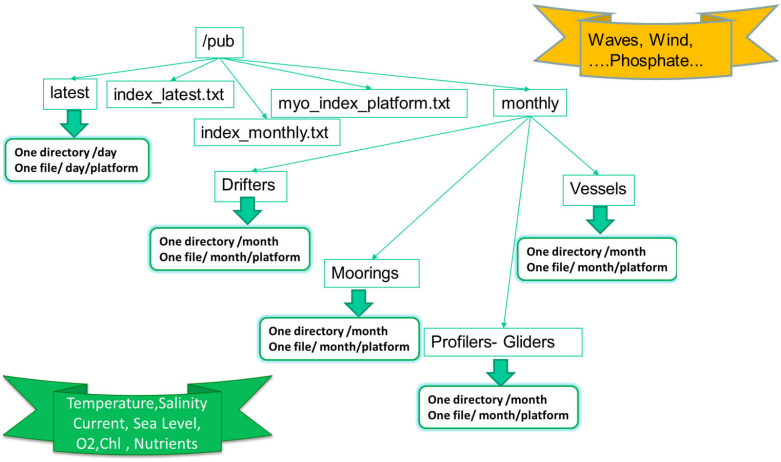

Figure 4 Structure of the FTP portal.

The monitoring tools developed for MyOcean benefit the ROOSs as the service is operated jointly. These tools monitor

- The availability of the portals: since the start of the V1 an availability of more than 95% has be reached on a trimestral basis for a commitment of 93% taking into account that there is no personnel on duty outside working hours and working days.
- The continuity of the data integration: this allows detecting when one data provider server is down and retrieving the data when back on-line.
- The delays in order to reach a 24–48 h delivery from observation date.

The permanent service improving loop that drives MyOcean activities will therefore benefit the ROOSs with lower additional activity performed at ROOS level.

A new data provider has to contact the ROOS portal manager and provide access to the data via an FTP server without needing to change the in-house format (as long as it contains enough metadata information). The conversion to common NetCDF format is taken on board by the MyOcean in-situ TAC partners as well as data integration on the portal.

Presently about 2500 platforms are transmitting observations on a global scale each day from a total of 8500 different platforms within a month. The numbers are different because some platforms do not transmit data every day (e.g. Argo floats transmit every 10 days, vessels do not transmit when they are in harbour).

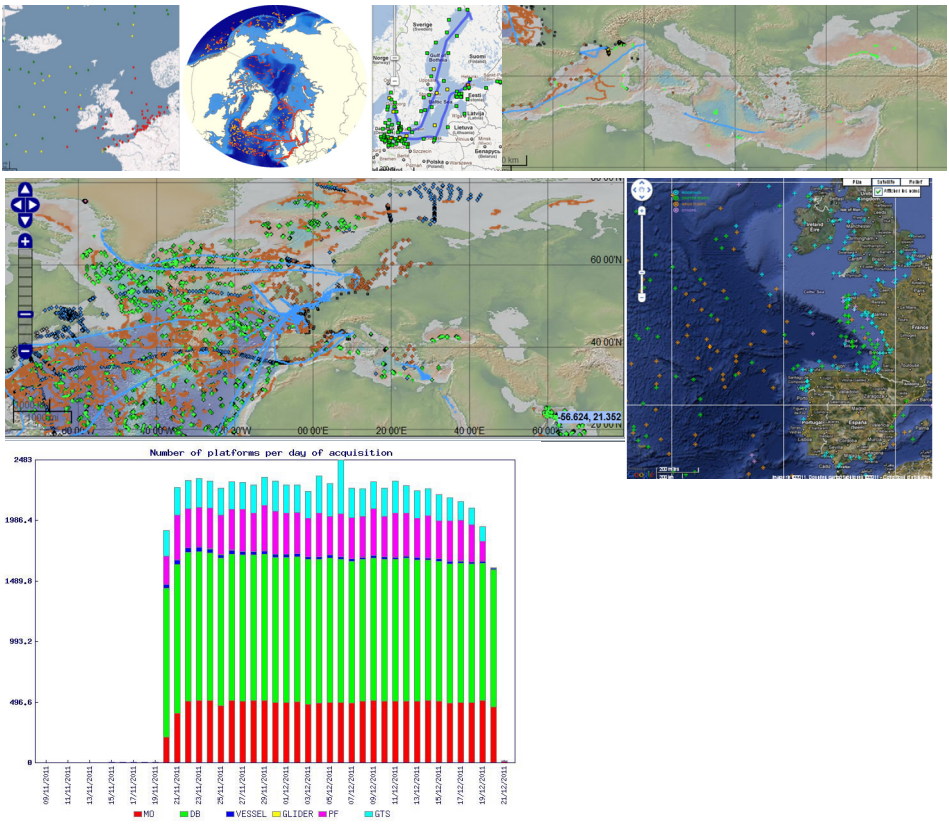

Figure 5 Data available in December 2011 in the different regional portals and at the European portal. 2500 platforms transmit observations at a global scale each day from a total of 8500 different platforms.
Red: Moorings and Tide gauges, Green: drifters, Dark blue: Vessels, Pink: Argo, Light blue: other platforms from GTS.

During 2011, MyOcean INS TAC partners have provided a service on the FTP servers with a rate higher than 98% availability over a month and a restart of less than one hour except once during a long break were it took more than a day to restart the service. Most of the user requests are answered within a day.

6. Future developments

This infrastructure developed jointly by MyOcean and EuroGOOS ROOSs has set up a useful service both for operational oceanography in Europe but also for the research community and the development of downstream services. It relies on an open and free data policy and the EUROGOOS ROOSs should encourage such a data policy.

In the coming years it will be strengthened within MyOcean II to enhance the assessment of the products and develop temperature and salinity time series for re-analysis activities. It will also be extended to coastal data within the JERICO project (www.jerico-fp7.eu) as well as in Mediterranean Sea within Perseus (www.perseus-fp7.eu). On the global

scale a better integration of the European glider data will be developed within the GROOM project. This infrastructure will be used by the EMODNET-PP project (www.emodnet-physics.eu) to provide a discovery and viewing service for fixed point stations and ferrybox data managed by MyOcean/EuroGOOS for real time and SeaDataNet for historical data.

It is important that this infrastructure is sustained jointly in the long term by the regions and the European Commission and not only through national funds complemented by FP projects as is the present situation.

Acknowledgements

This work is part of the MyOcean project. Additional observations are acquired outside MyOcean and especially by EuroGOOS ROOS institutes at the European scale.

References

Belbeoch, M. *et al*. (2010). "The JCOMM in situ Observing Platform Support Centre: A decade of progress and remaining challenges", in Proceedings of the "OceanObs '09: Sustained Ocean Observations and Information for Society" Conference (Vol. 2), Venice, Italy, 21–25 September 2009, Hall, J., Harrison D.E. & Stammer, D., Eds., ESA Publication WPP-306.

Pouliquen, S. *et al*. (2008) "Recommendations for a PAN-European data management system for operational oceanography within EuroGOOS" www.eurogoos.org/documents/eurogoos/downloads/recommendations_for_a_pan_eu_data_sysem_from_datameq-wg_v2.1.pdf

Pouliquen, S. *et al*. (2010). "Recommendations for in-situ data Near Real Time Quality Control" www.eurogoos.org/documents/eurogoos/downloads/recommendations_for_rtqc_procedures_v1_2.pdf

Pouliquen *et al*. (2011) "MyOcean In-Situ TAC User Manual" www.coriolis.eu.org/Data-Services-Products/MyOcean-In-situ-TAC/Documentation

Prandle, D., and N.C. Flemming (1998). "The science Base of EuroGOOS", EuroGOOS, publication N°6.

The MyOcean Thematic Assembling Centre: a new Integrated European Service to access satellite ocean colour data

R. Santoleri*[1], S. Colella[1], V. Forneris[1], E. Bohm[1], G. Volpe[1], C. Tronconi[1], P. Garnesson[2], A. Mangin[2], A. Lintu[3], F. Melin[3], F. Gohin[4], M. Taberner[5], and P. Walker[5]

[1]*Consiglio Nazionale delle Ricerche-Istituto di Scienze dell'Atmosfera e del Clima, Rome, Italy*
[2]*ACRI-ST, Sophie Antipolis, France*
[3]*Joint Research Centre, Ispra, Italy*
[4]*Institut français de recherche pour l'exploitation de la mer, Brest, France*
[5]*Plymouth Marine Laboratory, Plymouth, UK*

Abstract

The synoptic view and the regular data coverage provided by satellite data make them essential for monitoring the marine ecosystem. The MyOcean Ocean Colour Thematic Assembling Centre is a key component of the operational ocean observing and forecasting systems currently developed in Europe. The OCTAC is a distributed system built on the existing activities and services developed previously within the EC supported projects. The OCTAC provides Global and regional ocean colour products covering the Global ocean and European Seas. In this paper the OCTAC system and its products are described with the major scientific and technological steps taken to develop, maintain and improve the system and its products.

Keywords: ocean colour, satellite, operational oceanography, service

1. Introduction

Over the last 20 years, observation of the ocean by satellite sensors has become an essential element of ocean research and monitoring systems. Today physical properties of the ocean such as surface temperature and slope, wave height and surface winds are measured globally at high resolution and provide reliable inputs to ocean circulation models. The spatial synoptic view and the regular sampling afforded by satellite remotely-sensed data are unparalleled by other measurement systems in the monitoring of marine ecosystems. Since the launch of SeaWiFS, MODIS and MERIS missions, ocean colour data have contributed increasingly to investigating marine ecosystems, coastal and ocean productivity, and climate variability. Ocean colour sensors deliver data that can be used to generate a variety of oceanographic products (e.g. chlorophyll concentration, CDOM, Diffuse attenuation coefficient, etc.). These products are essential to monitor the state of the marine ecosystem at short and long time scales. Moreover, ocean colour data also enables detection and monitoring of marine hazards (e.g. pollution and harmful algal blooms).

* Corresponding author, email: r.santoleri@isac.cnr.it

Satellite measurements of ocean colour parameters, such as chlorophyll, are also needed in modelling of marine ecosystems to evaluate model output or to be assimilated into ecosystem models.

Access to long-term, continuous and near real time ocean colour data is considered one of the requirements of operational oceanography. This paper provides an overview of the Ocean Colour Thematic Assembly Centre (OCTAC), which is one of the observational components of the new operational ocean forecasting systems currently being developed by MyOcean in the framework of the European Global Monitoring for Environment and Security (GMES) Programme. MyOcean is delivering the data products and decision support information needed by governmental agencies, commercial organisations and individual citizens in order to ensure the safety of maritime operations, to manage the marine environment sustainably and to protect its resources.

OCTAC was designed to take advantage of the pre-existing pre-operational systems developed in Europe over the last few years in the framework of Member State and European and ESA projects. It will ensure a rapid evolution towards a common European ocean colour integrated service. OCTAC system design and implementation take into account MyOcean user and engineering requirements and present scientific consolidated knowledge. Research and development activities were planned to improve the quality of ocean colour products thus ensuring a long term system evolution.

In the following sections the OCTAC system and its products are described with the major scientific and technological steps taken to develop, maintain and improve the system and its products.

2. The Ocean Colour Thematic Assembling Centre

The main mission of OCTAC is to operate a European Ocean Colour Service for GMES marine applications providing global, pan-European and regional – NW Shelf, Arctic, Baltic, Mediterranean, Iberian-Biscay-Ireland (IBI) and Black Sea – high quality ocean colour products, accompanied by a suite of quality assurance items including accuracy.

OCTAC was designed to bridge the gap between space agencies providing ocean colour data and the MyOcean component dedicated to modelling and forecasting (i.e., the Modelling Forecasting Centres known as MFCs) as well as the gap between space agencies and organisations providing value-added services that require ocean colour-derived information.

To achieve the two objectives mentioned above, OCTAC generates not only products for MyOcean data assimilation but also for direct use by intermediate/end users (intergovernmental bodies, National Environmental Agencies, etc.) to monitor the marine state. OCTAC provides a series of products that satisfy these stakeholders' requirements and will be able to provide core parameters and indicators from present and future OC sensors.

One of the challenges that OCTAC has faced was to establish reliable pixel-level error bars, of each product and to improve the quality of ocean colour products for the European Seas. As a direct consequence of regional waters' OC complexities, the standard global OC products have been revised to meet the error requirements at the

regional scale. Improvement of regional products required tailored OC processing chains in addition to the global OC processing system.

OCTAC is designed as a distributed system composed of five Production Units and three Dissemination Units organised in a single TAC. The production of OC global, Pan-European and regional products is distributed among the PUs (see Table 1 for the relation between products and PUs). The regional OC processing chains use region-specific algorithms for satellite product retrieval. These processing chains were developed and are operated by different PUs.

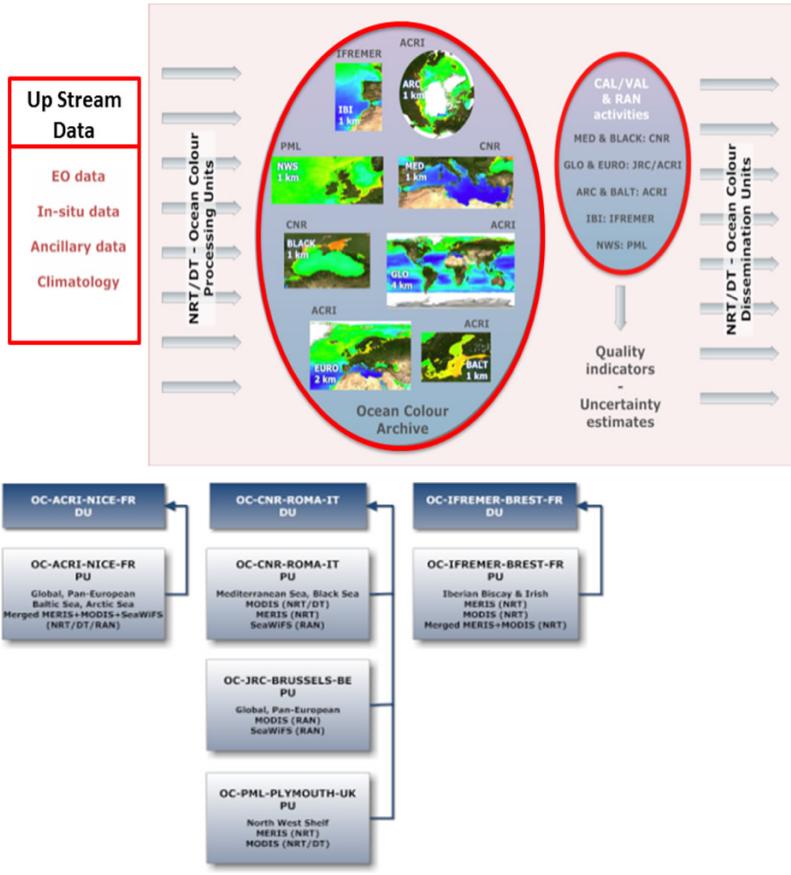

Figure 1 Overview of the OCTAC system (top) and PU/DUs organisation (bottom).

Each PU is responsible for its own processing chain and the QA of its products. The harmonisation and coordination of the distributed centres operations of the Cal/Val activities and service has made OCTAC an integrated and centralised sub-system providing a single ocean colour service to MyOcean users. The overview of the OCTAC system is shown in Figure 1.

2.1 OCTAC processing chains, Distribution System, Service Monitoring

All the PU processing chains have the same structure that can be divided into four main functions (Figure 2 left).

1. **Data ingestion**: Upstream data (Level 0, Level 1A, Level 2 Ocean Colour and auxiliary data from Space Agencies) are acquired by the system. Input data are checked. The process is completely automatic. Each PU has its own check of the input data depending upon the upstream provider. The main checks usually rely on delayed data especially for auxiliary data files. A database on the problematic upstream data is maintained at each PU. If one upstream is not available, depending on the problem, processing can be delayed or when possible an alternative upstream can be activated (automatic mechanism or operator depending on the PU).
2. **Products generation**: Depending on the upstream used, pre-processing can be required depending on input level/format of the data to harmonise inputs of the product generation module **Generate products**. The data sets (L2 products) to be used for the final products are generated for the different Ocean Colour Mission. Each PU produces the L2 data (regional/global product) using their own pre-existing chains. This is a completely automated process. Level 2 data are stored in an internal PU database used for products generation. For quality purposes, a database to collect in-situ data or establish climatology is also computed to perform QC and checks when end user products are generated.

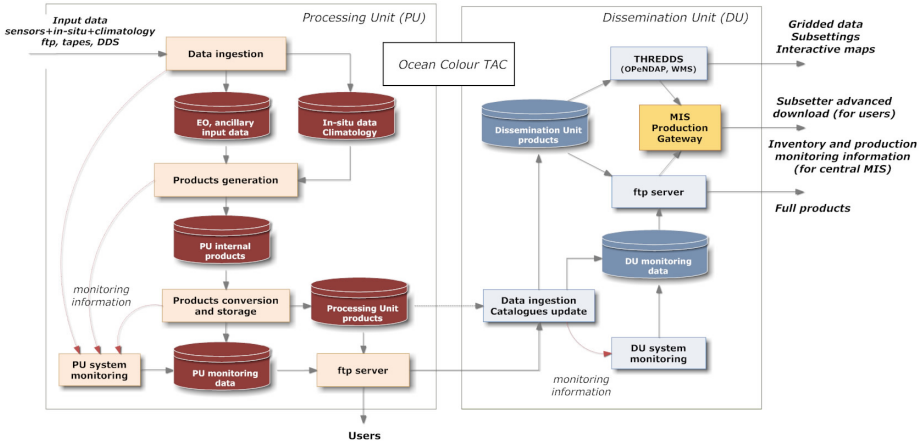

Figure 2 Generic OCTAC PU processing chain (left) and Dissemination Unit (right).

3. **Products conversion and storage**: Each PU produces L3/L4 data and quality flags of each OC pass over their region using pre-processed L2 products. Single passes are spatially binned and temporally binned to compute daily and multi-day products according to FTSS. Multi-sensor merged products are produced according to the FTSS. When data are missing, merged products are produced with degraded quality depending on the amount of missing input data. Each PU performs a QC activity as described in the OCTAC scientific calibration and validation plan. If anomalies are

detected, a warning is sent to the operator and appropriate actions are taken depending on the anomaly. The product are then transferred to the OCTAC DU.

4. **System Monitoring**: all events relative to data ingestion, products generation and conversion are stored. When anomalies are detected an exception is raised to the Dissemination Units and to the central OCTAC Service Desk.
5. **Data Dissemination**: the dissemination of the OC products to the users relies on the OCTAC Dissemination Units directly interfaced to the MyOcean central information system (MIS). A centralised OCTAC service desk has been organised to monitor the overall OCTAC production and to interface with the MyOcean service desk in contact with the users. The OCTAC service desk is a single point of contact for communication of incidents and to manage the service requests by users.

Each PU is responsible for its own processing chain and QC of its products. All PUs follow the same protocol for quality data assessment defined by the OCTAC. All the OC products produce and distribute data in the same format. Nomenclature of the products and files is the same independently of the PUs.

The entire OCTAC relies on three different OC sensors: MERIS, from ESA, and MODIS and SeaWiFS, both from NASA. Data from space agencies (L1 or L2) as well as ancillary data may be unavailable occasionally; in these cases products delivered by the OCTAC may be missing (due to lack of L1 or L2 upstream data) or with lower quality (in the case of lack of ancillary data). In either of these two cases, the OCTAC service desk alerts users for data unavailability/degradation via MyOcean central service.

2.2 OCTAC Products

The OCTAC provides Global and Regional ocean colour products covering the MyOcean regions: Global (GLO), North West Shelves (NWS), Arctic (ARC), Baltic (BAL), Mediterranean (MED), Iberian-Biscay-Ireland (IBI) and Black Seas (BS). In addition to global and regional products, OCTAC also delivers European products that cover the overall European Seas. Regional products differ from the global and the European products not only in their resolution and area coverage but also in the parameter values. Some of the regional datasets, such as MED, BS, NWS and IBI, are produced using higher quality region-specific algorithms in place of global OC algorithms that meet the error requirements at the regional scales of interest. Table 1 lists the ocean parameters available for each region.

OCTAC delivers three different versions of ocean colour products: the Near Real Time (NRT) products, the Delayed Time (DT) products, and the Reanalysis (RAN) products. NRT, DT or RAN products are generated by global and/or regional processing chains (see section 2.1) using different input data. As a consequence NRT, DT and RAN products are characterised by different scientific qualities. NRT is meant to provide users with products as soon as possible (within 24 hours of satellite data acquisition). These products are generated using the best ancillary data available (meteorological data) at the time of the processing (often only climatological fields are available). DT data are processed using consolidated ancillary data (meteorological field available 3–4 days after satellite acquisition) to improve the scientific quality of the products. DT products are made available to the user within 5 days the satellite acquisitions. NRT product are affected by larger errors with respect to DT products. Nevertheless, NRT data are very

useful for NRT coastal application, water quality monitoring, fishery application, and in-situ data acquisition. OCTAC has made ocean colour data re-analysis products available for climatic studies. Re-analysis products consist of a long time series produced re-processing the entire OC dataset with a fixed processing software configuration and a consistent time series of L2 products from space agencies. RAN product should be used for climatic studies or for analyses of the interannual variability of the ocean. The RAN products are generated all at once and are updated taking into account the space agency L2 re-processing scheduling. During MyOcean a new version of RAN data was made available in July 2011.

Table 1 List of ocean colour parameters associated with ocean regions and associated PUs. In the Covered Region column, G is GLO, M is MED, B is BS, N is NWS, I is IBI, E is Europe. In the PU column, A is ACRI, C is CNR, I is IFREMER, J is JRC, and P is PML.

Product	Covered region	PU
Rrs(λ): normalised remote sensing reflectance	G,E,M,B,N	A, C, J, P
Chl-*a*: Chlorophyll-*a* concentration (Chl-*a*)	All	All
Kd: diffuse attenuation coefficient at 490 nm	G,M B,N,E	A, C, J, P
b_{bp}: particulate backscattering coeff. at 443 nm	G, E	A, J
a_{ph}: absorption coeff. due to phytoplankton at 443 nm	G, E	J, P
a_{cdm}: absorption coeff. due to cdom and non-pigmented particles at 443 nm	G, E	A, J, P
a_t: total absorption coefficient	G, E	P
SPM: solid suspended matter	I	I
ZSD: Secchi depth	G, E	A
PAR: photosynthetically available radiation	G, E	J

3. Assessment of the Ocean Colour Product quality

OCTAC has focused on setting up a method for an off-line and on-line validation activity of multi-platform satellite OC products for all processing modes (NRT, DT and RAN). This required defining and implementing agreed common methods/principles/ metrics for validation and quality control of L3 and L4 products of each OCTAC PU.

3.1 Ocean colour product validation

The off-line validation aimed at qualifying the errors associated with ocean colour products by comparing them with in-situ observations. The off-line validation activity is focused on both operational DT and re-analysis products delivered to the users. This scientific validation is limited to the core products. Core products are the spectral normalised remote sensing reflectance (RRS) and the concentration of chlorophyll-*a* (CHL). The core products are validated using field measurements, obtained from international databases, maintained by space agencies or scientific programs, as well as from data collected by the OCTAC PUs. Validation is conducted with a match-up methodology, i.e., comparing the satellite product close to the field datum in space (pixels or grid points surrounding the field observation) and in time (a few hours). This validation is carried out using both satellite and field data collected over the duration of the satellite missions. Bias(δ), RMS(Δ), mean relative difference and mean absolute relative

difference were used as common matrix to compare satellite estimates to a reference in-situ data set. This enabled quality control of the errors associated with the OC core products in all regions.

Figure 3 shows an example of the scatter-plots of the satellite-derived versus in-situ chlorophyll concentration for new OCTAC SeaWiFS and MODIS global Re-analysis products. The RMS difference for log-transformed data is approximately 0.3 for globally-distributed data, consistent with the results of Gregg and Casey (2004). Nevertheless, the validation statistics have a regional variability (Zibordi *et al*., 2011). Figure 4 shows the scatter-plots of the DT satellite-derived versus in-situ chlorophyll concentration for the Mediterranean Regional Chlorophyll product. All of the three sensors show a good agreement with respect to in-situ data even if SeaWiFS shows better results. Δ (between 0.22 and 0.26) and δ (between –0.04 and 0.07) values for all the three sensors are comparable. Validation results of Global and IBI NRT products are analysed in Maritorena *et al*. (2010) and Gohin (2011) respectively.

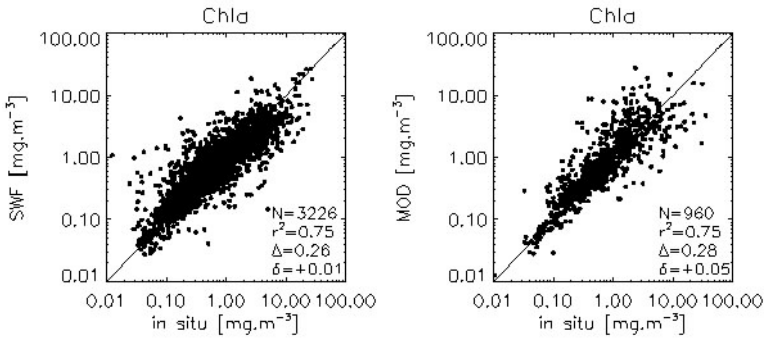

Figure 3 Satellite-derived versus in-situ chlorophyll concentration. Satellite values are the Global SeaWiFS and MODIS re-analysis products generated by JRC.

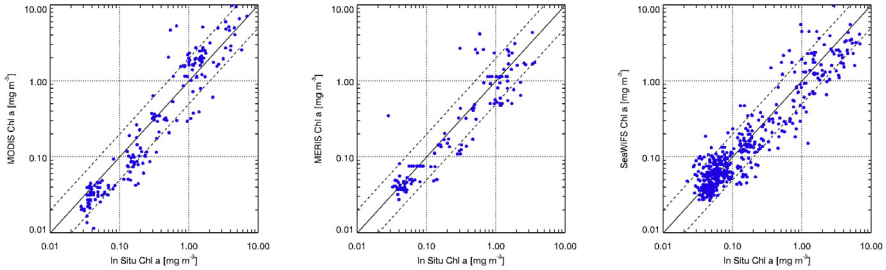

Figure 4 Satellite-derived versus in-situ chlorophyll concentration. Satellite values are the Mediterranean products produced by CNR using the three Mediterranean-adapted algorithms: MedOC4 (SeaWiFS), MedOC3 (MODIS) and MedOC4ME (MERIS) (Santoleri *et al*., 2008).

The results of the off-line validation activity allowed a characterisation of the core products (Rrs & Chl) OC data uncertainties at both the global and the regional scale, demonstrating that the OCTAC products fulfil the accuracy goal and showing a slight

improvement of V1 products available from MyOcean as of 2011 with respect to the previous version. A synthesis of the results obtained are also reported in the OCTAC Quality information documents produced by the OCTAC PUs and available to the user from MyOcean (www.myocean.eu.org).

3.2 3.1 Ocean Colour Product quality control

The online validation is applied to all the OCTAC operational products and consists of three parts: analysis of number of input data and their quality, quality of processing data, and consistency of physical signal. This check is made by the PU processing chains and validation metrics/statistics are automatically generated during the operational processing. Three types of consistency check are used by PUs, the first concerning data time consistency at the basin scale (region approach), the second on a pixel-by-pixel basis (pixel approach), both with respect to climatological fields, and the third relying on comparison between satellite-derived chlorophyll-*a* and fluorescence obtained from in-situ automatic coastal stations. The climatological fields used by OCTAC PUs are daily climatologies computed from long term satellite ocean colour datasets [1998–2010].

The mean, standard deviation and number of observations are computed for each day of the year and for each sea pixel. Figure 5 shows an example of the result. These methods aim at assessing the degree of data reliability based upon data time consistency.

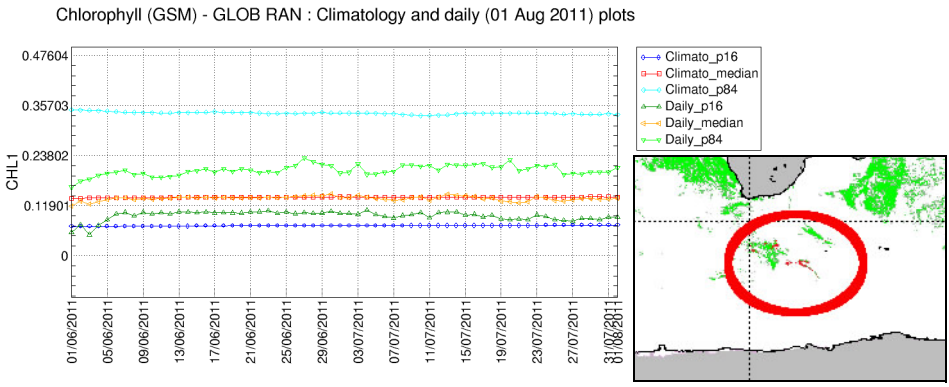

Figure 5 Comparison with climatology produced by ACRI PU: "region approach" at global scale (left panel); the "pixel approach" for a daily product (right panel). Green pixels are consistent with the climatology, red pixels are above the climatology.

A synthesis of the online validation activity performed by PUs enabled the quality of the operational products delivered between 1 July 2011 and 31 August 2011 to be viewed, showing that the quality of the products is reliable according to the used metrics. One element which needs to be clarified is that the quality assessed by this kind of approach is aimed at quantitatively indicating the time consistency of each product. This analysis does not provide absolute uncertainties due to the lack of an appropriate in-situ program to monitor the same quantities at the same spatial and temporal resolutions. That is, even if there was one or more operational sites, it would anyway be insufficient to operationally address this issue. On the other hand, this approach allows the possible identification of sensors drifts or shifts, in near-real time. Moreover, in the context of climate

studies, this approach can be used as a first order alarm system to identify possible natural changes which are not expected to occur. An automatic procedure can be set up to alert the responsible of the production in case of failure (missing upstream data or important anomalies with respect to climatology).

Acknowledgements

This work has been supported by the European Project "MyOcean: Development and pre-operational validation of upgraded GMES Marine Core Services and capabilities" funded by European Commission.

References

Gregg, W.W., and N.W. Casey (2004). Global and regional evaluation of the SeaWiFS chlorophyll data set. Remote Sens. Environ., 93, 463-479.

Gohin, F. (2011). Annual cycles of Chlorophyll-a, non-algal Suspended Particulate Matter and Turbidity observed from space and in-situ in coastal waters, Ocean Sci., 7, 705-732, 2011

Maritorena, S., O. Hembise Fanton d'Andon, A. Mangin, and D.A. Siegel (2010). Merged Ocean Color Data Products Using a Bio-Optical Model: Characteristics, Benefits and Issues. Remote Sensing of Environment, DOI: 10.1016/ j.rse.2010.04.002

Santoleri, R., G. Volpe, S. Marullo, and B. Buongiorno Nardelli (2008). Observing the Mediterranean Sea from space: ocean colour algorithms and chlorophyll variability, in Remote Sensing of the European Seas, edited by Vittorio Barale and Martin Gade, ISBN: 978-1-4020-6771-6, doi:10.1007/978-1-4020-6772-3_8, 103-116.

Zibordi, G., J.-F. Berthon, F. Mélin, and D. D'Alimonte (2011). Cross-site consistent in-situ measurements for satellite ocean color applications: the BiOMaP radiometric dataset. Remote Sens. Environ., 115, 2104-2115.

ENSURF: Multi-model sea level forecast – status and implementation for the IBIROOS and MOON regions, including MyOcean operational systems

B. Pérez Gómez*[1], E. Álvarez Fanjul[1], M.G. Sotillo[1], R. Brouwer[2], J. Beckers[2], D. Paradis[3], C. Balseiro[4], K. Lyons[5], M. Cure[5], and J. Nilsson[6]

[1]*Area de Medio Físico de Puertos del Estado, Madrid, Spain*
[2]*Deltares, Delft, The Netherlands*
[3]*Meteo-France, Toulouse, France*
[4]*MeteoGalicia, Santiago de Compostela, Spain*
[5]*Marine Institute, Galway, Ireland*
[6]*INGV, Rome, Italy*

Abstract

ENSURF is a multi-model application for sea level forecast that allows easy access and visualisation of storm surge or circulation models currently operational in Europe, as well as near-real time tide gauge data in the region. The system was developed and implemented within the ECOOP European Project based on the MATROOS visualisation tool. It includes the Bayesian Modelling Average (BMA) technique that generates an overall forecast probability density function (PDF) by making a weighted average of the individual forecasts PDFs; the technique needs the availability of sea level data from tide gauges in near-real time, with near-real time automatic quality control. We present here the validation results of this BMA technique and its ability to improve the independent deterministic forecasts. Recently a new source from the MyOcean project operational system for the IBIROOS region has been added for validation of the sea level component. The work has proved to be useful for detecting problems in some of the circulation models not previously well-calibrated with sea level data, to identify and confirm the differences on baroclinic and barotropic models for sea level applications and the general improvement of the BMA forecasts.

Keywords: sea level, surge, bayesian model average, integration of models and observations, tide gauges, near real time quality control.

1. Introduction

Recent studies have demonstrated the advantages of the multi-model and the ensemble approach for validation and improvement of predictive capabilities. On the other hand, several operational models provide a sea level forecast, as a main or secondary product, sometimes at common domains. Both facts provided the rationale for the creation of the ENSURF system (Ensembles SUrge Forecast), within the ECOOP European project (www.ecoop.eu/summary.php) (European Coastal-shelf sea Operational observing and forecasting system), Contract No. 3655, whose overall goal is to consolidate, integrate and further develop existing European coastal and regional seas operational systems.

* Corresponding author, email: bego@puertos.es

ENSURF represents a perfect example of this integration, not only because it involves different forecasting systems but also because it makes use of observations to improve the final forecasts thanks to the Bayesian Model Average technique.

Barotropic 2-D models (Flather, 1981, Flather, 1987, Alvarez-Fanjul *et al.*, 2001) have been the basis of the existing operational sea level forecasts during recent decades. Nevertheless, the recent improvement in computer skills and performance of 3D baroclinic models for current forecasts has led to the availability of sea level forecasts coming also from these more sophisticated and general models in some regions; validation of sea level output of general circulation models is critical for a correct characterisation of the sea surface elevation and consequently for an adequate description of the circulation patterns.

All these systems provide deterministic and independent forecasts of sea level for their specific regions, sometimes geographically coincident in part, but have not been compared and even less combined in order to improve their skills at the common domains or points.

ENSURF integrates some of these different models currently operational in Europe with tide gauge data for providing easy access to the sea level forecasts available at some specific harbours, validation with observations and improvement of these forecasts by means of the Bayesian Model Average Technique. The system was implemented for the NOOS and IBIROOS regions and it is running operationally at Deltares (noos.deltares.nl) and Puertos del Estado (ensurfibi.puertos.es) respectively, based on the MATROOS visualisation tool, developed by Deltares. Initially it was not possible to develop a component for the MOON region, due to the lack of enough operational models with output of sea level in the Mediterranean Sea. Nevertheless, in this work we have included the Western Mediterranean, where Spanish and French forecasts and data were available.

We present in this paper the implementation performed at Puertos del Estado for the IBIROOS region, for which it was necessary to select the locations of the storm surge forecasts for available tide gauges and to establish the data exchanges (real time measurements and forecasts) between partners. The system is currently operational and ready to incorporate more stations and sources in the future (Figure 1). We show also the first validation results of the different models and the performance of the Bayesian Model Average Technique as well as the first validation of the sea level forecast provided by MyOcean project operational model for the IBIROOS region (MyO IBI operational system) recently added as a new source to ENSURF.

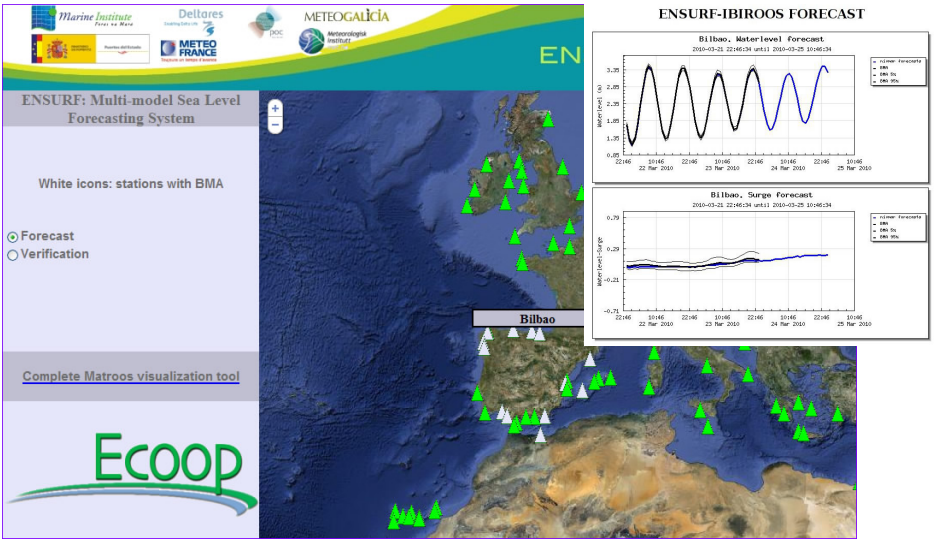

Figure 1 The ENSURF IBIROOS portal at ensurfibi.puertos.es, which displays the forecast including the BMA confidence interval or the verification with tide gauge data. The figure shows an example of a forecast for the Bilbao station, both for total and meteorological sea level.

2. Bayesian Model Average Technique

The Bayesian Model Average (BMA) is an ensemble calibration statistical technique which was first employed in social and health sciences, and later applied to dynamical weather forecasting models by Raftery in 2005 (Raftery *et al.*, 2005). In 2008 the technique was implemented for forecasting sea level at stations along the Dutch coastline, making use of six different forecasts from the NOOS region (Beckers *et al.*, 2008).

When selecting a particular model for prediction there is always a source of uncertainty that is normally ignored and hence underestimated. The Bayesian Model Average (Leamer, 1978; Kass and Raftery, 1995; Hoeting *et al.*, 1999) solves this problem by conditioning, not on a single "best" model, but on an ensemble of models, becoming a standard method for combining predictive distributions from different sources. Our uncertainty about the best of these sources is quantified by the BMA.

It is important to stress that the dominant approach to probabilistic weather forecasting has been the use of ensembles in which a model is run several times with different initial conditions or model physics (Leith, 1974; Toth and Kalnay, 1993; Molteni *et al.*, 1996; Hamill *et al.*, 2000). In our case, the approach is slightly different as we make use of existing operational systems based on different models and even physics, and of course more limited in the number of members.

The basic idea is to generate an overall forecast probability density function (PDF) by means of a weighted average of PDFs centred on the individual bias-corrected forecasts, as can be seen in the following expression:

$$forecast\ (overall,s,t\_fc)\ =\ \sum_{k} w(k) forecast\ (k,s,t\_fc)$$

$w(k)$ being the weight of model k. The mean of this total PDF is expected to have a smaller root mean square (RMS) error than those of the different models, i.e. there should be an improvement of the performance with respect to those of the individual forecasts. The weights used on this average represent the probability that a particular model will give the correct forecast PDF, and this is determined and updated operationally based on the performance of the models during a recent training period. Moreover, the overall PDF, being reasonably well-calibrated, can provide a forecast confidence interval which is important for many practical applications. Of course, the BMA weights can also be used to assess the usefulness of ensemble members and for their selection.

3. ENSURF IBIROOS sources and data

3.1 Sources or models used in the system

The sources initially contributing with operational sea level forecasts to the IBIROOS component of ENSURF are shown in Table 1. Seven different sources are provided by four different institutes from three countries in the region. As already mentioned, the characteristics of the models differ, some being barotropic and others baroclinic, and the model forcings may also differ, leading to different outputs of sea level (depending on just having meteorological forcing or including also the tide). Although details are not provided in this paper, they can be found in the ECOOP deliverable 7.4.1.

Institution	Source/Model	Output
OPPE	Nivmar / Hamsom model (barotropic) including tide gauge data assimilation	Surge + Total sea level
	Eseoat / POLCOMS model (baroclinic)	Total sea level
Meteo-France	Metfr_arpege /(barotropic, met forcing 0.25°)	Surge
	Metfr_aladin / (barotropic, met forcing 0.1°)	Surge
	Metfr_ecmwf (barotropic, met forcing 0.5°)	Surge
Marine Institute	Imi: ROMS model (baroclinic)	Total sea level
MeteoGalicia	Metga_sm: Mohid model (barotropic)	Surge

Table 1 Different sources initially available in ENSURF for the IBIROOS region, and used for the first tests of the BMA implementation.

The only baroclinic models available at the time of ECOOP project were the one from the ESEOAT system at Puertos del Estado (that uses POLCOMS circulation model) and the one from the Marine Institute system (based on the ROMS model). For these two models the tide is included, so a harmonic analysis of one year of model data was done at the tide gauge stations, and then subtracted to obtain the surge component. By doing this

the tide computed from the tide gauge data is always included and this observational tide is added to the surge component provided by the different models to obtain the total sea level forecast in ENSURF. This was also necessary because the BMA is only applied to the surge component.

Of course, implemented by different institutes in different countries, the domains of the models are also diverse (Figure 2), although sharing part of the coastline in some cases; these will be the coastlines and harbours where the advantage of multi-model approach to improve the forecasts will be explored.

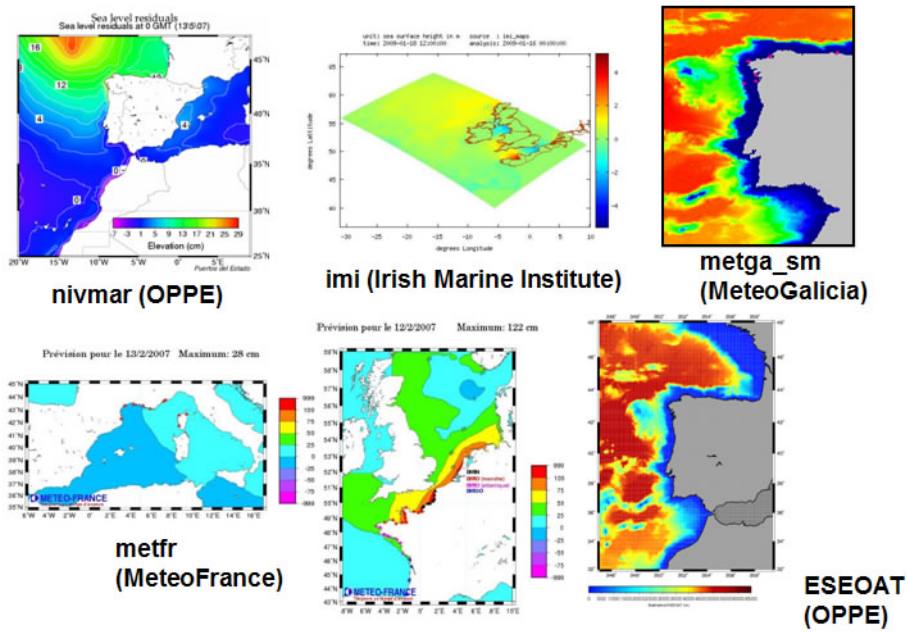

Figure 2 domains of the sources available for the ENSURF-IBIROOS component. Nivmar covers the whole Mediterranean Sea, but only results for the Western Mediterranean are presented.

All the models presented a bias when comparing with observations that were corrected before entering ENSURF. This bias was not present in the Nivmar system as it is the only one that corrects the bias operationally with the tide gauge observations, as in fact the BMA does itself.

3.2 Tide gauge data

A common set of tide gauge stations were selected for the reception of sea level data in near-real time. All the models must provide output at these special points if they fall within the model domain; the purpose of this is not just the validation of the different models with observations at the harbours, but also the implementation of the BMA for statistical forecast at these specific locations as it was explained before. The important role of tide gauge data for improving sea level forecasts at the coast has been recognised in the implementation of the Nivmar system (Alvarez-Fanjul *et al*., 2000), for example,

and is also mentioned by Mourre *et al*. (2006) who found that the use of tide gauges led to better global statistical performance of high-frequency barotropic models.

One of the critical steps for the use of tide gauge data in near-real time from different countries and institutes is the implementation of automatic quality control software that avoids wrong data entering the system and the BMA. Data sampling can vary from 10 to 60 minutes, and latency required can be of several hours. Time needs to be Universal Time. Automatic quality control of data in near-real time was implemented in the framework of the MyOcean project and is now in operation for the IBIROOS In-Situ Tac at Puertos del Estado. On the other hand, for each individual tide gauge entering ENSURF at least one year of data is required for previous computation of the tide and fixing the quality control parameters.

4. BMA experiments

The BMA is applied to the surge component of the sea level forecast because this component can be approximated by a normal distribution to a reasonable degree of accuracy, which is not the case for total sea level including tides.

The following BMAs were implemented in the region, taking into account the reliable sources available and their common domains (we will distinguish between Atlantic and Western Mediterranean coast):

Atlantic: available sources: *nivmar*, *eseoat*, *imi*, *metfr* (3) and *metga*. In this case, we have output from two baroclinic sources, *eseoat* and *imi*. Four BMAs were implemented (TP being the Training Period), avoiding *metga* and *imi* sources, due to the low Correlation Index that will be shown later. The maximum number of sources for the BMA is 5:

BMA0: eseoat and nivmar,	TP = 15 days
BMA_ibi1: eseoat, nivmar, metfr (3),	TP = 7 days
BMA_ibi2: "	TP = 4 days
BMA_ibi3: "	TP = 15 days

Mediterranean: available sources: *nivmar* and *metfr* (3). In the Mediterranean the four sources are barotropic. We used all the sources available, 4 in total, for the BMA implementation, changing also the TP, as in the Atlantic coast:

BMA_med1: nivmar, metfr (3),	TP = 7 days
BMA_med2:	TP = 4 days
BMA_med3:	TP = 15 days

The BMA was implemented at particular stations or harbours that were selected based on the availability of enough sea level forecasts or sources and automatic near-real time quality control of tide gauge data (Figure 3); the latter was initially available only for Puertos del Estado REDMAR network. All the BMAs were in operation during the ECOOP Training Operational Period (TOP).

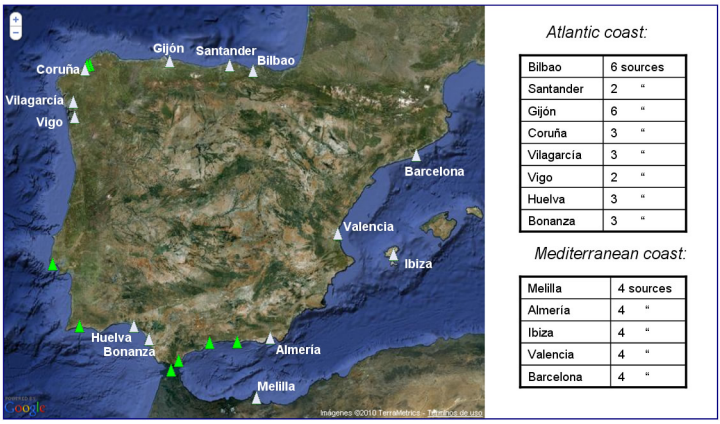

Figure 3 stations for which the BMA was implemented (white icons) for the first ENSURF-IBIROOS implementation, based on the availability of quality control of tide gauge data in near-real time, and more than two sources of forecast.

5. BMA validation results

Basic statistical parameters (Root Mean Square Error: RMSE, Correlation Index: CI, Maximum Error: RMAX and Mean difference: Bias) were computed from the comparison between the different models and the tide gauge observations, including the different BMAs, which have been treated here as additional sources, for the period September 2008 to December 2009. In order to synthesise all the data, we have averaged and plotted the CI and RMSE parameters of all the stations and sources on the Iberian Atlantic coast and on the Mediterranean coast (Figure 4).

If we pay attention to the capability of the BMAs implemented to outperform the individual forecasts, it can be seen from Figure 4 that this is in general the case for the Atlantic coast, with higher CI and lower RMSE for practically all of the BMAs, but more clearly for BMA_ibi2, the one with 4 days of training period; the best source is *nivmar*, which is not strange as it is the only source with a simple scheme of data assimilation for bias correction. For the Atlantic coast it is interesting to see also that Meteo-France forecasts, which are produced by a 2D barotropic model, without any kind of tide gauge data assimilation, perform better than the baroclinic models from ESEOAT and IMI. Nevertheless, the differences between these values of CI and RMSE are sometimes very small, and probably not statistically significant.

The results for the Mediterranean in Figure 4 show that the BMAs do not improve the results of *nivmar* so clearly in this case, with BMA_med2 using 4 days of training period the only one showing a slight improvement. On the other hand, Meteo-France results are poorer than in the Atlantic. One possible reason for the latter is the presence of a boundary on the Meteo-France model domain around Sardinia and Corsica which disturbs the results at these stations. Taking into account the experience with the *nivmar* system, we think the Mediterranean Sea should be completely covered by the model domain.

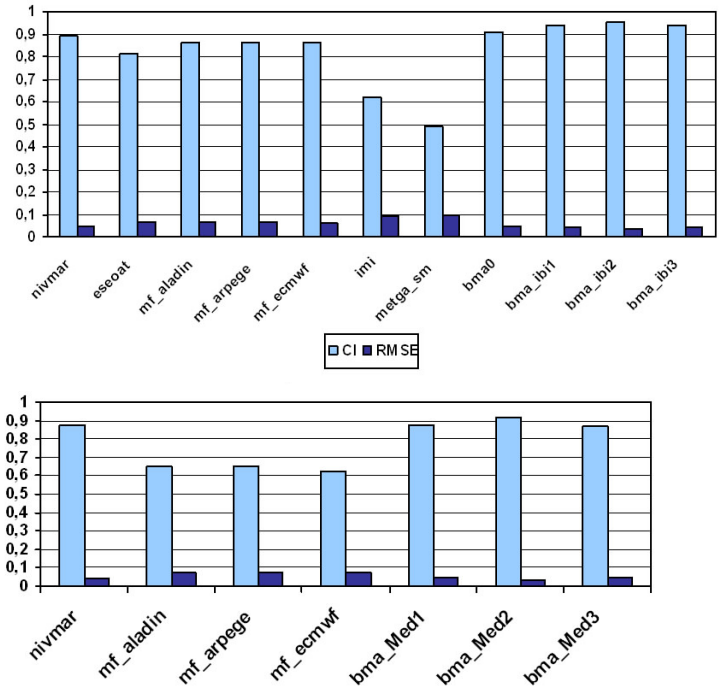

Figure 4 Mean CI (Correlation Index) and RMSE (Root Mean Square Error) for the sources and stations for September 2008 to December 2009. Top: Iberian Atlantic Coast, Bottom: Mediterranean Coast.

Gijón station	*Sept2008-Dec2009*		*Jan2009-Feb2009*	
Source	RMSE (m)	C.I.	RMSE (m)	C.I.
Nivmar	0.042	0.94	0.042	0.96
Eseoat	0.055	0.90	0.047	0.95
Mf-aladin	0.072	0.83	0.047	0.96
Mf-arpege	0.072	0.83	0.046	0.96
Mf-ecmwf	0.071	0.83	0.045	0.96
Metga_sm	0.080	0.74	0.045	0.96
Imi	0.102	0.58	0.052	0.97
BMA	0.036	0.96	0.038	0.97

Table 2 Statistical parameters of the validation for the whole TOP period (columns 2 and 3) and for just the stormy season January to February 2009 (columns 4 and 5), for the Gijón station. There is a general improvement of these parameters for the latter.

If we restrict our validation study to a stormy period, as can be seen in Table 2 for the Gijón station in Northern Spain, we get generally better statistical parameters even for the baroclinic models. And if we finally have a look to the performance during the peak of a storm then the best result is obtained from *nivmar*, which reproduces the peak better

than any of the different BMAs. This last result is important and should be explored in detail because the main objective of any forecast is the expected extreme value.

6. MyO IBI operational system in ENSURF

A first validation for the sea level component of the MyOcean operational forecast for the IBIROOS region has also been performed thanks to the addition of this new source to the ENSURF system. Table 3 shows the results of this validation for several stations, which vary from 0.037 m of RMSE at the Las Palmas station (Canary Islands) to 0.105 m at the Vigo station (North Western Spain). These are preliminary but encouraging results about the adequate performance of this system, based on the NEMO model, which will be included in the BMA studies in the near future. The surge component of the model has also been obtained by harmonic analysis of one year of model output at the harbours, which has allowed on the other hand checking the correct introduction of the tide forcing in the model.

Statistics from 2011-04-01 00:00:00 until 2011-08-04 00:00:00, analysis 0-999 hour

location	source	mean abs.error	mean	mean error	RMSE	min error	max error	count
Barcelona	IBI	0.03	-0.103	0	0.038	-0.041	0.079	13815
Bilbao	IBI	0.057	-0.077	-0	0.07	-0.074	0.186	13134
Coruna	IBI	0.051	0.057	0	0.064	-0.1	0.21	13498
Ferrol1	IBI	0.063	0.045	-0	0.081	-0.077	0.223	13622
Gijon	IBI	0.052	-0.024	-0	0.068	-0.098	0.242	13873
Hierro	IBI	0.028	0.004	0	0.035	0.071	0.049	10739
Huelva	IBI	0.058	0.088	0	0.073	-0.092	0.218	13799
Ibiza	IBI	0.073	0.024	0	0.085	0.05	0.16	13608
LasPalmas	IBI	0.029	0.014	0	0.037	0.01	0.14	13895
Malaga	IBI	0.038	0.029	0	0.048	-0.114	0.026	13693
Motril	IBI	0.036	0.027	0	0.045	-0.038	0.112	13881
Santander	IBI	0.036	-0.044	-0	0.046	-0.087	0.103	13436
Tenerife	IBI	0.043	-0.023	0	0.053	0.013	0.143	13699
Valencia	IBI	0.051	0.074	0	0.063	0.017	0.187	12902
Vigo	IBI	0.083	0.021	0	0.105	-0.333	0.257	13834
Villagarcia	IBI	0.051	0.033	0	0.064	-0.074	0.176	10333

Table 3 Statistical parameters provided by the MATROOS tool for MyO IBI operational system (surge component). Results are generally good, except at Vigo, where the RMSE reaches 10.5 cm.

7. Conclusions

ENSURF has proved its utility as a validation and multi-model forecast tool, and has become the first experience of exchange of operational forecasts for the IBIROOS region. It has enabled the detection of problems in existing operational models that had not been previously well-calibrated with respect to sea level observations and demonstrate that a better statistical forecast is feasible based on existing operational systems. The first validation results confirm the general idea that baroclinic models do not reach the good performance of barotropic models for storm surge applications.

The BMA generally provides an improvement with respect to the best of the forecasts, but it does not improve the peak of the storms, which will need further investigation, for example by checking the influence of the training period.

Finally the availability of near-real time data from tide gauges, with automatic quality control to avoid wrong data entering the system, becomes one of the main conditions to provide accurate forecasts of sea level at the harbours, something that became recently possible in IBIROOS within MyOcean project. On the other hand, ENSURF now includes the MyOcean operational systems for validation and use of the sea level component.

Acknowledgements

This work has been supported through the EU ECOOP project, Contract No. 36355. We would like to thank the personnel working at the different institutions who have collaborated in providing the sources to ENSURF. We thank also Ronan Creach (SHOM, France), Vibeke Hess (DMI, Denmark), Elizabeth Bradshaw (POL, UK) and Gonzalo Crisostomo (IGN, Portugal), for their support and cooperation in making the tide gauge data available. Finally, we thank José Antonio Zaballos for the development of the ENSURF-IBIROOS front page.

References

Álvarez Fanjul, E., B. Pérez, and I.R. Sánchez-Arévalo (2001). Nivmar: A storm surge forecasting system for the Spanish Waters. Scientia Marina, Vol 65, pp. 145−154.

Beckers, J.V.L., E. Sprokkereef, and K.L. Roscoe (2008). Use of Bayesian model averaging to determine uncertainties in river discharge and water level forecasts. Proc.4th International Symposium on Flood Defence: Managing Flood Risk, Reliability and Vulnerability. Toronto, Ontario, Canada, May 6−8.

Flather, R.A. (1981). Practical surge prediction using numerical models, pp. 21−43 in Floods Due to High Winds and Tides (ed. D. H. Peregrine). London: Academic Press, 109 pp.

Flather, R.A. (1987). Estimates of extreme conditions of tide and surge using a numerical model of the north-west European continental shelf. Estuarine, Coastal and Shelf Science, 24, 69−93.

Hamill, T.M., C. Snyder, and R.E. Morss (2000). A comparison of probabilistic forecasts from bred, singular-vector, and perturbed observation ensembles. Mon. Wea. Rev., 128, 1835−1851.

Hoeting, J.A., D. Madigan, A.E. Raftery, and C.T. Volinsky (1999). Bayesian model averaging: A tutorial (with Discussion). Statistical Science, 14, 382−401. [Corrected version.] Correction: vol. 15, pp. 193−195. The corrected version is available at http://www.stat.washington.edu/www/research/online/hoeting1999.pdf.

Kass, R.E., and A.E. Raftery (1995). Bayes factors. Journal of the American Statistical Association, 90, 773−795.

Leamer, E.E. (1978). Specification Searches, Wiley.

Leith, C.E. (1974). Theoretical skill of Monte-Carlo forecasts. Mon. Wea. Rev., 102, 409−418.

Molteni, F., R. Buizza, T.N. Palmer, and T. Petroliagis (1996). The ECMWF ensemble system: Methodology and validation. Quart. J. Roy. Meteor. Soc., 122, 73−119.

Mourre, B., P. De Mey, Y. Mènard, F. Lyard, and C. Le Provost (2006). Relative performance of future altimeter systems and tide gauges in constraining a model of North-Sea high-frequency barotropic dynamics. Ocean dynamics (2006) 56: 473–486.

Poole, D. and A.E. Raftery (2000). Inference for Deterministic Simulation Models: The Bayesian Melding Approach. Journal of the American Statistical Association; ABI/INFORM Global p. 1244.

Raftery, A.E., T. Gneiting, F. Balabdaoui, and M. Polakowsly (2005). Using Bayesian Model Averaging to Calibrate Forecast Ensembles. Am. Meteorological Soc. 133, 1155, 1174.

Toth, Z., and E. Kalnay (1993). Ensemble forecasting at the NMC: The generation of perturbations. Bull. Amer. Meteor. Soc., 74, 2317–2330.

An integrated approach to the study of high temporal variability coastal phenomena: Temporal variability of local diurnal upwelling driven by sea breeze along Civitavecchia coast

Riccardo Martellucci*, Simone Bonamano*, Viviana Piermattei, and M. Marcelli

Laboratory of Experimental Oceanology and Marine Ecology (DECOS), Tuscia University, Italy

Abstract

A modern approach to the study of coastal phenomena requires both an appropriate spatial and temporal resolution and a synoptic observation. For this reason, a rapid and high-resolution data acquisition is indispensable in order to describe the high variability of dynamical processes.

The traditional methods used in in-situ surveys are limited both in terms of the spatial and temporal sampling rate and in the duration of the observation. The development of remote sensing has permitted synoptic observations on large areas, but up to now in the coastal areas this approach suffers from a low spatial resolution and the lack of in-situ data for calibration of sensors.

The approach followed by this work consists of the integration between oceanographic and meteorological data, collected with a high temporal resolution, and coastal mathematical models, to describe and follow the evolution of high variability phenomena. The objective of this study is to analyse and describe the effect of the summer breeze on the coastal dynamics, in order to know if the upwelling phenomena driven by the sea breeze is included into the microscale.

This paper shows the data obtained during different summer surveys carried out between 2008 and 2010 along the Civitavecchia coast (Latium, central Tyrrhenian Sea), and intends to show how the sea breeze affects the spatial and temporal distribution of physical and biological variables. Oceanographic and meteorological data were acquired by a small vessel equipped with a multi-parametric probe and a weather station. In order to accurately characterise the wind field, meteorological data were integrated with those acquired by a network of ground weather stations.

Keywords: Upwelling, sea breeze, high-resolution data.

1. Introduction

Diurnal local upwelling driven by sea breeze often modulates significantly physical and biological nearshore processes.

During the summer, interactions between favourable land winds and coastal topography produce coastal upwelling: every day the winds, forcing along the coast, create upwelling and downwelling conditions, for a period of approximately 40 days. The

* Corresponding author, email: riccardomartellucci@gmail.com; simo_bonamano@unitus.it

upwelling/downwelling cycles have a very relevant importance relating to marine biological processes. For example, they are linked to recruitment pulses of both intertidal invertebrates and commercially important fish species (Rau *et al*., 2001).

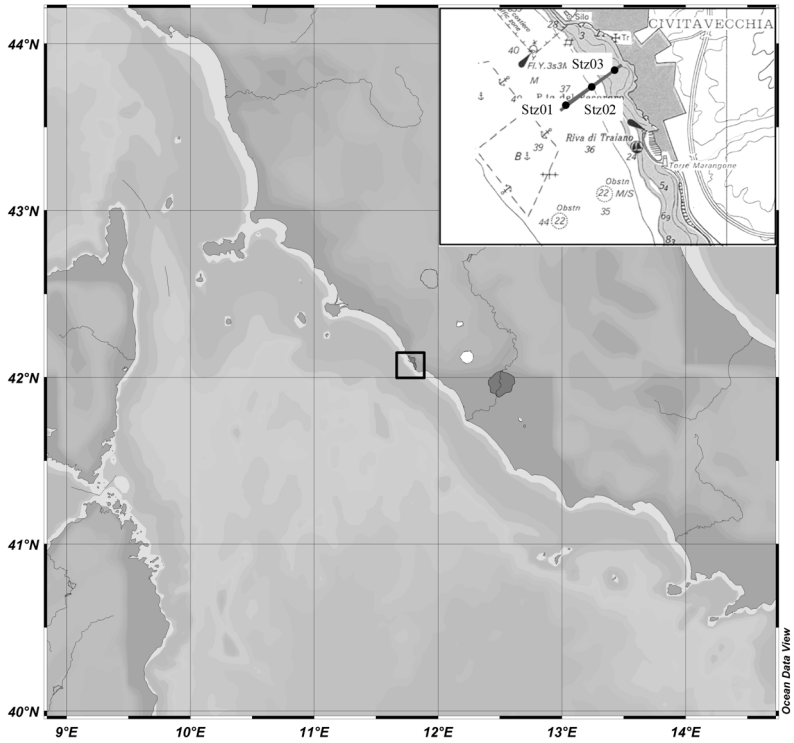

Figure 1 Map showing the location of study area, in the northern Latium coast (Italy) included between P. St. Agostino and Capo Linaro (Lazio, Italy). The sampling plan is shown on the top right.

Previous studies of the upwelling shadow and local wind forcing have focused on temporal scales longer than one day and thus they have not examined diurnal wind effects on inner shelf circulation (e.g. Graham and Largier, 1997; Drake *et al*., 2005).

Here we examine diurnal winds and their effects on local upwelling; documenting the effects of a diurnal sea breeze on the nearshore thermal structure of northern Lazio, Italy, during the investigations of various monitoring, carried out in August 2011. The results show that these kind of phenomena, according to Dickey (1991) would be collocated between microscale and mesoscale processes.

2. Results

Regional conditions during the study period (August 2010) were typical of upwellings during summer season (Figure 2). Data was collected at a meteorological measuring station, located within the port of Civitavecchia, (42°05.796' N, 11°47.132', 20 m elevation), able to measure temperature (Vaisala HMP50), wind direction and speed

(RM Young Wind Sentry Set), and atmospheric pressure (Vaisala PTB101B). The data collected show an alternation of winds from North-East South-East during the night, and West, during the day: a typical breeze cycle.

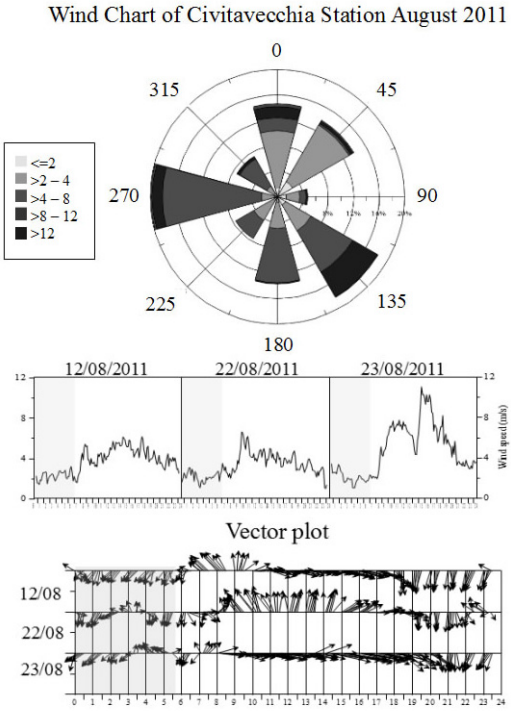

Figure 2 Time series of data at Civitavecchia station. Top: wind chart for August 2011; Middle: temperature variation over 3 days in August; Bottom: hourly wind speed and direction for 3 days in August.

In-situ surveys were carried out on board a vessel equipped with a meteorological station and, to describe physical and biological seawater characteristics, a multi-parameter probe (Ocean Seven 316 Multi-parameter Probe IDRONAUT).

The sampling plan (Figure 1) consists of three stations located at the 10, 20 and 30 m isobaths in order to obtain a high frequency time records; the oceanographic data were acquired every 30 minutes.

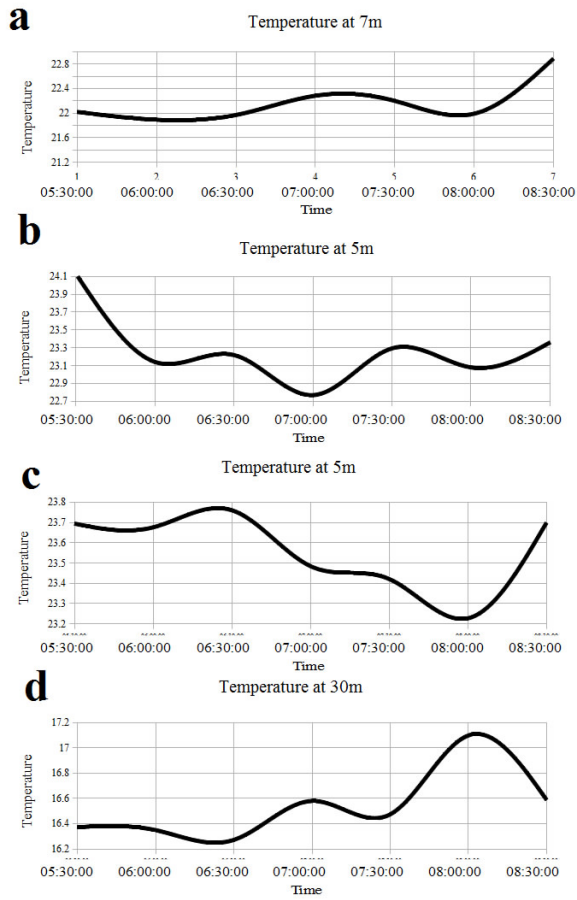

Figure 3 High-resolution time series on 23 August; a) st03; b) st02; c) and d) st01.

Figure 3 and Figure 4 show data elaborations for 23 August; this date is representative of local upwelling condition. The diurnal sea breeze signal is evident in Figure 3; which shows the variation of temperature with time. The temperature decreases with increasing time (Figure 3a, b, c): a phenomenon likely caused by the water upwelling from the underlying colder layers. Figure 3d shows the distribution of temperature at a depth of 30 m. The variable trend shows a temperature increase with time.

In both Figure 3 and Figure 4 we note the end of the upwelling condition that occurs at 8:00 AM. For this purpose, from the data processing, it is clear that the observed phenomena do not last more than six hours.

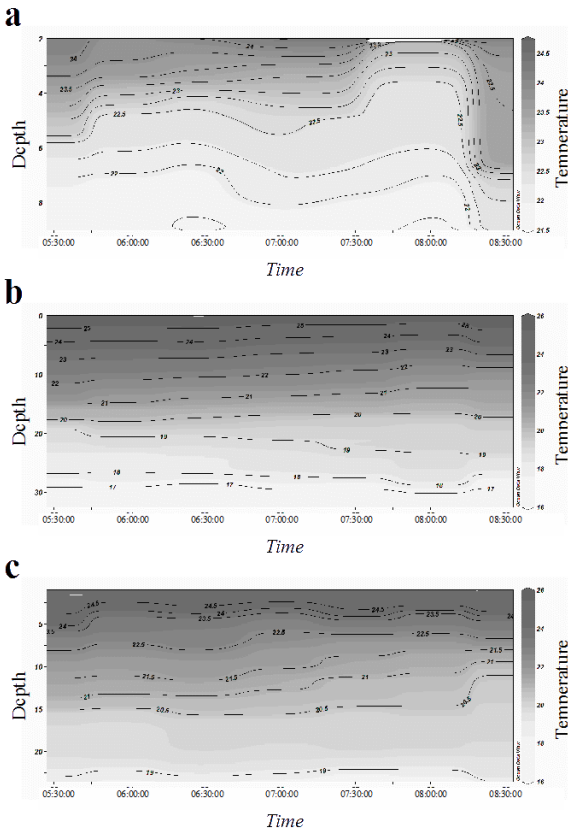

Figure 4 Upwelling on 23 August. a) st03; b) st01; c) st02

3. Conclusions

Large sea water temperature fluctuations were observed in the coastal area of Civitavecchia. Wind fields and temperature changes in water column suggest that the observed temperature fluctuations are due to coastal upwelling, driven by breeze.

Data analysis shows that the breeze upwelling has a life less of six hours, so these kind of phenomena, according to Dickey (1991), would be collocated between microscale and mesoscale processes. Otherwise it is clear that these diurnal fluctuations could not be attribute to the nearshore mixing process.

References

Dickey, T.D. (1991). The emergence of concurrent high-resolution physical and bio-optical measurements in the upper ocean and their applications. Rev Geophys 29: 383–413.

Drake, P.T., M.A. McManus, and C.D. Storlazzi (2005). Local wind forcing of the Monterey Bay area inner shelf. Continental Shelf Research 25, 397–417.

Graham, W.M., and J.L. Largier (1997). Upwelling shadows as nearshore retention sites: the example of northern Monterey Bay. Continental Shelf Research 17, 509–532.

Rau, G.H., S. Ralston, J.R. Southon, and F.P. Chavez (2001). Upwelling and the condition and diet of juvenile rockfish: a study using 14C, 13C, and 15N natural abundances. Limnology and Oceanography 46, 1565–1570.

Traganza, E.D., D.G. Redalje, and R.W. Garwood (1987). Chemical flux, mixed layer entrainment, and phytoplankton blooms at upwelling fronts in the California coastal zone. Continental Shelf Research 7, 89–105.

Woodson, C.B., D.I. Eerkes-Medrano, A. Flores-Morales, M.M. Foley, S.K. Henkel, M. Hessing-Lewis, D. Jacinto, L. Needles, M.T. Nishizaki, J. O'Leary, C.E. Ostrander, M. Pespeni, K.B. Schwager, J.A. Tyburczy, K.A. Weersing, A.R. Kirincich, J.A. Barth, M.A. McManus, and L. Washburn. (2007). Local diurnal upwelling driven by sea breezes in northern Monterey Bay. Continental Shelf Research 27 (2007) 2289–2302.

Downscaling methodology for coastal zones wave power assessment

F.M. Carli*[1], S. Bonamano[1], M. Marcelli[1], and M. Peviani[2]

[1]*Tuscia University*
[2]*RSE – Ricerca sul Sistema Energetico*

Abstract

Energy production from wave motion is one of the most challenging topics in applied oceanographic sciences. Despite its huge potentialities for development, at present there are very few projects that have reached a high grade of maturity.

In order to enable a faster market development, several barriers have to be faced; amongst which the evaluation of the effective wave energy potential deserves particular attention. This paper presents a methodology to assess the real wave energy potential in deep and shallow waters in a typical Mediterranean coastal environment. At the first stage, the methodology provides a wave power assessment in deep waters through the elaboration of wave gauge data, that draws bands of wave power distribution on a large scale area. The wave climates derived in the first part of the work are used as an input for numerical tools, aiming to evaluate the most promising sites as far as energy availability is concerned. In the second stage a regional characterisation is carried out. In this phase numerical models are used, to simulate wave propagation from deep to shallow waters, using bathymetric data from nautical charts, that allow the definition of the most suitable zones for wave energy production. Furthermore, interactions of wave spectrum with the shallow seabed and with the complex morphology of coastal zones need to be assessed with the highest possible accuracy, using detailed spatial resolution. Therefore, the third stage deals with a local scale analysis, allowing computation of the effective energy potential at a specific location. Finally, the fourth stage concerns the validation of the previous numerical outcomes with in-situ measured data. This research explains the details of the downscaling methodology and the pilot case study in the Northern Lazio coastal region (Italy).

Keywords: Wave power, coastal zone, electricity generation, numerical modelling, downscaling.

1. Introduction

The proposed downscaling methodology for coastal zone wave power assessment is articulated into four steps, as follows:

- Large scale assessment through the elaboration of data from offshore wave gauges, used for the elaboration of the Italian wave power atlas.
- Regional scale characterisation through wave propagation models and the identification of the most promising energetic zones.

* Corresponding author, email: fmcarli@unitus.it

- Local scale analysis though the evaluation of high resolution wave climate aiming to identify suitable sites for near-shore energy production.
- Validation of the methodology results through in-situ measurements.

The entire overview of the proposed methodology is presented in Figure 1.

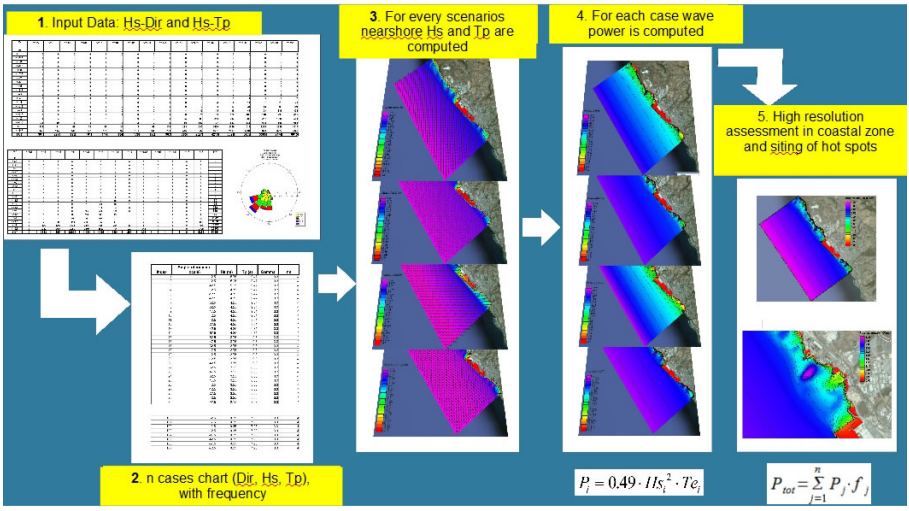

Figure 1 Scheme of the proposed downscaling methodology for coastal zones.

The main objective of this methodology is to assess the overall (annual and seasonal) wave energy potential at near-shore points where usually no data is available. In particular, the methodology is tested along the Northern Lazio coastal zone, with particular detail in Civitavecchia shores.

2. Data and methodology

To accomplish the first step of the methodology presented here, measured data are required. In Italy, the most extensive wave data service is the National Ondametric Web (RON) which runs an array of fifteen measurement buoys, placed around the coast. However, in order to make a comprehensive evaluation of the national offshore wave power, the RON dataset is not completely adequate, as both the time scale and the spatial scale are not always satisfactory. Measurement buoys were deployed at different times; in 1989 only eight instruments were installed, while others were added later and in different steps. Moreover some parts of the coast are still without wave gauge coverage. For this reason, wave data from the National Electricity Board were added to the dataset. The National Electricity Board (ENEL) has deployed an array of measurement instruments since the 1970s, in the proximity of power plants and other sensitive infrastructure along the coast. The addition of this data allows a more extensive analysis of the wave climate found in Italian waters.

The coverage of wave measurement buoys is shown in Figure 2.

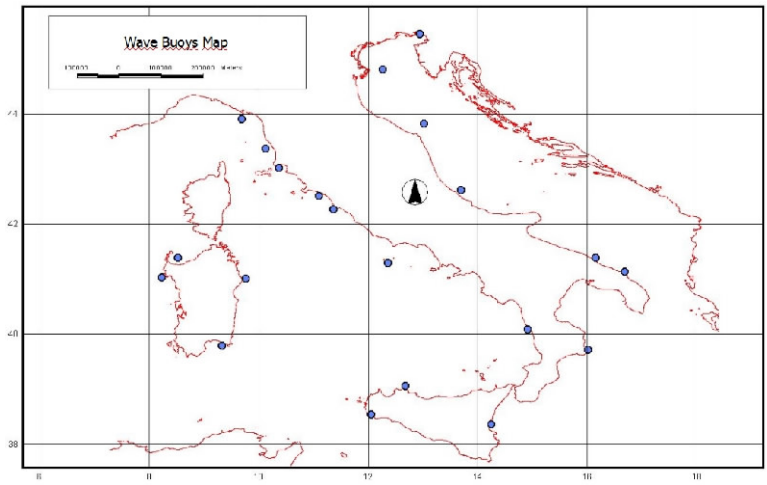

Figure 2 Wave buoy distribution.

Further steps of the methodology deal with the simulation of wave propagation from deep to shallow waters. For this work the STWAVE model, included in the SMS package, was used. STWAVE (STeady-state spectral WAVE model) is a steady-state finite difference model based on the wave action balance equation:

$\omega^2_r = g*k*\tanh(k*d)$

where: ω = angular frequency; g = gravitational acceleration; k = wave number; d = water depth.

The main model input is represented by a wave spectrum that is a statistical representation of a wave field and it is calculated from wave direction, significant height and peak period by different formulations (JONSWAP, TMA Shallow Water, etc).

STWAVE simulates depth-induced wave refraction and shoaling, current induced refraction and shoaling, depth- and steepness-induced wave breaking, diffraction, wind-wave growth, and wave-wave interaction and white capping that redistribute and dissipate energy in a growing wave field (Smith *et al*., 2001).

3. Application of the downscaling methodology

3.1 Large scale assessment, elaboration of the Italian wave power atlas

The first step of the methodology concerns the analysis of the available wave gauge data. The amount of data collected for the scope of this work needed to be screened and selected before being used in wave power computing. To have a clear view of the real wave climate in the area of a buoy, a range of operations were carried out, such as removing spikes and evaluating the functioning time percentage.

Once the out-of-scale data have been examined and eventually corrected, it is very important that the observing time series be made coherent by assessing any gaps in the data. Malfunctioning wave gauge buoys, problems with moorings, communication obstacles, and extreme weather conditions can result in gaps in the acquisition of spectral

parameters. For this reason obtaining a continuous and complete time series of data is quite difficult. The absence of some information was weighed and analysed and a differential distribution of the seasonally missing data established. In this way, it has been possible to obtain a reasonable distribution of credible data through the year.

From a theoretical point of view, in the field of wave climate assessment studies, several variances in the definition of the wave power were proposed. Differences are mainly due to the different interpretation of the spectrum and the associated approximation. The methodology adopted in this work is taken from the "Wave Data Catalogue for Resource Assessment in IEA-OES Member Countries" (2009), published by the Ocean Energy System - International Energy Agency (OES-IEA). In deep water, when depth is higher than half the wavelength (d>L/2), the wave power *P* can be computed in terms of significant wave height and energetic period:

$$P = \frac{\rho \cdot g^2}{64 \cdot \pi} \cdot Hs^2 \cdot T_e\left(\frac{W}{m}\right)$$

Seawater density is assumed to be ρ =1025 kgm^{-3}, and the gravity acceleration g = 9.81 ms^{-2}. Consequently wave energy flux for the length unit of wave front in computed as follows:

$$P = 0.49 \cdot Hs^2 \cdot T_e\left(\frac{W}{m}\right)$$

where *Hs* is expressed in metres and T_e in seconds.

In oceanographic datasets, energetic period is usually not specified so, when the spectrum shape is unknown, it has to be derived on the basis of other known parameters. For example, in the drawing of the "Atlas of UK Marine Renewable Energy Resources" (2004), the energetic period was assumed to be $T_e = 1.14 T_z$, where T_z is the average period of the spectrum.

In the present study, the energetic period is evaluated following the criterion described by Cornett (2008), that is a function of the peak period T_p as follows:

$$T_e = \alpha \cdot T_p$$

The α coefficient depends on the shape of the wave spectrum: α = 0.86 for a Pierson-Moskowitz one, with α tending to 1 with the narrowing of the spectrum. For example, Hagerman (2001) assumed $T_e = T_p$ in evaluating wave potential in southern New England. In the work of Cornett a more conservative assumption was made, for which α = 0.90, meaning $T_e = 0.9 T_p$, corresponding to a standard JONSWAP spectrum, considering a peak factor γ = 3.3.

By repeating this methodology for every wave gauge a global evaluation for Italian coasts was made possible (Table 1).

By assigning the available wave gauge data to the corresponding tract of the littoral, it was possible to derive the Italian wave power atlas, as reported in Figure 3.

Table 1 Wave power computing results

Station	Operator	Annual Mean Power (kW/m)
Alghero	RON	11,74
Mazara del Vallo	RON	5,49
La Spezia	RON	3,85
Ponza	RON	3,77
Palermo	RON	3,65
Fiume santo	ENEL	3,46
Crotone	RON	3,37
Cetraro	RON	3,15
Civitavecchia	RON+ENEL	3,12
Piombino	ENEL	3,08
Punta della Maestra	RON	2,75
Ancona	RON	2,60
Monopoli	RON	2,57
Catania	RON	2,43
Ortona	RON	2,33
Montalto	ENEL	2,28
Marina di Cecina	ENEL	2,18
Siniscola	RON	2,02
Brindisi	ENEL	1,49
Cagliari	RON	1,44
Punta Sdobba	ENEL	0,17

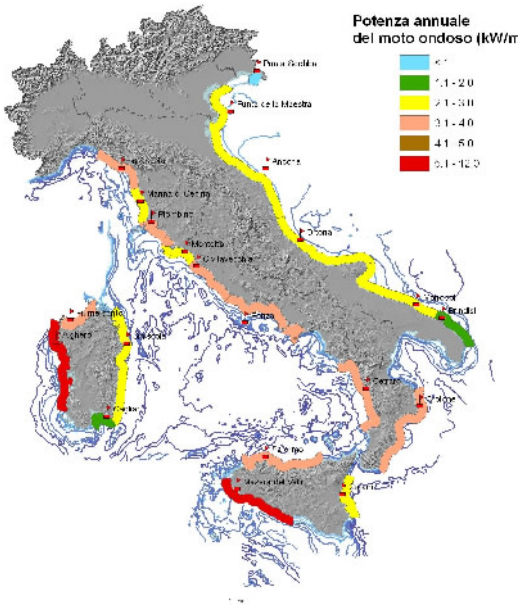

Figure 3 Italian wave atlas.

3.2 Regional characterisation

The second part of the methodology consists of the evaluation of the propagation of wave fronts approaching the coast. At this stage, the goal of the methodology is to make a qualitative description of the differences in the sea states, originating in the same area and reaching different tracts of littoral. The offshore boundary conditions are those produced in the first step, while the STWAVE numerical model is the tool through which simulations are carried out. The methodology was applied to the coast of Lazio Region, and wave power potential corresponding to two wave conditions is presented in Figure 4.

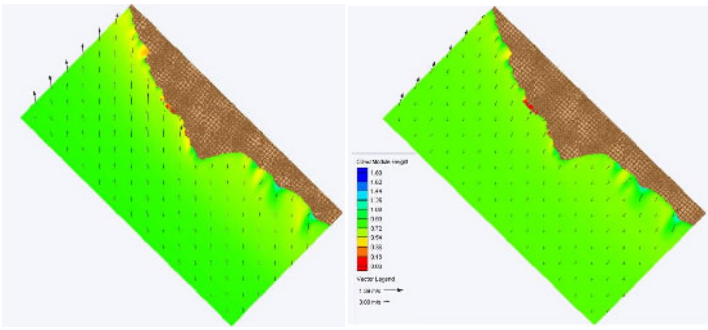

Figure 4 Wave power (KWm^{-1}) for Ostro (180°) and Libeccio (225°)

General considerations can be made when analysing the results. The fast deepening of the bathymetry makes wave trains maintain their spectral parameters up to a very close distance from the coastal line. When waves reach the shore, the local bathymetry trend affects wave height and period, and accordingly wave power. In some of the sites, a strong decrease in wave height is observed, where energy losses due to the friction effects of sea bottom are more intense. By contrast, in some locations a conservation, or even an increase in wave heights, can be observed. Model simulations can now be used to identify the most interesting areas for wave energy production.

3.3 Local scale analyses

At this stage, the most promising traits of littoral highlighted in the previous step were considered as new domains for high resolution simulations. The accuracy of bathymetric maps plays a key role at this point. For the scope of the present analysis the bathymetric map was drawn from in-situ surveys carried out with a single-beam tool, which allowed a 20 m grid spatial resolution.

When wave parameters are computed inshore it is possible to analyse the wave height distribution maps, allowing a qualitative and quantitative investigation of the most suitable sites. Model results are presented as wave power distribution maps, as shown in Figure 5. By simulating all wave scenarios throughout the year, it is possible to obtain the mean wave power distribution map, and interesting spots can thus be highlighted. Figure 5 provides the final results given by the integration of wave scenarios of a typical year, leading to the accumulated wave power map. In particular, the right part of Figure 5 shows a simulation detail of an interesting area for wave power generation (see the spot highlighted in violet).

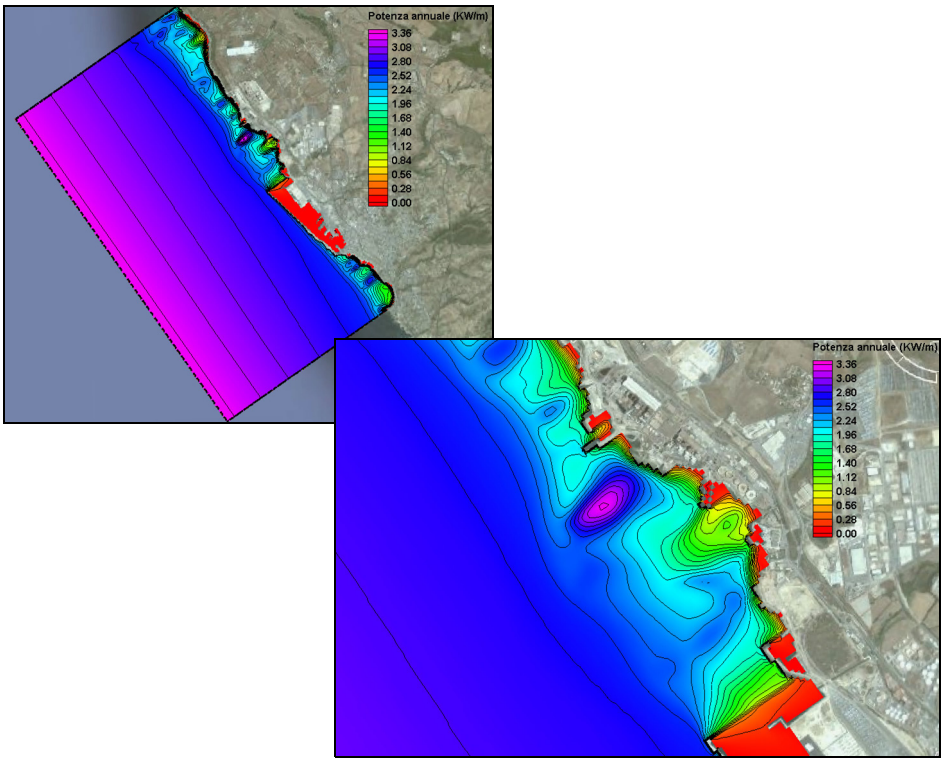

Figure 5 Left: annual mean power map. Right: a spot with high wave power.

Along most of the coast, wave power levels strongly decrease shorewards, as was predictable, but in the spot highlighted in Figure 5, they show a consistent similarity with wave power levels offshore. While wave heights generally slow down when approaching the coast, in certain bathymetric conditions, they can increase again as they move through shallow waters, and these locations are clearly indicated in the figure.

3.4 Validation of model results

The last stage of the methodology concerns the validation of model results. In order to be confident of the accuracy of the numerical simulations, an instrumental observation of near-shore wave parameters is necessary, as a final verification of the process. Verification for at least one point along the coast would allow a reasonable degree of confidence that, on the local scale, wave parameters are properly described by the model.

At present there are no wave buoys in Civitavecchia's coastal waters and an accurate validation has not been possible to date. A large series of observations have been made in the areas covered by the above analyses and these seem to confirm the results; the highlighted spot does actually demonstrate a higher wave height compared to neighbouring tracts of coast. However, these observations are still inadequate to affirm that the model results are correct. At the beginning of 2012, a wave gauge will be installed in the zone of investigation so that a very careful analysis of wave fronts approaching the coast

can be carried out. This will enable validation of the model results for wave heights and wave power generated by the model.

4. Conclusions

The implementation of the methodology process in a pilot coastal area has shown some significant issues. As regards the large scale assessment and the Italian Wave Atlas, factors like sectors exposure and fetch lengths are consistent with the magnitude of the computed available wave power. Indeed, as it was predictable on the basis of the preliminary observations, the western side of Sardinia presents the highest energetic field of the Italian coasts, where power levels can reach and exceed 10 kWm^{-1} while on the eastern side the available energy is low because of the sheltering effect of the island. High wave energy availability can be identified on the western side of Sicily as well, particularly as regards to the southern part, exposed for a wide length to south quadrant wave events (6 kWm^{-1}). Along the Adriatic coasts, power levels are very low, as predictable, both for a shorter fetch and for the morphological trend of Italian and Balkan coasts. Power levels usually do not exceed 3 kWm^{-1} and represent the lower values of the Italian seas. In the end, regarding the Tyrrhenian basin, values may vary consistently, with respect to the complex trend of the coastline and to the presence of several islands and archipelagos. In this basin power levels typically range from 2 and 5 kWm^{-1}.

As regards the modelling process, the downscaling approach avoided the information losses, which is one of the most challenging issues in numerical procedures. The dataset produced by wave buoys was used as input in the STWAVE model. Areas of interest that emerged during the regional analyses, were confirmed at the local scale. Moreover the local analyses enabled a comprehensive wave climate to be made for the identified sites, producing information on the wave train behaviour when they approach the coastline. At this stage the crucial importance of a very well-defined bathymetry has appeared as a bottleneck for the accuracy of results. In particular, in the Lazio northern coast a very interesting spot was highlighted, right north of the harbour. In this place wave power seems to keep the offshore levels which, as a yearly average, are between 3.30 and 3.40 kWm^{-1}, just like the offshore measurements. As soon as a wave buoy has been deployed, the results will be analysed in a more accurate process.

References

Cornett, A.M. (2008). “A Global Wave Energy Resource Assessment” – Canadian National Research Council.

Ocean Energy System – International Energy Agency (OES-IEA), (2009). “Wave Data Catalogue for Resource Assessment in IEA-OES Member Countries”

Peviani, M., F. Carli, and S. Bonamano (2011). “Wave Energy potential map along the Italian coast available for marine power generation” – paper presented at the HYDRO 2011.

Vicinanza, D., L. Cappietti, and P. Contestabile (2009). “Assessment of Wave Energy around Italy”, 8th European Wave and Tidal Energy Conference, Uppsala, Sweden.

Smith, J.M., A.R. Sherlock, and D.T. Resio (2001). “STWAVE: Steady-State Spectral Wave Model. User’s manual for STWAVE, Version 3.0”, Coastal and Hydraulics Laboratory, ERDC/CHL SR-01-1.

Sustained glider transects and data assimilation in the Levantine Sea

Daniel Hayes*[1], George Zodiatis[1], Pierre Testor[2], Angelos Hannides[1], and Gregory Konnaris[1]

[1]*Oceanography Center, University of Cyprus, Nicosia, Cyprus*
[2]*LOCEAN-IPSL/CNRS, Universite Pierre et Marie Curie, Paris, France*

Abstract

Between March 2009 and February 2011, over 3000 profiles of oceanographic parameters have been collected in the Eastern Levantine by the Oceanography Center, University of Cyprus autonomous underwater vehicles (gliders), most to 1000 m depth. Measurements include temperature, salinity, fluorescence (Chl-*a*) and optical backscatter at 470 nm and 700 nm. These profiles provide a detailed description in time and space of the general thermosaline characteristics as well as mesoscale features and variability that dominate the region. In particular, the Cyprus eddy has been characterised to an extraordinary level of detail multiple times. Daily temperature and salinity data from one glider mission have been assimilated in the Cyprus Oceanography Center ocean model using the 3DVAR technique. A five-month simulation produces a more realistic flow field when assimilating temperature and salinity from one glider.

Keywords: Gliders, operational oceanography, Mediterranean Sea, data assimilation, Cyprus eddy.

1. Introduction

In recent years, the Eastern Levantine basin has been examined using long-range autonomous underwater vehicles known as gliders. While previous work has provided the backdrop for the new experiments, it is clear that the primarily ship-based monitoring has been unable to adequately characterise the high temporal and spatial variability commonplace in the Levantine. The gliders, on the other hand, can collect information over seasons and at scales of 5−10 km in a single mission. This, along with numerical simulations, has led to a more definite and detailed description of the area. Ovchinnikov and Fedoseyev (1965) postulated the general cyclonic circulation around the circumference of the basin, with sub-basin scale features in the interior. Later, in the 1980s, the Physical Oceanography of the Eastern Mediterranean (POEM) cruises provided a more complete description of the vertical and horizontal distributions and movements of the water masses of the Levantine Sea. Four water types are present: the Levantine Surface and Intermediate Water (LSW and LIW) masses sandwiching the Atlantic Water (AW), with the Eastern Mediterranean Deep Water (EMDW) at the deepest observed levels (Robinson *et al*, 1991, POEM Group, 1992). Variability at basin scales, sub-basin scales, and the mesoscale has been recognised by many authors (Hecht *et al*., 1988). A picture has been established of intense mesoscale anticyclonic activity within a backdrop of the

* Corresponding author, email: dhayes@ucy.ac.cy

generally cyclonic circulation of the Levantine basin (Robinson and Golnaraghi, 1993; Zodiatis *et al*., 2005). These anticyclones typically contain warmer, saltier LIW, with subsurface meandering currents with an AW signature. The generation mechanism and evolution of the eddy field is not yet clear because of the difficulty in obtaining data sets with adequate resolution and coverage in time and space. Data sets have been collected by ship-based hydrographic sampling and have shed light on the variability of a particularly persistent eddy known as the Cyprus eddy. Anticyclonic features are clearly present in the annual hydrographic data from the Cyprus Basin Oceanography (CYBO) programme since 1996, with variable position, and sometimes with two or three such features (Zodiatis *et al*., 2005; 2010). A second eddy, known as the Shikmona eddy has been observed to pinch off from the coastal current of Israel and Lebanon. It appears as an eddy with strong surface signatures consistent with waters of coastal origin before dissipating (Gertman *et al*., 2010). However, anticyclones like the Cyprus eddy have little or no surface signature in the summer season because of the strong surface heating and evaporation, while in winter the surface signature is also very small because of the strong mixing with LSW (Brenner *et al*., 1991). The Mid-Mediterranean Jet (MMJ) has proven even more difficult to track because of its subsurface character, and its strong temporal variability.

2. Methods

Hydrographic data sets from ships in an active mesoscale eddy field are difficult to interpret, and remote sensing cannot provide a detailed view of eddy structure and dynamics, so in the Levantine base, an autonomous platform has been used: the ocean glider (Hayes *et al*., 2010; 2011). Gliders travel long distances over a programmed course while making measurements in the water column (Davis *et al*., 2002; Rudnick *et al*., 2004). Because it propels itself by modifying its buoyancy and its attitude, creating forward lift on the wings and body, it moves slowly and with high efficiency (about 20 km per day for up to 6 months). It moves in a sawtooth pattern at angles of 15–40 degrees from horizontal. When at the surface it exchanges data and commands with a land station using Iridium satellite communication. In the current study, two gliders of the Cyprus Oceanography Center, manufactured by the Seaglider Fabrication Center of the University of Washington were used (Eriksen *et al*., 2001). These gliders carry a suite of sensors consisting of Seabird Electronics unpumped conductivity and temperature (SBE-03, 04) and dissolved oxygen (SBE43) sensors, and a WetLabs BB2FVMG ECO puck for chlorophyll-a fluorescence and optical backscatter (470 nm and 700 nm). Dive-average currents (DAC) are computed based on GPS locations and an on-board model of the vehicle trajectory. The gliders are programmed to dive to 1000 m (when the bathymetry allows) over butterfly patterns south of Cyprus. The size of the pattern has been chosen to allow the glider to traverse any given leg of the pattern in a matter of 7–10 days. In this paper, a summary of the data collected with gliders, including the Cyprus eddy characteristics will be provided. Some supporting data from ship-based instruments will also be presented.

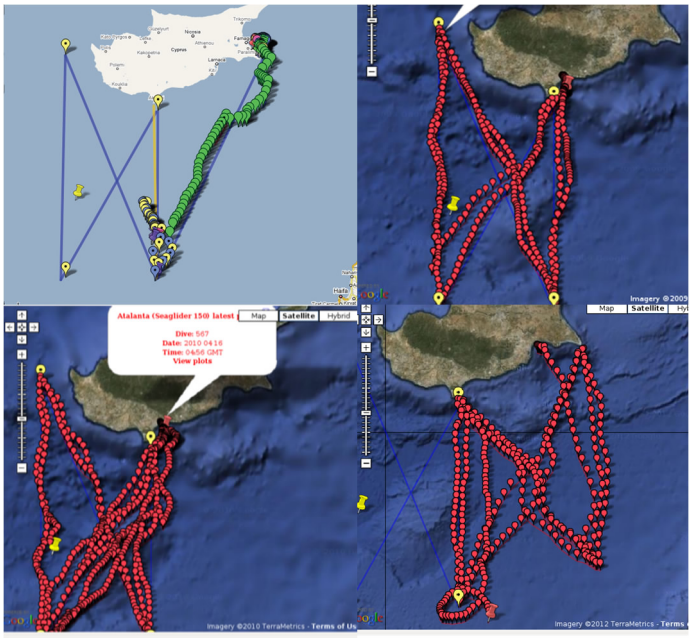

Figure 1 Map of OC-UCY glider surface positions from March 2009 – February 2011. A total of 1471 dives have been completed in these multi-month missions, most to 1000 m. See text for explanation of separate maps

3. Results and Discussion

With 23 extensive hydrographic cruises since 1996, the Cyprus Basin Oceanography programme (CYBO) provides an informative background regarding the expected location and properties of the Cyprus eddy (Zodiatis *et al*., 2005; 2010). The glider transects have been arranged according to the coverage and gaps of that programme (Figure 1). The first long mission was carried out by an OC-UCY glider in March–April 2009 for approximately 1 month and 177 dives (upper left in Figure 1). The V-shaped transect from the southeast tip of Cyprus to (33° N, 33° E) then north towards Cyprus did not reveal anticyclonic circulation. It did, however, indicate the presence of near-surface LIW, although it does not appear to have been locally formed. Water of nearly the same character was found in the eddy core in the 385 dives of the second glider mission from May to August 2009 (upper right Figure 1). The warmer and saltier LIW core of the eddy was evident most clearly at 300 dbar (~300 m), which is approximately the depth of widest eddy extent (80 km).

The “Eye of the Levantine” experiment in November–December 2009 was devised with this information in hand. In addition to the Cyprus glider in Figure 1 (lower left), a fleet of 5 additional gliders was deployed, along with surface drifters and profiling floats. Also, the TARA/Oceans research and sailing vessel was able to sample the eddy based on prior information from the glider fleet. The Cyprus eddy was again found near the Eratosthenes Seamount (Figure 2). The eddy typically has a radius of about 40 km and consists of a core of LIW extending down to 400 m. The slightly fresher AW is found

just below the thermocline, most noticeable in this section around the northern edge of the Cyprus eddy. Dissolved oxygen, optical scattering, and chlorophyll fluorescence typically show maximum values also in the layer just below the thermocline (not shown). The radius and maximum thickness of the eddy estimated are about 45 km and 300 m, respectively. The AW layer becomes appreciably thicker and more noticeable as the northern edge of the eddy is approached. In Figure 3, it is possible to see more results from this mission. In this case, the temperature and salinity at 300 dbar are plotted with colour-coded dots on a map, showing that from 21 December 2009, to 30 January 2010, seawater characteristics in the vicinity of the seamount changed. The southwest to northeast diagonal was completed from 5−14 January and shows clearly the higher temperature and salinity values over the seamount (shading), while the opposing diagonal (23−30 January) southeast to northwest shows a much weaker maximum.

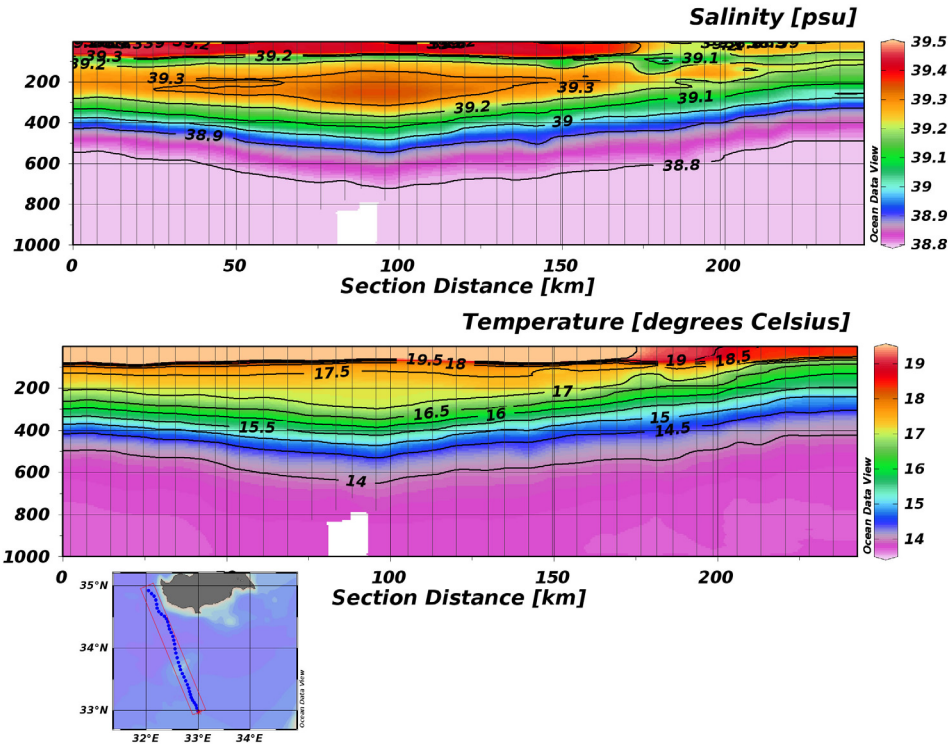

Figure 2 Vertical section of a) Salinity and b) Potential temperature from glider 150 ascents from December 1−23, 2009. The section begins at the south terminus of the transect. Positions at the end of each ascent are shown with vertical black lines.

Comparisons with ship-based measurements before, during, and after the EYE project indicate good agreement with the glider data, in particular Conductivity-Temperature-Depth (CTD) and Acoustic Doppler Current Profiler (ADCP) data from the Maria S. Merian cruise MSM 14/1 collected in the seamount area from mid-December 2009 to early January 2010 (Christiansen *et. al.*, 2011). Vertical profiles of temperature, salinity, and the TS-diagram all indicate very close agreement in the intermediate and deep water

masses, however, the AW and LSW changed significantly in 10 days between the sampling, probably because of horizontal advection. Because of the detailed information provided by the gliders in near real time, it was possible to direct the ship in order to optimise sampling of the eddy.

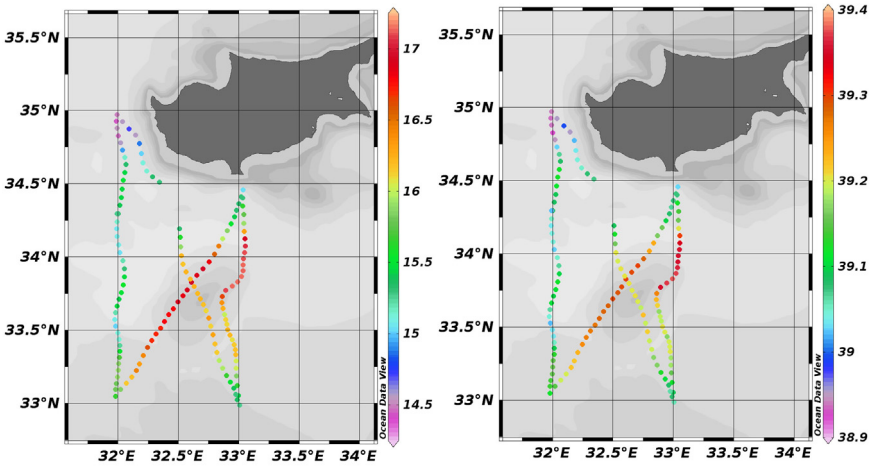

Figure 3 Surface map of a) Potential temperature and b) Salinity at 300 dbar at the surface positions of glider 150 from 21 December 2009 to 30 January 2010. The track begins southwest of Cyprus, and by the end of January is nearly back to the same position.

During MSM 14/1, a 76.8 kHz ADCP was used to measure current profiles during each CTD station. Vertical bin thickness was set to 16 m, the centre of the first bin is at 24 m. Fifty bins were collected, and the maximum range was 800 m. The Teledyne-RDI software WinADCP was used for the pre-processing ADCP data, including referencing to true currents in geographical coordinates using the ship GPS. A Matlab script was used to read and average the files produced by WinADCP. Currents were averaged for periods when the ship was carrying out CTD casts. The depth-averaged currents from the ADCP (approximately 16–800 m) compare well to the dive-averaged currents from Seaglider 150 (Figure 4c). The vertically-averaged currents are between 0.10 and 0.20 $m s^{-1}$ and show the anticyclonic rotation of the eddy. According to the glider-derived currents, the center of the eddy appears to have moved to the west a few km from January 5 to 17. It is also shown that the currents on the south side of the eddy are slightly more intense than the northern side, at least in the glider transect. Since gliders measure density profiles, it is possible to calculate the geostrophic velocity with an arbitrary reference level of 800 m (Figure 4a). The rotation of the eddy core is visible as well as the more intense and tightly focused southern edge of the eddy. The equivalent section of ADCP velocity (Figure 4b) shows excellent agreement, except the location of maximum geostrophic velocity on the southern edge was not sampled (33.75° N–38.0° N).

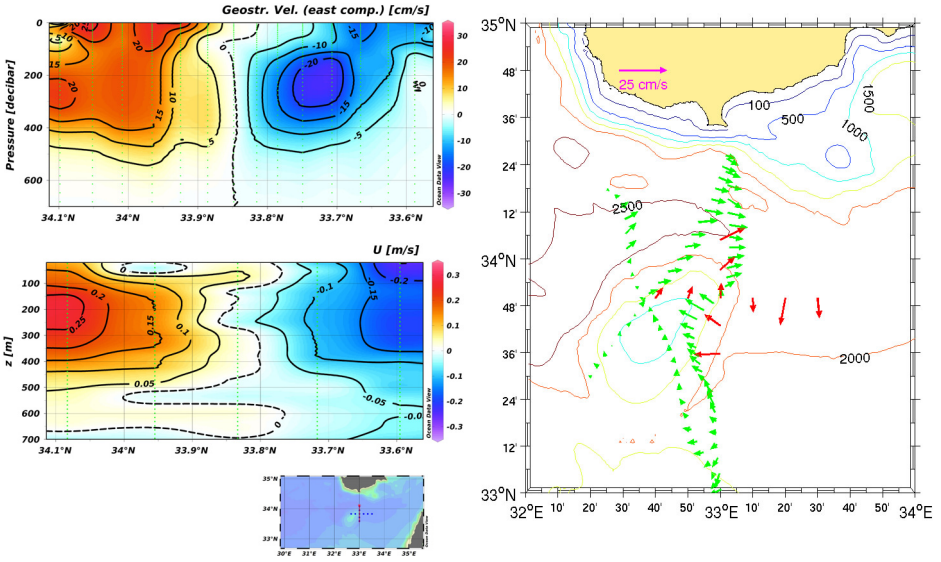

Figure 4 Vertical section of eastward geostrophic velocity from glider density profiles referenced to 800 dbar (a) compared with ADCP profiles from MSM 14/1 (b) and (c) Surface map of Glider-derived dive average currents (top 1000 m, green) and ship ADCP-derived currents vertically-averaged (top 800 m, red) overlaid on contours of bathymetry. Glider mission was 7−31 January, 2010, and MSM 14/1 was 4−5 January, 2010.

Following the 567 dives of the EYE of the Levantine Cyprus glider, a third long mission was initiated in October 2010 (Figure 1, lower right). These 357 dives further tracked the circulation features, including the Cyprus eddy, which was found east of its previous location (Figure 5), but with similar characteristics. Detailed structure of the eddy differed however, indicating an actively evolving and advecting feature of rich complexity.

For more accurate operational forecasts, as well as deeper understanding of the Cyprus eddy, the assimilation of the glider profiles directly into the CYCOFOS forecasting system at OC-UCY has been achieved. The assimilation of temperature and salinity profiles from one OC-UCY glider during the “Eye of the Levantine” project has been completed and compared to the control run of no assimilation. These runs were completed in hindcast mode, in which the model was initialised only at the beginning of the experiment (25 November, 2009, using the University of Athens 1/30° ALERMO model). Then a series of 1 day forecasts were carried out, using the current day’s meteorological forecast (the University of Athens 1/20° SKIRON model). During each run, differences between model and glider profiles were computed when observations were available. After each run, the data assimilation routine “OceanVar” (Dobricic and Pinardi, 2008) was called in order to compute the corrections to the three-dimensional temperature and salinity fields. The following run would read these corrected fields and linearly increment the fields that were read from the “restart” file over the first 20 time steps. The simulation lasted until the end of the last glider profile and continued for another 2 weeks without observations (last output 30 April 2010).

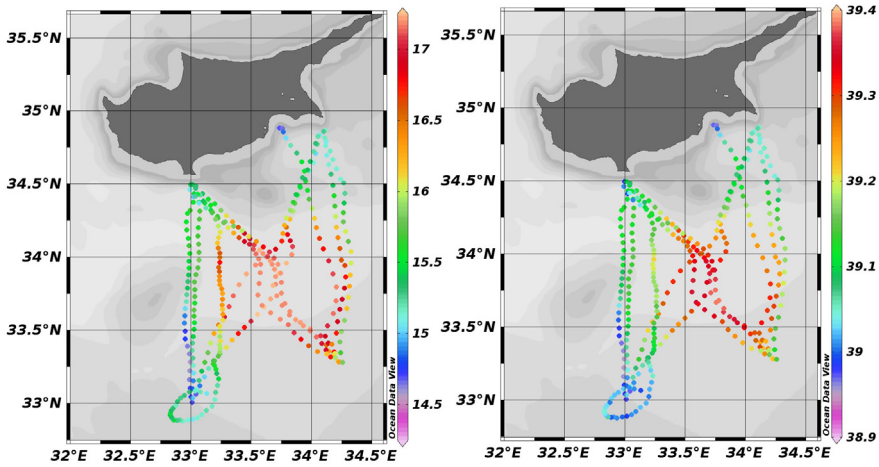

Figure 5 Surface map of a) Potential temperature and b) Salinity at 300 dbar at the surface positions of glider 150 from 12 October 2010 to 30 January 2011. The track begins southeast of Cyprus, and by the end (33°N, 33°E) is nearly through the third cycle through the pattern.

The open boundary conditions strongly influence the persistence of the eddy "inserted" by the data assimilation procedure. However, it is clear that after 5 months of running, the simulation did in fact improve upon the control run (Figure 6). In this figure the model output for temperature and currents at 280 m from both runs are shown. Note the increase in sea temperature south of Cyprus in the region of the Cyprus eddy when assimilating glider data. Further tests are required, in particular the assimilation of temperature and salinity from all six gliders and investigation of other open boundary condition specifications. The improvement of the estimated ocean state will be quantified by comparison with independent data, such as the trajectories of drifters deployed during the experiment compared to model-predicted trajectories, or satellite-derived sea level anomaly compared to model values.

An important first step has been taken. Hindcasts at the Cyprus Oceanography Center were successful in late 2009 and early 2010 in predicting the position and characteristics of the Cyprus eddy. This is despite the fact that the eddy was not present in the Mediterranean Forecasting System hydrodynamic model (from which the operational hydrodynamic model of the University of Athens and in turn that of OC-UCY are initialised). Because of the one-way nesting, the open boundary conditions applied were inconsistent with the presence of the eddy, causing unrealistic evolution. With the eddy present in the model and consistent boundary conditions, one can follow its evolution and compare to existing and future glider missions. More importantly, one can investigate the possible mechanisms responsible for the movement and dissipation of the eddy.

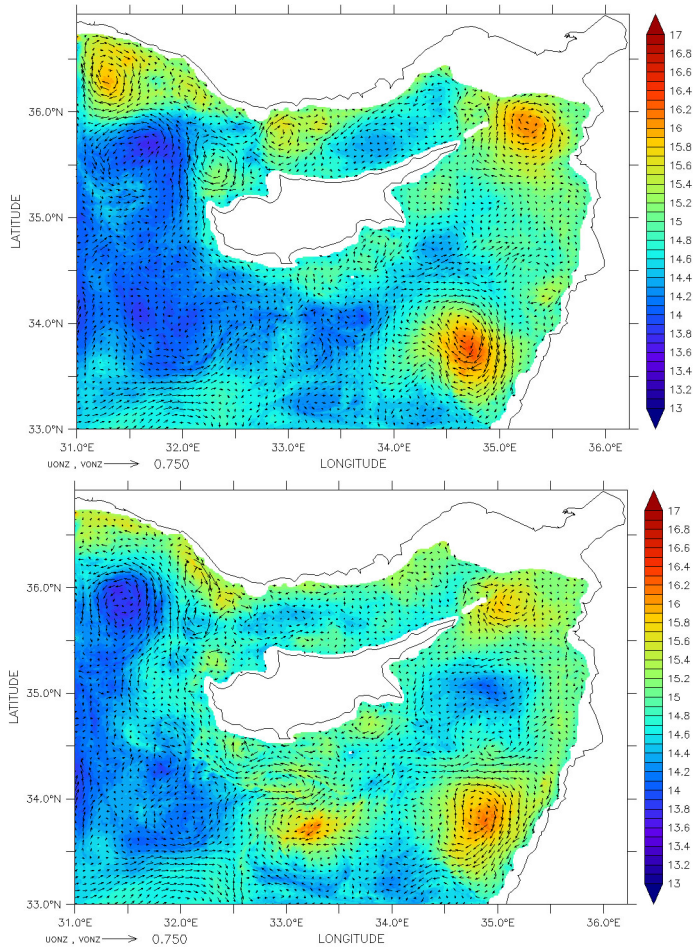

Figure 6 Temperature and currents at 280 m on 19 April 2010 for hindcast model initialised on 25 November 2009: a) the control run and b) the run assimilating daily glider temperature and salinity profiles from glider sg150.

4. Summary

This paper has given a brief overview of data collected in the open sea near Cyprus from 2009 to 2011. A set of four long missions, totalling nearly 1500 dives (3000 profiles) has been completed. Important information on the seasonal and longer timescales over a broad region has been collected. In particular, the Cyprus eddy, observed as a semi-permanent feature as far back as the 1980s from ships, has been examined in detail using gliders. It is an anticyclonic eddy with a core of relatively warm and salty Levantine Intermediate Water extending from just below the Levantine Surface and Atlantic Water to a maximum of 400 m. It is embedded in a generally cyclonic basin circulation, with other eddies often present. A meandering sub-surface current of Atlantic Water, attributed to the MMJ, is found around the upper periphery of the eddy. Further studies

examining the data in terms of ocean state determination using assimilation techniques are required to address questions of the eddy generation mechanism, the reasons for its location and permanence there, as well as the role of the bottom topography, in particular the Eratosthenes Seamount (Brenner, 1989). More glider missions will be carried out to supplement the operational ocean forecasting of OC-UCY, including data assimilation.

Acknowledgements

We would like to thank the scientists who participated in the "Eye of the Levantine" experiment for their willingness to provide instruments and expertise: L. Mortier, L. Beguery, K. Bernadet, F. D'Ortenzio, E. Mauri, F. Lekien, R. Gerin, P. Poulain and A. Lazar. The crew and scientists of the Marian S. Merian accommodated the requested sampling programme with limited time available. The data assimilation software was provided by Dr. Srdjan Dobricic of the Centro Euro-Mediterraneo per I Cambiamenti Climatici, Bologna, Italy.

References

Brenner, S. (1989). Structure and evolution of warm core eddies in the Eastern Mediterranean Levantine basin, J. Geophys. Res., 94: 12,593–12,602.

Brenner, S., Z. Rosentraub, J. Bishop, and M. Krom (1991). The mixed-layer/thermocline cycle of a persistent warm core eddy in the eastern Mediterranean, Dyn. Atmos. Oceans, 15: 457–476.

Christiansen, B., T. Brand., H. Christiansen, S.Christiansen, A. Denda, A. Fischer, K. H. George, D. Hayes, S. Hoffmann, E. Isaias, V. Kalogeropoulou, T. Kesselring, P. Lamont, N. Lampadariou, B. Martin, J. Montgomery, F. Peine, A. Schneehorst, A. Schuster, K. Sevastou, D. Solovyov, H. Stahl, J. Tiedke, R. Turnewitsch, K. Unger, G. Zodiatis (2011). Structure and function of pelagic and benthic communities of the eastern Mediterranean in relation to physical drivers and bottom topography, Cruise N. MSM14, Leg1, 17/12/2009–14/01/2011, Limassol-Limassol. Institut fur Meereskunde der Universitat Hamburg.

Davis, R., C.E. Eriksen and C.P. Jones (2002). Autonomous buoyancy-driven underwater gliders. p.37–58, in: "The Technology and Applications of Autonomous Underwater Vehicles", G. Griffiths, (Ed.), London: Taylor and Francis.

Dobricic, S. and N. Pinardi (2008). An oceanographic three-dimensional variational data assimilation scheme, Ocean modelling, 22 (3): 89–105.

Eriksen, C., T.J. Osse, T. Light, R.D. Wen, T.W. Lehmann, P.L. Sabin, J.W. Ballard, and A.M. Chiodi (2001). Seaglider: A long range autonomous underwater vehicle for oceanographic research, IEEE Journal of Oceanic Engineering, Special Issue on Autonomous Ocean Sampling Networks, 26(4).

Gertman, I., R. Goldman, Z. Rosentraub, T. Ozer, G. Zodiatis, D. Hayes, and P. Poulain (2010). Generation of Shikmona anticyclonic eddy from an alongshore current, Rapp. Comm. Int. Mer Medit., 39: 117.

Hayes, D, G. Zodiatis, G. Konnaris, A. Hannides, D. Solovyov, and P. Testor (2011). Glider transects in the Levantine Sea: Characteristics of the warm core Cyprus eddy, in OCEANS, 2011 IEEE-Spain: 1–9.

Hayes, D., P. Testor, G. Zodiatis, G. Konnaris, A. Hannides, L. Mortier, L. Beguery, F. D'Ortenzio, E. Mauri, F. Lekien, and others (2010). Glider transects in the Levantine Sea: A study of the warm core Cyprus eddy, Rapp. Comm. Int. Mer Medit., 39: 116.

Hecht, A., N. Pinardi, and A. Robinson (1988). Currents, water masses, eddies and jets in the Mediterranean Levantine Basin, J. Phys. Oceanogr., 18: 1320–1353.

Ovchinnikov, I. and A.F. Fedoseyev (1965). The horizontal circulation of the water of the Mediterranean Sea during the summer and winter seasons. p.185–201, In: "Basic Features of the Geological Structure, Hydrological Regime, and Biology of the Mediterranean", L. M. Fomin, (Ed.) Translated from Russian by the Inst. for Mod. Lang., Nav. Oceanogr. Off., Stennis Space Center, Miss.

POEM Group (1992). General circulation of the eastern Mediterranean, Earth Sci. Rev., 32: 285–308.

Robinson, A., and M. Golnaraghi (1993). Circulation and dynamics of the Eastern Mediterranean Sea; quasi-synoptic data-driven simulations, Deep-Sea Res. II, 40: 1207 1246.

Robinson, A., M. Golnaraghi, W.G. Leslie, A. Artegiani, A. Hecht, E. Lassoni, A. Michelato, E. Sansone, A. Theocharis, and U. Unluata (1991). The Eastern Mediterranean general circulation: features, structure, and variability, Dyn. Atmos. Oceans, 15: 215–240.

Rudnick, D, R.E. Davis, C.C. Eriksen, D.M. Fratantoni, M.J. Perry (2004). Underwater gliders for ocean research, Mar. Tech. Soc. J., 38 (2): 73–84.

Zodiatis, G., D. Hayes, I. Gertman, and Y. Samuel-Rhoads (2010). The Cyprus warm eddy and the Atlantic Water during the CYBO cruises (1995–2009), Rapp. Comm. Int. Mer Medit., 39: 202.

Zodiatis, G., P. Drakopoulos, S. Brenner, and S. Groom (2005). Variability of the Cyprus warm core eddy during the CYCLOPS project, Deep-Sea Res. II, 52: 2897–2910.

Towards the application of an operational sediment transport model for the optimisation of dredging works in the Belgian coastal zone (southern North Sea)

Dries Van den Eynde* and Michael Fettweis

Management Unit of the North Sea Mathematical Models, Royal Belgian Institute of Natural Sciences, Brussels, Belgium

Abstract

The Belgian Continental Shelf (BCS) is characterised by shallow waters, with an irregular bathymetry and systems of sand banks. The bottom sediments generally consist of fine to medium sand. In the coastal zone, high concentrations of fine-grained suspended particulate matter occur which are responsible for a significant siltation of the ports and navigation channels. Every year, about 11 million tons of dry material is dredged and dumped back into sea. The dumped matter is quickly resuspended and transported away from the dumping sites. A non-negligible part of it recirculates back towards the dredging places, raising the question of the efficiency of the dredging strategy.

To study this recirculation process, numerical models are developed, validated and used in an attempt to help the authorities in the choice of an optimum dredging methodology. A semi-Lagrangian two-dimensional sediment transport model is coupled to MUMM's three-dimensional baroclinic hydrodynamic models. Model results have been validated against observed dispersion of radio-active material dumped in the area as well as long term in-situ measurements. Other model applications dealt with the study of the mud balance in the BCS and the influence on it of dumping activities.

The selection of the optimal location for the dumping sites is an important concern. Optimal means: i) minimising recirculating to the dredging places, ii) confining the physical, chemical and biological effects and iii) keeping the distance between the dumping site and dredging places as short as possible. Different model simulations are carried out to investigate the influence of the position of the dumping sites and of the meteorological conditions on the recirculation process. A first step is made in the operational implementation of a tool that can help the authorities to make the best choice for the dumping site, taking into account the actual meteorological and hydrodynamic conditions.

Keywords: Dumping and dredging activities, dredging efficiency, operational forecasting, sediment transport modelling, southern North Sea, Belgium.

* Corresponding author, email: Dries.VandenEynde@mumm.ac.be

1. Introduction

The Belgian–Dutch coastal area is shallow, with water depths between 5 and 40 m and is characterised by strong vertical mixing and high tidal velocities. The sediment transport in the area is complex. High turbidity values (about a few hundred mgl^{-1}) are regularly observed between Oostende and Zeebrugge making the Belgian coastal waters one of the most turbid in the North Sea. Main Belgian sea ports (Oostende and Zeebrugge) and the main navigation channels towards the Westerschelde estuary must therefore be continuously dredged to maintain accessibility. Comparison between the natural input of the suspended particulate matter (SPM) in the coastal zone through (mainly) the Strait of Dover and the quantities dredged and dumped at sea show that an important part of the SPM is involved in the dredging/dumping cycle (Fettweis and Van den Eynde, 2003).

Dredging and dumping amounts to about 11 million tons of dry matter yearly, from which more than 70% is silt and clay. 10% of the total dredged quantity is dredged in the navigation channel connecting the port of Zeebrugge with the open sea and 62% in the port of Zeebrugge. The rest is extracted from the navigation channel towards the Westerschelde (22%) and the harbour of Oostende (5%).

Most of the dredged material is dumped back into the sea at selected dumping sites, from which the material is transported again, mainly in suspension. The dumping of this fine-grained material can disturb the nutrient dynamics in the water. A higher sediment concentration in the water column mainly influences the biota and filter-feeding organisms. At the dumping sites themselves, the benthos is disturbed due to burial.

Dredging works may be limited by reducing the sedimentation in harbours (transformation of the harbour entrance or current deflecting wall) or by applying a more efficient dumping scheme. The efficiency of a dumping place is determined by physical (sediment transport, hydrodynamics), economic and ecological aspects. An efficient dumping place has a minimal recirculation of dumped matter back to the dredging places, a minimal distance between the dumping place and the dredging area and a minimal influence on the environment.

Operational numerical hydrodynamic and sediment transport models can forecast the recirculation of dumped material during the next few days. The best dumping site can then be selected taking into account the present conditions.

This paper first briefly presents the numerical models. Then the results of model applications dealing with the evaluation of the efficiency of three different dumping schemes around Zeebrugge (east, west or as a function of tide) are presented and discussed. A fourth section is dedicated to a short presentation of a first implementation of an operational forecasting system. Finally, some conclusions and recommendations for further work are formulated.

2. Hydrodynamic and fine sediment transport forecasting tools

2.1 Main characteristics of the hydrodynamics and fine-grained sediment transport on the Belgian Continental Shelf

A detail of the bathymetry of the part of the BCS is shown in Figure 1. The water depth varies between three and about thirty metres. The navigation channels are dredged to

about fifteen metres below LAT (Lowest Astronomical Tide). The hydrodynamics of the Belgian coastal waters are determined mainly by tides, wind and wave activity. The tides are semi-diurnal and slightly asymmetrical. The mean tidal range at Zeebrugge is 4.3 m at spring tide and 2.8 m at neap tide. The tidal current ellipses are elongated in the coastal zone and become more broadly elliptical further offshore. The current velocities can reach more than 1 m s^{-1} at spring tide. The water column in the area is well mixed during the entire year. The freshwater outflow from the Westerschelde is low and has a long-term (1949–1997) annual mean of 107 m^3s^{-1}. The winds and consequently also the waves are mainly from the southwest or from the northeast. The winds are most of the time (90%) below 5 Bft (10.8 m s^{-1}). Significant wave height at Westhinder, 20 km from the coast, is 87% of the time below 2.0 m. The long term transport of the water is mainly to the northeast.

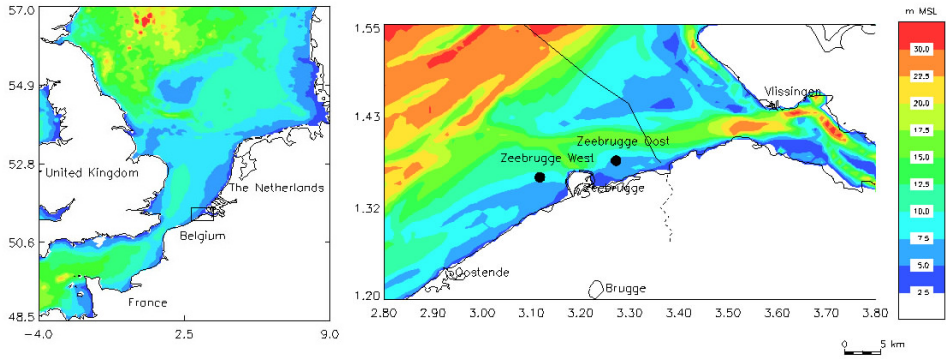

Figure 1 Left: Position of the study area. Right: Detail of the bathymetry of the 820 m × 772 m model grid of the Belgian Continental Shelf. Two possible dumping sites are indicated.

The surface sediments on the BCS consist mainly of medium to fine sand. Further from the coast, at water depths greater than 12 m, medium sand is found with a median grain size up to more than 400 µm. Nearer to the coast and east of Oostende, fine sands are found with a median grain size lower than 200 µm. In the eastern part large mud fields are found. These mud fields are partly correlated with the high turbidity zone between Oostende and the mouth of the Westerschelde.

2.2 Description of the numerical models

The core of the hydrodynamic models is the COHERENS code (Luyten *et al.*, 1999). Governing equations express conservation of mass, momentum, temperature and salinity. A transport equation for turbulent kinetic energy combined with an algebraic formulation for the length scale is used. These equations are solved using the mode splitting technique on an Arakawa-C model grid.

For operational purposes, three different implementation of the COHERENS code are used. Only the barotropic mode is turned on for the two-dimensional implementation, referred to as OPTOS-CSM, that covers the entire Northwest European Continental Shelf. Model forcing comes from the tide and the Numerical Weather Predictions (NPW) provided by the United Kingdom Meteorological Office. For the North Sea area as well as on the BCS, the full three-dimensional version of COHERENS is used. The North Sea

model, OPTOS-NOS, is forced along its open boundaries by OPTOS-CSM. Surface forcing is coming from the same NWP. Freshwater discharges (climatological values) from main European rivers are taken into account.

On the BCS, the model (referred to as OPTOS-BCS) is implemented on a grid with a resolution of about 1/84° in longitude (817–833 m) and 1/144° in latitude (772 m). Along the vertical, 20 σ-layers are used. Open boundary conditions are provided by OPTOS-NOS.

The OPTOS-BCS model was validated extensively, using 400 hours of current profiles on the BCS, measured with a bottom mounted Acoustic Doppler Current Profiler (ADCP), type Sentinel 1200 kHz Workhorse of RDInstruments (Dujardin *et al*., 2010).

The two-dimensional sediment transport model is a semi-Lagrangian model, based on the Second Moment Method (de Kok, 1994). In this method, all the material in a grid cell is represented by one rectangular mass, with the sides parallel to the direction of the model grid, and characterised by its zero order moment (total mass), its first order moments (position of mass centre) and its second order moments (the extension of the mass). Advection is represented by the advection of each of the sides of the rectangle. Diffusion is simulated by enlarging its extension. After each time step all material in a grid cell is recombined and represented by one new rectangle with the same zero, first and second order moments. The model can account for different sediment classes. In the applications reported in this paper, only mud, defined as the fraction smaller than 63 μm, is introduced. Erosion and sedimentation processes are governed by bottom friction, which is parametrised using an adaptation of the Bijker formula (Bijker, 1966). Erosion is modelled following Ariathurai (1974), while sedimentation is calculated using the formula from Krone (1966). The amount of material that is eroded depends on the erosion constant M ($\mathrm{kg\,m^{-2}\,s^{-1}}$) and of a critical bottom stress for erosion τ_s (Pa), while sedimentation uses parameters for the fall velocity of the sediment particles w_s ($\mathrm{m\,s^{-1}}$) and for the critical bottom stress for deposition τ_d (Pa). In this model, the critical bottom stress for erosion depends on the consolidation of the deposited material. The complete description of the consolidation model falls out of the scope of the present paper, but more information can be found in Fettweis and Van den Eynde (2003).

The critical bottom stress for erosion varies between 0.5 Pa for loosely deposited mud and 0.79 Pa for consolidated mud after 48 hours, the erosion constant M is set to $0.00012\ \mathrm{kg\,m^{-2}\,s^{-1}}$. The fall velocity is set constant and equal to $2\ \mathrm{mm\,s^{-1}}$. This rather high value implicitly accounts for flocculation processes and agrees with recent measured values. The critical bottom stress for deposition has a value of 0.5 Pa. This high value promotes the deposition of the sediments. The model was validated by comparing the model with in-situ measurements and by simulating radio-active tracer experiments (Van den Eynde, 2004).

3. Model simulations and results

3.1 Different scenarios

To demonstrate the possible useful application of the numerical models to select the most efficient dumping scheme, three different dumping strategies are evaluated. In the strategy “business as usual”, the material is dumped on the Zeebrugge-Oost dumping site

(ZBO), a site which is used at the present time, at a distance of about 4.5 km east of the harbour entrance. In a second dumping strategy, this site is moved to the west of Zeebrugge harbour (ZBW), at an equivalent distance with respect to the entrance. Both locations are indicated in Figure 1. In a third scenario (TDD), the dumping is tide dependent: during ebb (water transport to the west), the ZBW site is used, while during flood (currents to the east) material is dumped on ZBO site.

The efficiency of the dumping strategies is evaluated by calculating the recirculation from the dumping sites towards two dredging areas, i.e., the zone around the port (see Figure 2a) taken as a proxy for the recirculation to the harbour itself, and the zone around the navigation channels (see Figure 2b).

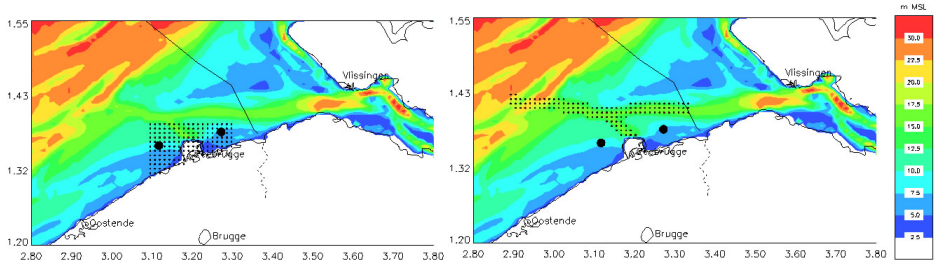

Figure 2 Two zones where the recirculation of the dumped material is being calculated. a: (left) Zone around Zeebrugge harbour; b: (right) Zone around the navigation channels.

A one month period, from 1 January – 1 February 2006, has been chosen. The period comprises two spring-neap tidal cycles with spring tides around 2, 16 and 31 January and neap tides around 9th and 24th January. The wind speed during the period stayed limited to less then 8 ms^{-1} most of the time, with wind peaks of more then 10 ms^{-1} on 10, 11, and 26 January. The wind direction was highly variable, with the winds coming most of the time from the south or the east. Simulations start at different dates during this period. Each simulation has a duration of 5 days and 5 hours (equivalent to the length of the actual model forecast).

Various surface forcing are considered: no wind forcing, realistic wind forcing, uniform in space and constant in time wind forcing (9 ms^{-1} from northwest, northeast or southwest). During each model run, 337.5 tons of mud is dumped according to one of the dumping schemes previously described. The efficiency of the dumping strategy is evaluated from the averaged amount of material found at the bottom in each dredging zone during the last day of the simulation.

Results from the simulations without wind forcing are presented in Figure 3. The last day averaged amount of material found at the bottom, in the two zones of interest and as a function of the starting date, is displayed. For the zone around the harbour of Zeebrugge (Figure 3, left), dumping on ZBO induces the largest recirculation of material. Concerning the two others dumping schemes (ZBW and TDD), results clearly indicate that the choice should be made according to the time start of the simulations. Sometimes it is better to dump continuously on Zeebrugge-West. Other times, it is better to use a tide dependent dumping strategy. For the zone around the navigation channels, the results vary more. The results indicate that dumping on ZBO at some times seems to be

the best choice. However, this is probably mainly due to the fact that the simulation is only executed over a short period of 5 days and 5 hours.

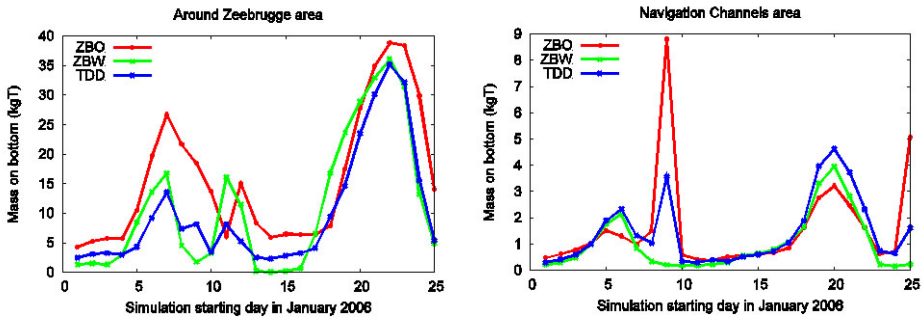

Figure 3 Amount of material on the bottom, averaged over the last day of the simulation, for the dumping at Zeebrugge-Oost (ZBO), at Zeebrugge-West (ZBW) or for tide dependent dumping (TDD) for the zone around Zeebrugge (left) and the zone around the navigation channels (right) and as a function of the starting date of the simulation. No meteorological conditions have been taken into account.

Results from the simulations made with different wind forcing are presented in Figure 4. Results are presented for one zone (around Zeebrugge) and two dumping schemes: ZBO (left) and ZBW (right). Also the influence of the meteorological conditions on the recirculation from the dumping sites is clear. The actual meteorological conditions can therefore influence the optimal dumping strategy to be applied.

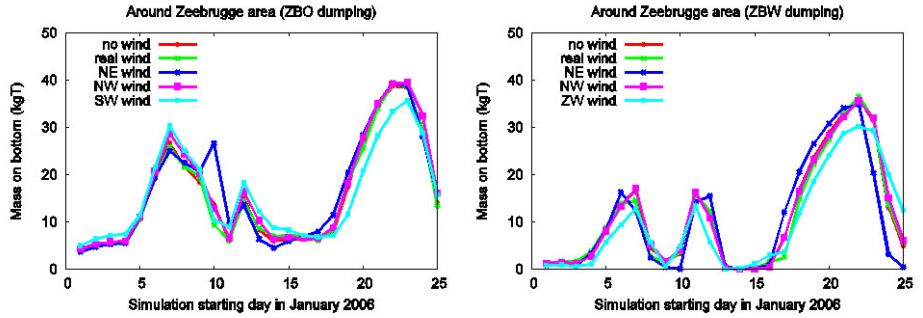

Figure 4 Amount of material on the bottom, averaged over the last day of the simulation, for the dumping at Zeebrugge-Oost (ZBO) (left) and at Zeebrugge-West (ZBW) (right) for the zone around Zeebrugge as a function of the starting date of the simulation for the different meteorological conditions.

4. Operational forecasts

To help the government to apply the most efficient dumping strategy, an operational tool is being set up, which can be used to decide where best to dump the dredged material, taking into account the actual situation. The model uses the operational forecasts of the currents and water elevations, which were executed twice a day, using the three-dimen-

sional hydrodynamic model, described above. The results of these operational currents and tidal elevations forecasts are presented on the MUMM website and are used for example for the operational forecasts of oil spills (Legrand and Dulière, 2012).

In addition to the hydrodynamic forecasts, every day two additional simulations are being executed now, using the sediment transport model. For the next five days, limited by the meteorological forecasts, the dispersion of the material is followed using the three dumping strategies. Automatically, an animation is prepared, presenting the evolution of the material in suspension and the material at the bottom during the simulated period, which can be consulted on a web site. An example of this movie for the dumping at Zeebrugge-Oost and Zeebrugge-West is presented in Figure 5. Furthermore, a table is automatically calculated and presented with the calculated recirculation averaged over the last day of the simulations, to the two zones, defined above. This table could be used to help the decision makers to decide which dumping strategy to follow during the next days, taking into account the actual situation and the actual hydrodynamic forecasts, to minimise the recirculation of the dredged material.

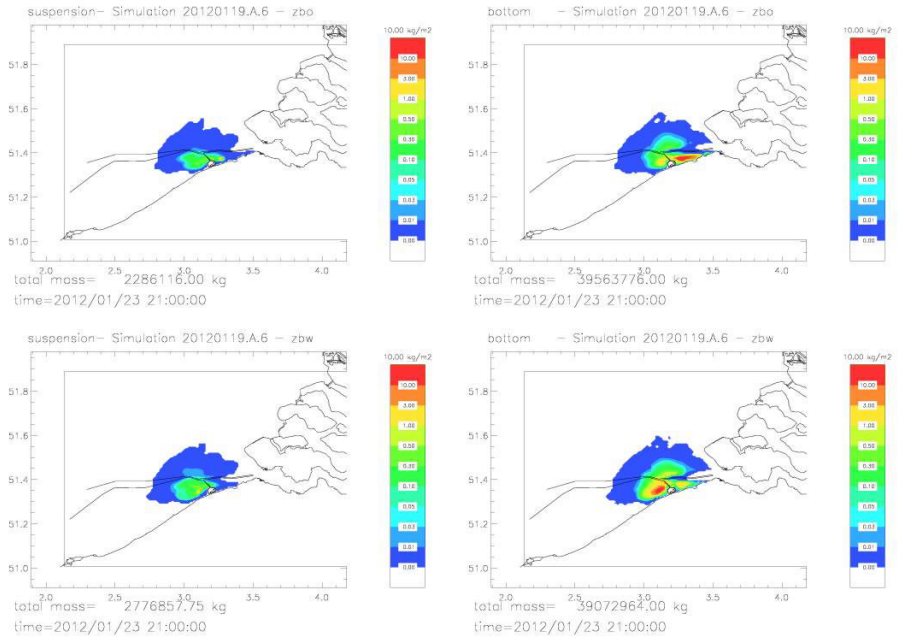

Figure 5 Operational forecasts of the dispersion of dredged material from two different dumping sites.

5. Conclusions and future work

This paper presents some work on the development of a tool that can be used to make the dumping of dredged material more efficient. For this purpose a semi-Lagrangian sediment transport model was set up, which follows the dumped material through the model grid, and which calculates the recirculation of the dumped material to predefined zones of interest, in this case the harbour of Zeebrugge and the navigation channels. Using operational hydrodynamic forecasts, also operational forecasts of the dispersion of

the dumped material are being produced. The results of these forecasts are easily accessible through a web site. This information then can be used by the responsible authorities, when deciding where to dump the dredged material.

It is clear that further research has to be carried out before the operational tool will be ready. First of all, the operational sediment transport model should be extended to include the influence of waves on the sediment transport. Furthermore, a good calibration of different model parameters and a proper validation of the model results has to be made. To this extent, a large scale measuring campaign is being set up, to measure the influence of the dumping site on the recirculation of the dumped material to the Zeebrugge harbour. These measurements will be of great importance to validate the operational sediment dispersion model.

Acknowledgements

This research was executed in the framework of the MOMO project, financed by the Coastal Waterways Division of the Ministry of the Flemish Community, Belgium. José Ozer and Frederic Francken from MUMM are acknowledged for the constructive remarks.

References

Ariathurai, C.R. (1974). A finite element model for sediment transport in estuaries. Ph.D. Thesis, University of California, Davis.

Bijker, E.W. (1966). The increase of bed shear in a current due to wave motion. In: Proceedings of the 10th Conference on Coastal Engineering, Tokyo, 746–765.

de Kok, J.M. (1994). Numerical modelling of transport processes in coastal waters. Ph.D. Thesis, Universiteit Utrecht, 158 pp.

Dujardin, A., D. Van den Eynde, J. Vanlede, J. Ozer, R. Delgado and F. Mostaert (2010). BOREAS – Belgian Ocean Energy Assessment, A comparison of numerical tidal models of the Belgian part of the North Sea. Version 2_0. WL Rapporten, 814_03. Flanders Hydraulics Research, Soresma & MUMM. Antwerp, Belgium, Belspo Contract SD/NS/13A, 62 pp.

Fettweis, M. and D. Van den Eynde (2003). The mud deposits and the high turbidity in the Belgian–Dutch coastal zone, southern Bight of the North Sea. Continental Shelf Research, 23, 669–691.

Krone, R.B. (1966). Flume studies of the transport of sediment in estuarial shoaling processes. Final Report, Hydr. Eng. Lab. And Sanitary Eng. Research Lab., Univ. California, Berkeley.

Legrand, S. and V. Dulière, 2012. OSERIT: a downstream service dedicated to the Belgian Coast Guard Agencies. This volume, page 181.

Luyten, P.J., J.E. Jones, R. Proctor, A. Tabor, P. Tett and K. Wild-Allen (1999). COHERENS: A Coupled Hydrodynamical-Ecological Model for Regional and Shelf Seas: User Documentation. Management Unit of the North Sea Mathematical Models, Brussels, 914 pp.

Van den Eynde, D. (2004). Interpretation of tracer experiments with fine-grained dredging material at the Belgian Continental Shelf by the use of numerical models, Journal of Marine Systems, 48, 171–189.

Oil-drift forecasting services

Monitoring oil spills at sea with optical satellite sensors: the PRIMI project Optical Observation Module

A. Pisano*[1], S. Colella[1], F. Bignami[1], R.H. Evans[2], and R. Santoleri[1]

[1]*CNR-ISAC UOS Roma, Italy*
[2]*The Rosenstiel School of Marine and Atmospheric Science, Miami, USA*

Abstract

The PRIMI project funded by the Italian Space Agency (ASI) has implemented an observation and forecast system to monitor marine pollution from hydrocarbon oil spills (OS) in the Italian Seas. The system consists of four components; two for OS detection via multi-platform SAR and optical satellite imagery, an OS displacement forecast subsystem based on numerical circulation models and a central archive that provides WEB-GIS services to users. The system also provides meteorological, oceanographic and ship detection information. The Optical Observation Module, based on MODIS and MERIS imagery, is described here. The idea of combining wide swath optical observations with SAR monitoring arises from the necessity to overcome the SAR reduced coverage of the monitoring area. This can be done now, given the MODIS and MERIS higher spatial resolution with respect to older sensors (250–300 m vs. 1 km), which enables the identification of smaller spills deriving from illicit discharge at sea. The procedure to obtain identifiable spills in optical reflectance images involves removal of natural variability to enhance slick–clean-water contrast, image segmentation/clustering and a set of criteria for the elimination of features which look like spills (look-alikes). The final result is a classification of oil spill candidate regions by means of a score based on the above criteria.

Keywords: oil spill, Mediterranean Sea, MODIS, MERIS, satellite, optical sensor.

1. Introduction

The main contribution to marine oil pollution is due to illegal discharges from ships cleaning their bilges underway, to cut harbour costs. 2 million tons of oil are illegally spilled annually and this accounts for about 45% of global oil pollution (REMPEC, www.rempec.org), while tanker and platform accidents contribute by only 5% and 2% respectively. In particular, the Mediterranean Sea hosts 25% of the world's sea-borne oil traffic, with up to 600000 tons of hydrocarbons illegally spilled in this basin every year (REMPEC, www.rempec.org).

Naval, aerial and Synthetic Aperture Radar (SAR) surveillance is generally adopted in monitoring maritime traffic and ocean pollution (Trieschmann *et al*., 2003; Ferraro *et al*., 2007; Girard-Ardhuin *et al*., 2003; Fiscella *et al*., 2000; Del Frate *et al*., 2000; Topouzelis *et al*., 2002; Karathanassi *et al*., 2007). SAR is particularly useful because of its all-weather and all-day observation capability and high spatial resolution (typically 10–100

* Corresponding author, email: andrea.pisano@artov.isac.cnr.it

m). However, SAR data are expensive, have relatively low coverage (long revisit times due to narrow 100–500 km bands). This calls for a multi-platform monitoring approach, including SAR as well as wider swath platforms, such as optical sensor satellites.

Optical oil spill detection is now possible, thanks to the increased spatial resolution (250–300 m) of the new generation MODIS (NASA TERRA and AQUA platforms) and MERIS (ESA ENVISAT platform) sensors (Hu *et al*., 2003; Shaban *et al*., 2009 and Coppini *et al*., 2011). Polluted waters may be detected because their water-leaving radiance differs from that of clean water (Otremba, 2009; Otremba and Piskozub, 2004); however, attempts to implement optical detection algorithms are few and recent (Grimaldi *et al*., 2009).

We present a new, highly automated, oil spill detection algorithm using MODIS and MERIS optical imagery, developed within the PRIMI project (Nirchio *et al*., 2009), funded by the Italian Space Agency (ASI). PRIMI has implemented a modular operational system (Figure 1) for marine oil pollution monitoring and forecast in the seas around Italy. The system consists of four modules, i.e. multi-platform SAR and Optical observation Modules (ERS, ENVISAT, RADARSAT, COSMO-SkyMed, MODIS TERRA and AQUA, MERIS), an oil spill displacement Forecast Module based on Mediterranean basin and sub-basin circulation models and an oil spill displacement/transformation lagrangian model and an Archive Module that provides WEB-GIS services to users (Nirchio *et al*., 2009).

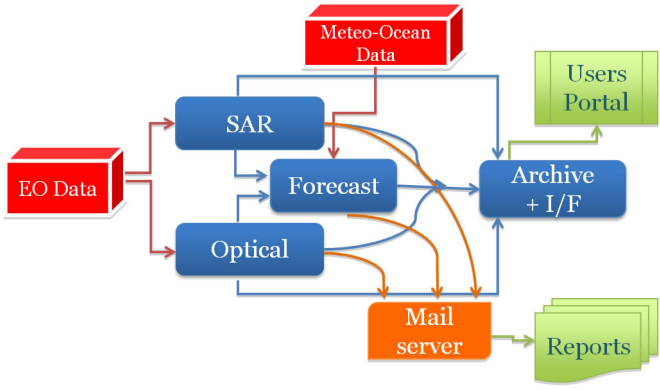

Figure 1 A modular operational system for marine oil pollution monitoring and forecast.

The PRIMI optical oil spill (OS) detection algorithm was developed and validated using an in-situ certified OS database. The algorithm pre-processes the imagery (declouding, destriping for MODIS, etc.), then enhances oil–water contrast by eliminating natural variability from input images ("image flattening"). Flattened images are then clustered into regions with common mode reflectance values. Next, cluster images are pruned of look-alikes and obvious non-slick regions, using a set of spectral and geometric feature parameters, thus leaving what we termed "OS candidates". Finally, a probability score is assigned to each OS candidate. Algorithm validation is briefly presented followed by a summary of the work and comments on future efforts.

2. Materials and methods

2.1 The oil spill in-situ certified database

A collection of in-situ oil spill observations was compiled, as reported by international and Italian Authorities responsible for OS monitoring (Table 1), for which we obtained MODIS and MERIS TOA reflectance imagery. OS events include: ROSES (www.boost-technologies.com/roses/report.php) report OSs (3 images), Lebanon 2006 spills (23 MODIS and images), OSs in the Italian seas (6 images; Italian Ministry of the Environment, 2002–2008), an OS off the Algerian coast (3 images; August 6–10, 2008) and five OSs visited by CNR's *R/V Urania* during the PRIMI validation cruise of August – September 2009 (5 images). A subset of the database has been selected to develop the algorithm (training OS database; 15 images, containing 60 OSs), while the remaining OSs were used to validate the methodology (validation OS database, 25 images, containing 101 OSs; Table 1). Each spill in each image was manually digitised as a Region of Interest using the ENVI ROI tool, thus obtaining position text files of OS pixels (Figure 2), to be used in algorithm development or validation.

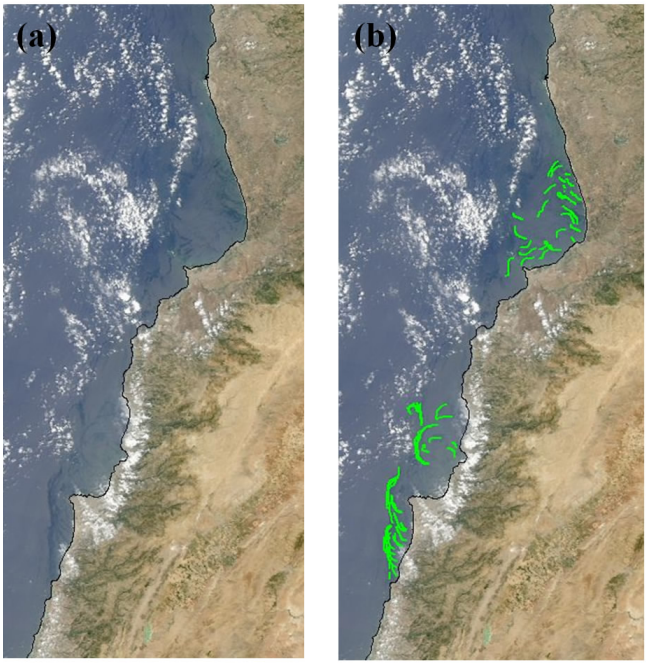

Figure 2 True colour images for the oil spill disaster of the Lebanon coast (a) MODIS TERRA (August 17 2006, 08:30 UTC) detail, low glint condition, (b) the same but with the oil spill ROI (green) manually digitized with the ENVI ROI tool.

Table 1 Training and validation dataset of MODIS and MERIS images relative to the in-situ oil spill observations. For each area the number of images and their relative number of OSs is shown.

Area	Training	Validation	MODIS	MERIS
Lebanon	12 (55 OSs)	11 (77 OSs)	14	9
Algeria	2 (4 OSs)	1 (1 OS)	2	1
Italian Ministry	1 (1 OS)	5 (10 OS)	6	-
ROSES	-	3 (3 OSs)	3	-
PRIMI cruise	-	5 (10 OSs)	5	-
Total	**15 (60 OSs)**	**25 (101 OSs)**	**30**	**10**

2.2 MODIS and MERIS data

MODIS L0 (TERRA and AQUA) and MERIS L1B data were downloaded from the NASA and ESA websites (modis.gsfc.nasa.gov; envisat.esa.int/instruments/meris) and processed with the SeaDAS v5.4 freeware to obtain L2 TOA reflectance $\rho_t(\lambda)$, Rayleigh reflectance $\rho_r(\lambda)$ and water-leaving reflectance $\rho_W(\lambda)$ at the wavelengths
λ_{MODIS} = (469, 555, 645, 859, 1240, 1640, 2130) nm and
λ_{MERIS} = (443, 560, 665, 681, 865) nm,
as well as Level 2 processing flags (l2_flags MODIS product for land and cloud, etc., detection), SST Quality Levels (qual-sst, MODIS only, for custom declouding) and θ_{sat}, θ_{sun}, ϕ_{sat}, ϕ_{sun}, i.e. satellite and sun zenith and azimuth angle maps. Spatial resolution is 250 or 500 m and 300 m for MODIS and MERIS products, respectively.

3. Oil Spill Detection Methodology

The OS detection algorithm includes:

1. Destriping of intermediate L1A MODIS products and computation of $\rho_t(\lambda)$, $\rho_r(\lambda)$, $\rho_W(\lambda)$ L2 products (with SeaDAS, for both satellites)
2. Cloud Masking
3. "Image flattening", i.e. elimination of the natural oceanic and atmospheric variability from $\rho_t(\lambda)$, which produces flattened $\rho_\varepsilon(\lambda)$ images
4. Clustering of $\rho_\varepsilon(\lambda)$
5. Feature Extraction in clustered image (pruning of obvious look-alikes)
6. OS Classification remaining features ("OS candidates").

3.1 Destriping and cloud masking

The well-known striping artefact in MODIS images (Figure 3) is due to hardware differences between the two faces of the rotating mirror, which reflects light from the scene to a line of N detectors (10, 20 and 40 detectors for the 1 km, 500 m and 250 m bands, respectively). Also, the detectors have hardware differences which cause further finer striping within each mirror scan stripe (Figure 3a and c). Therefore, a cross-swath data line is disturbed by detector striping, a ramp-like artificial trend, each ramp being slightly displaced from its neighbours, due to mirror side differences (Figure 3c).

Destriping has been implemented mainly for the MODIS 1 km bands (Weinreb, 1989; Antonelli, 2004, IMAPP Team cimss.ssec.wisc.edu/imapp/destripe.shtml), but did not prove satisfactory when we applied it to 250 m bands, since artefacts occurred which had the shape similar to small slicks. Therefore, we developed a custom destriping for the 250 m bands and applied it to the L1A level MODIS products. It consists in determining the slope and bias of the regression line best fitting each ramp and "rectifying" the ramp by subtracting the regression line from the signal (Figure 3c). The destriped L1A files were then fed into SeaDAS to obtain the L2 level products. Figure 3b obviously shows that destriping is not perfect; however it has proved sufficient for the OS detection algorithm.

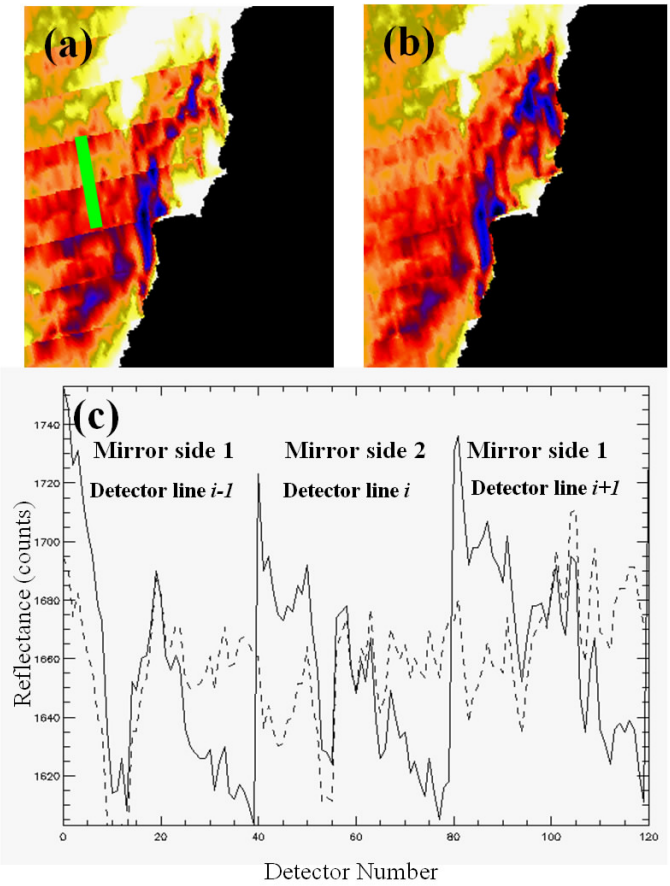

Figure 3 MODIS AQUA 2006 August 22 10:25 UTC L2 TOA reflectance (ρ_t) at 859 nm
(a) image showing striping. Green line refers to section across stripes given in (c) (each major stripe has 40 detectors, this being a 250 m resolution image). (b) Destriped image. (c) Section across stripes with striping ramps (solid line) across three swaths acquired by different mirror sides and due to sensor hardware differences and corrected reflectance after destriping (dashed line). Reflectance expressed in counts.

The custom cloud masking is based on the highly positive cloud-water contrast and was adopted because the standard MODIS and MERIS cloud flags were seen to sometimes mask OS pixels as clouds. All pixels in MODIS images for which one or more SST quality flags indicate bad SST are flagged. Next, declouding is completed using the reflectance standard deviation of the 3×3 box centred in each pixel. Since cloudy pixels have high reflectance with respect to surrounding water, pixels with high standard deviation are flagged as bad data. MERIS images are declouded only with the latter procedure.

3.2 Image flattening

Image flattening is the elimination of all reflectance signals in t extraneous to the response of oil and clean water, i.e. Rayleigh scattering, aerosols and oceanographic signals (e.g. presence of phytoplankton), in order to exhalt oil-water contrast. This is done by subtracting $\rho_r(\lambda)$, $\rho_W(\lambda)$ and $\rho_a(\lambda)$ from $\rho_t(\lambda)$ ($\rho_W(\lambda)$ is removed only for water-sensitive bands λ_{MODIS} = 469, 555 nm and λ_{MERIS} = 443, 560 nm). The aerosol signal ρ_a was eliminated by subtracting the signal of the aerosol-sensitive red band (λ_{MODIS} = 645 nm; λ_{MERIS} = 665 nm) from $\rho_t(\lambda)$.

The result of this procedure is a "flattened" image $\rho_\varepsilon(\lambda)$ (Figure 4), in which slicks are more contrasted and have finer detail than in $\rho_t(\lambda)$ (Figure 4a). The best OS enhancement is seen in the 859 nm and 865 nm bands for MODIS and MERIS respectively, which were thus chosen for the PRIMI Optical Module.

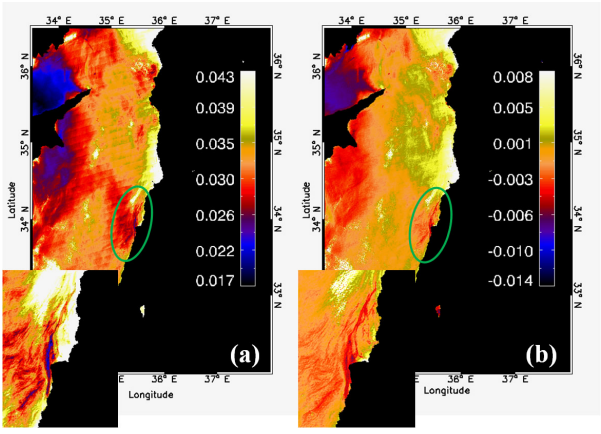

Figure 4 MODIS AQUA (August 22 2006 10:25 UTC), 859 nm band showing (a) ρ_t and (b) ρ_ε.The inset shows the Lebanon coastal oil spill in low glint condition (slick shown by green ellipse).

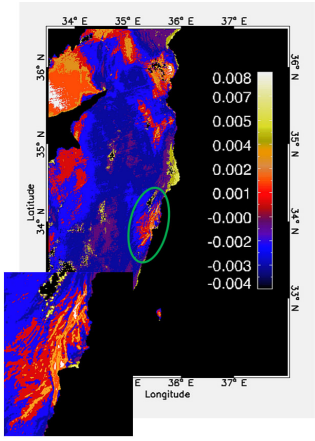

Figure 5 MODIS AQUA (August 22 2006 10:25 UTC), ρ_ε (859) cluster matrix. The clustering procedure found 10 clusters (different colours correspond to different reflectance mode values).

3.3 Clustering and segmentation

Flattened images were then clustered using the **mean shift** algorithm (Comaniciu, 2002). This procedure spatially subdivides the input $\rho_\varepsilon(\lambda)$ image in a set of clusters, each of which is composed of a number of (not necessarily connected) regions (Figure 5). Each

cluster is defined by a "mode" reflectance value, common to all its pixels. In practice, the quasi-continuum set of $\rho_\varepsilon(\lambda)$ values in the input map is reduced to a much smaller set of modes by means of the clustering algorithm.

3.4 Slick feature extraction (look-alike pruning)

We defined a set of geometric and spectral **feature parameters** in order to reject or retain the regions of the clustered image. For each parameter a threshold was empirically devised, with which each cluster region is either rejected or retained as an "OS candidate". First, each region was tagged as in either high or low glint illumination/view geometry, because slick-water contrast is brighter (darker) than water for high (low) glint. To do this we used the glint angle α, given by (e.g. Giglio *et al*., 2003):

$$\cos\alpha = \cos\theta_{sat}\cos\theta_{sun} - \sin\theta_{sat}\sin\theta_{sun}\cos\phi$$

where θ_{sat} and θ_{sun} are the satellite and solar zenith angles and $\phi = |\phi_{sat} - \phi_{sun}|$ is the sun-satellite relative azimuth angle, as seen from an image pixel. We empirically determined that high (low) glint conditions occurred for $\alpha < 17.5°$ ($\alpha > 17.5°$). This threshold proved to better separate positive from negative oil-water contrast regions than the standard MODIS and MERIS glint flags. Negative (positive) contrast regions in high (low) glint conditions are discarded using this method.

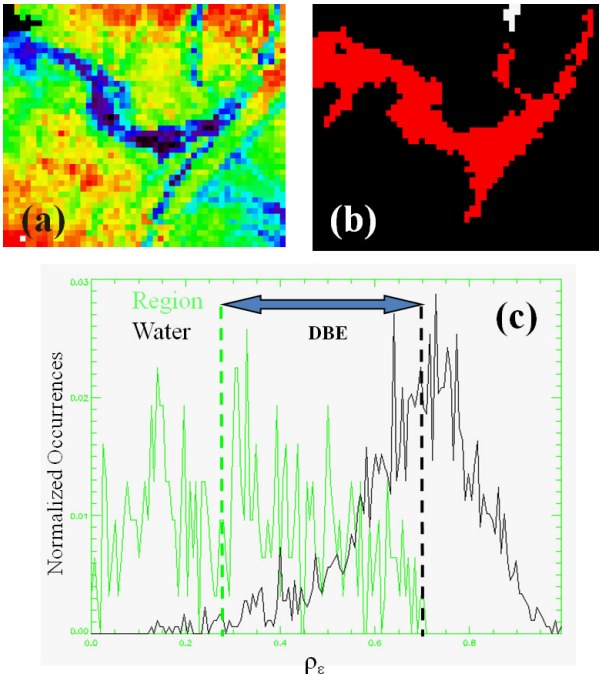

Figure 6 MODIS AQUA August 17 2005 12:15 UTC, low glint spill south of Elba island (northern Tyrrhenian Sea, slick in dark blue surrounded clean waters in green); (a) rhoeps-859 slick detail; (b) Oil spill ROI (red) manually digitized; (c) Slick (green curve) and surrounding water (black curve) rhoeps-859 normalized distribution histograms. Dashed lines indicate histogram baricenters and blue arrow indicates baricenter distance dbe, which in this case is approximately 0.3 – 0.7 = -0.4, indicating slick to be darker than surrounding water.

Next, the following parameters were computed for each region:

1. Area and perimeter (*A* and *P*)
2. Shape parameters combining *P* and *A*, e.g. $S_1 = P/A$ and $S_2 = 2\ln(0.25P)/\ln(A)$
3. Cloud Vicinity (*V*; slick distance from clouds)
4. Contrast (*C*; mean region reflectance to mean surrounding water reflectance ratio)
5. Baricenter Reflectance: the most frequent $\rho_\varepsilon(\lambda)$ value for the region and the surrounding water (Figure 6)
6. Region–water baricenter distance (*dbe*; difference between most frequent region and water reflectances; Figure 6).

S_1 and similar combinations of *P* and *A* (McGarigal and Marks, 1995) give a measure of e.g. region elongatedness, which is a typical feature of illegal spills, while S_2, the fractal dimension index, accounts for region patchiness (OSs are patchy).

Regions with contrast $C > 1$ ($C < 1$) for high (low) glint scenes were retained. Cloud vicinity *V* is used to discard regions close to clouds affected by cloud shadow or cloud straylight, which can be mistaken for slicks in low or high glint conditions respectively. The *dbe* tells us how much a region is on average darker or brighter than its surrounding water. Figure 7 shows that look-alike pruning with these parameters greatly reduces the number of regions likely to be true OSs (OS candidates).

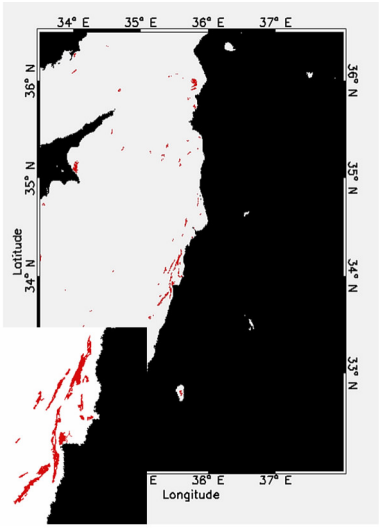

Figure 7 MODIS AQUA (August 22 2006 10:25 UTC), OS candidate matrix. The OS selection procedure finds 68 regions, as candidate oil spills.

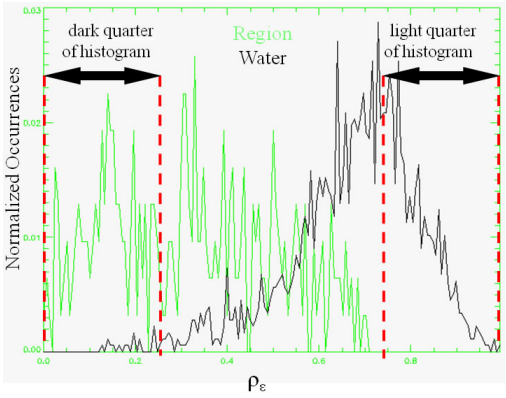

Figure 8 Slick (green curve) and surrounding water (black curve) ρ_ε (859) normalized distribution histograms, with histogram regions used for computation of d4r, d4w (histogram integrals on dark quarter) and l4r, l4w (histogram integrals on light quarter)

3.5 Automatic score assignment

Figure 7 shows also that threshold pruning does not eliminate all look-alikes. This is because oil spills are patchy, even within one image pixel, so reflectance from a pixel

within an OS is often an average reflectance resulting from a mix of polluted and clean water patches. This induced us to define "OS probability" scores, relative to a set of spectral parameters *p*, to be assigned to each OS candidate. Among the chosen parameters was the above defined *dbe*, but also a new set of "integral parameters" obtained using the $\rho_\varepsilon(\lambda)$ histograms of each region and surrounding water. As an example of the latter, we cite the value of the integrals of each histogram in the lower (darker) or higher (brighter) quarter of the $\rho_\varepsilon(\lambda)$ range relative to the two histograms and indicate how much a region histogram is darker or lighter than surrounding water: e.g. an OS candidate in low glint conditions is probably a true OS if the dark quarter is more populated by region pixels than water pixels (Figure 8).

Each parameter *p* was estimated for all known OS regions and look-alikes of our training OS database and its histograms were computed, i.e. $H_{OS}(p)$ and $H_{LA}(p)$ (Figure 9a; example relative to the *dbe*). Next, 0 to 1 scores were defined as:
$S(p) = H_{OS}(p)/[H_{OS}(p)+ H_{LA}(p)]$ (Figure 9b).

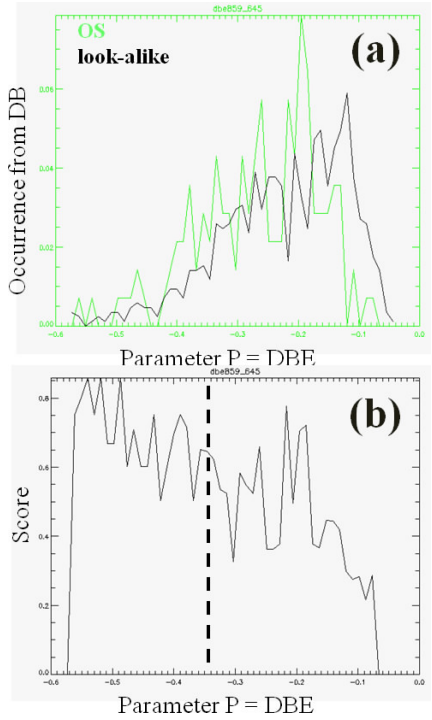

Figure 9 (a) Certified OS (green curve) and look-alike (black curve) dbe distribution for all no-glint images in the OS database.
(b) Score for dbe values, regions with dbes corresponding to high (low) score values will be classified as more probable oil spills (look-alikes). Similar scores are obtained for the high glint OS – look-alike database.

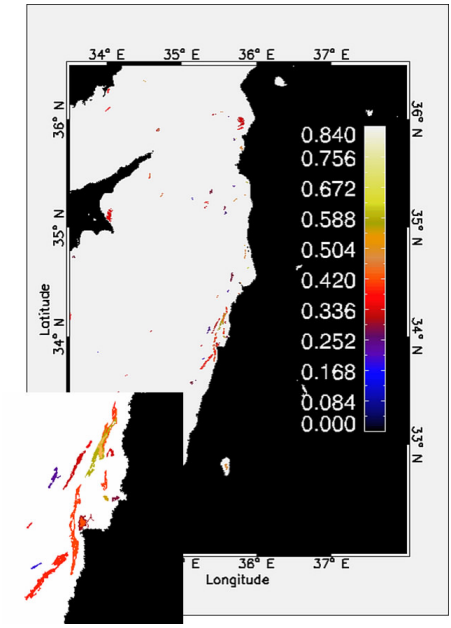

Figure 10 MODIS TERRA (July 23 2006 08:30 UTC) OS Score Matrix. Different colours correspond to different score values from 0 to 1.

When a new image is examined operationally, p is calculated for its OS candidates and $S(p)$ is found, using Figure 9b as a look-up table. Finally, a cumulative score is assigned to the OS candidate, as a linear combination of single $S(p)$ scores. Score assignment is exemplified in Figure 10 and our validation analysis indicates that true OSs are generally classified with higher scores than remaining look-alikes in the OS candidate image. During the PRIMI 6 month operational phase, optical images were processed daily and resulting score maps (Figure 10) were analysed by an operator. Also, reports containing the chosen OSs were issued automatically and sent to end users of the PRIMI system. 210 spills were reported operationally.

3.6 OS Detection Algorithm: Validation and Application

The PRIMI oil spill detection algorithm was tested on the validation subset of our OS database (Table 1) by computing a detection success percentage as

1. The ratio of detected spills to the known spills (Figure 11)
2. The ratio of detected pixels to ROI pixels in each image (Figure 12).

The average percent success is 78% and 65%, respectively. Moreover, OSs detected by SAR and MODIS (Table 1) and their displacement forecasts were verified and sampled in-situ during an *ad hoc* PRIMI cruise onboard the Italian CNR *R/V Urania*, in August–September 2009 (Southern Tyrrhenian and Strait of Sicily; not shown).

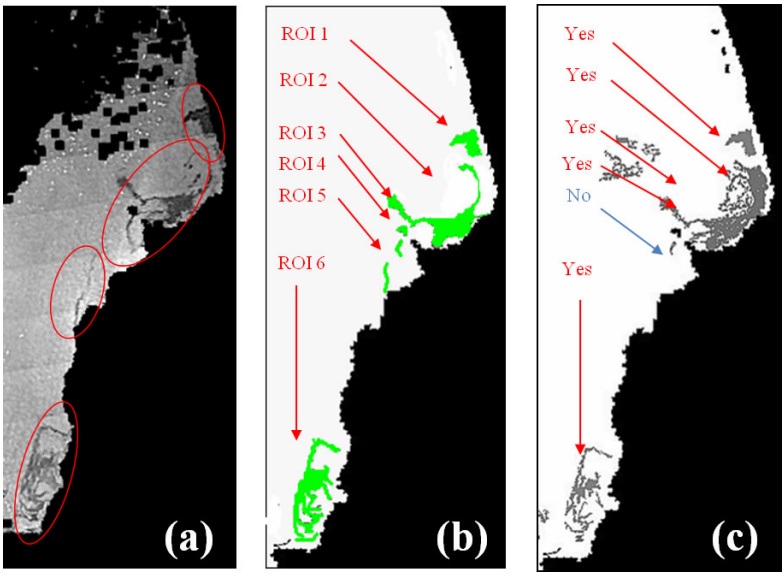

Figure 11 ρ_ε (859) from MODIS AQUA (August 2 2006) relative to the oil spill (in red ellipses) of the Lebanon coast (b) ROI matrix: green regions are oil spills signatures manually digitized. (c) Oil spill candidate matrix: land in black, sea in white and oil spill regions in grey.

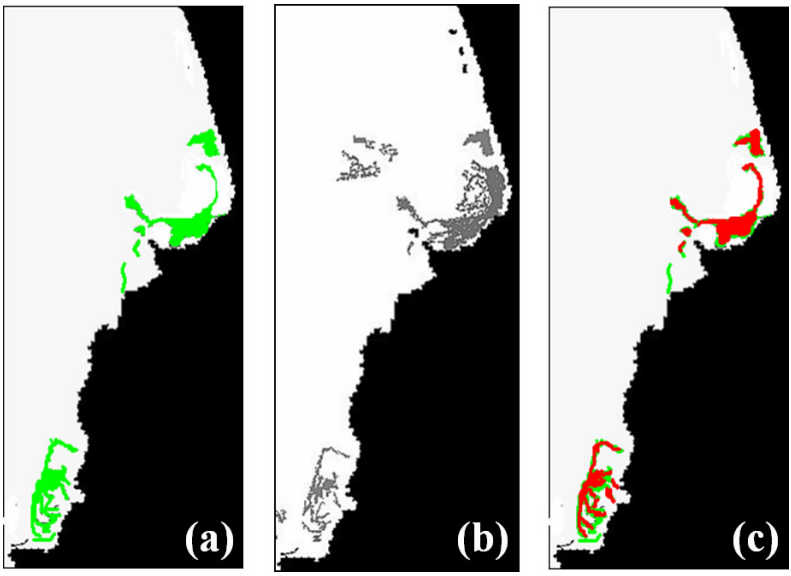

Figure 12 (a) ROI matrix: green regions are oil spills signatures manually digitized. (b) Oil spill candidate matrix: land in black, sea in white and oil spill regions in grey. (c) Comparison result: red pixels are common pixels belonging to both digitized pixels and detected pixels.

4. Summary and conclusions

We have described a new, highly automated oil spill detection methodology with MODIS and MERIS TOA reflectance imagery. After destriping (MODIS only) and cloud masking, images are "flattened" by eliminating natural variability, to enhance slick−clean water contrast. Next, flattened images are clustered and cluster regions are then pruned by means of a set of geometric and spectral feature parameters. However, since not all look-alikes are eliminated, due to e.g. slick patchiness, cumulative scores are computed as a linear combination of single feature parameter scores.

Validation results are encouraging, in that they show that the method was on average able to detect 78% of the OS and 65% of the total slick area in a given image. The PRIMI Optical Module developed in this work has been tested operationally for 6 months during the PRIMI project and 210 spills were reported.

A crucial point for improvement is to increase the number certified OS cases, to cover more geometric shapes and illumination-view situations and to develop more reliable pruning and score parameters.

Finally, the proposed algorithm may quite easily be adapted to other optical satellite sensors (e.g. hyperspectral) and/or updated for the next generation of optical satellites (e.g. Sentinel-3, VIISR).

Acknowledgements

We thank the crew of *R/V Urania* and technicians, for their fundamental role in the success of the PRIMI cruise.

References

Antonelli, P., M. di Bisceglie, R. Episcopo and C. Galdi (2004). Destriping MODIS data using IFOV overlapping, Proceedings of the IEEE International Geoscience and Remote Sensing Symposium (IGARSS), 7, 4568–4571, DOI: 10.1109/IGARSS.2004.1370171.

Comaniciu, D. and P. Meer (2002). Mean Shift: a robust approach toward feature space analysis. IEEE Trans. Pattern Analysis Machine Intell., 24, 603–619.

Coppini, G., M. De Dominicis, G. Zodiatis, R. Lardner, N. Pinardi, R. Santoleri, S. Colella, F. Bignami, D. R. Hayes, D. Soloviev, G. Georgiou and G. Kallos (2011). Hindcast of oil-spill pollution during the Lebanon crisis in the Eastern Mediterranean, July–August 2006. Marine Pollution Bulletin, 62, 140–153, doi:10.1016/j.marpolbul.2010.08.02.

Del Frate, F., A. Petrocchi, J. Lichtenegger and G. Calabresi (2000). Neural networks for oil spill detection using ERS-SAR data. IEEE Transactions on Geoscience and Remote Sensing, 38, 2282–2287.

Ferraro, G., A. Bernardini, M. David, S. Meyer-Roux, O. Muellenhof, M. Perkovic, D. Tarchi, and K. Topouzelis (2007). Towards an operational use of space imagery for oil pollution monitoring in the Mediterranean basin: A demonstration in the Adriatic Sea. Marine Pollution Bulletin, 54, 403–422.

Fiscella, B., A. Giancaspro, F. Nirchio, P. Paveseand P. Trivero (2000). Oil spill detection using marine SAR images. International Journal of Remote Sensing, 21, 3561–3566.

Giglio, L., J. Descloitres, C. O. Justice, Y. J. Kaufman (2003). An Enhanced Contextual Fire Detection Algorithm for MODIS. Remote Sensing of Environment, 87, 273–282.

Girard-Ardhuin, F., G. Mercier, and R. Garello (2003). Oil slick detection by SAR imagery: potential and limitation. Proceedings OCEANS 2003, 1, 164–169.

Grimaldi, C.L.S, D. Casciello, I. Coviello, T. Lacava N. Pergola and V. Tramutoli (2009). Near Real Time Oil Spill Detection And Monitoring Using Satellite Optical Data. Proceedings IGARSS 2009, 4, 709–712.

Hu, C., F. E. Moller-Krager, C. J. Taylor, D. Myhre, B. Murch, A. L. Odriozola *et al*. (2003). MODIS detects oil spills in Lake Maracaibo, Venezuela. EOS Transactions, American Geophysical Union, 84, 313–319.

Karathanassi, V., K. Topouzelis, P. Pavlakis, D. Rokos (2007). An object-oriented methodology to detect oil spills. International Journal of Remote Sensing, 27, 5235–5251, doi:10.1080/01431160600693575.

Lardner, R.W. and G. Zodiatis (1998). An operational oil spill model in the Levantine Basin (Eastern Mediterranean Sea). Int. Symp. Mar. Pollut. 10, 5–9.

Lardner, R., G. Zodiatis D. Hayes and N. Pinardi (2006). Application of the MEDSLIK Oil Spill Model to the Lebanese Spill of July 2006. European Group of Experts on Satellite Monitoring of Sea Based Oil Pollution. European Communities.

McGarigal, K. and B. J. Marks (1995). FRAGSTATS: spatial pattern analysis program for quantifying landscape structure. Gen. Tech. Rep. PNW-GTR-351. Portland, OR: U.S. Department of Agriculture, Forest Service, Pacific Northwest Research Station. 122 pp.

Nirchio F., G. V. Pandiscia, G. Ruggieri, R. Santoleri, F. Tataranni, P. Trivero, N. Pinardi, A. Masini, G. Manzella, and C. Castellani (2009). PRIMI (Pilot Project Marine Oil Pollution). Proceedings of the ISRSE 2009 33rd International Symposium on Remote Sensing of environment Sustaining the Millennium Development Goals, May 4–8, 2009, Palazzo dei Congressi Stresa, Lago Maggiore, Italy, http://isrse-33.jrc.ec.europa.eu/.

Otremba, Z. (2009). Influence of oil dispersed in seawater on the bi-directional reflectance distribution function (BRDF). Optica Applicata, 39, 123–128.

Otremba, Z. and J. Piskozub (2004). Modeling the bidirectional reflectance distribution function (BRDF) of seawater polluted by an oil film. Optics Express, 12, 1671–1676.

Shaban, A., M. Hamzé F. El-Baz and E. Ghoneim (2009). Characterization of an Oil Spill Along the Lebanese Coast by Satellite Images. Environmental Forensics, 10, 51–59.

Topouzelis, K., V. Karathanassi P. Pavlakis, and D. Rokos (2002). Oil Spill Detection: SAR Multi-scale Segmentation & Object Features Evaluation. Proceedings of the 9th International Symposium on Remote Sensing – SPIE, September 2002, Crete, Greece, 23–27.

Trieschmann, O., T. Hunsanger, L. Tufte, and U. Barjenbruch (2003). Data assimilation of an airborne multiple remote sensor system and of satellite images for the North- and Baltic sea. Proceedings of the SPIE 10th int. symposium on remote sensing, conference “remote sensing of the ocean and sea ice 2003”, 51–60.

Weinreb M. P., R. Xie, J. H. Lienesch and D. S. Crosby (1989). Destriping GOES Images by Matching Empirical Distribution Functions. Remote Sens. Environ., 29, 185–195.

Oil drift modelling, the M/V Godafoss accident

Göran Broström*[1], Ana Carrasco[1], and Silje Berger[2]

[1]*Norwegian Meteorological Institute (met.no)*
[2]*The Norwegian Coastal Administration (NCA)*

Abstract

The ship *M/V Godafoss* went aground in the outer Oslo fjord on February 17, 2011, and leaked about 110 m^3 of heavy fuel oil to the sea. There were a number of observations of the oil spill and in this study we evaluate the performance of the met.no oil drift and fate forecasting system toward these observations. Overall we find that the model system reproduced observations in a satisfactory way. Compared to a similar accident (the Full City) that took place in severe weather, we find much less beaching and slower development of the oil spill in this accident, which was in calm weather.

Keywords: Godafoss, oil spill, drift modelling, Oslo fjord.

1. Introduction

Oil spill accidents are an inevitable part of today's society. To minimise the impact of possible oil spill accidents most countries have contingency organisations to respond to oil spills when they occur. In Norway it is the Norwegian Coastal Administration (NCA) that is the national authority with the overall responsibility for monitoring oil spill and the remedial actions. One helpful tool in this work is oil spill models; these are helpful both for oil drift forecasting and for reconstructing the most likely oil spill path, which is useful for establishing the monitoring programme usually set up after an accident. In Norway there are several organisations that provide oil spill model solutions; one of them is the 24-7 operational oil spill model available at the Norwegian Meteorological Institute (met.no). This study evaluates some parts of this oil spill model towards observations.

Oil drift models are generally based on oil super particles that describe the drift and spreading of oil spills (Hackett *et al*., 2006; Reed *et al*., 1999). The spill is divided into discrete particles with the same mass that are released at different times and at slightly different positions thus creating an ensemble of particles. The particles are advected by a velocity field and the models also include a parametrisation of small scale turbulence by including random walk movements mimicking the turbulence fields. Algorithms for gravitational surface spreading of buoyant oil and vertical dispersion result in additional particle displacements. The properties of the oil will change in time due to e.g., complicated weathering processes that may for instance influence oil density and viscosity.

The most important forcing mechanisms for an oil drift forecast are probably the ocean currents, followed by the wind/wave conditions (sometimes including the Stokes drift): however, the importance of the different forcing variables may change with condition and location. For the met.no oil drift model it is generally the ocean currents that are

* Corresponding author, email: goran.brostrom@met.no

most important for the advection of the oil spill. An assessment of the oil drift model is thus in principle often an assessment of the ocean model. It is known that the atmospheric forecast or analysis is often quite accurate up to 48–72 h forward in time. For ocean currents the situation is more complicated, the combination of much smaller dynamical scales in the ocean and fewer observations implies that models for ocean currents often lack in predictability, which implies less accurate oil drift predictions. Nevertheless, even if ocean models have small dynamical scales there are certain cases that are well predictable. For instance, coastal currents are often very stable and are dynamically driven by e.g., slowly changing freshwater output along a long coastline and topographic steering (Walin *et al*., 2004). Another situation is under strong wind where the wind-driven flow becomes dominant. In the Full City accident (which was located quite close to the Godafoss accident), the accident happened in severe weather and this probably created a situation that was quite predictable for the large scale current system (here 5–10 km), and all three models that were compared for the oil spill in the Full City accident were quite accurate (Broström *et al*., 2011). The Godafoss accident was also close to land and the spill was of similar magnitude; the main difference is that Godafoss was in calm weather while Full City was in very windy conditions.

2. Observations

Godafoss went aground at about 18 UTC on February 17 (see Figure 1). The accident site at Kvernskjergrunn (59° 02.41 N, 10° 58.35 E) is just inside the Ytre Hvaler national park, a sensitive environmental area and a national reserve. Initial estimates of the amount of the spill was about 200–400 m^3 of heavy fuel oil (IFO 380). The early estimates were later revised, and the updated estimate from the NCA is that 112 m^3 of heavy fuel oil was released into the environment, and 55 m^3 out of this were recovered at sea (Report, 2011). A number of sea birds were soaked in oil: most of the oiled birds were eiders, it is estimated that approximately 1000 individuals were affected. The survey of the environmental effects is still going on.

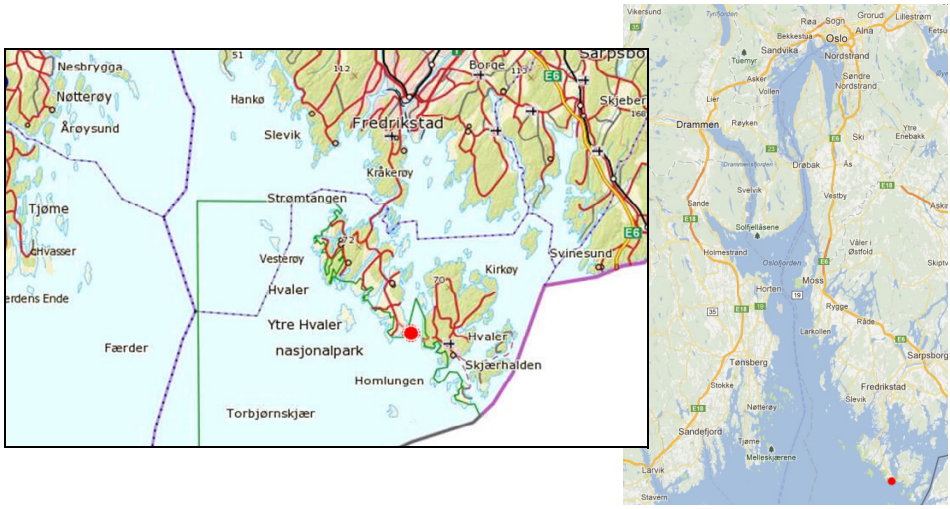

Figure 1 Map showing the position of the Godafoss accident (red dot).

There was some ice on the eastern Oslo fjord at the time of the accident and some of the recovery action was taken in ice conditions. The extent of the ice cover changed from day to day in this period. The ice conditions may have influenced the beaching of the oil in the calm weather conditions. Furthermore, the low temperatures and low wave exposure led to a low spreading property and low water uptake of the oil (Ramstad and Faksness, 2011).

2.1 Observation of the oil spill

The description of the oil movements presented here for the Godafoss accident are based on the observations made by the Norwegian Coastal Administration (NCA), most of the observations considered here were presented on their web page. Immediately after the accident the oil drifted out of the strait and then started to drift north-northwest and continued to move north-westwards during the first day (Figure 2a). During the following day the oil moved over to the western side of the outer Oslo fjord, and started to slowly drift south-westward along the coast (Figure 2b). The slow south-westward drift along the coast continued for at least two more days (Figure 2c, d). The main observations were about 10 km from the coast (Figure 2b–d): other areas were surveyed by aeroplane, helicopters and ships, but no further locations of oil were observed. Notably, the inner Oslo fjord was covered by ice so even if there were no observations of oil in the inner Oslo fjord area, there may have been oil underneath the ice. However, after the ice disappeared there were no indications that oil had drifted further north than observed in the first days after the incident.

It should be noted that the oil spill was not as large as in the Full City accident, and due to less spreading on the sea surface, lower wind speed and lower wave heights, the recovery at sea was more successful after the Godafoss incident. About 50% of the spill was recovered at sea, which is remarkable compared to the Full City incident that took place under strong wind conditions.

There were some reports of beaching of oil on the western side of the outer Oslo fjord; furthermore there were a few scattered observations of beaching all the way down to the southern tip of Norway, but these were mainly small amounts of oil. Although the distribution southwards along the coastline with scattered beaching of oil quite far south is similar to the Full City incident, the pattern of beaching is somewhat different. Beaching occurred more “compactly” than observed after the Full City incident. The spreading on the sea surface was less pronounced and the oil remained in patches, ply due to the combination of oil type, little wind and low temperatures. Patches of small extent, but with massive thick oil, were observed on the beaches.

Notably, the ice may have modified the pattern of beaching. In some areas it was observed that the ice acted as a barrier and blocked the oil from beaching. This is probably a phenomenon very specific to the extremely calm wind situation.

In other sites freezing occurred as oil drifted on the water surface. The oil was enclosed in the ice and moved along with the ice. Samples from the oil infested ice showed that even small amounts of oil in the ice cover were easy to detect by observation.

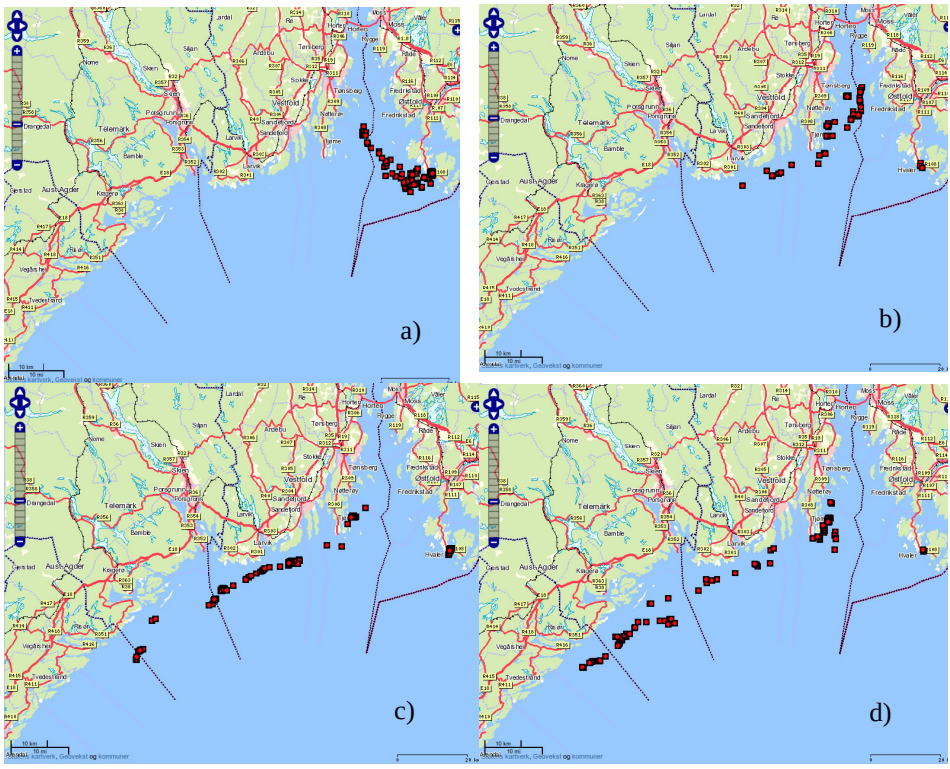

Figure 2 Observations made by NCA from the Godafoss accident. Red dots indicate positions of photographs taken by helicopter. Photographs were taken in areas where oil was observed, although later analysis showed that oil may not be detected in all photographs. However, here we simply assume that photographs were taken in vicinity of oil observations. The figures are for a) 18 February, b) 19 February, c) 20 February, and d) 21 February.

2.2 Atmospheric conditions during Godafoss accident

The atmospheric conditions were dominated by a high pressure system initially located over Finland (Figure 3a), but that slowly moved westward such that it covered the area from Oslo to St.Petersburg by midday on 19 Feb. By 20 Feb the high pressure become smaller and was located approximately over Bergen (Figure 3b). This weather situation gave rise to weak easterly (or east-southeasterly) winds over the outer Oslo fjord over the entire period covered in this analysis. Observations from Svenner lighthouse (met.no station 29950 on the western side of the Oslo fjord) show that the wind speed was about 8 ms^{-1} with a direction of 60° at the time of the accident and remained constant for a few hours. For the main part covered in this analysis the wind speed was about 5 ms^{-1}. The same conclusion, but with slightly lower wind is true for the Strømtangen lighthouse (met.no station 17000) on the eastern side of the Oslo fjord. The temperatures were cold during the entire period with temperatures between around –6 to –12 °C. The atmospheric model is consistent with these observations.

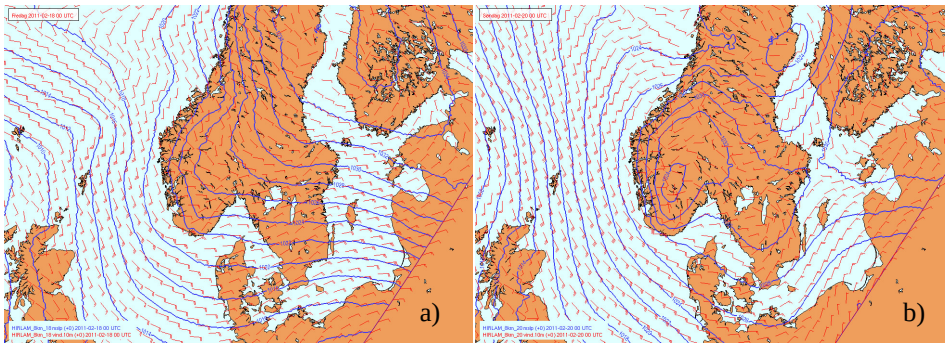

Figure 3 Sea level pressure and wind arrows from the HIRLAM 8 km run made at met.no. Results are from 00.00 on a) February 18 and b) 20 February.

2.3 Wave conditions during Godafoss accident

The wave conditions from the WAM 4 km model are presented in Figure 4. It is well known that wave conditions are very sensitive to ice cover, which efficiently dampens waves. This interaction mechanism is not described in the present wave model and areas covered in ice are masked out in the model (zero wave height). The most intense wave fields were simulated in the initial part of the accident, however, the highest waves were on the western side of the outer Oslo fjord, and in the area of the accident the significant wave heights were very low (i.e., zero wave height due to presence of ice). For the remaining period, the wave conditions were calm following the weak wind velocities over the area. Most likely the effect of the wave conditions on the oil spill was small in the simulations presented here. However, it is possible that there were some wave-ice interaction mechanisms at play that can be important for the movement of oil in ice covered areas; however, these processes are not described in the met.no modelling system, and it is difficult to judge the importance of these processes.

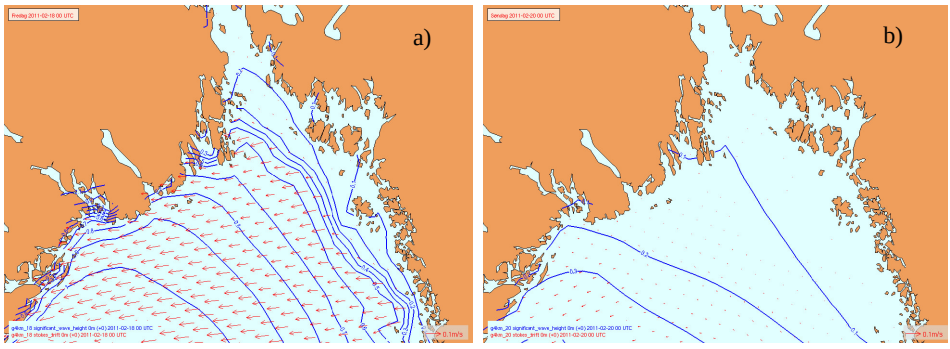

Figure 4 Significant wave height and Stokes drift vectors from the WAM 4 km run made at met.no. Results are from 00.00, on a) 18 February, and b) 20February. The contour line interval in significant wave height is 0.1 m.

2.4 Current conditions at Godafoss accident

The ocean current in this study is based on the operational ocean model at met.no (the MI-POM, Meteorological Institute-Princeton Ocean Model; Engedahl, 1995) run at the 1.5 km resolution. The current situation the days following the accident are shown in Figure 5. The model simulation does not show any clear ordered coastal current, something that is often found in this area. The model fields are rather chaotic, thus since met.no do not have observations or assimilation system to place ocean eddies correctly in space and time we should place some cautions on the accuracy of the ocean current field, at least at some distance from the coast. The current system close to the coast is less chaotic and possible more reliable.

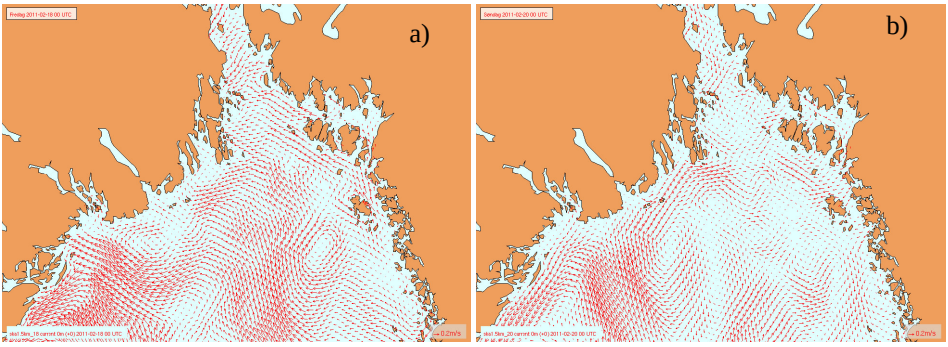

Figure 5 Current vector vectors from the MIPOM 1.5 km run made at met.no. Results are from 00.00 on a) 18 February, and b) 20 February.

3. Oil drift simulations for the Godafoss accident

3.1 First 36 hours

Several trial and error attempts showed that the model is quite sensitive to the initial position of the oil spill (which is very close to the model boundary). It is likely that the model does not describe all the fine details of the oil spill in the vicinity of a coast line, and thus not the fine scale dynamical features of the oil spill. Accordingly we decided to use three different starting points for the oil spill (see Figure 6a).

The oil-drift simulation correctly describes an initial north-northwest movement of oil, and the speed of the movements seems to be of the correct order (Figure 6a–d). The oil gets very close to the coast of the western side of the outer Oslo fjord, but there is no beaching of oil (as was observed). Although we do not get beaching of oil, the predictions are very accurate in the first 36 hours following the accident (i.e., compare Figure 2 and Figure 6). The observations are much more scattered than the modelled particles: this may be an indication that the horizontal diffusivities grounded in small scale eddies may not be parametrised correctly in the model. A higher horizontal diffusivity may produce more realistic results (this is consistent with the evaluation of the model for the Full City accident).

After 36 h the model predicts that oil moves out from the coast; however, it stays in a position outside the coast for a few days. The oil moves toward the coast on Feb 22, and

beaches on the coast on Feb 23. According to observations, the oil stayed in the area for a few days but all observations were made closer to the coast (helicopter surveillance did not show any sign of oil more then say 15 km from the coast).

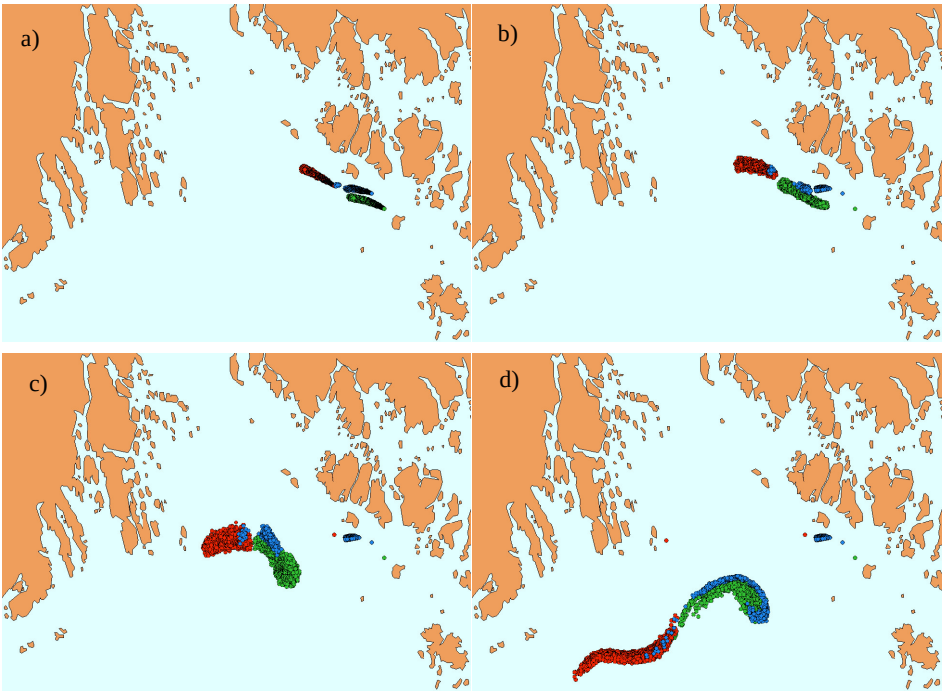

Figure 6 The simulated oil spill from the met.no oil drift model OD3D. The oil super-particles are shown as dots, the different colours represents different initial positions of the oil spill in the model. The plots are from 18 February for a) 00:00, b) 06:00, c) 12:00, and d) 19 February at 18:00.

3.2 Beaching

The model predicts major beaching of oil on Feb 23 (Figure 7): observations show some beaching in the area where the model simulates beaching; however, there were no observations of a major beaching and the observed beaching came earlier. It should be noted that there was ice along the coast and this may imply that there was more beaching but that these were not observed. Another remark we make is that neither the ocean model nor the oil drift model account for ice conditions. This represents a large uncertainty when evaluating the simulations; the simulated beaching would probably not occur if ice was included in the drift model so the trajectory dynamics can be correct, but the oil-drift model does not include critical components on how oil and ice interacts.

It is interesting to note that the beaching pattern is sensitive to the exact initial position of the spill in the model. This indicates that we need to initialise the oil-drift model using a certain spread of particles to capture the sensitivity of the simulation to the exact initial positions of the oil super particles.

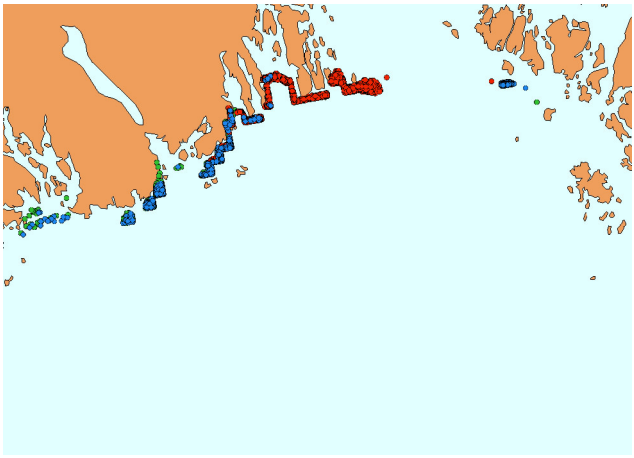

Figure 7 Oil drift simulation based on OD3D. Results are from Feb 23 at 12:00, and most particles have beached. The different colours represent different release positions.

4. Results and discussion

This study evaluated the met.no oil drift modelling system for the Godafoss accident. This accident happened in light wind conditions, and is thus somewhat different to nearby accidents that happened in strong wind conditions (i.e., Stafjord A (Hackett *et al*., 2008), Full City (Broström *et al*., 2011), and Golden Trader). We thus expect that the dynamics underlying the oil drift will be different in the Godafoss case as compared to these other accidents. The impact of the light wind is seen by the weak velocities of the oil drift, and the rather lengthy observations of oil on the ocean surface. It is also notable that the beaching of oil appears to be much smaller in the Godafoss than in the Full City accident. Notably, a significant fraction of the released oil was recovered, and the spilled amount was smaller. Another explanation is that the direction of the wind was out from the coast at the accident site, but also by the weak wind speeds so that oil was not forced toward the land but rather drifted with (slow) ocean currents. Interesting in this regard is also that beaching occurred more “compactly” than observed after the Full City incident. The oil remained in patches, possibly due to little wind and low temperatures.

As in the evaluation of the Full City accident, we note that the model does not describe beaching accurately in the vicinity of the accident site, and in areas where the oil particles get close to the coast in areas where beaching occurred but where the model does not predict any beaching. In both cases the accident sites were close to the coast (less then a few hundred metres) in areas with complex geometry.

Finally, one point of concern in this analysis is the quite thick ice in many parts of the Oslo fjord during the accident. Ice is not included in the present model setup and this unfortunately represents a major uncertainty in the present evaluation of the model system.

Acknowledgement

This study has been supported by the Norwegian Research council through the project OilWave 207541.

References

Broström, G., A. Carrasco, L.R. Hole, S. Dick, F. Janssen and coauthors (2011). Usefulness of high resolution coastal models for operational oil spill forecast: the "Full City" accident. Ocean Science 7, 1−16, doi:10.5194/os-7-1-2011.

Engedahl, H. (1995). Implementation of the Princeton Ocean Model (POM/ECOM3D) at the Norwegian Meteorological Institute. 5, Norwegian Meteorological Institute, Oslo, Norway.

Hackett, B., Ø. Breivik, and C. Wettre (2006). Forecasting the drift of objects and substances in the ocean. In: E.P. Chassignet and J. Verron (Editors), Ocean Weather Forecasting: An Integrated View of Oceanography. Springer, Dordrecht, The Netherlands, pp. 507–524.

Hackett, B., G. Zodiatis, P. Daniel, and G. Broström (2008). Oil spill fate forecasting in the MERSEA Integrated Project, Mercator newsletter, pp. 28−33. Ramstad, S., and L.-G. Faksness 2011. Godafoss: Karakterisering av oljeprøver, naturlige prosesser og mulige tiltaksalternativer, Trondheim.

Reed, M., Ø. Johansen, P.J. Brandvik, P.S. Daling, A. Lewis and coauthors (1999). Oil spill modelling towards the close of the 20th century: Overview of the state of the art. Spill Science & Technology Bulletin 5, 3−16.

Report, (2011). Oljeregnskap Godafoss 2011, oppdatert 14.10. Norwegian Coastal Authorities.

Walin, G., G. Broström, J. Nilsson, and O. Dahl (2004). Baroclinic boundary currents with downstream decreasing buoyancy: A study of an idealised Nordic sea system. Journal of Marine Research 62, 517−543.

Coupled currents-oil spill modelling: MEDSLIK-II model implementation and validation

M. De Dominicis*[1], N. Pinardi[2], G. Coppini[1], G. Zodiatis[3], and R. Lardner[3]

[1]*Istituto Nazionale di Geofisica e Vulcanologia, Bologna, Italy*
[2]*Corso di Scienze Ambientali, University of Bologna, Ravenna, Italy*
[3]*Oceanographic Centre, University of Cyprus, Cyprus*

Abstract

The success in the management of an oil spill depends on several factors including the ability to detect the spills and the capabilities to forecast the drift and transformations of oil over time. Transport, dispersion and transformation processes can be simulated using a Lagrangian oil spill model coupled with Eulerian circulation models. MEDSLIK-II simulates the transport of the surface slick governed by the water currents and by the wind. Forecasting of the Lagrangian trajectories relies on the accuracy of ocean currents. The advent of operational oceanography and accurate operational models of the circulation have made possible the knowledge of the ocean currents fields, which can be provided by the analyses and forecasts available hourly or daily by a forecasting Ocean General Circulation Model (OGCM), such as the Mediterranean ocean Forecasting System, MFS. MEDSLIK-II includes a proper representation of high frequency currents and wind fields in the advective components of the Lagrangian trajectory model, the introduction of the Stokes drift velocity and the coupling with the remote-sensing data to be used as initial conditions. Oil particles are also dispersed by turbulent fluctuation components that are parametrised with a random walk scheme. In addition to advective and diffusive displacements, the oil spill parcels' characteristics change due to various physical and chemical processes that transform the oil (evaporation, dispersion in water column, spreading, emulsification, adhesion to coast).

The model has been validated with data from surface drifters, and with satellite data in different Mediterranean regions. Moreover, the MEDSLIK-II model has been validated using in-situ data acquired during the PRIMI Project (PRogetto pilota Inquinamento Marino da Idrocarburi) validation cruise on oil spill detection and fate. The PRIMI cruise objective was to verify in-situ the oil slicks detected by satellite, presumably being the result of illegal tank flushing, in order to acquire in-situ data for validation of the oil spill model and the satellite detection system. During the cruise, several oil spills were detected and verified in-situ. The MEDSLIK-II model proved crucial to finding the oil slick within 12−24 hours of the satellite observation. The position of the detected oil slick moved several tens of kilometres in few hours and the ship had to be moved toward the predicted oil spill position in order to validate the detection and the forecast. The PRIMI cruise results highlighted the maturity of the MEDSLIK-II model in its ability to forecast the trajectory of oil slicks observed by satellite.

Keywords: Oil spill, Lagrangian model

* Corresponding author, email: michela.dedominicis@bo.ingv.it

1. Introduction

MEDSLIK-II has been designed to provide timely information on oil spill advection-diffusion and weathering in the ocean. The model has the potential to become part of an operational system providing detection of oil slicks and predictions of their movement and transformation, in order to manage emergencies and assess pollution levels.

Our work starts with the MEDSLIK model (Lardner and Zodiatis 1998; Lardner *et al*., 2006; Zodiatis *et al*., 2005; 2008) and presents some novel characteristics of MEDSLIK-II including an initialisation procedure by using remote sensing data and a proper representation of high-frequency currents, wave-induced currents and wind field corrections in the advective components of the particle trajectory equations.

This paper illustrates the advection diffusion processes, describes the transformation processes, and presents the MEDSLIK-II validation using in-situ data.

2. Transport processes: advection and diffusion

Oil transport at sea is governed by advection of the hydrodynamic field and dispersion generated by turbulence in the motion field. Oil concentration also varies according to numerous physical and chemical transformation processes. The use of a numerical model for hydrocarbon transport and diffusion at sea allows the evolution of the oil slick's position, as well as its concentration over time, to be predicted. MEDSLIK-II is a Lagrangian model, which means that the oil slick is represented by a large number of particles. Each single particle is transported by advection and turbulent dispersion. The particle trajectory equation is as follows:

$$d\mathbf{x}(t) = \begin{bmatrix} U(\mathbf{x}, t) \\ V(\mathbf{x}, t) \\ 0 \end{bmatrix} dt + d\mathbf{x}'(t) \qquad (1)$$

where U(**x**,t), V(**x**,t) are the components of the current velocity and d**x**'(t) is the particle displacement due to the turbulent flow component. Vertical velocity is taken to be so little that it can be overlooked, as it is two orders of magnitude smaller than the horizontal velocity components.

The particles composing the oil slick move horizontally, transported by the horizontal current field, which is generated by buoyancy, wind and waves. The first term of equation (1) may therefore be rewritten thus:

$$d\mathbf{x}(t) = [\mathbf{U}_c(\mathbf{x}, t) + \mathbf{U}_w(\mathbf{x}, t) + \mathbf{U}_s(\mathbf{x}, t)]dt + d\mathbf{x}'(t) \qquad (2)$$

where $\mathbf{U}_c(\mathbf{x}, t)$ is the marine current velocity generated by buoyancy and non-local winds, $\mathbf{U}_w(\mathbf{x}, t)$ is the velocity caused by local winds (Ekman current) and $\mathbf{U}_s(\mathbf{x}, t)$ is the wave-induced particle velocity (Stokes drift velocity).

In the past, the marine current velocities used were those of geostrophic and climatological currents. Oil slicks, however, are transported by marine surface currents (ageostrophic currents). It was therefore necessary in the past to add a wind correction,

$\mathbf{U}_w(\mathbf{x}, t)$, to the geostrophic currents in order to be able to reconstruct the ageostrophic Ekman current component correctly. The term $\mathbf{U}_w(\mathbf{x}, t)$ allows the parametrisation of surface Ekman currents for wind intensity and angle of deviation with respect to the wind direction.

With the advent of operational oceanography (Pinardi and Coppini, 2010) (Coppini *et al*., 2010) it has been possible to use advanced marine circulation models: ageostrophic currents can be supplied directly by analyses and forecasts from the Ocean General Circulation Model (OGCM). However, using the term $\mathbf{U}_w(\mathbf{x}, t)$ is still admissible in order to take into account processes at the air-sea interface that the Eulerian hydrodynamic model used does not resolve.

Oil slicks on the sea surface also move because of wave motion: the velocity generated by wave motion is called Stokes drift velocity, $\mathbf{U}_s(\mathbf{x}, t)$. This velocity has to be added to the current velocity produced by a Eulerian hydrodynamic model, unless the model is directly coupled with a wave model. Stokes drift velocity has been introduced into MEDSLIK-II using an analytical formula in which the Stokes drift velocity is expressed according to the wave spectrum. The JONSWAP (Joint North Sea Wave Project, Hasselmann *et al*., 1973) spectrum parametrisation was used, in which the spectrum is expressed according to the wind intensity and fetch. It has been assumed that the direction of wave propagation is the same as the wind direction.

The transport processes due to turbulent dispersion, the last term in equation (1), are represented by a random-walk model:

$$\begin{aligned} d\mathbf{x}'(t) &= [2n-1]\sqrt{6K_h dt} \\ d\mathbf{y}'(t) &= [2n-1]\sqrt{6K_h dt} \\ d\mathbf{z}'(t) &= [2n-1]\sqrt{6K_v dt} \end{aligned} \tag{3}$$

Where n is a random real number that can have any value between 0 and 1, and K_h and K_v are the horizontal and vertical diffusivity components.

3. Transformation processes

As well as sea-surface transport processes, physical and chemical processes also modify oil slicks by transforming the hydrocarbons. MEDSLIK-II allows the processes of spreading, evaporation, dispersion, emulsification and coastal absorption to be simulated.

Because of transformation processes, every particle composing the oil slick modifies some of its properties – for example, its volume.

When the oil first enters the sea, the slick spreads on the sea surface because of gravitational forces. As it is transported, lighter oil components disappear through evaporation and heavier ones emulsify with the water or are dispersed in the water column. MEDSLIK-II is also able to take into account absorption of oil by the coast should the slick reach it.

4. MEDSLIK-II model implementation

4.1 Initialisation from remote sensing data

The oil spill data required to define the oil spill initial conditions are: location, time, oil type, the area covered by the slick, the thickness of the slick, and the age of the oil spill from initial release into the sea. Most of this information can be provided from satellite images, especially the area covered by the slick.

MEDSLIK-II randomly inserts N particles within a slick polygonal area that can be constructed from Synthetic Aperture Radar (SAR) or optical images. An example of the initialisation using the real slick shape observed by satellite is given later.

A novel feature of MEDSLIK-II is its ability to initialise the oil properties (oil viscosity, initial oil volume, initial fraction of water mousse). In order to calculate these variables the age of the slick has to be hypothesised. Initialisation proceeds in two stages: first a simulation with weathering processes only is performed for a time period equal to the slick age, taking into account the wind and SST in the area where the spill is observed, but leaving the particles in the same positions. This will give the initial values, which can be used for forward integration of the model.

4.2 Meteorological and oceanographic forcings

The level of precision found when forecasting oil transport and transformation depends on the accuracy of the marine currents and the wind field. MEDSLIK-II requires the wind field, surface temperature and three-dimensional current field as input. The wind field, i.e., the components of wind velocity at 10 m above the sea surface, is supplied by a Eulerian general atmospheric circulation model, whilst currents and temperature are supplied by a Eulerian marine oceanic circulation model. MEDSLIK-II can use daily and hourly fields produced by the Mediterranean Forecasting System (MFS: gnoo.bo.ingv.it/mfs) (Pinardi *et al*., 2003), which has a horizontal resolution of 1/16°, or regional models with a higher spatial resolution. The fields of three oceanographic models can currently be used by MEDSLIK-II: the Adriatic Forecasting System (AFS: gnoo.bo.ingv.it/afs) (Oddo *et al*., 2006); the Sicily Channel Regional Model (SCRM) (Gaberšek *et al*., 2007); the Tyrrhenian Sea Model (Vetrano *et al*., 2010). These models are nested in the Mediterranean model and achieve a horizontal resolution up to 2 km.

MEDSLIK-II can also use current fields produced by a relocatable model, IRENOM (Interactive Relocatable Nested Ocean Model), which is nested within MFS and produces high-resolution (up to 1 km) currents. This model can be used in emergencies (e.g. accidents where there is a particular risk of a large oil spill), when it is necessary to have current fields with high horizontal resolutions in a given area of the Mediterranean.

The wind forcing used by MEDSLIK-II, which is produced by the ECMWF (European Centre for Medium-Range Weather Forecasts), consists of wind fields every six hours with a horizontal resolution of 0.5° or 0.25°.

5. MEDSLIK-II model validation

In this work the MEDSLIK-II model has been validated using data acquired in 2009 during an oceanographic survey organised in the Mediterranean Sea (Sicily area) in the framework of the PRIMI project (Santoleri *et al*., 2010). The cruise was organised to

visit oil slicks detected by the SAR and optical satellite observations and whose displacement was predicted by the MEDSLIK-II model, coupled with the oceanographic operational models available in the Mediterranean Sea. The cruise was planned in order to have the ship within selected satellite image frames at acquisition time, so as to maximise the number of monitorable oil spills. The satellite images were processed in order to give detailed slick information, such as the oil slick contour coordinates on board, and if available, the oil slick contours were used as input to the oil spill model simulation.

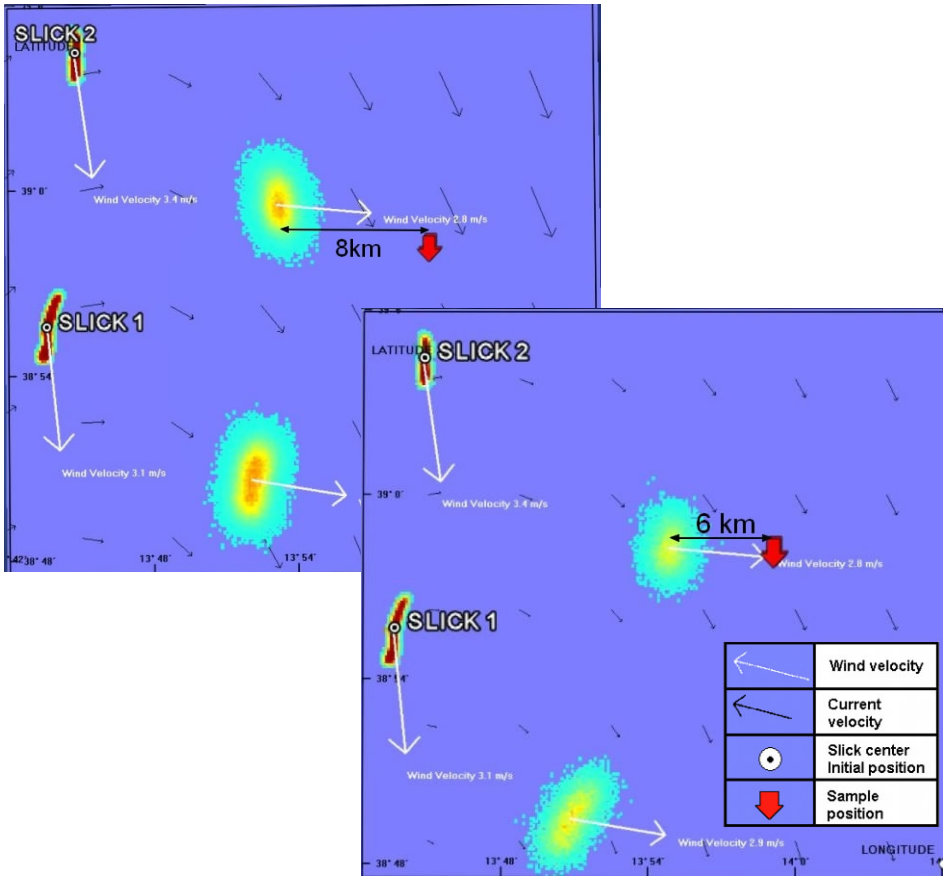

Figure 1 The oil spills labelled "slick1" and "slick2" correspond to slicks observed in the COSMOSKYMED image on 8 August 2009. The red arrows represent the sample collection positions on 8 August at 9:30. The wider two slicks are the predicted positions by MEDSLIK 29 hours after the satellite detection using the MFS currents (top) and using the Tyrrhenian Sea Model currents (bottom).

Two of the four slicks found near the position predicted by the MEDSLIK-II model will be presented in this section.

The first one was observed on 7 August 2009 at 10.00 UTC by the COSMOSKYMED satellite and was found in-situ 29 hours later. The predicted position of the slick was 8

km from the in-situ observation using the hourly surface currents produced by MFS. (Figure 1, top). When higher resolution Tyrrhenian Sea Model hourly fields are used, the slick trajectory is better reconstructed: the predicted position was 6 km from the observed slick position (Figure 1, bottom).

In the second case a slick was observed in-situ 6 hours after the satellite observation (ENVISAT acquisition on 18 August 2009 at 09.35). The distance between the sample collection position and the predicted slick centre is approximately 1 km. In this case due to the short period of the simulation the results were more accurate, although, as in the previous case, the comparison of model simulation results with in-situ observations shows that the simulated oil spill moved slower than the real slick.

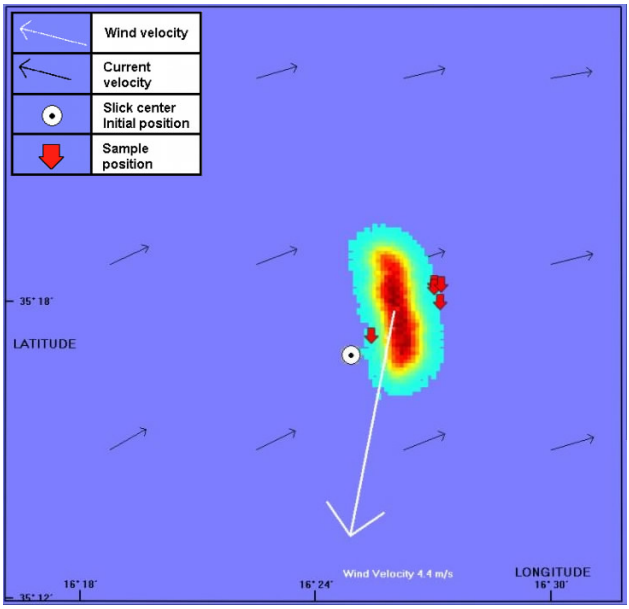

Figure 2 Predicted position after 6 hours (18.08.09 15:00 UTC) using the MFS surface currents. The red arrows represent the position of the collected samples.

6. Final remarks

In conclusion we have shown that the MEDSLIK-II model coupled with operational forecast as basic current fields for the transport process show skill in reproducing slick transport. We found that an hourly time frequency and an open ocean horizontal resolution of a few km is necessary to recover slick trajectories for 12–24 hours from the satellite observation. After this time, numerical errors due to the simple Euler forward numerical scheme used grow too fast, and re-initialisation of the solution should be required.

The MEDSLIK-II model proved crucial to finding the oil slick, because the position of the detected oil slick moved several tens of kilometres over a few hours and the ship had to be moved toward the predicted oil spill position in order to validate the detection and the forecast.

Acknowledgements

We gratefully acknowledge support from the ASI (Agenzia Spaziale Italiana) PRIMI project.

References

Coppini, G., M. De Dominicis, G. Zodiatis, R. Lardner, N. Pinardi, R. Santoleri, S. Colella, F. Bignami, D.R. Hayes, D. Soloviev, G. Georgiou, and G. Kallos (2010). Hindcast of oil spill pollution during the Lebanon Crisis, July–August 2006. Marine Pollution Bulletin.

Gabèrsek, S., R. Sorgente, S. Natale, A. Olita, M. Astraldi and M. Borghini (2007). The Sicily Channel Regional Model forecasting system: initial boundary conditions sensitivity and case study evaluation, Ocean Science, Vol. 3, pp.31–41.

Hasselmann, K., T.P. Barnett, E. Bouws, H. Carlson, D.E. Cartwright, K. Enke, J.A. Ewing, H. Gienapp, D.E. Hasselmann, P. Kruseman, A. Meerburg, P. Miller, D.J. Olbers, K. Richter, W. Sell, and H. Walden (1973). Measurements of wind-wave growth and swell decay during the Joint North Sea Wave Project (JONSWAP). Ergnzungsheft zur Deutschen Hydrographischen Zeitschrift Reihe, A8–12.

Lardner, R., G. Zodiatis, D. Hayes, and N. Pinardi (2006). Application of the MEDSLIK Oil Spill Model to the Lebanese Spill of July 2006. European Group of Experts on Satellite Monitoring of Sea Based Oil Pollution. European Communities.

Lardner, R., G. Zodiatis, L. Loizides, and A. Demetropoulos (1998). An operational oil spill model for the Levantine Basin (Eastern Mediterranean Sea), in: International Symposium on Marine Pollution.

Oddo, P., N. Pinardi, M. Zavatarelli and A. Colucelli (2006). The Adriatic Basin forecasting system, 2006, Acta Adriatica, 47: 169–184.

Pinardi, N., I. Allen, E. Demirov, P. de Mey, G. Korres, A. Lascaratos, P.Y. Le Traon, C. Maillard, G. Manzella, and C. Tziavos (2003). The Mediterranean ocean forecasting system: first phase of implementation (1998–2001). Pages 3–20 of: Annales Geophysicae-European Geophysical Society, vol. 21.

Pinardi, N., and G. Coppini (2010). Operational oceanography in the Mediterranean Sea: the second stage of development. Ocean Science, 6, 263–267.

Santoleri R., F. Bignami, E. Böhm, F. Nirchio, M. De Dominicis, and PRIMI Cruise Group "The PRIMI Project: August–September 2009 validation cruise on oil spill detection and fate." SEASAR 2010, 25–29 January, ESA-ESRIN, Rome, Italy.

Vetrano, A., E. Napolitano, R. Iacono, K. Schroeder, and G.P. Gasparini (2010). Tyrrhenian Sea circulation and water mass fluxes in spring 2004: Observations and model results, Journal of Geophysical Research, Vol. 115, C06023.

Zodiatis, G., R. Lardner, D. Hayes, G. Georgiou, G. Kallos, and N. Pinardi (2005). "Oil spill model predictions integrated with operational forecasting and observing systems in the Mediterranean" IMEMS – The 8th International Marine Environmental Modeling Seminar, pp 58, Helsinki, 23–25 August, 2005.

Zodiatis, G., R. Lardner, D. Hayes, G. Georgiou, N. Pinardi, M. De Dominicis, and X. Panayidou (2008). The Mediterranean oil spill and trajectory prediction model in assisting the EU response agencies, in: Congreso Nacional de Salvamento en la Mar, Cadiz, 2–4 October, libro de actas, pp.535–547.

MyOcean products in the CYCOFOS Decision Support System for Marine Safety

George Zodiatis*, Robin Lardner, Andreas Nikolaidis, Stavros Stylianou, Xenia Panayidou, Daniel Hayes, George Galanis and Georgios Georgiou

Oceanography Centre, University of Cyprus, Nicosia, Cyprus

Abstract

The MyOcean marine core service, implementing the GMES objectives, is composed of several regional forecasting centres including the Mediterranean, Black Sea and Baltic Sea. These centres provide the Member States national marine services, intermediate users, and end-users, with forecasting products for sea currents, temperature, salinity and sea level. The MyOcean regional products in the Mediterranean are used by the CYCOFOS upgraded hydro-dynamical modules for hierarchically high resolution downscaled forecasts in the Levantine and its sub-basins. The MyOcean regional and CYCOFOS downscaled forecasting products are used for downstream services, leading to the establishment of a Decision Support System for marine safety in the European seas. The CYCOFOS DESS downstream service provides: a) short, 24-hour forward and backward predictions of oil spills primarily in the Mediterranean, and secondary predictions upon request in the Black Sea and the Baltic Sea, using ASAR satellite images from ESA and EMSA-CSN and b) support to search and rescue centres for floating object predictions. The CYCOFOS DESS will contribute to the establishment of the Mediterranean Decision Support System for marine safety, in the framework of the relevant MED programme, using the MyOcean regional and downscaled products.

Keywords: ocean forecasting, flow models, oil spill models, marine safety.

1. Introduction

The general aim of the ocean component of GMES is to produce regular and systematic information on the state of the oceans, at global and European regional level, providing products for observational and model data, both available in near real time. The MyOcean project, under the GMES fast track services, is targeting the provision of core marine services (MCS) based upon common ocean state variables, from in-situ and satellite remote sensing observations and numerical models that are required to assist and to meet the needs of the response agencies. These needs are driven by the EU Directives, regional and international conventions and treaties related to the environment and civil protection, marine safety, policy making, assessment and implementation. In particular, MyOcean aims to provide products to assist services within key areas, such as Marine and Coastal Environment, Marine Safety, Marine Resources, Marine climate and seasonal forecasting.

The risk from oil spill pollution in the European seas, particularly in the Southern ones, such as the Mediterranean and the Black Sea, is high due, to the heavy traffic of

* Corresponding author, email: gzodiac@ucy.ac.cy

merchant vessels for transporting oil and gas, and the coastal and offshore installations related to the oil and gas industry. The response agencies for major oil pollution incidents at local, regional (REMPEC and BSS, HELCOM) and European (EMSA) levels, require operational reliable information on the movement and the evolution of the spilled oil. Moreover, the coastal Member States need to implement the EU directive 2005/35, regarding the identification of the responsible ships for illegal pollution. The operational ocean forecasts in oil spill and floating objects response have been proven to assist the response agencies in reducing the impact on the marine environment that may arise from such pollution incidents at sea. The initial response in oil spill incidents is to predict operationally where the slick will drift, where and when it will arrive, which resources will be threatened and how it looks at a give time interval. Such downstream predictions need validated high-resolution downscaled ocean forcing data, in addition to the meteorological one.

MyOcean regional products have been used operationally in CYCOFOS since January 2009, for initial and lateral forcing for its downscaled applications, for on-line validation purposes, for improving the CYCOFOS waves forecasts and for oil spill predictions. CYCOFOS consists of downscaled and downstream forecasting systems and has been operational since early 2002 (Zodiatis *et al*., 2002; 2003a; 2010). CYCOFOS is improved, validated and consolidated periodically (Zodiatis, *et al*., 2003b; 2008), following the developments in EU projects relevant to operational ocean forecasting, such as MFSTEP, ECOOP, MERSEA. The CYCOFOS downscaled and downstream products are accessible on-line at www.oceanography.ucy.ac.cy/cycofos.

The MyOcean CYCOFOS downscaled products provide predictions to the local, regional and the EU response agencies, such as REMPEC and EMSA, on the movement and the weathering of the oil spills, as well daily downscaled ocean forecast to sub-regional search and rescue centres operating in the Levantine Basin.

This paper aims to describe the upgraded CYCOFOS downscaled and downstream forecasting systems and to demonstrate the use of the MyOcean and CYCOFOS downscaled products in marine safety, supporting the relevant response and decision agencies.

2. CYCOFOS downscaled modules

2.1 Hydro-dynamical models

The CYCOFOS upgraded hydro-dynamical forecasting modules consist of three modelling systems with different resolutions, open boundaries and domains covering the Levantine Basin, the NE Levantine and the SE coastal zone of Cyprus. Two of the downscaled modules run independently of each other, with different MyOcean and surface forcing. This set-up is necessary in order to additionally provide a backup of the operational predictions, in case one of the two fail. The CYCOFOS hydro-dynamical forecasts are carried out operationally by CYCOM – the Cyprus Coastal Ocean Model (Zodiatis *et al*., 2003b; 2008). CYCOM is a modified version of the Princeton Ocean Model (POM) and since 2009 is initialised from MyOcean regional or sub-regional ocean forecasts and with higher resolution atmospheric surface fluxes.

For the CYCOFOS Levantine Basin hydro-dynamical model, the MyOcean regional daily averaged products have been used operationally for the initial and boundary conditions, along with the daily averaged ECMWF surface fluxes. This mode of operation allows 10-day, daily averaged forecasts to be completed daily with a grid resolution of 1 nm and 25 vertical sigma layers.

For the CYCOFOS NE Levantine the model is downscaled to 1 km, also with 25 vertical sigma layers. This hierarchically downscaled model uses the forecasting products from the sub-regional ALERMO model for initialisation, and for its two open boundaries, which is in turn nested within the MyOcean regional products. This mode of operation allows a 4 and a half day, 6 hour averaged forecast to be repeated daily. Initialisation is once a week, and a spin up of three days takes place with previous initial and boundary fields, along with the high frequency 5 km resolution SKIRON (Kallos and SKIRON group, 1998) surface forcing. This has been shown to increase the small scale hydrodynamic features, without significantly increasing the bias in the model relative to observations (Zodiatis *et al*., 2008).

A Variational Initialisation and FOrcing Platform-VIFOP (Auclair *et al*, 2000a; 2000b) has been implemented in order to downscale more accurately the initial and lateral fields to the CYCOM 1 km resolution grid domain. In particular, spurious gravity waves due to interaction of the interpolated flow field and the high resolution land mask are minimised. For the SE coastal zone of Cyprus, the model is downscaled to 500 m, with 16 vertical sigma layers. This hierarchically downscaled model uses the CYCOFOS 1 km model for initialisation and for its two open boundaries, which is in turn nested within the ALERMO sub-regional, and which is in turn nested within the MyOcean regional products. This mode of operation allows a 4 day, 6 hourly averaged forecasts to be repeated daily, using the SKIRON high-frequency surface forcing.

The MyOcean regional products, used for initialisation of the CYCOFOS hydrodynamical models, include the assimilation of in-situ observations, satellite sea level anomalies and the correction of the heat fluxes using satellite SST. The latter data are used for on-line validation of the CYCOFOS downscaled forecasts, in addition to the periodical off-line validation with in-situ observations (Zodiatis *et al*., 2008).

2.2 Wave models

The CYCOFOS wave module has been upgraded in order to provide higher resolution sea surface wave predictions at basin, sub-basin and coastal scales, minimising, at the same time, the necessary computational cost (Galanis *et al*., 2011). The latest parallel version of the wave model WAM (ECMWF version, cycle 33R1), which employs new parametrisation of shallow water effects, has been adopted in CYCOFOS since January 2009. The new CYCOFOS WAM model includes a novel advection scheme extended to account for the corner points of the grid boxes based on the Corner Transport Upstream scheme leading to a more uniform propagation of wave spectra in all directions (Bidlot and Janssen, 2003), new procedures for the estimation of the maximum expected wave height by means of the probability distribution of sea surface elevation, increased horizontal resolution of the SKIRON wind input at 0.05×0.05 degrees, and wave-current interaction. For the latter improvement, the sea surface currents from the MyOcean regional products in the Mediterranean have been incorporated in the wave integration,

providing a second independent forcing input for the wave model in addition to the wind speed and direction.

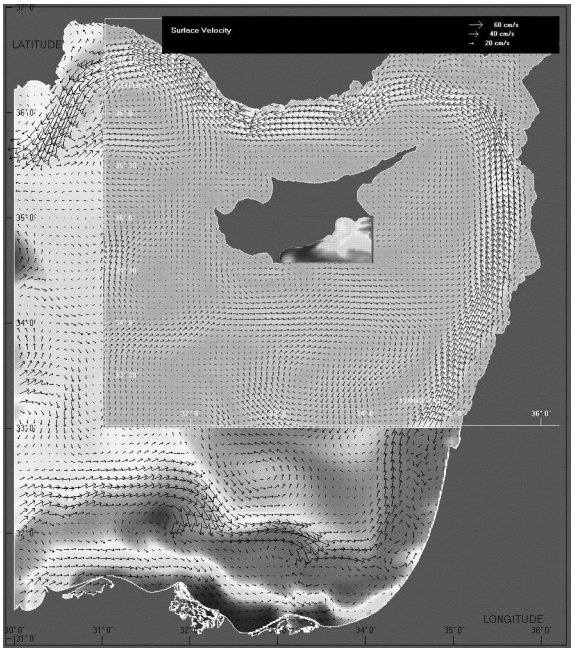

Figure 1 The MyOcean CYCOFOS downscaled hydro-dynamical models: example of the flow and sea temperature in the Levantine, NE Levantine and SE coastal zone of Cyprus on the 26 January 2012.

The resolution of the CYCOFOS new wave model has been increased, to 10 km, 5 km and 2.5 km, respectively for the Mediterranean, Levantine Basin and NE Levantine. The CYCOFOS wave models are nested hierarchically, where the NE Levantine wave model is nested within the Levantine Basin wave model, which is in turn nested within the Mediterranean one. This mode of operation allows a 4 day forecast to be repeated daily, providing 3-hourly predictions for the significant wave height and direction, maximum expected wave height, swell height and direction, wind driven wave height and direction, mean and peak wave period, mean swell and wind driven period, mean directional spread and wind speed and direction at sea level. The CYCOFOS new wave forecast in the Levantine is validated periodically with in-situ wave measurements (Galanis *et al*., 2011) and with other MOON wave forecasts of lower resolution.

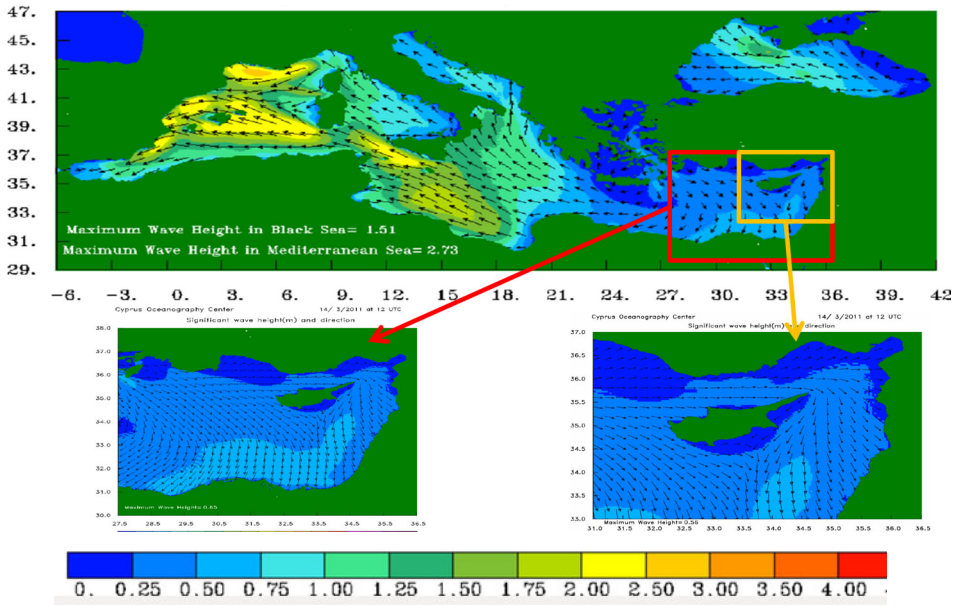

Figure 2 The CYCOFOS new wave forecasts in the Mediterranean (from regional, sub-regional, coastal) and the Black Sea, examples of the significant wave height and direction on the 14 March 2011 at 12:00 GMT.

3. CYCOFOS downstream DESS

3.1 Satellite monitoring for oil spills

In CYCOFOS, ASAR (Advanced Synthetic Aperture Radar) satellite data is received regularly from ESA ENVISAT and processed in house for possible oil slick detection in the Levantine Basin. These satellite data together with ASAR images from the EMSA-CSN portal are used operationally as input-source information in MEDSLIK and AutoMedTrack oil spill models for short forward and backward predictions. From 2007 until 2011 more than one thousand possible small or extended oil spills were detected in the Levantine, mostly at open sea areas.

ASAR is proven a useful tool for ocean oil spill detection due to its wide coverage, independence of day and night, and all-weather capability. The instrument is located on board the ESA ENVISAT satellite. The detection of oil spills by radar systems is based on the dampening effect oil has on surface waves. An oil slick at sea “smooths” the water surface and thus reduces the radar backscatter to the sensor. This creates a darker signature in the image which, after automatic processing, experienced analysts can then interpret as a possible oil slick. A condition for detecting mineral oil spills on the sea surface is that the wind is strong enough for the generation of waves of a minimum size (wavelengths in the centimetre to decimetre range). In addition there is also a maximum wind speed above which oil films become invisible to radar, since the dampening effect disappears against the wind-generated waves. CYCOFOS, in addition, is using the medium-resolution (250−500 m) MODIS satellite data for daily monitoring of possible

oil slicks in the Levantine, because of their unprecedented synoptic and repetitive coverage with a relative high spatial resolution.

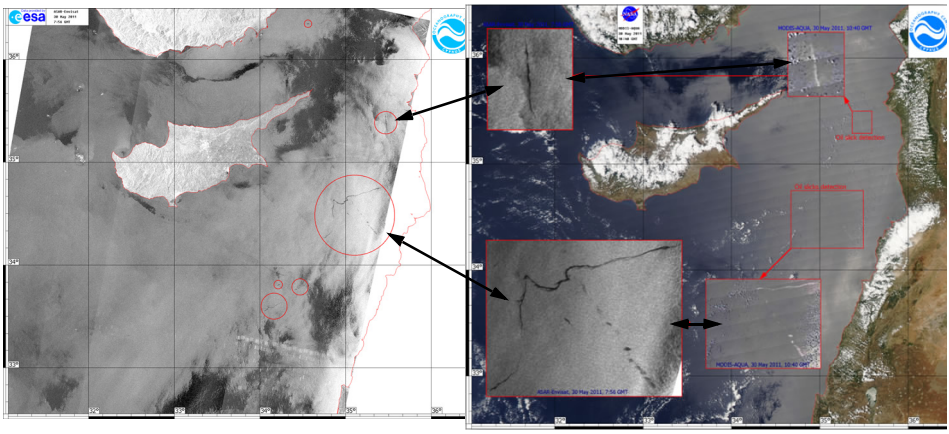

Figure 3 Left: ESA ASAR ENVISAT image on 30 May 2011 at 07:56 GMT showing the detection, after CYCOFOS processing, of several possible oil slicks in the most eastern part of the NE Levantine. Right: NASA MODIS AQUA image on 30 May 2011 at 10:40 GMT showing the detection, after CYCOFOS processing, of two oil spills, which are the same slicks as detected 3 hours later in the ASAR image. The detection of these oil spills from two different satellite observing platforms, confirms that the oil spills are indeed real ones.

3.2 Oil spill predictions

The well-established MEDSLIK oil spill and floating objects system (Lardner *et al*., 2006; Zodiatis *et al*., 2007) has been adapted to operationally use the MyOcean regional products in the Mediterranean and pre-operationally in the Black Sea, as well recently in the Baltic Sea, in order to support the response agencies for marine safety. MEDSLIK needs the currents, the sea surface temperature, the waves and the winds to proceed with the oil spills prediction. The MyOcean CYCOFOS downscaled products in the Levantine Basin and the NE Levantine are also used by AutoMedTrack, which constitutes an automatic version of MEDSLIK without any operator intervention, along with ASAR satellite data for short forward and backwards predictions. These predictions can be superimposed on the AIS traffic information to assist the response agencies in identifying the ship responsible for the detected oil slicks, contributing in this way to the implementation of EU Directive 2005/35.

For the wind forcing, MEDSLIK uses the SKIRON high frequency wind field that covers the Mediterranean and the Black Sea, as well as the ECMWF data, in a similar way as in the CYCOFOS downscaled modules. MEDSLIK also uses the CYCOFOS waves forecasts to count the Stoke's drift on the oil spill movement. The short forward and backward predictions of the oil spills drift in the Mediterranean are provided for viewing on-line on a dedicated CYCOFOS web page, together with the satellite images showing the detected possible oil slicks. The MyOcean regional products are downloaded for CYCOFOS downscaled and downstream applications via FTP and OpenDap, which are proven to be the most efficient way to access the MyOcean regional forecasts. The same method is used to access the SKIRON forecasts.

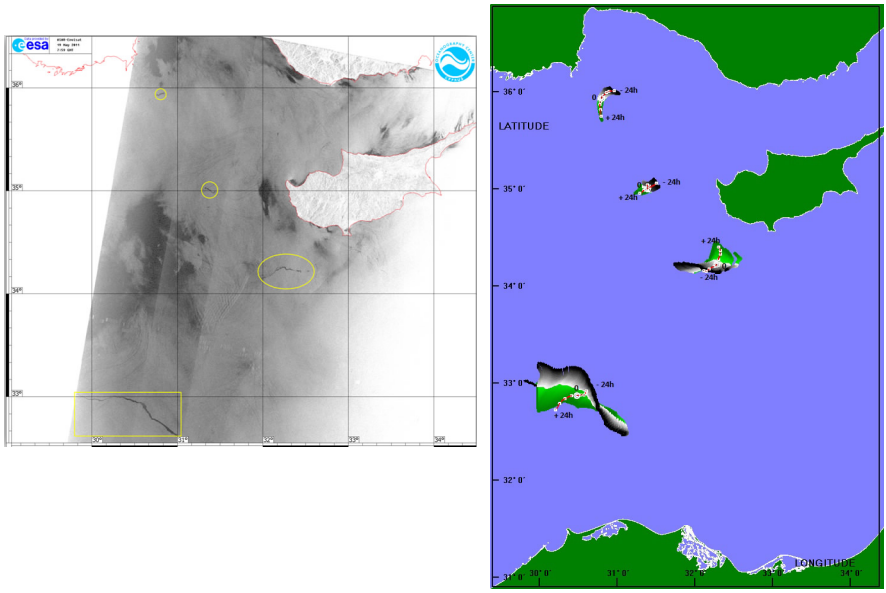

Figure 4 Left: ASAR ENVISAT image on 19 May 2011 at 07:59 GMT showing the detection by CYCOFOS of four possible oil slicks in the Levantine Basin. Right: The MEDSLIK 24-hour forward and backward predictions of the detected oil spills, using the ASAR images and the MyOcean CYCOFOS downscaled products along with SKIRON winds.

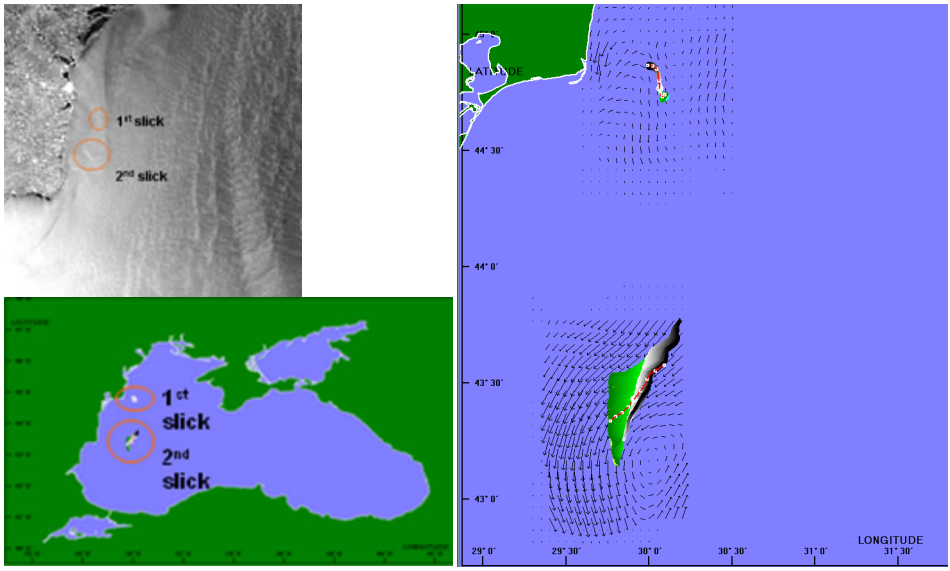

Figure 5 Top left: ASAR ENVISAT image on 11 January 2009 showing the detection by EMSA-CSN of two possible oil slicks in the western Black Sea. Bottom left and right: The MEDSLIK 24-hour forward and backward predictions of the detected oil spills, using the EMSA-CSN ASAR images and the MyOcean Black Sea regional products along with SKIRON winds.

3.3 Floating object predictions

MEDSLIK is used also by search and rescue centres in the region for operational prediction of the trajectory of various floating objects. To demonstrate the importance of using multiple virtual drifters in the predictions of floating objects, as well for inter-comparison purposes, seven virtual drifters were used simultaneously within a given radius of 5 km in MEDSLIK, along the physical trajectory of an Argo SVP type drifter, which was deployed from February to April 2008 in the NE Levantine. For the predictions, 24 hours ahead, of the trajectories of the virtual drifters, the CYCOFOS 6 hourly forecasts, which are nested in the MyOcean regional products, were used along with the high frequency SKIRON winds. The inter-comparison experiment showed that the prediction of all the virtual drifters in MEDSLIK were in most cases in good agreement with the in-situ drifter trajectory (Figure 6). However, in areas of high spatial current variability, only a limited number of the seven released virtual drifters were able to follow the actual in-situ drifter trajectory, while the rest of the virtual drifters were diverted due to the high resolution current's variability.

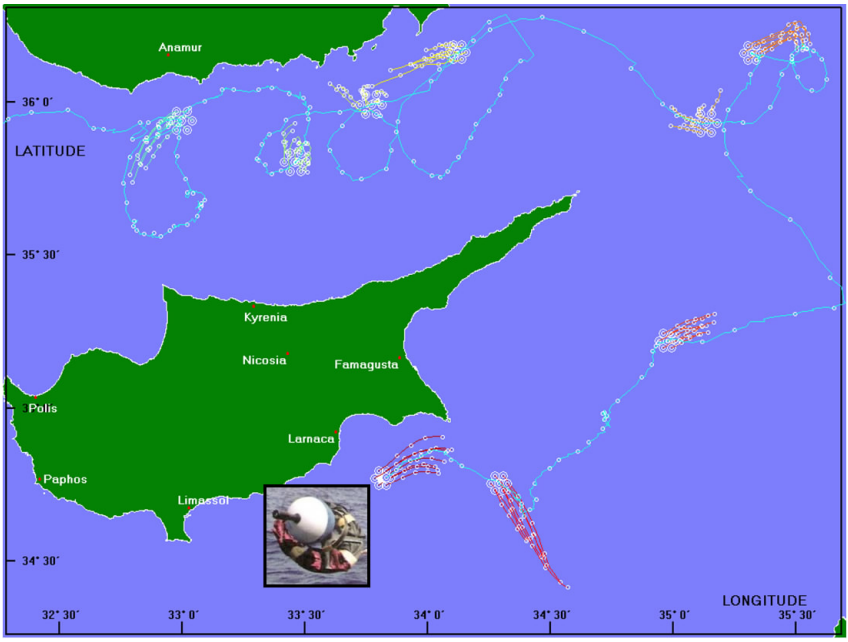

Figure 6 The inter-comparison of MEDSLIK multiple virtual drifters along the trajectory of an Argo SVP type drifter in the NE Levantine, from February to April 2008. For this application MEDSLIK used the CYCOFOS downscaled products from MyOcean and SKIRON winds.

4. Conclusion

The near real time provision of the MyOcean regional products in the Mediterranean made possible the upgrade of the CYCOFOS downscaled forecasting systems in the Levantine and its sub-region. This led to the establishment of an operational downstream service, a Decision Support System, for marine safety using the MEDSLIK and

AutoMedTrack oil spill and floating objects systems, and ASAR satellite data from ESA and EMSA-CSN. Moreover, the use of MyOcean products allowed the adaptation of MEDSLIK in the Black and the Baltic Sea too. The successful CYCOFOS/MEDSLIK implementation using MyOcean products in establishing the CYCOFOS-DESS, has initiate the regional efforts targeting the establishment of the Mediterranean Decision Support System for the Marine Safety (MEDESS4MS), jointly with operational partners and response agencies in the region, in the framework of a Mediterranean call addressing the marine safety.

References

Auclair, F., P. Marsaleix, and C. Estournel, (2000a). Truncation errors in coastal modelling: evaluation and reduction by an inverse method. J. Atmos. Oceanic Tech., 17, 1348−1367.

Auclair, F., S. Casitas and P. Marsaleix, (2000b). Application of an inverse method to coastal modelling. J. Atmos. Oceanic Tech., 17, 1368−1391.

Galanis, G., D. Hayes, G. Zodiatis, P.C. Chu Yu-Heng Kuo and G. Kallos (2011). Wave height characteristics in the Mediterranean Sea by means of numerical modeling, satellite data, statistical and geometrical techniques, Marine Geophysical Research, DOI: 10.1007/s11001-011-9142-0.

Holthuijsen, L.H., N. Booij and R. Padilla-Hernandez (1997). A curvi-linear, third-generation coastal wave model, Conf. Coastal Dynamics '97, Plymouth, 128−136.

Kallos G. and the SKIRON group (1998). The SKIRON forecasting system: VOL. I: Preprocessing ISBN 960-8468-15-9; VOL. II: Model description ISBN 960-8468-16-7; VOL. III: Numerical techniques ISBN 960-8468-17-5; VOL. IV: Paralellization ISBN 960-8468-18-3; VOL. V: Postprocessing ISBN 960-8468-19-1; VOL. VI: Procedures 960-8468-20-5

Lardner, R., G. Zodiatis, D. Hayes, and N. Pinardi (2006). Application of the MEDSLIK oil spill model to the Lebanese spill of July 2006. European Group of Experts on satellite monitoring of sea based oil pollution, European Communities ISSN 1018−5593.

Pinardi, N., and MFSTEP partners (2006). Mediterranean Forecasting System Toward Environmental Predictions (MFSTEP) status of implementation, European operational oceanography present and future, European Communities ISBN92-894-9788-2,286−294.

WAMDI Group (1988). The WAM model − a third generation ocean wave prediction model. J. Phys. Oceanogr., 18, 1775−1810.

World Bank (2007). Report No. 39787-LB, "Republic of Lebanon, Economic Assessment of Environmental Degradation due to July 2006 Hostilities",

Zodiatis G., R. Lardner, G. Georgiou, E. Demirov, and N. Pinardi (2002). Cyprus coastal ocean forecasting and observing system, in Building the European Capacity in Operational Oceanography, Proceedings of 3rd EuroGOOS Conference, Elsevier Oceanography Series, 36−45.

Zodiatis, G., L. Lardner, E. Demirov, G. Georgiou, G. Manzella, and N. Pinardi (2003a). "An Operational European Global Ocean Observing System for the Eastern Mediterranean Levantine Basin: The Cyprus Coastal Ocean Forecasting".

Zodiatis, G., R. Lardner, A. Lascaratos, G. Georgiou, G. Korres, and M. Syrimis (2003b). High resolution nested model for the Cyprus, NE Levantine Basin, eastern Mediterranean Sea: implementation and climatological runs, Annales Geophysicae, 21, 221–236.

Zodiatis, G., R. Lardner, D. Hayes, D. Soloviev, and G. Georgiou (2007). The successful application of the Mediterranean oil spill model in assisting the decision makers during the oil pollution crisis of Lebanon in summer 2006, Rapp.Comm.int. Mer Medit., 214,38.

Zodiatis, G., R. Lardner, D. Hayes, G. Georgiou, S. Sofianos, N. Skliris, and A. Lascaratos (2008). Operational ocean forecasting in the Eastern Mediterranean: implementation and evaluation, Ocean Science 4, 31–47.

Zodiatis, G., D. Hayes, R. Lardner, G. Georgiou, G. Kallos, S. Sofianos, N. Pinardi and X. Panayidou (2010). Marine core and downstream oceanographic services in the Eastern Mediterranean Levantine Basin and their success in assisting the EU response agencies, Proceedings of the 5th EuroGOOS conference, publication N. 28, 465–472.

Using surface drifters to validate an operational oil drift system in the Barents Sea

Lars R. Hole*[1], Kai H. Christensen[1], Igor Ivichev[1,2], Johannes Röhrs[1], Göran Broström[1], and Cecilie Wettre[1]

[1]*Norwegian Meteorological Institute*
[2]*Russian State Hydrometeorological Institute*

Abstract

A number of Isphere surface drifters were dropped during a campaign off the coast of Lofoten/Vesterålen in April 2010. The drifters are designed to behave like an oil spill. Some of the drifters survived in the sea for several months and the trajectory data have been used for comparison with the met.no oil drift model with a 4 km horizontal resolution in the ocean forcing fields. The model was restarted every 24 hours at the position of the drifter. The results show the transport distance made by the drifter in 24 hours is well predicted by the model ($r=0.84$), whereas the modelled oil slick trajectories have a tendency to turn $10-20°$ to the right compared to the observed trajectories. It is believed that improvements in the representation of the Coriolis-Stokes force and better horizontal resolution to resolve eddies will result in more reliable predictions of oil spill trajectories in the future.

Keywords: Surface drifters, oil spill, model trajectories, Barents Sea.

1. Introduction

In order to provide accurate oil spill forecasts, information about atmospheric conditions, waves and ocean dynamics is required. Several European operational oceanography and data assimilation systems have been implemented during the last few years. All these systems use different operational capacities, data streams and expertise (Daniel *et al*., 2005). At the Norwegian Meteorological Institute (met.no), the operational Princeton Ocean Model with a 4 km resolution has for several years been the main operational model, with model runs performed twice daily. The atmospheric model used to force the oil drift model is the Hirlam 8 km (run 4 times daily) while the wave model applied is the wave model project code (WAM 4 km), run 4 times daily. The Lagrangian oil drift system, Oil Drift 3 Dimensional model (OD3D), provides a forecast for a large ensemble of oil particles based on forcing from the above mentioned models. OD3D can be operated through a simple and user friendly web interface. These models will be described in more detail.

Satellite-tracked surface drifters provide useful information on the surface circulation and related water property transports in deep ocean regions (Riser and Rossby, 1983; Fratantoni, 2001; Reverdin *et al*., 2003; Zhurbas and Oh, 2003) and within marginal seas and on continental shelves. Here we present a simple comparison of observed trajectories

* Corresponding author, email: lrh@met.no

from semi-submerged surface drifters and oil drift simulation. The drifter experiment was carried out off the coast of Northern Norway in April–July 2010.

The data presented here were obtained as part of the BioWave project (Surface wave effects in the upper ocean and consequences for biological modelling) which is a collaboration between met.no and the Norwegian Institute of Marine Research (IMR) sponsored by the Research Council of Norway. The project was initiated to improve the mixed-layer dynamics of the numerical circulation models as applied to the physical forcing in ecosystem models and trajectory models such an OD3D. Wave-induced fluxes of momentum and energy give a more realistic description of the ocean currents and turbulent mixing in the upper layer of the ocean.

BarentsWatch is a Norwegian governmental programme established in order to provide a comprehensive environmental monitoring and warning system in the high north. One sub-project carried out by met.no has resulted in a largely extended domain for the operational oil drift service (Figure 1).

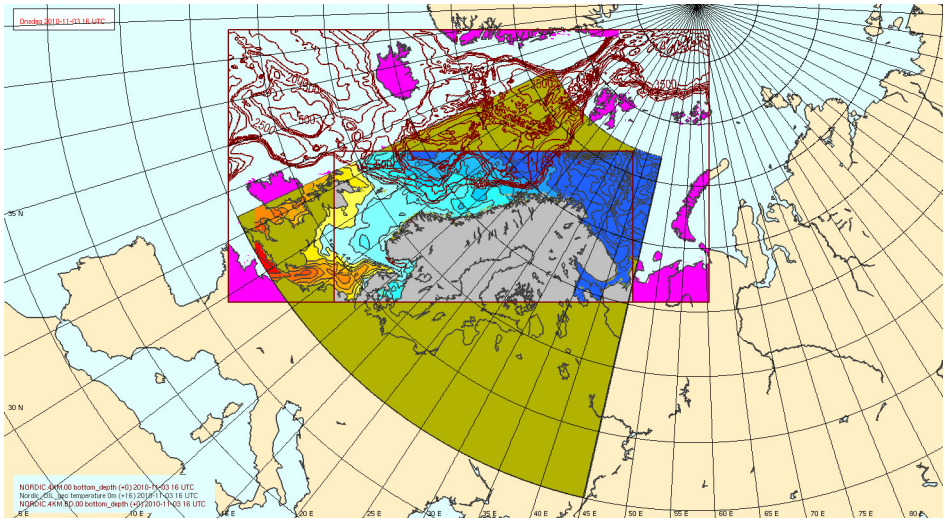

Figure 1 The extended domain of the met.no oil drift system. The small rectangle represent the old domain, while the large rectangle represent the new domain established during BarentsWatch.

2. Oil drift modelling

The HIRLAM 8 km atmospheric model is a hydrostatic grid-point model in which the dynamic core is based on a semi-implicit semi-Lagrangian discretisation of the basic dynamic equations (www.hirlam.org).

The wave model is based on the wave model project code (WAM) which describes the energy in different wave components (Komen *et al*., 1994; Phillips, 1977; Cavalieri, 2007): WAM belongs to the third generation wave models and accounts for the non-linear interaction between the wave components. The Stokes drift is calculated from an integration over the wave spectrum, the contribution from high frequency waves that are

not resolved by the model is calculated using a self-similar spectral shape of this part of the spectrum (Komen *et al.*, 1994; Phillips, 1977; Broström *et al.*, 2009).

The Princeton Ocean Model (POM) (Blumberg and Mellor, 1987) has been modified for operational use at met.no (Engedahl, 1995). The local model version MI-POM (Meteorological Institute Princeton Ocean Model) numerically solves the three-dimensional primitive equations in sigma coordinates (terrain-following coordinates) to describe the ocean dynamics. The model uses a 2.5-order turbulent mixing model (Melsom, 1996; Mellor and Yamada, 1982). The heat flux formulations have been adjusted for local conditions (Røed and Debernard, 2004); the model also includes a simple nudging scheme to assimilate satellite SST products. Tides are included by the eight harmonic components taken from a barotropic tidal model.

The oil drift model at met.no is based on OD3D which was developed in collaboration with SINTEF (Broström *et al.*, 2011, Martinsen *et al.*, 1994; Wettre *et al.*, 2001). OD3D is based on super-particles that represent the main characteristics of the oil. The particle drift is forced by wind, waves (including the Stokes drift), oceanic currents and stratification. The oil chemistry depends mainly on temperature, wind speed and significant wave height. The default model time step is 15 minutes and thus the numerical advection of particles, especially in areas with complex topography, is not very accurate. Furthermore, in the present operational setting, the model does not allow for oil particles to be inside the one half grid-point closest to the coast, for numerical reasons.

The OD3D model predicts the drift of oil particles, how they disperse in time and how much oil has been evaporated, submerged and beached. This study has focused on the advection and used a heavy oil type. In the "standard" operational set up, OD3D uses forcing data from the Nordic 4 km ocean model. However, it is expected that an ocean model with 4 km resolution will not perform well in the vicinity of rugged sections of the coastline or/and in archipelago areas. Therefore we have chosen to compare with a surface drifter which was at some distance from the shore. The oil drift model can be driven using various atmospheric, wave, and ocean models in a non-operational mode and in this study we will compare the performance using the Nordic 4 km model. Note that OD3D only accepts fields in geographic grids, i.e., in standard longitude-latitude grids. Thus, in order to generate inputs to OD3D all forcing fields must be interpolated to the same latitude-longitude domain.

The Isphere drifters (metocean.com) are robust, bi-directional buoys with a lifetime after deployment of 6–12 months. The drifters are tracked by the Global Positioning System (GPS) and the Iridium system transmits data with a transmission interval of 30 minutes. For this study, GPS positioning was most relevant, but SST was also reported. Tracking buoys are advected by the Lagrangian current that includes the wave-induced Stokes drift. The order of magnitude of the Stokes drift can be of the same as the Eulerian current judging from recently collected data in the Lofoten/Vesterålen area (Röhrs *et al.*, 2011).

3. Results

A scientific cruise was carried out in the Lofoten/Vesterålen area in 8–13 April on the Research Vessel Johan Hjort. Ten Isphere drifters were deployed during the cruise, but

several of them stranded after a few days (Figure 2). Although the Isphere drifters are considered expendable, most drifters were retrieved within 6 months of the study since they were labelled and were found by the public along the coast of Northern Norway. Two drifters terminated in Russia and have not been retrieved.

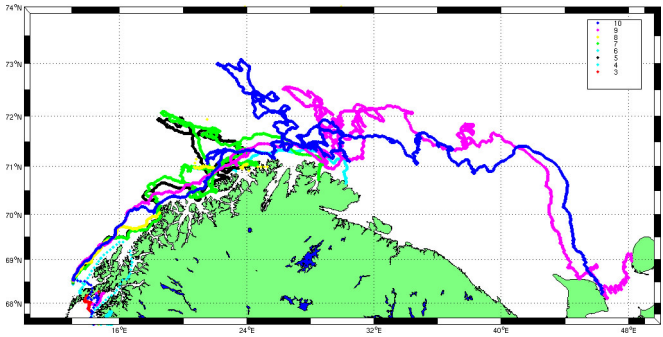

Figure 2 Trajectories of drifters launched during the BioWave cruise in April 2010. The plot includes data from August 2010.

The model experiment was carried out by a script that restarted OD3D at the position of the drifters at midnight every day for about 2 months after deployment (Figure 3). 500 particles were seeded between 0000 and 0030 UTC and the drifter location was compared with the location of the mass centre of the model particles. Since a 4 km ocean model was applied, we avoided near shore trajectories, as the complex coastal topography is not resolved here. The trajectories reported are from drifters advected by the North Atlantic current which is very near to the shore of Lofoten. Drifters in the current moved as fast as 80 km per day.

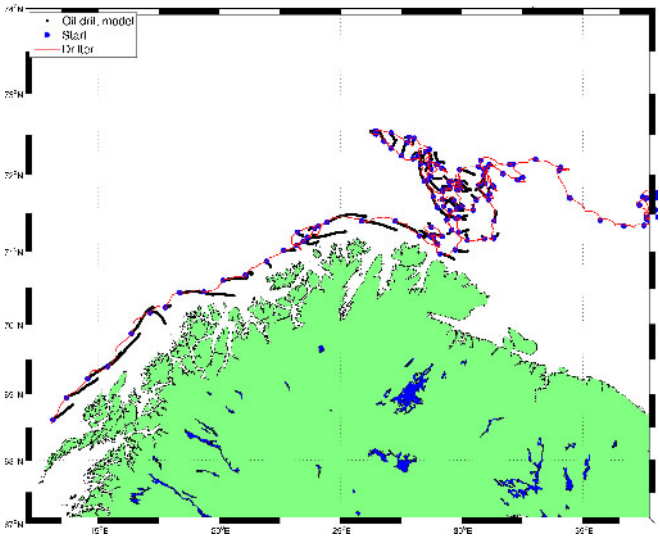

Figure 3 Example of observed drifter trajectory (thin line) and OD3D simulations (thick lines). Red dots indicate starting points of the simulations every 24 hours.

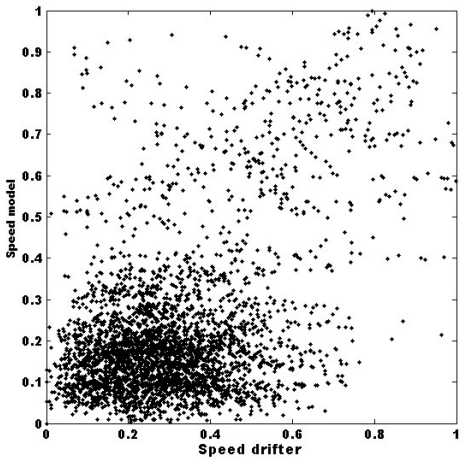

Figure 4 Scatter plot of observed and simulated 30-minute average drifter speed. The modelled speed is the speed of the mass centre of 500 particles.

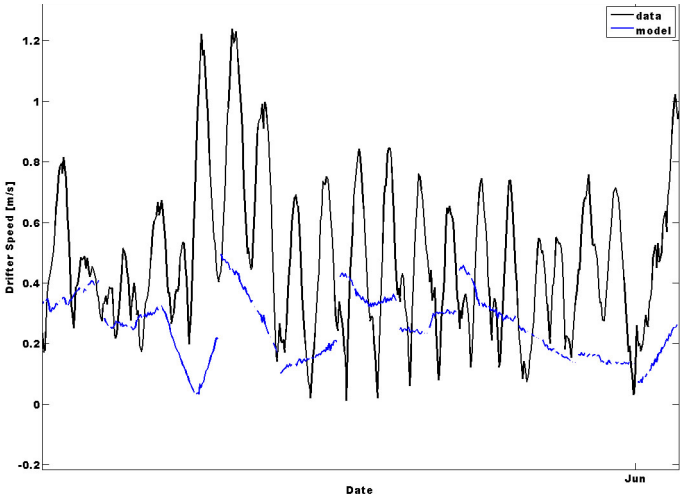

Figure 5 Time series of observed and simulated 30-minute average speed.

A scatter plot of 30-minute velocities from model and drifters indicate no correspondence between observed and modelled speeds (Figure 4). However, from the time series it appears that the drifter speeds displays a strong tidal signal which is not resolved by the model, since the model speed here is an average of 500 particles drifting in different directions (Figure 5). To average out this semi-diurnal signal, a new comparison was made for 24-hr average speeds (Figure 6). The same data (from drifter #9) are presented as a scatter plot in Figure 7 with a correlation of 0.84. A new model experiment was carried out where wind and Stokes drift was switched off in the model (Figure 8). An overall reduction in model speed of 11% was observed. The reason for the zero speed observed in July is that all model particles are stranded. Since the drifters

were advected by the Atlantic current, the Eulerian current seemed to be more important than the Stokes drift in this case. The Coriolis-Stokes effect can still be important for the drift direction of the spill and in some cases determine whether the oil strands or not.

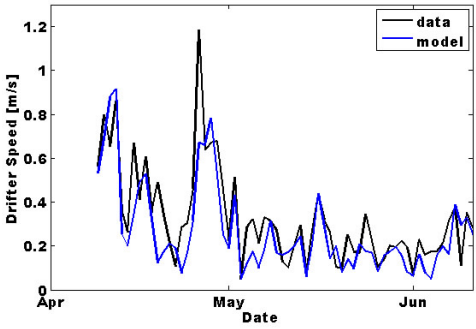

Figure 6 Time series of observed and simulated 24-hr average speed.

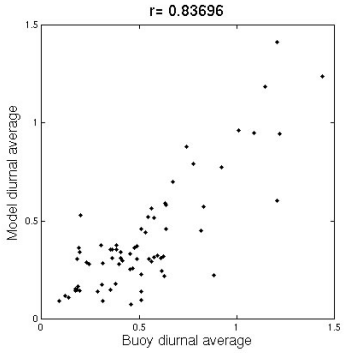

Figure 7 Scatter plot of observed and simulated 24-hr average speed

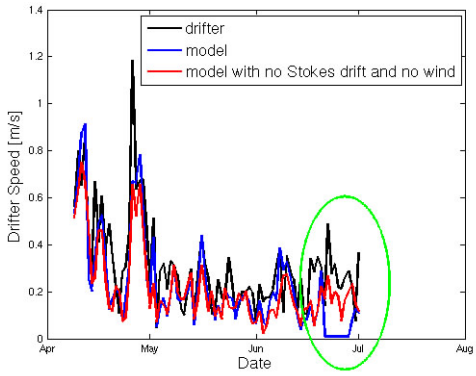

Figure 8 Time series of observed and simulated 24-hr average speed including a case with wind and Stokes drift turned off in the model.

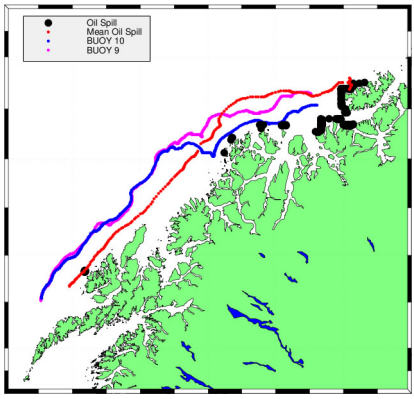

Figure 9 Observed and simulated 10-day trajectories. The modelled speed is the speed of the mass centre of 500 particles.

In all experiments the modelled 24-hr trajectory was typically 10−20° to the right of the observed trajectory. We attribute this to the fact that the Coriolis-Stokes effect is not well represented in the present MIPOM model system (Röhrs *et al*., 2011). In BIOWAVE, wave-induced fluxes will be implemented in the ocean circulation model using the theoretical framework of Broström *et al*. (2008). The operational wave prediction model at met.no will produce the necessary forcing fields for the ocean circulation model, and hence the wave model will act as a link between the atmosphere and ocean models. The ocean circulation model will subsequently deliver improved physical forcing fields for the operational ecosystem models used by IMR and met.no. From 2012, the operational ocean model at met.no will be a version of the Regional Ocean Model System (ROMS) community model (myroms.org), with 800 m horizontal resolution along the entire coast

of Norway. Thus we expect that eddies can be resolved better and that coastal scenarios can be more realistically represented in the model.

However, both observed drifter trajectories and simulations indicate very high northwards drift speeds since the Atlantic current is close to the coast in the region of interest. Figure 9 shows a 10-day oil drift simulation compared with two of the observed drifter trajectories. Lofoten/Vesterålen is under consideration for oil exploration, and our the results suggest that a oil spill in this region will be advected to North Cape within 10 days, probably with stranding along the route, with major environmental consequences. In the neat future, new simulations with the 800 metre ocean model (with improved Coriolis-Stokes representation) will be carried out, hopefully resulting in even more realistic scenarios.

Acknowledgements

This project was supported by the Norwegian government's BarentsWatch programme (barentswatch.blogspot.com) and the Research Council of Norway (RCN) through grant #ES446896 (BioWave). We are also grateful to crew members on *R/V Johan Hjort* and others who have helped undertake the measurements.

References

Blumberg, A.F., and G.L. Mellor (1987). A description of a three-dimensional coastal ocean circulation model, in: Three-Dimensional Coastal Ocean Models, edited by: Heaps, N. S., AGU Coastal and Estuarine Series, American Geophysical Union, Washington D.C.

Broström, G., A. Carrasco, L.R. Hole, S. Dick, F. Janssen, J. Mattsson, and S. Berger (2011). Usefulness of high resolution coastal models for operational oil spill forecast: The Full City accident. ECOOP Ocean Science Special Issue 2011. Ocean Sci., 7, 805–820.

Broström, G., K.H. Christensen, and J.E. Weber (2008). A quasi-Eulerian quasi-Lagrangian view of surface wave induced flow in the ocean, J. Phys. Oceanogr., 38(5), 1122–1130.

Broström, G., A. Carrasco, B. Hackett, and Ø. Sætra (2009). Using ECMWF products in global marine forecasting services, ECMWF newsletter, 118, 16–20.

Daniel, P, P. Josse, and P. Dandin (2005). Further improvement of drift forecast at sea based on operational oceanography systems, Coastal Engineering VII. The Built Environment volume 78. ISBN: 1-84564-009-8. Edited by C.A. Brebbia, and M. da Donceicao Cunha, 368 pp.

Engedahl, H. (1995). Implementation of the Princeton Ocean Model (POM/ECOM3D) at the Norwegian Meteorological Institute, Norwegian Meteorological Institute, Oslo, Norway.

Komen, G.J., L. Cavaleri, M. Donelan, K. Hasselmann, S. Hasselmann, and P.A.E.M. Janssen (1994). Dynamics and modelling of ocean waves, Cambridge University Press, Cambridge, 532 pp.,

Martinsen, E.A., A. Melsom, V. Sveen, E. Grong, M. Reistad, N. Halvorsen, Ø. Johansen, and K. Skognes (1994). The operational oil drift system at DNMI., Norwegian Meteorological Institute, Oslo, Norway, 125, 52.

Mellor, G.L., and T. Yamada (1982). Development of turbulence closure model for geophysical fluid problems, Rev. Geophys. Space Phys., 20, 851–875.

Melsom, A. (1996). A review of the theory of turbulence closure due to Mellor and Yamada, and its implementation in the Princeton Ocean Model, Norwegian Meteorological Institute, Oslo, Norway, 38, 47.

Phillips, O.M. (1977). The dynamics of the upper ocean, Cambridge University Press, Cambridge, 336 pp.

Reverdin, G., P.P. Niiler, and H. Valdimarsson (2003). North Atlantic Ocean surface currents, J. Geophys. Res., 108(C1), 3002, doi:10.1029/2001JC001020.

Riser, S.C., and H.T. Rossby (1983). Quasi-Lagrangian structure and variability of the subtropical western North Atlantic circulation, J. Mar. Res., 41, 127–162, doi:10.1357/002224083788222992.

Röhrs, J., K. Christensen, L.R. Hole, G. Broström, M. Drivdal, S. Sundby (2011). Observation based evaluation of surface wave effects on trajectory forecasts. Subm. Ocean Dynamics.

Røed, L.P., and J. Debernard (2004). Description of an integrated flux and sea-ice model suitable for coupling to an ocean and atmosphere model, Norwegian Meteorological Institute, Oslo, Norway, 51.

Wettre, C., Ø. Johansen, and K. Skognes (2001). Development of a 3-dimensional oil drift model at DNMI, Norwegian Meteorological Institute, Oslo, Norway, 50.

Zhurbas, V., and I.M. Oh (2003). Lateral diffusivity and Lagrangian scales in the Pacific Ocean as derived from drifter data, J. Geophys. Res., 108(C5), 3141, doi:10.1029/2002JC001596.

An integrated operational system for the Coast Guard management of oil spill emergencies in the Strait of Bonifacio

A. Ribotti*[1], A. Cucco[1], A. Olita[1], M. Sinerchia[1], L. Fazioli[1], A. Satta[1], M. Borghini[2], K. Schroeder[2], A. Perilli[1], B. Sorgente[1,3] and R. Sorgente[1]

[1]*Institute for Coastal Marine Environment/CNR, Oristano, Italy*
[2]*Institute of Marine Sciences/CNR, La Spezia, Italy*
[3]*National Park of La Maddalena Archipelago, Italy*

Abstract

An innovative operational forecasting system of marine circulation has been implemented in support of the local Coast Guard in the Bonifacio Strait for the management of maritime operations during oil spill emergencies. The area has an extraordinary environmental value but also extreme meteorological conditions due to a particular orography. Since it has a maritime status of International Strait, it is crossed every year by about 3500 oil, gas and chemical tankers. In case of accident, quick action is essential to avoid or mitigate an environmental and economic impact. The system described here can facilitate the planning and coordination of operations of the local authorities through the forecast of the oil slick displacement, due to wind and surface marine currents, and of the physical-chemical processes determining the fate of the oil at sea. A chain of nested operational models, from the basin to the coastal scale, is the core of the system. A Lagrangian module, coupled with the coastal hydrodynamic/wave model and embedding the weathering equations for the physical-chemical transformation of the oil, provides the estimates for its particles fate. Furthermore, oil spill scenarios, risk maps and a user-friendly Graphical User Interface help the Coast Guard develop a quick plan of action. The system was qualitatively validated in January 2011 when a heavy oil spill occurred in a harbour in north Sardinia, then moved along the coast for 10 days.

Keywords: oil spill, Bonifacio Strait, integrated system, forecasting, numerical modelling.

1. Introduction

The Strait of Bonifacio, located at the centre of the western Mediterranean Sea, separates Corsica from Sardinia and is limited to 7.5 km at its narrowest point (eastern opening) by the presence of tens of islands of different size and reefs, the most of them part of the La Maddalena Archipelago. Morphologically the coast is jagged and consists of frequent rias, cliffs and beaches of limited size that mainly develop in the lee of the prevailing winds from the W-NW (Astraldi *et al*., 1980; Figure 1).

* Corresponding author, email: alberto.ribotti@cnr.it

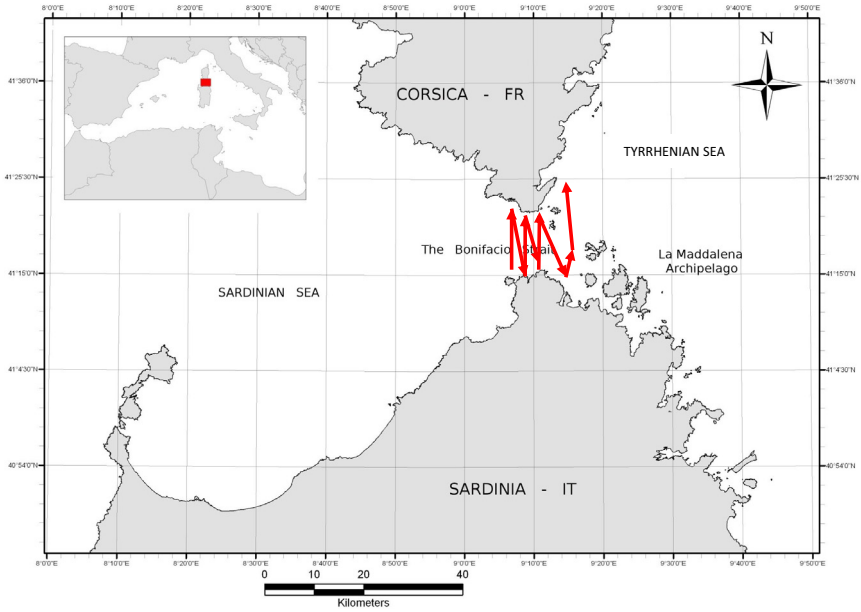

Figure 1 The area of the Strait of Bonifacio with the SADCP transects realised during the cruise Sicily09 shown in red.

In the Strait of Bonifacio, large-scale evolving weather patterns occur, often associated with the topography of Corsica and Sardinia that often generate unexpected and unpredictable weather. The strong northwestern Mistral and eastern winds, due to the Venturi effect, are of increased speed when they funnel through the Strait, and greatly influence the sea conditions particularly during the transit of vessels (Astraldi *et al*., 1980; Astraldi *et al*., 1983).

The Strait of Bonifacio has natural features of great significance and uniqueness. Despite its environmental importance, the maritime traffic is significant and mainly represented by merchant ships that transit the Strait along the route between Gibraltar and Spain to the Italian peninsula, and between Sardinia and Corsica with passenger ships (about 10 daily routes between Corsica and Sardinia). All this traffic intensifies during the summer, to include about 5000 leisure boats.

Actually it is not possible to prevent the passage of merchant ships through the Strait as the maritime traffic is regulated by the Montego Bay Convention (UNCLOS, 1982) that establishes the legal freedom of transit and innocent passage of all ships. But international regulations permit at least control of the characteristics of some vessels in transit, reducing the risk of spill of pollutants: the MARPOL 73/78 from IMO, amended in 1993 (IMO Assembly Resolution A.766(18) of November 4, 1993); the unilateral measure OPA 90, enacted after the Exxon Valdez accident in 1989; the 1993 bilateral agreement between Italy and France, formalised respectively with the Italian Ministerial Decree (DM hereafter) 26/02/1993 by the Ministero della Marina Mercantile and the French Arrêté Prefectoral No.1–93. In the two decrees, of similar content, specific measures were adopted to prohibit navigation in the Strait of Bonifacio of national merchant ships

carrying oil and other hazardous and noxious substances, as defined by international conventions in force in both countries (Directive 2002/59/EC and the MARPOL 73/78 Convention). Despite these limitations, an annual average of 3500 ships transit the Strait, mainly solid bulk cargo ships and Ro/Pax, with a gross tonnage ranging between 500 and 25000 tons (B. Sorgente, personal communication). from the analysis of data from the Vessel Traffic Service (VTS) data provided by the Italian Coast Guard in La Maddalena. It is provided jointly with the French authorities and represents a system in place to increase control for greater safety at sea and making it more efficient and prompt, together with reducing the risk of maritime accidents.

In order to reduce the risk of accidents in the area, several protected areas and national and international parks were established. On April 2010 the establishment of the International Park of the Strait of Bonifacio was defined by the Italian and French authorities and involving the two national protected areas realised in the 1990s. Furthermore, in 2006 the La Maddalena Archipelago and the islands of the Strait have been submitted to the World Heritage List of UNESCO (UNESCO Ref. 2028) and from July 2011 the Strait of Bonifacio and the surrounding areas have been recognised by the International Maritime Organization (IMO) as a "Particularly Sensitive Sea Area" (PSSA), a designation that allows further international measures to be taken to strengthen environmental protection. It is the first PSSA in the Mediterranean and the second international strait in the world.

In 2009 the Italian Ministry for the Environment funded a 2-year project named "SOS-Bonifacio" to manage emergencies at sea due to oil spills in the Strait of Bonifacio. The project aimed to build a new forecasting and monitoring system of the marine circulation for the management of environmental emergencies caused by oil spills, that can be accidental (collisions between ships, rocks, etc) or voluntary (discharge bilge waters, ballast waters, dirty tanks waters). This system facilitates the rapid planning and coordination of operations response against marine pollution by authorities, through the knowledge of the future estimates of an oil spill displacement at sea led by wind and sea currents, and the main physical-chemical processes which are applied to hydrocarbons. These response activities against marine pollution are provided in the "Local emergency operations plan against marine pollution by oil and other harmful substances" of the Coast Guard at La Maddalena. This plan is activated on the basis of art.11 of the Italian Law 979/82 of the "Regulations for the protection of the sea" in case of pollution or imminent threat of pollution of the sea caused by dumping, accidental event of oil or other harmful substances.

Furthermore, the realisation of "scenarios and risk maps" has quickly identified the most appropriate intervention strategies to be taken during an environmental emergency, given the high variability of possible events. Rapid action is essential to avoid a risk of pollution becoming real or developing into a serious threat to the coastline. The main objective is therefore the prevention and/or limitation of damages, aimed at conservation of marine resources in coastal waters, especially the most vulnerable areas of high environmental value typical of this area.

This paper gives a short description of the integrated system composed by observations and numerical models and by a nesting of basin, sub-regional and coastal models,

followed by its validation through observational data and its application during an oil spill event in north Sardinia. Some products are also described.

2. The integrated system

The system is composed mainly of an integrated numerical modelling component whose basic part works in the framework of the European project MyOcean (www.myocean.eu). Forecast results are finally collected by a Graphical User Interface (GUI) used by the local Coastal Guard to obtain all necessary information for correct management of the oil spill event.

The system aims to provide a prognostic tool for managing oil-spill emergencies giving an estimate of the chemical and physical evolution, both in space and in time, of a possible oil spill in the study area for up to a maximum of 72 hours, in order to know its movements well in advance. It also traces the source of pollution when the event has already occurred through a backward investigation, supporting in the identification of vessels that illegally discharge their waste water into the sea.

2.1 The numerical models

The simulation of study scenarios in the Strait of Bonifacio, the creation of maps of probability of impact/stranding of an oil spill and the numerical prediction of its evolution for transportation and distribution are realised through an integrated nested numerical system from basin to coastal scale.

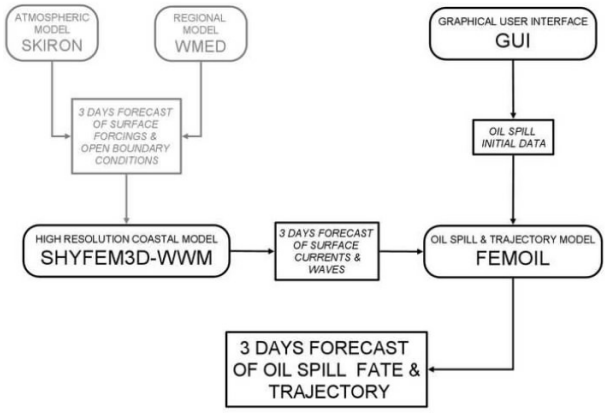

Figure 2 The flow chart describing the BOOM system composed by a hierarchy of different types of numerical models, based on structured and unstructured grids, and a Graphical User Interface.

The coastal system, named Bonifacio Oil-spill Operational Model (BOOM) is composed of a hierarchy of different types of numerical models, based on structured and unstructured grids, and a GUI to facilitate the set-up and analysis of simulations (Figure 2). The core of BOOM is composed of a set of finite element numerical models, including a three dimensional coupled hydrodynamic-wave model (the SHYFEM3D-WWM, called SHYFEM hereafter) with Lagrangian trajectory and weathering modules (named FEMOIL). The tools are used to operationally provide the hydrodynamics and the funda-

mental variables controlling the oil-spill fate and to forecast its dispersion in the Bonifacio coastal area.

SHYFEM is a finite element hydrodynamic numerical model validated and calibrated in previous studies (Ferrarin *et al*., 2004, Cucco *et al*., 2006, 2011). It is coupled one to the other in order to simulate the mutual influence between the marine circulation and the wave component, of extreme importance in the simulation of transport processes of pollutants in a coastal environment.

It can reproduce and predict the space-time variability of the water circulation and sea conditions in the coastal area with a spatial resolution less than 0.1 km and a number of vertical levels to properly resolve the surface layer, whose dynamics are the main mechanism of transport and dispersion of hydrocarbons. The coastal system provides two daily forecasts, to a maximum of 3 days each, of the barotropic current velocities and waves in the Bonifacio Strait area (including the La Maddalena Archipelago) with steps of 6 hours. The coupled model reproduces well the tide and wind induced water circulation in the study area where it is applied in order to reproduce the barotropic current velocities and waves. However in the Strait both the tidal forcing and the baroclinic contribution are negligible. The first is very weak as its associated current velocities range between 0.03 and 0.05 ms^{-1} (Gerigny *et al*., 2011) while the average and the maximum measured current speeds are 0.5 ms^{-1} and 1.46 ms^{-1}, respectively. The second is negligible because of the very low fresh water inputs in the area.

Numerical simulations are carried out over a computational domain that represents the area of work (09°6.899'–09°37.06' E and 41°6.2'–41°25.683' N) by means of a finite element staggered grid. The numerical grid consists of 40000 nodes and 70000 triangular elements and is characterised by different spatial resolutions ranging from 10 m, for the smallest channels in the La Maddalena Archipelago, to few kilometres in the offshore areas inside and outside the Bonifacio Strait. The SHYFEM considers the offshore perimeter of the computational domain as open boundary and is forced by an astronomic tide imposed at the open boundary and by a wind intensity and direction imposed as surface boundary conditions. Meteorological data are provided by atmospheric simulations carried out at the National & Kapodistrian University of Athens by means of the SKYRON-MOON (SKIRON hereafter) high spatial resolution atmospheric numerical model (10 km of resolution; Kallos *et al*., 1997).

In order to obtain as realistic as possible a description of the dynamics at coastal scale, the SHYFEM is nested, at its open boundaries, with the simulation and forecast ocean numerical circulation model at a sub-regional scale (WMED hereafter) with a resolution of about 3 km of the western Mediterranean basin, then again one-way asynchronously nested, in the framework of the European project MyOcean, at lateral boundaries with the analysis and forecast regional circulation NEMO model with 5 km of spatial resolution developed at INGV in Bologna (Pinardi *et al*., 2003). This downscaling technique adequately solves the smallest dynamic scales limited to an area of interest, without necessarily having to also solve the regional dynamics, through the use of the off-line numerical coupling technique (known as one-way nesting).

This approach is necessary to obtain a high quality product, as the spatial and temporal variability of the marine circulation in the Strait of Bonifacio is strongly influenced by

both the atmospheric forcing at the air−sea interface and the evolution of the offshore current flows.

The WMED gives a 5-day forecast of the mean fields of temperature, salinity, speed and other physical parameters, starting from 00:00 UTC. The simulation of the WMED is based on the 3D ocean circulation model called Princeton Ocean Model (POM, developed by Blumberg and Mellor, 1987). At the surface boundary its forecast is forced through momentum fluxes, heat and "water" calculated by the hourly fields of the atmospheric parameters (wind speed, wind direction, humidity, cloud coverage, solar radiation, etc.) simulated by the ECMWF forecast numerical model. The calculation of fluxes at the air-sea interface is asynchronously realised through the use of an interactive algorithm based on the bulk formulae. The WMED forecasting numerical system works in Slave Mode and near-real-time, i.e. the simulation model is re-initialised daily by using the daily numerical fields produced by NEMO and that "assimilated" data are available within 3 days from the real acquisition date of the data. Due to acquisition and calculation times, the forecast comes about 6 hours later.

Similarly, a sub-regional numerical simulation system of the wave field provides a 5-day forecast of the wave height and direction in the western Mediterranean area at steps of 3 hours. Numerical simulations of wave height and direction are carried out over a domain with a finite elements grid between longitude 003°−016° E and latitude 36.5°−44.5° N. Open boundary, astronomic tide and meteorological data are the same as for the coastal wave model.

The numerical simulation of transport and diffusion of oil spills is based on a three-dimensional module of Lagrangian particles that provides the chemical and physical transformation of an oil slick. The BOOM oil spill model receives as input the bi-dimensional wind fields and the three-dimensional oceanographic fields. When they refer to forecast fields, the transport and distribution of oil spills obtained and the model output give a numerical information on the space-time evolution of the oil spill distribution and on its chemical and physical evolution processes.

2.2 System validation through observations

The numerical simulation forecasts are verified through a comparison with field data for water current (ADCP), CTD or satellite and drifters, then generating a database with information at different sea and wind conditions.

For the surface circulation, eight experiments with surface Lagrangian drifters have been carried out inside and outside the Strait during springs and autumns with variable wind regimes representative of the meteorological conditions in the Strait. This was necessary to validate the results of the SHYFEM numerical simulations and for a correct estimation of three coefficients (wind drift factor, surface current factor and wave drift factor). For these coefficients a proper calibration is necessary for each specific application, as suggested by Price *et al*. (2006), minimising the discrepancies between model results and experimental data. For each drifter trajectory (in green in Figure 3 for comparison with a drifter experiment) a set of simulations was performed, releasing, at each drifter position (in blue), a defined number of Lagrangian particles (in grey) then reproducing their path (in red) within the time interval between field observations. The number of released particles was selected in relation to the size of the grid element containing each drifter

position in order to compute the mean distance between particles and drifter position. On average, about 10000 particles were seeded for each drifter position and more than 80 groups of particles were released in the whole set of simulations reproducing the trajectories of the 8 drifters. An exhaustive description of the validation method is found in Cucco *et al*. (2011). The rifters were Technocean Argo floats equipped with GPS telemetry and ARGOS satellite for the acquisition of surface temperature and positions every 20 minutes, with the experiments ranging between 4 hours and over 2.5 days.

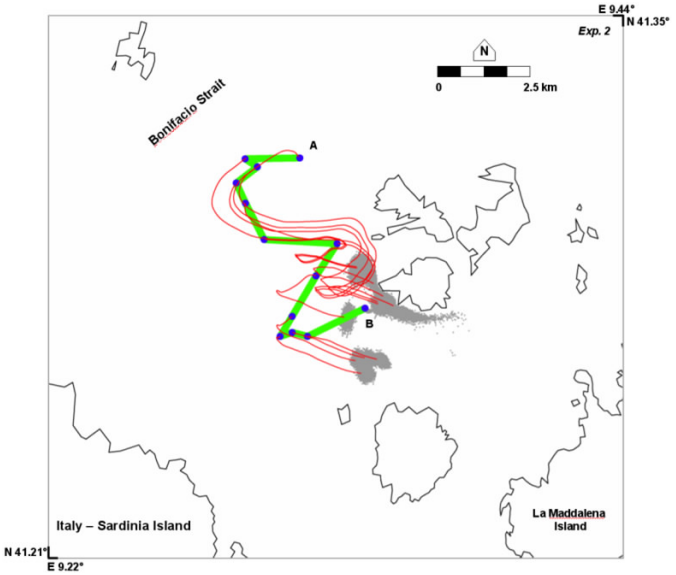

Figure 3 Comparison between drifter paths during an experiment at sea (the green line represents the observed trajectory and the blue circles the available drifter positions) and the slick path (the red line is the mean trajectory followed by each set of released particles; the grey dots show the final position of all the particles at the end of the experiment) for the same weather conditions.

In order to acquire information on the current field below the surface, u and v vertical sections have been acquired in November 2009 in the Strait area through a Workhorse Sentinel (300 kHz) Shipboard ADCP (SADCP) mounted on the *Urania* research vessel during the cruise Sicily09 (Figure 1). The SADCP acquisition was along seven transects mainly perpendicular to the Strait axis. The vertical profiles of current speed were on 40 z-levels, between 11 and 167 m in depth in cells each 4 m wide. They provided good information on water stratification and speed at each level, but particularly between cells 1 to 15 depending by the bottom depth ranging from 100 m to about 40 m. The speed values are initially referred to a coordinate system fixed with the instrument and then transformed into a geographic coordinate system, known pitch and roll of the vessel. Data have been acquired every second and then averaged over a time interval of 5 minutes. For the acquisition of ADCP data the Data Acquisition System (VMDAS) was used, processed using the Common Oceanographic Data Access System (CODAS) developed at Hawaii University. Current speeds and water transport along the main

transects have then been calculated and used to qualitatively verify model outputs and study the local circulation (see Cucco *et al.*, 2011).

A further step is to check the level of agreement of the high resolution atmospheric forcing SKIRON of the coastal coupled models with real local winds from the remote meteorological station of Guardia Vecchia, located on La Maddalena island, through comparison for a period of about seven months (22/04– 30/11/2009). This was done by extracting data of the SKIRON closest grid point to the station of Guardia Vecchia. The analyses show a good agreement between the two datasets both for the intensity and wind directions. The comparison of the two frequency polar histograms of appearance of the winds (Figure 4) show that the model is more concentrated along a few directions while the local data show a wider range. Further, the maximum speeds at Guardia Vecchia come from westerly-southwesterly winds (angle <270°) with 24 ms^{-1} while for SKIRON they predominantly blow from the west (270°) with maximum speeds of 35 ms^{-1}. This difference in speeds may be due to the position of the local weather station that underestimates the winds from north-east and east, and is therefore not necessarily to be attributed to an overestimation of the model. Even the temporal trend of the wind speed is well simulated by the numerical model (Figure 5) and the periods of maximum and minimum speeds correspond to those measured at Guardia Vecchia. From Figure 5b, which correlates the wind speed with the direction, it can be clearly seen that there are two main directions of about 270° (west) and 100° (east south-east) with also the highest speeds. The two data sets show a good agreement, justifying the use of SKIRON as meteorological forcing in the Strait area.

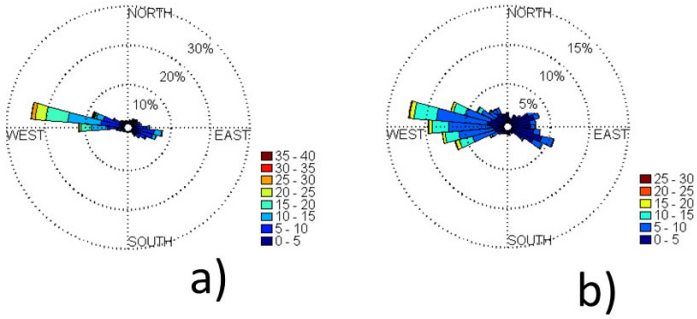

Figure 4 Frequency polar histograms of the winds in ms^{-1} for the period 22/04–30/11/2009 obtained from a) the SKIRON numerical model in the grid point at 41.20°N, 009.40°E and b) measured at the Guardia Vecchia meteorological station located at 41.22°N, 009.40°E.

Finally the system was qualitatively validated in the field during an oil spill event that occurred on 10 January 2011 when about 45.6 m^3 of heavy fuel oil was spilled in the harbour of Porto Torres (north-west Sardinia) from an oil tanker. The warning was not issued by the vessel until 24 hours after the spill occurred, so the slick moved northwards along the Sardinian coast reaching Santa Teresa di Gallura, at the entrance of the Bonifacio Strait, a week later (Figure 6). The area of interest was partially out of the grid of the coastal model, so the western boundary was extended in order to cover the whole Gulf of Asinara.

The transport of oil was correctly forecast along the whole path, as proved by laboratory chemical analyses provided with oil samples collected from several strandings coincident with those simulated.

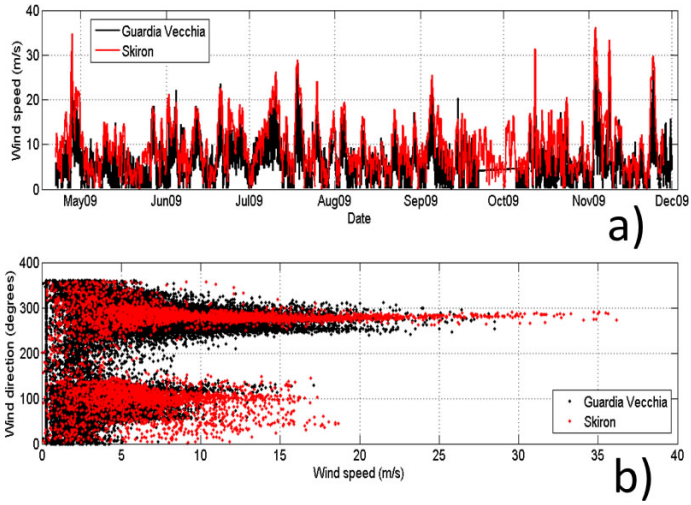

Figure 5 a) Time series of the wind speed at the Guardia Vecchia meteorological station (black) and from SKIRON (red) for the period 22/04–30/11/2009; b) wind speed and direction at Guardia Vecchia (black) and from SKIRON (red) for the same period.

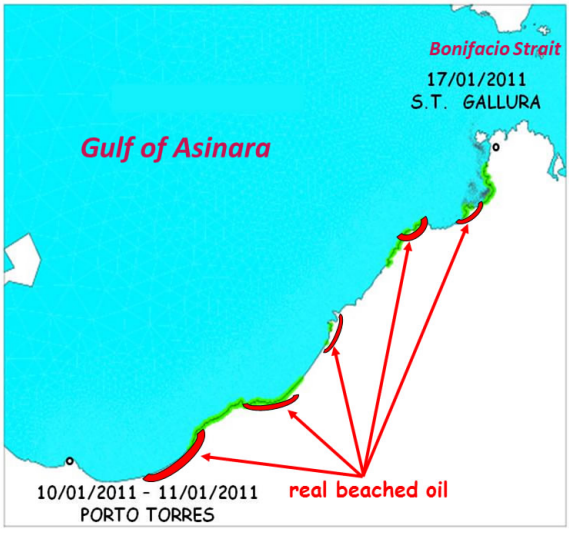

Figure 6 Simulation of the whole path of the oil slick stranded along the northern Sardinia coast (in green) compared with real beached oil (in red). The accident occurred on 10 January and the slick moved along the northern coast of Sardinia reaching Santa Teresa di Gallura on 17 January.

3. The products: Graphical User Interface

The main product obtained from the system is a user-friendly graphical interface used to create scenarios, start numerical model simulations and analyse the results (Figure 7). Usually the use of simulations generated by complex numerical models requires interaction with computer codes and high-level processes. For this reason it is limited to users able to work through blocks of machine code commands. The GUI is designed to enable a user, even with modest computer skills, to easily interact with the numerical model. In order to make the forecasting system operational it was therefore necessary to for it to be accessible to all users, even if not expert programmers, and facilitate the process of selection of scenarios, launch of the simulation and analysis of the generated results. The GUI has been designed through the "object-oriented" approach and implemented in Java. These choices have two advantages: the first is the modularity of the system (easier to upgrade or modify the interface with new functions) and independence of the operating system (Windows, Unix, Linux, Sun, etc.) on the PC where the interface is installed.

Specifically the process of creating the simulations and analysis of the results of the forecasting model is in four distinct phases.

During **phase 1** the user enters those specifications related to the scenario to be simulated (simulation name, geographical coordinates, number and type of pollutant, etc.) in the input menu of the GUI and the area (in m^2) of the observed slick of pollution. In the current BOOM system, it is assumed that the spot is circular. The radius in metres of the spill is automatically calculated and passed to the hydrodynamic model to fill the area of interest with the particles of pollutant. At this step the user can use the specifications previously used and saved in a file or generate new ones. After specifying the initial conditions, the user can launch the simulation.

In **phase 2** the GUI automatically generates a file containing the requested specifications and passes it to the hydrodynamic numerical model that runs the simulation of pollutant dispersion.

Results are produced in the form of digital files during **phase 3** of the process.

Finally, in **phase 4**, through the output section of the GUI, the user has a tool to graphically display the results generated by the simulation.

The GUI consists of two main areas on the screen: the input where the user specifies a scenario (phase 1) and the output (phase 4) where the user analyses the results of simulations generated by the numerical model (Figure 7), inside an interactive and geo-referenced map. The intermediate steps (phases 2–3), of communication with the model, are automatically performed without any input from the user, who can initialise the simulation over a period ranging between ±24 hours from the last midnight.

The GUI can be used in two ways: forecast and backward mode. The forecast mode allows the user to obtain the scenario on the characteristics and position of the slick from the point and time of discharge to the following 72 hours as described above.

The backward mode provides a useful qualitative information to the Coast Guard to find the vessel responsible for pollution at sea. This numerical technique trace back to the estimate of the start date and of the possible area of an oil spill in the sea, known type and amount of oil pollution identified and the affected area.

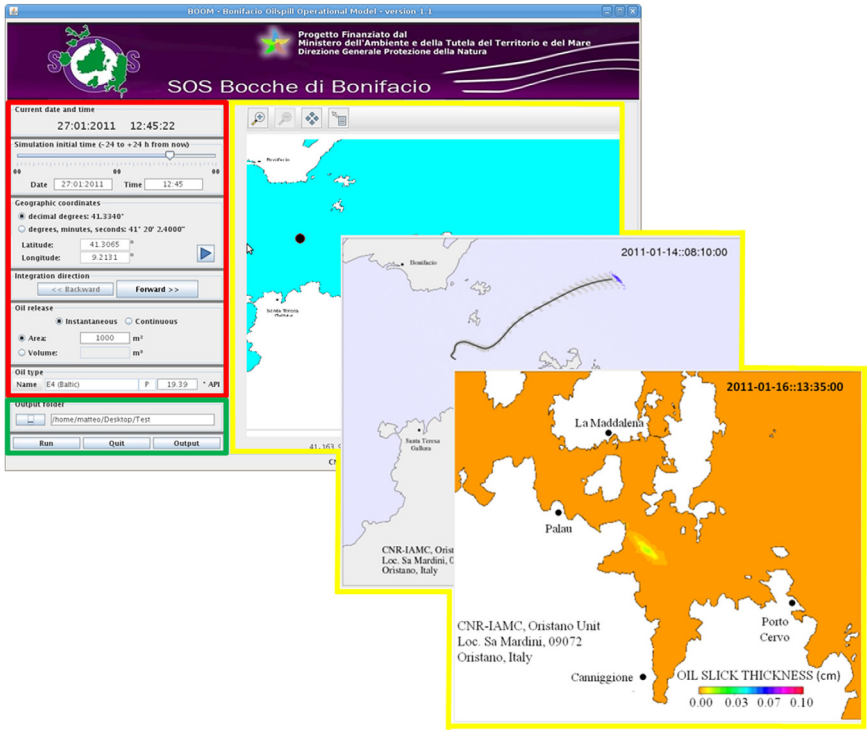

Figure 7 The area marked in red is where the user specifies the scenario inserting the date of the event, its geographic position and the extension and type of hydrocarbon; the green part is where simulations are launched with two possibilities: forward mode to forecast the pollution risk areas and backward mode to trace the source of pollution; the areas in yellow show where the results are displayed through maps of hydrocarbon dispersion and diffusion and through hydrological (temperature, salinity, current speed, etc.) and risk maps.

4. Conclusions

An operational system has been realised to provide support to the Italian Coast Guard in managing oil-spill emergencies and enabling rapid identification of operational priorities and rationalisation of resources in the coastal area of the Strait of Bonifacio.

Such an operational system consists in an integrated numerical tool, whose core is organised in a set of fully coupled high resolution numerical models based on the finite element method. The models include a 3D hydrodynamic model, a wind-wave model, a Lagrangian trajectory model and a module for reproducing the main weathering processes interesting the oil slick. The system allows, through interaction with an easy to use Graphical User Interface, an operational forecast of the fate of oil spills in the whole area of the Bonifacio Strait and La Maddalena Archipelago.

The innovative approach consists of the use of operational finite element numerical models with a spatial resolution of up to 10 metres, fully nested with an open ocean operational model based on the finite differences method, for reproducing the transport processes occurring in coastal areas characterised by a complicated geometry. The

system has been used during the oil spill emergency that occurred in mid-January 2011 in northwest Sardinia when about 50 m^3 of oil spilled from an oil tanker in the harbour of Porto Torres.

Currently the system produces, daily and operationally, a 3-day forecast of wind and wave fields, surface water circulation, temperature and salinity for the area of interest. Furthermore, it had been used to investigate the consequences of oil-spills events, to produce risk maps identifying the most exposed areas to the risk of oil impact in relation to both the season and the type and quantity of spilled oil and as a tool for tracking back the surface trajectories of oil slicks through the backward investigation technique.

Simulation results of oil spill scenarios will provide the local Coast Guard with information on the fate oil spills, those most probable in the area. In particular, the hourly maps of oil slick position and those showing which areas would be most probably impacted, as a function of different meteorological conditions, provide a useful tool to improve the management of oil spill emergencies at sea. For this reasons, the local Coast Guard in La Maddalena has used the simulations in its “Local anti-pollution plan for 2009" sent to the Italian Ministry for Environment. These simulations will be used to predict the trajectory of the oil in advance, assisting decision makers in planning the best remedial action to minimise oil pollution, while reducing time response and costs.

Further information is also provided by the risk analysis and the coastal risk index tools, which allow the local Coast Guard to identify the areas most exposed to the risk of oil impact during the year. These are also useful for the identification of the areas most suitable for concentration of instruments and resources.

Finally, even if the backward investigation with VTS data cannot exactly pinpoint the initial position of the oil spill, it still provides information on the most probable path followed by the oil slick since its detection. This assists in identification of polluters.

All the tools described define the system as a useful instrument for any local Coast Guard in the management of oil spill events in a coastal area like the Bonifacio Strait and La Maddalena Archipelago, characterised by a wonderful marine and terrestrial environment daily threatened by the passage of tens of vessels.

Acknowledgements

Special thanks go to the local staff at Capitaneria di Porto – Coast Guard in La Maddalena for their support and supply of meteorological data. This work is part of the European project MyOcean funded by EU – VII Framework Programme (contract FP7-SPACE-2007-1) and of the project SOS-BONIFACIO (contract DEC/DPN 2291 of 19/12/2008) funded by the Directorate General for Nature Protection of the Italian Ministry for Environment, Land and Sea. Finally we must also thank our wallets without which we would not be able to carry out this research.

References

Astraldi, M., A. Bruschi, G. Buffoni, G.M.R. Manzella and C. Stocchino (1980). Circolazione delle correnti nell'Arcipelago di La Maddalena. CNEN-RT/FI, 80, 8, 1–20.

Astraldi, M., A. Bruschi, G. Buffoni, A. Esposito, G. Gasparini, G.M.R. Manzella, R. Meloni and C. Stocchino (1983). Circolazione nei canali dell'Arcipelago della Maddalena. Atti V Convegno AIOL, Chiavari

Blumberg, A.-F., and G. Mellor (1987). A description of a three-dimensional coastal ocean circulation model. In: Heaps NS (ed), Three-dimensional Coastal Ocean Models, Coastal Estuarine Science, AGU, 1–16.

Cucco, A., and G. Umgiesser (2006). Modeling the Venice Lagoon residence time. Ecological Modelling. 193, 34–51.

Cucco A., M. Sinerchia, A. Ribotti, A. Olita, L. Fazioli, B. Sorgente, A. Perilli, M. Borghini, K. Schroeder and R. Sorgente (2011). A high resolution real time forecasting system for predicting the fate of oil spills in the Strait of Bonifacio (western Mediterranean), in press on Marine Pollution Bulletin.

Ferrarin, C., and G. Umgiesser (2005). Hydrodynamic modeling of a coastal lagoon: the Cabras lagoon in Sardinia, Italy, Ecological Modelling, 188, 2–4, 340–357.

Gerigny, O., B. Di Martino, and J.C. Romano (2011). The current dynamics inside the Strait of Bonifacio: Impact of the wind effect in a little coastal strait. Continental Shelf Research 31, 1–8.

Kallos, G., S. Nickovic, A. Papadopoulos, D. Jovic, O. Kakaliagou, N. Misirlis, L. Boukas, N. Mimikou, E. Anadranistakis, and M. Manousakis (1997). The regional weather forecasting system Skiron: An overview, in: Proceedings of the Symposium on Regional Weather Prediction on Parallel Computer Environments, 109–122, Athens, Greece.

Pinardi N., I. Allen, E. Demirov, P. De Mey, G. Korres, A. Lascaratos, P.-Y. Le Traon, C. Maillard, G.M.R. Manzella, and C. Tziavos (2003). The Mediterranean ocean forecasting system: first phase of implementation, Ann. Geophys., Special Issue: Mediterranean Forecasting System Pilot Project (MFSPP), 21, 3–20.

Price, J.M., M. Reed, M.K. Howard, W.R. Johnson, Z. Ji, C.F. Marshall, N.L. Guinasso Jr., and G.B. Rainey (2006). Preliminary assessment of an oil-spill trajectory model using a satellite tracked, oil-spill simulating drifters. Environmental Modelling & Software 21, 258–270.

UNCLOS, 1982, United Nations Convention on the Law of the Sea, 10 December 1982, www.un.org/depts/los/convention_agreements/convention_overview_convention.htm, 202 pp.

Monitoring and modelling marine biogeochemical processes

Ocean colour discrimination of harmful algal blooms in European waters: classification of MODIS and MERIS data

A.A. Kurekin*[1], P.I. Miller[1], and H. van der Woerd[2]

[1]*Plymouth Marine Laboratory, UK*
[2]*Water Insight, Netherlands*

Abstract

This paper presents a novel methodology for identifying harmful algal blooms (HABs) from satellite optical images. It uses ocean colour and inherent optical properties (IOPs) derived from the Moderate Resolution Imaging Spectrometer (MODIS) and Medium Resolution Imaging Spectrometer (MERIS) data to discriminate between harmful, harmless and no bloom cases. Discrimination of HABs is carried out using a Linear Discriminant Analysis classifier trained on satellite observations of *Karenia mikimotoi* and *Phaeocystis* phytoplankton species, which form dense monospecific HABs. The performance of HAB discrimination is evaluated by using further satellite datasets.

Keywords: remote sensing, ocean colour, harmful algal blooms, *Karenia mikimotoi*, *Phaeocystis*, MERIS, MODIS

1. Introduction

Monitoring water quality in European oceanic and coastal waters is a task of high importance for monitoring agencies and a focus of public interest in recent years. It is also a subject of several European Directives and conventions (Directive 2000/60/EC; Directive 2008/56/EC). Development of an efficient monitoring service is also demanded for the needs of fisheries, aquaculture and tourism that are directly affected by the water quality. Algal blooms can be harmful to humans, and their harmfulness depends on the concentration and dominant species of organisms present, the affected area and time interval of bloom event. In high concentrations harmful algae may cause respiratory irritation for humans, shellfish neurotoxic poisoning, fish mortality and can lead to significant economic losses by damaging fish farms and degrading coastal tourism sites (Stumpf *et al*., 2003; Miller *et al*., 2006).

The efficiency of water quality monitoring methods is usually measured in terms of observation regularity, spatial coverage, low false alarm rate, and ability to identify the composition of algal bloom. In-situ methods for water quality analysis cannot satisfy these requirements as they are limited in spatial and temporal coverage. The requirements of users to obtain HAB information in near real time and to monitor large areas can be met by using optical remote sensing methods (Miller *et al*., 2006), and the techniques that have been developed within the EC AquaMar project.

It has been demonstrated in Park *et al*. (2010) that the analysis of daily chlorophyll-a concentration can be applied to detection of high biomass algal blooms from satellite

* Corresponding author, email: anku@pml.ac.uk

optical images. However, the approach based on using chlorophyll-a concentration (Park *et al*., 2007) is not suitable for discrimination between harmful and harmless algal bloom events.

This paper approaches the challenging task of identifying harmful algal species composition by applying a machine learning approach (Duda *et al*., 2001) that uses satellite data for training a classification algorithm. This is applicable to species that form dense monospecific blooms and hence may cause a characteristic colouring of the water due to their concentration, cell size, pigmentation or scattering properties. The methodology for HAB discrimination is based on using four classes: "harmful bloom", "harmless bloom", "no bloom" and an "unknown" class that includes unclassified data. It has been tested in European waters and can be extended to new areas. The study is focused on *Karenia mikimotoi* and *Phaeocystis globosa* HAB species, but the methodology can be adapted to other species which form dense monospecific blooms.

2. Methodology for HAB discrimination

The discrimination of HAB is based on ocean colour data acquired by the MODIS and MERIS sensors. The satellite images are processed by SeaDAS version 6.2 and Plymouth Marine Laboratory (PML) proprietary software to generate normalised water leaving radiance data $nLw(\lambda)$ for MODIS and MERIS spectral bands. The water leaving radiances $nLw(\lambda)$ are used as features for HAB discrimination. The inherent optical properties (IOPs) of water, such as the total absorption $a(\lambda)$ and backscattering $b_b(\lambda)$ coefficients are also included in the feature set to help improve discrimination efficiency. The absorption and backscattering are retrieved from the ocean colour data by applying an IOP model based on slope and spectral signatures and is applicable to turbid European waters (Smyth *et al*., 2006).

The additional features derived as the spectral slopes between two neighbouring wavelengths are used to improve robustness to sensor calibration and atmospheric correction errors as well as to overcome limitations of linear classifiers (Duda *et al*., 2001). These features are calculated as the spectral ratios of

water leaving radiances $R_L(i,j)=nLw(\lambda_i)/nLw(\lambda_j)$,

absorption $R_a(i,j)=a(\lambda_i)/a(\lambda_j)$ and

backscattering $R_b(i,j)=b_b(\lambda_i)/b_b(\lambda_j)$.

The main stages of generating feature sets from satellite data are schematically shown in Figure 1. The features are calculated on a pixel by pixel basis forming a three dimensional array with the first two dimensions corresponding to spatial coordinates in a Mercator projection and the third dimension corresponding to the feature index.

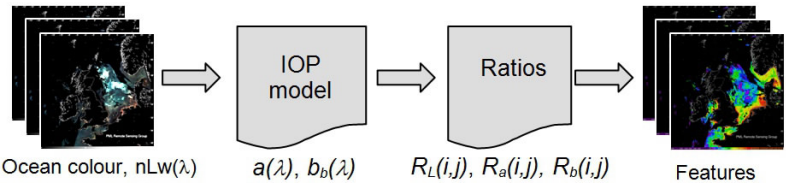

Figure 1 A block-diagram of generating a feature set including normalised water leaving radiances, absorption, backscattering IOPs and spectral ratios between neighbouring wavelengths.

Classification of the feature vector composed of water leaving radiances, absorption, backscattering and spectral ratios is carried out by a Linear Discriminant Analysis (LDA) classifier (Duda *et al*., 2001; Bandos *et al*., 2009). The LDA classifier is based on the assumption that the distribution of features is Gaussian with the same covariance matrix for all classes. Before classification the features in the high dimensional feature space are projected into a space of much lower dimension to maximise the between-class distance and minimise within-class distance simultaneously. The classifier provides good performance for linearly separable classes and easily handles training data with unequal number of samples in each class by estimating the prior probability of class samples. In addition it has low computational complexity and is relatively simple for implementation.

The performance of an LDA classifier strongly depends on the selection of features and the dimensionality of feature space. Due to the "curse of dimensionality" its efficiency can deteriorate if too many features are used for classification (Duda *et al*., 2001). Hence, a reduced number of most important features have to be selected to improve the classifier performance. This is achieved by applying a Stepwise Discriminant Analysis (SDA) algorithm implemented in the statistical package 'klaR' (Weihs *et al*., 2005) to the training data at the classifier training stage. The SDA algorithm selects the most important features from the original set automatically. It uses the probability of correct classification criterion to select the best combination of features iteratively by adding more significant or removing less significant features one by one.

The unknown parameters of LDA classifier are estimated by training, using the preliminary classified fragments of satellite images. The classification of training data is based on in-situ sampling and visual interpretation of ocean colour scenes and chlorophyll-a products. The scenes are labelled manually as "harmful bloom", "harmless bloom" and "no bloom" regions. The main stages of training procedure is summarised in Figure 2. It includes selection and identification of training image scenes, sampling training data, feature selection and training LDA classifier.

Classification of new scenes is carried out on a pixel by pixel basis. For each pixel in the satellite image the features selected at the training stage are calculated and processed by the LDA classifier. The classifier estimates probabilities of "harmful bloom", "harmless bloom" and "no bloom" classes for each tested sample. Assuming that the distribution of features is Gaussian, the probability for each class is calculated as

$$p\left(\frac{c_i}{\mathbf{x}}\right) = \frac{\exp(-0.5\|\mathbf{x}-\boldsymbol{\mu}_i\|^2)P(c_i)}{\left(\sum_{j\,=\,1..3}\exp(-0.5\|\mathbf{x}-\boldsymbol{\mu}_j\|^2)\right)P(c_j)}, \; i=1..3 \tag{1}$$

where $\mathbf{x}$ is a vector to be classified and i is the mean value of the i-th class in the discriminant space.

For input data that cannot be considered as any of the "no bloom", "harmless bloom" or "harmful bloom" categories the classifier will produce false alarms. To reduce the classifier false alarm rate for these data we introduced an additional "unknown" class. The probability of "unknown" class samples is evaluated at the final stage of classifi-

cation. This is achieved by calculating the distance $d_{\min}$ between the input sample and the mean of the nearest class in the discriminant space, and finding the probability that for the samples of this class the distance is less than $d_{\min}$. This probability becomes higher when the distances from mean value π_i is increased, so it can been considered as a measure of dissimilarity with "no bloom", "harmless bloom" or "harmful bloom" classes. Assuming that the distribution of features in the discriminant space is Gaussian, the probability of "unknown" class is calculated as

$$p\left(\frac{c_u}{x}\right) = \chi^2_{cdf}(d^2_{\min}, n_d), \tag{2}$$

where $\chi^2_{cdf}(...)$ is a cumulative density function of chi-squared distribution and n_d is the dimension of discriminant space equal to 2 for three classes.

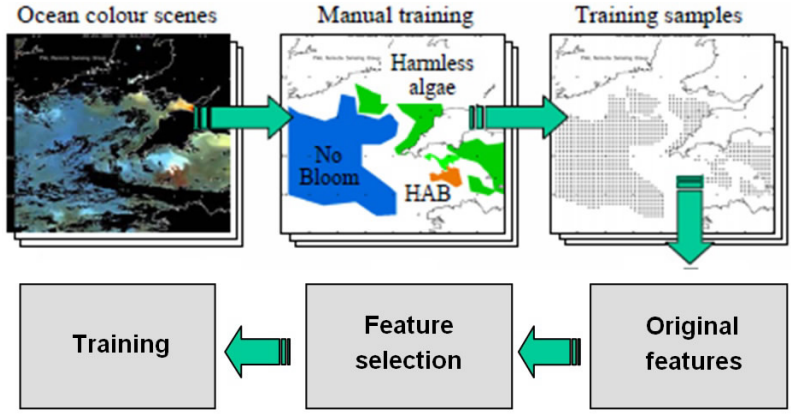

Figure 2 The training procedure for the HAB discrimination technique based on LDA classifier

The probability of detection maps generated by the developed classification technique for "harmful bloom", "harmless bloom", "no bloom" and "unknown" classes are presented as a palette-based 8-bit images in the Portable Network Graphics (PNG) format with the probabilities 0..1 mapped to 0..255 pixel values. To simplify visual analysis of classification results a composite classification image is generated that represents probabilities of "harmful bloom", "harmless bloom" and "no bloom" classes using a combination of red, green and blue primary colour components, with the "unknown" class shown in grey.

3. Results and discussion

The developed methodology has been applied to discriminate *Karenia mikimotoi* algal blooms in the UK waters in summer 2010 and *Phaeocystis globosa* blooms in the Dutch coastal waters in spring 2008 using ocean colour data acquired by MODIS Aqua and MERIS sensors.

3.1 Training results

Training for the LDA classifier has been carried out using several images of *Karenia mikimotoi* bloom events observed in years 2002–2004 in the UK Southwest waters. The images have been labelled as "harmful bloom", "harmless bloom" and "no bloom", and sub-sampled by a factor of 8 to avoid redundancy of training data and reduce processing time. The training data set includes 1993, 1495 and 433 samples for each class respectively. The same labelled areas have been used to produce MODIS and MERIS training data sets.

The training data set has been applied to train LDA classifier, and to evaluate its performance. The 5-fold cross validation method has been used to estimate classification probabilities to avoid biased results (Duda *et al*., 2001). The confusion matrix for the MODIS training data set is given in Table 1. The diagonal elements in the table show the probability of correct classification in percent for all three classes. The highest probability achieved for the "no bloom" class and the lowest for "harmless bloom". It follows from Table 1 that the *Karenia* HAB is most often misclassified as a "harmless bloom" and there is a 17.49% probability that the "harmless bloom" class is misclassified as a "no bloom". The total probability of correct classification for MODIS data is Pt = 87.6%.

Table 1 The confusion matrix for the *Karenia mikimotoi* classifier and MODIS training data

True class:	**Classified as:**		
	no bloom	harmless bloom	*Karenia* HAB
no bloom	93.24	6.76	0.0
harmless bloom	17.49	80.98	1.53
Karenia HAB	0.22	15.05	84.73

Similar results have been obtained for the MERIS training data set with the probability of HAB correct classification higher by 4%.

The training data for *Phaeocystis globosa* blooms are obtained by analysis of in-situ measurements along the Dutch coastal waters provided by Water Insight Company, the Netherlands, and applying the Chl-*a* and HAB cell concentration measurements to identify and label HAB regions in satellite images.

The confusion matrix for the *Phaeocystis globosa* classifier indicates better classification accuracy in comparison with *Karenia mikimotoi*. For the MODIS training data set the probability of HAB correct classification has been improved by about 14% while the total probability of correct classification is reduced to Pt = 87.3%. For the MERIS training data Pt = 88.81%.

3.2 HAB discrimination results

The independent tests have been carried out to evaluate the efficiency of *Karenia mikimotoi* and *Phaeocystis globosa* discrimination in MODIS and MERIS scenes. The probability map of HAB generated by LDA classifier is given in Figure 3a. It demonstrates the *Karenia mikimotoi* bloom event in the English Channel on 26 August 2010 that has been confirmed by in-situ measurements. The low probability of HAB is shown in the image in blue and high probability in red indicating the presence of *Karenia*

mikimotoi in high concentration. The intermediate probability levels in the image indicate the early and subtle signs of HAB development.

To verify the efficiency of using linear classifier for HAB discrimination, an alternative nonlinear classification technique based on Support Vector Machine (SVM) (Vapnick, 1998) has been tested. The HAB probability map generated by the SVM classifier is presented in Figure 3b. It shows that a more complicated nonlinear classifier, such as SVM does not provide significant advantages in HAB discrimination.

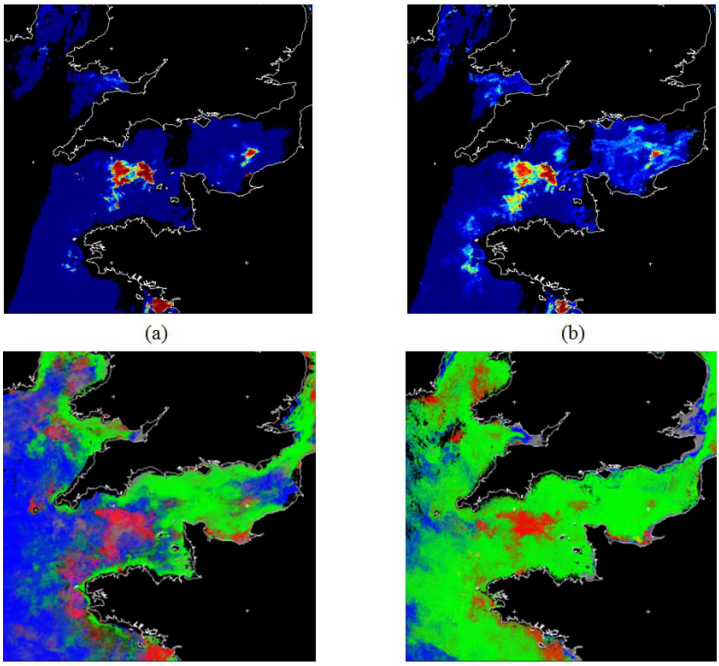

Figure 3 *Karenia mikimotoi* discrimination results: HAB probability map generated by (a) LDA and (b) SVM classifiers; weekly composite classification maps for (c) MODIS and (d) MERIS sensors.

Figure 3c and Figure 3d present weekly composite of classification maps generated using MODIS and MERIS data. Visual analysis of these images indicates that the level of HAB false alarms is lower for the MERIS sensor.

The weekly experimental results of *Phaeocystis globosa* discrimination in the Dutch coastal waters are given in Figure 4. Joint analysis of the 'false colour' image in Figure 4a and chlorophyll-a concentration image in Figure 4b reveals patches of intense *Phaeocystis* bloom in combination with high sediment concentration in coastal waters. The probability of detection map generated by LDA classifier trained on *Phaeocystis* species using MERIS data is shown in Figure 4c. The map demonstrates good agreement with the 'false colour' and chlorophyll-a images and low false alarm rate of HAB discrimination. The composite classification map in Figure 4d shows grey areas mainly along the shore classified as "unknown" that can be explained by the presence of sediment.

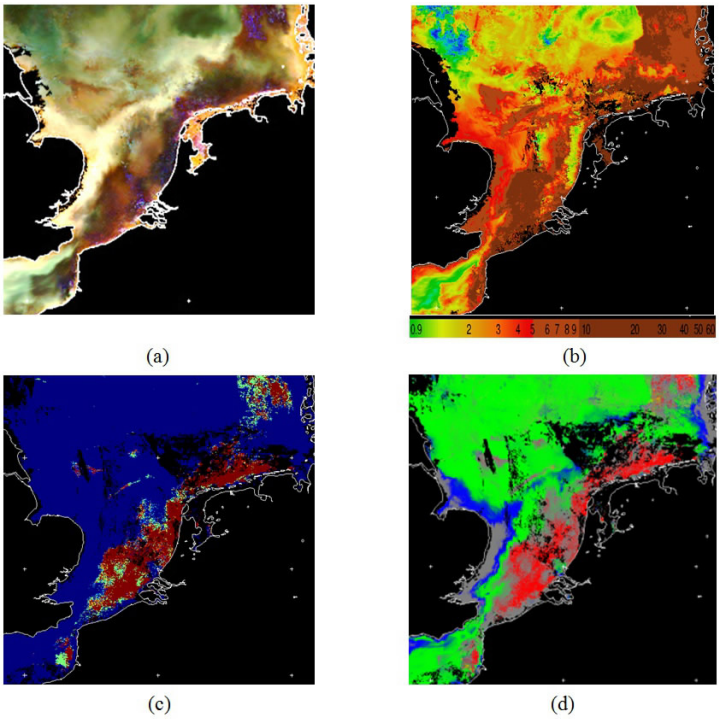

Figure 4 *Phaeocystis globosa* discrimination: (a) enhanced 'false colour' image of HAB scene; (b) chlorophyll-a concentration; weekly composites of (c) HAB probability map and (d) classification map.

4. Conclusions

The paper presents a novel methodology for automatic discrimination of *Phaeocystis globosa* and *Karenia mikimotoi* HAB in European waters using ocean colour and IOP data, producing spatial probability maps for "harmful bloom", "harmless bloom", "no bloom" and "unknown" classes. It has been tested on MODIS and MERIS sensor data and demonstrated the advantages of using MERIS data for HAB discrimination. A comparison with an alternative nonlinear SVM discrimination technique has been carried out and confirmed the efficiency of using linear classification approach for HAB discrimination. The developed methodology uses a machine learning technique that extends its application to wider range of HAB species and different sensors.

Acknowledgements

The authors are thankful to Water Insight Company for providing HAB in-situ monitoring data for *Phaeocystis globosa* species. We would like to gratefully acknowledge funding of this work through the EC Framework 7 AquaMar project.

References

Directive 2000/60/EC of the European Parliament and of the Council (2000), eur-lex.europa.eu/LexUriServLexUriServ.do?uri=OJ:L:2000:327:0001:0072:EN:PDF

Directive 2008/56/EC of the European Parliament and of the Council (2008), eur-lex.europa.eu/LexUriServ/LexUriServ.do?uri=OJ:L:2008:164:0019:0040:EN:PDF

Stumpf, R.P., M.E. Culver, P.A. Tester, M. Tomlinson, *et al*. (2003). Monitoring *Karenia* brevis blooms in the Gulf of Mexico using satellite ocean color imagery and other data, Harmful Algae, vol.2, 147−160.

Miller, P.I., J.D. Shutler, G.F. Moore, and S.B. Groom (2006). SeaWiFS discrimination of harmful algal bloom evolution, International Journal of Remote Sensing, vol. 27, No. 11, 2287−2301.

Park, Y., K. Ruddick, and G. Lacroix (2010). Detection of algal blooms in European waters based on satellite chlorophyll data from MERIS and MODIS, International Journal of Remote Sensing, vol. 31, Issue 24, 6567−6583.

Park, Y., and K. Ruddick (2007). Detecting algae blooms in European waters, Proceedings of Envisat Symposium, Montreux, Switzerland ESA SP-636.

Duda, R.O., P.E. Hart, and D.G. Stork (2001). Pattern classification, 2nd edition, Wiley, New York, ISBN 0-471-05669-3.

Smyth, T.J., G.F. Moore, T. Hirata, and J. Aiken (2006). Semianalytical model for the derivation of ocean color inherent optical properties: description, implementation, and performance assessment, Applied Optics, vol. 45, No.31, 8116−8131.

Bandos, T.V., L. Bruzzone, and G. Camps-Valls (2009). Classification of hyperspectral images with regularised linear discriminant analysis, IEEE Transactions on Geoscience and Remote Sensing, 47(3), 862−873.

Weihs, C., U. Ligges, K. Luebke, and N. Raabe (2005). klaR Analyzing German Business Cycles. In Baier, D., Decker, R. and Schmidt-Thieme, L. (eds.). Data Analysis and Decision Support, 335−343, Springer-Verlag, Berlin.

Vapnick, V.N. (1998). Statistical learning theory. John Wiley and Sons Inc.

Operational nowcasting of Harmful Algal Blooms in the Baltic Sea using satellite data from MERIS and MODIS – improving bloom detection

Martin Hansson*, Per Pemberton, and Bertil Håkansson

Swedish Meteorological and Hydrological Institute, Oceanographic Unit

Abstract

In the Baltic Sea, summer blooms of nitrogen-fixing cyanobacteria, dominated by *Aphanizomenon* sp. and *Nodularia* sp., are a natural and regular phenomenon. However, in recent years, intense and widespread blooming has caused concern due to their nuisance and toxic content, as well as their effect on nitrogen inputs and the eutrophic state of the Baltic Sea. The Swedish Meteorological and Hydrological Institute are operating a daily satellite-based monitoring service of cyanobacterial blooms in the Baltic Sea during the summer period. The main data source has been the AVHRR (NOAA) sensor, which is reliable but has a low spatial and radiometric resolution. To improve the service, data from MERIS (ENVISAT) and MODIS (AQUA EOS), which has a higher spatial and radiometric resolution, has been included and combined. The disadvantage of using MERIS or MODIS separately is the longer revisit intervals and smaller swath width compared to AVHRR, which makes it difficult to get daily coverage. By combining MODIS and MERIS this problem can be less severe from an operational point of view. A method to detect cyanobacterial blooms in MODIS data using normalised water leaving radiance in the 551 and 670 nm bands, has been made operational and adapted to similar MERIS bands (555 and 665 nm). Differences between MERIS and MODIS data are generally small and dissimilarities are often due to discrepancy in flag definitions. Future work will focus on data availability since both sensors are operating beyond their technical lifetime.

Keywords: operational satellite monitoring, cyanobacterial blooms, MODIS, MERIS.

1. Introduction

Nowcasting of harmful algal blooms (HABs) is important both for the public and for environmental management. In the Baltic Sea summer blooms of nitrogen-fixing cyanobacteria, dominated by *Aphanizomenon* sp. and *Nodularia* sp., are a natural and regular phenomenon, see Figure 1. However, in recent years, intense and widespread blooming has caused concern due to their nuisance and toxicity, as well as their effect on nitrogen inputs (Kahru *et al*., 1994; Finni *et al*., 2001; Kononen, 2001).

The Swedish Meteorological and Hydrological Institute has since 2002 been operating a daily satellite monitoring service of potentially harmful algal blooms in the Baltic Sea. (Hansson and Håkansson, 2007) The system has been developed to support both the public and the Swedish Marine Information Offices, providing near real time information about the present algal situation. The main data source has been the NOAA satel-

* Corresponding author, email: martin.hansson@smhi.se

lites and the AVHRR sensors, which gives daily full coverage of the Baltic region. The AVHRR sensor has been a reliable but coarse instrument, due to low spatial and radiometric resolution (Hansson, 2006; Håkansson, 2000).

Figure 1 Cyanobacterial blooms in the Baltic Sea are dominated by *Aphanizomenon* sp. (non-toxic) and *Nodularia* sp. (toxic!) forming patchy surface accumulation. Photo: Swedish coast guard.

Other satellite sensors, such as MERIS or MODIS onboard ENVISAT and AQUA EOS PM-1 respectively are more suitable for nowcasting purposes of blooms, with both higher spatial resolution and narrower bands in the visible part of the spectrum. The disadvantage of using MERIS or MODIS separately is the revisit interval, 1–2 days for AQUA-MODIS and 3 days for MERIS, and smaller swath width (1150 km and 2330 km respectively) compared to AVHRR (~2900 km). This means that it is not possible to get continuous daily full coverage of the Baltic region. The high presence of clouds at these latitudes makes each overpass important to fill gaps where data is missing.

2. Data and Method

Methods to detect surface accumulations of cyanobacteria in the Baltic Sea have been developed for several satellite sensors: CZCS, AVHRR, SeaWIFS (Kahru, 1997), and MODIS data. The detection scheme to classify blooms in MODIS data (Kahru *et al*., 2007) relies on a combination of threshold value masking of normalised water leaving radiance (nLw) in two bands; 551 and 670 nm. For the 551 nm band, where the radiation penetrates a few metres down in the water column, (Kahru *et al*., 2007) estimated a threshold of nLw(551) > 0.8 $mWcm^{-2}\pi m^{-1}sr^{-1}$ by visual inspection of RGB composite images. The water signal in this channel is sometimes affected by shallow depths which gives a false high signal from the bottom. It is also sensitive to turbid waters, which has a strong signal, such as river plumes or sediment-rich coastlines. Because of water's strong absorption properties at 670 nm the radiation does not penetrate as deeply as band 551 nm. Hence, this gives a signal from the water surface that can be used to detect surface accumulations and also to filter out bottom reflection when combined with the 551 nm band. For the 670 nm the authors (Kahru *et al*., 2007) used the turbid water flag from

MODIS which corresponds to a threshold of nLw(670) > 0.18498 $mWcm^{-2}\pi m^{-1}sr^{-1}$. This method can therefore be used to distinguish between blooms at the surface and blooms present just below the surface; subsurface blooms.

This classification method for detection of blooms in MODIS imagery has been adopted for the similar bands 560 nm and 665 nm of the MERIS sensor full resolution level 2 data. By combining nLw data from MODIS and MERIS the problem with daily data coverage of the Baltic region can be minimised.

The MERIS data used were the FRS L2 products downloaded from EOLi (Earth Observation Link), which is the European Space Agency's client for earth observation catalogue and ordering services. MODIS L2 data was collected from NASA's Ocean Color Web. MERIS surface reflectance (Rho_wn) data was converted to normalised water leaving radiance (nLw) by using equation (1).

$$nLw = (Rho\_wn * F0 * \cos(SzA))/\pi, \quad (1)$$

where F0 is the downwelling solar irradiance and SzA is the solar zenith angle (pers. comm. Ludovic Bourg, EOHelpdesk).

The method used to detect blooms in MODIS and MERIS imagery was tested for well-known blooms in the Baltic Sea, Figure 2. The same analysis was carried out for the other dates and showed consistent results.

Figure 2 Cyanobacterial bloom in the Baltic Sea. RGB-composite of MERIS FRS L1 bands XYZ from 31 July 2008, 09:32 UTC.

3. Results

The normalised water leaving radiance (with clouds and land masked out) for the MODIS bands 551 nm and 670 nm are compared with the MERIS bands 560 nm and 665 nm in Figure 3 and Figure 4. Both sensors show similar structures with high values in the central Baltic Proper, southeast of the islands Öland and Gotland and the southwest of the Bothnian Sea for the 560/551 nm band. The 665/670 nm bands show high values in similar areas but not as distinct and widespread as the 560/551 nm bands. Both sensors have difficulties detecting the bloom close to eastern Swedish coast, northwest of Gotland. The heavy bloom on 31 July along the Swedish east coast was also observed and reported by media and several monitoring authorities in Sweden. In the MODIS image this area is masked out as clouds whereas the MERIS image has negative values of the water reflectance. In the MERIS image three other such areas are also evident: in the Gulf of Finland, in the Central Baltic Proper and in the Gulf of Riga. All these areas appear to be free from clouds in the L1 RGB composite, see Figure 2. Data from MODIS is also missing from the same site in the southeast Baltic Proper.

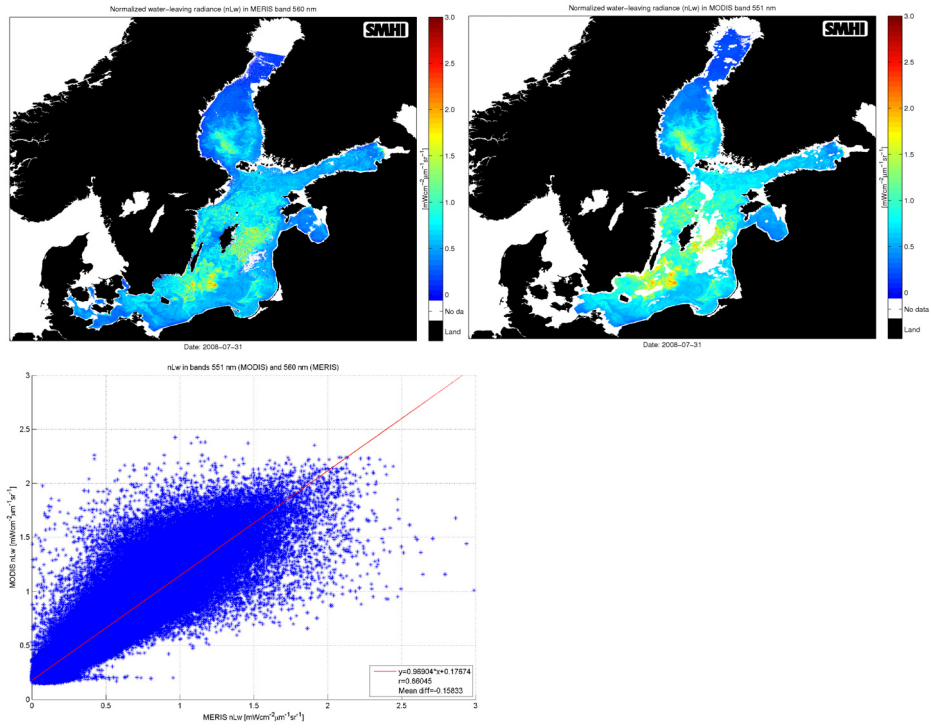

Figure 3 Top: Normalised water leaving radiance; left: nLw(560) from MERIS 09:32 UTC. Right: nLw(551) from MODIS 10:50 and 10:55 UTC. Bottom: Scatter plot of MODIS nLw (551 nm) and MERIS (560 nm).

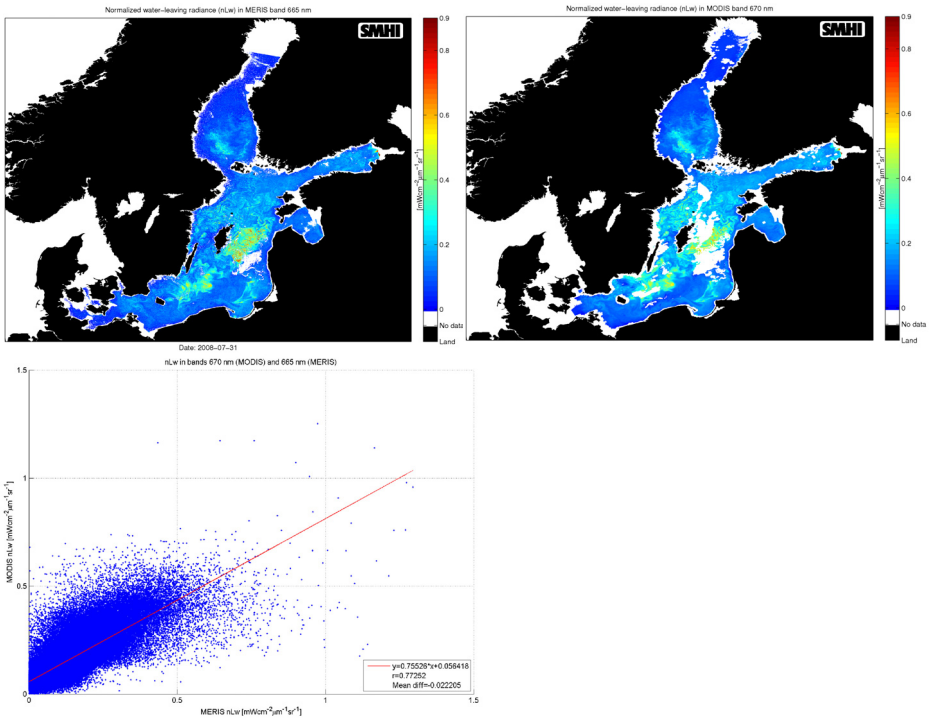

Figure 4 Top: Normalised water leaving radiance, nLw(665) from MERIS 09:32 UTC. Bottom: Normalised water leaving radiance, nLw(670) from MODIS 10:50 and10:55 UTC. Bottom: Scatter plot of MODIS nLw(670 nm) and MERIS nLw(665 nm).

Before applying the band threshold the water leaving radiances have to be masked with the appropriate flags to remove pixels with suspicious values or where the processing has failed. Kahru *et al*. (2007) uses a set of MODIS flags, which are denoted 'valid ocean'. Not all of these flags are available for MERIS although in most cases similar flags exist and were used. In Figure 5 these two flag sets are compared and it can be seen that the MODIS mask excludes a lot more than the MERIS flag set. MODIS seems to mask out quite large areas in the central part of the Baltic Proper and along the Swedish east coast. When applying the individual thresholds, see Figure 6, it can be seen that they compare quite well overall. However there are regional differences which are mainly due to differences in masking or due to erroneous values (South east Baltic Proper, the Gulf of Riga and a small part of the Gulf of Finland) from the MERIS sensor.

This is also true for the combined thresholds which in the end produce a classification that is generally quite good but has some shortcomings as discussed above. Thus, the gaps due to flag set differences and the erroneous values seem to compensate for when an overlap between MODIS and MERIS exists. The areas east and northeast of the island Gotland and along the Swedish east coast, which are masked out by MODIS, are valid in the MERIS data and the blooms in these areas have been marked – compare the RGB-image, valid ocean and the detection results in Figure 2 and Figure 5–Figure 6.

To compare the two data sets, all available images from one blooming season, 1 June – 31 August 2008, were analysed using data from both MODIS and MERIS, applying the same classification method to both datasets.

Comparison of MODIS and MERIS nLw data on a pixel to pixel basis shows that there is little difference between the two data sets, although the difference increases as the time between the over flights increase.

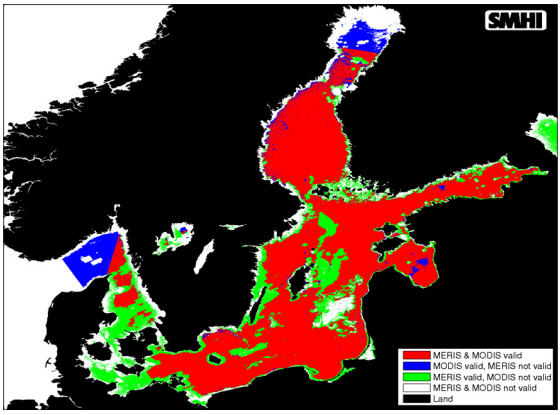

Figure 5 Comparison of valid ocean flags for MODIS used by Kahru *et al*. (2007) and similar flags found for MERIS. Note that not all flags defined for MODIS are available for MERIS. Red show valid ocean areas in both data sets, blue (MODIS) and green (MERIS) represent where each flag set alone indicate valid ocean. In white areas both flag sets are non valid.

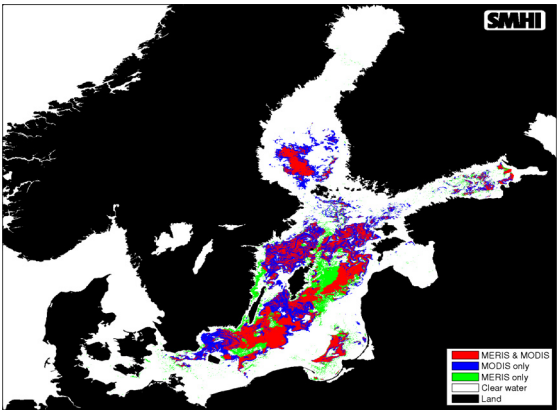

Figure 6 Comparison of detection results on 31 July 2008. Surface blooms detected in both MERIS (560/665 nm) and MODIS (551/670 nm) data are marked with red, blue (MODIS) and green (MERIS) represent where each data set alone has detected surface bloom. MERIS is from 09:32 UTC and MODIS from 10:50 and 10:55 UTC.

3.1 Implementation

The daily monitoring service of algal blooms in the Baltic Sea is operational from 1 June to 31 August. All MERIS and MODIS data that is available from the day before, covering the Baltic region, is collected via FTP boxes (Near Real-Time service at OceanColorWeb, NASA and the MERIS rolling archive at ESA) to SMHI. Data from yesterday is convenient to use, since a new bloom map can be made available directly around 09:00 local time and the public and environmental managers can then get updated information about the algal situation early in the morning. It is also practical for the operator who does not have to wait for additional satellite data which can delay the production.

Usually two satellite data sets from one overpass are needed to cover the Baltic regions and depending on what data that is available the system can handle one or two data sets from each sensor. The MERIS surface reflectance data is converted to nLw using equation (1), and both MODIS and MERIS data is mapped to a equal area projection covering the Baltic Sea. Flags from both datasets are used to eliminate clouds or other conditions in which bloom detection is either not possible or likely to produce errors. Error pixels are marked as no data.

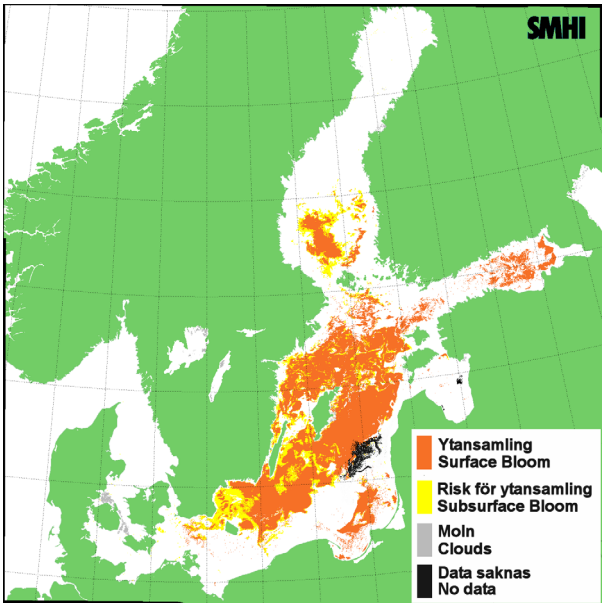

Figure 7 Bloom map for 31 July 2008. Orange show areas which are affected by surface blooms and yellow indicate subsurface blooms. Clouds are grey and areas with no data are black.

The combined bloom maps (Figure 7) present the occurrence of surface and subsurface blooms, clear water, clouds and areas with no data. When an overlap exists, bloom observations are prioritised. However, surface blooms go before subsurface and clouds and ‘no data’ is only marked if detected in both data sets in overlapping areas or detected in non-overlapping areas. The operator performs a quality control of the bloom map and writes the report, which is published on the web. A week composite, presenting a stacked

image of the bloom observations during the last seven days, is also published. If data from both MODIS and MERIS is absent due to swath outside the Baltic regions, sensor or data delivering malfunction, data from NOAA-AVHRR can still be used in the service as a backup. This certifies that a daily bloom map always can be produced during the blooming season, see Figure 8.

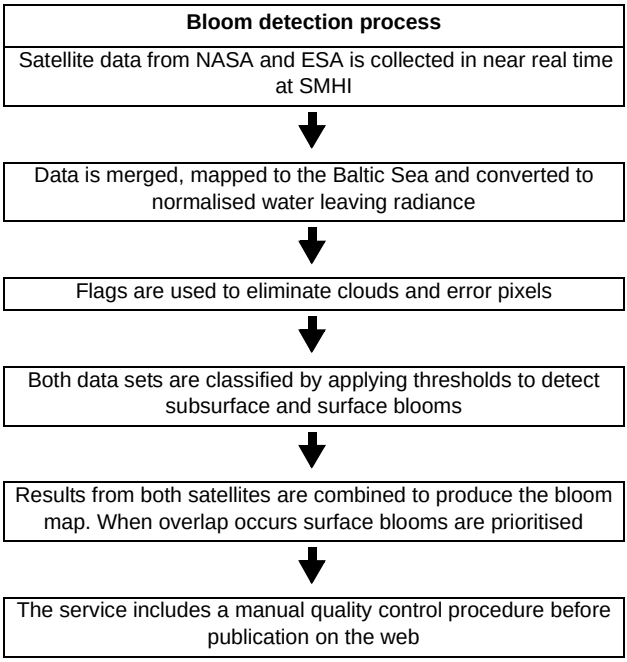

Figure 8 The bloom detection process.

4. Conclusions

MERIS and MODIS data have higher spatial and radiometric resolution compared to NOAA-AVHRR, which gives a more accurate and detailed view of the algal situation. However, due to the revisit interval and the swath width the two sensors must be combined in the service to achieve a daily coverage of the Baltic Sea during the blooming season.

The detection scheme developed by Kahru *et al*. (2007) for MODIS data has been adapted to MERIS data. In order to improve the monitoring service, MODIS and MERIS data have been combined to produce daily bloom maps. Differences between MERIS and MODIS nLw data are generally small; dissimilarity in bloom classifications are often due to discrepancies in flag definitions of valid ocean pixels. The flag sets for valid ocean must be further examined to minimise this problem. Future work will focus on the satellite data availability. Since both MERIS and MODIS are operating beyond their technical lifetime it is necessary to introduce other similar satellite data or include new missions into the service as soon as data is made available.

Acknowledgements

We would like to acknowledge the Swedish Space Board for funding of the development and implementation project to improve the algae monitoring service.

References

Finni, T., K. Kononen, R. Olsonen, and K. Wallström (2001). The History of Cyanobacterial Blooms in the Baltic Sea. Ambio 30, No.4–5.

Hansson, M. (2006). Cyanobakterieblomningar i Östersjön, resultat från satellitövervakning 1997–2005, SMHI Oceanografi rapport nr 82, ISSN 0283-7714.

Hansson, M., and B. Håkansson (2007). The Baltic Algae Watch System – a remote sensing application for monitoring cyanobacterial blooms in the Baltic Sea. J. Appl. Remote Sens., Vol. 1.

Håkansson, B. (2000). "Satellite remote sensing of coastal oceans: water quality and algae blooms". Seas at the millennium: An Environmental evaluation, Elsevier Science Ltd. 3, pp. 293–302.

Kahru, M., U. Horstmann, and O. Rud (1994). Satellite Detection of Increased Cyanobacteria Blooms in the Baltic Sea: Natural Fluctuation or Ecosystem change? Ambio 23, No. 8.

Kahru, M. (1997). Using Satellites to Monitor Large-Scale Environmental Change: A case study of the Cyanobacteria Blooms in the Baltic Sea. Monitoring algal blooms: New techniques for detecting large-scale environmental change, Landes Bioscience.

Kahru, M., O.P. Savchuk, and R. Elmgren (2007). Satellite measurements of cyanobacterial bloom frequency in the Baltic Sea: Interannual and spatial variability. Mar. Ecol. Prog., 343, pp 15–23.

Kononen, K. (2001). Eutrophication: Harmful Algal Blooms and Species Diversity in Phytoplankton Communities, Examples from the Baltic Sea. Ambio 30, No. 4–5.

Bio-optical model development: implementation to real time operation in the Black Sea

V. Suslin*[1], T. Churilova[2], M. Ivanchik[1], and G. Korotaev[1]

[1]*Marine Hydrophysical institute of NASU, Sevastopol, Ukraine*
[2]*Institute of Biology the Southern Seas of NASU, Sevastopol, Ukraine*

Abstract

The vertical diffuse attenuation coefficient, $K_d(490)$, is one of the key parameters required for modelling of water quality, hydrodynamic and biological processes in the sea. This paper shows that the standard satellite product of $K_d(490)$ was underestimated in comparison with $K_d(490)$ values simulated by the regional model during the diatom bloom in the Black Sea. Using data from the SeaWiFS colour scanner, a regional relationship between the model value of $K_d(490)$ and the ratio of the standard satellite products of remote sensing reflectances, $R_{rs}(490):R_{rs}(510)$, has been obtained.

Keywords: Black Sea, diffuse attenuation coefficient, ocean colour data, SeaWiFS.

1. Introduction

Remote sensing of the ocean in the visible domain and data processing is being continuously developed. Recent satellite multispectral measurements provide an overview of any world area once or twice a day with a spatial resolution of 1 km or higher. Ocean colour datasets are available on the internet with ~ 6 hours delay. At present a few ocean colour scanners (MODIS-Terra since February 2000; MODIS-Aqua since July 2002 and MERIS-Envisat since May 2002) are operating. Taking into account the SeaWiFS (operated between September 1997 and December 2010), the ocean colour data set includes bio-optical products of the upper layer of the world ocean for more than one decade (Level-2). The quality of ocean colour products is continuously being advanced resulting from instrument calibration giving a correction of output products and from refining the atmosphere correction and bio-optical algorithms (Reprocessing).

To get an adequate estimation of the water, a bio-optical features revision is required of the optical constants and use of the relationships between bio-optical parameters for open ocean waters (O'Reilly *et al*., 2000, Lee *et al*., 2002, Maritorena *et al*., 2002) and for selected areas of world ocean, in particular for the Black Sea (Suetin *et al*., 2002, Churilova *et al*., 2007, Suslin *et al*., 2008, 2009). The development of regional bio-optical algorithms is required because optical parameters and relationships between bio-optical characteristics for the Black Sea significantly differ from those for open ocean waters (Suetin *et al*., 2002; Churilova *et al*., 2007, Suslin *et al*., 2008; 2009).

The downwelling diffusive attenuation coefficient at 490 nm, $K_d(490)$, is one of the standard ocean colour products (Oceancolor, GlobColour). $K_d(490)$ is one of the key parameters that determines the thermodynamics of the upper sea layer (Kubryakov *et al*., 2010), and the light field in the sea (Churilova *et al*., 2009) which in turn affects the

* Corresponding author, email: slava.suslin@gmail.com

primary synthesis of organic matter (Finenko *et al*., 2009, 2010, Churilova *et al*., 2011) and the ecosystem of the sea (Dorofeev *et al*., 2011).

For the open ocean, the relationships between in-situ $K_d(490)$ measurements and the ratio of remote sensing reflectances have been statistically analysed (O'Reilly *et al*., 2000). The result of this is used for calculating the $K_d(490)$ standard product. Optical features of the Black Sea differ from open ocean parameters:

a) Higher light absorption of coloured dissolved organic matter, CDOM, (Suetin *et al*., 2002, Kopelevich *et al*., 2004 Churilova *et al*., 2007)

b) Specific absorption at 530−560 nm, which is likely to be caused by phytoplankton (Suslin *et al*., 2011).

Due to the above mentioned optical peculiarities of the Black sea it requires the development of a regional model of $K_d(490)$ based on remote sensing data – remote sensing reflectance, R_{rs}. The aim of this work is to develop this regional model.

2. Methods

The value of $K_d(490)$ is calculated by the following equation:

$$K_d = -\frac{1}{E_d} \cdot \frac{dE_d}{dz} \tag{1}$$

where E_d is the downwelling radiance, and z is the depth.

$$E_d = \int_0^{2\pi} d\varphi \int_0^{\pi/2} L(\theta, \varphi) \cdot \cos(\theta) \cdot \sin(\theta) d\theta \tag{2}$$

where θ and φ are vertical and azimuth angles of radiance, $L(\theta, \varphi)$. Moreover, the $K_d(490)$ value could be calculated using inherent optical properties (IOPs) of the water (Ivanov, 1975, Gordon, 1989):

$$K_d = \frac{a + b_b}{\mu} \tag{3}$$

where a and b_b are the total light absorption and backscattering coefficients of sea water, respectively, and π is the averaged cosine of downwelling radiance, which is equal 0.8.

The regional model includes input parameters – level 2 SeaWiFS R2010.0 products of 1998 (Level-2), which are used in a $0.035 \times 0.025°$ grid (longitude × latitude) with two-week averaging. For the averaging, data corresponding to the following criteria were used:

1. The water leaving radiance at all channels after atmosphere correction must be >0
2. The iteration number of the atmosphere correction procedure must be < 10
3. The stray light pixels are not used

4. Glint-contaminated measurements are not used

For analysis six sea regions were used: 5 in deep waters:

1: 42.93°–43.5° N and 30.85°–31.66° E;
2: 42.9°–43.5° N and 36.1°–36.9° E;
3: 41.9°–42.5° N and 38.4°–39.2° E;
4: 42.9°–43.5° N and 33.7°–34.5° E;
5: 42.2°–42.8° N and 29.8°–30.6° E)

and one on the north-western shelf (44.55°–45.125° N and 30.85°–31.655° E).

In-situ measured chlorophyll-a concentration obtained during bio-optical monitoring of the Black Sea (region 5) on ship opportunities (Churilova *et al*., 2004) were used in this research.

3. Results and discussion

The $K_d(490)$ value was calculated by equation (3) using SeaWiFS data from 1998 for region 5 (Figure 1). THe light backscattering coefficient of suspended particles was calculated using SeaWiFS data and the equation described in (Suetin *et al*., 2002). To calculate the total light absorption coefficients (as a sum of colored dissolved organic matter and non-algal suspended particles, CDM, and phytoplankton absorption) an approach described in Suslin *et al*. (2008) was used. Light backscattering and absorption coefficients of pure water were taken from Morel *et al*. (1977) and Pope *et al*. (1997) respectively.

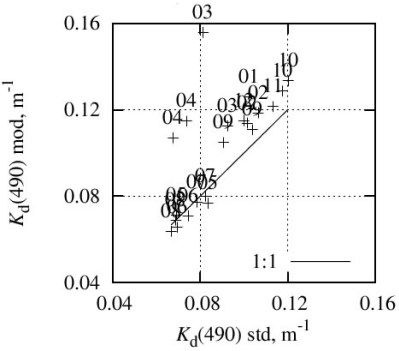

Figure 1 Comparison of standard product $K_d(490)$*std* with values calculated by equation (3) in region 5 of the Black Sea in 1998 based on SeaWiFS data. The numbers correspond to the month of the year and the line is 1:1.

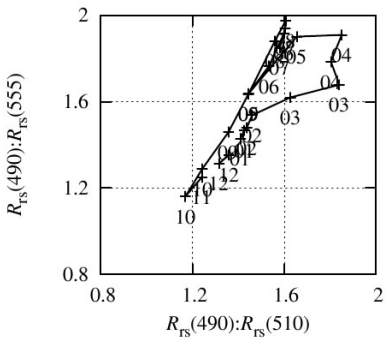

Figure 2 Relationship between $R_{rs}(490):R_{rs}(510)$ and $R_{rs}(490):R_{rs}(555)$ in 1998 in region 5of the Black Sea based on SeaWiFS data. The numbers correspond to the month of the year.

The comparison of the $K_d(490)$ standard product, $K_d(490)$*std*, with $K_d(490)$ values simulated by the regional bio-optical model (Churilova *et al*., 2007), $K_d(490)$*mod* shows good agreement in summer and disagreement in spring (Figure 1). The SeaWiFS $K_d(490)$ (in m^{-1}) was calculated by:

$$K_d(490) = 10^{\alpha_0 + \alpha_1 \cdot X + \alpha_2 \cdot X^2 + \alpha_3 \cdot X^3 + \alpha_4 \cdot X^4} + 0.0166 \quad (4)$$

where $X = \lg[R_{rs}(490)/R_{rs}(555)]$, $\alpha_0 = -0.8515$, $\alpha_1 = -1.8263$, $\alpha_2 = 1.8714$, $\alpha_3 = -2.4414$, $\alpha_4 = -1.0690$ – constants for the spectral channels of SeaWiFS (KD). Equation (4) was obtained as a result of fitting relationship between in-situ measured $K_d(490)$ and the R_{rs} ratio for two channels at 490 and 555 nm (O'Reilly *et al*., 2000). The operational algorithm for deriving $K_d(490)$ was updated using in-situ data from NOMAD version 2 (KD). The algorithm form describes the polynomial best fit that relates the log-transformed geophysical variable to a log-transformed ratio of remote-sensing reflectances.

Because $K_d(490)$ measurements corresponded to case 1 waters (Morel *et al*., 1997), the $R_{rs}(490):R_{rs}(555)$ ratio is correlated to the total light absorption coefficient of the sea at 490 nm. However it is not typical for the Black Sea (Suslin *et al*., 2008) due to specific phytoplankton absorption at 555 nm, which is higher than the values for case 1 waters (Bricaud *et al*., 1995). This fact causes the relationship between $R_{rs}(555):R_{rs}(510)$ and $R_{rs}(510):R_{rs}(490)$ shown for region 5 (Figure 2).

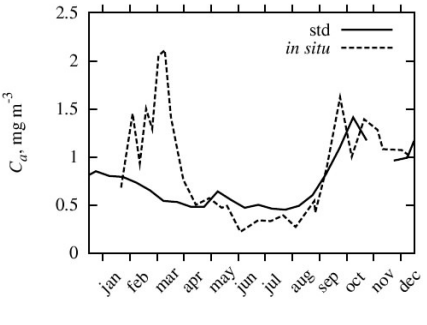

Figure 3 Dynamics of chlorophyll-a concentration in 5th deep-water region of the Black Sea in 1998: SeaWiFS standard product – std; in-situ measured data (Churilova *et al*., 2004)

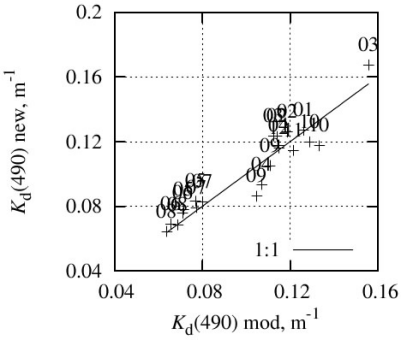

Figure 4 As Figure 1, but $K_d(490)$*new* was calculated by equation (4), where $R_{rs}(490):R_{rs}(555)$ ratio is estimated by equation (5).

In region 5 in spring 1998 diatoms blooming was observed and chlorophyll-a concentrations were high (~2 mgm^{-3}) (Figure 3). This resulted in an increase in the total light absorption coefficients which in turn (equation (3)) lead to an increase in $K_d(490)$ values. In Figure 3 it is evident that the standard algorithm underestimates chlorophyll-a concentrations in spring and does not "see" the spring maximum. In summer, when chlorophyll *a* concentrations are about one order less than in winter–spring time, the main contribution to the total absorption introduces the CDM component, whose contribution is much larger at 490 nm than at 555 nm. The latter causes a good correspondence between the standard and modelled estimates of $K_d(490)$ values. It turns out that this feature is absent in the Black Sea if equation (4) is rewritten in terms of the $R_{rs}(490):R_{rs}(510)$ ratio. The ratio $R_{rs}(490):R_{rs}(510)$ corresponds well to the total absorption by phytoplankton and by *CDM* for all seasons (Figure 4), while the ratio $R_{rs}(490):R_{rs}(555)$ is not appropriate for winter and spring time due to the phytoplankton

specific absorption at 555 nm (Suslin *et al*., 2008). The ratio $R_{rs}(490):R_{rs}(555)$ can only be used for summer, when the relative contribution of phytoplankton to the total absorption is smallest for the year and *CDM* determines the total light absorption.

In equation (4), the ratio $R_{rs}(490):R_{rs}(555)$ was replaced by $R_{rs}(490):R_{rs}(510)$ following:

$$y = A \cdot x + B \tag{5}$$

where $y=R_{rs}(490):R_{rs}(555)$, $x=R_{rs}(490):R_{rs}(510)$, $A=1.85$, and $B=-1.0$.

Equation (5) was found empirically (with determination coefficient $r^2=0.95$) using summer data for all five deep-water regions of the Black Sea for the lifetime of SeaWiFS (Figure 5).

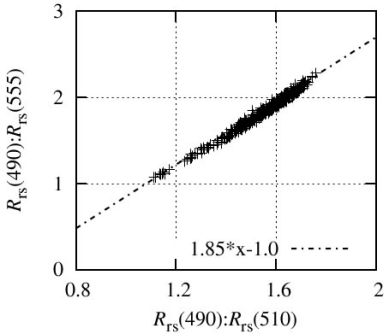

Figure 5 Relationship between $R_{rs}(490):R_{rs}(510)$ and $R_{rs}(490):R_{rs}(555)$ obtained in the five deep-water regions during the summer months of the lifetime of SeaWiFS.

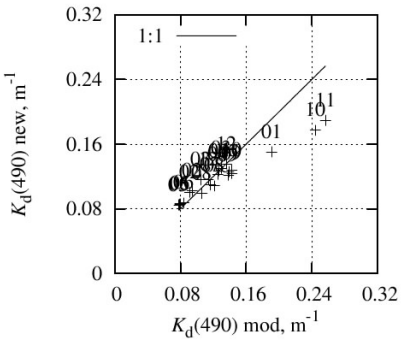

Figure 6 As Figure 4 but for the north-western shelf region of the Black Sea.

As has been shown above when *CDM* dominates in total light absorption the standard product $K_d(490)$*std* is practically equal to $K_d(490)$ obtained using regional bio-optical model (*mod*) and "*new*": $K_d(490)std \approx K_d(490)mod \approx K_d(490)new$. The *CDOM* domination occurred in the coastal and north-western shelf waters of the Black Sea (Churilova *et al*., 2007). A comparison of the $K_d(490)$*new* and $K_d(490)$*mod* values for the north-western shelf in 1998 is shown in Figure 6, where it is evident that the error is less than 20 which corresponds to the accuracy of equation (3). Thereby equations (4) and (5) can retrieve $K_d(490)$ with appropriate (< 20%) accuracy for all seasons and for different regions of the Black Sea. It should be noted that the difference between $K_d(490)$*std* and $K_d(490)$*new* in spring is not only typical for 1998, but also observed in other years (Suslin *et al*., 2011).

The approach described above of the standard product correction (using $R_{rs}(490):R_{rs}(510)$ instead of the $R_{rs}(490):R_{rs}(555)$ ratio) has been used to obtain correct $K_d(490)$ maps based on the SeaWiFS data from September 1997 to December 2010 with two-week averaging (Black Sea Color). Figure 7, shows some examples of these $K_d(490)$*new* maps in comparison with the SeaWiFS $K_d(490)$*std*. The $K_d(490)$*new* and $K_d(490)$*std* maps differs significantly for spring values in deep-waters region, while summer and autumn $K_d(490)$ values are in a good agreement with the exception of some

coastal waters where slight differences in $K_d(490)$ values are observed (Figure 7).

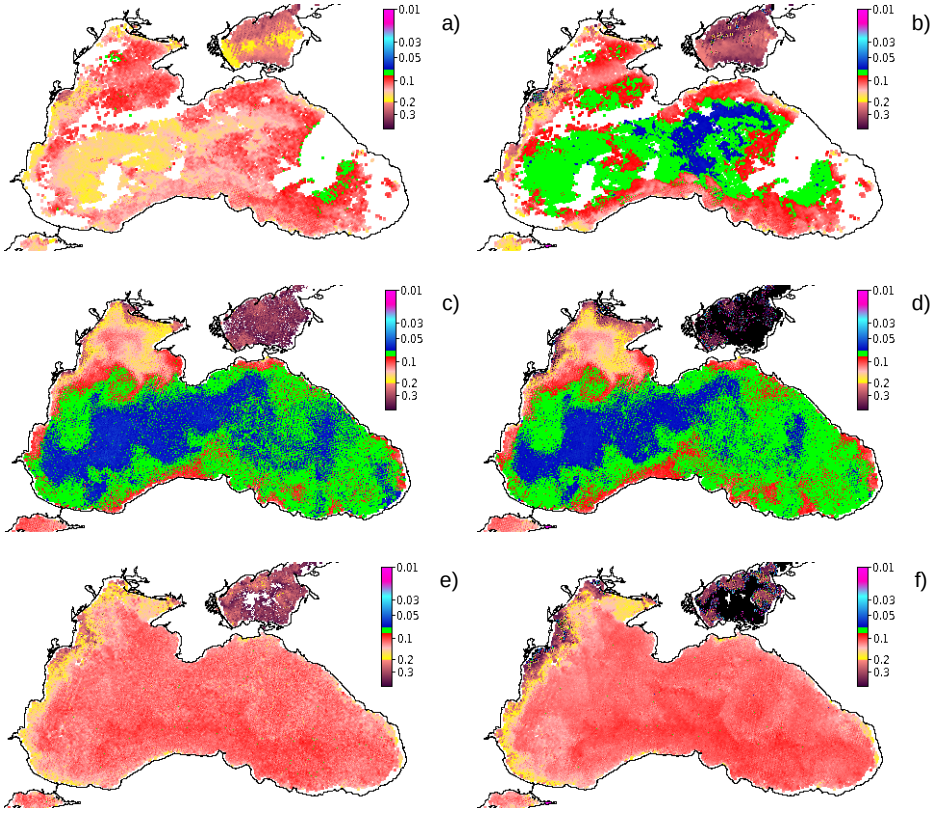

Figure 7 Maps based on SeaWiFS data for 1998. a) and b): second half of March; c) and d): second half of August; e) and f): second half of October (Left maps – new approach; Right maps: standard product).

4. Conclusions

It has been shown that the standard $K_d(490)$ product in the Black Sea during the winter–spring bloom is underestimated in comparison with $K_d(490)$values simulated by the regional bio-optical model. It has been shown that replacing the ratio at 490:555 with the ratio at 490:510 allows an estimation of the value with appropriate accuracy (~20%) in all seasons and in different regions of the Black Sea. Using this approach, two-week averaged maps of $K_d(490)$ for the entire SeaWiFS operation period have been obtained.

Acknowledgements

The research was supported by the NASU projects “Operational Oceanography”, GSA Ukraine “Metodika-M”, FP 6 project “SESAME”, “MyOcean” (FP7/2007–2013 grant agreement no. 218812) and “ODEMM” (FP7 project #244273).

References

Black Sea Color, blackseacolor.com

Bricaud, A., M. Babin, A. Morel *et al*. (1995). Variability in the chlorophyll-specific absorption coefficients of natural phytoplankton: Analysis and parametrisation. JGR, Vol. 100, No.C7, 13321–13332.

Churilova, T., G. Berseneva, and L. Georgieva (2004). Variability in bio-optical characteristics of phytoplankton in the Black Sea. Oceanology. V. 44, No. 2, 192–204 (translated into English from "Okeanologia")

Churilova, T.Ya., V.V. Suslin, G.P. Berseneva, and S.F. Pryahina (2007). Parametrisation of light absorption by phytoplankton, non-algal particles and coloured dissolved organic matter in the Black Sea. Proc. 4th Int. Conf. ONW'2007, Nizhny Novgorod, September 11–15, 2007, 70–74.

Churilova. T.Ya., V.V. Suslin, and H.M. Sosik (2009). Spectral model of underwater irradiance in the Black Sea. Marine Hydrophys. Journal, No.6, 33–46 (in Russian).

Churilova, T., V. Suslin, O. Rylkova, and A. Dzhulay (2011). Spectral features of downwelling radiance and chromatic adaptation of phytoplankton in the Black Sea. Proc. of VI Int. Conf. ONW'2011, St. Petersburg, Russia, September 6–9, 2011, Publishing house of "Nauka" of RAS, 117–121.

Level-2, Ocean level-2 data products, oceancolor.gsfc.nasa.gov/DOCS/ ocformats.html#3

Dorofeev, V., T. Oguz, T. Churilova, V. Suslin, A. Kubryakov, and G. Korotaev (2011). The MyOcean Black Sea coupling of dynamics and ecosystem. Mercator Ocean Quarterly Newsletter, No.40, 26–35.

GlobColour (2007). MERIS, www.globcolour.info

Gordon, H.R. (1989). Can the Lambert-Beer law be applied to the diffuse attenuation coefficient of the ocean water? Limnol. Oceanogr, Vol. 34, No. 8, 1389–1409.

Finenko, Z.Z., V.V. Suslin, and T.Ya Churilova (2009). The regional model to calculate the Black Sea primary production using satellite colour scanner SeaWiFS. Marine Ecological Journal, No. 1, 81–106 (in Russian).

Finenko, Z.Z., V.V. Suslin, and T.Ya. Churilova (2010). Estimation of phytoplankton productivity in the Black Sea based on satellite data. Doklady Akademii Nauk, V. 432, No. 6, 845–848 (in Russian).

Ivanov. A.P. (1975). Physical Foundations of hydrooptics. Minsk, Nauka i Tekhnika 503 p. (in Russian).

KD, Diffuse attenuation coefficient for downwelling irradiance at 490-nm, oceancolor.gsfc.nasa.gov/REPROCESSING/R2009/kdv4/

Kopelevich, O.V., V.I. Burenkov, S.V. Ershova *et al*. (2004). Application of SeaWiFS data for studying variability of bio-optical characteristics in the Barents, Black and Caspian Seas. DeepSea Res, II 51, 1063–1091.

Kubryakov, A., V. Suslin, T. Churilova, and G. Korotaev (2010). Effects of Penetrative Radiation on the Upper Layer Black Sea Thermodynamics. MyOcean Science Days, Toulouse, 1–3 December 2010, mercator-myoceanv2.netaktiv.com/MSD_2010/ Abstract/ Abstract_KUBRYAKOVa_MSD_2010.doc

Lee, Z.P., K.L. Carder, and R. Arnone (2002). Deriving inherent optical properties from water color: A multi-band quasi-analytical algorithm for optically deep waters. Applied Optics, 4, 5755–5772.

Maritorena, S., D.A. Siege, and A. Peterson (2002). Optimization of a Semi-Analytical Ocean Color Model for Global Scale Applications. Applied Optics, 41(15), 2705–2714.

Morel, A., and L. Prieur (1997). Analysis of variations in ocean color. Limnol. Oceanog. V. 22, No.4, 709–722.

Reprocessing, oceancolor.gsfc.nasa.gov/WIKI/OCReproc.html.

Level-2, Ocean Color Products and Algorithms, Standard Products, oceancolor.gsfc.nasa.gov/cgi/algorithms.cgi.

Oceancolor, Oceancolor web site, oceancolor.gsfc.nasa.gov/

O'Reilly, J.E. and 24 Coauthors. (2000). SeaWiFS Postlaunch Calibration and Validation Analyses, Part 3. NASA Tech. Memo. 2000-206892, Vol. 11, S.B. Hooker and E.R. Firestone, Eds., NASA Goddard Space Flight Center. 49 p.

Pope, R.M., and E.S. Fry (1997). Absorption spectrum (380–700 nm) of the pure water. II. Integrating cavity measurements. Applied Optics, V. 36, 8710–8723.

Suetin, V.S., V.V. Suslin, S.N. Korolev, and A.A. Kucheryavy (2002). Estimation of variability of water optical properties in the Black Sea in summer 1998 using data of the satellite instrument SeaWiFS. Marine Hydrophys. J., No. 6, 44–54 (in Russian).

Suslin, V.V., T.Ya Churilova, and H.M. Sosik (2008). The SeaWiFS algorithm of chlorophyll-a in the Black Sea. Marine Ecological J., V. VII, No. 2, 24–42 (in Russian).

Suslin, V.V., T.Ya Churilova, and S.F. Pryahina (2009). Seasonal variability of the slope in absorption spectra of color detrital matter in the deep part of the Black Sea based on SeaWiFS and MODIS data sets. Current Problems in Optics of Natural Waters: Proc. 5th Int. Conf. (St. Petersburg), 136–138.

Suslin, V., T. Churilova, M. Ivanchik, S. Pryahina, and N.A. Golovko (2011). Simple Approach for Modeling of Downwelling Irradiance in the Black Sea Based on Satellite Data. Proc. of VI Int. Conf. ONW'2011, St. Petersburg. Russia, September 6–9, 2011, Publishing house of “Nauka” of RAS, 199–203.

Impact of irregular sampling by MERIS on eutrophication monitoring products for WFD and MSFD applications

Dimitry Van der Zande*, Geneviève Lacroix, Xavier Desmit, and Kevin Ruddick

Royal Belgian Institute of Natural Sciences, MUMM, Brussels, Belgium.

Abstract

The chlorophyll-a 90 percentile product (CHL-P90) gained importance in describing the eutrophication state of the Belgian part of the North Sea when Water Framework Directive requirements were transposed into Belgian law in July 2010. A MERIS based CHL-P90 product was developed to answer this need for information as MERIS provides a better temporal and spatial coverage compared to in-situ monitoring and thus is potentially better suited to provide a P90 estimate. However, the irregular availability of satellite chlorophyll-a observations both in space and time due to cloudiness, quality flagging, sensor malfunction, etc. has to be considered as it impacts the product accuracy. This impact is two-fold and dependent on (1) the availability of observations during the actual phytoplankton bloom and (2) a proportional distribution of observations in the bloom and non-bloom period.

This effect of irregular sampling on the accuracy of CHL-P90 was studied in detail in simulations. The MIRO&CO-3D ecosystem model was used to generate realistic time series of chlorophyll-a concentrations with high temporal resolution in the most important Belgian monitoring stations. These time series were sub-sampled using the actual observation density of the MERIS satellite in Belgian waters. Results show that a mean relative error of 25.4% on the CHL-P90 estimate can be expected due to the effects of irregular sampling. The results of this study were used to improve the CHL-P90 algorithms by adding a weighing procedure taking into account irregular sampling issues to reduce these errors to 9.9%.

Keywords: chlorophyll-a P90, MERIS, Water Framework Directive, Belgium

1. Introduction

The Water Framework Directive (WFD) and the Marine Strategy Framework Directive (MSFD) are currently the most important drivers for monitoring the coastal and offshore waters in Europe with the objective of reaching a 'good environmental status' (Gohin *et al*., 2008). Human-induced eutrophication is one of the criteria for assessing the extent to which good environmental status is being achieved. Eutrophication can be defined as the enrichment of water by nutrients causing an accelerated growth of algae and higher forms of plant life to produce an undesirable disturbance to the balance of organisms present in the water and to the quality of the water concerned, and therefore refers to the undesirable effects resulting from anthropogenic enrichment by nutrients (OSPAR, 1998).

* Corresponding author, email: Dimitry.vanderzande@mumm.ac.be

In June 2010, WFD requirements (Directive, 2000) for the Belgian Coastal Zone (BCZ) were transposed into Belgian law (Royal Decree 23.06.2010) thus structuring/guiding the water quality monitoring programmes. The eutrophication status is established by monitoring the chlorophyll-a (CHL) concentration as it is a proxy of phytoplankton biomass. More specifically, the indicator of choice is the chlorophyll-a 90 percentile (CHL-P90) over the phytoplankton growing season (i.e. March−November inclusive) expressed in $\mu g l^{-1}$. The CHL-P90 is the CHL concentration below which 90 percent of observations fall. While in-situ data acquisition is still considered as the main monitoring tool there is a growing tendency to use optical remote sensing as a supporting tool to achieve the monitoring requirements because of severe resource constraints of available ship time and manpower (Sorensen *et al*., 2002). For example, in Belgium, in-situ measurements are collected 5−7 times on average per growing season at 10 stations distributed in the BCZ (Ruddick *et al*., 2008c). These numbers are too low to calculate CHL-P90 values with sufficient accuracy. Hence the need for additional information sources.

The algal1 and algal2 products from MERIS are now considered sufficiently mature for use in applications in the turbid Belgian waters (Ruddick *et al*., 2008a, 2008b). The MERIS data enables the calculation of CHL-P90 pixel-by-pixel resulting in a map product which is expected to provide more accurate CHL-P90 estimates due to an increased temporal and spatial resolution compared to the in-situ data (Park *et al*., 2010). Subsequently, this map product provides the policy makers with the means to objectively and quantitatively report on the WFD and MSFD guidelines for reaching a 'good environmental state' by 2020.

However, the irregular availability of satellite CHL observations both in space and time due to cloudiness, quality flagging, sensor malfunction, etc. has to be considered (Sirjacobs *et al*., 2011) as it impacts the accuracy of CHL-P90. This impact is two-fold and dependant on (1) the availability of observations during the actual phytoplankton bloom and (2) a proportional distribution of observations in the bloom and non-bloom periods. Figure 1 illustrates this by showing how a different timing of 50 samples on the same CHL time series can result in significantly different CHL-P90 estimates. From this example it is obvious that sufficient sampling of the bloom period is crucial for generating an accurate CHL-P90 product but can still lead to errors in case of under- or oversampling compared to the non-bloom period.

The main objective of this study is to perform a detailed sensitivity analysis on the CHL-P90 product considering irregular sampling and to use the results to develop a correction procedure to improve the CHL-P90 product. Simulation techniques were used to ensure the availability of sufficient reference data. The MIRO&CO-3D ecosystem model (Lacroix *et al*., 2007) provided CHL time series with a high temporal resolution (i.e. 30 minutes) in five Belgian monitoring stations for a full growing season in the arbitrarily chosen year 2006. These five time series were generated taking into account processes such as wind- and tide-induced variability, complex biological interactions etc. and were subsequently sub sampled using actual pixel-specific MERIS sampling frequency during the growing season of 2003 to 2010. This resulted in more than 20000 sub-sampled CHL time series which could be directly compared to the five MIRO&CO-3D time series to perform the accuracy analysis.

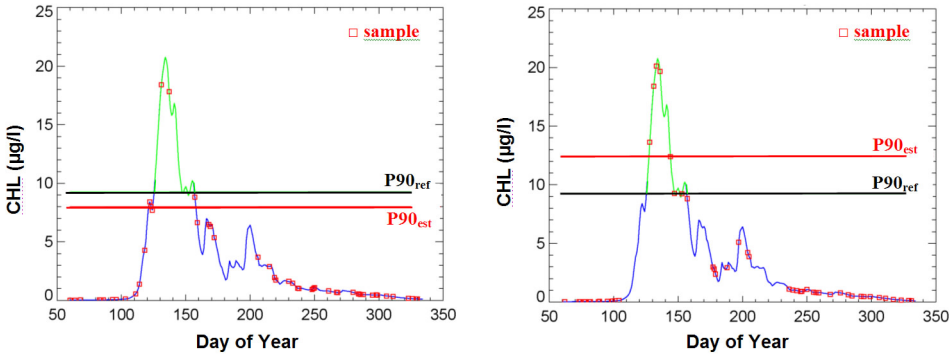

Figure 1 Illustration of the impact of two different timings of 50 samples on the same CHL time series on CHL-P90 estimates. Blue/green line: time series of CHL computed by MIRO&CO-3D model (Lacroix *et al*., 2007) for the year 2006 for a single Belgian monitoring station (51.27°N–2.91°W) with the phytoplankton bloom marked in green. $P90_{ref}$ (black line) and $P90_{est}$ (red line) are the percentile 90 computed respectively from the daily data and from a subsample of 50 data.

2. Materials and Methods

2.1 Belgian Coastal Zone

The Belgian Coastal Zone (BCZ) is located in the Southern Bight of the North Sea (SNS) and covers approximately 3454 km^2 with an average depth of 20–30 m. The BCZ is influenced directly by the Scheldt river (and other small Belgian rivers) inputs as well as indirectly by waters discharges from French rivers such as the Seine and the Somme and the Dutch Rhine/Meuse system (Lacroix *et al*., 2004). The river nutrient input causes eutrophication in the BCZ leading to high-biomass algal blooms, mainly the *Haptophycea Phaeocystis globosa* that spreads over the entire area in spring (Lancelot *et al*., 1987).

2.2 MIRO&CO-3D model

The MIRO&CO-3D model is a combination of the 3D hydrodynamical model described in Lacroix *et al*. (2004) based on the COHERENS model (Luyten *et al*., 1999) and the biogeochemical MIRO model (Lancelot *et al*., 2005). The MIRO&CO-3D ecosystem model was used to generate simulated time series of chlorophyll-a concentrations with high temporal resolution for five Belgian monitoring stations. The model is capable of simulating the transport and dynamics of inorganic and organic nutrients, phytoplankton, bacterioplankton and zooplankton biomass in the SNS (Lacroix *et al*., 2007). For this theoretical study, the BCZ was subdivided in five zones around the five in-situ monitoring stations using the nearest neighbour interpolation. For each zone a typical CHL time series during the phytoplankton growing season was generated capturing the main variations in the BCZ (Figure 2). While these time series are theoretical, we believe that they capture the main phytoplankton dynamics present in the BCZ, generally with an intensive *Phaeocystis globasa* bloom during the spring followed by a less intensive summer Diatoms bloom (Lancelot *et al*., 2005). Remote Sensing observations show that bloom intensity decreases with increasing distance from the coast (Rousseau *et al*., 2006;

Ruddick *et al*., 2008c). The CHL time series are presented in Figure 2 (right) showing a phytoplankton biomass peak around day 134 (i.e. 12 May) for the different zones.

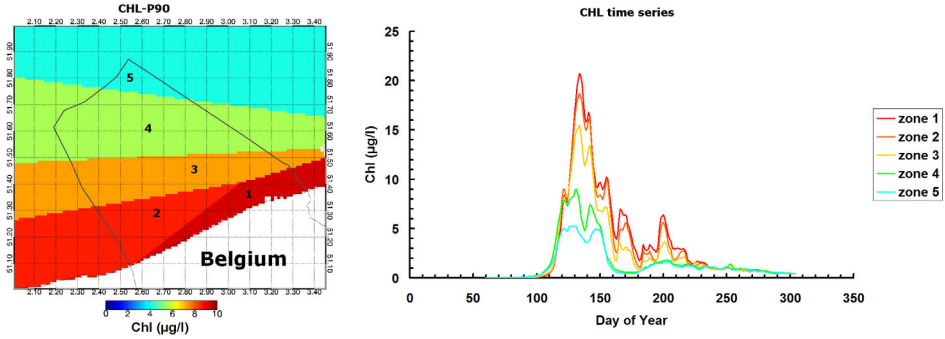

Figure 2 Left: CHL-P90 computed from daily MIRO&CO-3D data for the year 2006 for five zones around the five in-situ monitoring stations using the nearest neighbour interpolation, catching the main variations in algal bloom intensities in the BCZ (represented by the black line). Right: Daily time series of CHL computed by MIRO&CO-3D (Lacroix *et al*., 2007) at the 5 chosen stations. The colour scale referring to the 5 zones is the same for both diagrams.

2.3 MERIS sampling frequency

Satellite images are widely used in operational oceanography and in ecosystem dynamics studies due to their extensive spatial and temporal coverage. The Medium Resolution Imaging Spectrometer (MERIS) instrument provides level 2 algal products (CHL in $\mu g l^{-1}$) (Doerffer and Schiller, 2007) for both case 1 and case 2 waters on a daily basis with a spatial resolution of 1 km and a theoretical daily temporal resolution for the BCZ. However, satellite remote sensing is subject to one major limitation: cloud presence can totally or partially cover the area of interest. For the BCZ this generally results in a high percentage of missing data in the daily images. This missing data is not evenly distributed over the year, and thus biases any simple averaging calculations. To study the impact of gaps in the observation continuity on the CHL-P90 product quality, the actual MERIS sampling frequencies per pixel for the years 2003 to 2010 were applied to the five simulated CHL time series described in section 2.2. This resulted in more than 20000 subsampled CHL time series accompanied with the detailed model data needed to perform the accuracy analysis.

2.4 Standard CHL-P90 product

CHL-P90 values were calculated pixel-by-pixel from the mean and standard deviation (σ) of the CHL time series over the growing season by the approximation:

$$\text{CHL-P90} = \text{Mean} + 1.28 * \sigma \quad (1)$$

with a minimum of 2 CHL values per pixel. The mean and standard deviation σ are computed in log transformed space. This statistical approach is an approximation for a log-normal distribution of selecting the CHL value in a time series such that 90% of the observations are equal or less than this value. It requires considerably less computing resources as no actual time series need to be stored for each pixel, speeding up the

processing significantly. It delivers accurate CHL-P90 values when the sampling is regularly distributed over the growing season and when the underlying distribution is log-normal.

2.5 Weighted CHL-P90 calculation

In this approach a quality assessment of the satellite-based CHL time series is taken into account when generating the CHL-P90 product to compensate for irregular sampling. In a first step a key period (KP) is defined as the period containing the main algal bloom. In this study this period is defined as the period starting 14 days before and ending 14 days after the maximum CHL observation (Figure 3). This arbitrary definition of the KP is region-specific and needs to be adjusted using prior knowledge of the local phytoplankton dynamics from model results or in-situ/Remote Sensing (RS) data. It is important that this period is sufficiently sampled to obtain a valid CHL-P90 estimate.

Next, the key period proportion (KPP) is calculated as follows:

$$KPP = \frac{Nrdays_{KP}}{Nrdays_{GS}} \tag{2}$$

where $Nrdays_{KP}$ is the total number of days of the KP (i.e. 28 days around the day of max CHL for the BCZ) and $Nrdays_{GS}$ is the total number of days in the phytoplankton growing season (i.e. 275 days). The arbitrarily chosen KPP equals 10.18%. Knowing the KP, the KPP for the MERIS time series can be calculated in a similar fashion as well as the relative difference (RD) between KPP and KPP_{MERIS}:

$$KPP_{MERIS} = \frac{NrObservations_{KP}}{NrObservations_{GS}} \qquad RD = \frac{KPP_{MERIS} - KPP}{KPP} \tag{3}$$

where $NrObservations_{KP}$ is the total number of CHL observations in the KP and $NrObservations_{GS}$ is the total number of CHL observations in the complete phytoplankton growing season.

The KPP_{MERIS} can be calculated for each pixel and can be compared to the KPP per zone resulting in a quantification of sampling irregularities represented by the weight indices WI_{KP} and WI_{NKP} for the key period and the non-key period respectively:

$$WI_{KP} = \frac{KPP_{MERIS}}{KPP} \qquad WI_{NKP} = 1 - \frac{KPP_{MERIS}}{KPP} \tag{4}$$

The KP is undersampled by MERIS in the case of $WI_{KP} < 1$ which would result in an underestimation of the CHL-P90 using the standard method. Conversely, overestimation of the CHL-P90 is expected in the case of $WI_{KP} > 1$. This information can be used to improve the CHL-P90 procedure by giving all the observations a weight which is the inverse of the respective WI in order to compensate for the sampling irregularities.

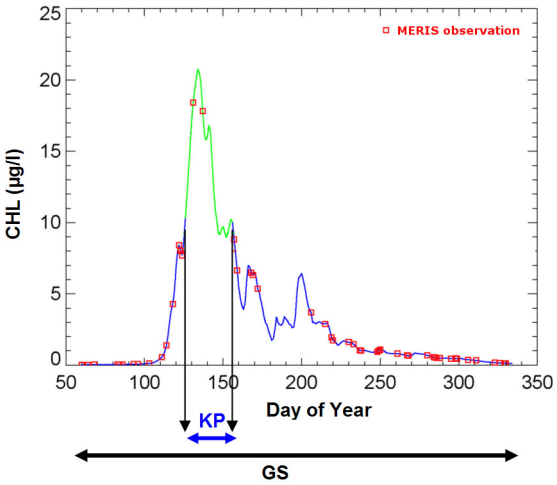

Figure 3 The region specific key period (KP) is defined as the period in the phytoplankton growing season (GS) containing the main algal bloom. Blue/green line: time series of CHL computed by MIRO&CO-3D model (Lacroix *et al*., 2007) for the year 2006 for a single Belgian monitoring station (51.27°N–2.91°W) with the key period marked in green. Red squares correspond to the dates where MERIS observations are available for the year 2003 in this case.

Finally, the CHL values are ranked from low to high with their weights cumulated and normalised (W_{norm}). The weighted CHL-P90 value is then defined as the CHL value where W_{norm} equals 0.90 with the possibility to linearly interpolate between the two closest CHL values above and below the W_{norm} of 0.90 if this is not the case.

3. Results and Discussion

Figure 4 shows an overview of the different map products which are relevant to the generation of the CHL-P90 product. The product has been generated for the years 2003 to 2010. Only data from the years 2004 and 2005 are shown here as means of demonstration. The available number of MERIS observation per pixel and per growing season for the BCZ is shown in the first column. This illustrates the annual variations in terms of data availability due to cloud cover. Significantly more observations per pixel were available for 2004 compared to 2005. Sampling irregularities are described by the weight index WI_{KP} but are best visualised in a relative fashion using RD which is calculated by comparing the KPP_{MERIS} to KPP (Figure 4 column 2). Red, green and blue pixels represent CHL time series where the KP is oversampled, correctly sampled and undersampled respectively compared to the KPP which equals 10.18% in this particular case. In 2004 the KP is oversampled near the coast and undersampled in the centre of the BCZ. For 2005 we mainly observe an undersampling of the KP which has the expected impact on the quality of the standard CHL-P90 product (Figure 4 column 3) which in case of ideal sampling should be identical to the reference data (Figure 2, left). While for both 2004 and 2005 the same reference CHL time series were used, the standard CHL–P90 maps are significantly different as a result of different sampling frequencies. This demonstrates the need for a correction procedure as mean relative errors of up to 16%

and 30% due to sampling issues were observed for 2004 and 2005 respectively (error maps not shown).

Using the weighted CHL-P90 approach, the information on sampling irregularities provided by the KPP is taken into account for each pixel separately enabling a weighing factor to be calculated. The results of this approach are presented in the fourth column of Figure 4 showing a closer fit of the weighted CHL-P90 product with the reference CHL-P90 map (Figure 2, left) compared to the standard CHL-P90 product. It can be concluded that the weighting approach works for a large number of sampling situations. Most of the over-estimations are eliminated but some under-estimations are still present, as can be seen in the top left corner of the weighted CHL-P90 map for 2004 and in different areas for 2005. These areas are characterised by a critical unavailability of observations during the actual phytoplankton bloom. Such pixels could be identified and discarded by using a threshold as a quality control as no statistically robust CHL-P90 estimate can be made using those specific CHL time series. The artificial boundary fronts seen in these maps are present in the original (simulated) dataset defining the 5 used zones and are not generated by the weighting procedure proposed here.

Figure 5 shows the mean relative errors of the standard and weighted CHL-P90 products which are calculated for the years 2003 to 2010 by directly comparing the estimated CHL-P90 values to the values obtained from the MIRO&CO-3D model and subsequently calculating the average for the BCZ. For the standard CHL-P90 product this error ranges from 16% to 35% with a mean error of 25.4% and for the weighted CHL-P90 product this ranges from 6% to 19% with a mean error of 9.9%. This results in a decrease in relative errors of 15.5%.

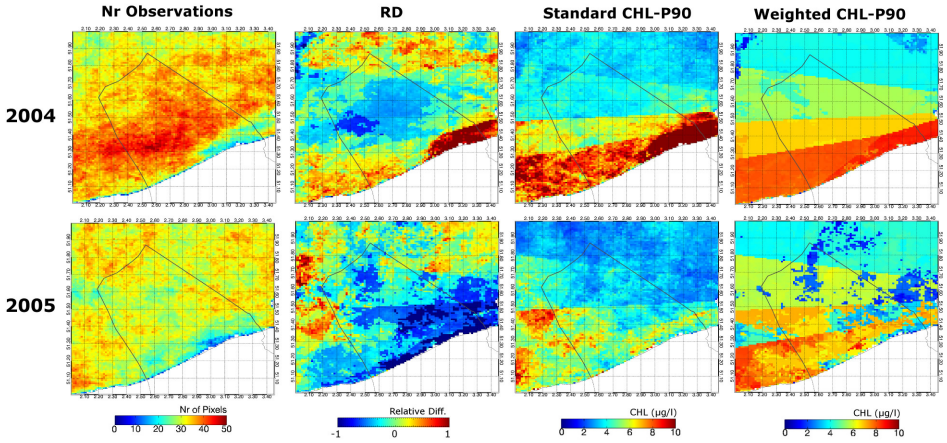

Figure 4 Overview of different map products relevant to the generation of the CHL-P90 product for the years 2004 and 2005. Column 1 presents the data availability in terms of number of MERIS observations during the growing season of the respective years. In column 2 the relative difference between KPP_{MERIS} and KPP (RD) provides a descriptor of sampling irregularities considering the key period. Column 3 and 4 respectively present the standard and weighted CHL-P90 product.

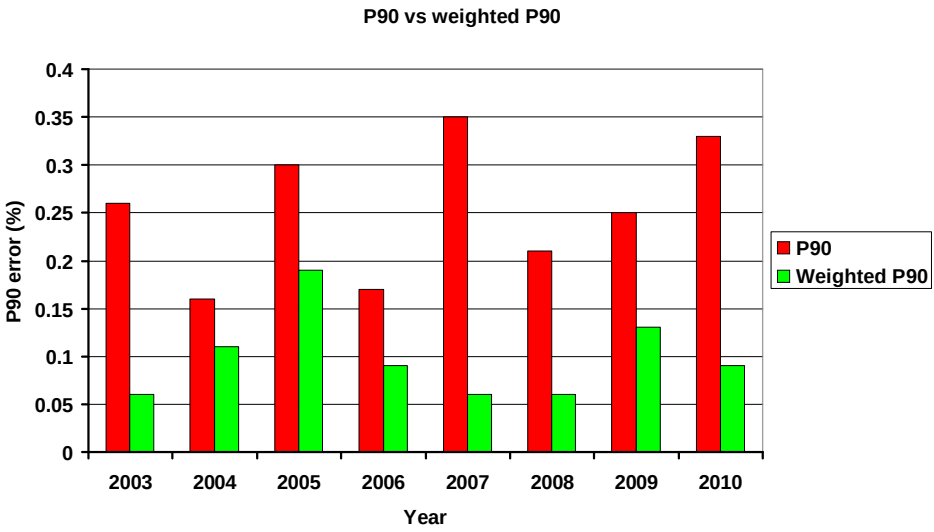

Figure 5 Mean relative errors of the standard (red) and weighted (green) CHL-P90 products for the years 2003−2010.

4. Conclusions

With the CHL-P90 product gaining importance in describing the eutrophication state of the European seas for WFD and MSFD applications, product quality has become an essential concern of potential users. While most studies have considered only the accuracy of individual satellite CHL measurements, this study has focused on the additional errors generated in multitemporal products. The sensitivity study performed in this work allowed more insight into the impact of sampling irregularities on the final product which should be considered carefully as significant errors were found. The proposed weighting approach provides a tool to take into account sampling issues resolving a significant part of this problem without the need for additional data except for the identification of the key period. Obviously a CHL-P90 product can only be generated if sufficient observations during the algal bloom period or key period are available.

This theoretical study was performed in a simulated environment raising the question of how the developed methodology can be transformed into an operational status. This only requires the knowledge of the region specific key period which could be obtained from in-situ data sets (e.g. SmartBuoys, traditional point sampling, etc.), ecological models (e.g. MIRO&CO-3D) or the remote sensing data itself by using pixels with well-defined time series. Next, theoretical look-up-tables need to be generated for estimated CHL-P90 errors in terms of the number of observations and KPP for different phytoplankton dynamics (i.e. bloom intensity, length of bloom, etc.). These look-up-tables can then be used to generate an error map to accompany the CHL-P90 map product. The combination of the weighted CHL-P90 map and a (theoretical) error map could then be considered as a more complete product needed by policy makers for WFD and MSFD reporting requirements.

Acknowledgements

This study was supported by the AquaMar project funded by Seventh Framework Program (FP7).

References

Directive (2000). Directive 2000/60/EC of the European Parliament and of the council of 23 October 2000 establishing a framework for community action in the field of water policy. Official Journal 22 December L327/1, Brussels: European Commission.

Doerffer, R., and H. Schiller (2007). The MERIS Case 2 water algorithm. International Journal of Remote Sensing, Vol. 28, pp. 517–535.

Gohin, F., B. Saulquin, H. Oger-Jeanneret, L. Lozac'h, L. Lambert, A. Lefebvre, P. Riou, and F. Bruchon (2008). Towards a better assessment of the ecological status of coastal waters using satellite-derived chlorophyll-a concentrations. Remote Sensing of Environment, Vol. 112, Issue 8, pp. 3329–3340.

Lacroix, G., K. Ruddick, J. Ozer, and C. Lancelot (2004). Modelling the impact of the Scheldt and Rhine/Meuse plumes on the salinity distribution in Belgian waters (Southern North Sea). Journal of Sea Research, 52: 149–163.

Lacroix, G., K. Ruddick, N. Gypens, and C. Lancelot (2007). Modelling the relative impact of rivers (Scheldt/Rhine/Seine) and Channel water on the nutrient and diatoms/*Phaeocystis* distributions in Belgian waters (Southern North Sea). Continental Shelf Research, Vol. 27, Issue 10–11, pp. 1422–1446.

Lancelot, C., G. Billen, A. Sournia, T. Weisse, F. Colijn, M.J.W. Veldhuis, A. Davies, and P. Wassman (1987). *Phaeocystis* blooms and nutrient enrichment in the continental coastal zones of the North Sea. Ambio. Vol. 16, Issue. 1, pp. 38–46.

Lancelot, C., Y. Spitz, N. Gypens, K.G. Ruddick, S. Becquevort, V. Rousseau, G. Lacroix, and G. Billen (2005). Modelling diatom and *Phaeocystis* blooms and nutrient cycles in the Southern Bight of the North Sea: The MIRO model. Marine Ecology Progress Series 289, pp. 63–78.

Luyten, P.J., J.E. Jones, R. Proctor, A. Tabor, P. Tett, and K. Wild-Allen (1999). COHERENES documentation: a coupled hydrodynamical-ecological model for regional and shelf seas: user documentation. MUMM internal document, MUMM, Brussels, P. 903.

OSPAR (1998). OSPAR Agreement 1998-18. OSPAR Strategy to Combat Eutrophication. www.ospar.org

Park, Y., K. Ruddick, and G. Lacroix (2010), Detection of algal blooms in European waters based on satellite chlorophyll data from MERIS and MODIS. International Journal of Remote Sensing, Vol. 31, Issue 24, pp 6567–6583.

Rousseau, V., Y. Park, K. Ruddick, W. Vyverman, J.-Y. Parent and C. Lancelot (2006). Phytoplankton blooms in response to nutrient enrichment. In: Current status of Eutrophication in the Belgian Coastal Zone. Editor(s): V. Rousseau, C. Lancelot, D. Cox.

Ruddick, K., G. Lacroix, C. Lancelot, B. Nechad, Y. Park, S. Peters and B. Van Mol (2008c). Optical remote sensing of the North Sea. In: Remote sensing of the European Seas. Springer-Verlag. Editor(s): V. Barale and M. Gade.

Ruddick, K., Y. Park, R. Astoreca, A. Borges, G. Lacroix, C. Lancelot, and V. Rousseau (2008b). Applications of the MERIS algal2 product in Belgian waters. Proceedings of the 2nd MERIS-(A)ATSR workshop, 2008, Frascati, Italy. ESA Special Publication SP-666. 4p.

Ruddick, K., Y. Park, R. Astoreca, G. Neukermans, and B. Van Mol (2008a). Validation of MERIS water products in the Southern North Sea: 2002–2008. Proceedings of the 2nd MERIS-(A)ATSR workshop, 2008, Frascati, Italy. ESA Special Publication SP-666. 8p.

Sirjacobs D., A. Alvera-Azcarate, A. Barth, G. Lacroix, Y. Park, B. Nechad, K. Ruddick, and J.-M. Beckers (2011). Cloud filling of ocean color and sea surface temperature remote sensing products over the Southern North Sea by the Data Interpolating Empirical Orthogonal Functions methodology. Journal of Sea Research, Vol. 65, pp. 114–130.

Sorensen, K, G.G. Severinsen, G. Aertebjerg, V. Barale, and C. Schiller (2002). Remote Sensing's contribution to evaluating eutrophication in marine and coastal waters. European Environment Agency, 41p.

Monitoring chlorophyll concentrations with POSEIDON system's optical instruments

P.G. Drakopoulos*[1], K. Nittis[2], G. Petihakis[2], D. Kassis[2], P. Pagonis[2], D. Ballas[2], and M. Ntoumas[2]

[1]*Department of Optics, TEI of Athens*
[2]*Institute of Oceanography, HCMR*

Abstract

In a specially designed experiment optical data from the POSEIDON system Cretan Sea station, above water surface reflectance measurements and in-situ chlorophyll-a profiles were collected and combined in order to evaluate the existing remote sensing chlorophyll retrieval algorithms. It was found that both SeaWiFS and MODIS global algorithms overestimate the chlorophyll concentration by >35%, but another more interesting finding was that the algorithms, developed specifically for the Mediterranean, underestimate the concentration by a similar factor. Further investigation is under way.

Keywords: ocean optics, remote sensing, operational oceanography

1. Introduction

Algal biomass distribution is an important factor for the assessment of marine environment condition. Traditionally, a proxy to this distribution is chlorophyll concentration, which in turn can be estimated with the implementation of optical methods. More specifically, this is achieved either by monitoring the stimulated fluorescence of chlorophyll or simply the effect it has in the colour of the ocean. Satellite-collected ocean colour data provide a cost effective way for this purpose provided that the chlorophyll retrieval algorithms have been validated for the region of interest. Drakopoulos *et al*. (2003) found that for the Cretan Sea oligotrophic Case I waters, the global SeaWiFS algorithm overestimates in-situ chlorophyll by ~37%. In time new empirical relations tuned to the Mediterranean waters have been developed (MedOC4 for SeaWiFS, and MedOC3 for MODIS; Volpe *et al*., 2007, Santoleri *et al*., 2008).

In order to monitor algal biomass for the needs of the prognostic system Poseidon, optical sensors have been installed at an operational level on the multi-parameter observation platform (E1-M3A) in the Cretan Sea (Nittis *et al*., 2010). This platform is moored in 1400 m depth, 20 miles north of Iraklion, at exactly the same location that the SeaWiFS global chlorophyll retrieval algorithm was investigated 10 years ago. The availability of new optical measurements and the lack of proper validation of ocean colour products for that region led us to undertake this relevant experiment. Its scope was oriented towards assessing the performance of the newly developed local algorithms. It was executed during the regular maintenance visit to the E1-M3A platform in March 2011. The purpose of this paper is to report the preliminary results.

* Corresponding author, email: pdrak@teiath.gr

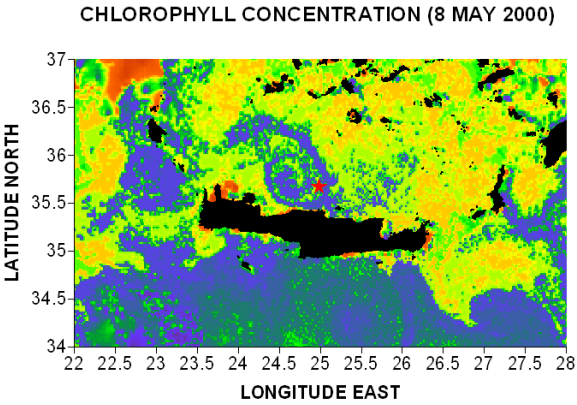

Figure 1 Location of the E1-M3A platform.

2. Instruments

The basic optical instruments installed on the multi-parameter observation platform E1-M3A and utilised in this experiment are (Drakopoulos *et al*. 2009):

- OCR-507 irradiance meter monitoring solar irradiance at seven wavelengths 412, 443, 490, 555, 665, 683, 705 nm. It is installed 2.2 m above sea surface and is equipped with an anti-fouling shutter.
- OCR-507 radiance meter monitoring water leaving radiant flux over the above mentioned seven wavelengths. It is installed at a depth of 40 cm below the sea surface and is equipped with an anti-fouling shutter.
- LI-193SA PAR photometers and FLNTU fluorometers installed at depths 25, 50, 75, 100 m.

In addition an Ocean Optics HR4000 portable spectroradiometer was utilised. The radiance measurements were performed with an 8° FOV Gershun tube attached to the end of the fibre. For downwelling irradiance estimation, the diffuse reflectance of a calibrated Spectralon plate was measured. Complimentary data included in-situ vertical profiles obtained with an SBE25 CTD equipped with PAR, transmittance and fluorescence sensors. Chl-*a* concentration profiles were calibrated against concurrent water samples from six visits on location during 2010–2011.

3. Methods

The remote sensing chlorophyll concentration is given by (e.g. D'Ortenzio *et al*., 2002):

$$C = 10^{(a_0 + a_1 R + a_2 R^2 + a_3 R^3 + a_4 R^4)} \quad (1)$$

where the *a* coefficients are algorithm-dependent and *R* is related to the ratio of blue to green remote sensing reflectances. This concentration is comparable to the weighted in-situ concentration:

$$C_w = \frac{\int_0^{\tau} C(z)\exp(-2kz)dz}{\int_0^{\tau}\exp(-2kz)dz} \quad \text{where } \tau = \frac{1}{k_{\mathrm{PAR}}} = \frac{z_e}{4.6} \approx 19 \text{ m} \tag{2}$$

with the limit of integration (optical depth) during the experiment estimated from PAR profiles.

The above the water surface (Mobley 1999 protocol) and below surface remote sensing reflectance were calculated following:

$$R_{rs}(0+) = \frac{L_w(0+)}{E_d(0+)} = \frac{[L_u(0+) - \rho L_{\mathrm{sky}}(0+)]R_g}{\pi L_d(0+)}$$

$$R_{rs}(0+) = \frac{L_w(0+)}{E_d(0+)} = \frac{0.54L_u(0-)}{E_d(0+)} \tag{3}$$

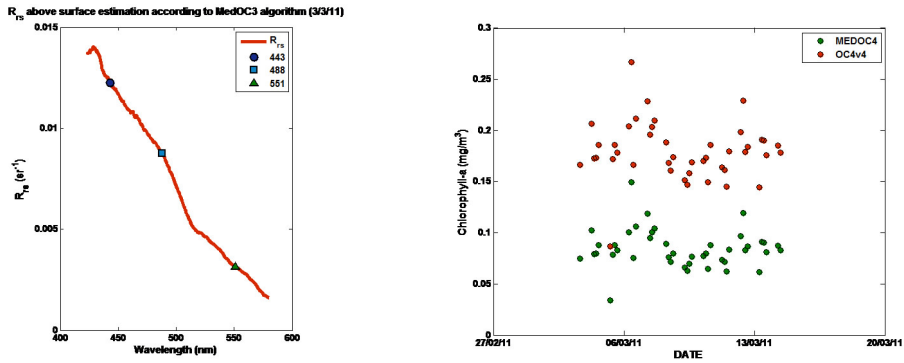

Figure 2 Left: Typical above surface remote sensing reflectance during the experiment. Right: Time series of chlorophyll concentration at the M3A location monitored by the OCR7 radiometers and estimated using the MEDOC4 (solid circles) and OC4v4 (transparent circles) algorithms. The starting date is 3 March 2011, which was the day of the experiment.

4. Results

The corresponding depth integrated weighted concentration was found to be:

$$C_w = 0.12(\pm 0.02)\ \mathrm{mg\,m^{-3}} \tag{4}$$

This value is also expected to be calculated by the radiance measurements (both above and below surface) provided that the retrieval algorithms used are properly tuned.

The tabulated results are in $\mathrm{mg\,m^{-3}}$. Both the above and under surface measurements gave comparable results. Undoubtedly, the global algorithms OC4v4 and OC3 overes-

timate concentration (~35%). Surprisingly enough, it was found that the regional algorithms for the Mediterranean Sea are also biased and underestimate the ground truth by a similar amount. This figure was also evident in concurrent MODIS pictures readily processed with the MedOC3 algorithm and archived in the site of CNR.

Algorithm	Above surface	Below surface	MODIS pictures	In-situ optically weighted
OC4v4	0.14	0.16		
MedOC4	0.06	0.07		0.12
OC3	0.13	-		
MedOC3	0.05	-	~0.06	

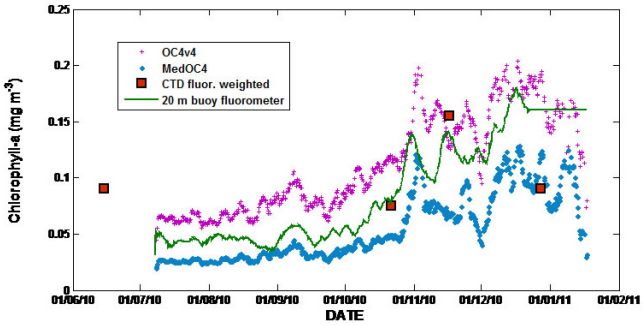

Figure 3 Available data before the current experiment. In-situ collected data fall, on average, in between the values obtained from buoy reflectance measurements evaluated according to the two different algorithms.

5. Conclusions

The main conclusion is that all global algorithms overestimate the chlorophyll concentration (35%) in the Cretan Sea. Moreover, the newly developed regional algorithms underestimate concentration (>35%) at least for concentrations of the order of 1 $mg\,m^{-3}$. The agreement with in-situ and remote sensed estimations points toward adequacy of atmospheric correction algorithms. The discrepancy can be attributed to the local phytoplankton community structure and distribution.

New visits to the site are scheduled for the near future, in order to accumulate enough data for estimating local empirical coefficients. Refined optical measurements, such as collection of profiles with a hyperspectral absorption-transmission meter, should aid the investigation towards explaining the causes behind the peculiarities of the local water colour.

References

D'Ortenzio, F., S. Marullo, M. Ragni, M.R. d'Alcala, and R. Santoleri (2002). Validation of empirical SeaWiFS algorithms for chlorophyll-alpha retrieval in the

Mediterranean Sea. A case study for oligotrophic seas, Remote Sensing of Environment, 82(1), 79–94.

Drakopoulos, P., G. Petyhakis, V. Valavanis, K. Nittis, and G. Triantafyllou (2003). Optical variability associated with phytoplankton dynamics in the Cretan Sea during 2000 and 2001. in: "Building the European Capacity in Operational Oceanography", Elsevier Oceanogr Series No 69, Elsevier BV: 554–561.

Drakopoulos, P., G. Petihakis, V. Zervakis, K. Nittis, and POSEIDON system (2009). Environmental monitoring with new generation optical instruments, Proceedings of the Second International CEMEPE and SECOTOX, Mykonos Island, Greece, 395–399.

Mobley, C.D., (1999). Estimation of the remote-sensing reflectance from above-surface measurements. Appl Opt, 38, 7442–7455

Nittis, K., L. Perivoliotis, G. Korres, D. Ballas, A. Papadopoulos, G.Triantafyllou, P. Pagonis, K. Tsiaras, G. Petihakis, and P. Drakopoulos (2010). POSEIDON II: Upgrading the monitoring and forecasting services in the Eastern Mediterranean Sea. Proceedings of the 5th International Conference of EuroGOOS, EuroGOOS publication n. 28, ISBN 978-91-974828-6-8, p.392–398

Santoleri, R., G. Volpe, S. Marullo, and B. Buongiorno Nardelli (2008). Open Waters Optical Remote Sensing of the Mediterranean Sea, in: "Remote Sensing of the European Seas", edited by: Barale, V., and Gade, M., Springer, 103–114.

Volpe, G, R. Santoleri, V. Vellucci, M. Ribera d'Alcalà, S. Marullo, amd F. D'Ortenzio, (2007). The colour of the Mediterranean Sea: Global versus regional bio-optical algorithms evaluation and implication for satellite chlorophyll estimates, Remote Sensing of Environment 107, 625–638.

Indexes


L - Z
Regular Fee 300 EUR
Student Fee 250 EUR
Accompanying Person 50 EUR

Index of Authors

Index of Keywords

W

List of Participants

Mario Adani
Justin Ahanhanzo
Andres Alonso-Martirena
Enrique Alvaréz Fanjul
Cecilia Ambjörn
Philip Axe
Jesper Baasch-Larsen
Pierre Bahurel
Tomasz Balcerzak
Rosa Barciela
Mike Bell
Francesco Bignami
Simone Bonamano
Goran Brostrom
Erik Buch
Filippo Carli
Pablo Cerralbo
Pedro Costa
Alessandro Crise
Aleksandra Czyz
Nick D'Adamo
Hans Dahlin
Michela De Dominicis
Viktor Dorofeyev
Panos Drakopoulos
Dominique Durrand
Peter Ehlers
Weiwei Fu
Lennart Funquist
Marcos Garcia Sotillo
Santiago Gaztelumendi
Fanny Girard-Ardhuin
Stanislav Glushchenko
Patrick Gorringe
Colin Grant
Tom Gross
Mark Grunwald
Guenole Guevel
Jari Haapala
Bruce Hackett
Thomas Hammarklint
Torill Hamre
Martin Hansson
Daniel Hayes
Lars Robert Hole
Edison Hudson
Frank Janssen
Johnny Johannessen
Magdalena Kaminska
Dimitris Kassis
Petros Katsafados
Holger Klein
Nicolai Kliem
Tarmo Kõuts
Piotr Kowalczuk
Nils Melsom Kristensen
Wlodzimierz Krzyminski
Alexander Kubryakov
Andriy Kurekin
Iréne Lake
Pierre-Yves Le Traon
Sebastien Legrand
Shao Hua Lin
Urmas Lips
Patrick Macdonald
Detlev Machoczek
George Malz
Giuseppe Manzella
Marco Marcelli
Arne Melsom
David Mills
Tim Moltmann
Kostas Nittis
Glenn Nolan
Aleksi Nummelin
Harm Oterdoom
Atanas Palazov
Elena Pallares
Anastasios Papadopoulos
Laura Pederson
Begoña Pérez
Wilhelm Petersen
Sian Petersson
George Petihakis

Jan Piechura
Viviana Piermattei
Nadia Pinardi
Sylvie Pouliquen
Yuriy Ratner
Alberto Ribotti
Marie-Helene Rio
Friedrich Rochleder
Lars Petter Roed
Stein Sandven
Rosalia Santoleri
Christoph Schreyer
Johannes Schulz-Stellenfleth
Jun She
John Siddorn
David Storkey
Vyacheslav Suslin
Marina Tonani
Dries Van den Eynde
Dimitry van der Zande
Kees van Ruiten
Henning Wehde
Marcin Wichorowski
Zdenka Willis
Evgeny Vyazilov
George Zodiatis